MARTIN MARIETTA ENERGY SYSTEMS LIBRARIES
3 4456 0134418 5

CENTRAL RESEARCH LIBRARY
DOCUMENT COLLECTION

cy. 2

ORNL-4682
UC-10 — Chemical Separations Processes
for Plutonium and Uranium

OAK RIDGE NATIONAL LABORATORY
CENTRAL RESEARCH LIBRARY
DOCUMENT COLLECTION
LIBRARY LOAN COPY
DO NOT TRANSFER TO ANOTHER PERSON
If you wish someone else to see this document, send in name with document and the library will arrange a loan.
UCN-7969
(3 3-67)

CHEMICAL TECHNOLOGY DIVISION

ANNUAL PROGRESS REPORT

FOR PERIOD ENDING MARCH 31, 1971

OAK RIDGE NATIONAL LABORATORY
operated by
UNION CARBIDE CORPORATION
for the
U.S. ATOMIC ENERGY COMMISSION

Printed in the United States of America. Available from
National Technical Information Service
U.S. Department of Commerce
5285 Port Royal Road, Springfield, Virginia 22151
Price: Printed Copy $3.00; Microfiche $0.95

This report was prepared as an account of work sponsored by the United States Government. Neither the United States nor the United States Atomic Energy Commission, nor any of their employees, nor any of their contractors, subcontractors, or their employees, makes any warranty, express or implied, or assumes any legal liability or responsibility for the accuracy, completeness or usefulness of any information, apparatus, product or process disclosed, or represents that its use would not infringe privately owned rights.

INTRA-LABORATORY CORRESPONDENCE

OAK RIDGE NATIONAL LABORATORY

ORNL-4682
Errata

CHEMICAL TECHNOLOGY DIVISION ANNUAL PROGRESS REPORT

FOR PERIOD ENDING MARCH 31, 1971

Please make the following corrections to your copy of the subject report:

On page 39 the title for Chapter 2 is incorrect. The attached correct title is printed on gummed stock and may be glued directly on the page.

On page 225, line 22 in the left-hand column, the reference callout should be 17 instead of 19. Reference 19 should be shown as a superscript callout after the last word of the centered heading that appears in the right-hand column of page 226, and should have been included at the bottom of that page.

Bew
7/21/71

UCN-430
(3 5-61)

ORNL-4682

Contract No. W-7405-eng-26

CHEMICAL TECHNOLOGY DIVISION

ANNUAL PROGRESS REPORT

for Period Ending March 31, 1971

D. E. Ferguson — Division Director
K. B. Brown — Assistant Division Director
R. G. Wymer — Chemical Development Section A Chief
R. E. Blanco — Chemical Development Section B Chief
M. E. Whatley — Unit Operations Section Chief
H. E. Goeller — Process Design Section Chief
R. E. Brooksbank — Pilot Plant Section Chief

JULY 1971

OAK RIDGE NATIONAL LABORATORY
Oak Ridge, Tennessee
operated by
UNION CARBIDE CORPORATION
for the
U. S. ATOMIC ENERGY COMMISSION

MARTIN MARIETTA ENERGY SYSTEMS LIBRARIES
3 4456 0134418 5

Reports previously issued in this series are as follows:

ORNL-2392	Period Ending August 31, 1957
ORNL-2576	Period Ending August 31, 1958
ORNL-2788	Period Ending August 31, 1959
ORNL-2993	Period Ending August 31, 1960
ORNL-3153	Period Ending May 31, 1961
ORNL-3314	Period Ending May 31, 1962
ORNL-3452	Period Ending May 31, 1963
ORNL-3627	Period Ending May 31, 1964
ORNL-3830	Period Ending May 31, 1965
ORNL-3945	Period Ending May 31, 1966
ORNL-4145	Period Ending May 31, 1967
ORNL-4272	Period Ending May 31, 1968
ORNL-4422	Period Ending May 31, 1969
ORNL-4572	Period Ending May 31, 1970

Contents

SUMMARY vii

1. MOLTEN-SALT REACTOR PROCESSING 1
   - 1.1 Molten-Salt Breeder Reactor Flowsheet Analysis 2
   - 1.2 Measurement of Distribution Coefficients in Molten-Salt–Metal Systems 10
   - 1.3 Estimated Free Energies of Formation of Some Lanthanide and Actinide Halides Using Distribution Coefficient Data 14
   - 1.4 Solubilities of Thorium and Neodymium in Lithium-Bismuth Solutions 15
   - 1.5 Protactinium Oxide Precipitation Studies 17
   - 1.6 Reductive Extraction Engineering Studies 20
   - 1.7 Development of the Metal Transfer Process for Removing Rare Earths 24
   - 1.8 Contactor Studies of a Simulated Molten-Salt– Liquid-Bismuth System 29
   - 1.9 Axial Dispersion in Simulated Continuous Fluorinators 31
   - 1.10 Development of a Frozen-Wall Continuous Fluorinator 33
   - 1.11 Design of a Processing Materials Test Stand and the First Molybdenum Reductive Extraction Equipment 35
   - 1.12 Removal of Uranium from Molten Salt by Oxide Precipitation 36
   - 1.13 Reduction of Iron Fluoride in Molten Salt by Countercurrent Contact with Hydrogen in a Packed Column 37

2. DEVELOPMENT OF AQUEOUS PROCESSES FOR LMFBR FUELS 39
   - 2.1 Shipping 40
   - 2.2 Head-End Processing 42
   - 2.3 Removal of Volatile Fission Products 49
   - 2.4 Dissolution and Feed Preparation 53
   - 2.5 Solvent Extraction with TBP 59
   - 2.6 Off-Gas Treatment 61
   - 2.7 Radiation, Shielding, and Criticality Studies 69
   - 2.8 Engineering Studies 73

3. DEVELOPMENT OF METHODS FOR REPROCESSING HTGR FUELS 80
   - 3.1 Head-End Reprocessing Studies with Unirradiated Fuel 80
   - 3.2 Head-End Reprocessing Studies with Irradiated Fuels 84

3.3 Procurement of HTGR Fuel for Head-End Studies 92
3.4 Design Support for Head-End Studies 94

4. WASTE TREATMENT AND DISPOSAL 95
4.1 Radioactive Waste Repository 95
4.2 Engineering, Economic, and Safety Evaluations 99
4.3 High-Level Radioactive Waste 103
4.4 Combustion of Plutonium-Bearing Solid Wastes 105
4.5 Incorporation of Intermediate-Level Wastes in Polyethylene 109

5. TRANSURANIUM-ELEMENT PROCESSING 114
5.1 TRU Operations 114
5.2 Isolation and Purification of TRU Products 117
5.3 Special Projects 118
5.4 Development of Chemical Processes 119
5.5 Transplutonium-Element Research 121
5.6 Collaborative Research with the Transuranium Research Laboratory 130

6. DEVELOPMENT OF THORIUM FUEL CYCLE 133
6.1 Recycle of the Alcohol Used in the Microsphere-Forming Column 133
6.2 Development of Prototype Equipment for TURF 134
6.3 Preparation of Microspheres in Nonfluidized-Bed Columns 137
6.4 Preparation of Test Materials 140
6.5 ^{233}U Storage, Purification, and Distribution 142

7. SOL-GEL PROCESSES FOR THE URANIUM FUEL CYCLE 144
7.1 Preparation of UO_2 Sol by the CUSP Process 144
7.2 Development of the UO_2-PuO_2 Sol-Gel Process 149
7.3 Microsphere-Forming Studies 154
7.4 Preparation of UO_2-PuO_2 Materials 158

8. CONVERSION STUDIES IN THE LMFBR FUEL CYCLE 160
8.1 Technical and Economic Evaluation 160
8.2 Conversion by Homogeneous Reduction 160

9. PREPARATION OF $^{233}UO_2$ FOR LIGHT-WATER BREEDER REACTORS 163
9.1 Process Development and Flowsheets 163
9.2 Plant Modifications 165
9.3 Design of Equipment for the UO_2 Conversion Line 165
9.4 Receipt and Storage of ^{233}U Feed Material 166
9.5 Plant Safety 166
9.6 Site Preparation 167

10. SEPARATIONS CHEMISTRY RESEARCH 168
10.1 New Separations Agents 168
10.2 Recovery of Uranium from Commercial Phosphoric Acid 170
10.3 High-Resolution Rare-Earth Separations 173
10.4 Displacement Elution with Aminopolyacetic Acids 174
10.5 Isotope Enrichment by (n,γ) Reactions in Molecular Sieves 174
10.6 Distribution Equilibria and Mechanisms 175
10.7 Relative Potentials of the Bk(IV)-Bk(III) and Ce(IV)-Ce(III) Couples 177
10.8 Lanthanide and Actinide Hydroxides 177
10.9 Kinetics of Metal-Ion Extractions by Organophosphorus Acids 179

11. CHEMICAL APPLICATIONS OF NUCLEAR EXPLOSIVES 182
11.1 Copper Ores 182
11.2 Recovery of Oil from Shale 185
11.3 Natural-Gas Storage 186

12. BIOCHEMICAL TECHNOLOGY 187

MACROMOLECULAR SEPARATIONS 187
12.1 Preparation of Crude Bovine Liver Transfer Ribonucleic Acid 187
12.2 New Chromatographic Systems for the Separation of Transfer Ribonucleic Acids 189
12.3 Miniature Chromatographic Systems for Tracer-Labeled Transfer Ribonucleic Acids 190
12.4 Separation of Ribosomal Ribonucleic Acids 191
12.5 Purification of Five Leucine Transfer Ribonucleic Acids from *E. coli* 193
12.6 Flowsheet Development and Large-Scale Purification of *E. coli* Transfer Ribonucleic Acids 194
12.7 Distribution of Purified Transfer Ribonucleic Acids 196

BODY FLUIDS ANALYSES PROGRAM 197
12.8 Prototype Analyzers 197
12.9 Separation Systems 197
12.10 System Components 202
12.11 Identification of Body Fluid Constituents 203
12.12 Applications and Experimental Results 205
12.13 Data Acquisition and Analysis 207

WATER POLLUTION STUDIES 209
12.14 Preparation of Samples 210
12.15 Analytical Systems 210
12.16 Identification of Refractory Organics 214

13. SPECTROPHOTOMETRIC STUDIES OF SOLUTIONS OF LANTHANIDES AND ACTINIDES 215
13.1 High-Energy Absorption Bands of H_2O and D_2O 215
13.2 Spectral Studies of the Actinides 215
13.3 Emission Spectra of the Actinides 216
13.4 Densities of Aqueous Rare-Earth Solutions to 340°C 216
13.5 Protonic Wave Functions and Spectra 216

14. PREPARATION AND PROPERTIES OF ACTINIDE OXIDES 218
14.1 Thoria Desintering Studies 218
14.2 Adsorption of Nitric Acid on the Surface of Urania 223
14.3 Preparation of Carbides and Carbonitrides 224

15. CHEMICAL ENGINEERING RESEARCH 229
15.1 Mass Transfer of Water from Sol Droplets 229
15.2 Dehydration of Individual Sol Droplets in a Minicolumn 231
15.3 Production of Sol-Gel Microspheres of Small Uniform Size 234
15.4 Pulsed Clone Contactor 234
15.5 Axial Dispersion in Packed Columns for Contacting Liquids with a High Density Difference 235
15.6 Multicomponent Mass Transfer in Electrolyte Systems 237
15.7 Chemical Engineering Research Studies Related to MSR Processing 239

16. REACTOR EVALUATION STUDIES 240
16.1 Oak Ridge Systems Analysis Code 240
16.2 Optimal Dispatching of Electric Power Generating Plants 241
16.3 Economic Integration of Nuclear Reactors in Electric Utility Systems 241

17. MISCELLANEOUS PROGRAMS 242
17.1 Quality Assurance Program 242
17.2 Evaluation of the Radiation Resistance of Selected Protective Coatings (Paints) 242
17.3 Resource Studies 245
17.4 Environmental Quality Program: Productive Uses of Waste Heat 246
17.5 Systems Analysis of a Nuclear Energy Center 247
17.6 Applications of ^{252}Cf 248

PUBLICATIONS, SPEECHES, AND SEMINARS 250

ORGANIZATION CHART 261

Summary

1. MOLTEN-SALT REACTOR PROCESSING

1.1 Molten-Salt Breeder Reactor Flowsheet Analysis

We have developed an improved protactinium isolation method in which the ^{233}Pa is held for decay in a secondary fluoride salt that is physically and chemically isolated from the reactor. Representative operating conditions and partial fuel cycle costs are given for this system. Calculations that show the effects of important process parameters for the metal transfer process for rare-earth removal were made. A flowsheet that uses the improved protactinium isolation method and the metal transfer process was devised. A method for combining and fluorinating the waste streams from the two parts of the flowsheet was developed, thus eliminating several potential routes for loss of fissile material from the system.

Oxide precipitation is being studied as an alternative to the fluorination–reductive extraction method for isolating protactinium and for subsequently removing uranium from the fuel salt of an MSBR. Two possible flowsheets based on oxide precipitation have been developed, and the effects of several parameters on the operation of the process have been investigated.

The importance of the uranium inventory in the processing plant was evaluated. It was concluded that a processing plant uranium inventory as high as 5 to 10% of the reactor uranium inventory should not rule out an otherwise attractive processing system.

1.2 Measurement of Distribution Coefficients in Molten-Salt–Metal Systems

The distribution of selected lanthanide and actinide elements between liquid bismuth solutions and molten lithium halide salts was studied in support of the development of a metal transfer process for removing rare-earth fission products from MSBR fuel salt. Data obtained with LiCl as the salt phase confirmed earlier indications that the distribution behavior of the di- and trivalent elements was not markedly affected by temperature changes. It was found that the californium species in the LiCl was primarily in the 2+ oxidation state both at 640 and at 700°C. Results of studies with LiCl-LiF solutions as the salt phase at 640°C showed that the distribution behavior of the di- and trivalent elements was relatively insensitive to variations in the LiF concentration between 0 and 4 mole %. On the other hand, distribution coefficients for thorium decreased by about a factor of 100 as the LiF concentration was increased from 0 to 4 mole %.

1.3 Estimated Free Energies of Formation of Some Lanthanide and Actinide Halides Using Distribution Coefficient Data

Distribution coefficient data were used in conjunction with published thermochemical data to estimate standard free energies of formation (ΔG^f) for several lanthanide and actinide chlorides and bromides. The ΔG^f values obtained for $LaCl_3$, $ThCl_4$, $ThBr_4$, UCl_3, UBr_3, and $PuCl_3$ generally were in reasonable agreement with values reported in the recent literature. However, our ΔG^f values for $LaBr_3$, $NdCl_3$, and $NdBr_3$ were not in accord with estimates made by others.

1.4 Solubilities of Thorium and Neodymium in Lithium-Bismuth Solutions

Measurements of the solubilities, both individual and mutual, of thorium and rare earths in lithium-bismuth solutions were made in support of the development of the metal transfer process. At 450 to 700°C, the solubilities of both thorium and neodymium increased as the lithium concentration in the solution increased from 0 to 25 at. %. The mutual solubilities of thorium and neodymium were measured in lithium-bismuth solutions at 640°C. The solubilities obtained were much higher than those required in the stripping of rare earths from the LiCl acceptor salt into lithium-bismuth solutions.

1.5 Protactinium Oxide Precipitation Studies

Isolation of protactinium from MSBR fuel salt by oxide precipitation is being studied. Two methods were used to estimate the solubilities, at various temperatures, of Pa_2O_5 in $LiF\text{-}BeF_2\text{-}ThF_4\text{-}UF_4$ (71.8-16-12-0.2 mole %) that was also saturated with UO_2. These solubilities define the lowest protactinium concentrations attainable without attendant precipitation of uranium and thorium oxides. Our preliminary results at about 600°C indicate that most of the protactinium can be precipitated from the salt without precipitation of UO_2.

1.6 Reductive Extraction Engineering Studies

Experimental work in the flow-through reductive extraction facility was continued after the original packed column had been replaced with a modified column packed with ¼-in. Raschig rings.

A set of pressure drop measurements was made with only salt flowing through the column; these measurements will be used in future comparisons to detect possible iron deposition in the column. Uranium was added to the $LiF\text{-}BeF_2\text{-}ThF_4$ salt in the form of an $LiF\text{-}UF_4$ eutectic in preparation for mass transfer experiments with uranium. The first mass transfer experiment resulted in essentially no transfer of uranium as the result of an error in adding thorium reductant to the bismuth prior to the run. The second experiment, UTR-2, was the first successful demonstration of the reductive extraction of uranium into bismuth in a flowing system. Greater than 95% of the uranium was extracted into the bismuth phase, which initially contained a 140% stoichiometric excess of reductant. The next two runs for study of uranium extraction included six periods of steady-state operation covering metal-to-salt flow ratios ranging from 0.75 to 2.05.

The data could be correlated by an HTU model based on the assumption that the uranium transfer rate was controlled entirely by the diffusive resistance in the salt phase. The observed HTU values ranged from 0.77 to 2.1 ft and were inversely proportional to the metal-to-salt flow rate ratio. Flooding data obtained during the countercurrent flow of salt and bismuth in the packed column were in good agreement with predictions based on studies with a mercury-water system.

Preparations were begun for mass transfer experiments in which the rate of exchange of zirconium isotopes will be measured between salt and bismuth phases otherwise at equilibrium in a packed column.

1.7 Development of the Metal Transfer Process for Removing Rare Earths

The first two engineering experiments involving the metal transfer process for the removal of rare earths from a single-fluid MSBR fuel salt have been completed. In the first experiment, approximately 50% of the lanthanum and 25% of the neodymium originally in the fluoride salt were extracted; however, the rare earths did not collect in the lithium-bismuth stripping solution as expected. The distribution coefficients for lanthanum and neodymium between the fluoride salt and the thorium-saturated bismuth were relatively constant and were in agreement with expected values. The distribution coefficients for lanthanum and neodymium between the chloride salt and the thorium-saturated bismuth were higher than anticipated initially but approached the expected values toward the end of the experiment.

The second experiment operated satisfactorily for about three months before it was shut down for inspection. During that period, more than 85% of the lanthanum and more than 50% of the neodymium originally in the fuel carrier salt were removed and deposited in a lithium-bismuth solution. There was no measurable accumulation of thorium (<10 ppm) in the lithium-bismuth solution, thus demonstrating that the rare earths can be removed without significant removal of thorium. The thorium-lanthanum decontamination factor was about 10^5. The distribution coefficients for lanthanum and neodymium between the fluoride salt and the thorium-saturated bismuth were relatively constant and in agreement with expected values. The distribution coefficients for lanthanum and neodymium between LiCl and thorium-saturated bismuth were somewhat higher than expected. When the vessel was disassembled for inspection after the run, the condition of the interior of the vessel was generally good; however, the components made of thin carbon steel (the lithium-bismuth container and the sparge tubes) showed some evidence of corrosion.

The third engineering experiment for development of the metal transfer process is presently being designed. This experiment will use flow rates that are 1% of the estimated flow rates for a 1000-MW(e) reactor. Mechanical agitators will be used to promote efficient contacting of the salt and metal phases. The three vessels required for the experiment will be made of carbon steel; one of the vessels has already been fabricated.

1.8 Contactor Studies of a Simulated Molten-Salt–Liquid-Bismuth System

Studies of hydrodynamics in packed columns during the countercurrent flow of high-density liquids are being made in order to evaluate and design contactors for processing systems based on reductive extraction. Data obtained by an MIT Practice School group show that the slip velocity with nonwetted packing is dependent on the −0.167 power of the continuous-phase viscosity rather than independent as was previously assumed. Knowledge of the dependence of slip velocity on the continuous-phase viscosity allowed calculation of the power dependence of the difference in densities of the phases on slip velocity. A power dependence of 0.5 was calculated rather than the previously assumed dependence of 1.0. Studies with packing wet by the metal phase indicate a substantial reduction in interfacial area between the phases and an increase in the slip velocity.

A program has been initiated for the development of mechanically agitated salt-metal contactors as an alternative to packed columns presently considered for the MSBR processing system. Studies to date have been concerned primarily with selection of a contactor design for the third metal transfer experiment. Tests with mercury and water using a four-bladed flat-paddle agitator located in the mercury-water interface frequently resulted in a stable dispersion of very small mercury droplets and entrainment of water in the mercury. We have begun studies of a contactor which has a paddle operating in each phase, well away from the interface, at a speed that does not result in the dispersion of either phase.

1.9 Axial Dispersion in Simulated Continuous Fluorinators

Studies of the effect of column diameter on axial dispersion in open bubble columns were extended to include a 6-in.-diam column, and additional data were obtained on the effect of the viscosity of the liquid. The dispersion coefficient values obtained with a 6-in.-diam, 72-in.-long column were about three times the values measured at the same superficial gas velocity in a 3-in.-diam column; the data show little dependence on superficial gas velocity at low gas velocities. The dispersion coefficient in a 6-in.-diam column is not noticeably affected by changing the viscosity of the liquid from 0.9 to 12 cP. The same change in viscosity in a 1.5- or a 2-in.-diam column results in a 20% decrease in dispersion coefficient. However, since the diameter of continuous fluorinators will be 6 in. or larger, the viscosity of the liquid will not affect the dispersion coefficient.

1.10 Development of a Frozen-Wall Continuous Fluorinator

Twenty-eight runs have been made with the simulated continuous fluorinator to determine heat generation rates in nitric acid (used as a stand-in for molten salt), in the pipe surrounding the acid column (representing the fluorinator wall), and in four different induction coils. Air was also bubbled through the nitric acid at rates up to 2.16 scfm, producing bubble volume fractions up to 18%, to determine the effect of bubbles on heat generation rate in the acid. Efficiencies predicted for heating molten salt in a fluorinator using the best coil design ranged from 31.1% with no bubbles to 27.6% with 15% bubbles in the salt. These efficiencies are sufficiently high to operate a fluorinator having a 4.5-in.-diam molten zone and a 1.5-in.-thick frozen salt layer using an available generator.

Rate constants for the corrosion of Ni-200 and Ni-201 in gaseous fluorine at 1 atm pressure were calculated from literature data, assuming that the reaction follows a parabolic rate law; the calculated rate constants were correlated with temperature, assuming an Arrhenius temperature dependence. The resulting data were then used to estimate average corrosion rates when the NiF_2 protective film is periodically destroyed. Average corrosion rates of 2.9 mils/year and 0.97 mil/year for Ni-200 and Ni-201, respectively, were estimated at 450°C (a typical fluorinator wall temperature) when the NiF_2 film was assumed to be destroyed 52 times annually. These corrosion rates are acceptable for long-term fluorinator operation.

1.11 Design of a Processing Materials Test Stand and the First Molybdenum Reductive Extraction Equipment

A cooperative project is in progress between the Chemical Technology and the Metals and Ceramics Divisions to develop molybdenum fabrication techniques and build a small packed-column system. Fabrication methods have been selected and are now being developed for molybdenum. A plastic flow-test model of part of the system has been tested. The final design of the system will be started in the near future.

1.12 Removal of Uranium from Molten Salt by Oxide Precipitation

We are presently designing an engineering-scale experiment to study the precipitation of uranium oxide from

MSBR fuel salt from which the protactinium has been previously removed. In this experiment, uranium will be precipitated from 2 liters of fuel salt in a single-stage batch operation by contact with an argon-steam mixture. The design of the precipitator vessel is described.

1.13 Reduction of Iron Fluoride in Molten Salt by Countercurrent Contact with Hydrogen in a Packed Column

Equipment to study the continuous purification of molten-salt mixtures in a packed column was put into operation. Ten flooding runs were made with argon or hydrogen and $LiF-BeF_2$ (66-34 mole %). Iron fluoride was added to the system, and two hydrogen reduction runs were made. Accumulated oxide was removed from the salt and equipment by H_2-HF treatment. After thorium had been added to the salt to form $LiF-BeF_2-ThF_4$ (72.0-14.4-13.6 mole %), nine additional runs were made.

2. DEVELOPMENT OF AQUEOUS PROCESSES FOR FAST REACTOR FUELS

2.1 Shipping

Impact tests made with model casks of all-steel construction have shown that seals can be installed in such a way that deformation of the cask body will not bring about deformation of the critical sealing surfaces. This leads us to believe that satisfactory mechanical sealing systems can be devised. Two large-scale heat transport tests have been operated to demonstrate exceptionally low temperature variations both within the fuel subassembly boundary and within the spaces between the subassembly and the cask fuel cavity boundary. Much lower heat dissipation capacities were shown to be available when gaseous heat transport media were used.

2.2 Head-End Processing

A comparison of the decay heat generation rates for a typical PWR fuel (Diablo Canyon) assembly and several LMFBR assemblies was made using the computer code ORIGEN, and the center-rod temperatures were compared as a function of decay time using the computer code HEX.

The thermal conductivity of sheared stainless-steel-clad porcelain (simulating sheared LMFBR fuel) was measured in air and in argon, and the thermal conductivity of sheared stainless steel rod was measured in argon. The validity of using stainless-steel-clad porcelain as a stand-in for stainless-steel-clad urania is being checked by measuring and comparing the conductivities of the two systems.

A plasma torch with a sensing-probe tracking device and carriage is currently being considered as the most favorable instrument for deshrouding LMFBR fuel assemblies. The torch successfully cut a prototype shroud corner (longitudinally) without damaging the prototype fuel rod array.

Material for thermal conductivity measurements was produced by shearing AI reference prototype core rods (porcelain filled), ¼ in. OD by 15-mil wall, into ½-in. lengths. Measurements showed that the packing density, void fraction, and quantity of dislodged core were 1.66 g/cc, 55%, and 11.5% respectively.

Shearing forces of 11,607 and 14,171 psi were measured on unclad prototype (porcelain) fuel rods (AI reference) having cross-sectional areas of 0.036 and 0.078 in.^{2} respectively.

In a series of tests with the single-rod hot-cell shear, little difference was observed in the force required to shear single rods of empty, porcelain-filled, or irradiated $(U,Pu)O_2$-filled stainless steel tubing.

A program proposal was written for the study of the removal, deactivation, and disposal of sodium present with spent LMFBR fuels. In addition, a state-of-the-art literature review was made, and scoping-type experiments were performed.

2.3 Removal of Volatile Fission Products

Small samples of unirradiated LMFBR $(U,Pu)O_2$ pellets containing 20 and 25 mole % PuO_2 were oxidized isothermally and by programmed heating in a thermal-gravimetric balance. The final O/M ratio was deduced from the observed weight gain. The oxidation kinetics are very rapid at about 400°C up to an O/M ratio between 2.3 and 2.4; however, further oxidation appears to be very dependent on temperature and composition. Pulverization of the fuel occurs only during the second stage of oxidation, in which the U_3O_8 phase is formed.

In voloxidation experiments with sieved fractions of 20% PuO_2–80% UO_2 fuel that had been irradiated to 1800 MWd/ton, larger particles (>30 mesh) of fuel released ^{85}Kr more readily and completely (up to about 60% at 550°C) than did <100-mesh particles. More than 98% of the tritium in the fuel samples was released by the voloxidation treatments. Only 2 to 4% of the calculated yield of tritium was found, however, indicating that most of the tritium escaped from the fuel during irradiation.

A 4-hr oxidation at 450°C removed more than 99% of the tritium but only about 12% of the ^{85}Kr from pellet

fragments from a UO_2 blanket rod from the Shippingport PWR. The low release of ^{85}Kr is attributed to the lack of significant restructuring of the fuel during irradiation.

A rotary calciner, which has been obtained for voloxidation studies, was operated with sheared prototype LMFBR fuel (porcelain-filled stainless steel tubes) to determine the solids holdup under steady-state operating conditions. For a slope of $\frac{1}{8}$ in./ft and a rotational speed of 4 rpm, the residence time is about 50 min and is independent of the feed rate for bulk holdup volumes up to 25% of the calciner volume.

2.4 Dissolution and Feed Preparation

Leaching of unirradiated FTR-type pellets for 18 hr with boiling 8 *M* HNO_3 left about 1.5% of the uranium and 15% of the plutonium undissolved. Oxidizing the fuel at 450 or 750°C or heating the fuel at 1450°C in argon–4% H_2 did not affect the amounts dissolved. In dissolution tests with irradiated coprecipitated fuel, about 0.2% of the plutonium did not dissolve. The rate of dissolution and the quantity of plutonium dissolved increased as the burnup of irradiated sol-gel microspheres was increased; ^{106}Ru became more insoluble as the burnup was increased.

Studies of the volatilization of iodine from nitric acid solutions showed a large decrease in volatility as the concentration of iodine in the solution was decreased. The residual ^{131}I in the solution does not exchange readily with fresh nonradioactive iodine added to the system. Isotopic exchange was achieved by autoclaving the solution at 135 to 150°C.

A state-of-the-art study was made of existing equipment and concepts for the dissolution of sheared nuclear power fuels. As part of the study some new dissolver concepts were developed.

2.5 Solvent Extraction with TBP

Coefficients for the extraction of Pu(IV) with TBP from 3 to 4 *M* HNO_3 were essentially independent of temperature; however, in extractions from 0.3 *M* HNO_3, the coefficient decreased by a factor of 4 as the temperature was increased from 30 to 60°C. At acid concentrations from 0.3 to 3 *M*, uranium coefficients were about a factor of 2 lower at 60°C than at 30°C. The efficiency of stripping plutonium with 0.3 *M* HNO_3 was appreciably improved by increasing the temperature, apparently because this favored disproportionation of the Pu(IV). Hydroxylamine nitrate was the most effective of several reductants examined as aids in stripping plutonium.

2.6 Off-Gas Treatment

Calculations and preliminary tests indicate that cold trapping at −75 to −125°C offers a potentially attractive method for collecting into a small volume most of the iodine and tritium (as tritiated water) that are released during shearing and voloxidation of LMFBR fuel.

Efficient trapping of methyl iodide from air streams was obtained by passing the air through a column of refluxing 16 *M* HNO_3, which decomposes the methyl iodide and oxidizes the iodine to the nonvolatile iodate form. Although optimum operating conditions for the system have not yet been established, decontamination factors of 10^4 and higher were consistently obtained at air flow rates through a 1-in.-diam column of 1.5 liters/min or less.

Studies of catalytic oxidation of organic compounds that may be present in off-gas streams showed the importance of the gas residence time in the catalyst bed. Prolonged heating of Hopcalite catalyst appreciably decreased its catalytic efficiency in the oxidation of butane and methane in air.

Highly efficient trapping of methyl iodide and I_2 was obtained with silver zeolites and alumina sorbents treated with silver nitrate at temperatures of about 200°C. Long-term tests were started to determine if these sorbents will maintain high iodine trapping efficiency on prolonged exposure to air containing organic (and other) potential sorbent bed poisons.

Studies with macroreticular resins continued to show that these materials have high capability for absorbing I_2 from dry air streams; sorption is much less efficient from wet air. One of the resins, Amberlite XAD-12, sorbed methyl iodide efficiently from dry air. This resin also sorbed iodine effectively from water.

Recent tests indicate that the appreciable volatilization of iodine from I_2-caustic solutions reported previously was apparently due to organic iodides that are formed by reaction of highly reactive hypoiodite with organic impurities in the system.

An iodine removal system, consisting of a catalytic oxidation step to destroy organics, followed by charcoal beds for iodine removal, was installed and operated on the combined TRU vessel and cubicle off-gas (~400-cfm) stream. Iodine-131 decontamination factors approaching 10^4 were demonstrated during the first month of operation, consistent with previous experiences with small-scale systems of this design. Removal efficiencies were, however, decreased by factors of 10 to 100 after three months of continuous operation. This loss of efficiency with time had been observed for previous small-scale systems. The charcoal

beds will be replaced by silver zeolite during the coming year, and a significant improvement in both initial efficiency and bed life is expected.

2.7 Radiation, Shielding, and Criticality Studies

The objective of this series of studies is to provide basic nuclear data to support the design and development of the LMFBR fuel cycle. The studies of radiation properties and shielding requirements of LMFBR fuels involve correlation of basic nuclear data, including decay schemes, neutron cross sections, energy spectra of radiation sources, and thermal power; development of computer programs for the calculation of transient concentrations of radionuclides; calculation of attenuation kerma of shield materials of interest; and application of these data to LMFBR fuel cycle processes. The criticality studies involve compilation and correlation of basic data, liaison with experimental groups, development and verification of computational techniques, and development of criticality parameters and control techniques for specific process applications.

During the past year, we have been evaluating the accuracy of the ORIGEN program and developing parametric data for use in the design of radiation shields. We have also been developing parametric data for heterogeneous systems of $(U + Pu)O_2$ in water and fissile solutions to complement the data for homogeneous systems that were reported previously.

2.8 Engineering Studies

A study was made of the feasibility of the interim reprocessing of fuels from the Fast Test Reactor (FTR or FFTF) and other conceptual Follow-On LMFBR's in the Nuclear Fuel Services (NFS) plant, West Valley, New York. The study showed that the *present* NFS head-end equipment and facilities (including plant alterations planned for 1973) are inadequate for the reprocessing of LMFBR fuels. The downstream aqueous Purex facilities and equipment are capable of handling LMFBR fuels, although some of the steps (e.g., plutonium isolation and packaging) and the waste effluents limit the reprocessing rates.

Some mechanical modifications and other development work must be accomplished before long-decayed (one year or more) LMFBR fuels may be reprocessed. The reprocessing of short-decayed fuel in the existing system, even with the most extensive modifications envisioned as being reasonable, would result in excessive radioactive emissions as well as lead to other problems.

The NFS facilities would require only minimal modifications if the fuel supplied to the plant were long-decayed and could be guaranteed to be free of sodium. For example, a new fuel receiving and cleaning facility would not be required. Sodium-free fuel of a post-irradiation time of 365 days or longer could be processed if a disassembly capability was added to the process mechanical cell or if the bundle shear was suitably altered to ensure that the shroud of each subassembly was cut into small discrete pieces that would pass through the restricted throat of the shear. However, the reprocessing of sodium-activated spent fuel after a long decay period would not permit the overall demonstration of the technology required for shorter-decayed fuels.

Overall, it could be concluded that the processing limitations at NFS and the modifications that would be required are of such a magnitude that, for the shorter-decayed fuels, the addition of a new reprocessing head-end facility (for receiving and cleaning the fuel and for carrying out all the process steps through feed adjustment) would probably be more desirable than renovation of the existing facilities.

3. DEVELOPMENT OF METHODS FOR REPROCESSING HTGR FUELS

3.1 Head-End Reprocessing Studies with Unirradiated Fuel

In small-scale tests, simulated TRISO-TRISO fuel was crushed in the hammer mill set to produce either $-\frac{3}{4}$- or $-\frac{3}{8}$-in. product. Breakage of the fissile particle coatings was less than 1% in the $-\frac{3}{4}$-in. product and 3.4% in the $-\frac{3}{8}$-in. product.

Pitch-bonded BISO-TRISO fuel was crushed to $-\frac{3}{8}$ in. in the hammer mill and burned in the fluidized-bed reactor. All of the BISO-coated ThC_2 kernels were converted to a fine ThO_2 powder. Leaching tests showed an average breakage of 2.6% of the TRISO-coated particles in the crushing and burning steps.

Tests were carried out in the 2-in.-diam fluidized-bed burner to determine the maximum burning rate as a function of oxygen partial pressure and superficial gas velocity. The reagent gas composition was held constant at 70% oxygen–30% diluent; the wall temperature was held at 750 ± 25°C. The highest burning rate obtained by holding the superficial gas velocity at 1.25 fps was 30.1 kg of carbon per square foot per hour at a bed overpressure of 18 psig. When the superficial velocity was increased to 1.75 fps, the burning rate increased to 47.5 kg ft^{-2} hr^{-1} at a bed overpressure of 22 psig.

Detailed process chemical flowsheets were prepared for the head-end and Acid-Thorex pilot plants for

TURF. Calculations were based on the assumption that all the bred ^{233}U needed to produce 12 kg of $(Th,U)O_2$ microspheres per day would be recovered from spent Fort St. Vrain reactor fuel.

The major problem in off-gas decontamination is removal of the very large volume of carbon dioxide from the relatively minor amounts of other gases to permit safe disposal of the carbon dioxide. The ratio of volumes and the physical similarity of carbon dioxide, krypton, and xenon practically preclude the use of possible separation processes such as sorption on charcoal, absorption in Freon, and preferential permeation through membranes. The following more promising processes are being studied: (1) liquefaction of the CO_2 fraction, coupled with gas rectification; (2) reversible sorption of CO_2 in hot K_2CO_3-$KHCO_3$ solution; and (3) solidification of the CO_2.

3.2 Head-End Reprocessing Studies with Irradiated Fuels

Head-end methods are being developed for the reprocessing of HTGR fuels. Both the Fort St. Vrain and the 1100-MW(e) reference reactor fuels are included in the development program. An important programmatic change that occurred in the past year is the firm decision by Gulf General Atomic (GGA) to use bonded graphite fuel sticks rather than loose fuel particles in the graphite elements. Fort St. Vrain fuel sticks contain TRISO-coated (i.e., an SiC layer sandwiched between two isotropic carbon layers) $(U,Th)C_2$ and ThC_2 particles. The SiC coating remains intact during the burning step, and methods are being developed to physically separate the particles. The 1100-MW(e) reference fuel consists of TRISO-coated fissile particles ($^{235}UC_2$) and BISO-coated (i.e., two pyrocarbon layers) ThC_2 and fertile $(^{233}U,Th)O_2$ particles. The basic concept remains the same; that is, for minimum power cost, the driver ^{235}U fuel should be maintained separate from the bred ^{233}U and thorium in the fuel cycle. Burning the BISO-coated $(U,Th)C_2$ particles in a fluidized bed may convert them into a finely divided oxide powder; the $(^{233}U,Th)O_2$ particles may retain their shape. Methods are being developed to separate the fissile particles, the alumina used in the fluidized-bed burner, and the fertile particles (or residue).

Seven types of unirradiated and irradiated fuel compacts have been received from the Dragon Project for use in hot-cell studies of HTGR head-end reprocessing. Four of the unirradiated compacts have been studied, and work has started on two of the irradiated compacts.

A flowsheet in which the fuel is sawed into several pieces, the pieces are crushed and burned, and the particles are separated and then finally leached was tested on compact 14719, type 19M, a TRISO UC_{10}–TRISO ThC_2 compact. Sawing broke essentially all the coated particles in the path of the blade. Crushing to ~$^1/_8$-in. feed and burning in the fluidized-bed burner broke about 6 to 9% of the TRISO-coated UC_{10} particles and 20 to 24% of the TRISO-coated ThC_2 particles. No handling problems were experienced.

The saw-crush-burn-separate-leach flowsheet was also tested on compact 22396, a BISO-coated $(U,Th)O_2$ compact. The breakage due to the saw and the crusher was 1.2%. There were no operating problems; however, the oxide kernels (which contained large voids) fractured on burning such that about 15 to 17.5% collected in the alumina fraction.

On crushing compacts 14397 (TRISO UC_{20}) and 14158 [BISO $(5Th/U)C_{2.4}$], we found the breakage of the fuel particles to be <0.1 and 4% respectively. The middle-size crusher fractions of each compact were divided equally, and the two compacts were combined by mixing the appropriate crushed samples to give duplicate samples for burn-separate-leach tests. Breakage of the TRISO particle, leading to crossover of uranium from that particle into the oxide burner product from the BISO particle, was less than 1.7%. Results of leaching the sieved burner products showed that 3 to 11% of the leachable heavy metals stayed with the SiC-coated particles (fissile fraction), 52 to 58% with the oxide produced by burning the BISO particle, and 32 to 45% with the alumina used in the fluidized-bed burner. Losses to insoluble residues were less than 0.1%.

3.3 Procurement of HTGR Fuel for Head-End Studies

We are negotiating with Gulf General Atomic to obtain some reject Fort St. Vrain reactor fuel elements for use in small-scale head-end engineering studies.

Two irradiation programs to provide irradiated materials for head-end studies and for evaluating coated-particle fuel are under way: (1) Two capsules containing several combinations of candidate coated-particle 1100-MW(e) HTGR fuel were placed in the ETR during the third quarter of FY 1971. They are scheduled for discharge late in the first quarter of FY 1972. (2) Seven recycle test elements (RTEs) have been inserted in the Peach Bottom reactor. RTE 7 will be discharged in April 1971. It contains particle combinations typical of Fort St. Vrain fuel and will provide

the earliest determination of the behavior of such fuel during head-end reprocessing.

3.4 Design Support for Head-End Studies

Design support for HTGR head-end studies has been limited to three efforts: (1) evaluation of scale-up potential of burners being considered for development to industrial capacity, (2) design of a whole-element burner and a CO_2 sorption column, and (3) planning of schedules and of manpower requirements to meet the needs of the National HTGR Fuel Recycle Program Plan.

4. WASTE TREATMENT AND DISPOSAL

4.1 Radioactive Waste Repository

We have been involved in a rather substantial effort leading to the establishment of a national repository for radioactive wastes in a bedded salt formation near Lyons, Kansas. While the Chemical Technology Division has participated to some extent in virtually all phases of this project, our major responsibilities have been centered in the conceptual design and safety analysis of the repository, in a survey of the sources and characteristics of transuranium-contaminated solid ("alpha") wastes, and in experimental investigations needed to establish criteria for packaging those alpha wastes to be stored in the repository.

4.2 Engineering, Economic, and Safety Evaluations

During the past year, we have extended our studies of the economics of high-level waste management to include consideration of fluidized-bed calcination as a method for solidifying the wastes, and we have revised an earlier study on shipment of solidified wastes to include provisions for neutron shielding. Also, a theoretical analysis was made of the leaching of the radionuclides from solid wastes.

4.3 High-Level Radioactive Waste

As a part of our program to measure and evaluate the properties of high-level aqueous wastes and the solidified products made from these wastes, we continued to study the thermal conductivity of waste solids and the solubility of boron in aqueous waste. We also initiated studies on energy storage and buildup of electric charges in waste solids.

4.4 Combustion of Plutonium-Bearing Solid Wastes

Pressurized aqueous combustion is a promising method for converting burnable contaminated waste to a noncombustible solid residue suitable for shipment and final storage. A process based on this method can provide a high degree of containment and achieve large reductions in both the volume and the weight of waste to be stored. The most common constituents of contaminated waste, cellulosic materials and polyethylene, are sufficiently oxidized by treatment for about 1 hr at 217°C. Rubber, Bakelite, and epoxy required higher temperatures. For a continuous or semicontinuous process at 235°C, the pressure could be as low as about 460 psig. Titanium is promising as a material of construction.

An engineering design survey showed that the continuous method of operation would be the most practical for a full-scale plant handling 1 ton or more of waste per day. However, such a plant will require development of some components. It is therefore recommended that a semicontinuous pilot plant be built to handle 0.1 ton of waste per day to demonstrate feasibility of the process and to provide design data for the full-scale plant. This work would proceed concurrently with the development of components required for the continuous plant.

4.5 Incorporation of Intermediate-Level Wastes in Polyethylene

The incorporation of intermediate-level wastes in polyethylene was successfully demonstrated in five ~2-hr pilot plant tests. The nonradioactive pilot plant used for incorporation of wastes in asphalt was modified to accept molten polyethylene. A 20 wt % sodium borate solution was used to simulate power reactor wastes. Wastes were processed at rates of 35 to 65 lb/hr to produce products containing 19 to 32 wt % waste solids at evaporator temperatures of 185 to 200°C. A product composition of ~20% solids and a temperature of 200°C were found to be the best conditions. Low-melting polyethylene (DYDT, softening point ~100°C) was used. Material balances ranged from 95 to 105%, and product leach rates after nine weeks were as low as 6×10^{-4}, expressed as the fraction sodium leached $(cm^2/g)^{-1}$ day^{-1}. These initial leach rates appear favorable as compared with those obtained for similar products manufactured in laboratory equipment. Although equipment performance was satisfactory, it appears that the flexibility of the process and product quality could be increased substan-

tially if equipment that could operate at higher temperatures were available.

5. TRANSURANIUM-ELEMENT PROCESSING

Production for the USAEC Heavy Element Program is centered in two facilities at ORNL: the High Flux Isotope Reactor (HFIR) and the Transuranium Processing Plant (TRU). In previous years, heavy elements were recovered primarily from materials irradiated in HFIR; during this period, a total of 75 mg of californium was produced. During the current report period, the unique facilities at TRU were used to recover about 200 mg of ^{252}Cf for the commercial sales program that is being promoted at the Savannah River Plant. The other associated elements, berkelium, einsteinium, and fermium, were contributed to the research effort and distributed through normal channels.

5.1 TRU Operations

The major effort during this report period was the processing of 164 curium slugs that had been irradiated as part of the Californium-I program at the Savannah River Plant (SRP). This program is attempting to establish a commercial market for ^{252}Cf. The irradiated slugs contained about 430 g of ^{244}Cm (550 g of total curium) and 200 mg of ^{252}Cf. This is about three times the quantity of curium and four times the quantity of californium that we had processed in any previous year. The TRU operations group was expanded by about one-third to handle the increased processing load; the increased operating costs are being borne by the AEC Division of Production. Expanded operations will continue for about a one-year period, during which an additional 400 mg of ^{252}Cf will be recovered from other Californium-I materials. A significant effort will also be devoted to the production of transuranium elements from HFIR targets for use in research.

Most of the ^{252}Cf from the slugs was returned to SRP. The curium will be purified further, converted to oxide, and then returned to SRP. The other transuranium elements, 25 mg of ^{249}Bk, 400 μg of ^{253}Es, and about 3×10^9 atoms of ^{257}Fm, were distributed to researchers through the Transplutonium Committee. Ninety-six shipments were made during this report period. In addition to the slugs that were processed, about 22 g of ^{243}Am and 50 g of ^{244}Cm were converted to oxide and fabricated into targets for the HFIR.

The processes and equipment used to process the slugs were generally the same as those used to process HFIR targets. The slugs are similar to HFIR targets in that they contained aluminum-clad pressed compacts of actinide oxides and aluminum powder.

Some new equipment was installed, and the existing equipment was modified. These changes were made partly to make it possible to process the SRP-Californium-I materials and partly for general improvement of the TRU facilities. Changes and new equipment required for the SRP materials included (1) two new larger slug chutes, (2) a larger-capacity equipment rack for use in separating and purifying the transuranium elements, (3) modifications to the waste system so that the high-level wastes could be segregated and stored separately, and (4) a new 14.4-ton cask for use in shipping the SRP-Californium-I slugs to ORNL.

General improvements to the TRU processing facilities included the installation of (1) four 20-liter-capacity tantalum-lined product storage tanks, (2) an iodine retention system that is capable of handling the entire 400-cfm vessel off-gas flow, (3) a pneumatically actuated rabbit system for transferring californium between the TURF californium facility and TRU, and (4) a shielded facility for decontaminating targets and sources prior to shipment.

Seventeen targets containing americium and curium, one special target, and eight rabbits were fabricated.

During this report period, three targets failed during irradiation in the HFIR. One of them was a 90%-dense plutonium target whose failure was anticipated by our mathematical model for target failures. However, the other two targets, in which the pellets were pressed to 80% of theoretical density, should not have failed according to the model. Investigation of these failures is incomplete.

5.2 Isolation and Purification of TRU Products

The final purification of transplutonium products, the isolation of second-growth isotopes, and the fabrication of actinide shipping packages and neutron sources are performed in cell 5 in TRU, the californium facility at TURF, and in the supporting shielded-cave facilities. In addition to main-line products, 65 μg of ^{253}Es and about 1.3 mg of ^{248}Cm were isolated from highly purified californium; about 900 μg of ^{249}Cf was separated from ^{249}Bk. Resin-loading–calcination techniques were used to prepare over 20 shipping packages and 13 neutron sources. An additional 6 neutron sources were prepared by the quartz bead method.

5.3 Special Projects

Special projects include nonroutine productions, special preparations, special irradiations in the HFIR, and fabrication of neutron sources using ^{252}Cf. During the current report period, these projects included fabrication of 22 ^{252}Cf neutron sources containing from 1 μg to 5 mg of ^{252}Cf and irradiation of eight rabbits (three containing ^{253}Es, two containing ^{244}Pu, two containing ^{241}Am, and one containing ^{252}Cf).

5.4 Development of Chemical Processes

Progress in the development of a resin-loading–calcination technique to produce curium oxide for HFIR targets was encouraging. Results show that, with either of two resins (Dowex 50W or Amberlite IRC-50), curium oxide particles can be produced by loading the resin to saturation with curium from a dilute nitrate solution. After loading, the resin is carefully heated to decompose the resin matrix and then calcined at the appropriate temperature to form the dense oxide (~50% of the theoretical crystal density).

Studies were continued to evaluate the separation of actinides from fission product lanthanides by displacement elution with aminopolyacetic acids. Promising results were obtained in rare-earth studies with the chelate ethylenediaminetetraacetic acid (EDTA) when diethylenetriaminepentaacetic acid (DTPA) was used as an organic barrier. The DTPA can be easily removed from the product eluates. An alternative process for the separation and purification of berkelium and californium was also developed. This method, which combines solvent extraction with oxidation by a solid (PbO_2), is convenient for the purification of small amounts of ^{249}Bk and ^{252}Cf, and it may be applicable for processing large quantities of material.

In additional studies, we evaluated cation exchange techniques for removing lithium from curium products obtained from the LiCl-based anion exchange process. Results of this work indicate that the method may be particularly suitable when actinide oxides for use in HFIR targets are prepared by the resin-loading–calcination process.

5.5 Transplutonium-Element Research

A systematic study of actinide element chemistry and of comparative lanthanide element chemistry is being made to increase our basic understanding of actinide systems. This program includes the investigation of problems involving solution chemistry, with particular emphasis on the formation of complexes and on the preparation of solid actinide compounds that will be characterized by x-ray diffraction, electron microscopy, thermogravimetry, differential thermal analysis, and metallographic examination.

The investigation of lanthanide and actinide sulfate complexes by amine extraction was completed except for final refining of the calculation of the formation constants. In a parallel investigation of actinide thiocyanate complexes by di(2-ethylhexyl)phosphoric acid extraction, overall formation constants, β_1 and β_3, were evaluated for mono- and trithiocyanate complexes of Am, Cm, Bk, Cf, and Es. Apparent formation constants, β_2, evaluated for dithiocyanate complexes were smaller (especially at the higher atomic numbers), and their deviations of fitting were relatively large, making the existence of dithiocyanate complexes of these elements questionable. The formation constants of the trithiocyanate complexes and of all the sulfate complexes show a "tetrad" grouping of the elements curium to einsteinium, analogous to "tetrad" grouping of the lanthanides from gadolinium to holmium. This suggests that these complexes, but not the mono- and dithiocyanates, are inner-sphere complexes.

Studies of the preparation and properties of lanthanide and actinide hydrides and metallides were continued. The dissociation pressure of two-phase ErH_2 + $Er\text{-}H_2$ solid solution was found to be

$$\log_{10} P\,(\text{torrs}) = -(11{,}000 \pm 150)/T\,(^\circ\text{K}) + 10.19 \pm 0.07\,.$$

From this, $\Delta H = -50.3$ kcal per mole of H_2 and $\Delta S = -33.4$ cal/deg per mole of H_2, in reasonably good agreement with literature values. X-ray diffraction of a sample approximating stoichiometric ErH_2 showed a face-centered cubic structure (CaF_2 type) with a_0 = 5.128 Å. Erbium compounds with S, Se, As, and Sb and Am compounds with As and Se were prepared by vapor-solid reaction. These compounds are ready for further treatment by melting. Erbium arsenide was obtained as a single phase with a_0 = 5.743 Å. The other initial products were all mixtures. The americium-selenium reaction product was of special interest since x-ray diffraction indicated the presence of AmSe (fcc), which has not been reported previously.

A study was made to prepare and identify the various oxides of californium. Loading californium onto a single cation-exchange resin bead from a highly purified californium chloride solution, burning out the resin matrix, and calcining in air at 1200°C produced Cf_2O_3 in a body-centered cubic structure with a lattice

parameter of about 10.802 ± 0.006 Å. Heating this material in air to >1400°C converted the Cf_2O_3 to a monoclinic structure with lattice parameters of a_0 = 14.121 ± 0.015 Å, b = 3.592 ± 0.004 Å, c = 8.809 ± 0.007 Å, and β = 100.34 ± 0.08°. Californium dioxide was prepared by oxidizing a reactive form of Cf_2O_3 with either molecular oxygen at high pressures (~100 atm) or with atomic oxygen produced in an electrical discharge tube. The CfO_2 had a face-centered cubic structure with a_0 = 5.310 ± 0.002 Å. Upon standing, this material spontaneously converted to a rhombohedral structure with lattice parameters of a_0 = 5.372 ± 0.003 Å and α = 89.92 ± 0.04°.

The thermal stability and decomposition of several lanthanide and actinide compounds were studied during this report period. Additional data were obtained for the trihydroxides of these elements by thermogravimetric techniques. In the earlier work, hydroxides prepared from nitrate salts were used, and it was found that the residual nitrate decomposed at a temperature very near to that at which one of the decomposition steps of the hydroxide occurs. This problem was corrected by preparing the hydroxides from a chloride medium, since the residual chloride decomposed at higher temperatures than the hydroxide. Thermal decomposition of some berkelium compounds was also investigated. Since the entire quantity of berkelium available (~1 mg) was used in each decomposition studied, supporting chemical analyses could not be obtained; thus it was necessary to estimate the composition by comparing the results with lanthanide preparations made in an identical manner. Thermal decompositions of cerium, gadolinium, terbium, and berkelium chlorides, nitrates, and oxalates were carried out. Additional work was done on the sulfates and hydroxides of these elements.

Electron microscopy and electron diffraction have been used to investigate the oxides, hydrous oxides, and hydroxides of the lanthanides and actinides. Recent work has centered on preparing the hydroxides of berkelium and cerium from 1-mg amounts of material. The preparation of cerium and berkelium trihydroxides is complicated by the ease with which the metal ions can be oxidized by air to the tetravalent oxidation state in basic media. Both the trihydroxides and the hydrous dioxides of these two elements were prepared and examined by electron microscopy. In addition, the oxides of several lanthanides and actinides have been examined by electron diffraction. From these studies, it was possible to identify einsteinium sesquioxide and to assign a tentative lattice parameter of 10.72 Å for the body-centered cubic structure.

5.6 Collaborative Research with the Transuranium Research Laboratory

Several research projects were conducted in collaboration with the Transuranium Research Laboratory. The half-life of ^{246}Cm decaying by alpha emission was determined to be (4.655 ± 0.40) × 10^3 years. The partial half-lives of ^{248}Cm were determined to be (3.703 ± 0.032) × 10^5 years for alpha decay and (4.115 ± 0.034) × 10^6 years for spontaneous fission. Measurements and calculations have shown that the first excited (J = 7) energy level in the $5f^{10}$ electronic configuration of Es^{3+} in an aqueous solution of 1 M $HClO_4$ is at 9600 cm^{-1}. Single crystals of $Am_2(SO_4)_3 \cdot 8H_2O$, $Am(ClO_4)_3 \cdot XH_2O$, and $Pr(ClO_4)_3 \cdot XH_2O$ have been prepared and will be analyzed by x-ray diffraction, absorption spectrophotometry, and thermogravimetry to determine coordination numbers.

6. DEVELOPMENT OF THE THORIUM FUEL CYCLE

Sol-gel processes are being developed for use in preparing fuel spheres of ThO_2, ThO_2-UO_2, and UO_2 for HTGR fuel elements. Spheres of all three compositions were prepared for use in irradiation tests and in preparing test elements for use in head-end reprocessing studies. The addition of an ion exchange step in the treatment of the 2-ethyl-1-hexanol (2EH) used for sphere preparation results in an improved 2EH recycle process. The preparation of spheres in a nonfluidized column was investigated in a 28-ft-high column with 2EH temperatures of 25 to 70°C. Process and equipment development and design were continued for refabrication of 10 kg of ThO_2-$^{233}UO_2$ spheres per day in the Thorium-Uranium Recycle Facility. In connection with the preparation of material for use in fuel cycle studies, ThO_2-UO_3 sol containing 100 kg of oxides was made using natural uranium. Good operation was experienced at rates up to 1.5 kg of ThO_2-UO_3 per hour.

6.1 Recycle of the Alcohol Used in the Microsphere-Forming Column

The successful continuous formation of gel spheres requires control of the composition of the 2-ethyl-1-hexanol (2EH) fluidizing medium, that is, the concentrations of the nitric and formic acids (which enter the 2EH from the sol droplets), water, and surfactants. The water content of the 2EH has been controlled by distillation previously, but reactions with acid in the

still have led to undesirable surfactant and alcohol decomposition. During the past year, we have developed and demonstrated the use of ion exchange to remove nitric and formic acids from the alcohol prior to distillation. This step is a significant process improvement and makes possible more trouble-free continuous operation of the sphere-forming system.

6.2 Development of Prototype Equipment for TURF

Processes and equipment have been demonstrated for the preparation of ThO_2-UO_3 sols and formation of them into microspheres at the design capacity, 10 kg of oxide per day, of the Thorium-Uranium Recycle Facility (TURF). Flowsheets of the sol preparation process and the sphere-forming process have been prepared, based on the TURF design throughput, to aid in evaluating the materials and waste handling problems to be expected.

In development studies, the solvent extraction equipment designed to operate at a capacity of 10 kg of oxide per day was shown to be capable of operation at up to 30 kg/day.

Use of an in-cell periscope for viewing the gel sphere-forming operations through a wall of a hot cell is being tested. Demonstration of drying and firing the gel beads requires additional equipment development. We are selecting prototype designs for evaluation.

6.3 Preparation of Microspheres in Nonfluidized-Bed Columns

Uranium dioxide microspheres smaller than 200 μ in diameter may find application as fuel for future HTGR's. We have been studying the use of nonfluidized-bed columns as an improved approach to preparing spheres in this size range from oxide sols. In our studies, we have used a 28-ft column and both UO_2 and ThO_2 sols.

Although analytical solutions to the equations governing water extraction from sol droplets are not possible, values of droplet and column variables can conveniently be calculated using a computer. The calculated values of gelation time, column temperature, product sphere diameter, and column length are in good agreement with the values obtained experimentally. It appears that product spheres up to 200 μ in diameter can be prepared readily in columns of reasonable length (i.e., less than 30 ft) and at practicable temperatures (less than 70°C).

6.4 Preparation of Test Materials

Fuel microspheres of enriched urania, urania-thoria, and thoria were prepared for a variety of needs in the thorium fuel cycle program. A major accomplishment was the preparation of over 100 kg of ThO_2-UO_3 sol using the amine solvent extraction process. In this effort, it was shown that the capacity of the existing equipment (0.5 kg of oxide per hour) could be increased more than twofold by merely increasing the size of the interstage digester. It was also demonstrated that repeated startups and shutdowns could be conducted with no deleterious effects on the product sol.

6.5 ^{233}U Storage, Purification, and Distribution

New storage space for ^{233}U in the form of solids and liquids has been added to the storage, purification, and distribution facility. The facility can now store 454 kg of ^{233}U as solid with an average density of 1 g/cm^3 and 900 kg as nitrate solution having a concentration of 250 g/liter. There is also now an interim storage vault that can hold up to 70 kg of ^{233}U in shipping containers.

Twenty-seven shipments, containing a total of 831 kg of ^{233}U, were received during the year. Twenty-one shipments, containing 15 kg of ^{233}U, were made from the facility.

7. SOL-GEL PROCESSES FOR THE URANIUM FUEL CYCLE

Sol-gel processes are ideally suited for the preparation of LMFBR fuel since they can be readily adapted to continuous and remote operations for processing materials behind shielding. In the processes under development, sols are prepared by the controlled extraction of nitrate from uranium nitrate and plutonium nitrate solutions, which are the products from fuel reprocessing plants. The sols are then converted into the desired forms required for subsequent fabrication into recycle fuel elements; this form usually consists of high-density oxide microspheres for use in Sphere-Pac operations.

7.1 Preparation of UO_2 Sol by the CUSP Process

Development work on the CUSP (concentrated urania sol preparation) process during the last year has been directed primarily at the characterization of sols produced in engineering-scale equipment and at the evaluation of various types of contactors used for extracting nitrate to form the sol. There has been no need to make any appreciable changes in the process,

since it continues to produce satisfactory urania sols. Studies of sol properties were made on 52 sols produced in a mechanically stirred J-column contactor, 45 sols produced in a spray-column contactor, 8 sols produced in a packed-column contactor containing ceramic Berl saddles which are aqueous wettable, and 10 sols produced in a packed-column contactor containing non-aqueous-wettable Teflon rods. In all cases the sols were approximately 1 *M* in concentration. Sols prepared in the J-column contactor were fluid for the longest time after preparation, with an average shelf life of 5.75 months. The average shelf life for sols prepared in the spray-column contactor was 3.5 months and for sols prepared in the packed-column contactor was about 1.9 months. Properties of 2 and 3 *M* UO_2 sols prepared by concentrating 1 *M* UO_2 sols were compared. When the sol concentration was increased by a factor of 3, the conductivity (or free acid content) increased only 30 to 40%. This indicates enhanced adsorption of nitric acid by the sol particles as the free acid is increased. Doubling the concentration from 1 to 2 *M* increased the viscosity from 1.3 to 2.0 cP. The 3 *M* UO_2 sol was much more viscous (~7 cP) and became thixotropic on aging a week.

A small amount of extraneous material, commonly called "crud," is formed during preparation of sol by the CUSP process. Altering the type of contactor used for nitrate extraction did not have an appreciable effect on the amount of crud formed. In laboratory tests, it was found that this extraneous material could be effectively removed by treating the sol with an equal volume of *n*-hexanol. The crud transfers to the *n*-hexanol, from which the sol can be easily separated.

Since preparation of sols at higher concentrations would increase the capacity of the sol-making equipment and the sphere-forming equipment, preliminary investigations were made to prepare 1.8 *M* UO_2 sol instead of 1 *M* UO_2 sol, which is normally produced. Two sols at ~1.8 *M* UO_2 were produced. Both were fluid, had shelf lives of 1.0 and 1.5 months, and produced good spheres in the forming column. These results are encouraging, but if sols of this concentration are to be produced routinely, additional development is required, especially to optimize the feed preparation method for producing sol.

7.2 Development of the UO_2-PuO_2 Sol-Gel Process

In continued laboratory work to develop solvent extraction processes for the preparation of mixed UO_2-PuO_2 sol, we are studying a process in which CUSP urania sol is pretreated to remove excess formate and is then mixed with a plutonia sol produced by an alcohol extraction process (APEX). Development efforts were concentrated on (1) modification of the APEX process to produce low-nitrate sol, (2) laboratory experiments to prepare UO_2-PuO_2 microspheres, and (3) mixed-sol compatibility studies.

It was discovered that several primary characteristics of APEX sol could be improved by seeding, in which a portion of a normally prepared APEX sol is added to feed solution during the initial extraction of a subsequent sol preparation. This technique can produce sol in which the primary crystallites are arranged in aggregated micelle structures. This type of structure results in rapid denitration and crystallite growth when the sols are taken to dryness and heated. Low-nitrate sols can be prepared (NO_3^-/Pu $\cong$ 0.2) with average crystallite diameters of ~60 Å when a sol with the appropriate aggregate structure is taken to dryness and heated for 30 to 90 min at temperatures in the range of 180 to 230°C. This is in direct contrast to the behavior of regular APEX sols, which show no detectable change in crystallite size nor any significant reduction in the NO_3^-/Pu mole ratio when heated at these temperatures for much longer times. The specially prepared sols with low nitrate-to-plutonium mole ratios and with larger crystallites exhibit greatly improved mixed-sol shelf life. For example, the time to gelation for 0.9–1 *M* sol (80% UO_2–20% PuO_2) at 25°C is increased from <1 hr for regular APEX sol to five to eight days for the modified products. It is even possible to form pure plutonia microspheres which calcine to dense, crack-free products. This has not been possible with high-nitrate plutonia sols, including regular APEX sols, because of extensive cracking and disintegration of the spheres during calcination.

Excellent results were also obtained in small-scale experiments when these larger crystallite sols were mixed with CUSP sols and formed into microspheres. Because of the improved shelf life, a series of mixed CUSP-APEX microsphere-forming runs were made in which the sols were not cooled to 5°C, as is required when regular APEX sol is used. High yields (90–95%) of calcined microspheres were consistently obtained in these experiments.

Studies were continued in an effort to understand the variables that affect the shelf life of mixed CUSP-APEX sols and the mechanisms responsible for gelation. We previously demonstrated that mixed-sol instability is a function of formic acid concentration, and various tests indicated that the instability is related to a redistribution of the nitrate and formate anions when the UO_2 and PuO_2 sols are mixed. The initiating step appeared to involve a preferential association of $HCOO^-$ (or

HCOOH) with PuO_2 crystallites and a release of NO_3^-. During this report period, a study of colloidal charge was initiated. The results obtained correlate well with previous work and tend to substantiate that anion redistribution and imbalance are related to mixed-sol gelation. The instrument used for this work was a Streaming Current Detector manufactured by Waters Association, Inc. Several techniques were used to analyze streaming-current data obtained by titrating PuO_2 sols with HNO_3, and efforts were initiated to correlate these results with data obtained by the conductometric titration of sols. The relationships found are of interest because they indicate that there is an equilibrium between nitrate in the aqueous phase and nitrate sorbed on plutonia micelles, and that the equilibrium is a function of the total nitrate concentration. A preliminary interpretation of the conductometric titration curves obtained indicates that this technique can be used to determine HNO_3 concentrations in PuO_2 sols and the equilibrium between NO_3^- in the aqueous phase and nitrate sorbed on the plutonia.

7.3 Microsphere-Forming Studies

Investigations were continued on the development and demonstration of microsphere forming from CUSP urania sols. It was established in laboratory-scale experiments that satisfactory microspheres can be formed from CUSP sols in 2-ethyl-1-hexanol (2EH) that has an apparent pH within the range of 2.0 to 6.0 and a temperature in the range of 30 to 55°C and that contains ~0.3 vol % Span 80, ~0.1 vol % Ethomeen S/15, and 0.5 to 1.5 vol % H_2O. The principal operating problems encountered during long-term operation of sphere-forming columns with CUSP sols are (1) excessive cracking of the gel microspheres during drying and firing and (2) sticking, clustering, or coalescence of partially dried spheres in the forming column. Cracking of the gel spheres can be caused by a number of different conditions. It has been found that the amount of cracking can be greatly decreased or eliminated by more thorough drying in the sphere-forming column, either by increasing the temperature or by increasing the residence time of the gel spheres in the column. Problems with sticking, clustering, and coalescence in the sphere-forming column can be mostly eliminated by controlling the surfactant and water concentrations and by preventing the buildup of surfactant degradation products in the 2EH. Although we have not yet established the optimum method for accomplishing this, considerable progress has been made by developing methods of treating 2EH from the sphere-forming column for recycle. During operation of engineering-scale equipment, it was demonstrated that nitric acid and formic acid were effectively removed by passing 2EH from the sphere-forming column through a bed of ion exchange resin. This prevents the accumulation of excessive amounts of formic acid (which is extracted from CUSP sols) and eliminates degradation of Ethomeen S/15 which takes place if nitric acid is allowed to remain in the 2EH during azeotropic distillation to remove water. Unfortunately, Span 80 is lost during this treatment (probably by hydrolysis), and periodic additions are required. However, this results in a continual buildup of Span 80 degradation products. We plan to control the concentration of Span 80 and its degradation products by continuously bleeding off a small stream of 2EH and replacing it with purified 2EH containing the appropriate amounts of surfactants. The waste 2EH stream will be treated by distillation to purify it for recycle.

Fewer problems are usually encountered if gel spheres are not fluidized in the forming column. However, the size of the microspheres is limited by the height of a nonfluidized column. A 28-ft nonfluidized column was used to prepare up to 145-μ-diam UO_2 spheres at a forming temperature of 25°C and 200-μ-diam UO_2 spheres at 70°C.

Production of PuO_2 spheres was carried out with relatively trouble-free operation of the sphere-forming column, but problems of the same type encountered with UO_2 sols are also present when forming spheres from mixed UO_2-PuO_2 sols.

7.4 Preparation of UO_2-PuO_2 Materials

We still must rely on the precipitation-peptization process and the precipitation-peptization-baking process for preparing enriched urania sols and plutonia sols respectively. Facilities are not yet available for preparing enriched urania sols by the CUSP process or for preparing high-nitrate plutonia sols by the APEX process. During this report period, about 7 kg of plutonium was converted into high-quality PuO_2 sols, and about 9 kg of enriched uranium was converted into urania sols. These materials were used to prepare UO_2, PuO_2, and $(U,Pu)O_2$ microspheres and for the preparation of $(U,Pu)O_2$ powder for the preparation of pellets.

Approximately 2.5 kg of $(U,Pu)O_2$ microspheres with a Pu-to-(Pu + U) ratio of 0.25 were prepared for Argonne National Laboratory; one-third of the material was <44-μ-diam microspheres, and the rest was 350- to 595-μ-diam microspheres. About 550 g of $(U,Pu)O_2$ microspheres (400 to 595 μ in diameter) with a

Pu-to-(Pu + U) ratio of 0.27 were prepared for testing the U-Fines method of fuel fabrication, in which all plutonium is contained in the large spheres and the <44-μ-diam spheres are pure UO_2. Plutonium used to prepare 4 kg of sol had an isotopic content of ~23% ^{240}Pu and ~3.5% ^{241}Pu. This was formed into high-density PuO_2 microspheres (~200 μ in diameter) without overexposure to operating personnel, despite the high level of gamma activity associated with the heavy plutonium isotopes.

8. CONVERSION STUDIES IN THE LMFBR FUEL CYCLE

8.1 Technical and Economic Evaluation

Preliminary analysis of the interrelations of fuel conversion processes with the fuel reprocessing and refabrication processes indicates that some sort of conversion process should be carried out at the reprocessing plant. It is likely that this is desirable both from an economic and a safety point of view. Shipment of liquid forms of plutonium may not be acceptable in the future. A report on this work is in preparation.

8.2 Conversion by Homogeneous Reduction

Studies have been made to demonstrate the feasibility of chemical reduction of nitrate and uranyl ions in pressurized solutions to produce powders suitable for use in making pellet fuels. A semicontinuous system that allows continuous feed introduction, temperature and pressure control, and batch product removal was developed and utilized to prepare oxides for use in tests. Ethylene glycol, ethyl alcohol, and hydrazine were employed as reductants over a temperature range of 150 to 210°C and at pressures up to 250 psig. Oxides of uranium and of uranium-cerium and uranium-thorium were prepared and pressed into satisfactory pellets by pressing at pressures of 10,000 to 15,000 psi. The cerium and thorium were used as alternative stand-ins for plutonium. Pellets with densities up to about 95% of theoretical were obtained. This density is the same as that obtained under the same pelletizing conditions with a so-called standard, sinterable UO_2 powder. Preparations are under way to extend these studies to systems containing plutonium.

9. PREPARATION OF $^{233}UO_2$ FOR LIGHT-WATER BREEDER REACTORS

ORNL participation in the Light Water Breeder Reactor (LWBR) Program, under contract with Bettis Atomic Power Laboratory (BAPL), involves (1) the receipt and storage of approximately 750 kg of ^{233}U (475 kg as UNH and 275 kg as UO_2), (2) the purification of this material in small batches (~20 kg of ^{233}U per week) to remove ^{232}U daughters, (3) the conversion of the UNH to ceramic-grade UO_2 powder at the rate of about 20 kg of ^{233}U per week, (4) the packaging and shipping of the UO_2 to BAPL for blending with thoria and pressing into pellets, and (5) the recovery of ^{233}U from the $^{233}UO_2$ scrap generated at ORNL and the $^{233}UO_2$-ThO_2 scrap generated at BAPL.

During the past year, additional storage facilities were constructed, and all the feed material (750 kg of ^{233}U) was received and stored. A dissolver capable of dissolving 50 kg of ThO_2-UO_2 in a 12-hr cycle was constructed and is presently being installed in the processing cell. Modifications to the existing solvent extraction purification equipment and installation of an ion exchange system will be completed in the early part of April 1971. Construction of the oxide conversion equipment will be completed by July 1, 1971. The facility is scheduled to begin qualifying runs in July 1971, and production will begin in December 1971.

10. SEPARATIONS CHEMISTRY RESEARCH

New separations methods are being developed, principally for uses in radiochemical processing but also for other purposes extending from extractive metallurgy to biochemical separations. The program in separations chemistry divides into three parallel, interdependent, and frequently overlapping types of research activity: (1) descriptive chemical studies (Sects. 10.1, 10.3, 10.5, 10.6) of the reactions of substances to be separated and of separations reagents, of the controlling variables in particular separations, and of potential new reagents and methods; (2) development (Sects. 10.2–10.4) of selected separations and methods into specific complete processes, both where no workable process exists and where existing processes can be improved, carried where warranted to the point that large-scale performance can be predicted; and (3) fundamental chemical studies (Sects. 10.6–10.9) of the species, equilibria, and reaction mechanisms involved in separations systems, both to increase knowledge and to help define potential applications.

10.1 New Separations Agents

We are continuing to investigate, for potential utility in solvent extraction or other separations methods, compounds that are (1) newly available commercially,

(2) submitted by manufacturers for testing, or (3) specially procured for testing of class or structure.

Extractions of iron(III) and technetium(VII) chloride, nitrate, and sulfate by the corresponding methyltrioctylphosphonium (MTOP) and dodecylbenzyltrioctylphosphonium (DDBTOP) salts and of vanadium(IV) chloride and sulfate by the corresponding MTOP salts were similar to extractions by the analogous Adogen 464 (methyltrialkylammonium) salts. Coefficients were slightly higher for extractions with MTOP salts than with the corresponding DDBTOP salts.

The previously known synergistic extraction of lithium ion by a β-diketone–phosphine oxide mixture, limited to high pH, has been extended to neutral salt solutions (pH 7 and even slightly lower) by substituting a highly fluorinated diketone for the simple diketone. The separation factors for lithium chloride from sodium, potassium, rubidium, and cesium chlorides were greater than 10^3 in extractions at high lithium loading with 0.2 *M* heptafluorodimethyloctanedione + 0.1 *M* trioctylphosphine oxide in benzene.

Preliminary tests of a new commercial complexing agent, 1,2-diaminopropanetetraacetic acid (PDTA), in cation exchange extraction with HDEHP and chromatography with Dowex 50 indicate that it is a strong complexing agent, giving enhanced separation factors for the trivalent actinides.

10.2 Recovery of Uranium from Commercial Phosphoric Acid

Bench-scale development of a process for recovering uranium from wet-process phosphoric acid by extraction with di(2-ethylhexyl)phosphoric acid plus trioctylphosphine oxide in an aliphatic diluent was essentially completed. The process consists of two cycles. In the first cycle, the uranium is reduced with ferrous iron to strip it from the solvent. This strip product solution is relatively concentrated in uranium and is highly amenable to processing with the same solvent in a second cycle. In the most recent work, the second cycle was demonstrated in a mixer-settler system. Uranium was directly precipitated from the solvent as ammonium uranyl tricarbonate, which was calcined to give a product analyzing 97.5% U_3O_8. Chemical reagent costs for the process are estimated at about $0.85 per pound of U_3O_8.

10.3 High-Resolution Rare-Earth Separations

The pressurized ion exchange technique was successfully applied to the simultaneous separation of all the rare earths in milligram quantities (except tracer Pm) within 2 hr, in contrast to about one week required by the methods at present used for such separation. The high resolution was obtained by use of 25- to 60-μ resin (Dowex 50-X8), and still finer resin could be used. Elution was by α-hydroxyisobutyrate in concentration gradient. Pressures in the order of 500 psi provided fast flow (6 to 16 ml cm^{-2} min^{-1}) through the resin.

10.4 Displacement Elution with Aminopolyacetic Acids

Use was demonstrated of the amphoteric diethylenetriaminepentaacetic acid (DTPA) in cation form as a barrier ion in displacement elution of lanthanide ions (stand-ins for actinides) with ethylenediaminetetraacetic acid (EDTA) from a cation exchange column. About half as much eluant volume (and half as much time) was needed to start elution of the first lanthanide ion with $DTPA^+$ as was needed with Cu^{2+} as the barrier ion, and the use of $DTPA^+$ did not add a metallic contaminant to the eluted lanthanide. (Use of H^+ as the barrier ion, which also would avoid contamination, is precluded by precipitation of EDTA in acid.)

10.5 Isotope Enrichment by (n,γ) Reactions in Molecular Sieves

Lanthanide isotope product yields of ~70% can be obtained consistently with enrichment factors of ~100. Similar actinide product yields can be obtained, but the enrichment factors have been lower. For significant production of actinide isotopes, either (1) enrichment factors must be much larger or (2) neutron exposures must be increased by factors of 10^3 or more – if the zeolite structure can tolerate that. Study of radiation damage has been started. Increase of the enrichment factors must come almost entirely from decrease of the elution of unchanged target ions along with the product ions. Although tests are still in progress, results suggest that drying of the loaded zeolite for irradiation typically causes a few percent of the target ions to migrate to exchangeable sites. An alternative is irradiation in water, which has not been examined.

10.6 Distribution Equilibria and Mechanisms

A comparison of di(2-ethylhexyl)phosphoric acid (HDEHP) with two phenylphosphonic ester acids for intragroup separations of lanthanides and actinides was completed, and a paper describing the results is in press. The extractive power increases in the order HDEHP < 1-methylheptyl phenylphosphonic acid (HMeH[ΦP]) < 2-ethylhexyl phenylphosphonic acid (HEH[ΦP]).

HMeH[ΦP] is superior to both the others in separating tracer-level europium from cerium and californium from curium, in extractions from several different solutions. However, neither phenylphosphonic acid is suitable for separating natural lanthanides at the usual high concentrations, because of limited solubilities of the complexes formed.

Study is in progress on several different methods for investigating the formation of weak metal-ion complexes, that is, those that are formed to an important extent only in the presence of moderate to high ligand concentrations. Many such complexes are important in chemical processing. These methods include distribution equilibria with fixed or varying ionic strength, electromigration, spectrophotometry, and (receiving the principal current attention) "tagged-ligand transfer." In the last, the ligand in the aqueous phase of a solvent extraction system is tagged radioactively. The ligand/metal transfer ratio is determined, corrected for transport of ligand via other paths, and extrapolated back to zero time to show the average ligand/metal association number in the species that cross the interface. Tests in the known iron(III)-chloride system gave Cl/Fe = 3 at 4 *M* Cl^-. Tests in the europium-chloride system gave surprisingly high chlorine/europium values of 6 to 8 at 5 to 9 *M* Cl^-. This is still under study.

Liquid-scintillation alpha counting was extended to the analysis of transplutonium actinides in aqueous thiocyanate-perchlorate solutions, using an extractive scintillator with HDEHP as the extractant. Americium-241 results were precisely confirmed by gamma counting. Berkelium-244 (0.125 MeV beta) and ^{253}Es (6.6 MeV alpha) were determined simultaneously.

10.7 Relative Potentials of the Bk(IV)-Bk(III) and Ce(IV)-Ce(III) Couples

Study was completed of the difference between the formal potentials of the Bk(IV)-(III) and Ce(IV)-(III) couples, and a paper reporting the results is in press. Cerium(IV) is the stronger oxidant at all nitric acid concentrations below ~7.5 *M*, with a maximum difference of ~0.08 V at 2 *M*. In perchloric acid the potential difference shifted only slightly, with ~0.11 V maximum at 4 *M*. Measurements in phosphoric and sulfuric acids, initially encouraging, were prevented by the degree of complex formation.

10.8 Lanthanide and Actinide Hydroxides

The basicities of americium and curium were compared with those of the natural lanthanides and yttrium by measurement of pH during NaOH titration of very dilute solutions of their nitrates and of some of their chlorides. Americium behaved approximately like promethium, while curium was considerably less basic than any of the lanthanides. The tendency of the lanthanides to precipitate as basic salts was greatest in the middle of the group, where stoichiometry was about 0.85 for complete titration. Stoichiometry of americium was about 0.80 and that of curium about 0.70, indicating its precipitation mostly as $Cm(OH)_2NO_3$ or $Cm(OH)_2Cl$.

Calculated solubility products and solubilities of the hydroxides, based on observed stoichiometries rather than on an assumed $M(OH)_3$ composition, were constant throughout most of the course of titration for all of these elements except curium.

10.9 Kinetics of Metal-Ion Extractions by Organophosphorus Acids

Study was completed of iron extraction from acid perchlorate solutions, by HDEHP, under conditions of iron loading far from saturation and from equilibrium. A paper reporting the results is in press. In addition to the measurements with quiescent interface previously summarized in these progress reports, key points were cross-checked by dispersion mixing with a flat-blade turbine in a baffled cell under conditions that have been standardized for scaleup. The latter results were similar to those with the quiescent interface at low HDEHP concentrations but differed at higher concentrations, especially in that the component of zero order (with respect to iron) prominent with the quiescent interface was slight or absent with total dispersion. We have attributed the zero-order component to saturation of the interface by an intermediate reaction species and accordingly suggest that the changing interfaces of rapidly splitting and recoalescing droplets may not have time to reach saturation.

11. CHEMICAL APPLICATIONS OF NUCLEAR EXPLOSIVES

11.1 Copper Ores

In a small-scale demonstration of a column leaching–solvent extraction–electrowinning flowsheet for re covering copper from simulated nuclear-broken ore, only small fractions of the radionuclides were leached from the ore even though they were added to the ore column in soluble form. The radioactivity of the solvent extract and of the copper strip product solution was barely above background. The radioactivity of the electrolytic copper metal products was extremely low, being detectable only in a special low-level counting facility.

11.2 Recovery of Oil from Shale

Increasing the exposure time of Green River oil shale to tritiated hydrogen from 44 to 85 days had no effect on the tritium contamination of the shale or of the oil retorted from the shale. The contamination of both the shale and the oil had increased as the shale exposure time was increased to 44 days. Contamination from tritiated methane or tritiated ethane, which was about an order of magnitude less than from tritiated hydrogen, was not affected by increasing the shale exposure time from 7 to 25 days.

11.3 Natural-Gas Storage

We have begun laboratory studies of the behavior of radionuclides in natural-gas reservoirs formed with nuclear explosives. Initial tests with shale of low permeability showed that tritiated water penetrates the pores and fractures of the shale and is not easily removed by purging with air. The tritium contamination of methane stored in contact with contaminated shale was extremely low.

12. BIOCHEMICAL TECHNOLOGY

MACROMOLECULAR SEPARATIONS

12.1 Preparation of Crude Bovine Liver Transfer Ribonucleic Acid

A method for preparing crude tRNA from calf liver has been developed. The best products had total amino acid acceptance and 3′-terminal adenosine content values comparable with those of product obtained from *E. coli.* The yield from calf liver, however, was only about 6% of the yield from a comparable weight of *E. coli* cells.

12.2 New Chromatographic Systems for the Separation of Transfer Ribonucleic Acids

Improved separation of tRNAs by reversed-phase chromatography has been achieved through the use of a new plastic support, polychlorotrifluoroethylene. Two new chromatographic systems using this support, designated RPC-5 and RPC-6, yield sharper separations of multiple isoaccepting tRNAs and less overlap of adjacent tRNA peaks.

12.3 Miniature Chromatographic Systems for Tracer-Labeled Transfer Ribonucleic Acids

A small reversed-phase chromatographic system for the separation of $[^3H]$- or $[^{14}C]$ aminoacyl-tRNAs has been developed. This system has the advantages of speed (chromatographic runs can be completed in 30 to 60 min), sensitivity (as little as 3.5×10^{-9} g or 60×10^{-6} A_{260} unit of phenylalanyl-tRNA has been detected as a chromatographic peak), and excellent resolution of isoaccepting tRNAs. The system has been applied to samples of *E. coli* tRNAs and calf liver tRNAs.

12.4 Separation of Ribosomal Ribonucleic Acids

Reversed-phase chromatography has been applied to the separation of 5S rRNA and has been adapted for use on an analytical scale for the rapid (about 30-min) separation of small amounts (0.1 A_{260} unit) of 16S and 23S rRNAs. Compared with other techniques, this method is more rapid and gives more effective resolution while using only small amounts of material, which can be recovered.

12.5 Purification of Five Leucine Transfer Ribonucleic Acids from *E. coli*

The five chromatographically resolvable leucine tRNAs of *E. coli* were purified. Except for $tRNA_2^{Leu}$ (which was present only in minor amounts), the tRNAs were estimated to be 80 to 100% active. In ribosome binding experiments, $tRNA_1^{Leu}$ and $tRNA_2^{Leu}$ recognized the codon CUG, and $tRNA_5^{Leu}$ recognized UUG. The $tRNA_3^{Leu}$ and $tRNA_4^{Leu}$ did not recognize any of the known leucine codons.

12.6 Flowsheet Development and Large-Scale Purification of *E. coli* Transfer Ribonucleic Acids

An improved flowsheet for the purification of tRNAs from *E. coli* was developed and partially demonstrated on a large scale. Ten separate tRNAs were purified to an activity greater than 1200 picomoles per A_{260} unit. Several of the tRNAs from the middle of the chromatograms were recovered by repeated chromatography on reversed-phase columns using different operating conditions to maximize the separation of specific tRNAs. A total of about 10 g of purified formylmethionine, glutamic acid, and phenylalanine tRNAs was obtained from large-scale tests.

12.7 Distribution of Purified Transfer Ribonucleic Acids

A total of 5.5 g of purified tRNAs was distributed in 162 shipments.

BODY FLUIDS ANALYSES PROGRAM

12.8 Prototype Analyzers

Eleven prototype analyzers either built at ORNL or built according to ORNL construction plans are now in operation in other laboratories. We plan to place three additional prototype analyzers during the next report period.

12.9 Separation Systems

A useful new separation concept is the use of an anion exchange and a cation exchange column in series, with concurrent elution of both columns after the initial loading phase. Such an arrangement gives higher resolution and a significant decrease in required operating time. Another new concept is to use multiple parallel columns in the same instrument, thereby increasing the sample throughput rate. We have found neutral resins to be useful in concentrating the trace organic compounds in urine, so that an additional 50 to 60 chromatographic peaks can be resolved in a separate elution. Parametric studies have continued.

12.10 System Components

We have developed a flow UV-photometer-fluorimeter that can continuously monitor the column eluate for UV absorbance and for fluorescence. The conceptual design of a multiple-channel, dual-beam, dual-wavelength UV photometer has been completed, and a two-channel system is being fabricated.

12.11 Identification of Body Fluid Constituents

Sixty-nine compounds separated from normal and pathologic body fluids by the UV-analyzer have been positively identified.

12.12 Applications and Experimental Results

Body fluids from subjects with various different pathologic states have been analyzed on both the UV-analyzer and the carbohydrate analyzer. The metabolites of ingested nicotinic acid were established, urinary metabolites of patients with orotic aciduria were investigated, and an infant with the lack of galactokinase was found to excrete large amounts of sucrose. The linearity of the UV-analyzer was found to be within 5%, and the standard deviation of elution position was found to be less than 2% for most compounds.

12.13 Data Acquisition and Analysis

An on-line digital computer is being used routinely to evaluate two channels of chromatographic data continuously in real time. The data analysis computer program has been revised to include a more efficient determination of peak area, determination of the beginning of a peak, and the elution volumes of each peak.

WATER POLLUTION STUDIES

12.14 Preparation of Samples

The two-step concentration procedure using vacuum evaporation followed by freeze-drying, reported last year, has been adopted as the technique for concentrating sewage effluent samples. It has been tested for maintenance of sample integrity. Tests for total noncarbonate carbon in samples before and after concentration indicate recovery of more than 85% in the concentrate.

12.15 Analytical Systems

The concentration step in sample preparation was shown to be reproducible and to maintain sample integrity. The UV-analyzer was adapted for use in the analysis of refractory organics in sewage effluents, and a modified Mark II UV-analyzer was constructed and delivered to the Advanced Waste Treatment Research Laboratory of the Water Quality Office.

12.16 Identification of Refractory Organics

By the use of two-column anion and cation exchange chromatography, nine compounds have been tentatively identified in primary sewage effluent. The identification of three other compounds has been confirmed by gas chromatography and mass spectral data. Good gas chromatographic and mass spectral data have been obtained for an additional compound, but it has not been identified.

13. SPECTROPHOTOMETRIC STUDIES OF SOLUTIONS OF LANTHANIDES AND ACTINIDES

Spectrophotometric techniques for studying aqueous solutions, especially of the lanthanides, actinides, and transition elements, are being developed and exploited. Studies of non- or low-alpha-active solutions at temperatures less than 100°C are accomplished by regular techniques, while a special spectrophotometer system has been built for studying the lanthanide and actinide

solutions at temperatures to 380°C with associated pressures to 10,000 psi. These systems have been used in a standard laboratory for studying temperature effects (25 to 380°C) on aqueous lanthanide nitrates, the uranyl ion, and on the near-infrared absorption bands of H_2O and of D_2O, which interfere with the spectral studies of the metal ions. Previously unreported bands were found for UO_2^{2+} as well as for H_2O and D_2O.

In conjunction with the spectrophotometric studies, the densities of aqueous solutions of lanthanides and actinides are being measured over the temperature range 25 to 400°C.

In our continued study of protonic wave functions and spectra, the protonic transition types constituting so-called vibrational and rotational structure have been identified. Effects of external electric and magnetic fields on electrons and protons of neutral and ionized hydrides were calculated. A multiplet theory for a single configuration for symmetric wave functions was developed. Work on selection rules for protonic transitions was extended to include photoeffect, with the conclusion that protons can be photoejected from molecules in the same way as are electrons; however, the cross section is large only at frequencies near the resonance frequency.

14. PREPARATION AND PROPERTIES OF ACTINIDE OXIDES

14.1 Thoria Desintering Studies

Sol-gel thoria (and some other related oxides), after being sintered to >99% of theoretical density, may be "desintered" to a considerably lower density by further firing in air. Desintering occurs by the formation of small, mostly closed pores. The usual explanation for such pore formation, that is, high-pressure "bubble" formation by trapped gas, appears to be inadequate for some aspects of thoria desintering for several reasons, especially the following: (1) the faceted pores are typically elongated instead of approaching a spherical shape and (2) firing in vacuum after firing in air causes some redensification instead of further dedensification. (Further dedensification would be expected since ΔP_{ext} = 1 atm is a significant fraction of estimated P_{int} ≈ 4–40 atm.) An alternative explanation based on other types of internal stresses is being examined; however, no conclusions have been reached thus far.

14.2 Adsorption of Nitric Acid on the Surface of Urania

The ideal Donnan potential relation between adsorbed and free nitric acid that was found to be valid for thoria sols,

$$pH_{apparent} = 2[\log (HNO_3)_{free}] - \log (HNO_3)_{total},$$

did not fit urania sols. Typically, chemical analyses showed larger $(HNO_3)_{total}$ than predicted by the equation. A part of the difference is attributed to the presence of formic acid as a holding reductant in the urania sols and to some unavoidable oxidation during the tests (in spite of the holding reductant). However, the fraction of the urania that is amorphous varies for different sols, and the "excess" nitrate correlates roughly with this fraction. The resulting assumptions that HNO_3 associated with amorphous urania is kinetically unavailable and that all rapidly equilibrating HNO_3 adsorption occurs only on crystalline urania lead to the calculation of (−2.5 ± 0.5) kcal per mole of HNO_3 with 12% of the metal-ion surface sites occupied. This compares with about −6.5 kcal per mole of HNO_3 on thoria.

14.3 Preparation of Carbides and Carbonitrides

In continued laboratory studies of the preparation of plutonium and uranium-plutonium carbides and carbonitrides, the feasibility of producing these compounds from colloidal solutions of metal oxide and carbon particles was demonstrated. Since the colloidal solutions contain very small primary particles (<500 Å) and provide intimate contact of the reactants, the reaction rates should be more rapid and uniform than those obtained by merely mechanically mixing the components. In addition to the preparation of carbides from the reactants, the studies have shown that nitrogen can be introduced during the conversion step to form carbonitrides. The latter reactions were most successful when the C/M ratio in the final products was >0.4, with (C + N)/M ≈ 1. With plutonium, the carbon requirement for a single-phase carbonitride is much lower, and it was more difficult to achieve the desired conversion. Efforts have been made to follow the carbothermic reactions more closely and to relate the importance of the initial experimental parameters to the conversion. Plutonium appears to differ from uranium in the carbothermic reduction by being converted to the carbide in two steps rather than in a single step.

Reaction kinetics determined for UC + N_2, UC_2 + N_2, and UO_2 + C were applied to the fluidized-bed conversion of, for example, sol-gel $(U_{0.8}Pu_{0.2})O_2$-C shards to (U,Pu)(C,N) that was successfully pressed and

sintered into 89%-dense pellets free of any second phase.

Two successive reactions, previously unreported, were found in the conversion of UO_2 with C and N to U(C,N):

$$UO_2 + 0.78C + 0.27N_2 \rightarrow UO_{1.22}N_{0.54} + 0.78CO$$

and

$$UO_{1.22}N_{0.54} + 1.68C \rightarrow UC_{0.46}N_{0.54} + 1.22CO$$

(1700°C, P_{N_2} = 380 torrs, P_{CO} = 10 torrs). The intermediate $UO_{1.22}N_{0.54}$ is a composition in a solid-solution field including UO_2.

Conditions were determined for accurately predictable reduction of $(U,Pu)O_2$ to hypostoichiometric $(U,Pu)O_{2-x}$ with hydrogen and also via the (faster) C-CO-CO_2 system.

15. CHEMICAL ENGINEERING RESEARCH

15.1 Mass Transfer of Water from Sol Droplets

The mass transfer of water from single droplets of water or thoria sol into several alcohols (covering a range of Schmidt numbers) has been studied. Results have shown that the transfer rates are controlled by resistance in the alcohol film surrounding the droplet. A generalized correlation for the mass transfer coefficient between rigid spheres and a flowing stream and a specific correlation for the gelation time of sol droplets are presented.

15.2 Dehydration of Individual Sol Droplets in a Minicolumn*

A tapered Plexiglas column with an overall height of 8 in. and a minimum diameter of 1/8 in. was used to observe in situ the dehydration and gelation of single droplets of sol. The formation of flat spots and pits was reflected in the diametral shrinkage rate and the settling velocity. Diametral shrinkage rates are in general agreement with those observed earlier by Clinton. Two types of skin formation were noted: one typical for gels showing the "cherry pit" defect and the other typical for gels showing the "raisin" defect. Rotation of the droplets during gelation eliminated deformation from the former cause but not from the latter. Settling velocities were in reasonable agreement with values calculated from drag coefficient relationships. Internal circulation within droplets was observed, and its cessation, leading to stagnant droplets, was noted. The formation and growth of surfactant caps were observed directly, and their effect on settling velocity was determined.

*This work was done at the Swiss Federal Institute for Reactor Research (EIR), Würenlingen, Switzerland, by a Chemical Technology Division staff member who was on assignment to the EIR Plutonium Project under a cooperative agreement between EIR and ORNL.

15.3 Production of Sol-Gel Microspheres of Small Uniform Size

Ultrasonic vibrations and possible electrical disturbances are being considered to break a liquid (in liquid) jet into very small uniform droplets. Such droplets of sol could then be used to prepare very small uniform microspheres. Preliminary experiments using 18- to 25-kHz vibrations have shown that droplet size can be controlled, but higher frequencies will be needed to obtain droplets as small as 25 to 80 μ with reasonable flow rates.

15.4 Pulsed Clone Contactor

A novel compact liquid-liquid contactor suitable for use in a glove box was designed and briefly tested. The device performed satisfactorily in terms of throughput capacity and stage efficiencies during operation with Amsco–15% TBP and uranyl nitrate.

15.5 Axial Dispersion in Packed Columns for Contacting Liquids with a High Density Difference

Axial dispersion coefficients have been measured during the countercurrent flow of mercury and water through a column filled with various packing materials (1/4-, 3/8-, and 1/2-in. Raschig rings and 1/4-in. solid cylinders). This system is similar to reductive extraction columns, such as those proposed for use in processing molten-salt breeder reactors, which employ high-density fluids that frequently do not wet the packing. The data are in reasonable agreement with a correlation developed several years earlier by other investigators studying aqueous-organic solvent systems.

A new design for a device that reduces axial mixing was tested. Our earlier designs had been effective in reducing mixing, but they had also reduced the column capacities to an undesirable degree. The new design was shown to give adequate column capacity with approximately the same effectiveness in reduction of mixing.

15.6 Multicomponent Mass Transfer in Electrolyte Systems

Calculation procedures are being developed for analyzing the transfer of several components with electrical charges (e.g., ions) between an electrolyte and a solvent phase. These procedures should be useful in treating extraction systems using "liquid ion exchange" solvents and in reductive extraction systems. These systems are complicated by the number of components frequently involved (usually more than two) and by the electric charge on the diffusing ions.

15.7 Chemical Engineering Research Studies Related to MSR Processing

Studies that are related to MSR processing but are supported entirely or partially by Chemical Engineering Research funds are briefly summarized. These studies are described in more detail in Sect. 1.

16. REACTOR EVALUATION STUDIES

This program, which is a joint effort with the ORNL Reactor Division, has the primary purpose of assisting the USAEC in evaluating the technical feasibility and economics of various nuclear power concepts being developed, or being considered for development, under the U.S. Civilian Power Program. Work in this Division during the past year was devoted primarily to performing production calculations with the Oak Ridge Systems Analysis Code and developing systems analysis models for electric utility systems in cooperation with other members of the Joint Systems Analysis Study Group (Tennessee Valley Authority, Commonwealth Edison Company, Westinghouse Atomic Development Corporation, and ORNL).

17. MISCELLANEOUS PROGRAMS

17.1 Quality Assurance Program

Quality assurance procedures based on program requirements given in RDT F2-2T are being written and applied to projects, particularly those involving reactor support work, within the Chemical Technology Division. The appropriate level of quality assurance effort is determined and reflected in the quality level assigned to each project. More than 30 experiments in the Division have been examined and assigned quality levels. Seminars and discussions have been held with Division personnel; these personnel are now acquainted with the intent and scope of Division procedures and are working within them.

17.2 Evaluation of the Radiation Resistance of Selected Protective Coatings (Paints)

The comparative resistances of 108 protective coating systems to gamma radiation were determined. Selective systems of epoxies, modified phenolics, and polyurethanes were found to withstand exposures of up to 7×10^9 rads in deionized water and to 1×10^{10} rads in air.

Test procedures for evaluating protective coatings for use in reactor containment facilities were developed and incorporated in a proposed standard, American National Standards Institute standard No. ANSI 101.2-1970, "Protective Coatings (Paints) for Light Water Reactor Containment Facilities."

17.3 Resource Studies

A wide-range program was begun partly as a National Science Foundation activity and partly as an independent effort to evaluate the long-term situation in regard to the availability of mineral resources and the future potentials for substitution and recycle to extend resource horizons of critical materials. Much of this work has been done in cooperation with Resources for the Future, Inc. (RFF). H. E. Goeller spent the summer of 1970 at the RFF offices in Washington, D.C., working with Joel Darmstadter, Hans Lansberg, and Samuel Schurr, who are economists on the RFF staff.

17.4 Environmental Quality Program: Productive Uses of Waste Heat

The Environmental Quality Program was established in response to the increasing involvement of the Atomic Energy Commission in assessing the total impact of nuclear power plants on the environment. Productive uses of waste heat relate to the utilization of this heat as a resource instead of rejection of it as a waste. Potential benefits to agriculture, aquaculture, and urban applications are discussed.

17.5 Systems Analysis of a Nuclear Energy Center

A systems analysis approach was developed for (1) optimizing a combination of industrial activities for a nuclear energy center as a function of energy cost and (2) determining the economic impact of the center on its economic region. Results indicate that, for an assumed base power rate of 4.1 mills/kWhr and comparable costs for steam, the total energy demand for industries located in the center would be about 890 MW(e). The impact of this center (capital cost $461 million) on its economic region would be significant,

particularly on the demands for additional capital by the government and public services sectors.

17.6 Applications of ^{252}Cf

A program is being instituted using ^{252}Cf as the neutron source in a capture-gamma activation analysis technique for detecting trace elements. Also, studies using the DOT computer program are being conducted to optimize, with regard to geometry and materials of construction, a thermal-neutron radiography design incorporating a ^{252}Cf source.

1. Molten-Salt Reactor Processing

Oak Ridge National Laboratory is developing a molten-salt breeder reactor (MSBR) which would operate on the ^{232}Th-^{233}U fuel cycle to produce low-cost power while producing more fissile material than is consumed. The reactor would use a molten fluoride salt (72-16-12 mole % LiF-BeF_2-ThF_4) as the fuel and graphite as the moderator. If the reactor is to operate as a breeder, ^{233}Pa must be isolated from the region of high neutron flux during its decay to ^{233}U. Also, the rare-earth fission products must be removed on a 25- to 100-day cycle. The Chemical Technology Division is responsible for developing an on-site processing plant to economically effect these operations. Processes that employ liquid-liquid extraction of the reactor salt with a bismuth phase containing reductants appear to offer the best means to this end and have been the major subjects of our studies.

During this report period we have continued to evaluate and develop a flowsheet based on fluorination–reductive extraction for protactinium isolation and the metal transfer process for rare-earth removal. The portion of the flowsheet dealing with protactinium isolation was simplified considerably by retaining the isolated protactinium in a secondary salt, rather than in bismuth, at a point intermediate in the protactinium extraction column. This change results in a process that will be much easier to operate and will effect a significant reduction in plant cost.

Additional data on the distribution of rare earths between liquid bismuth solutions and molten LiCl confirm that these materials distribute favorably. We have shown that temperature does not markedly affect distribution and that our previous extrapolation of distribution data to conditions involving lithium concentrations in bismuth as high as 50 at. % appears to be valid.

Data were obtained on the effect of the LiF concentration on the distribution of solutes, including lanthanum, neodymium, and uranium, between LiCl-LiF solutions and liquid bismuth. This information confirmed earlier indications that LiF in concentrations below about 4 mole % has little effect on the behavior of di- and trivalent solutes but that the thorium–rare-earth separation factor decreases with increasing LiF concentration. The mutual solubilities of thorium and neodymium in lithium-bismuth solutions at 640°C appear to be much higher than those required in the extraction of rare earths from LiCl by contact with lithium-bismuth solutions.

Our first two engineering experiments for study of the metal transfer process for removing rare earths from single-fluid MSBR fuel salt were completed. In the first experiment, the rare earths (La and Nd) were extracted from the fluoride salt at about the predicted rates, and approximately 50% of the lanthanum and 25% of the neodymium were removed. The rare earths did not collect in the lithium-bismuth solution as expected; we believe that this was the result of oxide contamination in the system. The second experiment, which demonstrated all of the important aspects of the process, was operated for about three months before it was shut down for inspection. During that period more than 85% of the lanthanum and 50% of the neodymium originally in the fuel carrier salt was removed and deposited in a lithium-bismuth solution. There was no measurable accumulation of thorium (<10 ppm) in the lithium-bismuth solution, thus demonstrating that the rare earths can be removed without significant removal of thorium. The thorium-lanthanum decontamination factor was about 10^5. The distribution coefficients between the salt and metal phases in the system were in reasonable agreement with expected values. A third engineering experiment, which will use flow rates that are about 1% of those required for a 1000-MW(e) MSBR, is being designed and fabricated.

Our work on contactor development was quite successful during this reporting period. Flooding data obtained during the countercurrent flow of bismuth and molten salt in a 24-in.-long, 0.082-in.-ID column packed with ¼-in. molybdenum Raschig rings are in good agreement with flooding rates predicted from studies with mercury and water. These studies indicate

that the flow capacity of packed-column contactors is sufficiently high for use in MSBR processing systems. Using the same column, we also demonstrated the extraction of uranium from molten salt by bismuth containing reductants in a flow system. Greater than 95% of the uranium was extracted from a molten-salt stream by countercurrent contact with a bismuth stream. Data on the extraction of uranium from salt by countercurrent contact with bismuth containing reductant were effectively correlated by an HTU model that assumed the major resistance to uranium transfer to be in the salt phase. These data indicate that the mass transfer performance of packed columns is adequate for MSBR processing systems at metal-to-salt flow rate ratios of about 0.3 or greater. Preparations were begun for mass transfer studies in packed columns using an improved experimental technique that involves measuring the rate of exchange of zirconium isotopes between salt and metal streams otherwise at equilibrium.

We have continued our efforts to develop a frozen-wall continuous fluorinator. Studies of heat generation and heat transfer in a simulated fluorinator system have shown that radio-frequency heating can be used to provide the internal heat source required for studies with nonradioactive systems. A relatively large continuous fluorination experiment is planned.

We have begun considering oxide precipitation as an alternative to the fluorination–reductive extraction method for isolating protactinium and for subsequently removing uranium from MSBR fuel salt. The utility of flowsheets based on oxide precipitation is largely dependent on the development of methods for separating oxide precipitate from molten-salt streams.

Studies on a number of topics related to MSR processing are supported wholly or in part by funds from the AEC Division of Research. These include work on (1) distribution of protactinium between salt and bismuth phases and protactinium oxide precipitation studies, supported by Chemistry of Protactinium in Molten Fluoride Systems, (2) hydrodynamics and mass transfer in packed columns and continuous reduction of iron fluoride in molten salt in packed columns, supported by Chemical Engineering Research Studies, and (3) axial dispersion in open bubble columns and continuous fluorinator development, supported by Fluoride Salt Separation Technology.

1.1 MOLTEN-SALT BREEDER REACTOR FLOWSHEET ANALYSIS

A flowsheet in which fluorination is used for removing uranium and reductive extraction is used for isolating protactinium from MSBR fuel salt has been described.[1,2] However, it has been found that a considerable simplification in the flowsheet and a significant reduction in partial fuel cycle cost can be achieved by holding the isolated protactinium in a secondary salt phase rather than in bismuth as previously considered. A flowsheet has been developed using this improved protactinium isolation method and the metal transfer process described previously.[3] We have also observed that the waste streams from the protactinium isolation and the rare-earth removal portions of the new flowsheet can be conveniently combined for uranium recovery prior to disposal, thus decreasing the probability of loss of fissile material. Oxide precipitation is being considered as an alternative method for selectively removing protactinium from MSBR fuel salt and for subsequently removing uranium from the fuel salt prior to the removal of rare earths. Two conceptual flowsheets based on oxide precipitation have been developed. Topics related to promising MSBR processing flowsheets are discussed in the remainder of this section.

Protactinium Isolation Using Fluorination and Reductive Extraction

Analysis of the previously reported[2] fluorination–reductive extraction flowsheet for isolating protactinium from MSBR fuel salt revealed several undesirable features and suggested an improved method for removing fission product zirconium and for retaining ^{233}Pa during its decay to ^{233}U. In that flowsheet, zirconium was extracted into the bismuth stream exiting from the lower column of the protactinium isolation system and was removed from this stream by hydrofluorinating a small fraction of the bismuth in the presence of salt that was withdrawn from the system. Since the bismuth stream also contained protactinium and uranium, the portion of the stream that was hydrofluorinated represented a compromise between (1) maintaining an acceptably low zirconium concentration in the bismuth in the lower part of the column and (2) transferring acceptably small amounts of protactinium and uranium to the waste salt from which these materials were recovered. The remaining bismuth was hydrofluorinated in the presence of salt that was

1. L. E. McNeese, *MSR Program Semiannu. Progr. Rep. Feb. 28, 1970,* ORNL-4548, pp. 282–88.

2. M. J. Bell and L. E. McNeese, *MSR Program Semiannu. Progr. Rep. Aug. 31, 1970,* ORNL-4622, pp. 199–202.

3. *Chem. Technol. Div. Annu. Progr. Rep. May 31, 1970,* ORNL-4572, pp. 4–5.

decontamination

reductive extraction

recycled to a point ahead of the fluorinator in order to remove the uranium as UF_6. This operation also resulted in the recycle of zirconium, which, under operating conditions of interest, was oxidized and reduced several times before its removal. Such recycling resulted in a significant increase in the quantity of reductant required for isolating the protactinium.

We have observed that the flowsheet can be simplified by hydrofluorinating the entire bismuth stream in the presence of a secondary salt stream, as shown in Fig. 1.1. Salt is withdrawn from the reactor on a ten-day cycle and is fed to a fluorinator where about 99% of the uranium is recovered. The salt from the reactor is held up about 30 min before fluorination in order to decrease the heat generation rate due to fission product decay from 56.4 to 15.6 kW/ft^3. The salt is then fed to an extraction column where protactinium, zirconium, and the remaining uranium are extracted into a bismuth stream containing a reductant. Subsequently, the bismuth stream is hydrofluorinated in the presence of a second salt stream, which results in transfer of the extracted materials to the salt. Reductant is added to the recovered bismuth, and the resulting metal stream is recycled to the extraction column as in the previous flowsheet. The secondary salt stream is circulated through a hydrofluorinator, a fluorinator, and a protactinium decay tank. The fluorinator is used to maintain an acceptably low uranium concentration in the protactinium decay tank. Salt is withdrawn from the decay tank periodically to remove zirconium and other fission products that accumulate in the tank. The salt is held for a sufficient period before final discard to allow ^{233}Pa to decay to ^{233}U, which is recovered from the salt by batch fluorination.

These flowsheet modifications offer the following advantages over the previous flowsheet:

1. The bismuth inventory in the system is greatly reduced, thus avoiding a significant inventory charge.

Li_2BeF_4 Li separated

ORNL DWG 70-2811R1

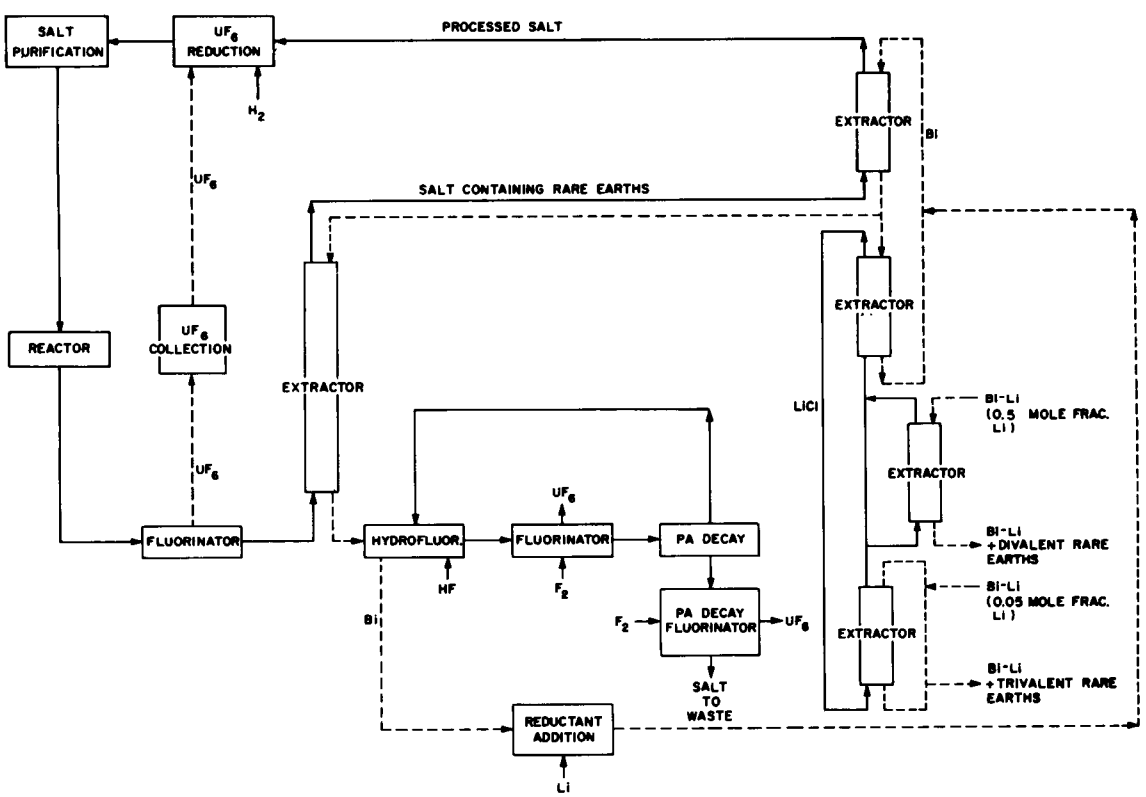

Fig. 1.1. Improved flowsheet for processing a single-fluid MSBR by fluorination–reductive extraction and the metal transfer process. The isolated protactinium is held for decay in a secondary salt stream.

2. The protactinium decay tank can be fabricated from a nickel-base alloy rather than molybdenum, which will result in a considerable saving in the cost of the installed equipment.
3. Control of the protactinium isolation system is greatly simplified.
4. Zirconium will not be recycled in the lower part of the protactinium isolation system, thus reducing the consumption of reductant.
5. The isolated protactinium is retained in such a manner that maloperation of the extraction column cannot return large quantities of protactinium to the reactor.
6. The flowsheet is simplified; recycle of fuel salt containing uranium, zirconium, and protactinium to the primary fluorinator is avoided. Operation of the secondary salt circuit is restricted only by heat removal and inventory considerations.
7. Very efficient hydrofluorination of the bismuth stream would permit the initial salt inventory in the protactinium decay tank to contain natural lithium rather than ^{7}Li.

Representative operating conditions and partial fuel cycle costs have been determined for the revised protactinium isolation system. Both the quantity of reductant required and the rate at which fuel carrier salt must be removed from the reactor to compensate for the LiF added by the protactinium isolation system depend on the fraction of the uranium that is removed from the fuel salt by the primary fluorinator. For a uranium removal efficiency of 95%, the lithium reductant requirement is 370 moles/day and fuel carrier salt must be withdrawn at the rate of 0.3 ft^3/day. For a uranium removal efficiency of 99%, the reductant requirement is 200 moles/day and salt must be discarded at the rate of 0.16 ft^3/day. In the former instance, the chemical and inventory charges for the fluorination–reductive extraction system amount to 0.047 mill/kWhr. These charges are reduced to 0.034 mill/kWhr for the higher fluorinator efficiency. In each case, the salt inventory in the protactinium decay tank is about 150 ft^3. The uranium inventory in the tank is about 0.1% of the reactor inventory.

Rare-Earth Removal Using the Metal Transfer Process

Salt leaving the protactinium extraction column is essentially free of uranium and protactinium but contains the rare earths. This stream is fed to the metal transfer process (see Fig. 1.1), which has been described previously.[3] Calculations have been made to show the effects of several variables on the performance of the process. The quantity that was used as a measure of processing plant performance was the breeding gain (breeding ratio minus 1). Figure 1.2 shows the effect of the number of stages in the fuel salt–bismuth and the LiCl-bismuth contactors on the breeding gain. It is obvious that little benefit is realized from using more than three stages in each contactor; thus three stages are considered optimum.

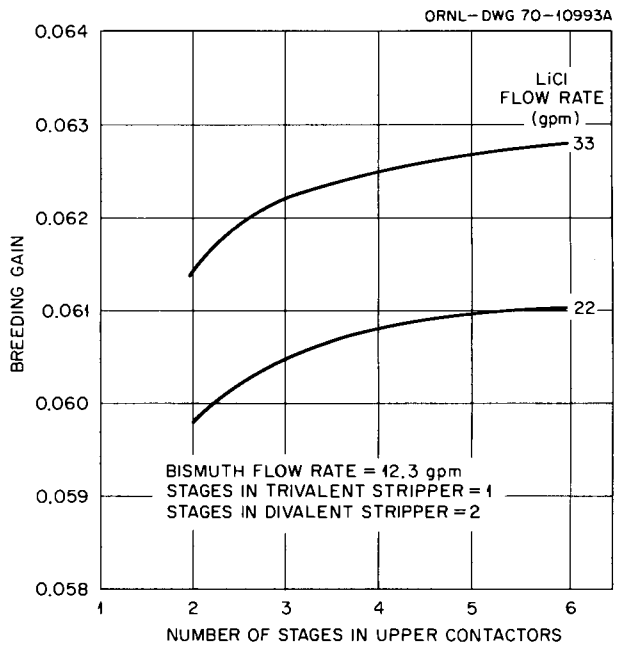

Fig. 1.2. Effect of number of stages in the fuel-salt–bismuth and LiCl-bismuth contactors on MSBR performance.

The effects of the bismuth and LiCl flow rates are shown in Fig. 1.3. A substantial increase in the breeding gain is obtained by increasing the bismuth flow rate from 8.3 to 12.4 gpm; however, further increases in the flow rate do not produce corresponding gains in reactor performance. The breeding gain is relatively insensitive to increases in the LiCl flow rate above 33 gpm. These results led us to select bismuth and LiCl flow rates of 12.4 and 33 gpm, respectively, for the reference processing conditions. For these flow rates, the metal-to-salt flow ratio in the fuel salt–bismuth contactor is 14.1. The column will be packed with ½-in. Raschig rings and will be 7 in. in diameter. The LiCl-bismuth contactor, which will also be packed with ½-in. Raschig rings, is about 14 in. in diameter.

The presence of fluoride in the LiCl causes a significant decrease in the thorium distribution coeffi-

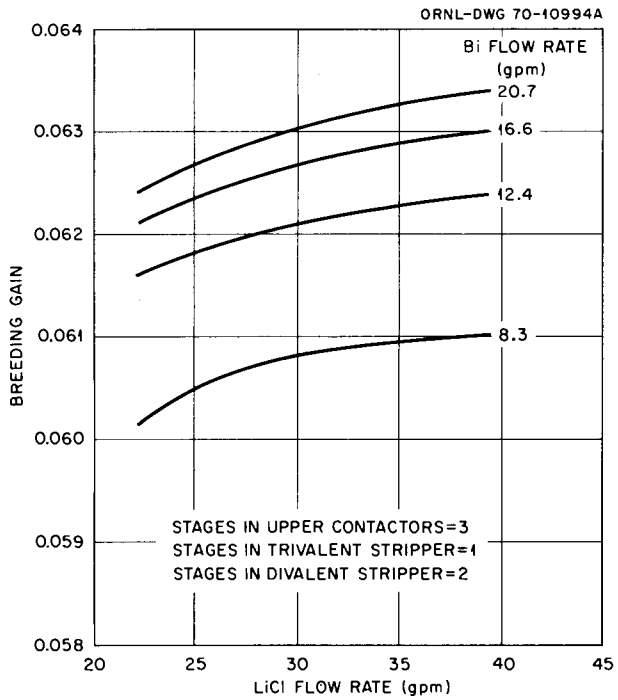

Fig. 1.3. Effects of LiCl and bismuth flow rates in the metal transfer system on MSBR performance.

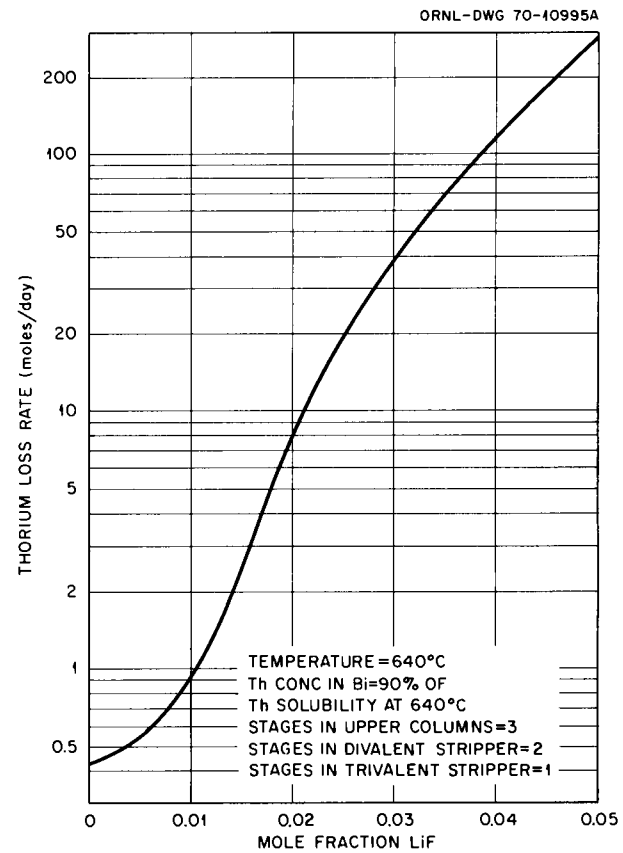

Fig. 1.4. Effect of LiF contaminant in LiCl on thorium loss rate in the metal transfer process.

cient.[4] As a result, an increase in the rate at which thorium transfers to the LiCl is observed as the LiF content in the LiCl is increased. This is undesirable since the thorium is subsequently extracted, along with rare earths, from the LiCl into the lithium-bismuth solutions that are discarded. As shown in Fig. 1.4, the thorium transfer rate increases from 0.41 mole/day with no LiF in the LiCl to 280 moles/day when the LiCl contains 5 mole % LiF. It is likely that the LiF concentration in the LiCl will have to be kept below about 2 mole %, which corresponds to a thorium transfer rate of 7.7 moles/day. Discard of thorium at this rate would add 0.0013 mill/kWhr to the fuel cycle cost. The effect of the presence of fluoride in the LiCl on the removal of rare earths is negligible; in fact, the rare-earth removal efficiency increases slightly as the fluoride concentration in the LiCl increases.

The bismuth and LiCl in the metal transfer process are essentially captive phases and will contain appreciable quantities of fission products when the processing system reaches steady state. The fission product concentration in the bismuth leaving the upper contactor is about 0.0003 mole %, and the corresponding total heat generation is about 1.7 kW. This bismuth phase will have a volume of about 3.6 ft^3; the resulting specific power (470 W/ft^3) is negligible. The fission product concentration in the LiCl leaving the second contactor is about 0.3 mole %. The total heat generation rate in the LiCl is 305 kW; the maximum specific power is about 15 kW/ft^3. The total heat release rate in the lithium-bismuth solution (50 at. % Li) used for removal of the divalent rare earths is 460 kW; this phase is circulated through an 18-ft^3 holdup volume for heat removal. The maximum specific power is 25.6 kW/ft^3, which results primarily from decay of ^{140}Ba and ^{140}La. The total heat release rate in the lithium-bismuth solution (5 at. % Li) used for removal of the trivalent rare earths is about 1.1 MW; this phase is circulated through a 27-ft^3 holdup volume for heat removal. About 75% of the heat results from decay of ^{140}La, ^{141}Ce, and ^{143}Ce. The maximum specific power in this phase is about 40.7 kW/ft^3.

4. L. M. Ferris, *MSR Program Semiannu. Progr. Rep. Feb. 28, 1970,* ORNL-4548, pp. 290–91.

Combination of Discard Streams from the Protactinium Isolation System and the Metal Transfer System

The flowsheet shown in Fig. 1.1 requires that about 40 moles of LiF be added daily to the secondary salt, in which the protactinium is held for decay, in order to obtain a suitable liquidus temperature. Lithium fluoride purchased at a relatively low expense could be used for this addition; however, we have observed that an acceptable liquidus temperature can also be obtained by hydrofluorinating the lithium-bismuth stream from the divalent rare-earth stripper in the presence of the secondary salt. This operation adds 50 moles of LiF and about 1.1 moles of rare-earth fluorides to the decay tank per day. With this addition, the composition of the secondary salt is 72-24-3 mole % $LiF\text{-}ThF_4\text{-}ZrF_4$, 1 mole % divalent rare-earth fluorides, and 360 ppm of trivalent rare-earth fluorides. The salt has a liquidus temperature of 570°C; at this temperature, the rare-earth fluoride concentration is well within the rare-earth solubility. The total heat generation in the secondary salt is 5.2 MW; about 4.0 MW results from ^{233}Pa decay and about 1.2 MW from decay of fission products. The total secondary salt volume is about 175 ft^3, and the specific power in the salt is 30 kW/ft^3.

We have also observed that it is possible to combine all waste streams from the metal transfer system and the protactinium isolation system for uranium recovery prior to disposal, as shown in Fig. 1.5. In this operation, waste salt from the protactinium decay tank would be combined with the fuel carrier salt discard stream. The lithium-bismuth stream from the trivalent rare-earth stripper would be hydrofluorinated in the presence of the resulting salt, and the combined stream would be held for protactinium decay. The protactinium concentration in the combined streams would be only 500 ppm initially, and the specific heat generation rate would be acceptably low. The salt in the waste holdup tank would be fluorinated before discard to recover uranium. The composition of the discarded salt would be 74.7-13.5-9.5-0.8 mole % $LiF\text{-}ThF_4\text{-}BeF_2\text{-}ZrF_4$, 1.2 mole % trivalent rare-earth fluorides, and 0.3 mole % divalent rare-earth fluorides. Although the liquidus temperature of the salt is near 500°C, the salt temperature would have to be maintained at about 600°C so that the trivalent rare-earth fluorides would not precipitate. This processing scheme would require that salt be discarded at the rate of 60 ft^3 every 220 days.

Removal of Protactinium and Uranium from Fuel Salt by Oxide Precipitation

Ross, Bamberger, and Baes[5] have shown that protactinium can be precipitated selectively as Pa_2O_5 from

5. R. G. Ross, C. E. Bamberger, and C. F. Baes, Jr., *MSR Program Semiannu. Progr. Rep. Aug. 31, 1970*, ORNL-4622, p. 92.

ORNL DWG 71-2858

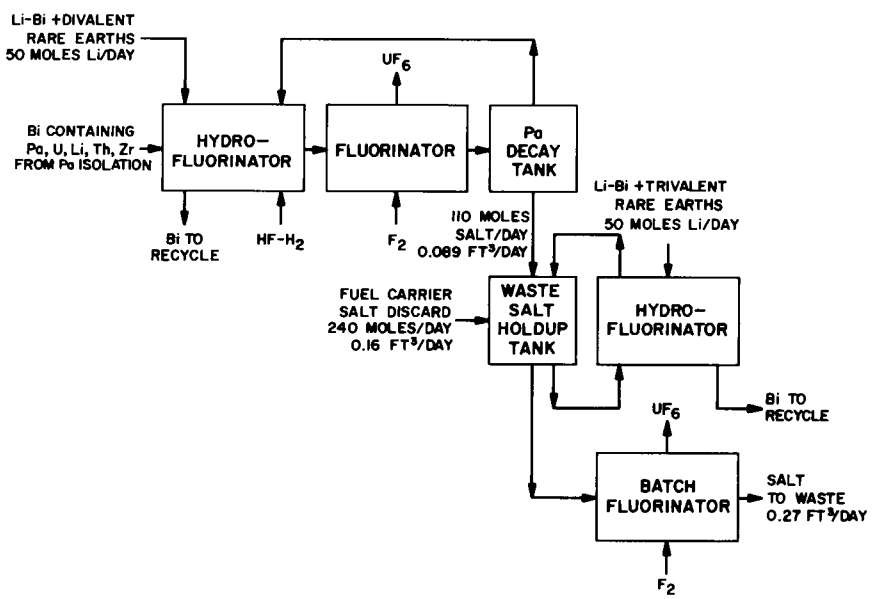

Fig. 1.5. Method for combining waste streams from protactinium isolation and rare-earth removal processes. Flow rates are shown for an assumed uranium removal efficiency in the primary fluorinator of 99%.

MSBR fuel salt by the addition of oxide to salt containing Pa^{5+}. Bamberger and Baes[6] have also found that uranium oxide can be precipitated from protactinium-free fuel salt (i.e., fuel salt from which protactinium has been previously removed), with the attendant precipitation of only a small fraction of the thorium. However, if most of the uranium is precipitated from the salt in a single operation, a large quantity of ThO_2 will also be precipitated. Precipitation of large quantities of thorium can be avoided by use of a multistage countercurrent precipitator. Calculations have been made on the performance of a multistage precipitator using the equilibrium data of Bamberger and Baes[6] for UO_2-ThO_2 solid solutions in contact with fuel salt. Typical results for the effects of temperature and number of stages on system performance are shown in Fig. 1.6. These results indicate that greater than 99% of the uranium can be removed from MSBR fuel salt with relatively few stages and that the oxide stream produced will have a UO_2 concentration of greater than 90%. A decrease in performance is observed with increasing temperature. Thus we conclude that oxide precipitation can be considered as an alternative method to fluorination and reductive extraction for the isolation of protactinium and removal of uranium from the fuel salt of an MSBR.

A possible flowsheet and typical operating conditions are shown in Fig. 1.7. Fuel salt is withdrawn from the reactor on a three-day cycle, and protactinium is removed by precipitation as Pa_2O_5. Part of the salt is processed on a 30-day cycle for rare-earth removal by the metal transfer process. Most of the uranium must be removed from this stream prior to removal of the rare earths. The separated uranium is then recombined with the processed salt leaving the metal transfer system and is returned to the reactor. The Pa_2O_5 precipitate is hydrofluorinated in the presence of a captive salt phase, which circulates through the protactinium decay tank and through a fluorinator in order to maintain an acceptably low uranium inventory in the decay tank. Part of the salt in the decay tank must be returned to the reactor to compensate for salt that is transferred to the tank with the Pa_2O_5 precipitate.

As shown in Fig. 1.8, the protactinium removal time for this system depends on the precipitator efficiency and the rate at which fuel salt is transferred to the protactinium decay tank along with the Pa_2O_5. A removal time of about five days can be obtained if 60% of the protactinium is removed from the salt in the

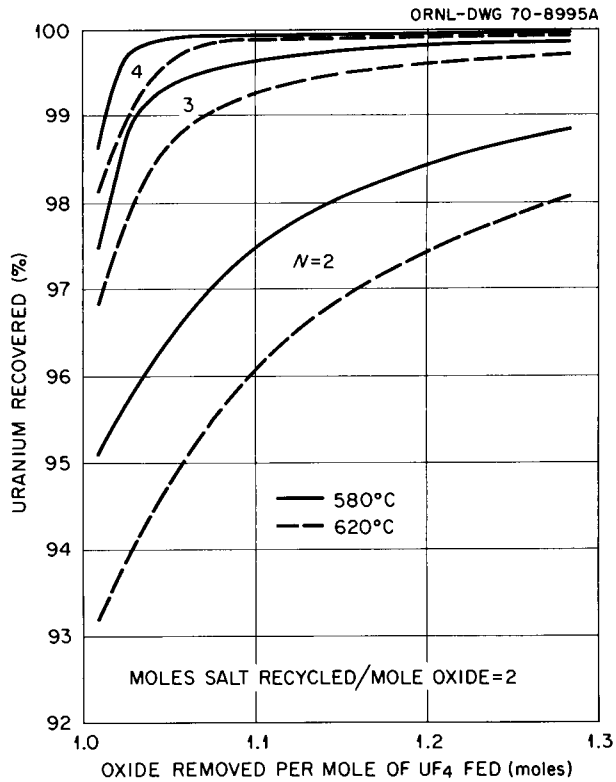

Fig. 1.6. Effect of temperature, number of stages, and oxide removal rate on percentage uranium recovered in an oxide precipitator.

precipitator, provided the salt transfer rate to the protactinium decay tank is as low as 10 to 20 moles/day (a salt-to-oxide flow rate ratio of 2 to 4). A precipitator efficiency of about 80% would be required if the rate of salt transfer to the decay tank were as high as 600 moles/day. The uranium inventory in the decay tank depends on the efficiency of the fluorinator in the protactinium isolation loop and on the amount of fuel salt transferred to the protactinium system with the precipitate, as shown in Fig. 1.9. This uranium inventory will be only a small fraction of the uranium inventory in the reactor, and the associated inventory charge will be less than 0.001 mill/kWhr for a wide range of operating conditions.

Isolation of protactinium by oxide precipitation can also be achieved without the use of a fluorinator, as shown in Fig. 1.10. In this flowsheet, the Pa_2O_5 precipitate is hydrofluorinated in the presence of uranium-free salt leaving the metal transfer system. The resulting salt stream then passes through a decay tank, where it is held up two to four days before being recycled to a point ahead of the precipitator in order to return ^{233}U to the reactor. Since the salt flow rate

6. C. E. Bamberger and C. F. Baes, Jr., *J. Nucl. Mater.* 35, 177 (1970).

through the protactinium decay tank must be relatively large in order to limit the uranium inventory in the decay tank, high precipitator efficiencies are required; a precipitator efficiency of about 96% would be required to obtain a protactinium removal time of five days. Uranium inventories in the protactinium isolation system using this flowsheet will be 0.5 to 1.0% of the reactor fissile inventory; corresponding inventory charges will be 0.002 to 0.004 mill/kWhr.

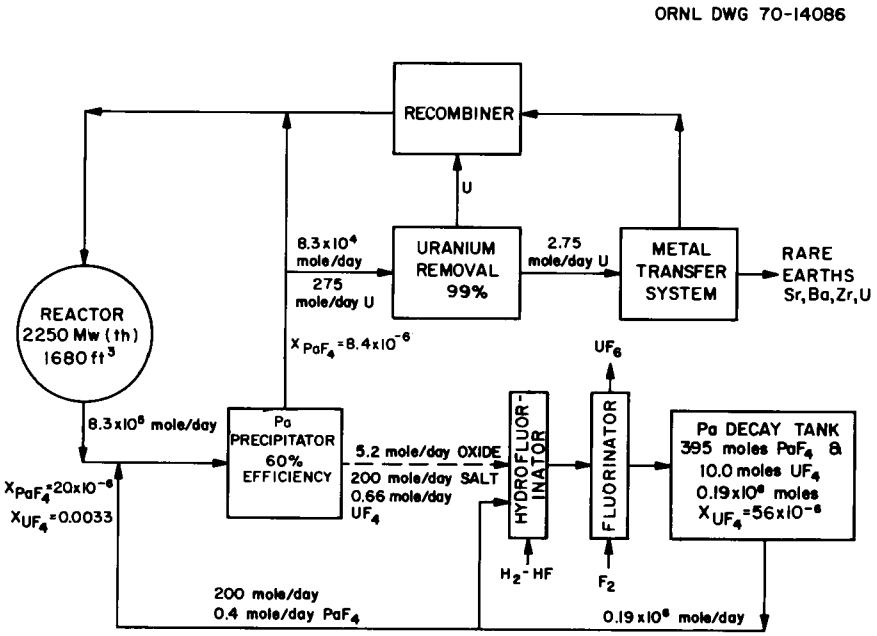

Fig. 1.7. Flowsheet for protactinium isolation using fluorination and oxide precipitation.

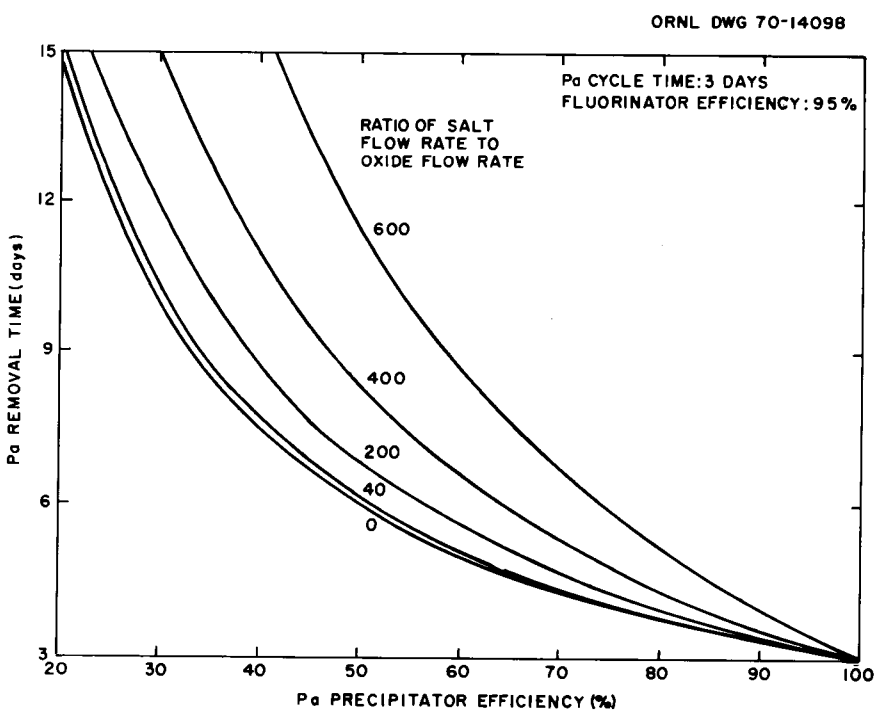

Fig. 1.8. Effects of precipitator efficiency and fuel salt transfer rate on protactinium removal time for the fluorination–oxide-precipitation flowsheet.

ORNL DWG 70-14099

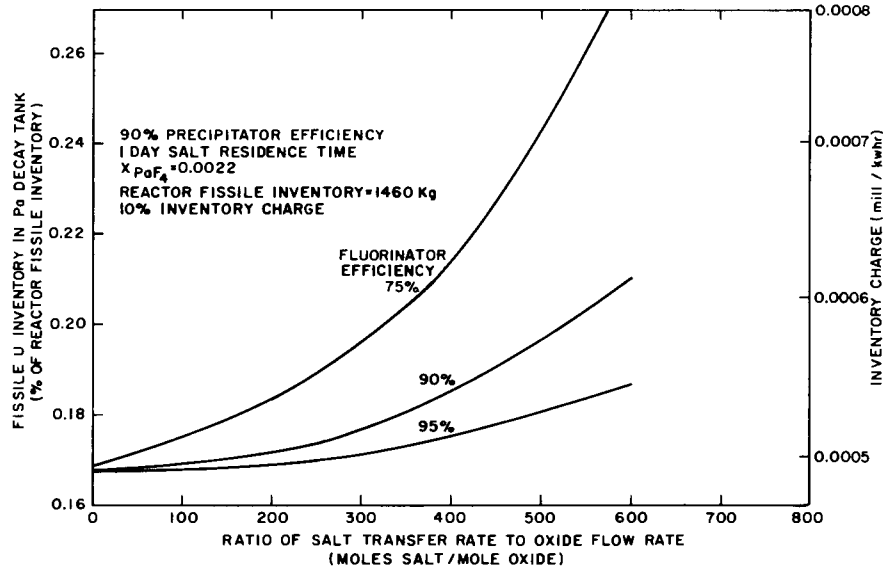

Fig. 1.9. Effect of secondary fluorinator efficiency and fuel salt transfer rate on uranium inventory for the fluorination–oxide-precipitation flowsheet.

ORNL DWG 70-14087

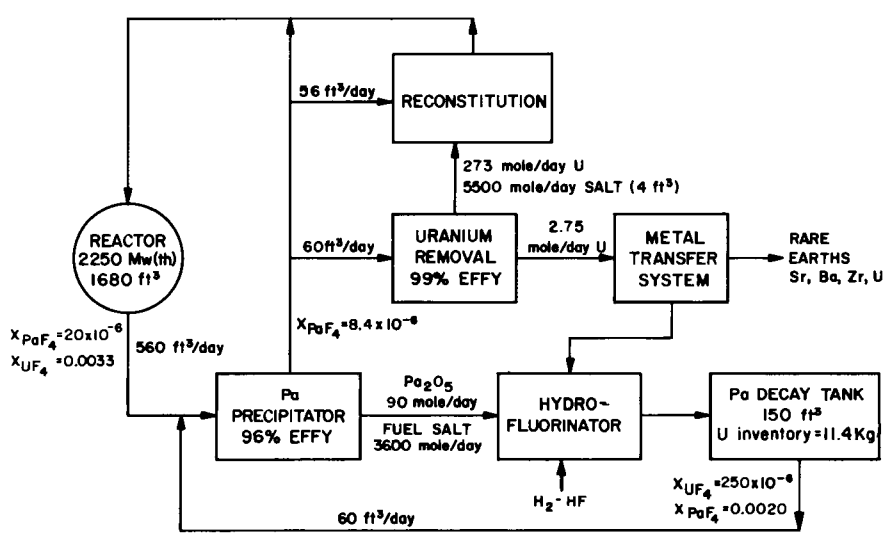

Fig. 1.10. Flowsheet for protactinium isolation using oxide precipitation.

Importance of Uranium Inventory in an MSBR Processing Plant

The MSBR processing flowsheets considered thus far have uniformly resulted in very low uranium inventories in the processing plant, that is, inventories that are usually below 1% of the uranium inventory in the reactor. Since several potential processing systems might result in uranium inventories as large as 5 to 10% of the reactor inventory, we have investigated the importance of uranium inventory in an MSBR processing plant. The major effects of an increased uranium inventory are (1) an increase in inventory charges on fissile material and (2) an increase in the reactor

ORNL DWG 71-2860

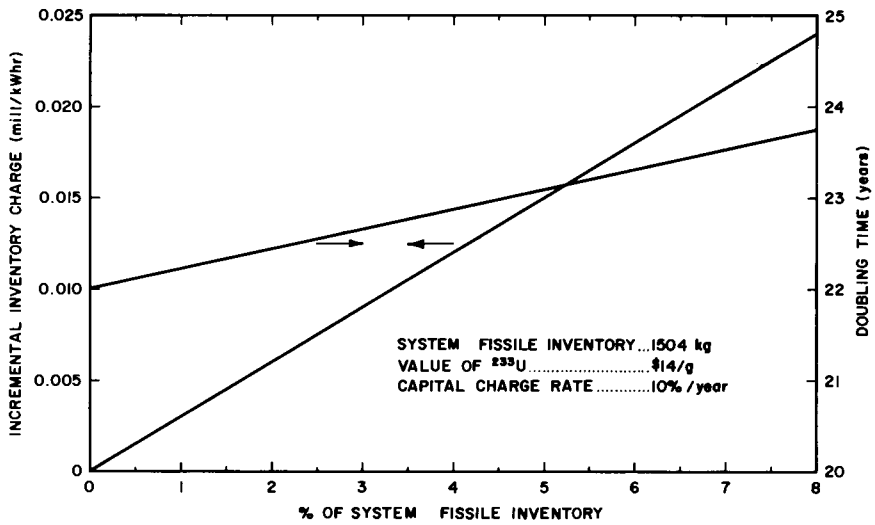

Fig. 1.11. Effect of ^{233}U inventory in processing plant on system doubling time and inventory charges.

doubling time. The variation of each of these quantities with processing plant uranium inventory is shown in Fig. 1.11. The fissile inventory (which includes the ^{233}Pa in the processing plant) was assumed to be 1504 kg for the reference reactor and processing plant, the value of ^{233}U was taken to be $14/g, and the capital charge rate was assumed to be 10%/year. The calculated system doubling time for the limiting case of a zero uranium inventory in the processing plant was 22 years. It is seen that a processing plant uranium inventory of 5% of the system fissile inventory would increase the fuel cycle cost by 0.015 mill/kWhr and would increase the system doubling time from 22 to 23.1 years. A uranium inventory of 10% of the system fissile inventory would result in a fuel cycle cost increase of 0.03 mill/kWhr and an increase in doubling time from 22 to 24.2 years. Thus, while there is incentive for maintaining a low uranium inventory in the processing plant, it does not appear that a uranium inventory as high as 5 to 10% of the system fissile inventory would rule out an otherwise attractive processing system.

1.2 MEASUREMENT OF DISTRIBUTION COEFFICIENTS IN MOLTEN-SALT–METAL SYSTEMS

Studies of the basic chemistry relating to the metal transfer process[7,8] for the removal of rare earths from MSBR fuel salt were continued during the past year. In these studies, more measurements of the equilibrium distribution of lanthanide and actinide elements between liquid bismuth solutions and molten LiCl or LiBr were made. Data were also obtained on the effect of fluoride concentration on the distribution of uranium and several lanthanide elements between LiCl-LiF and bismuth solutions. These latter measurements should be useful in predicting how the metal transfer process would be affected if the LiCl acceptor salt became contaminated with fluoride fuel salt.

It has been shown before[8-11] that at a given temperature the distribution coefficients for component M,

$$D_M = \frac{\text{mole fraction of M in bismuth phase}}{\text{mole fraction of M in salt phase}}, \qquad (1)$$

can be expressed as

$$\log D_M = n \log N_{Li} + \log K_M{}^* , \qquad (2)$$

in which N_{Li} is the mole fraction of lithium in the bismuth phase, n is the valence of M^{n+} in the salt phase, and $\log K_M{}^*$ is a constant. Most of the values of n and $\log K_M{}^*$ obtained in our recent studies using various salt phases are given in Table 1.1. The original data, as

7. L. E. McNeese, *MSR Program Semiannu. Progr. Rep. Feb. 28, 1970,* ORNL-4548, p. 277.

8. D. E. Ferguson and staff, *Chem. Technol. Div. Annu. Progr. Rep. May 31, 1970.* ORNL-4572, p. 1.

9. L. M. Ferris et al., *J. Inorg. Nucl. Chem.* 32, 2019 (1970).

10. L. M. Ferris, F. J. Smith, and J. C. Mailen, *MSR Program Semiannu. Progr. Rep. Feb. 28, 1970,* ORNL-4548, p. 289.

11. L. M. Ferris and F. J. Smith, *MSR Program Semiannu. Progr. Rep. Aug. 31, 1970,* ORNL-4622, p. 204.

Table 1.1. Values of n and log K_M* obtained in measurements of the equilibrium distribution of several solutes between bismuth solutions and molten lithium halide salts

Element	Composition of salt phase (mole %)			Temperature (°C)	n	log K_M*
	LiCl	LiF	LiBr			
La	100	0	0	640	3	7.796 ± 0.4
Nd					3	8.374 ± 0.4
U					3	11.197 ± 0.4
Np					3	10.33 ± 0.1
Pu					3	10.126 ± 0.1
Am					~3	~10.16 ± 0.2
Cm					3	9.406 ± 0.1
Cf					~2	~5.38 ± 0.2
Th	0	0	100	640	4	14.8 ± 0.7
Pa					4	15.7 ± 0.8
U					3	10.6 ± 0.5
La	99.5	0.5	0	640	3	7.607 ± 0.4
Nd					3	8.568 ± 0.4
U					3	10.954 ± 0.4
La	98.0	1.99	0	640	3	7.878 ± 0.4
Nd					3	8.064 ± 0.4
U					3	11.329 ± 0.4
La	97.4	2.65	0	640	3	7.789 ± 0.4
Nd					3	8.310 ± 0.4
U					3	11.624 ± 0.4
La	95.7	4.33	0	640	3	7.372 ± 0.4
Nd					3	7.805 ± 0.4
U					3	11.480 ± 0.4
La	91.2	8.82	0	640	3	7.182 ± 0.4
Nd					3	7.521 ± 0.4
U					3	10.340 ± 0.4
La	82.6	17.41	0	640	3	6.458 ± 0.4
Nd					3	6.739 ± 0.4
U					3	8.604 ± 0.4
La	73.9	26.07	0	640	3	5.494 ± 0.4
Nd					3	6.354 ± 0.4
U					3	8.758 ± 0.4
U	100	0	0	675	3	10.11 ± 0.3
La	100	0	0	700	3	7.185 ± 0.1
Nd					3	7.831 ± 0.1
Sm					2	2.756 ± 0.1
Eu					2	2.133 ± 0.1
Th					4	13.772 ± 0.1
Pa					4	15.8 ± 0.4
U					3	10.192 ± 0.1
Np					3	10.369 ± 0.1
Pu					3	10.223 ± 0.1
Cm					3	9.589 ± 0.1
Cf					2	5.43 ± 0.2

plots of log D_M vs log N_{Li}, obtained at 700°C for plutonium, curium, and californium with LiCl as the salt phase are shown in Fig. 1.12. Generally, the values of n obtained (Table 1.1) were those expected; an exception was californium, which existed primarily in the 2+ oxidation state at 640°C and was almost totally divalent at 700°C (Fig. 1.12). These results confirm our earlier evidence[12] for the existence of Cf(II) under the experimental conditions employed.

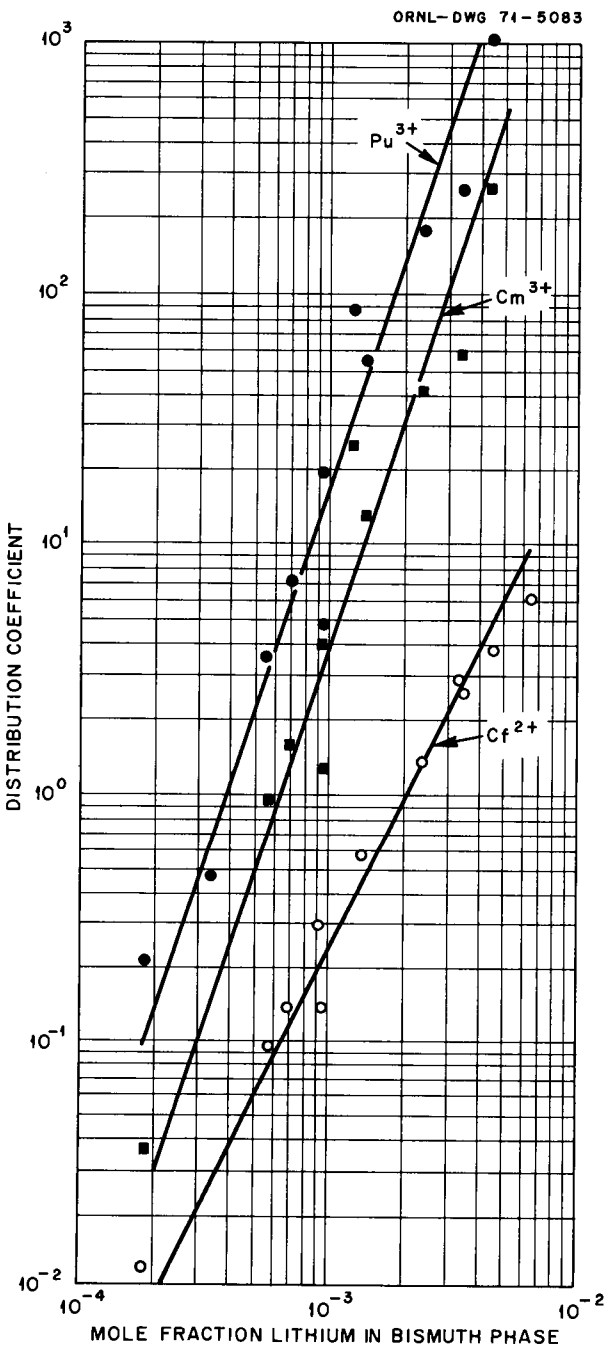

Fig. 1.12. Equilibrium distribution of plutonium, curium, and californium between molten LiCl and liquid bismuth solutions at 700°C.

Table 1.2. Temperature dependence of log K_M* for several elements: log $K_M^* = A + B/T(°K)$

Temperature range 625 to 750°C

Salt	Element	A	B	Standard deviation of log K_M*
LiCl	Ba^{2+}	−0.6907	2,189	0.02
	La^{3+}	−2.6585	9,697	0.1
	Nd^{3+}	−3.3568	10,900	0.08
	Sm^{2+}	0.7518	1,950	0.05
	Eu^{2+}	−0.1584	2,250	0.05
LiBr	Ba^{2+}	−0.0733	1,333	0.02
	Nd^{3+}	4.4046	4,297	0.1

The data given in Table 1.1, when used in conjunction with previously reported data,[8,10,11] allowed us to determine the temperature dependence of log K_M* for several elements. With each element for which sufficient data were obtained, the relationship log $K_M^* = A + B/T(°K)$ was obeyed. Values of A and B for several elements, obtained with either LiCl or LiBr as the salt phase, are given in Table 1.2. These data confirm earlier indications[8,10,11] that the distribution behavior of the di- and trivalent elements is rather insensitive to temperature changes and that the distribution coefficients for a given element at a given temperature are about the same with LiCl and LiBr. On the other hand, the available data indicate that the values of log K_M* for tetravalent elements such as thorium and protactinium are more strongly dependent on temperature than the values for the di- and trivalent elements.

The effect of LiF concentration on log K_M* for several elements is shown graphically in Fig. 1.13. The values of log K_M* for lanthanum, neodymium, and uranium are those given in Table 1.1; the data for thorium and europium were reported previously.[8,11] As seen in Fig. 1.13, the values of log K_M* for the di- and trivalent species did not vary markedly when the LiF concentration was in the range of 0 to about 4 mole %. However, the value of K_{Th}* decreased by about 2 orders of magnitude as the LiF concentration was increased from 0 to 4 mole %. These data indicate that contamination of the LiCl acceptor salt with fluoride fuel salt in amounts that are equivalent to 4

12. J. C. Mailen and L. M. Ferris, "Distribution of Transuranium Elements between Molten Lithium Chloride and Lithium-Bismuth Solutions: Evidence for Californium(II)," *Inorg. Nucl. Chem. Lett.* (in press).

ORNL DWG 71-2861

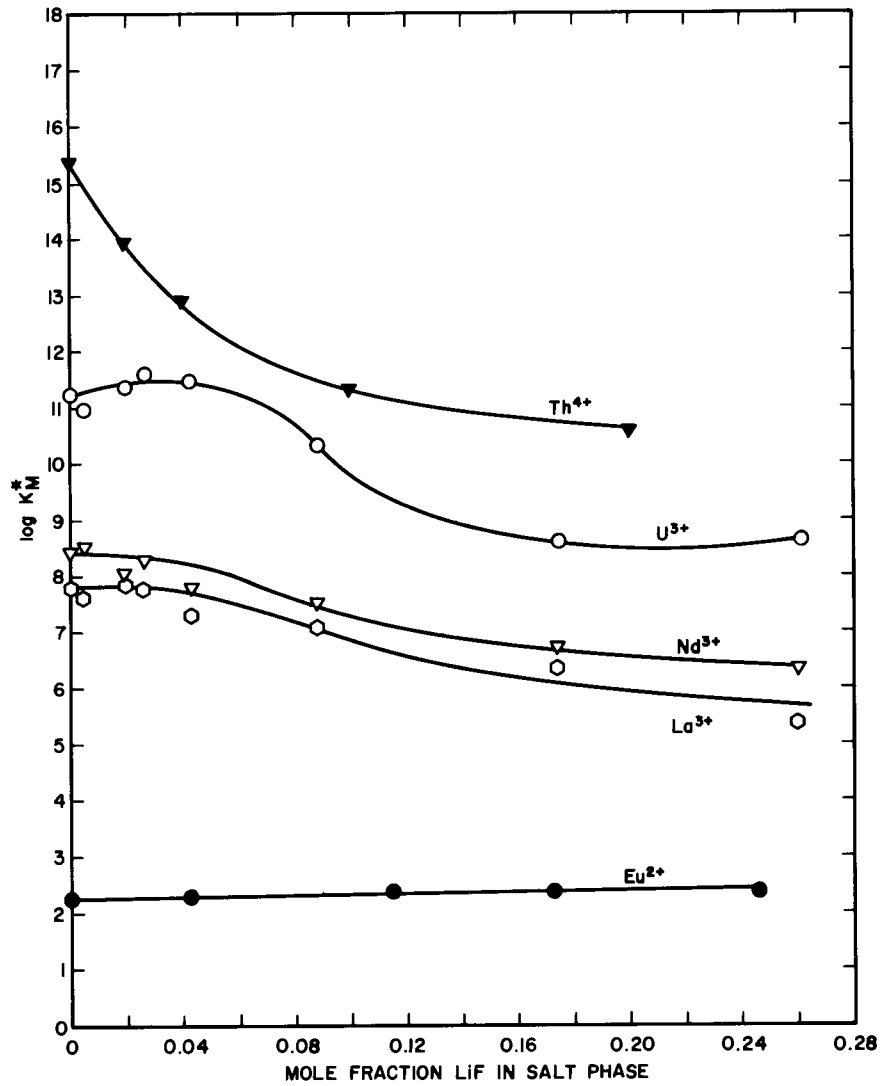

Fig. 1.13. Variation of log K_M* with salt composition. Salt phase was an LiCl-LiF solution; data obtained at 640°C except for europium, which was obtained at 650°C.

mole % LiF or less will not affect the extent to which the rare earths are removed in the metal transfer process. The presence of fluoride in the acceptor salt would, however, cause a decrease in the thorium–rare-earth decontamination factor.

In another report[11] we presented values of log K_{Pm}* that were obtained in an experiment at 640°C involving several LiCl-LiF solutions as the salt phase and also estimated the neodymium-promethium separation factor (D_{Nd}/D_{Pm}) to be 3 ± 2. The LiF concentration in the solutions ranged from about 2 to 18 mole %. Inspection of the gamma spectra of samples taken in this experiment revealed that a significant amount of ^{147}Nd was present along with the promethium. Analysis of these spectra showed the neodymium-promethium separation factor to be independent of the LiF concentration in the salt and yielded an average separation factor of 8.3 ± 1.8. Assuming that this separation factor is also valid with LiCl as the salt phase, we estimate log K_{Pm}* = 7.66 ± 0.4 at 640°C. This estimate indicates that promethium would behave much like lanthanum in the metal transfer process.

1.3. ESTIMATED FREE ENERGIES OF FORMATION OF SOME LANTHANIDE AND ACTINIDE HALIDES USING DISTRIBUTION COEFFICIENT DATA

The general reaction for the distribution of an element M between a liquid bismuth phase and an LiCl or LiBr salt phase can be written as

$$MX_n(\text{salt}) + n\text{Li(Bi)} = \text{M(Bi)} + n\text{LiX(salt)}\,, \qquad (3)$$

in which X is Cl or Br and (salt) and (Bi) denote the respective phases. At a given temperature, the equilibrium constant for reaction (3) can be written as

$$K = \frac{N_M \gamma_M a_{LiX}{}^n}{N_{MX_n} \gamma_{MX_n} N_{Li}{}^n \gamma_{Li}{}^n}\,, \qquad (4)$$

in which a is the activity, N denotes mole fraction, and γ is an activity coefficient referred to the designated pure solid or liquid. In the systems investigated, LiX was practically a pure phase; hence a_{LiX} was essentially unity. The concentration of the solute in both the bismuth and salt phases was very low, as was the concentration of lithium in the bismuth phase; therefore the respective activity coefficients were practically constant. Assuming that the activity coefficients are constant and that $a_{LiX} = 1$, and substituting Eq. (1) into Eq. (4), we obtain in logarithmic form:

$$\log K = \log D_M - n \log N_{Li} + \log \gamma_M - \log \gamma_{MX_n} - n \log \gamma_{Li}\,. \qquad (5)$$

Substitution of Eq. (2) into Eq. (5) yields

$$\log K = \log K_M{}^* + \log \gamma_M - \log \gamma_{MX_n} - n \log \gamma_{Li}\,. \qquad (6)$$

The Gibbs standard free energy change for reaction (3) is

$$\Delta G^\circ = n\,\Delta G^f{}_{LiX} - \Delta G^f{}_{MX_n} = -(2.3RT) \log K\,, \qquad (7)$$

in which ΔG^f is the free energy of formation of the designated compound. From Eqs. (6) and (7), we obtain

$$\Delta G^f{}_{MX_n} = n\,\Delta G^f{}_{LiX} + (2.3RT)\,[\log K_M{}^* + \log \gamma_M - \log \gamma_{MX_n} - n \log \gamma_{Li}]\,. \qquad (8)$$

In our work, values of $\log K_M{}^*$ have been obtained for several elements using LiCl or LiBr as the salt phase. Free energies of formation for liquid LiCl and LiBr are available from the JANAF tables.[13] Activity coefficients for several metals in liquid bismuth solution are also available from the literature.[14–18] We have estimated[19] values of $\log \gamma_{MX_n}$ for dilute solutions of MX_n in LiCl and LiBr from published phase diagrams and the results of emf studies.

Values of ΔG^f for several lanthanide and actinide chlorides and bromides were estimated by incorporating the above information in Eq. (8). These values are compared with those from the literature in Table 1.3. Within the estimated uncertainties, the ΔG^f values obtained in this work for $LaCl_3$, $ThCl_4$, $ThBr_4$, and UBr_3 are in good agreement with the values reported by others.[20–22] In the temperature range 640–700°C, our estimates of $\Delta G^f{}_{UCl_3}$ are only about 5 kcal/mole less negative than the values quoted by Brown.[21] Our value at 640°C is in agreement with that measured by Egan et al.[22] At 640°C, our value for $\Delta G^f{}_{PuCl_3}$ is in good agreement with the values quoted by others;[21,23] however, our value at 700°C is about 7 kcal/mole less negative than the literature values. Our values of ΔG^f

13. *JANAF Thermochemical Tables,* Clearing House for Federal Scientific and Technical Information, U.S. Dept. of Commerce, August 1965.

14. V. I. Kober et al., *Zh. Fiz. Khim.* **42,** 686 (1968).

15. V. A. Lebedev, I. F. Nichkov, and S. P. Raspopin, *Zh. Fiz. Khim.* **42,** 690 (1968).

16. V. A. Lebedev et al., *Sov. J. At. Energy* **27,** 59 (1969).

17. M. S. Foster, S. E. Wood, and C. E. Crouthamel, *Inorg. Chem.* **3,** 1428 (1964).

18. L. M. Ferris, J. C. Mailen, and F. J. Smith, *Estimation of Activity Coefficients for Barium and Several Lanthanide Elements in Liquid Bismuth from Distribution Coefficient and Thermochemical Data,* paper submitted for publication.

19. L. M. Ferris, J. C. Mailen, and F. J. Smith, *Estimated Free Energies of Formation of Some Lanthanide and Actinide Halides at 600 to 800°C Using Molten Salt–Liquid Metal Distribution Coefficient Data,* paper submitted for publication.

20. C. E. Wicks and F. E. Block, *Thermodynamic Properties of 65 Elements – Their Oxides, Halides, Carbides, and Nitrides,* U.S. Bur. Mines Bull. 605 (1963).

21. D. Brown, *Halides of the Lanthanides and Actinides,* p. 244, Wiley, New York, 1968.

22. J. J. Egan, W. McCoy, and J. Bracker, "The Standard Molar-Free Energy of Formation of Some Chlorides of Mg, Ce, U, and Th by Solid-State EMF Techniques," in *Thermodynamics of Nuclear Materials,* p. 163, IAEA, Vienna, 1962.

23. F. L. Oetting, *Chem. Rev.* **67,** 261 (1967).

Table 1.3. Comparison of our estimated ΔG^f values with those from other sources

Compound[a]	Temperature (°C)	$-\Delta G^f$ (kcal/mole) This work	Other sources
$LaCl_3(s)$	650	202 ± 4.6	205 (ref. 20)
	750	198 ± 4.6	200 (ref. 20)
$LaBr_3(s)$	640	174 ±4.6	158 (ref. 20)
			182 (ref. 24)
$NdCl_3(s)$	640	185 ± 5.5	197 (ref. 20)
			192 (ref. 25)
	700	183 ± 5.5	194 (ref. 20)
			189 (ref. 25)
$NdBr_3(s)$	640	157 ± 5.5	149 (ref. 20)
			175 (ref. 24)
$ThCl_4(s)$	640	216 ± 4.5	221 (ref. 21)
	700	214 ± 4.5	216 (ref. 21)
$ThBr_4(s)$	640	183 ± 5.4	180 (ref. 21)
$UCl_3(s)$	640	160 ± 4.4	166 (ref. 21)
			158 (ref. 22)
	675	161 ± 4.4	165 (ref. 21)
	700	158 ± 4.4	163 (ref. 21)
$UBr_3(s)$	640	136 ± 4.8	134 (ref. 21)
$PuCl_3(s)$	640	178 ± 4.4	181 (ref. 21)
			180 (ref. 23)
	700	171 ± 4.4	178 (ref. 21)
			177 (ref. 23)

[a]s denotes solid.

for $LaBr_3$, $NdCl_3$, and $NdBr_3$ generally are not in accord with estimates made by others.[20,24,25]

1.4 SOLUBILITIES OF THORIUM AND NEODYMIUM IN LITHIUM-BISMUTH SOLUTIONS

In the metal transfer process[7,8] being developed for removal of rare earths from MSBR fuel salt, lithium-bismuth solutions having high lithium concentrations (5 to 50 at. %) would be used to strip the rare earths (along with any thorium present) from the LiCl acceptor salt. Therefore, we are determining the solubilities, both individual and mutual, of rare earths and thorium in lithium-bismuth solutions.

24. L. Brewer et al., "The Thermodynamic Properties of the Halides," in *The Chemistry and Metallurgy of Miscellaneous Materials. Thermodynamics* (ed. by L. L. Quill), NNES, Div. IV, vol. 19B, p. 76, McGraw-Hill, New York, 1950.

25. A. Glassner, *The Thermochemical Properties of the Oxides, Fluorides, and Chlorides to 2500°K*, ANL-5750 (1957).

ORNL DWG 71-2883

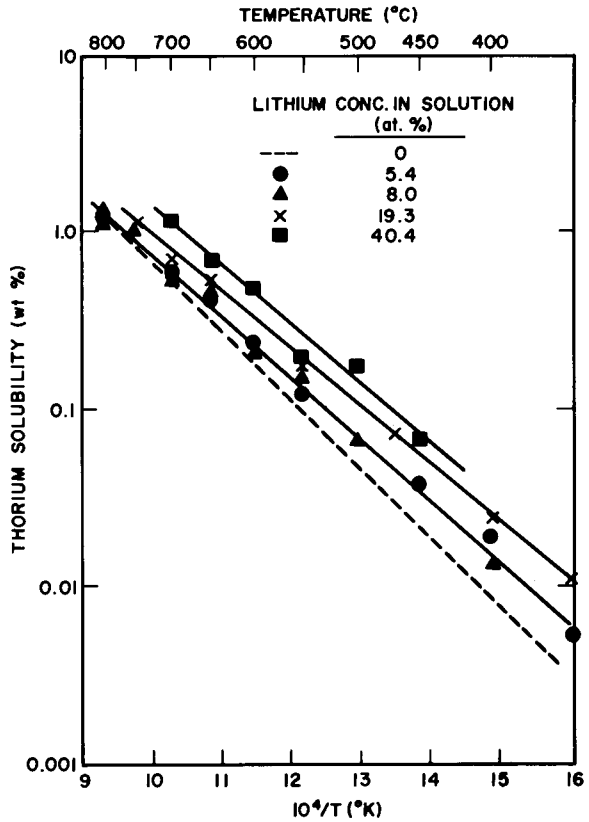

Fig. 1.14. Thorium solubility in lithium-bismuth solutions. Data for 0 at. % lithium taken from ref. 26.

Solubilities of thorium and neodymium in several lithium-bismuth solutions were measured using the procedure and apparatus described elsewhere.[26] The results are summarized in Tables 1.4 and 1.5 and are shown graphically in Figs. 1.14 and 1.15. At each temperature below 750°C the thorium solubility in lithium-bismuth solutions increased by about a factor of 3 as the lithium concentration in the solution increased from 0 to about 40 at. %. Similarly, the neodymium solubility increased regularly as the lithium concentration increased from 0 to 25 at. %. However, when the lithium concentration was increased from 25 to 38 at. % at 640°C, the neodymium solubility decreased to about the same value that was obtained with pure bismuth as the solvent (Fig. 1.15). We are redetermining the neodymium solubilities in Li-Bi (40-60 at. %) to confirm this behavior.

26. C. E. Schilling and L. M. Ferris, *J. Less-Common Metals* **20**, 155 (1970).

ORNL DWG 71-2872

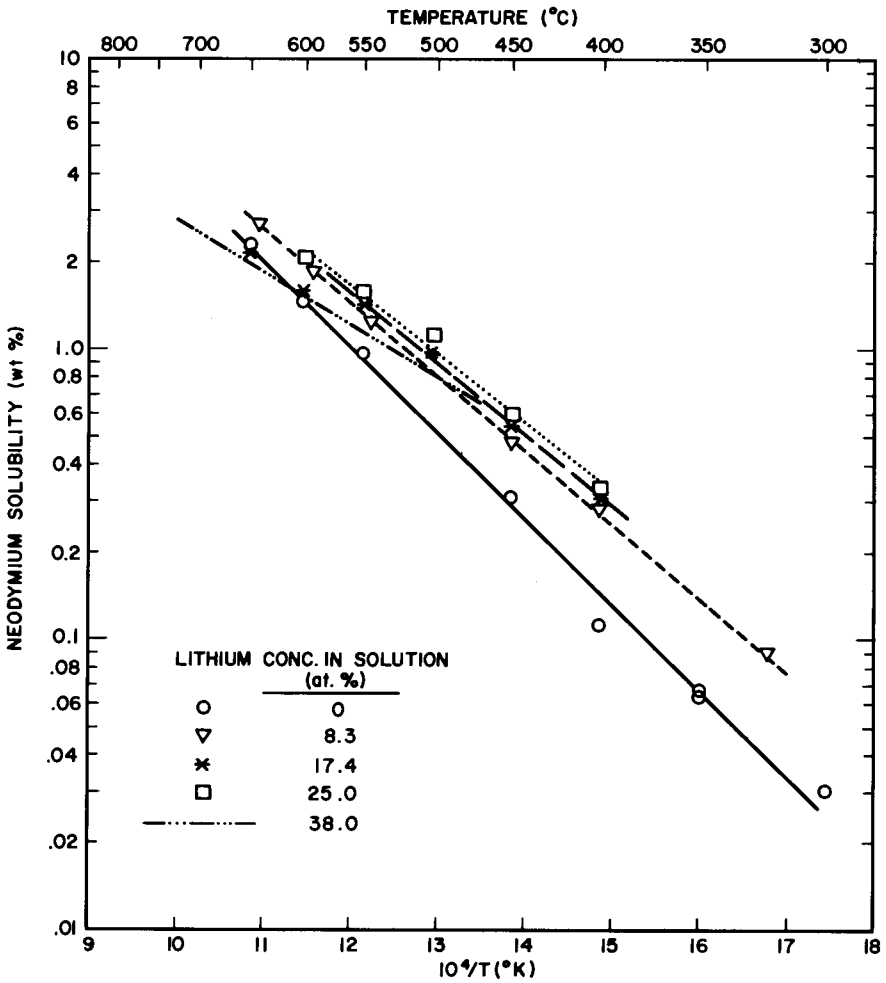

Fig. 1.15. Solubility of neodymium in lithium-bismuth solutions. The solubility of neodymium in lithium-bismuth (38-62 at. %) was taken from ref. 11. The solubility of neodymium in bismuth (lithium = 0 at. %) should be considered preliminary.

Table 1.4. Solubility of thorium in liquid lithium-bismuth solutions

Li concentration in solution (at. %)	Temperature range (°C)	Thorium solubility, log S_{Th} (wt ppm) = $A + B/T$(°K)	
		A	B
0[a]	350–800	7.708	−3852
5.4	350–800	7.073	−3205
8.0	350–800	7.073	−3205
19.3	400–750	7.133	−3164
40.4	450–750	7.473	−3333

[a]Reference 26.

Table 1.5. Solubility of neodymium in liquid lithium-bismuth solutions

Li concentration in solution (at. %)	Temperature range (°C)	Neodymium solubility, log S_{Nd} (wt ppm) = $A + B/T$(°K)	
		A	B
0[a]	500–700	6.68	−2200
8.32	400–700	7.19	−2531
17.4	450–700	7.11	−2435
25.0	450–700	7.07	−2379
38[b]	475–700	6.26	−1809

[a]Preliminary data.
[b]Reference 11.

A series of experiments was conducted in an attempt to measure the mutual solubilities of thorium and neodymium at 640°C in lithium-bismuth solutions having lithium concentrations ranging from 0 to 20 at. %. The mutual solubility limit was approached by making incremental additions of neodymium to the thorium-saturated liquid lithium-bismuth solution. The data obtained in this series of experiments were somewhat scattered, due primarily to the difficulty in analyzing for thorium at a relatively low concentration (less than 0.35 wt %) in the presence of neodymium at a high concentration (up to about 2 wt %). However, the following general conclusions can be drawn from the data: (1) Neodymium, in concentrations below about 1 wt %, appeared to have no effect on the thorium solubility (about 0.35 wt %) in lithium-bismuth solutions at 640°C; as the neodymium concentration was increased from 1 to about 2 wt % (saturation), the thorium concentration decreased almost linearly from about 0.35 to about 0.1 wt %. (2) The effect appeared to be reversible. Additions of thorium to lithium-bismuth solutions saturated with neodymium caused a decrease in the neodymium concentration to about 1 wt % as the thorium concentration increased to about 0.35 wt %.

The above results indicate that the mutual solubility of thorium and rare earths should be much higher than required in the solution, Li-Bi (5-95 at. %), proposed[7,8] for stripping of the trivalent rare earths (La, Pm, Nd) from the LiCl acceptor salt.

1.5 PROTACTINIUM OXIDE PRECIPITATION STUDIES

We are investigating oxide precipitation methods (instead of fluorination and reductive extraction) for the isolation of both uranium and protactinium from MSBR fuel salt. It has been shown[5] that Pa^{4+} dissolved in a molten $LiF\text{-}BeF_2\text{-}ThF_4$ solution can be oxidized to the 5+ state either by hydrofluorination or by reaction with NiO. Furthermore, addition of oxide to a salt solution containing Pa^{5+} results[5] in precipitation of pure, or nearly pure, Pa_2O_5. The solubility product for Pa_2O_5 appears to be much lower than that for UO_2; hence, Pa_2O_5 can be precipitated in preference to UO_2.[5,11] Measurements at various temperatures of the solubility of Pa_2O_5 in MSBR fuel salt that is saturated with UO_2 are being made. Accurate measurements are extremely important in that the Pa_2O_5 solubility defines the lowest protactinium concentration attainable at a given temperature without changing the uranium and thorium concentrations in the salt. Solubilities of Pa_2O_5 at UO_2 saturation of the salt can be obtained in two ways. One method consists of the direct measurement of the equilibrium quotient (Q) for the reaction

$$\tfrac{5}{4}UF_4(d) + \tfrac{1}{2}Pa_2O_5(c) = PaF_5(d) + \tfrac{5}{4}UO_2(ss)\,, \qquad (9)$$

for which

$$Q_9 = \frac{N_{PaF_5(d)}\,N^{5/4}_{UO_2(ss)}}{N^{5/4}_{UF_4(d)}}$$

if Pa_2O_5 is present as a pure solid phase. In these expressions, N, d, c, and ss denote mole fraction, dissolved species, pure crystalline solid, and $ThO_2\text{-}UO_2$ solid solution respectively. The other method involves combining the equilibrium quotients for the following two equilibria:

$$\tfrac{5}{4}ThF_4(d) + \tfrac{1}{2}Pa_2O_5(c) = PaF_5(d) + \tfrac{5}{4}ThO_2(c)\,, \qquad (10)$$

$$UF_4(d) + ThO_2(ss) = UO_2(ss) + ThF_4(d)\,, \qquad (11)$$

for which

$$Q_{10} = \frac{N_{PaF_5(d)}}{N^{5/4}_{ThF_4(d)}}$$

and

$$Q_{11} = \frac{N_{ThF_4(d)}\,N_{UO_2(ss)}}{N_{UF_4(d)}\,N_{ThO_2(ss)}}\,.$$

Previously,[11] we reported preliminary data from an experiment in which Pa_2O_5 was precipitated from $LiF\text{-}BeF_2\text{-}ThF_4\text{-}^{233}UF_4$ (71.8-16-12-0.22 mole %) that initially contained about 110 wt ppm ^{231}Pa. Complete data from this experiment, along with the derived values of log Q_9, are given in Table 1.6. In the first part of this experiment, small amounts of UO_2 were added incrementally at 600°C to about 100 g of salt which had been extensively hydrofluorinated to ensure that the protactinium was in the 5+ oxidation state. The protactinium concentration in the salt declined regularly with each addition of UO_2 until it reached a steady value of about 2.5 wt ppm (Table 1.6, samples 1–7). The protactinium concentration in the salt should become practically constant when the oxide concentration in the salt becomes high enough to cause precipitation of a UO_2-containing solid. These results

Table 1.6. Precipitation of Pa_2O_5 from $LiF-BeF_2-ThF_4-UF_4$ (71.8-16-12-0.2 mole %)

Initial weight of salt: 100 g

Sample	Temperature (°C)	Pa concentration in salt (wt ppm)	$10^6 N_{PaF_5}$	$10^3 N_{UF_4}$	Total UO_2 added to system (mg)	log Q_9 (footnote *a*)
1	600	111	30.4	2.68	0	
2	600	110	30.1		10.8	
3	600	100	27.5		10.8	
4	600	66.9	18.3	2.37	22.8	
5	600	14.2	3.87		31.6	
6	600	2.5	0.69	2.39	41.6	−2.91
7	600	2.7	0.73		51.0	
8	655	11.4	3.12	2.33	51.0	−2.24
9[b]	600	118	32.3	2.49	0	
10	551	4.8	1.32	2.21	113	−2.59
11	577	9.7	2.65	2.10	113	−2.26
12	605	3.1	0.86	2.08	113	−2.74
13	632	7.4	2.03	2.13	113	−2.38
14	658	7.8	2.12	2.05	113	−2.34

[a] $Q_9 = \dfrac{N_{PaF_5} N_{UO_2}^{5/4}}{N_{UF_4}^{5/4}}$; N_{UO_2} was about 0.95 in each case.

[b]System extensively hydrofluorinated after taking sample 8.

indicate that about 98% of the protactinium was precipitated before attendant precipitation of a UO_2-containing solid occurred. The temperature of the system was then raised to 655°C, and sample 8 was withdrawn. After this, the system was again extensively hydrofluorinated, and about 113 mg of UO_2 was added. The temperature of the system was varied between 550 and 660°C, and filtered samples of the salt were taken at each temperature (Table 1.6, samples 10–14). At least 24 hr was allowed for the attainment of equilibrium at each temperature. In calculating values of log Q_9 it was assumed (1) that the system was at equilibrium in each case, (2) that the protactinium in the salt was in the 5+ oxidation state, and (3) that the solid phase was a mixture of pure Pa_2O_5 and a UO_2-ThO_2 solution whose composition could be calculated from the uranium concentration in the salt and the expression

$$\log Q_{11} = \log\left[\frac{N_{UO_2(ss)} N_{ThF_4(d)}}{N_{UF_4(d)} N_{ThO_2(ss)}}\right] = \frac{2101 + 550 N_{UO_2(ss)}}{T} \qquad (12)$$

reported by Bamberger and Baes.[6] This calculation showed that $N_{UO_2(ss)}$ varied only from 0.93 to 0.97; the average value was 0.95. The average UF_4 concentration in the salt was 0.22 mole %. We believe that equilibrium was not achieved at 551 and 577°C and, therefore, that our values of log Q_9 at these temperatures (Table 1.6) are much too high.

We also measured the solubility of Pa_2O_5 in $LiF-BeF_2-ThF_4$ (72-16-12 mole %) in the presence of excess ThO_2 and NiO using the general technique just described. These solubilities and the values of log Q_{10} derived from them are summarized in Table 1.7. Our values for the solubility of Pa_2O_5 are higher than those of Ross, Bamberger, and Baes[5] at temperatures above about 675°C but, being more dependent on temperature, indicate lower solubilities at the lower temperatures.

Also given in Table 1.7 are values of log $Q_9 = \frac{5}{4}$ log Q_{11} + log Q_{10} that were obtained from the measured values of log Q_{10} and values of log Q_{11} that were calculated from Eq. (12) using $N_{UF_4(d)} = 0.0022$. A plot of all of our values of log Q_9 vs $1/T$(°K) is shown in Fig. 1.16. A least-squares fit yielded log $Q_9 = 8.849 - 9859/T$(°K), with a standard deviation of 0.47. This expression gives values of log Q_9 that are significantly

different from those estimated by Ross et al.,[5] particularly at temperatures below about 650°C. In addition, the uncertainty in the values of this important equilibrium quotient is much larger than that required for a detailed analysis of the oxide precipitation process for the isolation of protactinium from MSBR fuel salt.

Table 1.7. Values of log Q_9 calculated at N_{UF_4} = 0.0022 from measured values of log Q_{10} and log Q_{11}

Temperature (°C)	Pa^{5+} concentration at ThO_2 saturation of salt		$10^6 Q_{10}$	log Q_{10}	log Q_{11} (footnote *a*)	log Q_9 (footnote *b*)
	Wt ppm	$10^6 N_{PaF_5}$				
654	1.6	0.438	6.20	−5.207	2.812	−1.692
678	14	3.829	54.2	−4.265	2.730	−0.852
738	62	16.96	240	−3.619	2.536	−0.449

[a] Q_{11} evaluated at N_{UF_4} = 0.0022.
[b] log Q_9 = $\frac{5}{4}$ log Q_{11} + log Q_{10}.

ORNL DWG 71-2862

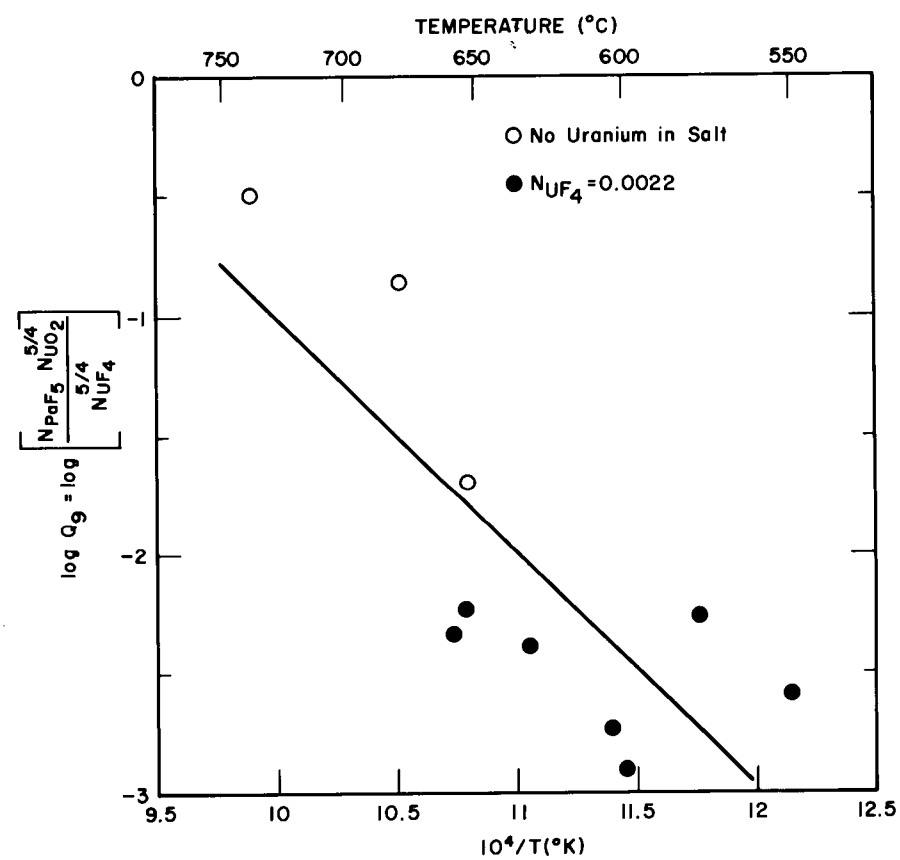

Fig. 1.16. Values of the equilibrium quotient for the reaction $\frac{1}{2}Pa_2O_5(c) + \frac{5}{4}UF_4(d) = PaF_5(d) + \frac{5}{4}UO_2(ss)$ when the UF_4 concentration in $LiF\text{-}BeF_2\text{-}ThF_4$ (72-16-12 mole %) is 0.22 mole %.

1.6 REDUCTIVE EXTRACTION ENGINEERING STUDIES

We have continued our experimental work in the flow-through reductive extraction facility after making system modifications that were described previously.[27] The principal modification consisted of installing a column packed with ¼-in. molybdenum Raschig rings in place of the column packed with ¼-in. molybdenum solid cylinders. A final hydrodynamic experiment (HR-12) was carried out to measure pressure drop through the column when only salt (72-16-12 mole % $LiF-BeF_2-ThF_4$) was flowing through it. Since only a small pressure drop was expected, it was necessary that the bismuth-salt interface at the bottom of the column be depressed below the salt inlet. This was accomplished by routing the argon off-gas flow through a mercury seal to pressurize the top of the column, the salt overflow sampler, and the salt receiver. Observed pressure drops through the column were 2, 2.5, and 5 in. H_2O at salt flow rates of 68, 127, and 244 ml/min respectively; values predicted by the Ergun equation[28] for these flow rates were 0.5, 1, and 2 in. H_2O respectively. These measurements will be used for future comparison to detect possible iron deposition in the column.

In preparation for the first mass transfer run (UTR-1), a sufficient quantity of $LiF-UF_4$ eutectic mixture was added to the salt feed tank to produce a uranium concentration of 0.0003 mole fraction, and thorium metal was added to the bismuth in the treatment vessel. Hydrodynamically, run UTR-1 was successful. A uniform flow rate of each phase was maintained at 105 ml/min (~62% of flooding) for 90 min; during this period, seven sets of simultaneous samples (salt out, bismuth out) were taken from the flowing-stream samplers. The flow rates were then increased to 129 ml/min (~76% of flooding) for 50 min. Surprisingly, however, analyses of flowing bismuth samples showed that only a small fraction (≤0.5%) of the uranium was extracted from the salt phase. Subsequent investigation revealed that a cube of thorium metal had blocked the charging port in the treatment vessel and that there was essentially no reductant in the bismuth phase during the experiment.

Thorium metal was added directly to the bismuth feed tank in preparation for the next mass transfer run. Dissolution of the thorium was slow, requiring a total of about 300 hr (including 120 hr at 650°C). Operating conditions and results for run UTR-2 are summarized in Table 1.8. About 95% of the uranium was extracted into the bismuth phase, which initially contained a 140% stoichiometric excess of reductant. Conditions for the experiment were chosen such that a relatively large fraction of the uranium would be extracted, although these conditions are not optimum for the determination of mass transfer performance. This experiment was important in that it was the first successful demonstration of the reductive extraction of uranium into bismuth in a flowing system.

Prior to run UTR-3, 122.5 g of thorium metal was added to the treatment vessel, which contained about 10% of the salt (1.5 liters) and most of the bismuth (~17 liters) present in the system. The thorium dissolved in the bismuth at a very low rate (~0.3%/hr),

27. *MSR Program Semiannu. Progr. Rep. Feb. 28, 1970,* ORNL-4548, p. 298.

28. S. Ergun, *Chem. Eng. Progr.* **48**, 89 (1952).

Table 1.8. Data obtained from uranium mass transfer experiments in an 0.82-in.-ID by 24-in.-high column at 600°C

	Uranium concentration in salt (ppm)			Salt flow rate (cm^3/min)	Bismuth flow rate (cm^3/min)	Metal-to-salt flow rate ratio	Fraction of flooding	Fraction of U extracted from salt	Fraction of U remaining in salt
	Salt feed, X_i	Salt effluent, X_O	Maximum equilibrium value,[a] X^*						
UTR-2	808	40	~0.8	52	247	4.75	0.77	~0.95	~0.05
UTR-3	2100	159	3.6	100	205	2.05	0.87	0.92	0.076
		445	9.4	160	195	1.22	1.04	0.79	0.212
		561	10.3	220	200	0.91	1.23	0.73	0.267
UTR-4	1680	524	9.7	149	140	0.94	0.85	0.69	0.312
		439	7.2	118	117	1.0	0.69	0.74	0.261
		626	9.7	210	157	0.75	1.07	0.63	0.373

[a]Calculated as the concentration that would be in equilibrium with the observed concentrations of reductant (lithium) and uranium in the bismuth effluent.

which was nearly equivalent to the rate observed in the bismuth feed tank prior to run UTR-2. In order to improve the contact between thorium and the bismuth, an additional 119 g of thorium (contained in a 1-in.-diam perforated steel basket) was suspended in the bismuth. The resulting dissolution rate was about ten times the earlier rate; about 85% of the thorium dissolved in a 22-hr period. Samples of the bismuth phase showed a range of thorium concentrations and suggested the existence of a concentration gradient in the bismuth pool. The final thorium concentration in the bismuth is believed to have been 1200 ppm. The thorium-bismuth solution and the salt were then transferred to the feed tanks. The solubility of thorium in the bismuth at the feed tank temperature (540°C) is about 900 ppm. The final uranium concentration in the salt feed tank was 2100 ppm.

During run UTR-3, bismuth was fed to an 0.82-in.-ID by 24-in.-high extraction column at the rate of about 200 cm^3/min, and salt was fed to the column at the rates of 100, 160, and 220 cm^3/min. Under the first combination of operating conditions, five sets of samples were taken of the salt and bismuth streams leaving the column; however, only one set of samples was taken under each of the other combinations of conditions, after a salt volume equivalent to three column volumes had passed through the column. As shown in Table 1.8, the fraction of the uranium extracted from the salt decreased from 0.92 to 0.73 as the salt flow rate was increased.

The thorium dissolution rate in the treatment vessel prior to run UTR-4 was about the same as that observed prior to run UTR-3. Some nonuniformity in thorium concentration was observed in the bismuth. The final thorium concentration in the bismuth feed tank was about 1100 ppm, and the uranium concentration in the salt feed tank was 1680 ppm. During run UTR-4, the system was operated at three sets of salt and bismuth flow rates. Eleven pairs of samples were taken from the salt and bismuth streams leaving the column. The fraction of extracted uranium ranged from 63 to 74%, as shown in Table 1.8.

Watson has noted[29] that the uranium extraction data from runs UTR-3 and -4 can be correlated in terms of the height of an overall transfer unit based on the salt phase (HTU) if several assumptions are made. The chief assumption is that the rate at which uranium transfers to the bismuth phase will be controlled by the diffusive resistance in the salt film when the extraction factor is high and when the salt film is composed largely of nontransferring ions. In runs UTR-3 and -4, a small amount of uranium was added to the salt after it had been equilibrated with the bismuth phase; no significant transfer of lithium and thorium occurred in the column. In this case, the overall transfer coefficient based on the salt phase is equal to the individual salt film transfer coefficient. By definition, the HTU and the number of overall transfer units based on the salt phase (NTU) developed in the column are related as

$$H = \mathrm{HTU} \cdot \mathrm{NTU}\,, \tag{1}$$

where H is column length. If it is assumed that uranium is the major component transferring from the salt and that the controlling resistance to transfer is in the salt phase, HTU can be written as

$$\mathrm{HTU} = \frac{V_s}{ka}, \tag{2}$$

where V_s is the superficial velocity of the salt in the column and ka is the product of the overall mass transfer coefficient based on the salt phase and the interfacial area between the salt and bismuth phases per unit column volume. It has been previously[30] observed that the dispersed-phase holdup is approximately proportional to the flow rate of the dispersed phase except at conditions near flooding. We would, therefore, expect the interfacial area between the salt and the bismuth phases to be proportional to the bismuth flow rate, so that

$$ka = k' V_{\mathrm{Bi}}\,, \tag{3}$$

where k' is a constant and V_{Bi} is the superficial velocity of the bismuth in the column. The number of overall transfer units, based on the salt phase, developed in the column is defined as

$$\mathrm{NTU} = \int_{X_i}^{X_o} \frac{dX}{X^* - X}, \tag{4}$$

where

X = uranium concentration in the bulk salt,

X^* = uranium concentration in the salt in equilibrium with the bulk bismuth phase,

X_i = uranium concentration in the salt fed to the column,

29. J. S. Watson, ORNL, personal communication.

30. J. S. Watson and L. E. McNeese, *MSR Program Semiannu. Progr. Rep. Aug. 31, 1970*, ORNL-4622, p. 214.

X_o = uranium concentration in the salt leaving the column.

As shown in Table 1.8, the value of X^* at the bottom of the column is much smaller than the value of X_o; thus one would expect that $X^* \ll X$ throughout the column. In this case, Eq. (4) would become

$$\mathrm{NTU} = -\ln \frac{X_o}{X_i} . \tag{5}$$

Combining Eqs. (1), (2), (3), and (5) and rearranging yields the relation

$$\ln \frac{X_o}{X_i} = -k'H \frac{V_{\mathrm{Bi}}}{V_s} , \tag{6}$$

which states that a semilogarithmic plot of the fraction of the uranium remaining in the salt vs the bismuth-to-salt flow rate ratio should yield a straight line having a slope of $-k'H$. This line would pass through an ordinal value of 1.0 at a bismuth-to-salt flow rate ratio of zero.

As shown in Fig. 1.17 the data from runs UTR-3 and -4 are well represented by Eq. (6). For these data, the constant k' has the value of 0.0529 in.$^{-1}$. The product of the overall transfer coefficient, based on the salt phase, and the interfacial area is given by the relation

$$ka = 0.0529 V_{\mathrm{Bi}} , \tag{7}$$

where ka is the overall rate constant based on the salt phase, sec^{-1}, and V_{Bi} is the superficial velocity of the bismuth in the column, in./sec. Values for the overall rate constant for the present data range from 0.012 to 0.021 sec^{-1} and compare favorably with a preliminary value of 0.0076 sec^{-1} measured[31] for the transfer of uranium from a 96.2-3.6-0.2 wt % Cd-Mg-U solution to a molten salt (50-30-20 mole % $MgCl_2$-NaCl-KCl) at temperatures ranging from 560 to 610°C.

The HTU values for the data from runs UTR-3 and -4 are given by the expression

$$\mathrm{HTU} = \frac{18.9}{V_{\mathrm{Bi}}/V_s} , \tag{8}$$

where HTU is the height of the overall transfer unit based on the salt phase, in., and V_{Bi}/V_s is the bismuth-to-salt flow rate ratio. The HTU values range from 0.77 ft at a flow rate ratio of 2.05 to 2.1 ft at a flow rate ratio of 0.75.

31. T. Johnson et al., *Chem. Eng. Div. Semiannu. Rep. January–June 1965*, ANL-7055, p. 44.

In order to measure mass transfer rates in the column under more closely controlled conditions and under conditions where the controlling resistance is not necessarily in the salt phase, preparations were begun for experiments in which the rate of exchange of zirconium isotopes will be measured between salt and bismuth phases otherwise at equilibrium. Residual reductant was removed from the treatment vessel by hydrofluorinating the salt and bismuth for 20 hr with 70-30 mole % H_2-HF. Following the usual H_2 sparge for reduction of iron fluoride, the two phases were transferred to the feed tanks. A hydrodynamic experiment (UTR-5) was then carried out (1) to remove from the system any bismuth having a high thorium concentration and (2) to test the sampling and analysis techniques under conditions where no mass transfer should occur. Surprisingly, the reported uranium concentrations of salt samples removed from the column

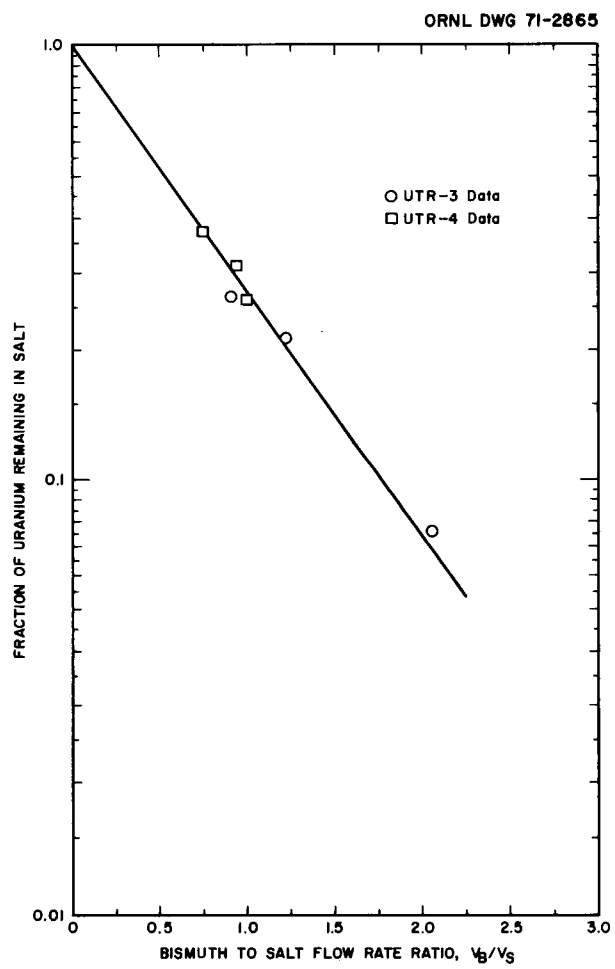

Fig. 1.17. Mass transfer of uranium from LiF-BeF_2-ThF_4 (72-16-12 mole %) to bismuth containing reductant at 600°C in an 0.82-in.-diam, 24-in.-long packed column.

ORNL DWG 71-2840R1

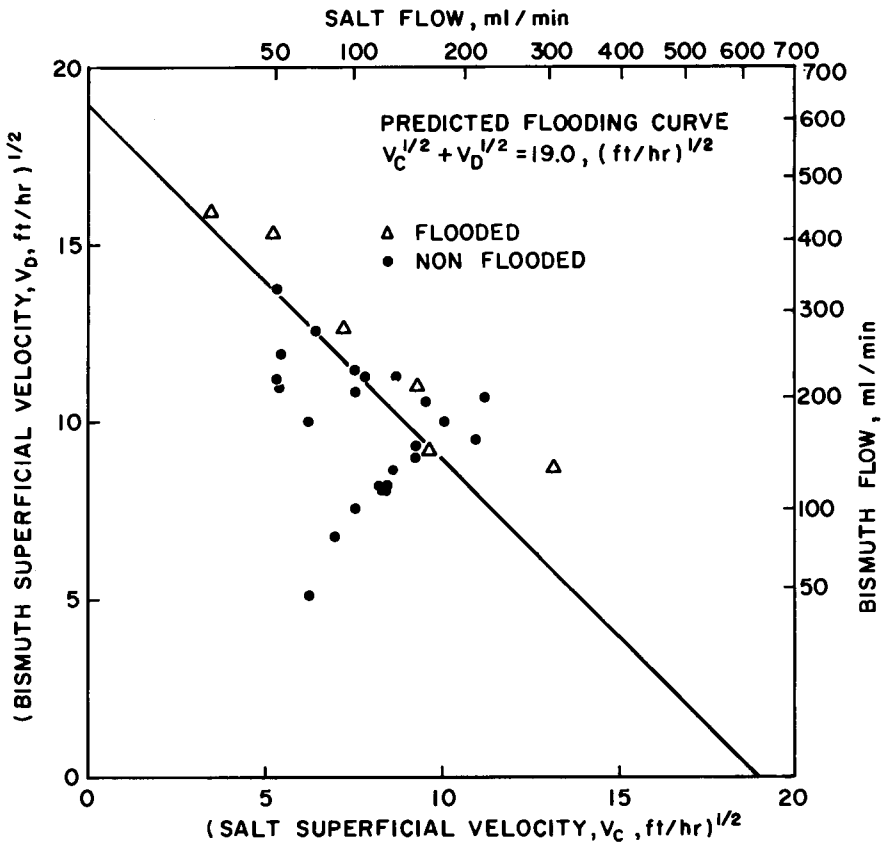

Fig. 1.18. Summary of flooding data with salt and bismuth in an 0.82-in.-diam, 24-in.-long column packed with ¼-in. Raschig rings.

effluent varied by ±35% from the average value, which was in excellent agreement with the indicated uranium concentrations of the salt feed and catch tanks.

An additional run (UTR-6) was made in order to further test the sampling and analysis techniques and to obtain hydrodynamic data. In this run, salt and bismuth were fed to the column at flow rates of 125 and 117 cm^3/min, respectively, for a 38-min period. During this period, seven pairs of samples were taken of the salt and bismuth streams leaving the column. Analysis of these samples showed a scatter in uranium concentration similar to that observed in run UTR-5. The flows of salt and bismuth were stopped following the initial operating period in order to freeze the drain line leaving the specific gravity pot. Operation was then resumed with a bismuth flow rate of 209 cm^3/min and a salt flow rate of 149 cm^3/min. Salt samples were taken periodically for bismuth analysis. The apparent dispersed-phase holdup, as indicated by the pressure drop across the column, stabilized at 30%. A bismuth concentration in the salt of about 5 ppm was observed during this period. When the salt flow rate was increased to 151 cm^3/min, the apparent bismuth holdup increased to about 60% before the specific gravity pot began to fill with bismuth, a clear indication that the column was flooded. A bismuth concentration in the salt of about 10 ppm was observed during the latter period.

The flooding data obtained during this reporting period are shown in Fig. 1.18, along with flooding data obtained previously. The data are well represented by the predicted flooding relation (denoted by the line in Fig. 1.18) resulting from work with mercury and aqueous solutions.[32]

Both phases were returned to the treatment vessel after run UTR-6, and sufficient thorium was added to extract about 50% of the uranium and zirconium from the salt phase. The thorium dissolution rate was about

32. J. S. Watson and L. E. McNeese, *MSR Program Semiannu. Progr. Rep. Aug. 31, 1970,* ORNL-4622, p. 213.

one-half that observed prior to runs UTR-3 and -4. A draft tube was installed in the treatment vessel in order to improve mixing of the phases. The basket containing the thorium was removed after about 156 g of thorium had dissolved. The treated salt and bismuth were then transferred through the system in order to bring the salt and bismuth in the entire system to equilibrium before the start of the ^{97}Zr tracer experiments. After both phases had been returned to their respective feed tanks, we withdrew samples that showed an average zirconium concentration of 165 ppm in the salt and a zirconium distribution ratio of 1.0, which are satisfactory conditions for the tracer experiments.

The initial attempt at producing ^{97}Zr by irradiation of $^{96}ZrO_2$ resulted in an activity about four times that expected for ^{97}Zr. The discrepancy was traced to an outdated value for the thermal-neutron cross section for ^{96}Zr, that is, 0.05 b as compared with a more recent value of 0.2 b. After a suitable interval, the original 20-mg charge of $^{96}ZrO_2$ was reirradiated for 2 hr to produce a calculated ^{97}Zr-^{97}Nb activity of 13.7 mCi. Counting rates for ^{97}Zr were measured for samples taken from the salt feed tank at intervals following the addition of tracer to the tanks. Mixing of the tracer in the 15-liter salt volume was about 75% complete within 2 hr. The irradiation yield of ^{97}Zr-^{97}Nb was about 30% higher than expected. The ^{97}Zr counting rate, which was greater than 200,000 counts per minute per sample, indicates that counting precision in future experiments should be good.

At the time the first ^{97}Zr tracer experiment was begun, a leak appeared in the salt feed line at a location near the salt feed tank. An attempt to transfer the salt from the tank by an alternate line disclosed a second leak. The resulting salt spills caused the Calrod heaters on the tank to fail and extensively damaged the nickel aluminide coating on the exterior of the tank.

The tank was removed from the system for examination and disposal since the damage from the salt made salvage impractical. Examination, by the Metals and Ceramics Division, of a metal specimen cut from the outer shell of the tank revealed that, although two years of operation at about 600°C had produced considerable graphitization of the steel, ductility and apparently tensile strength were not significantly impaired. A new salt tank was fabricated and installed in the system. The transfer lines were attached to the new tank by 0.5-in.-OD sleeves to prevent the occurrence of a similar failure. Insulation was stripped from all transfer lines to allow inspection, and all lines that were more than moderately oxidized were replaced.

1.7 DEVELOPMENT OF THE METAL TRANSFER PROCESS FOR REMOVING RARE EARTHS

Two engineering experiments (MTE-1 and -2) for the study of the metal transfer process for removing rare earths from single-fluid MSBR fuel salt were completed. The main objectives of these experiments were (1) demonstration of the selective removal of rare earths from fluoride salt containing thorium fluoride, (2) collection of the rare earths in a lithium-bismuth solution, and (3) verification of previous distribution coefficient data. All of these objectives were accomplished. Both experiments were performed in the 6-in.-diam carbon-steel vessel shown schematically in Fig. 1.19. The vessel had two compartments that were interconnected at the bottom by a pool of bismuth saturated with thorium. One compartment contained fluoride salt (72-16-12 mole % LiF-BeF_2-ThF_4) to which tracer quantities of ^{147}Nd and sufficient LaF_3 to produce a concentration of 0.3 mole % had been added. The other compartment contained LiCl, as well as a cup containing a lithium-bismuth solution. During operation, LiCl was circulated through the lithium-bismuth cup at the rate of about 25 cm^3/min. The concentration of reductant (35 at. % lithium) in the lithium-bismuth was sufficiently high that, at equilibrium, essentially all of the neodymium and lanthanum would have been extracted from the LiCl that was circulated through the lithium-bismuth cup.

The quantities of materials used in the two experiments are given in Table 1.9. The LiCl was purified prior to use by contact with bismuth saturated with thorium at 650°C. Both the carbon-steel vessel and the bismuth were treated with hydrogen at 650°C to remove oxides. The argon used as cover gas for the

Table 1.9. Materials used in metal transfer experiments MTE-1 and -2

	Run No.	Volume (cm^3)	Moles (g)
Fluoride salt	MTE-1	709	36.6
(LiF-BeF_2-ThF_4-LaF_3, 72-15.7-12-0.3 mole % plus ^{147}Nd tracer)	MTE-2	789	40.7
Bismuth saturated with thorium	MTE-1	797	36.8
	MTE-2	799	36.9
LiCl	MTE-1	1042	36.6
	MTE-2	1042	36.6
Li-Bi (35 at. % Li)	MTE-1	192	11.1
	MTE-2	164	9.5

ORNL DWG 70-12503-RI

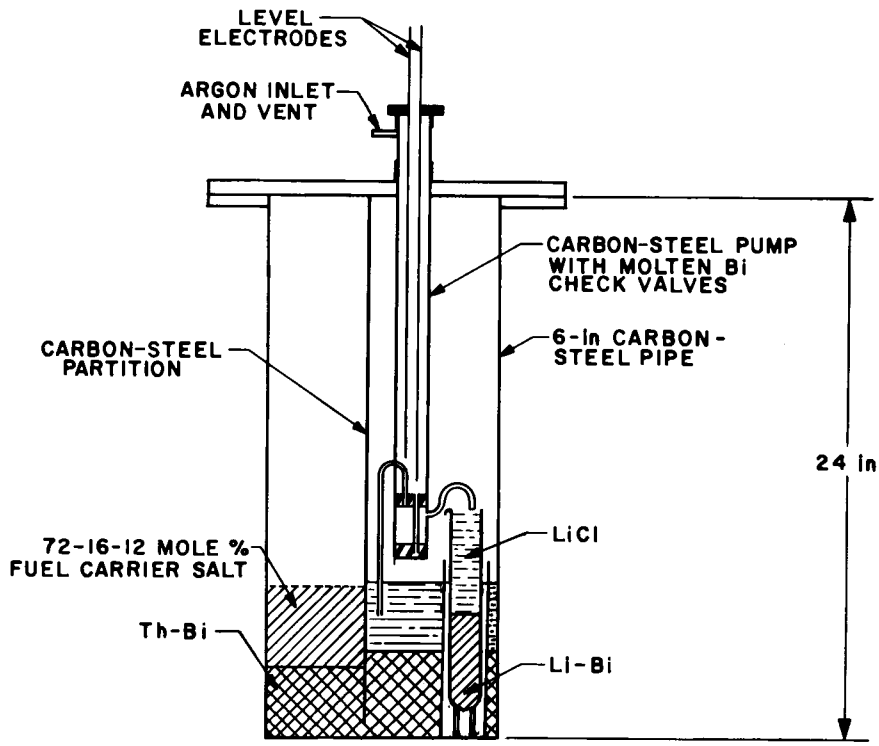

Fig. 1.19. Carbon-steel vessel for use in the metal transfer experiments.

experiment was purified by passage through a bed of uranium turnings at 600°C and a bed of molecular sieves. The equipment and operating conditions used for the two experiments were similar with the following exceptions:

1. a quartz pump having sapphire check valves was used to circulate the LiCl in experiment MTE-1, whereas a carbon-steel pump having molten bismuth check valves was used in MTE-2;
2. simple sparge tubes were used in MTE-1 to promote contact between the salt and bismuth phases, while in run MTE-2 gas-lift sparge tubes were used to disperse the metal into the salt phase;
3. the quantity of ^{147}Nd tracer added to the fluoride salt was increased in MTE-2 to 7 mCi (from the 2 mCi used in MTE-1) to facilitate the detection of the tracer;
4. the operating temperature was about 660°C in MTE-1 and about 650°C in MTE-2.

In the first experiment (MTE-1), the LiCl was pumped through the lithium-bismuth container for 3 hr at a flow rate of 25 cm^3/min. Pumping was then stopped, and the system was allowed to approach equilibrium during a 4-hr period. At this point, filtered samples of the salt and metal phases were taken. During the pumping and equilibration periods, the bismuth-thorium phase was forced to flow back and forth between the fluoride and chloride compartments at a rate equivalent to 10% of the metal volume every 7 min in order to promote mixing in the bismuth-thorium phase. The duration of the experiment was one week, during which the LiCl pump was operated 50.5 hr. The distribution coefficients for lanthanum and neodymium between the fluoride salt and the thorium-saturated bismuth were relatively constant throughout the run; the respective averages, 0.044 and 0.073, were in good agreement with expected values. The distribution coefficients for lanthanum and neodymium between the LiCl and the thorium-saturated bismuth were higher than anticipated during the first part of the run but approached the expected values near the end of the run.

Approximately 50% of the lanthanum and 25% of the neodymium (after correcting for ^{147}Nd decay) originally present in the fluoride salt were removed during

the run; however, the lanthanum and neodymium did not collect in the lithium-bismuth as expected. After the run was completed, most of the lanthanum and neodymium that had been removed from the fluoride salt was found in a $\frac{1}{8}$-in.-thick layer of black material located at the interface between the LiCl and the bismuth-thorium. The composition of the material (wt %) was: 3.6% La, 7.7% Th, 12.0% Li, 59.1% Cl, 4.4% O, 0.95% Si, 0.54% Fe, and about 12% Bi. It is believed that oxides introduced into the system from the quartz pump or from moisture and air introduced when the system was opened for maintenance before the run may account for the accumulation of the rare earths in the black material.

In the second experiment (MTE-2), quartz was eliminated from the system by the use of a carbon-steel pump, and contact between the salt and metal phases was improved by the use of gas-lift sparge tubes. During this experiment, the neodymium and lanthanum originally added to the fluoride salt transferred to the lithium-bismuth solution as expected. The experiment was operated for about three months before it was shut down for disassembly and inspection. During this time, the pump was operated 441 hr, and 702 liters of LiCl was circulated through the lithium-bismuth container. The sequence of operations carried out consisted of pumping the LiCl through the lithium-bismuth container for 3 hr at a flow rate of 25 cm^3/min, then stopping the pumping, and allowing a period of 4 hr for the system to approach equilibrium before filtered samples of the salt and metal phases were taken. This sequence was repeated three shifts per day during the first week and two shifts per day during the second week of operation. For the remainder of the three-month period, the pump was operated during the entire day shift and the system was allowed to approach equilibrium at night and on weekends.

The rate of accumulation of rare earths in this solution is shown in Fig. 1.20. There was essentially no accumulation of lanthanum or neodymium in the solution until operation of a gas-lift sparge tube was initiated (after about 50 liters of LiCl had been circulated through the lithium-bismuth compartment). After 400 liters of LiCl had been circulated (about

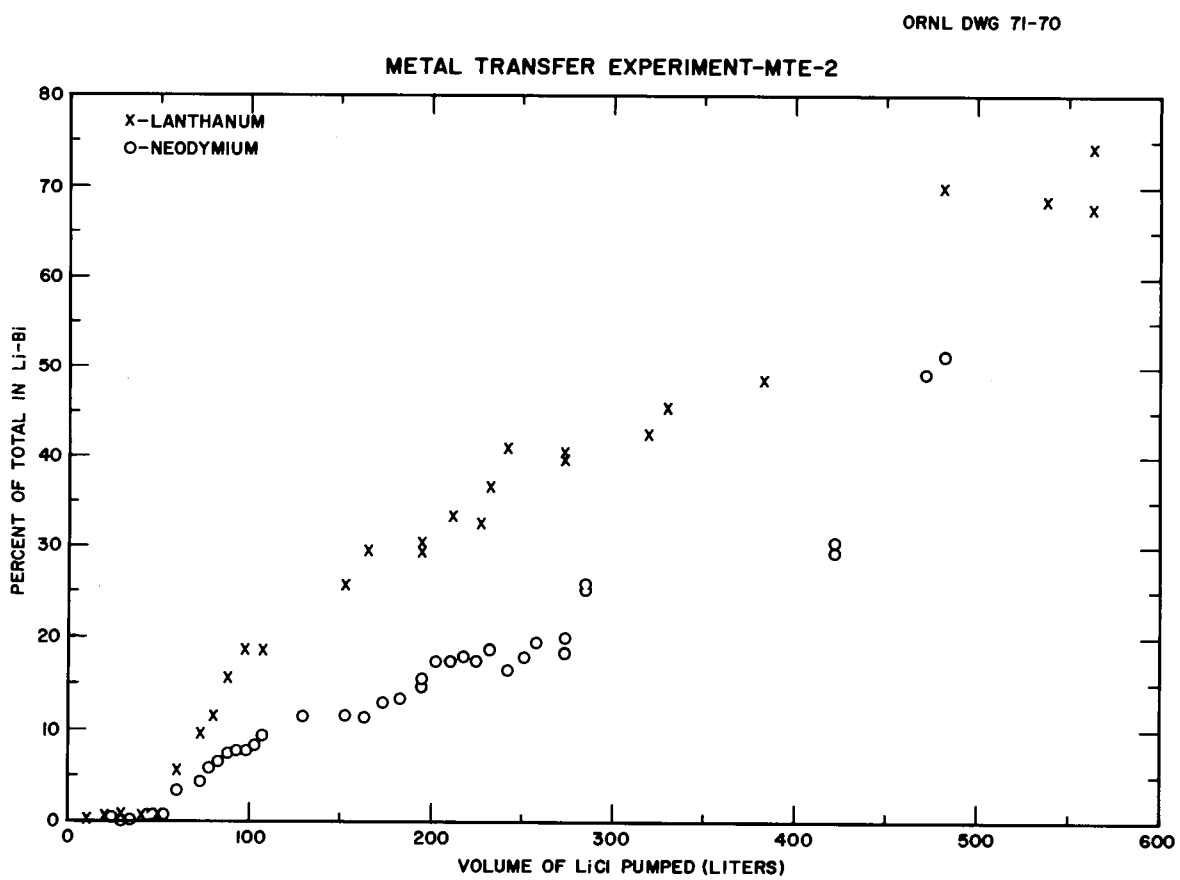

Fig. 1.20. Rate of accumulation of lanthanum and neodymium in the lithium-bismuth solution.

two-thirds through the run), about 50% of the lanthanum and 30% of the neodymium originally in the fluoride salt was found to be in the lithium-bismuth solution. During this time, 70 to 100% of the lanthanum and neodymium initially charged to the system could be accounted for by filtered samples taken of each phase, indicating that most of the rare earths remained in solution. During the last one-third of the run, the rare earths continued to accumulate in the lithium-bismuth solution, but the rate of accumulation could not be determined accurately because a leak developed in the lithium-bismuth cup, allowing about 30% of the solution to flow into the area between the cup and holder. The extent of removal of lanthanum from the fluoride salt is shown in Fig. 1.21, which indicates that more than 85% of the lanthanum had been removed at the end of the experiment; about 50% of the neodymium was also removed. Approximately 10 to 20% of the rare earths were removed from the LiCl as it was circulated through the lithium-bismuth compartment. There was no measurable accumulation of thorium (<10 ppm) in the lithium-bismuth solution during the experiment, thus demonstrating that the rare earths can be deposited in this solution without significant amounts of thorium also being deposited. The thorium-lanthanum decontamination factor was about 10^5. The distribution coefficients for lanthanum and neodymium remained relatively constant during the experiment. The average values of the distribution coefficients for lanthanum (0.05) and neodymium (0.06) between the fluoride salt and the bismuth-thorium solutions are in good agreement with expected

ORNL DWG 71-63

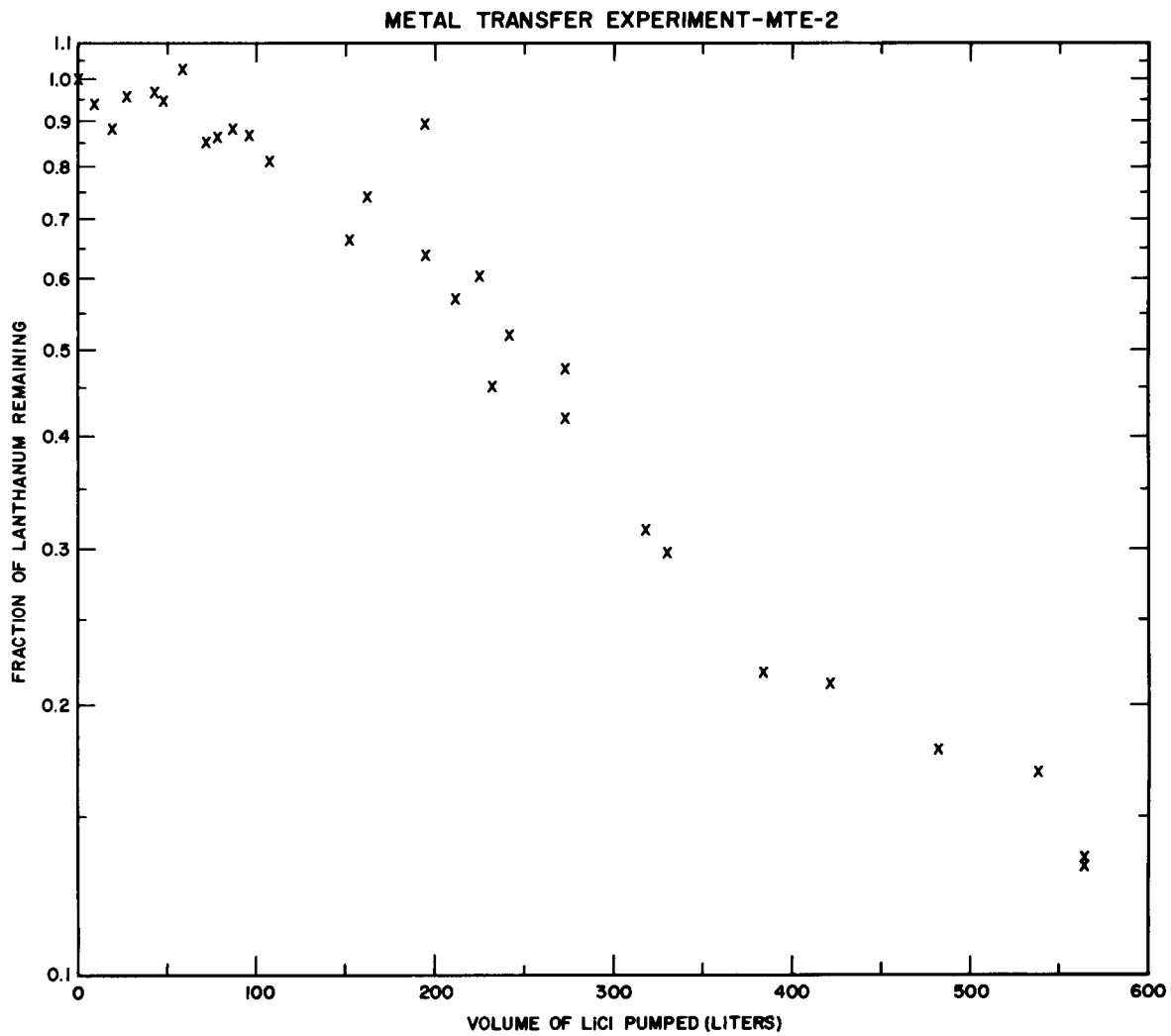

Fig. 1.21. Rate of removal of lanthanum from the fluoride salt.

values. The average values of the distribution coefficients between the LiCl and the bismuth-thorium solution were somewhat higher than expected for lanthanum (3.1) and near the expected value for neodymium (4.8). During the run, the lithium concentration in the lithium-bismuth solution decreased from 35 to 13 at. %. Only a small fraction of this decrease was due to the reaction of lithium with rare-earth chlorides; the principal reason for the decrease has not yet been determined. The bismuth-thorium phase remained saturated with thorium throughout the run, indicating that there was no excessive loss of thorium from the bismuth phase during the experiment.

Eight days before the end of the experiment, 1 vol % fluoride salt was added to the LiCl compartment to simulate entrainment of fluoride salt in the bismuth. Concentrations of beryllium, thorium, and fluoride in the LiCl were determined periodically after the addition of fuel carrier salt to the LiCl near the end of the experiment, as shown in Table 1.10. During the 93-hr period in which the LiCl was not circulated through the lithium-bismuth container, the beryllium concentration remained constant at the initial value of 490 ppm and the thorium concentration decreased, as expected, from the initial value of 9480 ppm to a value of 644 ppm. When circulation of the LiCl was resumed, the beryllium concentration in the LiCl began to decrease; after 27 hr of operation, a concentration of 135 ppm was observed. The thorium concentration in the LiCl at this time was 171 ppm.

The pump and other components of the system operated satisfactorily during the run. After the experiment was completed, the carbon-steel vessel was cut apart for inspection. The general condition of the inside surfaces was good. The salt and bismuth phases were sharply defined, and there was no evidence of accumulated impurities at the salt-bismuth interface as had been observed in MTE-1. The inside of the main vessel showed very little evidence of corrosion; however, holes had developed in some of the sparge tubes and other components made of thin (~0.030 in.) carbon steel.

The third engineering experiment for development of the metal transfer process for removing rare earths from MSBR fuel carrier salt is being designed. The experiment (MTE-3) will use flow rates that are 1% of the estimated flow rates for a 1000-MW(e) reactor. The experiment, shown schematically in Fig. 1.22, will use mechanical agitators to promote efficient contact of the salt and metal phases. Fuel carrier salt containing rare-earth fluorides will be circulated between one side of the salt-metal contactor and a fluoride salt reservoir. Lithium chloride containing rare-earth chlorides will be circulated between the other side of the salt-metal contactor and a rare-earth stripper, where the rare earths will be extracted into a lithium-bismuth solution.

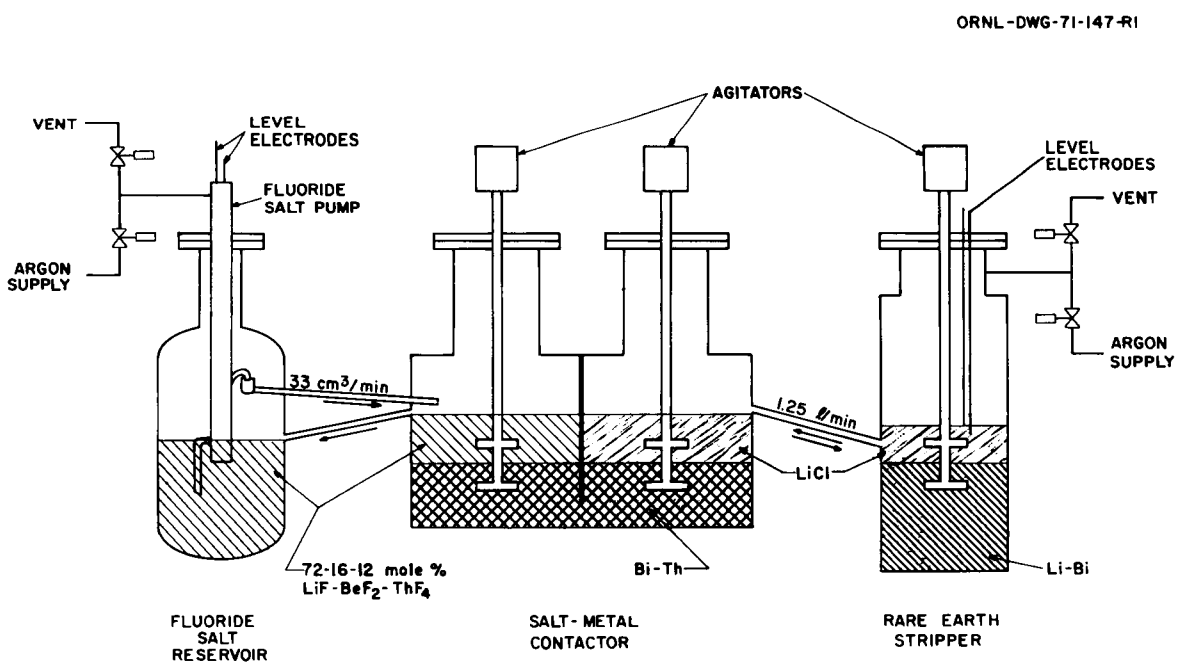

Fig. 1.22. Flow diagram for metal transfer experiment MTE-3.

Table 1.10. Variation of beryllium, thorium, and fluoride concentrations in the LiCl after addition of 1 vol % fuel carrier salt

Time after addition (hr)	Pumping time (hr)	Fluoride (wt %)	Beryllium (ppm)	Thorium (ppm)
0	0	0.98[a]	490[a]	9480[a]
19.8	0	1.49	490	7200
45.4	0	1.08	500	1100
69.7	0	1.81	320	
93	0	2.03	490	644
115.9	5.9	2.34	470	
163.9	20.3	1.07	120	1400
188.8	27.4	0.91		350
188.8	27.4	1.7[b]	135[b]	171[b]

[a]Calculated values based on the amount of fluoride salt added.

[b]Salt taken from vessel after experiment was concluded.

The experiment will use approximately 35 liters of fluoride salt, 6 liters of thorium-bismuth solution, 6 liters of LiCl, and 5 liters of lithium-bismuth solution having a lithium content of about 40 at. %. The system will require three process vessels, each of which will be made of carbon steel. The largest vessel (the fluoride salt reservoir), which will contain approximately 32 liters of salt, has been fabricated. The remaining 3 liters of fluoride salt will be contained in the salt-metal contactor. The fluoride salt will be recirculated continuously from the reservoir to the contactor at the rate of about 33 cm^3/min by a pump similar to the one used in the second metal transfer experiment. The salt-metal contactor will be a 10-in.-diam two-compartment vessel having a mechanical agitator in each compartment.

1.8 CONTACTOR STUDIES OF A SIMULATED MOLTEN-SALT–LIQUID-BISMUTH SYSTEM

Pressure Drop, Holdup, and Flooding in Packed Columns

Studies of the hydrodynamics in packed columns during the countercurrent flow of high-density liquids are being made in order to evaluate and design contactors for processing systems based on reductive extraction. We have previously[32,33] reported studies in which mercury and water were used to simulate bismuth and molten salt in columns packed with $^3/_{16}$-, $^1/_4$-, $^3/_8$-, and $^1/_2$-in. Raschig rings and with $^1/_8$- and $^1/_4$-in. solid right circular cylinders. These studies have shown that the dispersed-phase holdup and the column throughputs at flooding can be correlated[32] on the basis of a constant slip velocity in the following manner:

$$\frac{V_c}{1-X} + \frac{V_d}{X} = V_s , \tag{1}$$

$$V_{c,f}^{1/2} + V_{d,f}^{1/2} = V_s^{1/2} , \tag{2}$$

where

V_c = superficial velocity of the continuous phase,

V_d = superficial velocity of the dispersed phase,

V_s = slip velocity,

X = dispersed-phase holdup,

f = subscript denoting superficial velocities at flooding.

These relations were previously[32] extended to cover dispersed-phase holdup and throughput at flooding with salt-bismuth systems by assuming that, for a given packing size, the slip velocity was (1) independent of the viscosity of the continuous phase, (2) proportional to the difference in the densities of the phases, and (3) proportional to the packing void fraction. Although the resulting relations predicted flooding rates that were in excellent agreement with flooding rates measured with bismuth and molten salt, it was realized that the agreement did not constitute verification of the assumed effects of the continuous-phase viscosity and the difference in the densities of the phases.

During this reporting period, data showing the dependence of slip velocity on continuous-phase viscosity were obtained by an MIT Practice School group. A 2-in.-diam, 24-in.-long column packed with $^3/_8$-in. Teflon Raschig rings, which were not wet by either phase, was used in the study. The experimental system was modified so that water or water-glycerin solutions could be recirculated through the column at constant temperature by installation of a heat exchanger and an aqueous-phase surge tank. Data were obtained with glycerin solutions having viscosities of 7.5 and 15 cP, as well as with water (which has a viscosity of 1 cP), since repacking a column can alter the slip velocity by as much as 10%.

The results obtained were similar to those observed previously for mercury and water. The dispersed-phase holdup could be correlated in terms of a constant slip velocity for the three cases involving nonwetted packing. The relative standard deviations for the slip

33. J. S. Watson and L. E. McNeese, *MSR Program Semiannu. Progr. Rep. Feb. 28, 1970*, ORNL-4548, p. 302.

velocities were about ±10%; no dependence on the flow rate of either phase was noted. The variation of slip velocity with continuous-phase viscosity is shown in Fig. 1.23, which indicates that the slip velocity is proportional to the –0.167 power of the continuous-phase viscosity. As expected, the dependence is not large. However, neglect of this effect was significant in the earlier extrapolation from a water-mercury system to a salt-bismuth system since the continuous-phase viscosity changed by a factor of 12.

After the dependence of slip velocity on the continuous-phase viscosity was known, it was possible to reevaluate the dependence of slip velocity on the difference in the densities of the two phases by using the two data points afforded by the mercury-water and the salt-bismuth data. If it is assumed that the dependence of slip velocity on the difference in densities is a power-type dependence, a power of 0.5 is calculated. This result is interesting in that it is the same as the dependence of drop terminal velocity on the difference in densities in the inertial region, where the drag coefficient is essentially constant. The final relation for predicting the variation of slip velocity with packing void fraction, the difference in the densities of the phases, and the continuous-phase viscosity is, then,

$$V_s = V_s\,(\text{Hg-H}_2\text{O})\left(\frac{\epsilon}{\epsilon_{\text{ref}}}\right)\left(\frac{\mu}{\mu_{\text{H}_2\text{O}}}\right)^{-0.167} \times \left(\frac{\Delta\rho}{\Delta\rho_{\text{Hg-H}_2\text{O}}}\right)^{0.5}, \quad (3)$$

where

V_s = slip velocity,

$V_s(\text{Hg-H}_2\text{O})$ = slip velocity for mercury-water for the packing size considered,

ϵ = packing void fraction,

ϵ_{ref} = void fraction for packing for which $V_s(\text{Hg-H}_2\text{O})$ was determined,

μ = viscosity of continuous phase,

$\mu_{\text{H}_2\text{O}}$ = viscosity of water at 20°C,

$\Delta\rho$ = difference in the densities of the phases,

$\Delta\rho_{\text{Hg-H}_2\text{O}}$ = difference in the densities of mercury and water at 20°C.

Slip velocity values calculated from Eq. (3) can then be used with Eqs. (1) and (2) for determining the throughputs at flooding and the dispersed-phase hold-up.

The effect of wetting of the packing by the nominally dispersed phase was also evaluated with ⅜-in. copper Raschig rings that had been etched with nitric acid to promote wetting of the packing by the mercury. Complete wetting of the packing was obtained by the mercury, which was saturated with copper. (The solubility of copper in mercury is quite low, and no important changes in other physical properties should occur.) After a few hours of operation, solids could be seen at the water-mercury interface below the column; these solids were believed to be copper oxide formed as

ORNL DWG 71-2867

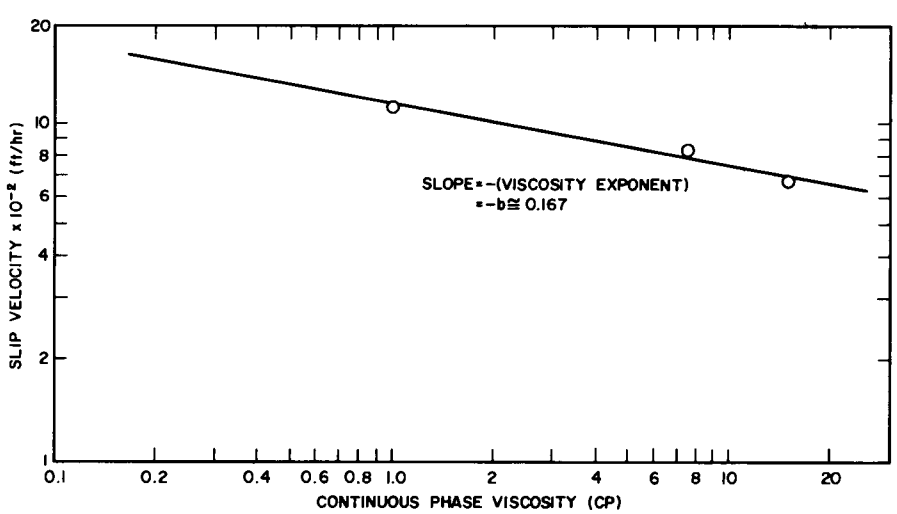

Fig. 1.23. Variation of slip velocity with continuous-phase viscosity in a 2-in.-diam column packed with ⅜-in. Raschig rings.

the result of the reaction of dissolved copper with oxygen in the system. Periodic additions of nitric acid to the system quickly removed the solids.

The interfacial area was decreased substantially when the packing was wet by the mercury. No dispersion of the mercury was observed; the interfacial area was essentially the packing surface area. The slip velocity (and hence the throughput at flooding) was considerably greater than with nonwetted packing. It is not obvious that the slip velocity is independent of the flow rates of the two phases. Since only nine metal holdup measurements were taken, a quantitative analysis of holdup is not possible. From the limited data, metal holdup appears to be less dependent on the superficial velocity of either the water or the mercury than one would expect with a constant superficial velocity.

Axial Dispersion in Packed Columns

Measurements of axial dispersion in packed columns during the countercurrent flow of fluids having high densities and a large density difference were made with $\frac{1}{4}$-in. solid cylinders and with $\frac{1}{4}$-, $\frac{3}{8}$-, and $\frac{1}{2}$-in. Raschig rings. Mercury and water were used to simulate the behavior of bismuth and molten salt. Axial dispersion is not important for metal-to-salt flow rate ratios of about 10 or less; however, the effect can be significant at higher flow rate ratios. Devices that can be inserted at intervals along the length of a column to reduce the effect of axial dispersion to any desired level have been developed. Details of these developments are reported in Sect. 15.5.

Development of Mechanically Agitated Salt-Metal Contactors

A program has been initiated for the development of mechanically agitated salt-metal contactors as an alternative to packed columns presently considered for MSBR processing systems. This type of contactor is of particular interest for use in the metal transfer process since designs can be envisioned in which the bismuth phase would be a near-isothermal internally recirculated captive phase. It is believed that such designs will require less molybdenum fabrication technology than would a counterpart system based on packed columns.

Studies to date have been concerned primarily with selection of a contactor design for the third metal transfer experiment (MTE-3), discussed in Sect. 1.7, which will have bismuth and salt flow rates that are about 1% of the estimated rates for a 1000-MW(e) MSBR. Several scouting tests were carried out with water and mercury in vessels having diameters of 4 to 7 in., and a mockup of the contactor proposed for experiment MTE-3 was built for additional study with mercury and water. The mockup consists of an 8-in.-diam vessel having a central partition that extends to within $\frac{1}{2}$ in. of the bottom of the vessel. The first tests with the mockup were made with a flat four-bladed paddle located in the mercury-water interface. The paddle, 1.5 in. in diameter, was located inside a 3-in.-diam, 3-in.-high shroud containing four 0.3-in.-wide, 3-in.-long baffles. The design was chosen to maximize the extent of dispersion of the mercury in the water, thereby maximizing the interfacial area between the two phases. The system was tested with agitator shaft speeds up to 1600 rpm. It was found that, under these operating conditions, a stable dispersion of very small mercury droplets was frequently formed. Also, at all but the lowest mixer speeds, a dispersion of water droplets in the mercury was formed, and these droplets were pumped from one chamber of the mockup to the other. Such pumping cannot be tolerated in the metal transfer process since it would result in the mixing of chloride and fluoride salts. The tendency of the salt-bismuth system to form emulsions may be quite different from that of the water-mercury system; however, it was concluded that the contactor should operate under conditions that minimize the likelihood of formation of emulsions.

The contactor design that has the greatest potential for achieving good mass transfer with minimum dispersion appears to be the Lewis cell[34] – a contactor with a paddle in each phase, located well away from the interface. With such a contactor, the phases would be agitated as vigorously as possible without actually causing dispersion of one phase in the other. The contactor mockup has been modified in order to study the hydrodynamics of this contactor.

The mass transfer performance of this type of contactor is known[34] for a number of agitated, nondispersed two-phase systems, and the results can be correlated in terms of the Reynolds numbers and viscosities of the two phases. Overall mass transfer coefficients for the salt-bismuth system predicted by this correlation appear to be adequate for MSBR processing operations.

1.9 AXIAL DISPERSION IN SIMULATED CONTINUOUS FLUORINATORS

Axial dispersion is important in the design of continuous fluorinators, which are envisioned as open

34. J. B. Lewis, *Chem. Eng. Sci.* 3, 248–59 (1954).

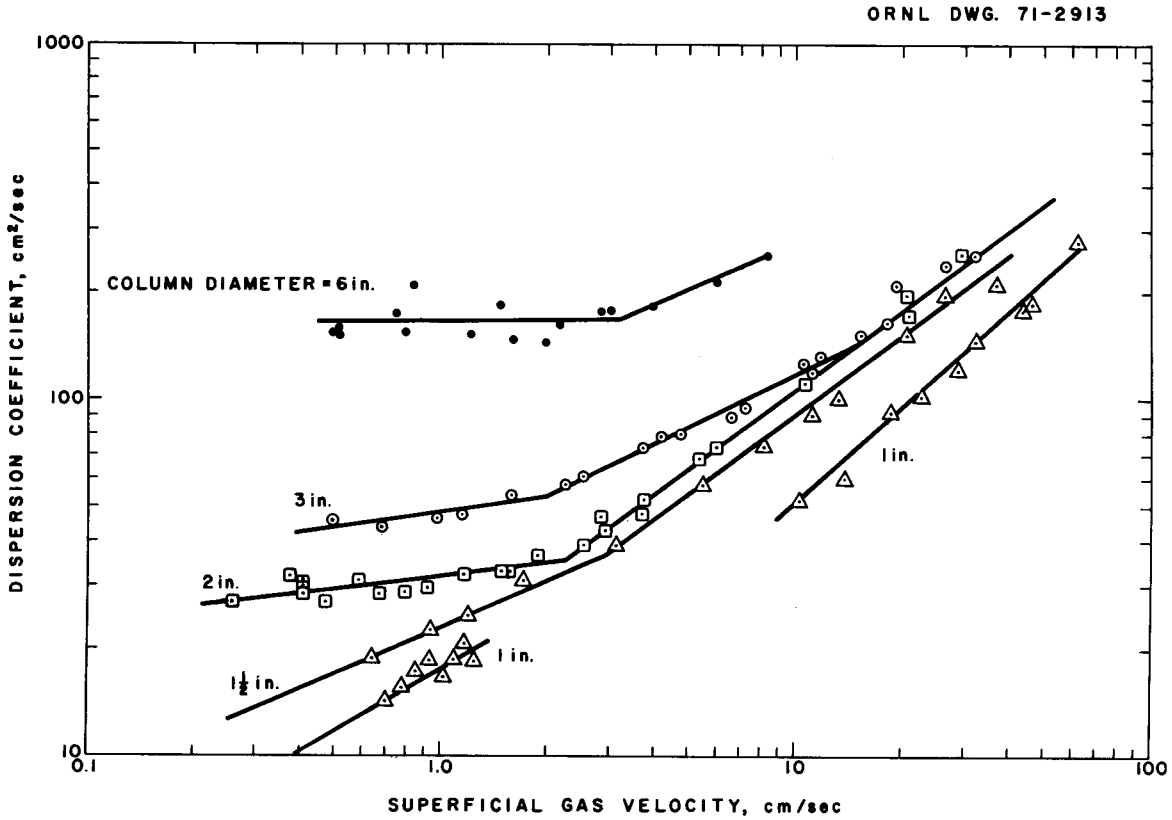

Fig. 1.24. Variation of dispersion coefficient with superficial gas velocity and column diameter in open bubble columns.

columns through which fluorine is bubbled countercurrent to a flow of molten salt. We have previously reported data[35-37] showing the variation of dispersion coefficient with changes in gas and liquid flow rates, physical properties of the liquid, column diameter, and gas inlet diameter. During this reporting period our efforts were directed toward developing an improved experimental technique, which was then used to study the variation of dispersion coefficient with changes in column diameter, gas inlet design, and liquid physical properties. The experimental technique is a transient one that involves injecting a small quantity of KCl solution at the top of the column and observing the rate of buildup of tracer at the bottom of the column. The KCl concentration is measured with a small conductivity probe. Earlier studies,[35] which used a steady-state technique, demonstrated that the axial dispersion coefficient is not dependent on the superficial velocity of the liquid in the range of interest; hence, the transient studies were carried out with no flow of liquid through the column. This was particularly useful for studying the effect of the physical properties of the liquid since relatively small volumes of solution were required.

The variation of dispersion coefficient with column diameter and superficial gas velocity is shown in Fig. 1.24 for column diameters ranging from 1 to 6 in. and superficial gas velocities ranging from 0.25 to 64 cm/sec. The effect of changes in the viscosity of the liquid in the range 0.9 to 15 cP was determined with water-glycerin solutions. Viscosity had little effect in 3- and 6-in.-diam columns; however, increasing the viscosity from 1.0 to 15 cP reduced the dispersion coefficient in 1.5- and 2-in.-diam columns by as much as 20%. Since the diameter of continuous fluorinators will be 6 in. or larger, the viscosity of the liquid will not affect the dispersion coefficient. The effect of surface tension was studied using butanol and isopropanol solutions; the dispersion coefficient was found to decrease as the surface tension was decreased. The number and size of the gas inlets were found to be important only for gas superficial velocities below the slugging region.

35. *MSR Program Semiannu. Progr. Rep. Aug. 31, 1969,* ORNL-4449, p. 240.

36. *MSR Program Semiannu. Progr. Rep. Feb. 28, 1970,* ORNL-4548, p. 307.

37. *MSR Program Semiannu. Progr. Rep. Aug. 31, 1970,* ORNL-4622, p. 216.

1.10 DEVELOPMENT OF A FROZEN-WALL CONTINUOUS FLUORINATOR

An experiment to demonstrate the operation of a continuous fluorinator having a layer of frozen salt deposited on its walls for protection against corrosion will use high-frequency induction heating to provide an internal heat source in the molten salt. Estimates of the performance[38] of a frozen-wall fluorinator having an induction coil embedded in the frozen salt near the fluorinator wall indicate that this may be an acceptable heating method. Because of uncertainties in the effect of bubbles in the molten salt and in the amount of heat that will be generated in the metal walls of the fluorinator, heat generation rates are being measured in a simulated fluorinator. In this simulation a 31 wt % HNO_3 solution, which has electrical properties similar to molten salts, is used to simulate molten salt in the fluorinator vessel. Four induction coil designs have been tested, and the effect of bubbles in the nitric acid has been determined with one of the better coil designs.

Rates of corrosion were estimated for Ni-200 and Ni-201 in gaseous fluorine at a pressure of 1 atm, using data from the literature.

38. J. R. Hightower, Jr., et al., *MSR Program Semiannu. Progr. Rep. Aug. 31, 1970,* ORNL-4622, pp. 219–21.

Induction Heating Studies

The induction-heated simulated fluorinator consisted of a 5-in.-OD by 5-ft-long glass tube inserted in an induction coil and placed inside a 5-ft-long section of 8-in.-diam 304 stainless steel pipe. The nitric acid inside the glass tube represented the molten-salt zone of the fluorinator, the space between the glass tube and the pipe wall (which contains the induction coil) represented the frozen salt layer, and the pipe represented the fluorinator vessel wall. The acid was circulated through the glass column, where it was heated by the induction coil, and through a heat exchanger, where the heat was removed. The heat generation rate in the acid was determined from a heat balance on the acid as it passed through the column. The pipe representing the fluorinator wall was equipped with a jacket through which cooling water passed. The heat generated in the pipe was calculated from the change in temperature of the water as it passed through the jacket. The induction generator operated at a nominal frequency of 400 kHz.

The characteristics of the coils tested are given in Table 1.11. Coils I, II, and III consisted of a number of smaller 5.6-in.-ID, 3-in.-long coils connected in parallel to headers carrying water and rf current to each small section. These three coils covered the acid column uniformly. Coil IV consisted of ten 5.6-in.-ID, 4-in.-long

Table 1.11. Characteristics of induction coils which were tested

Coil	Material	Number of small coils	Number of turns in each small coil	Diameter of conductor (in.)	Diameter of header (in.)
I	Monel	17	~6.3	1/4	5/8
II	304-L SS	18	6	3/8	1/2
III	304-L SS	18	6	3/8	1/2
IV	Copper	10	~11.8	1/4	5/8

Table 1.12. Summary of results from induction heating tests in simulated fluorinator

Coil	Bubble volume fraction	Effective resistance of acid (Ω)	Effective resistance of coil (Ω)	Effective resistance of pipe (Ω)	Efficiency of heating acid (%)	Predicted efficiency of heating molten salt (%)
I	0	0.0143	0.0617	0.0121	16.2	28.8
II	0	0.00845	0.0514	0.0076	12.5	24.7
III	0	0.0168	0.0559	0.0106	20.2	37.0
III	0.1	0.0150	0.0559	0.0106	18.4	34.3
III	0.15	0.0141	0.0559	0.0106	17.5	32.9
IV	0.0	0.118	0.0727	0.0401	51.1	31.1
IV	0.15					27.6

coils. The smaller coils were arranged in such a manner that there was a 2-in. space between each coil. Coils I, III, and IV had adjacent smaller sections wound in the opposite directions; coil II had all smaller sections wound in the same direction.

Twenty-eight runs have been made with the simulated fluorinator to determine the heat generation rates in the column of acid, in the pipe surrounding the acid, and in the induction coils. The results were expressed in terms of effective resistances of each component (acid, pipe, and coil). The effective resistance is defined as the ratio of the heat generation rate (in watts) to the square of the coil current in amperes (rms). The efficiency of heating the acid is found by dividing the resistance of the acid by the sum of the resistances of the acid, pipe, and coil. The results obtained in the runs are summarized in Table 1.12, which shows (1) the average effective resistances at 20°C of the acid, of the coil, and of the pipe; (2) the efficiency of heating the nitric acid; and (3) the predicted efficiency of heating molten salt in a nickel fluorinator after correcting for differences in conductivities between the simulated and the actual systems. In some of the runs with coil III, air was bubbled through the nitric acid at rates up to 2.16 scfm, resulting in bubble volume fractions as high as 18%. Typical fluorinators will operate with a bubble volume fraction of about 15%. Also shown in Table 1.12 is the effect of bubble volume fraction on the efficiency of heating the nitric acid and on the predicted efficiency of heating molten salt in a nickel fluorinator.

The predicted efficiencies for heating molten salt shown in Table 1.12 are for a 5-ft-long fluorinator having a 4.5-in.-diam molten-salt zone, a 1.5-in.-thick frozen salt layer, and a 50°C temperature difference across the salt layer. In such a fluorinator, about 1265 W must be generated in the molten salt. If a coil similar to coil IV were used, a total coil current of 100 A and a generator capable of generating at least 4600 W would be required. These requirements are entirely reasonable and could be fulfilled by the present generator. In the next phase of experimental work, we will attempt to form and maintain frozen salt films in equipment containing a static salt volume.

Estimated Corrosion Rates in Continuous Fluorinators

Nickel is the preferred material of construction for fluorinators since it exhibits greater resistance to attack from gaseous fluorine than other materials. Its resistance to attack by fluorine results from a tightly adhering film of the NiF_2 corrosion product through which fluorine must diffuse to react with the metallic substrate. The rate of reaction with nickel is greatly reduced, although not to zero, once a protective NiF_2 film is formed on a nickel surface exposed to gaseous fluorine. The purpose of the frozen salt film in a continuous fluorinator is to prevent the protective NiF_2 film from being washed away by the molten salt. (No benefit is assumed for any added resistance to fluorine diffusion which may be offered by the frozen salt film.) However, it is likely that the protective NiF_2 film will be destroyed unintentionally several times during the operating life of a fluorinator, resulting in relatively high corrosion rates during the period required for the formation of a new NiF_2 film. Therefore, we have estimated the expected corrosion rates which result from periodic destruction of the NiF_2 film during operation of a continuous fluorinator.

Data for the corrosion of Ni-200 and Ni-201 exposed to gaseous fluorine at a pressure of 1 atm were collected from the literature[39–44] and were used to calculate rate constants for the reaction between nickel and fluorine at 1 atm pressure in the temperature range 360 to 700°C, the reaction was assumed to follow a parabolic rate law. It has been shown[39] that the reaction of high-purity nickel with fluorine initially follows a parabolic rate law from 300 to 600°C but that, after a certain exposure time, the reaction rate decreases and follows a third- or higher-order rate law. Thus the assumption of a parabolic relation takes into account the time dependence of the reaction rate but should yield conservatively high estimates of the extent of corrosion.

The extent of corrosion of nickel in fluorine was assumed to be described by the equation

$$d = k\sqrt{t}\,, \qquad (1)$$

39. R. L. Jarry, W. H. Gunther, and J. Fischer, *The Mechanism and Kinetics of the Reaction between Nickel and Fluorine,* ANL-6684 (August 1963).

40. *Chem. Eng. Div. Summary Rep. July, August, September, 1958,* ANL-5924 (1958).

41. *Chem. Eng. Div. Semiannu. Rep. January–June 1964,* ANL-6900 (August 1964).

42. W. H. Gunther and M. J. Steindler, *Laboratory Investigations in Support of Fluid-Bed Fluoride Volatility Processes. Part XIV. The Corrosion of Nickel and Nickel Alloys by Fluorine, Uranium Hexafluoride, and Selected Volatile Fission Product Fluorides at 500°C,* ANL-7241 (December 1966).

43. F. T. Miles et al., *Progr. Rep. of the Reactor Sci. and Eng. Dep.,* BNL-176, pp. 17–18 (March 1952).

44. P. D. Miller and W. E. Berry, *A Survey of Corrosion in the Fluidized-Bed Volatility Process,* BMI-X-362 (November 1965).

where

d = depth of nickel attacked by F_2, mils;

t = time of exposure of nickel metal to gaseous fluorine, measured from the time when no NiF_2 film exists;

k = parabolic rate constant, mils $hr^{-1/2}$.

Rate constants were calculated for 41 measurements for which the exposure times ranged from 5 hr to 960 hr. Most of the exposure times were in the range of 30 to 150 hr. Fourteen measurements had been made to determine the rate of corrosion of Ni-201 in the temperature range 380 to 700°C; exposure times varied from 5 to 132 hr. The calculated rate constants are given elsewhere.[45] The best least-squares representations of the data, which showed considerable scatter, are given below:

$$\ln k = 0.3773 - \frac{3691}{T} \quad \text{for Ni-200}, \tag{2}$$

$$\ln k = 4.3083 - \frac{7836}{T} \quad \text{for Ni-201}, \tag{3}$$

where k has units of mils $hr^{-1/2}$ and T has units of °K. The largest deviations of individual data points from these two equations were about an order of magnitude higher and an order of magnitude lower.

If n is the number of times per year that the NiF_2 film is destroyed, the extent of corrosion experienced each year (8760 hr) is given in mils by

$$D = nk\sqrt{\frac{8760}{n}} \tag{4}$$

and is the average corrosion rate per year. If the NiF_2 film were destroyed 52 times per year, the average corrosion rates at 450°C (the approximate wall temperature that will be used in a frozen-wall fluorinator) would be 2.9 mils/year for Ni-200 and 0.97 mil/year for Ni-201. If the film were destroyed 12 times annually, the average corrosion rates would be 1.4 mils/year and 0.47 mil/year for Ni-200 and Ni-201 respectively. According to these results, Ni-201 seems to be more resistant to corrosion than Ni-200; however, either material shows satisfactory corrosion resistance if the NiF_2 film is kept intact for periods having an average length as great as one week. It appears that the anticipated corrosion rate would be influenced much more strongly by the length of time that a protective NiF_2 film is absent in the presence of fluorine and molten salt than by the frequency of destruction of the NiF_2 film in the absence of fluorine.

1.11 DESIGN OF A PROCESSING MATERIALS TEST STAND AND THE FIRST MOLYBDENUM REDUCTIVE EXTRACTION EQUIPMENT

Molybdenum has been selected as the most promising material of construction for reprocessing equipment that must resist corrosion by bismuth. A cooperative project is in progress between the Chemical Technology and the Metals and Ceramics Divisions to develop the fabrication techniques for molybdenum and to build a small packed-column system. The project will test the suitability of molybdenum as a material of construction and will provide engineering data on packed-column performance with a molten-salt–bismuth system.

The preliminary concepts[46] for the test stand and molybdenum equipment remain unchanged. A report describing the conceptual design and the fabrication development program has been prepared.[47] A limited amount of additional preliminary design work has been done to assist the Metals and Ceramics Division's fabrication development program.[48]

The molybdenum fabrication methods that have been selected for development are as follows: The 3⅞-in.-OD vessel heads will be produced by back extrusion (forging) with integral bosses for nozzle attachments. Shop fabrication of the vessels will be done using electron beam welding with back brazing of the welded joint to reinforce the brittle welds that are characteristic of molybdenum. The braze alloy will be a specially developed corrosion-resistant iron-base alloy. Vessel girth welds will be reinforced externally with brazed bands. Field welding of the molybdenum tubing will be done with a compact orbiting-arc tube welding machine. These welds will also be reinforced by induction-brazed bands. A limited number of tube-fitting-type connectors made of molybdenum have been tested but have not been very satisfactory, primarily because of galling of the threads. Additional fabrication development work is required before the final design of

45. L. E. McNeese, *Engineering Development Studies for Molten Salt Breeder Reactor Processing No. 9*, ORNL-TM-3259 (in preparation).

46. D. E. Ferguson et al., *Chem. Technol. Div. Annu. Progr. Rep. May 31, 1970*, ORNL-4572, pp. 35–36.

47. E. L. Nicholson, *Conceptual Design and Fabrication Development Program for the Molybdenum Reductive Extraction Equipment Test Stand*, ORNL-TM-3392 (in press).

48. M. W. Rosenthal et al., *MSR Program Semiannu. Progr. Rep. Aug. 31, 1970*, ORNL-4622, pp. 189–97, 212–13.

the equipment is started. It is expected that detailed design of the equipment will start in the near future.

A one-third-scale model of the test stand was made to assist fabrication and design studies. Preliminary designs were prepared for the head pots and for the molybdenum-to-steel transition joints at the containment vessel top flange. A full-scale transparent plastic model of the bismuth head pot and the top portion of the extraction column was tested with mercury and water to simulate molten bismuth and salt. Gas-lift performance was satisfactory over the desired mercury flow rate range of about 0.05 to 1.1 liters/min. Performance of the head pot was generally satisfactory in that liquid flow rate fluctuations in the gas-lift discharge were smoothed out and a quiet pool of liquid was maintained above the metering orifice. Very little liquid was entrained in the off-gas from the head pot.

1.12 REMOVAL OF URANIUM FROM MOLTEN SALT BY OXIDE PRECIPITATION

Oxide precipitation is being considered as an alternative to the fluorination–reductive extraction method for isolating protactinium and removing uranium from MSBR fuel salt prior to rare-earth removal. An engineering-scale oxide precipitation experiment is being designed to study uranium removal from fuel salt from which the protactinium has been removed. In this experiment, 0.3 mole of uranium will be precipitated from 2 liters (100 moles) of salt in a single-stage batch system. The source of oxide will be a steam-argon mixture that will be introduced through a draft tube to promote contact of the solid phase with the liquid phase. We will obtain information on (1) the rate of precipitation of UO_2 from fuel salt, (2) the chemical composition and hydrodynamic behavior of the precipitate, (3) steam utilization, and (4) the general characteristics of precipitator operation. We have planned a subsequent experiment in which multistage, countercurrent operation of a UO_2-ThO_2 precipitator will be studied.

Operation of a precipitator was simulated in a 4-in.-diam glass column (using air, a 50 wt % glycerol–water solution, and iron powder as the gas, liquid, and solid phases respectively) to assist in the design of the draft tube for the vessel. Experiments with this system indicated that the sides of the precipitator vessel should be tapered near the bottom to bring the solids under the draft tube and that the tube should extend to within a few millimeters of the bottom of the vessel. An all-nickel precipitator vessel incorporating these features (see Fig. 1.25) has been designed. Precipitation will take

ORNL DWG 71-2871

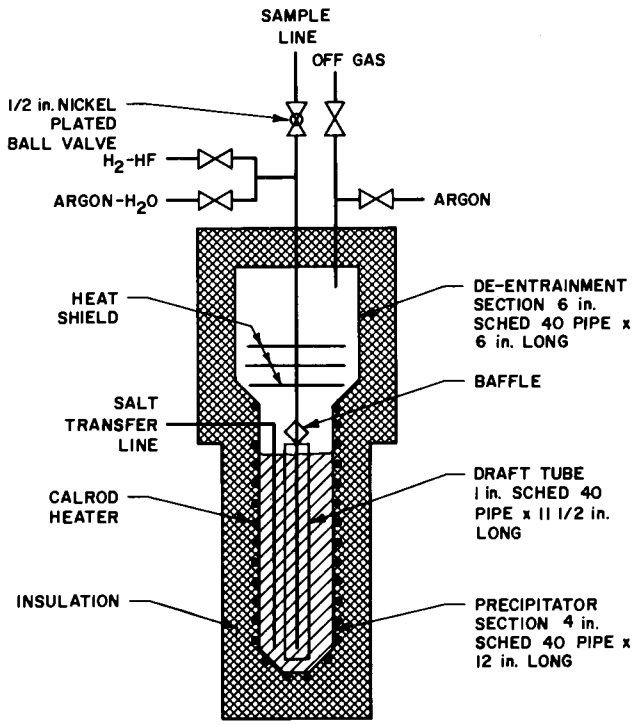

Fig. 1.25. Schematic diagram of precipitator vessel for the first uranium oxide precipitation experiment (OP-1).

place in the lower part of the vessel, which consists of a section of 4-in. low-carbon sched 40 nickel pipe. The upper part of the vessel is designed to permit deentrainment of salt from the gas stream and is fabricated from a 6-in.-long section of 6-in. sched 40 L nickel pipe. Gas is introduced into the system through a section of ½-in.-diam nickel tubing that extends to within ⅝ in. of the bottom of the vessel and then flows upward through a draft tube made of 1-in. sched 40 pipe.

A baffle is mounted on the gas inlet tube to prevent gross quantities of entrained salt from reaching the upper part of the vessel. Heat shields are also mounted on the gas inlet tube to prevent excessive heat loss to the head of the vessel. The gas inlet tube is fitted with a ½-in. nickel-plated ball valve through which samples of salt and oxide may be taken. Several methods for obtaining samples of the solid phase were tested with the glycerol-water-iron system, and results indicate that samples of the precipitate can be obtained satisfactorily.

The remainder of the system will consist of a salt feed-and-catch tank; the argon, hydrogen, and HF supply systems; the argon saturation system; the off-gas

disposal system; and scrubbers for measuring the HF concentration of various gas streams. The equipment, now being fabricated, will be installed in Building 3541.

1.13 REDUCTION OF IRON FLUORIDE IN MOLTEN SALT BY COUNTERCURRENT CONTACT WITH HYDROGEN IN A PACKED COLUMN

Flooding Studies

The equipment being used to study the continuous purification of molten-salt mixtures has been described previously.[49] During the flooding runs, salt flow rates of 50 to 400 cm^3/min were used with argon or hydrogen flow rates of up to 7.5 or 30 liters/min respectively; the temperature was 700°C in each case. The pressure drop across the column increased linearly with increases in gas flow rate, as shown in Fig. 1.26, which summarizes the best data from the ten runs. The salt flow rate was found to have only a minor effect on pressure drop. The maximum throughput in these runs was about 19% of the calculated flooding rate. Under these conditions, the combined pressure drop in the off-gas line and in the column was sufficient to depress the salt-gas interface below the seal loop in the exit line from the column. Increasing the off-gas line size and providing a deentrainment pot corrected this limitation.

Iron Fluoride Reduction Studies

The iron concentration in the salt was increased to about 400 ppm by the addition of iron fluoride prior to making 11 reduction runs. Data from these runs are given in Table 1.13. Although column operation was erratic, reasonable values were obtained for the mass transfer coefficients. These coefficients are about twice those obtained by the M.I.T. Practice School group in 1968 using a 3.375-in.-ID column. The last nine runs were made with $LiF\text{-}BeF_2\text{-}ThF_4$ (72.0-14.4-13.6 mole %). After the first three runs, the iron analyses became erratic, probably because some of the reduced iron particles passed through the sampler filter or because the samples had been contaminated with iron during sample preparation.

49. R. B. Lindauer et al., *MSR Program Semiannu. Progr. Rep. Feb. 28, 1970,* ORNL-4548, p. 329.

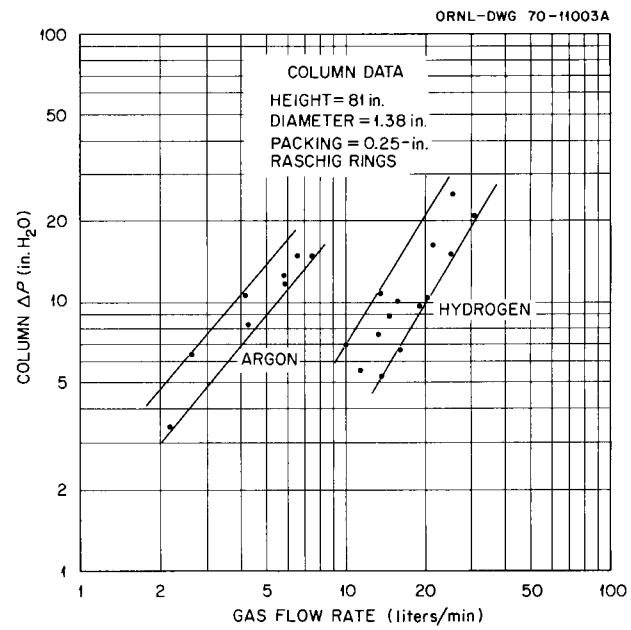

Fig. 1.26. Column pressure drop during countercurrent flow of molten salt (66-34 mole % $LiF\text{-}BeF_2$) and either argon or hydrogen.

Oxide Removal

Three H_2-HF treatments were made to remove oxide. The first was a batch treatment in the feed tank after the first flooding run. Plugging of the liquid level dip tube in the feed tank and of the feed line to the column indicated the presence of insoluble oxide in the tank. Nine hours of sparging with 4% $HF\text{–}H_2$ removed about 500 ppm of oxide from the salt. During the $LiF\text{-}BeF_2$ studies, the pressure drop across the column had doubled, indicating an accumulation of BeO on the packing. After the thorium was added to the salt, the salt was contacted countercurrently in the column with 10% $HF\text{–}H_2$ at 600°C. During the 2.75-hr treatment, 100 ppm of oxide was removed; the HF utilization was 15%. However, considerable oxide remained in the system, as shown by a sharp rise in the pressure drop across the column after three additional runs. To provide further opportunity for insoluble oxide in the column to be dissolved as oxide was removed from the salt and to allow dissolution of the BeF_2 produced, the column was filled with molten salt and H_2-HF was passed through the salt for 18 hr. Oxide was then removed at an average rate of about 15 ppm/hr, with a maximum HF utilization of 5%. After this treatment, the pressure drop across the column returned to normal and remained low for the remaining runs.

Table 1.13. Data from iron fluoride reduction runs

Column temperature, 700°C

Run No.	Date	Gas flow rate (std liters/min)		Salt flow rate[a] (cm^3/min)	Analyses of filtered samples (ppm iron)		Percent of batch contacted	Mass transfer coefficient,[b] k_l (ft/hr)
		H_2	Ar		Feed	Product		
1	7/27	20		100	425	307	71.4	0.018
2	7/28	13.5		100	307	228	72.9	0.016
3	10/22	16.6		100	220	158	75.3	0.015
4	11/3	14.6		210	158	373	84.7	
5	11/4	18.2		161	373	137	68.8	
6	11/5	4.5	4.5	106	137	110	81.8	0.011
7	11/6	3.9	3.9	142	110	70	81.8	0.030
8	11/9	24.0		103	70	75	86.5	
9A	11/13	4.5	4.5	93	75	55[c]	79.4[d]	0.012
9B	11/13	3.5	3.5	136				
10	11/17	14.1		105	69[e]	77[c]	81.8	
11	11/19	3.1	4.5	117	207	339 104[c]	81.2	

[a]The first two runs used $LiF\text{-}BeF_2$; the remaining runs used $LiF\text{-}BeF_2\text{-}ThF_4$.

[b]Based on outside surface of Raschig rings only since salt is considered to be nonwetting; k_l is 78% of these values if entire area of the Raschig rings is used as the basis.

[c]Average of flowing-stream samples; no batch samples were taken after the run.

[d]A value of 100% is used in calculating k_l since samples are of flowing-stream type.

[e]Calculated from flowing-stream samples from previous runs.

2. Development of Aqueous Processes for LMFBR Fuels

Beginning in the 1980's, reprocessing of large quantities of fissile material from LMFBR reactors will be required. The problems that will be encountered during the reprocessing of this material will be different from those that have been encountered with light-water reactor (LWR) fuels for the following reasons: (1) The major fissile material in LMFBR reactors is plutonium rather than ^{235}U. (2) The fissile content of the LMFBR fuel is higher, by a factor of about 7 in the core section and by a factor of about 3 when all the material to be processed is considered, than that of the LWR fuel. (3) The average fission product content will be somewhat higher (the localized fission product content may be three times higher) than that encountered in LWR fuel. (4) The specific power of the LMFBR is higher, by a factor of about 5, than that of the LWR. (5) Processing of the LMFBR fuel after short decay periods will be advantageous, owing to the high fissile content (and high inventory costs) of the core material.

The Purex solvent extraction process, which is employed by nearly every major fuel processing facility in existence today, will be applicable in the processing of LMFBR fuels. It appears feasible, with plant modifications, to process fuel from early LMFBR reactors, where preprocessing decay is acceptable, in existing fuel reprocessing facilities.

Aqueous reprocessing is most economically accomplished in large central facilities to which fuel is shipped from various reactor sites. The problem of fuel shipment, which is difficult even with LWR fuels, is aggravated in the case of LMFBR fuels by the high specific power of the fuel and the need to ship after only short decay times. We are working toward development of equipment and techniques for shipment that will ensure safety and containment under accident conditions.

The preparation of LMFBR fuel for solvent extraction is more difficult than that of LWR fuel because of increased heat generation, vastly increased amounts of radioiodine (if the fuel is processed after short decay periods), and the presence of substantial quantities of relatively difficult-to-dissolve plutonium and fission products. We are making studies of the dissolution rates for irradiated fuel and of equipment that will be suitable for the accomplishment of certain of the mechanical operations (e.g., shearing). Improved containment of each equipment item and reduction of the quantity of contaminated off-gas are among the primary goals.

Disposal of the tritium that is produced during the fissioning of uranium and plutonium is not currently a problem because of the relatively small amount being produced. However, when the nuclear capacity expands by several orders of magnitude and the size and number of processing facilities increase, there will be a definite need to minimize the discharge of tritium to the environment. A process that, hopefully, will isolate the tritium prior to its dilution with dissolver solution is under development. (If the tritium becomes mixed with the dissolver solution, its isolation and recovery will be impractical.) This process involves an oxidative heat treatment, which will also liberate other volatile fission products such as iodine, xenon, and krypton.

The treatment of off-gas is a major consideration in the processing of fuels that have been cooled less than 120 days. Removal efficiencies for radioiodine of 10^8 will be required for large-scale plants which process fuel that has been cooled for about 30 days. While no processing facility in existence today has the capacity (or the need) for this degree of removal, the recent development of several efficient iodine trapping systems, for example, the nitric acid scrub and the silver zeolite sorber, gives us confidence that such a plant is not beyond reasonable attainment. In the processing of short-decayed fuels, substantial quantities of radioactive xenon will also be present in the off-gas streams; it, along with ^{85}Kr, can be removed by various proven means and by other rare gas removal methods that are being developed.

Our work has been directed, in a considerable measure, toward clear definitions of the problems and a delineation of the most profitable areas of investigation.

In the future we expect to develop the equipment and the process flowsheet conditions that are required to demonstrate safe and economic shipment and the processing of short-cooled LMFBR fuel. While this is a challenging problem, we are confident that the solution lies in the extension of current practice and/or technology.

2.1 SHIPPING

The shipment of radioactive materials is an essential part of any nuclear power system. Even if each reactor, or reactor complex, were equipped with its own reprocessing and refabrication facilities, it would be necessary to transport the radioactive waste streams produced at the facility to permanent disposal areas. (The probability of locating all the power generating stations in the vicinity of permanent radioactive waste disposal sites is very low.) Hence, integration of power generating and fuel reprocessing facilities could theoretically eliminate the shipment of only one of the several categories of radioactive materials.

Three avenues are apparent for minimization of the hazard associated with the shipment of radioactive materials in general, and LMFBR spent fuel in particular. These are: (1) shipment in a form that is essentially nondispersible, (2) shipment in a container that is highly resistant to damage by both internal and external forces, and (3) shipment by a method that will essentially preclude exposure of the shipment to abnormal conditions. Long-decayed LWR fuels contain relatively small amounts of harmful fission products in a dispersible form. On the other hand, short-decayed LMFBR fuels are expected to contain large amounts of noxious fission products in a dispersible condition. Our efforts pertaining to fuel shipment have been centered on guaranteeing the retention of cask contents under highly abnormal circumstances. However, we are not overlooking the possibility of increasing assurance against accidental release of fission products through the control of material form and shipment method.

The principal hazard associated with the shipment of radioactive material is the possibility of dispersal. Hence, if the radioactive material being shipped is in a form that is very difficult to disperse, hazard to the general public is minimal. Oxide fuels retain almost all fission products with the exception of the more volatile ones, that is, the noble gases, iodine, and possibly cesium. (The oxide fuels are very slowly attacked by water.) If the oxide fuels are shipped without prior treatment to remove the available volatile fission products, the containment system must be of such construction that it offers adequate protection against the release of radioactive gases.

Reduction of the probability of exposure of a shipment to abnormal conditions can be achieved by any number of administrative procedures; however, possibly the most promising method is barge shipment, in which the cask is carried beneath the water level. In barge shipment, speeds are held to modest levels, falling from high places onto an unyielding surface is precluded, and protection from fire is guaranteed by immersion in water.

Cask Integrity Tests

Several metallic seals are being studied in an effort to determine their adequacy under normal and accident conditions. One of these seals, a modified Grayloc, was installed in four $\frac{1}{6}$-scale model casks, as shown in Fig. 2.1, and tested under impact conditions by being dropped in various orientations from a height of 30 ft onto an unyielding surface. Leak rates for the seals were determined before and after impact by using a helium leak detection system generally capable of measuring leaks approaching 10^{-10} cc/sec. Table 2.1 presents the measured leak rates of the four casks following the conditions specified. At the very low leak rates observed here, the numbers preceding the exponents have little significance.

ORNL-DWG 70-12483RA

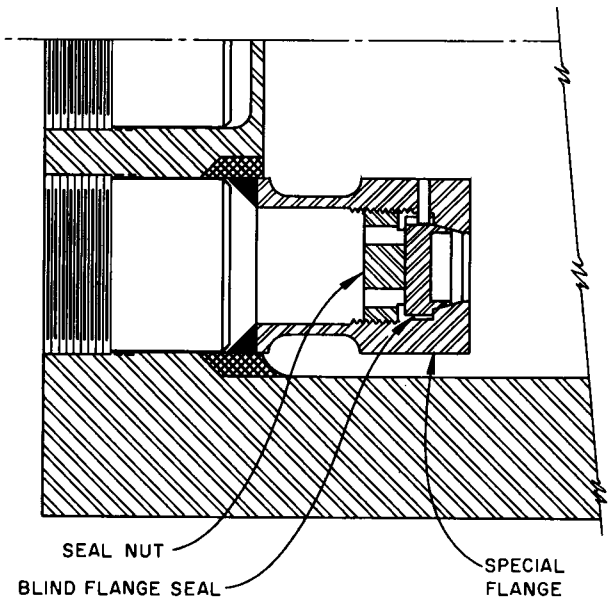

Fig. 2.1. Sectional view of seal as installed in $\frac{1}{6}$-scale model casks.

Table 2.1. Observed leak rates of seals installed in model casks[a]

Condition	Helium leak rate (cc/sec)			
	Cask A	Cask B	Cask C	Cask D
Initial	4.9×10^{-10}	4.9×10^{-10}	4.9×10^{-10}	4.9×10^{-10}
After first edge impact	2.3×10^{-9}	*b*		
After second edge impact on same surface	2.2×10^{-9}			
After additional impact on fresh surface	*b*	*b*		
Retest	6.2×10^{-10}	6.2×10^{-10}	6.2×10^{-10}	6.2×10^{-10}
After end impact			2.7×10^{-8}	$<7.4 \times 10^{-10}$
After opening, inspection, and resealing			4.8×10^{-9}	6.6×10^{-9}
After side impact	2×10^{-9}	$<3.9 \times 10^{-9}$	$<3.9 \times 10^{-9}$	$<5.1 \times 10^{-9}$

[a]Model casks were made of steel, unbuffered, and dropped 30 ft onto unyielding surface. Model scale was ~1/6. Seal was modified Grayloc with clear opening of 1.1 in. diameter.

[b]Impact was performed, but leak rate data are not available.

Cask A was dropped twice on the same point on an edge close to the seal (the center of gravity was directly above the point of impact); as a result, the seal loosened very slightly, causing the leak rate to increase to approximately 2×10^{-9} cc of helium per second. Later, cask A was dropped on a different zone of the edge. Cask B was dropped twice on edges adjacent to the cask seal. Casks C and D were dropped on end (normal to the landing surface), which produced much higher *g* forces than were observed in the case of impact on the edges. In one case, the leak rate increased to approximately 3×10^{-8} cc of helium per second, while no increase was observed in the second case. The two models were opened, inspected, resealed, and leak-checked. No damage to the sealing mechanism or to the interior of the cask cavity was perceptible.

All four casks were then subjected to a 30-ft free-fall side impact. Although, in each case, the four casks came to rest in a near-horizontal position, none of them had a perfectly flat landing. Leak tests and visual observations after the drop indicated that the seal was not affected by the impact. Peak decelerations in the models were 4000 to 5000 *g*, which would indicate a deceleration in a full-size cask of ~700 *g*. Visual indications of external damage to the cask structure were slight.

We interpret these results, as well as the results from earlier tests with various scale models of steel casks[1] (sans seals), to establish that any deformation resulting from credible impact accidents will be observable only in the outer portions of the cask structure and that mechanically isolated seals will suffer no deformation of the sealing surface. Under conditions of zero (or negligible) seal deformation, the maintenance of a seal is dependent upon its resistance to predictable loads. The equipment to withstand the imposed loads can be analyzed by techniques that are as well established and as well understood as those used for pressure vessels. Hence, we believe that a seal capable of surviving any credible impact load can be installed in a full-scale cask.

1. *Chem. Technol. Div. Annu. Progr. Rep. May 31, 1970,* ORNL-4572, p. 42.

Heat Transport

Two large test systems were operated to collect information on heat transport both within the subassembly and within the fuel cavity. The first of these consisted of an electrically heated mockup of an Atomics International Reference Oxide Reactor fuel subassembly mounted inside a 10-in.-diam pipe. Some of the results of tests made with a variety of coolants are displayed in Fig. 2.2. The fuel rod emissivity both before and after exposure to sodium was ~0.45. When using atmospheric-pressure argon and helium as primary coolants, thermal convection–conduction accomplished 38 and 72%, respectively, of the total heat transported within the subassembly boundary when the central fuel rod temperature was 1000°F.

The second large-scale test device was a half-length full-scale mockup of the fuel cavity of a 37-subassembly LMFBR fuel shipping cask. Some of the initial data taken with this system are displayed in Fig. 2.3.

ORNL DWG 70-9017-R2

COOLANT	HEAT INPUT	EQUIV. DECAY	TEMPERATURES, °F									
SODIUM	10.1 kw	28 DAYS	514	528	537	552	560	567	517	552	527	518
HELIUM	2.1	300	151	224	397	798	840	1002	311	617	120	97
ARGON	1.2	520	148	250	451	819	749	998	182	426	208	109
VACUUM	0.69	875	185	184	542	872	786	996	333	639	112	92

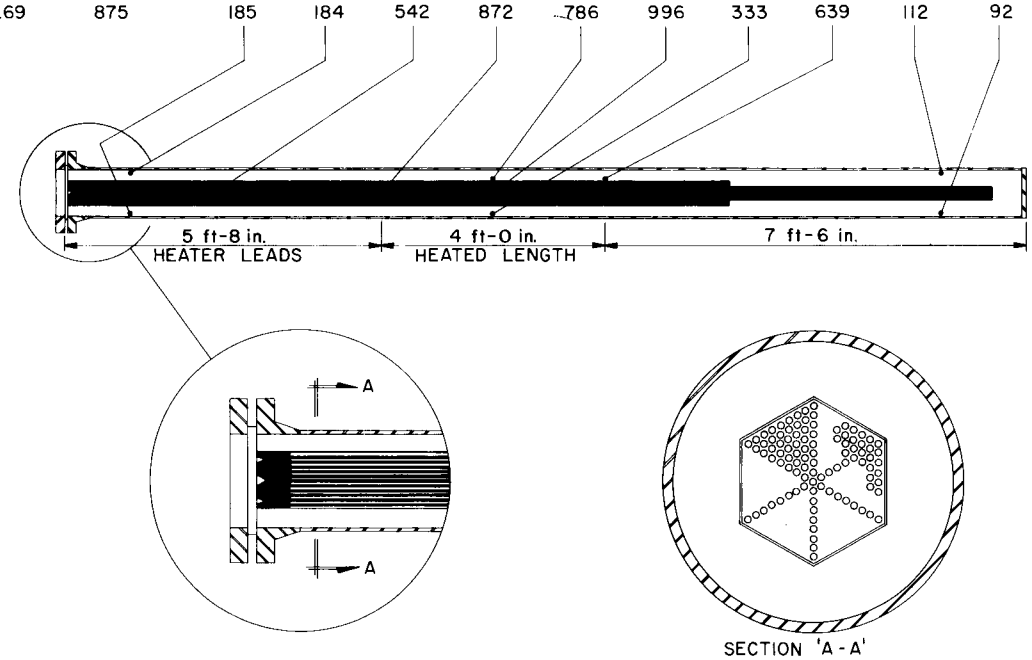

SINGLE SUBASSEMBLY CASK MOCKUP

Fig. 2.2. Temperatures observed in an electrically heated mockup of an Atomics International reference oxide reactor subassembly installed in a 10-in. pipe.

Because the observed absolute temperatures are not pertinent, whereas the temperature variation within the fuel cavity is the object of the investigation, all the temperatures are reported as variations from the maximum observed temperature. Temperature variations at the same physical level, but at different distances from the heated portion of the mock fuel subassemblies, can be seen to be quite small (generally less than 10°F); on the other hand, an appreciable temperature difference exists between points at different elevations. Temperature variation between points as a function of total power input appears to be less than a first power function. The temperatures at the extreme cold end of the fuel cavity are not displayed because peculiarities in the design of the system cause heat loss in this area to be excessive and because the observations are thought to be erroneous.

2.2 HEAD-END PROCESSING

The development and evaluation of candidate head-end steps for reprocessing spent Fast Test Reactor (FTR) and other LMFBR Follow-On fuels were continued. The main efforts were centered on heat dissipation, thermal conductivity measurements, dismantling of multitubular assemblies, shearing, sodium deactivation, and study of closures for equipment isolation.

Decay Heat Dissipation

A comparison of the decay heat generation rates for a typical PWR fuel (Diablo Canyon) assembly and several LMFBR fuel assemblies was made using the computer code ORIGEN (Fig. 2.4). Center-rod temperatures for

ORNL DWG 71-3786

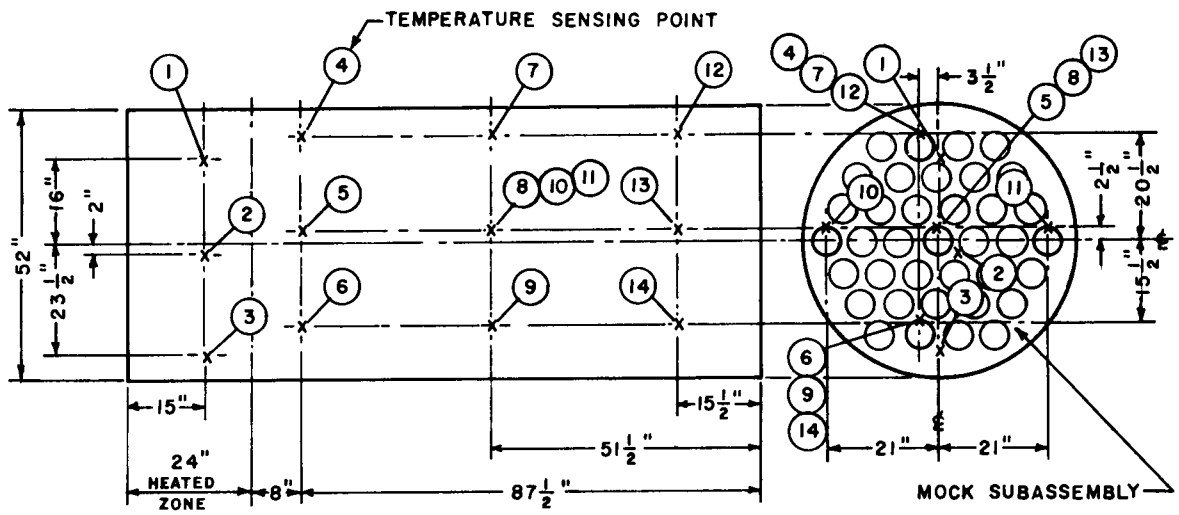

Temperature[a] Variation from Maximum

Point No.	Total Power Input 92.5 kW	150 kW	182 kW
1	0	0	0
2	-18	-20	-24
3	-51	-70	-78
4	-12	-4	-14
5	-19	-17	-27
6			-70
7	-16	-5	-16
8	-19	-16	-26
9			-66
10	-32	-17	
11	-23		
12	-22	-11	-22
13	-24	-20	-29
14			-67

[a] Temperatures are in °F.

Fig. 2.3. Observed variations in temperature in mock 37-subassembly fuel shipping cask cavity when filled with liquid sodium.

these fuel assemblies are shown in Fig. 2.5 as a function of decay time. Calculations were performed using the HEX code, which assumes radiative heat transport only between the rods within the array. Although the total heat release for the PWR assembly is higher than for the LMFBR assemblies, the heat release per unit of rod area (which is the important factor in the temperature calculations) is lower.

Thermal Conductivity Measurements

Head-end processing of LMFBR fuel by the shear-leach approach involves the shearing of fuel rods into short pieces to facilitate leaching of the urania-plutonia from the stainless steel cladding. Heat transfer calculations involving these fuel pieces, as in the calculation of temperatures attained in baskets of sheared fuel, require

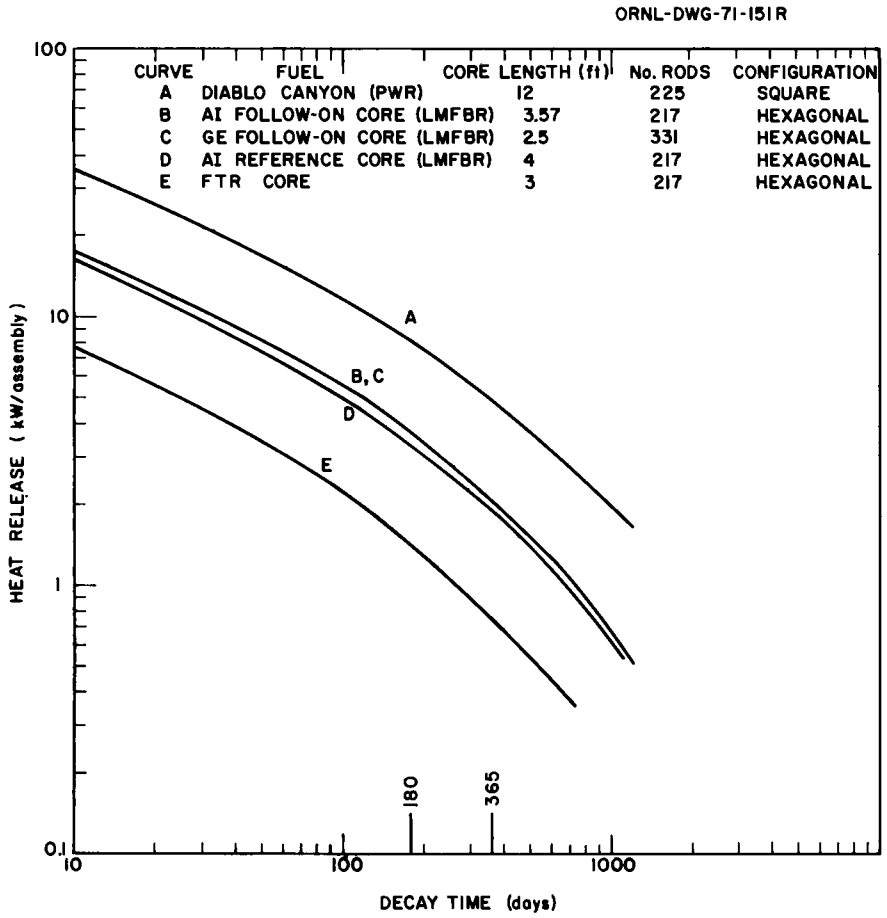

Fig. 2.4. Heat release of LMFBR fuel vs heat release of a typical LWR fuel.

knowledge of the effective thermal conductivity of the chopped fuel pieces. Thermal conductivity results obtained to date for the materials are given in Fig. 2.6. (Porcelain was used as a stand-in for urania-plutonia.)

The increase in thermal conductivity in air from that observed in argon (curve *A* vs curve *D*) is greater than can be accounted for by the different physical properties of the two gases. A partial explanation concerns the oxidation of the stainless steel cladding in air, which results in a higher emissivity and enhances radiative heat transport. A comparison of curves *B* and *E* with the same cover gas, argon, indicates that the thermal conductivity of the solid material significantly affects the effective thermal conductivity of the chopped pieces [k = 0.88 Btu hr^{-1} ft^{-1} (°F)$^{-1}$ at 400°F for porcelain; k = 10.2 Btu hr^{-1} ft^{-1} (°F)$^{-1}$ at 400°F for 304 stainless steel]. Curve *C* shows data taken with chopped UO_2 fuel pieces ½ in. in diameter and 1 in. long. As compared with results obtained with porcelain (curve *E*), the effective thermal conductivity of the UO_2 pieces is as much as 100% greater at high temperatures. The difference in geometry would not suffice to explain this difference in effective thermal conductivity. While the differing thermal conductivities of porcelain and UO_2 [k = 1.5 Btu hr^{-1} ft^{-1}(°F)$^{-1}$ for UO_2] might account for the difference at low temperatures (where conduction is important), it would not at high temperatures (where radiation and gas-phase convection are dominant).

Dismantling of Multitubular LMFBR Fuel Assemblies

Studies and scoping-type investigations of various means for dismantling fuel assemblies were continued. The concept of cropping the ends and removing the hexagonal shroud (~⅛ in. thick) by slitting in order to remove the fuel rods for single or multirod shearing was studied. This concept offers the advantages of employing a small, inexpensive shear instead of a massive bundle shear. With a small shear, decay heat dissipation could be easily controlled by processing fewer rods per array. However, disassembly may be feasible only for

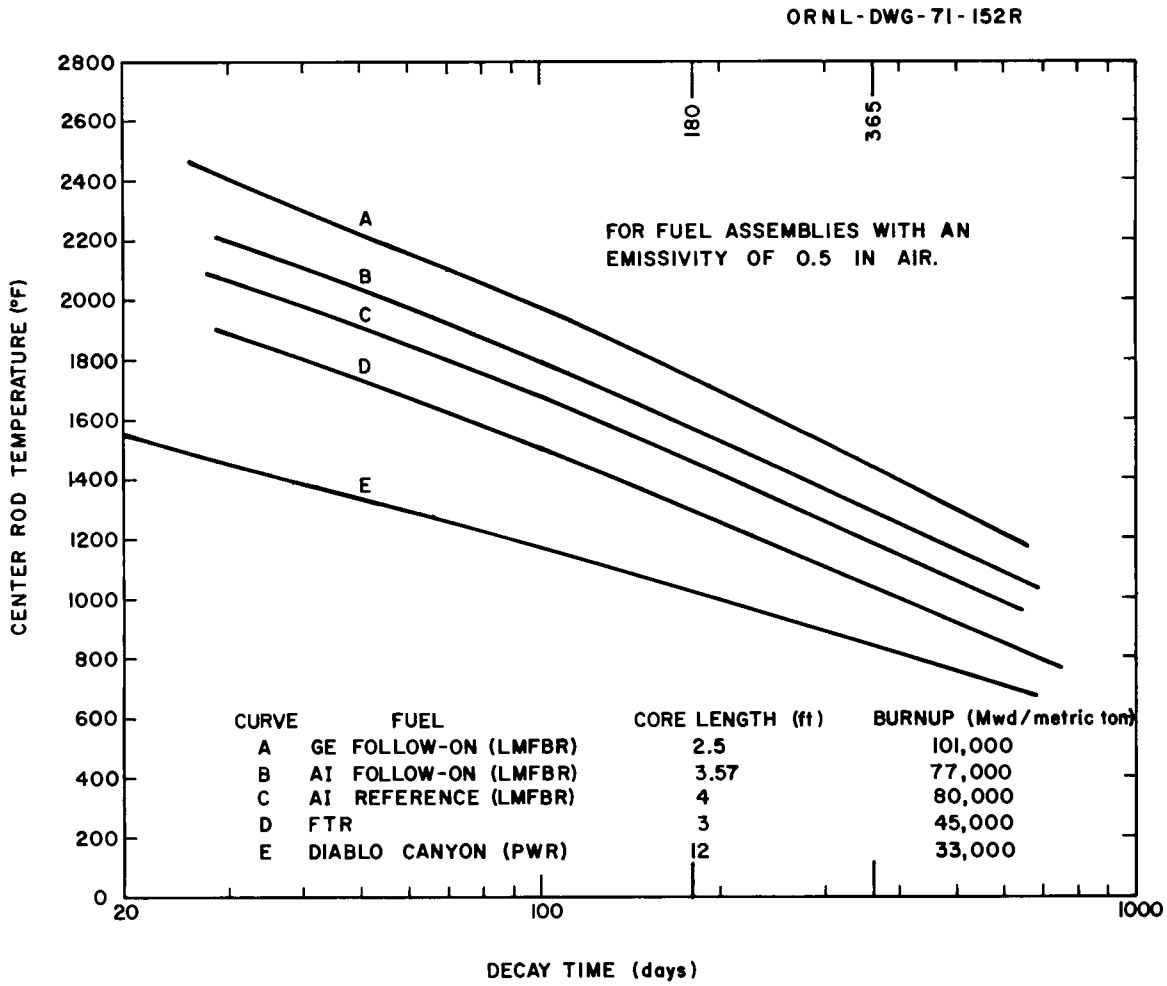

Fig. 2.5. Comparison of center-line temperatures of LMFBR fuel and a typical LWR fuel.

FTR fuel and Atomics International (AI) fuels that are free of grids. Disassembly does not appear to be feasible for the most recent General Electric and Westinghouse fuel concepts, which employ grids spot-welded to the flow duct or shroud.

A plasma-arc torch has been the leading candidate for use in longitudinal slitting at the hexagonal corner of the shrouds. Thus a plasma cutting unit (~250 A; 250 V, maximum working voltage) was installed, and shakedown tests were made. Results indicate that shrouds can be slit without cutting into the fuel rods within the shroud.

A tracking mechanism to guide the torch is a requirement for successful torch use. Commercial tracking mechanisms that can maintain the required torch position along a bowed and/or twisted assembly sheath are being investigated. It has been estimated that a bow of 8 to 12 in. per 18-ft assembly length may occur in LMFBR assemblies. A torch tracking sensitivity of ~2 to 10 mils is presently desired in order to prevent cutting into the fuel cladding. Two types of commercial tracking units are being investigated: (1) a mechanical sensing probe type to automatically control both vertical and horizontal positions and (2) a photoelectric sensing device. Burned (light-absorbing) spots on the shrouds may cause erroneous readings in a photoelectric sensing unit; therefore, mechanical sensing probe units are currently being considered as the most favorable tracking devices.

Shearing

In continuing studies of bundle (intact) shearing of fuel assemblies, three moving[2] blades were fabricated and three fixed blades were designed. These blades are to be evaluated for breaking of the assembly shroud

2. Ibid., p. 50.

ORNL-DWG 71-5781

CURVE	MATERIAL	GEOMETRY	VOID FRACTION	BULK DENSITY (g/cm^3)	COVER GAS
A	SS-CLAD (15-mil wall) PORCELAIN	1/4 in. diam. x 1/2 in. LONG	0.52	1.78	AIR
B	SOLID SS	1/4 in. diam. x 1 in. LONG	0.50	4.0	ARGON
C	SS-CLAD (35-mil wall) UO_2	1/2 in. diam. x 1 in. LONG	0.65	3.32	ARGON
D	SS-CLAD (15-mil wall) PORCELAIN	1/4 in. diam. x 1/2 in. LONG	0.52	1.78	ARGON
E	SS-CLAD (15-mil wall) PORCELAIN	1/4 in. diam. x 1 in. LONG	0.57	1.5	ARGON

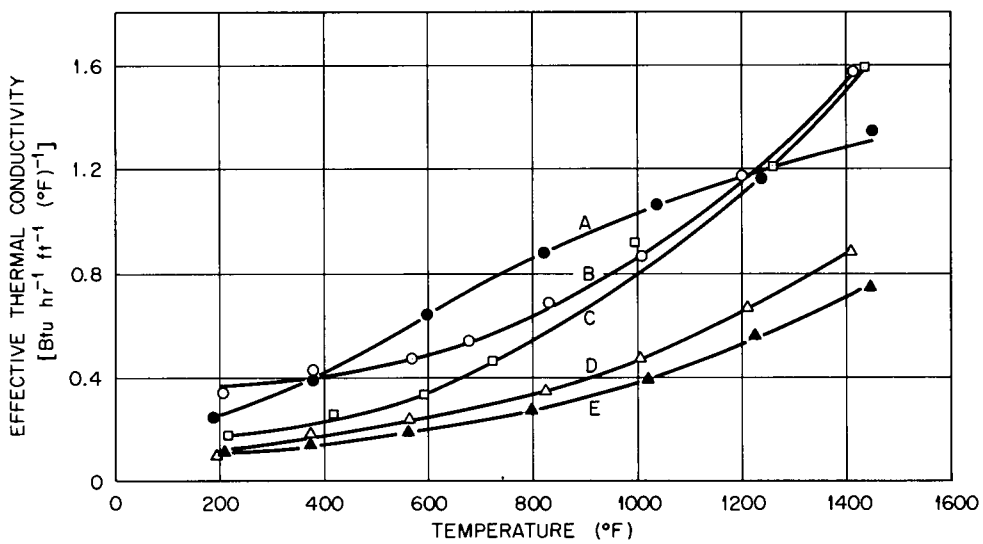

Fig. 2.6. Thermal conductivities of some prototype LMFBR fuels.

into small discrete pieces after the modifications of the ORNL 250-ton shear are complete. These modifications include new gags, feed envelope, blade holder, and shear faceplates.

Material for use in LMFBR thermal conductivity tests was sheared with the ORNL multirod shear. AI prototype rods, ¼-in.-OD by 15-mil-wall type 304 stainless steel tubing containing porcelain pellets, were sheared into ½-in. lengths. The packing density and the void fraction of the sheared material (with fines removed) were 1.66 g/cc and 55% respectively; 11.5% of the porcelain was dislodged.

Shearing force data were obtained by shearing single unclad ceramic rods (prototypes of AI core and inner-blanket fuel rods) with a single-rod shear designed for use in a hot cell. These data were intended to supplement existing information in arriving at the shearing force requirements for both LMFBR and LWR reprocessing facilities. Shearing stresses of 11,607 and 14,171 psi were measured for core and inner-blanket rods having cross-sectional areas of 0.036 and 0.078 in.^{2} respectively. The ceramic material had a density of 2.52 g/cc and a hardness of 7 to 9 on the Mohs scale (equal to the hardness of quartz and topaz).

Additional information was compiled on the force required to shear single rods of unfilled, porcelain-filled, or irradiated $(U,Pu)O_2$-filled stainless steel tubing. Table 2.2 and Fig. 2.7 show new data, along with previously reported values for unirradiated empty and porcelain-filled tubing. Little difference in behavior due to irradiation was observed. Rods containing Vipak powder or sol-gel material prepared by the Sphere-Pac method offered little resistance over that of empty tubing.

In many experiments, $(U,Pu)O_2$ fuel free of cladding is desired. The single-rod hot-cell shear was used to cut irradiated specimens into ⅛-in.-long pieces. In cutting pieces of this length, the shear crushes and dislodges the mixed oxides; the cladding segments can then be separated by screening. Fuel of the highest linear heat ratings and burnups produced more fines than otherwise similar fuels (Table 2.3). An investigation of

Table 2.2. Results of single-rod shearing tests

Manufacturer	Fuel specimen	Cladding material	Fuel in cladding	Burnup (MWd/metric ton)	Applied shearing force (lb)
GE	F1C	Incoloy-800	20% PuO_2 pellets	1,800	1068
GE	F1D	316 SS	20% PuO_2 pellets	1,800	960
GE	F1E	347 SS	20% PuO_2 pellets	1,800	1005
GE	F1F	Incoloy-800	20% PuO_2 powder	1,800	620
NUMEC	19-1	316 SS	Empty plenum	100,000	1020
NUMEC	19-5	316 SS	Empty plenum	100,000	1010
PNL	X-1	304 SS	25% PuO_2 pellets	3,630	780
PNL	59-5	304 SS	25% PuO_2 pellets	14,500	740
ORNL	43-112	304 SS	15% PuO_2 Sphere-Pac	5,000	420
ORNL		304 SS	Porcelain		880

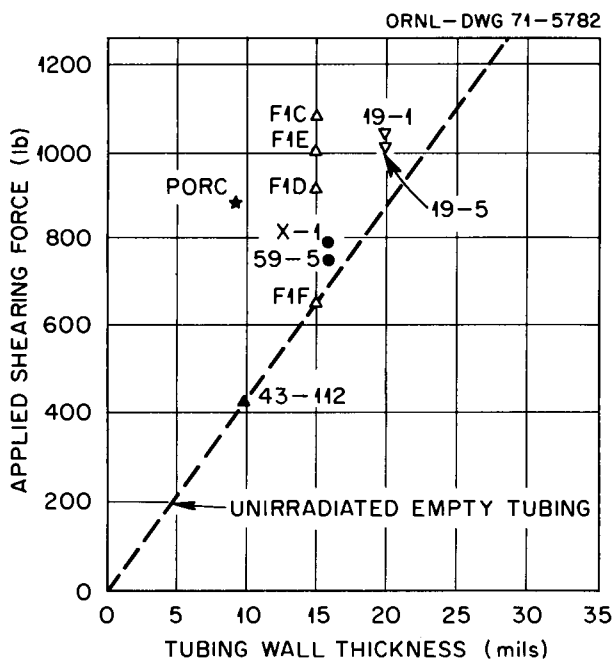

Fig. 2.7. Results of single-rod shearing tests.

differences in the chemical behavior of the different size ranges of crushed fuel has begun (see Sect. 2.4).

Deactivation of Sodium

A program proposal was written for the study of the removal, deactivation, and disposal of sodium present with spent LMFBR fuels. Its scope includes:

1. A literature search to review the chemistry, methods for handling, and existing means of deactivation and disposal of sodium.
2. The tabulation of known LMFBR fuel types and geometries, with an assessment of the quantity of sodium likely to be retained on the surfaces.
3. The calculation of the amount of energy that is released from reactions of sodium and an estimation of the quantity of sodium, purity, temperature, and surface characteristics.
4. The performance of deactivation methods of interest, and an analysis of each method for applicability to LMFBR reprocessing concepts.

Design efforts for a sodium-purification-loop–dry-box facility have progressed. The loop will provide pure sodium to a test pot that is a part of the glove-box assembly in which metallic specimens are to be soaked in sodium under a dry argon atmosphere. The loop will remove any sodium oxide generated by cold trapping. The cover gas will be monitored for oxygen, moisture, and hydrogen content. This facility will fall in the modified Quality Level 2 category. Fabrication of components should be in progress by the early part of FY 1972.

Sodium-soiled specimens will initially be deactivated by reaction with a moist inert carrier gas in small-scale equipment or by oxidation in an experimental voloxidizer unit.

Scoping-Type Sodium Deactivation Tests

A series of experiments was conducted to qualitatively determine the feasibility of reacting small amounts of sodium with nitric acid. Such a situation could occur if sheared defective (sodium-logged) fuel rods were placed in a dissolver without prior removal or deactivation of sodium. Ten-gram quantities of sodium

Table 2.3. Size distribution of irradiated fuels sheared into $\frac{1}{8}$-in. lengths

Experiment No.	Burnup (MWd/metric ton)	Linear heat rating (kW/ft)	Fuel type	Treatment	Distribution of standard sieve sizes (wt %)							
					+10	+30	+60	+65	+80	+100	+200	−200
F1F	1,800	16.4	Vipak	As fabricated	65			20				15
				Crushed		23.5	24.7		6.4	2.9	15.1	27.4
43-112-1	5,000	8.4	Sol-gel	As fabricated			75.3					24.6
				Crushed			77.8	22.2[a]				
43-112-3	6,800	13.6	Sol-gel	As fabricated			73.8					26.2
				Crushed			76.3	23.7[a]				
43-115-4	42,000	13.4	Sol-gel	As fabricated			74.1					25.9
				Crushed			61.1	38.9[a]				
PNL X-1	3,680	5.3	Pellet	As fabricated	100.0							
				Crushed		33.2	25.3			12.4	29.1[a]	
PNL 59-5	14,500	11.5	Pellet	As fabricated	100.0							
				Crushed			48.4			10.7	41.0[a]	

[a]Smaller sizes not determined.

encapsulated in argon-filled 0.5-in.-OD X 0.025-in.-wall X 5.5-in.-long carbon-steel tubing were used in each test.

When 4 to 8 *M* HNO_3 was used to a depth of 4 in. in 55-gal stainless steel drums (open or partially open tops), observed reactions ranged from strong (acid was expelled to a height of 20 ft) to mild (acid was not expelled). Weaker acids and/or an argon cover gas allowed the milder reactions. Presumably, the hydrogen-oxygen reaction was predominant in the released energy.

Mild reactions occurred when the sodium capsule was tamped with a 2.5-ft depth of sheared porcelain-filled stainless steel prototype fuel using 2 and 4 *M* nitric acid. In these tests, which were designed to simulate actual dissolver conditions, the fuel bed was not disturbed. An argon cover gas was used.

The presence of carbon-steel chips in similar experiments produced violent explosions with an accompanying expulsion of prototype fuel. The probable cause of such an energy release was the nitrous oxide–hydrogen reaction. (The action of nitric acid on carbon steel produces nitrous oxide. Nitrous oxide is also produced in the dissolution of urania-plutonia.) These results strengthen our desire to ensure that little or no sodium enters a dissolver.

State-of-the-Art Literature Review of Sodium Deactivation and Removal Methods

We have completed a literature review and study of deactivation and disposal information on sodium and its compounds. During the study, it was assumed that one or all of several different physical and chemical sodium collection and deactivation operations would be considered for application to the various LMFBR fuel head-end processing steps. Particular attention was directed toward establishing the relative worth of processes that (1) remove sodium from the exterior of an LMFBR fuel assembly, of fuel rods, and/or of any discarded fuel hardware and (2) remove sodium from the interior of fuel rods that are manufactured with sodium bonding and/or are sodium-logged due to venting or to failure of the cladding.

In the study, physical deactivation and chemical deactivation methods for sodium cleaning were considered separately. The principal physical deactivation methods that were reviewed included:

1. Mechanical methods, in which a high-velocity inert gas or liquid stream is used to dislodge sodium present on exterior surfaces.
2. Distillation methods in an inert gas or in vacuum, where considerations focus on the rates of oxidation vs vaporization of sodium, the heat transfer environment, and the geometry of the fuel shape that has to be cleaned of sodium.
3. Dipping techniques, utilizing a molten form of a low-melting alloy, metal, or molten salt (such as NaK, mercury or lead, and $NaCl\text{-}CaCl_2$), in which the residual liquid metal remains liquid at all handling temperatures.

Table 2.4. Major sodium deactivation techniques for each head-end processing step

Cask cleaning on-site	Receiving and cleaning	Cropping, deshrouding, decanning, and singularizing	Shearing	Voloxidation[a]	Dissolution
Mechanical methods	Mechanical methods	Steam-bearing carrier gas	Flushing techniques	Burning (oxidation)	Water or water vapor reactions
Steam-bearing carrier gas	Dipping techniques	Alcohols	Dipping techniques	Vaporization into an inert carrier gas	
Dipping techniques	Flushing techniques	Flushing techniques	Steam-bearing carrier gas		
Flushing techniques	Steam-bearing carrier gas	Dipping techniques	Alcohols		

[a]It may be possible to bypass all the other cleaning and deactivation schemes and deactivate the sodium present on the exterior of the fuel, as well as internal sodium exposed by the shearing operation, by a simple oxidation step. This method produces no hydrogen and does not produce volumes of caustic waste solutions that must be concentrated and stored.

4. Flushing techniques in liquid ammonia (a process that would exhibit rather high vapor pressures) or in heavy oils in conjunction with ultrasonic techniques.

The important chemical deactivation methods reviewed were:

1. Water and water vapor reactions, in which the imminent hazards to be taken into consideration are those associated with the high heat of chemical reaction and the large amount of hydrogen that is evolved.

2. Reactions with alcohols, preferably the multichained or highly branched types. Dowanol-EB, C_4H_9-O-C_2H_4-OH, has recently been used at various sites to deactivate sodium from the surfaces of LMFBR fuel material.

3. Oxidation of the sodium on the surfaces of an LMFBR fuel assembly by oxygen.

The above physical and chemical deactivation techniques were classified according to their applicability or relative importance to each phase of the head-end processing scheme (Table 2.4). The first procedure in each processing phase is presently considered the most favored.

2.3 REMOVAL OF VOLATILE FISSION PRODUCTS

As the nuclear power industry grows and the number and size of the fuel reprocessing plants increase, the release of radioactive noble gases, tritium, and iodine to the environment will become a much more important consideration than at present. In the future, the removal of essentially all radionuclides from the plant off-gas may be required. Efficient retention of iodine, which requires careful control even in present reprocessing plants, will become much more critical when short-cooled LMFBR fuels are processed.

Tests were described previously[3,4] of a new head-end processing step (termed voloxidation) designed to release volatile fission product gases from the fuel prior to aqueous processing. The objective of this step is to transfer most of the iodine, krypton, xenon, and tritium from the fuel into a relatively small volume of gas from which they can be efficiently removed in concentrated form for storage or permanent disposal. Conceivably, this objective can be met by heating the oxide fuel to some reasonable temperature in flowing oxygen. Use of this treatment appears to be of particular advantage with respect to tritium control since it would avoid large dilution of the tritiated water with water in the fuel dissolution step.

Oxidation of Unirradiated Fuels

Unirradiated sintered fuel specimens containing 20 and 25 mole % PuO_2 were oxidized isothermally and by programmed heating in a thermal-gravimetric balance. The final O/M ratio was deduced from the observed weight gain. The phases produced by the oxidation were identified by means of x-ray diffraction.

3. *Chem. Technol. Div. Annu. Progr. Rep. May 31, 1969,* ORNL-4422, p. 67.

4. *Chem. Technol. Div. Annu. Progr. Rep. May 31, 1970,* ORNL-4572, p. 54.

Coprecipitated and mechanically mixed fuels of the composition $U_{0.8}Pu_{0.2}O_2$ were oxidized to O/M ratios of ~2.55, the value expected if this composition obeys the published phase diagram for the U-Pu-O system. The O/M ratio of ~2.55 corresponds to a composition on the tie line between U_3O_8 and PuO_2 in the ternary system. Oxidation kinetics were very rapid while crossing the MO_{2+x} and $M_4O_9 + MO_{2+x}$ phase fields in the system and were relatively temperature insensitive over the temperature range 450 to 600°C. No pulverization of the fuel occurred during this stage of the oxidation. The ease of entry into the $M_4O_9 + M_3O_8$ phase field, however, was very temperature dependent, and total oxidation was achieved in 20 min or less in 100-mg specimens only at temperatures of 600°C or greater. All of the pulverization observed occurred during this stage of the oxidation. Very fine powders were produced during this stage of the process.

The oxidation of unirradiated homogeneous $U_{0.75}Pu_{0.25}O_2$ has been studied only for mechanically mixed fuel, and this material could not be oxidized beyond O/M = 2.36, which represents the edge of the $M_4O_9 + M_3O_8$ phase field. This material, after oxidation, consisted of an M_4O_9 phase having a lattice parameter a = 5.428 Å, which agrees with data that have been reported for this system.

Programmed-rate heating experiments provided similar results, which are shown in Fig. 2.8 for all three types of fuel. X-ray diffraction results indicated that the materials represented by curves *A* and *B* consisted of two phases, with M_3O_8 the major one and a cubic phase the minor. The material from curve *C* consisted only of an M_4O_9 phase, as expected, since the material was not pulverized by the oxidation procedure.

Some FTR-type pellets (mechanically mixed, 25% PuO_2) were oxidized in air at 750°C for 7 hr; this treatment reduced them to a fine powder. The powder was sieved, and the Pu/U ratio was determined for each fraction. About 96% of the material was finer than 200 mesh. Within experimental error, the plutonium concentration was uniform in all size fractions (Table 2.5); hence there is probably no plutonium segregation due to the voloxidation treatment. This conclusion is in agreement with the conclusion inferred from our dissolution tests.

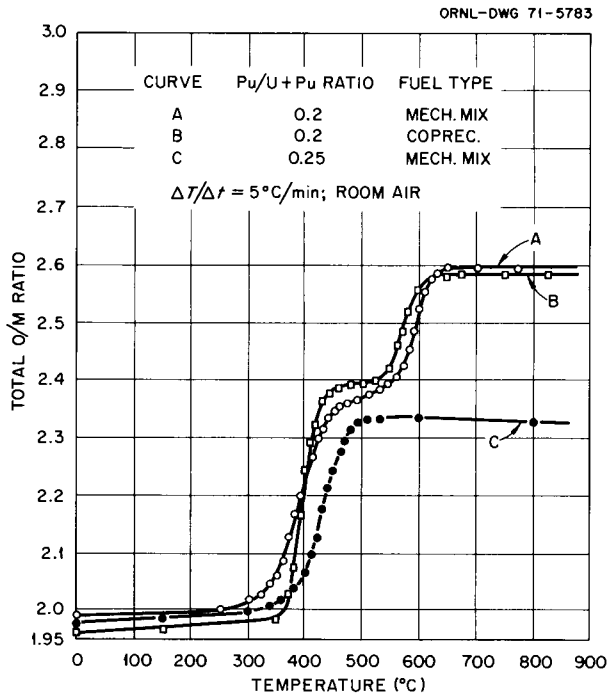

Fig. 2.8. Programmed-rate oxidation of UO_2-PuO_2 pellet fragments.

Table 2.5. Particle size distribution of FTR pellets after oxidation in air at 750°C for 7 hr

Screen size	Weight retained (g)	Amount retained (%)	Pu/U ratio
+80	0.0392	0.70	0.31
+100	0.0211	0.37	0.31
+200	0.1551	2.75	0.32
+325	1.3386	23.74	0.36
+400	0.7653	13.57	0.35
−400	3.3204	58.88	0.33
Total	5.6397	100	0.33 (original)

Voloxidation of Irradiated Fuels

Studies of the effect of oxidation variables on the release of volatile fission products were made with coprecipitated 20% PuO_2–80% UO_2 fuel that had been irradiated to about 1800 MWd/ton by the General Electric Company as their experiment F1F. The fuel rods were sheared in short lengths to release the fuel, which was then crushed and sieved. The plutonium, uranium, and ^{144}Ce concentrations were essentially the same for each of several different fractions over the size range of +30 to −200 mesh. The ^{137}Cs concentration, however, was about 70% higher in the −200-mesh fraction than in the +30-mesh fraction.

A 2^3 factorial voloxidation experiment was run with sieved fractions. Parameters of the tests were:

Particle size	Large, +30 mesh; small, −200 mesh
Time	16 and 4 hr
Temperature	550 and 350°C
Oxidant	Air

Statistical analysis of the results, based on the percent of the total ^{85}Kr in the fuel which was released during voloxidation, indicated that the major effect (95% confidence level) was particle size. The temperature and time-temperature interactions had a lesser effect (90% confidence level), while the time after 4 hr had a very small effect. The actual time required to release the ^{85}Kr may be as short as 1 hr, since the major conversion of UO_2 to U_3O_8 occurs in this time span. Contrary to expectations, the larger lumps of fuel (>30 mesh) released ^{85}Kr more readily and completely (up to about 60% at 550°C) than did the <100-mesh particles, which released up to 32% (Fig. 2.9). Based on the quantities of ^{85}Kr released and the proportion of large to small particles in the fuel, we calculated that from 37 to 39% of the ^{85}Kr would be released from a mixture of the two sizes; actual measurements showed that 41% of the ^{85}Kr was released when ½-in.-long segments of fuel rod were oxidized in the hot cell.

Additional experiments are planned to investigate these effects, which may be due to restructuring of the fuel during irradiation. It is possible that the ^{137}Cs-rich small particles came from the cooler outer radius of the inner portion. Variations in the quantity of ^{85}Kr released may also be related to the agglomeration of gas bubbles at grain boundaries, cracking, and other thermal effects.

Tritium Removal. Voloxidation removed tritium effectively from LMFBR fuel specimens. In tests with specimens that had been irradiated to 3630 or 14,500 MWd/ton, the amounts of tritium in the fuel solutions after dissolution of the voloxidized fuel were only 0.03 to 0.05% of the calculated amounts formed during irradiation (Table 2.6). Samples of the fuels that were

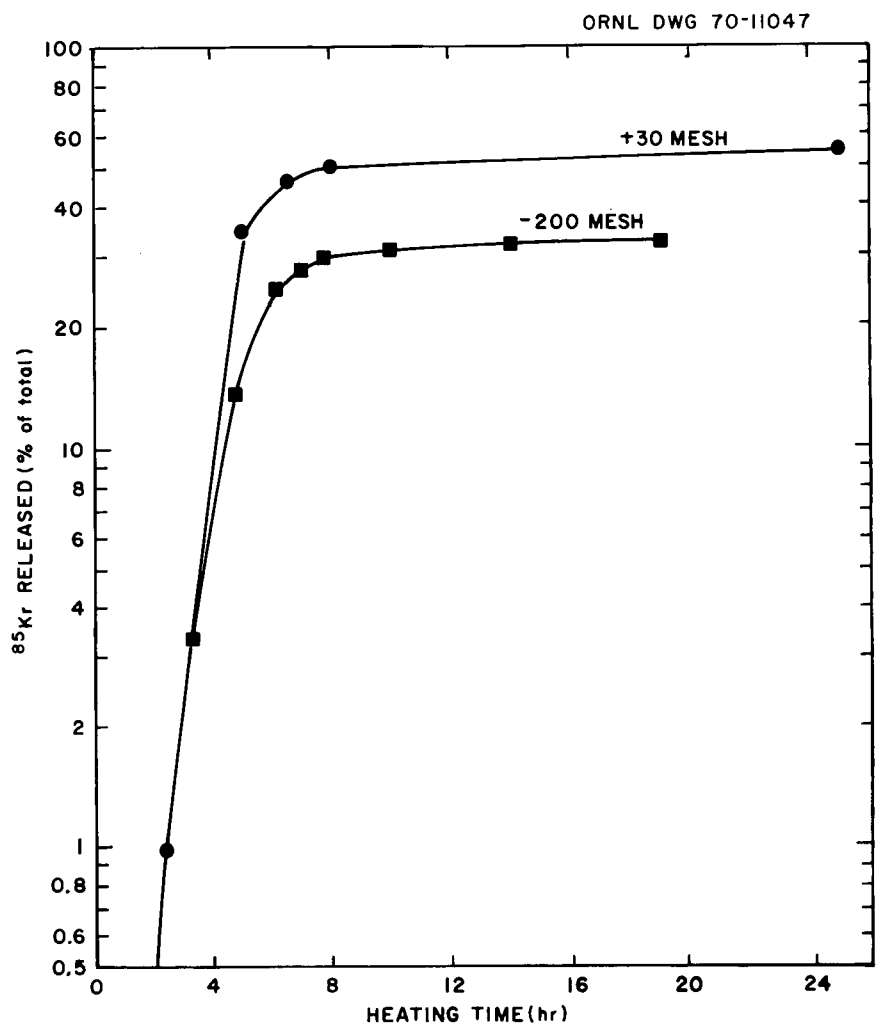

Fig. 2.9. Release of ^{85}Kr from 1800-MWd/ton $(U,Pu)O_2$ during oxidation with air at 550°C.

Table 2.6. Tritium content of solutions of oxidized fuel[a]

Fuel rod	Burnup (MWd/ton)	Irradiated in reactor	Linear heat rate (kW/ft)	Tritium in fuel solution	
				dis min^{-1} $[g(U,Pu)O_2]^{-1}$	Percent of total tritium[b]
				$\times 10^5$	
PNL X-1	3,630	EBR II	5.3	1.0	0.05
PNL 59-5	14,500	GETR	11.5	2.5	0.03

[a]Crushed 25% PuO_2–75% UO_2 pellets oxidized for 6 hr in air at 650°C and dissolved in HNO_3.
[b]Based on calculated amount produced during irradiation.

dissolved directly (without voloxidation) gave solutions with tritium concentrations equivalent to about 2 to 4% of the calculated yields. Apparently, more than 95% of the tritium had escaped from the fuel during irradiation. Based on the amounts present in the irradiated fuels, the voloxidation treatment (6 hr in air at 650°C) removed more than 98% of the tritium.

LWR Fuels. Voloxidation treatment (4-hr oxidation at 450°C) of pellet fragments from a blanket rod from core 1 of the Shippingport PWR, which operated at a linear heat rating of 4.85 kW/ft, released more than 99% of the tritium but only about 12% of the ^{85}Kr during the conversion from UO_2 of about 95% theoretical density to <200-mesh U_3O_8 powder. We attribute the low release of ^{85}Kr to the microdispersion of the krypton at the individual fission sites; restructuring of the fuel would have moved the fission gases to the grain boundaries, where they could be more easily released upon oxidation of the UO_2 to U_3O_8 powder. We will continue the studies as more typical BWR and PWR fuels become available.

Voloxidation Equipment

An electrically heated cylindrical-shaped rotary calciner (6.5 in. in diameter by 7.5 ft long; 1–12 rpm; maximum temperature, 800°C) was purchased for investigation of processing parameters in the voloxidation step. The calciner can be operated with a reducing or an oxidizing atmosphere, and the interior is equipped with lifting flights to cascade material through the gas stream. Six runs were made with the unit using 1-in. sheared lengths of porcelain-filled stainless-steel-clad prototype LMFBR fuel to determine the solids holdup under steady-state operation conditions.

Data from four of the six runs are summarized in Table 2.7. In each of the runs, sheared prototype fuel was fed into the calciner at a constant rate until the weight of material being discharged from the calciner per unit time was essentially constant. Steady state was reached in 2 to 3 hr. At the end of a run the amount of material remaining in the calciner was removed and weighed. The residence time of the sheared prototype fuel is about 50 min for a feed rate up to 400 g/min; however, at feed rates higher than 500 g/min, material is apparently forced through the rotating retort tube at a faster rate, causing a decrease in the residence time. Apparently this feed rate, or one near it, floods the unit.

Table 2.7. Steady-state operation of the rotary calciner (voloxidizer) with prototype LMFBR fuel[a]

Time-averaged feed rate[b] (g/min)	Run time (hr)	Volume holdup fraction[c]	Residence time[d] (min)
83	3.5	0.06	48.3
183	5.5	0.15	52.5
354	3.2	0.26	48.4
536	3.0	0.36	43.2

[a]Calciner: slope = ⅛ in./ft; 4 rpm; total volume = 43.2 liters. Simulated fuel: 0.25-in.-diam × 15-mil-wall-thickness stainless steel tubing filled with porcelain (0.215 in. diam × 1.5 in. long; bulk pour density of 1.5 g/cc).
[b]Total weight of material fed (g)/total running time (min).
[c]Bulk volume of fuel in calciner at steady state (cc)/total volume of calciner (cc).
[d]Weight of material in calciner at end of run (g)/time-averaged feed rate (g/min).

During run 5, a fixed volume of the sheared prototype fuel was fed into the calciner every minute at a time-averaged feed rate of 650 g/min. After 50 min of operation, the sheared pieces had accumulated at the rear of the calciner to the extent that no additional material could be fed through the vibrating feeder.

In run 6, sheared prototype fuel was hand-fed to the calciner at a time-averaged feed rate of 179.2 g/min for 4.5 hr. The discharge rate was equal to the feed rate after 3 hr. At that time, 75 sheared fuel lengths (180 g), which had been painted yellow, were fed to the calciner. The first piece came out of the calciner after 32 min, and half of the color-coded material had been discharged after 49.2 min. All but one piece had been discharged after 85 min. After 4.5 hr of operation, the volume holdup fraction within the calciner was 0.14 and the calculated residence time was 50.7 min, in agreement with the data of Table 2.7.

For a fixed slope and rotational speed, the fuel residence time in the calciner is independent of the feed rate for bulk holdup volumes up to about 25% of the total volume available. The normally recommended[5] volume holdup fraction for rotary dryers is between 0.05 and 0.15. With a required residence time of 50 min and a volume holdup fraction of 0.1, the rotary calciner throughput with sheared stainless-steel-clad UO_2-PuO_2 fuel (bulk density = 4.5 g/cc) is estimated to be 23.4 kg/hr. For a required residence time of 2.5 hr, the throughput with the same fuel would be decreased to 7.8 kg/hr.

2.4 DISSOLUTION AND FEED PREPARATION

Data on the leaching of irradiated fast reactor fuels are relatively limited. Information is needed concerning the dissolution rate and the metal recoveries to be expected as a function of the preparation history, the irradiation conditions, and the postirradiation temperature history of the fuel. We are procuring irradiated oxide fuels from as many sources as possible for testing. In addition to metal recovery data, information concerning the composition and physical characteristics of the leach residues is being obtained. Particular attention is also being given, both in laboratory and hot-cell studies, to the behavior of iodine in the dissolver-condenser system and to the use of fumeless dissolving techniques for minimizing the volume and fume content of the off-gas to allow easier separation and containment of the iodine, ^{85}Kr, and ^{133}Xe.

Dissolution Rate Studies with Unirradiated UO_2-PuO_2 Pellets

Dissolution experiments with unirradiated FTR-type (mechanically blended 25% PuO_2–75% $^{238}UO_2$) pellets obtained from WADCO were completed. The pellets were leached with boiling 8 *M* HNO_3 (1) in the "as received" condition, (2) after oxidation at 450 or 750°C in air, or (3) after being heat treated for 7 hr at 1450°C in argon–4% H_2. None of these treatments had a significant effect on the leaching results. After leaching for 18 hr, 1 to 1.5% of the uranium and 14 to 15% of the plutonium remained undissolved. Initial dissolution rates were faster for the oxidized pellets due to a resulting increase in surface area; however, the final values were unchanged. The results were fitted to an equation of the type

$$R = S_1 e^{S_2 t} + S_3 e^{S_4 t} + S_5 ,$$

where R represents the percent remaining as a function of time t, in minutes. A typical fit, with the constants for both uranium and plutonium, is shown in Fig. 2.10.

A summary of the data from these experiments is shown in Fig. 2.11. The 16% of the plutonium and the 1.3% of the uranium that remain undissolved after extensive leaching represent the 5% of the total weight of undissolved $(U,Pu)O_2$ previously reported by Lerch, at WADCO,[6] and by us.[7] On the basis of these results, we conclude that the dissolubility of the pellets in boiling 8 *M* HNO_3 is not significantly affected by voloxidation or the heat treatment at 1450°C. Similar pellets manufactured by Nuclear Materials and Equipment Corporation are being characterized under the same conditions.

Hot-Cell Tests

Analysis of the plutonium in the residues from dissolution experiments with the General Electric F1 group coprecipitated 20% PuO_2–80% UO_2 (1800 MWd/ton) fuel rods (14 experiments) and with fuel rods that had been oxidized (10 experiments) showed little difference due to the voloxidation treatments. We found 0.21 ± 0.12% of the plutonium in the residues from the untreated fuel and 0.19 ± 0.08% in the residues from the fuel that had been oxidized. The Pu/(U + Pu) ratios in the residues were about the same as in the original fuel; this contrasts with other leaching results with unirradiated, mechanically blended pellets which left a plutonium-rich residue.

Dissolution of Sol-Gel Microspheres. We have been determining the effects of irradiation on the dissolution

5. H. Perry, *Chemical Engineer's Handbook*, 4th ed., sect. 20, p. 20, McGraw-Hill, New York, 1963.

6. C. R. Cooley, *Application of Aqueous Technology to LMFBR Separations Processes, Progress Report for August 1970*, WHAN-IR-26-AUG (September 1970).

7. *LMFBR Fuel Cycle Studies Progress Report for September 1970, No. 19*, ORNL-TM-3180.

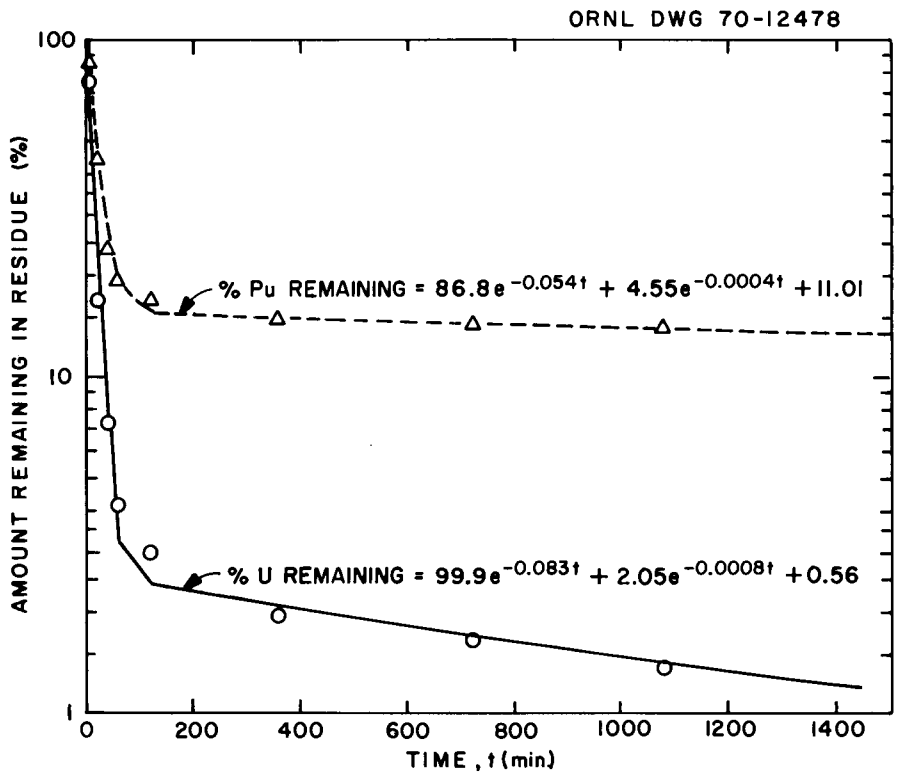

Fig. 2.10. Rate of leaching of plutonium and uranium from FTR-type pellets with boiling 8 *M* HNO_3.

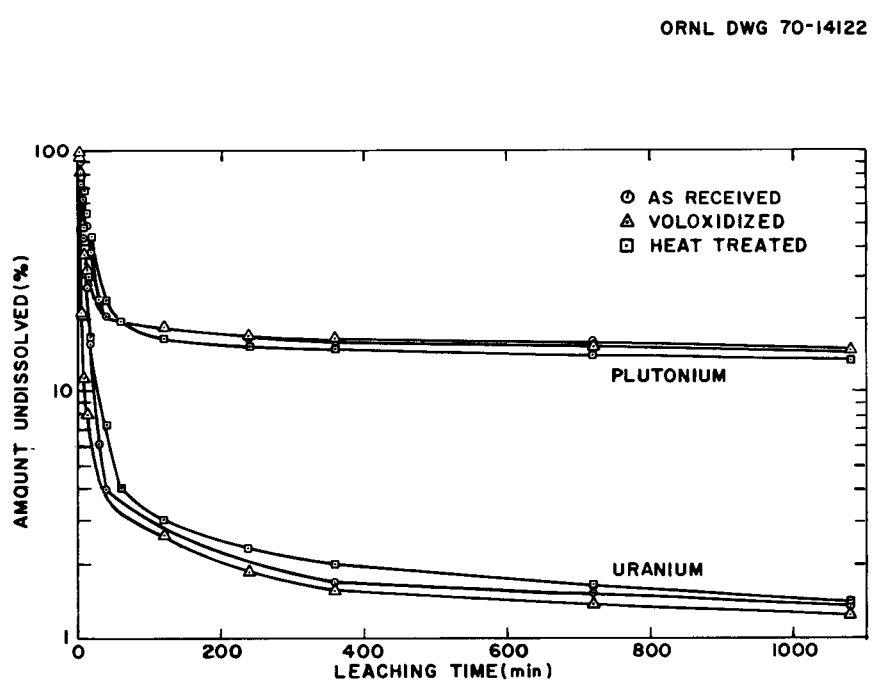

Fig. 2.11. Dissolubility of FTR "Reference" pellets in boiling 8 *M* HNO_3.

of 15% PuO_2–85% UO_2 sol-gel microspheres in boiling 8 M HNO_3. In the experiments, we dissolved both unirradiated microspheres and declad sieved microspheres that had been irradiated to 0.6% and 4.2% FIMA (fissions per initial metal atom) as ORNL experiments 43-112 and 43-115. Figures 2.12 and 2.13 show the quantities of undissolved plutonium and ^{106}Ru as a function of leaching time and particle size. The uranium curves, which are not shown, have similar shapes; however, the amounts dissolved at equivalent leaching times are about a factor of 10 lower.

Equations have been formulated for the dissolution of the plutonium in the coarse (C) and fine (F) fractions of the 15% PuO_2–85% UO_2 sol-gel microspheres. The equations are of the form $R = S_1 e^{S_2 t} + S_3 e^{S_4 t} + S_5$, where R is the percent of the plutonium remaining as a function of time, t. The calculated values of the constants are:

Run No.	S_1	S_2	S_3	S_4	S_5
43-112-1C	98	−0.055	0.11	−0.00057	1.89
43-112-3C	98	−0.046	0.16	−0.0025	1.84
43-112-1F	98	−0.200	1.07	−0.00020	0.93
43-112-3F	98	−0.162	1.09	−0.001	0.91
43-115-4C	98	−0.119	0.03	−0.0002	1.97
43-115-4F	98	−0.160	0.09	−0.0004	1.91

For the runs with low-burnup material (43-112), the coarse fraction dissolved at an average rate $R = 98e^{-0.050t} + 0.135e^{-0.0015t} + 1.87$; the average rate for the fine fraction was $R = 98e^{-0.181t} + 1.08e^{-0.0006t} + 0.92$.

The rate of dissolution and the quantity of plutonium that dissolved appeared to increase with irradiation for both the coarse and the fine fractions of microspheres, while ^{106}Ru became more insoluble as the burnup was increased. However, the dissolution behavior of the 43-112-1 coarse fractions was different from that of the 43-112-3 coarse fractions. We think that this is related to differences in fabrication rather than irradiation effects because the plutonium dissolution curves of both the low-burnup samples of fine microspheres were identical. In addition, ^{106}Ru behavior was replicated for each of the coarse and fine fractions of the two rods at low burnup.

The greater solubility of the plutonium in the coarse fraction over that in the fine fraction, regardless of burnup, is a peculiarity of these old (1966) batches of microspheres. The residues from these particular batches of 15% PuO_2–85% UO_2 fuel contained from 30 to 74% PuO_2. The overall plutonium concentrations of the two samples of fine fractions after irradiation were 13.9 and 14.7%. Newer (1970) batches that we have tested have dissolved completely. Comparison of the dissolubilities of the "reconstituted" fuel (obtained by adding the results of coarse and fine fractions together) indicates that a higher fuel operating temperature and a higher burnup decreased the amount of insoluble plutonium (Table 2.8).

Table 2.8. Comparison of the dissolubilities of reconstituted fuel

Fuel rod No.	Linear heat rate (kW/ft)	Burnup (% FIMA)	Amount insoluble after 6 hr of leaching (%)	
			Uranium	Plutonium
43-112-1(F+C)	8.4	0.50	0.04	0.34
43-112-3(F+C)	13.6	0.68	0.02	0.29
43-115-4(F+C)	13.4	4.20	0.01	0.03

Fumeless Dissolution of UO_2 Pellets

Uranium dioxide pellets were dissolved in nitric acid in a closed system maintained at a constant pressure by adding oxygen at the rate it was being consumed. The dissolution of UO_2 can be written as follows:

$$2UO_2 + 6HNO_3 \rightarrow 2UO_2(NO_3)_2 + NO + NO_2 + 3H_2O\ .$$

In a closed system and in the presence of excess oxygen, the net reaction becomes:

$$2UO_2 + 4HNO_3 + O_2 \rightarrow 2UO_2(NO_3)_2 + 2H_2O\ .$$

In the laboratory experiments, sufficient oxygen was supplied to a dissolver to maintain a constant pressure that was equivalent to about 2 in. H_2O below atmospheric pressure. The nitrogen oxides formed during the dissolution reacted with oxygen and redissolved in water in a downdraft condenser that was fitted to the dissolver. The uranium dissolved at the rate of about 1.5 g/min at 75°C in the flask and condenser, each of about 500 ml capacity. As the dissolution proceeded, the temperature was increased to maintain a high dissolution rate. Total dissolution of the UO_2 in 6 M HNO_3 to produce a Purex feed solution (~350 g/liter U, 2.5 N HNO_3) required about 4 hr.

Volatilization of Iodine from Feed Solutions

Variables affecting the volatilization of iodine from nitric acid solutions are being studied as guidelines for the development of methods for achieving efficient

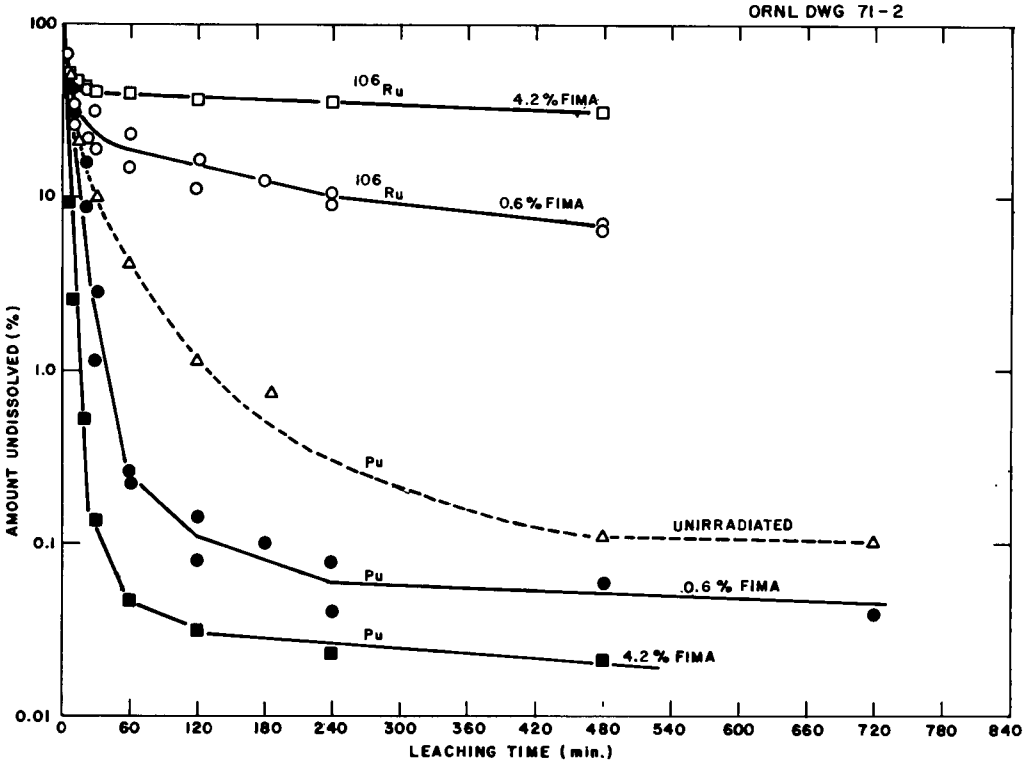

Fig. 2.12. Dissolution of sol-gel 15% PuO_2–85% UO_2 microspheres in boiling 8 *M* HNO_3. Coarse (>250-μ) fraction.

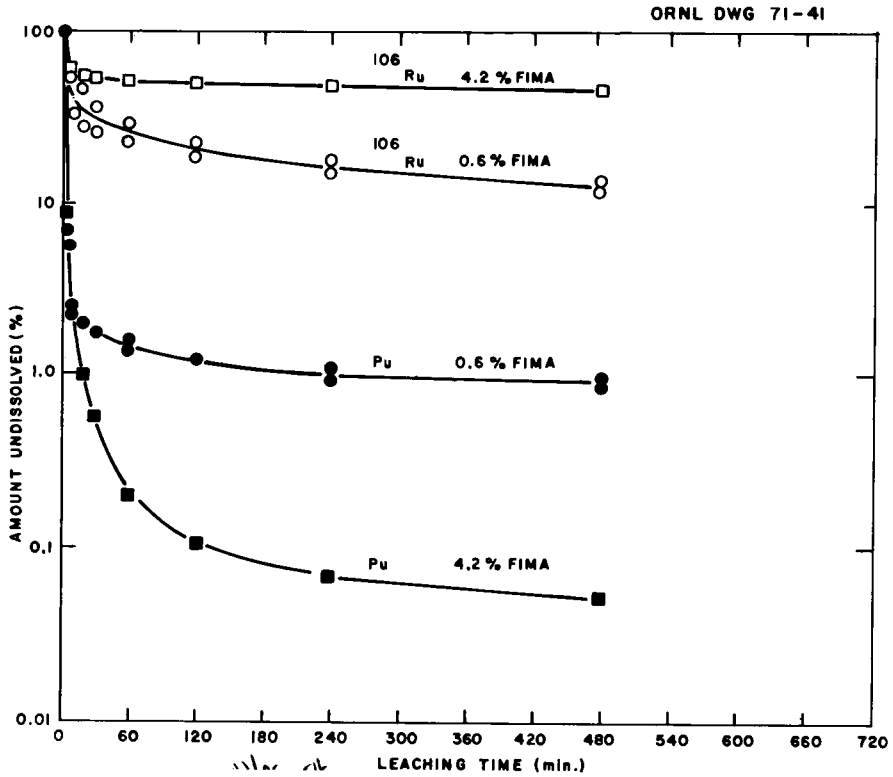

Fig. 2.13. Dissolution of sol-gel 15% PuO_2–85% UO_2 microspheres in boiling 8 *M* HNO_3. Fine (<250-μ) fraction.

removal of iodine from the solvent extraction feed solution. Separation of essentially all of the iodine from the uranium and plutonium prior to solvent extraction would greatly facilitate attainment of the very high processing plant retention factors for iodine that will be needed in processing short-cooled fuels.

As described previously,[8] we have experienced difficulties in volatilizing iodine completely from 4 *M* HNO_3 solutions that initially contained ^{131}I-traced I_2 at a concentration of about 10^{-4} *M*. The ^{131}I remaining after volatilization of most of the iodine (by distilling a small fraction of the solution or by sparging) does not exchange readily with fresh carrier iodine added to the system. The hydrolytic reaction

$$I_2 + H_2O \rightleftharpoons HOI + H^+ + I^-$$

may be the source of the difficulty. Rapid oxidation of the I^- by the nitric acid solution (catalyzed by some ever-present concentration of nitrite) essentially prevents the above reaction from being a true equilibrium. The ^{131}I is thereby trapped to some degree as HOI (or some derivative), with reversibility to the I_2 form being prevented by the lack of a true equilibrium in the hydrolytic reaction. Tests also have shown that small amounts of chloride impurity in the nitric acid solution can greatly increase the amount of the nonvolatile nonexchangeable iodine formed. Presumably the presence of chloride results in the formation of ICl or ICl_2^-.

As shown in Fig. 2.14, volatilization of iodine from 4 *M* HNO_3 becomes more difficult as the iodine concentration in the solution is decreased. In these tests, N_2O_3 was bubbled slowly into the solution to maintain the iodine in the I_2 state. The value of the iodine partition coefficient ($H = C_L/C_g$), corresponding to the initial portion of the volatilization curve, increased from 10 to 150 as the iodine concentration in the initial solution was decreased from 2.5×10^{-4} to 2.5×10^{-8} *M*. The partition coefficient is calculated from the equation

$$H = \frac{V_g}{V_L \ln (C_0/C)},$$

where the *C* refers to the aqueous iodine concentration and V_g and V_L are the respective volumes of gas and liquid involved in the distillation (or gas sparging) process. The partition coefficient *H* has a limiting value

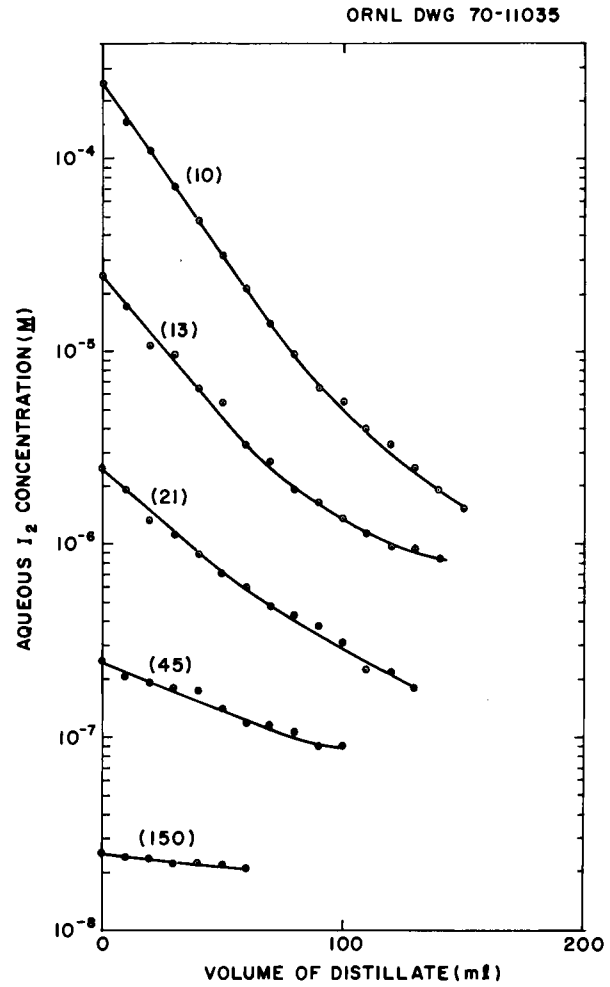

Fig. 2.14. Effect of initial iodine concentration on volatilization of iodine from 4 *M* HNO_3 by distillation. Initial solution volume was 4 liters. Numbers in parentheses show the approximate iodine partition coefficient for the initial portion of the curve.

of H_s at I_2 saturation, defined by the equation

$$H_s = \frac{C_s RT}{p^0},$$

where C_s is the saturation concentration (moles/liter) and p^0 is the saturation pressure of solid I_2. The value of H_s at 100°C has been calculated to be 8.9, which is in reasonable agreement with the value of 10 for the run with the highest I_2 concentration in Fig. 2.14.

The differences in the solubility of iodine (I_2) in water and in nitric acid concentrations ranging from 4 up to 16 *M* are not significantly large at 25°C (Table 2.9). This signifies that the differences in H_s are also not large. (We assume that the iodine is completely in

8. *Chem. Technol. Div. Annu. Progr. Rep. May 31, 1970,* ORNL-4572, pp. 58–60.

Table 2.9. Solubility of iodine in water and nitric acid solutions at 25°C

Solvent	Iodine solubility[a] (10^{-3} *M* units)	
H_2O	1.48	1.50 (21)
4 *M* HNO_3	1.65	1.81 (20)
8 *M* HNO_3	1.85	1.85 (17) 1.83 (41)
12 *M* HNO_3	1.63	1.93 (20)
16 *M* HNO_3	1.71	2.35 (20)

[a]The first column of values was determined (by filtering off solid I_2 and measuring the activity of the filtrate) almost immediately after addition of the KI. The numbers in parentheses after the values in the second column indicate the time, in hours, at which the solubility values listed in this column were determined.

the I^0 state, a condition which is maintained only with difficulty at high nitric acid concentrations.) The H_s value at 25°C for 4 *M* HNO_3, assuming a C_s value of 1.7 $\times 10^{-3}$ *M*, is 93.

Steam distillation tests, similar to those yielding the data for Fig. 2.14, were carried out at nitric acid concentrations of 8, 10, 12, and 16 *M*. The volatility of iodine from 8 *M* acid is similar to that from 4 *M* acid, although somewhat more nitrite must be used to maintain the desired I^0 oxidation state. Distillation from 10 *M* HNO_3 is difficult unless frequent additions of nitrite are made to the solution (after cooling down below the boiling point) to reduce any iodate formed. Distillation from 12 to 16 *M* acid is almost impossible, due to the difficulty of keeping the iodine in the I^0 state.

Studies of the exchange of fresh carrier iodine with the ^{131}I that remains in the solution after volatilization of most of the iodine have shown that the exchange is reasonably rapid at temperatures of 135°C and higher (Table 2.10). Autoclaving of the solution, therefore, may be a feasible method of achieving a high degree of iodine removal. The solution would pass from the autoclave to a flash evaporator. If 99% of the ^{131}I can be removed in one distillation step (during or following dissolution), then a second distillation after addition of cold iodine (for isotopic dilution) followed by autoclaving may be capable of achieving 99.99% removal. A small laboratory autoclave has been constructed and will be operated to determine the effects of time, temperature, and possibly other variables [such as radiation density, fission products, impurities, and major fuel constituents (U, Pu)] on the isotopic exchange kinetics.

Table 2.10. Effect of autoclave treatments on exchange of carrier iodine with ^{131}I

Procedure: 5 ml distilled from a total of 35 ml of solution after specified autoclave treatment. Original solution in all tests was a 4 *M* HNO_3–5 $\times 10^{-4}$ *M* I_2 solution. (A previous distillation treatment had converted most of the ^{131}I to the nonvolatile nonexchangeable form; carrier iodine was then added to the specified concentration.)

Autoclave time (hr)	Percent of initial ^{131}I remaining after distillation test with autoclave temperature of –			
	110°C	125°C	135°C	150°C
0.16		61.2		29.2
0.5		57.9	33.0	16.4
1.0		39.6		9.6
1.5		29.4		
18	22.9	5.5		

Dissolution Equipment

An extensive state-of-the-art study was made of existing equipment and concepts for the dissolution of sheared nuclear power reactor fuels.[9] No system was found to have all the necessary attributes for processing sheared LMFBR fuels. As part of the study, some new dissolver concepts were developed. These concepts represent current approaches to continuous dissolution methods and hopefully have the necessary features to meet the requirements of residence time, mixing, fuel feeding, transport and discharge, criticality, and off-gas collection.

It appears that an effective dissolver for LMFBR fuels could be developed from a combination of the desirable features found in the existing equipment and concepts and those exemplified by the new concepts.

Forward Mixing in a Continuous Dissolver. A mathematical study of forward mixing of sheared fuel was made to determine whether rotary, "cement-mixer" type, continuous dissolvers should, as a class, be discounted for consideration in LMFBR reprocessing concepts. Several variations of the cylindrical, longitudinally baffled design have been proposed as new LMFBR dissolution concepts. In these concepts, sheared fuel is transported through a dissolver by the rotary motion of the unit. Should extensive forward mixing occur, pieces of sheared fuel could be discharged

9. W. S. Groenier, *Equipment for the Dissolution of Core Material from Sheared Power Reactor Fuels,* ORNL-TM-3194 (March 1971).

without adequate dissolution time; this could significantly decrease the overall leach efficiency.

Treating the unit as a series of well-mixed stages, it was concluded that, although both forward mixing and back mixing do occur between stages, they do not significantly affect the quantity of off-specification product from a unit having many stages. The amount of material that is involved in interstage mixing at any time can be determined from the probability age distribution function. Similarly, the overall age distribution of the product can be calculated. For example, for a typical urania-plutonia dissolution-rate-vs-time relation, the amount of fuel undissolved after 10 hr decreases from about 1% for a 2-stage unit to about 0.01% for a 20-stage unit, and to about 0.002% for a system exhibiting no forward mixing.

The utility of a dissolver having forward mixing will primarily depend upon the length of a stage, which is not known at this time. The relative complexity of systems that feature a positive material transfer will also have a bearing on the acceptance of rotary dissolvers.

Table 2.11. Effect of temperature on plutonium stripping with 0.3 *M* HNO_3

Organic: 15% TBP–85% *n*-dodecane containing 5.2 g of Pu(IV) per liter
Aqueous: 0.3 *M* HNO_3
Contact: Batch at an aqueous/organic phase ratio of 2/1

Temperature (°C)	Organic plutonium concentration (g/liter)	Pu(IV) in aqueous (% of total[a])	Plutonium stripping coefficient, S_o[a]
25	0.503	>99	4.4
30	0.487	99	4.6
35	0.497	98	4.3
40	0.437	~90	5.0
45	0.414	86	5.2
50	0.383	80	5.8
55	0.340	74	6.6
60	0.302	68	7.2

[a]Total plutonium in aqueous was about 2.2 g/liter. Amount of Pu(IV) present was determined by TTA extraction; presumably the balance of plutonium was Pu(III) + Pu(VI) since other identification tests showed no significant amount of polymer present.

2.5 SOLVENT EXTRACTION WITH TBP

Emphasis in the solvent extraction studies has been centered on establishing flowsheet conditions for the interim processing of LMFBR fuels in an existing plant. The reference first-cycle solvent extraction flowsheet is based on the use of 15% TBP and feeds of low plutonium concentration in existing geometrically unrestricted equipment. Neutron absorbers might also be used for criticality control. The overall process calls for the coextraction and partitioning of plutonium from uranium in the first cycle, followed by two TBP cycles for further purification of the plutonium. Laboratory studies of these flowsheets with simulated feeds are essentially complete, but tests with radioactive feeds to verify their suitability are needed. Emphasis in the laboratory studies is shifting to definition of the most suitable flowsheets for use in plants designed specifically for processing LMFBR fuels. Alternatives to TBP extraction for plutonium isolation such as, for example, high-pressure ion exchange will also be examined.

Recent studies have been concerned primarily with improving the efficiency of stripping plutonium from TBP and with determining the effect of variations in temperature on the extraction and stripping processes.

Effect of Temperature

Because of the relatively high plutonium concentrations, operation at higher than ambient temperatures is necessary at certain points in the flowsheet to ensure that third-phase formation does not occur.[10] Tests were made with plutonium and uranium separately to more accurately define the effect of temperature on the extraction of each.

Plutonium(IV) extraction from moderately concentrated HNO_3 (3 to 4 *M*) was essentially independent of temperature. However, in extractions from 0.3 *M* HNO_3, the coefficient decreased by a factor of about 4 as the temperature was increased from 30 to 60°C. Apparently the large effect at low acidity is due to an increase in disproportionation of Pu(IV) to less-extractable species as the temperature is increased (see stripping data of Table 2.11).

Uranium extraction coefficients at acid concentrations of 0.3 to 3 *M* and at low uranium loadings decreased by a factor of about 2 as the temperature was increased from 30 to 60°C; at high solvent loadings, the effect was much less (Fig. 2.15). These data were fitted by computer to an equation readily applicable to the SEPHIS computer code[11] for simulation of a Purex extraction cascade. The uranium extraction coefficient, E_{T_2}, at low loadings (<15% of saturation, assuming 2 moles of TBP per mole of U) can be calculated for

10. *Chem. Technol. Div. Annu. Progr. Rep. May 31, 1970,* ORNL-4572, p. 61.

11. Ibid., p. 60.

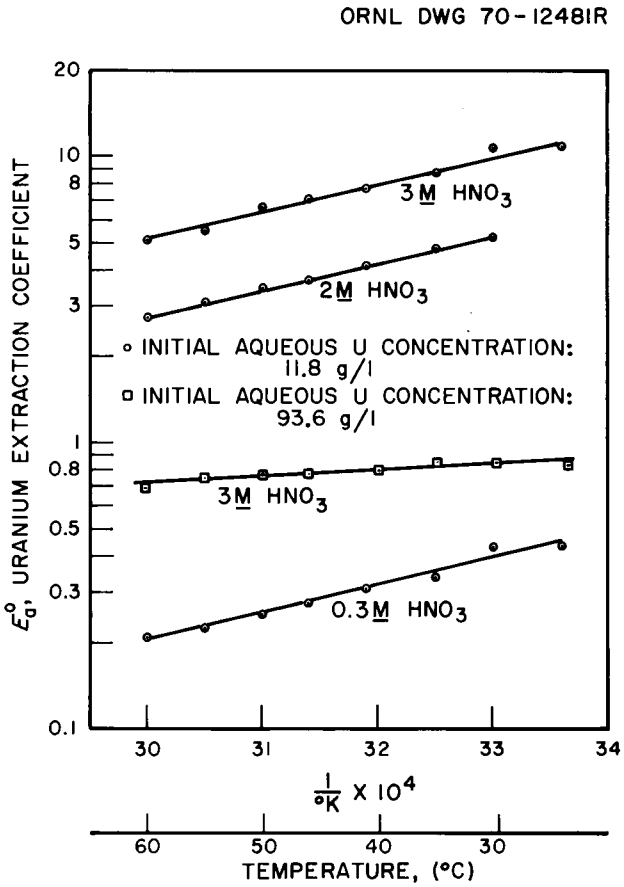

Fig. 2.15. Effect of temperature on uranium extraction from nitric acid with 15% TBP–85% *n*-dodecane. Phase ratio of 1/1.

temperatures between 25 and 60°C:

$$E_{T_2} = E_{T_1} \times e^{2220(1/T_2 - 1/T_1)} ,$$

where T is the absolute temperature and E_{T_1} is the experimentally determined extraction coefficient at 25°C.

Plutonium Stripping

The minimum acid concentration for stripping plutonium has been set at 0.3 *M* to decrease the possibility of forming undesirable plutonium polymer in the stripping system. The stripping coefficient at this acidity increases as the temperature is increased. This apparently is at least partly caused by disproportionation of Pu(IV) to Pu(III) and Pu(VI) at this low acidity, the extent of disproportionation increasing as the temperature is increased. This is shown in the data of Table 2.11; the fraction of the total plutonium in the aqueous strip solution that was present as Pu(IV) decreased from more than 99% at 25°C to about 68% at 60°C.

Table 2.12. Plutonium stripping with various reagents

Organic: 15% TBP–85% *n*-dodecane containing about 0.2 g of Pu per liter
Contact: Batch at an organic/aqueous phase ratio of 2/1

Stripping solution	Pu stripping coefficient, S_o[a]			
	23°C		40°C	
	1 min	3 min	1 min	3 min
0.3 *M* HNO_3	1.6	1.5		
0.3 *M* HNO_3–0.02 *M* hydroxylamine nitrate	8.1	9.5	15	37
0.3 *M* HNO_3–0.02 *M* hydroxylamine nitrate–0.01 *M* hydrazine	6.2	7.8	13	31
0.3 *M* formic acid	3.2			
0.3 *M* acetic acid	4.0			

Although stripping with dilute acid alone is practicable, reduction of at least part of the plutonium has the advantages of increasing the stripping efficiency and allowing the preparation of more concentrated plutonium product solutions. Reducing agents and potential complexing agents have been tested as aids in stripping; emphasis has been centered on reagents that subsequently can be converted to nonobjectionable compounds. Hydroxylamine nitrate appears to be the most effective of the reductants tested, although the reduction reaction is known[12,13] to be slow. Increasing the temperature from 23 to 40°C appreciably increased the reaction rate (Table 2.12). Both formic and acetic acids stripped plutonium more effectively than nitric acid. Formic acid, like hydroxylamine nitrate, can be readily destroyed to yield products that would not contaminate the plutonium.

Third-Cycle Demonstration

A batch countercurrent demonstration of the third TBP cycle was made with simulated third-cycle feed at 40 to 45°C using the total stages available in a glove box (five for extraction, one for scrubbing, and five for stripping). The plutonium was stripped with 0.3 *M* HNO_3–0.02 *M* hydroxylamine nitrate–0.01 *M* hydrazine. Plutonium recovery in the extraction step was apparently considerably higher than 99.5% (Table 2.13)

12. J. M. McKibben and J. E. Bercaw, *Hydroxylamine Nitrate as a Plutonium Reductant in the Purex Solvent Extraction Process*, DP-1248 (January 1971).

13. R. L. Walser, *The Hanford Purex Plant Experience with Reductants*, ARH-SA-69 (July 17, 1970).

Table 2.13. Batch countercurrent third-cycle extraction and stripping at 40–45°C

Organic: 15% TBP–85% *n*-dodecane
Feed solution: 41.3 g of Pu per liter; 4 *M* HNO_3; 0.04 *M* Fe^{3+}
Scrub solution: 2 *M* HNO_3
Strip solution: 0.3 *M* HNO_3–0.02 *M* hydroxylamine nitrate–0.01 *M* hydrazine
Organic/feed/scrub/strip: 30/30/4/15
Contact time: 2 min

Stage No.	Organic phase		Aqueous phase	
	Pu (g/liter)	HNO_3 (*M*)	Pu (g/liter)	HNO_3 (*M*)
Strip-5	0.11	0.019	8.9	0.40
-4	2.9	0.028	25.5	0.37
-3	12.4	0.043	44.3	0.41
-2	22.8	0.025	63.1	0.59
-1	34.4	0.039	76.7	0.64
Scrub	40.5	0.079	30.1	2.42
Extr.-1	43.6	0.11	23.9	3.80
-2	23.9	0.25	6.0	3.90
-3	4.9	0.39	0.69	4.09
-4	0.89	0.42	<0.2	3.99
-5	0.10	0.41	<0.2	3.71

but was not measured accurately because of appreciable interference from americium that was present in the raffinate. No third-phase formation occurred even though the 15% TBP solvent had a plutonium concentration at the feed stage of 43.6 g/liter (at 23°C, third-phase formation occurs at a solvent loading of about 25 g per liter). About 99.7% of the plutonium was stripped in five stages at an organic/aqueous phase ratio of 2/1 to give a product solution containing about 77 g of plutonium per liter. The strip solution contained hydroxylamine nitrate to provide partial reduction of the plutonium and thereby improve the stripping efficiency in the last strip stages. Use of an additional one or two stages apparently would have provided complete recovery of plutonium from the solvent.

2.6 OFF-GAS TREATMENT

The retention or control of iodine is one of the major problems to be solved in the development of short-decay processing capability for LMFBR fuels. Overall plant retention factors approaching 10^8 will be required for ^{131}I when 30-day-decay fuel is processed. In order to achieve an iodine retention of this order, new and highly reliable systems for removing iodine from all plant effluent streams must be developed. A significant reduction in the volume of all plant effluents, as compared with past experience, will be necessary to improve the economics of the required treatment systems.

Increased emphasis on reducing all discharge from processing to levels that are "as low as practicable" has generated interest in removal systems applicable to tritium removal. Numerous potential methods for control of volatile fission product emissions are being studied. During this report period, laboratory studies were conducted on cold trapping for tritium and iodine removal, iodine removal by scrubbing with concentrated nitric acid, and the application of various solid sorbents for iodine removal. An engineering-scale (400-cfm) iodine removal system using solid sorbents was installed and successfully operated on the TRU cubicle and vessel off-gas stream.

Cold Trapping of Iodine and Tritium Oxide

Calculations show that cold trapping at a temperature in the range of –75 to –125°C offers a potentially attractive method for collecting into a small volume most of the iodine and tritium oxide from the oxidizing gas stream effluent from a fuel voloxidation treatment system (see Sect. 2.3). A cold trap was constructed and has been operated at temperatures in the range of –60 to –85°C with I_2 at concentrations of 0.25 to 1 mg per liter of N_2. Effluent gas is sparged through 1 *M* NH_4OH–0.1 *M* $(NH_4)_2S_2O_3$ solutions to collect uncondensed I_2. The cold trap is eluted with nitrogen to remove the collected iodine. Depending on the total gas flow rate, iodine decontamination factors varied from 45 to 190 under the conditions mentioned above. Other tests were performed in which water vapor was added to the gas stream at concentrations of 1 to 5 mg per liter of N_2 and carbon dioxide was added at 0 or 90 mg per liter of N_2. However, in no case did more than 3% of the injected iodine emerge from the short stainless steel gas-mixing system. Although it has not yet been proved, it is likely that the iodine reacted, in the presence of water, with the stainless steel. This suggests an additional technique for removing iodine from a gas stream.

Scrubbing Methyl Iodide from Air with Concentrated Nitric Acid

Hot concentrated nitric acid is an effective agent for the destruction of methyl iodide, with the iodine being retained in solution in the pentavalent form. An iodine trapping process based on the use of nitric acid, which is available in the processing plant, therefore appears attractive for the removal of methyl iodide and free

iodine from various gas streams expected to be encountered in fuel reprocessing, particularly in the head end of the plant, where the amount of iodine to be handled would be large. Several process variations have been considered, but the one which we prefer involves use of refluxing concentrated nitric acid.

The destruction of methyl iodide by concentrated nitric acid presumably proceeds by the following reactions:

$$CH_3I \xrightarrow{HNO_3} CO_2 + \tfrac{3}{2}H_2O + \tfrac{1}{2}I_2 \ ,$$

$$I_2 + 5NO_3^- + H_2O + 3H^+ \rightleftharpoons 2IO_3^- + 5HNO_2 \ .$$

The first reaction is irreversible; the second, however, represents an equilibrium involving nitrous acid, the concentration of which determines how much of the free iodine is converted to the nonvolatile iodate form. The advantage of the refluxing concentrated nitric acid system is that the nitrogen oxides (hence the nitrous acid) are effectively stripped out of solution.

Preliminary tests in which air that contained methyl iodide was bubbled through nitric acid solutions established that 16–17 *M* acid is much more effective than lower acid concentrations and that the reaction rate increases rapidly as the temperature is increased (Table 2.14).

A series of gas-liquid countercurrent scrub tests was made in a 1-in.-diam column that contained 2 ft of stainless steel packing; the CH_3I concentration in the air stream was varied from 50 to 20,000 ppm. The decontamination factor (DF) increased from 50 at the lowest concentration to about 10^3 at the highest concentration.

A schematic of the equipment used to trap methyl iodide from air with refluxing 16 *M* HNO_3 (the azeotropic composition) is shown in Fig. 2.16. A silver zeolite bed was used to trap any iodine that escaped from the system. A large number of runs were made to identify the more important variables affecting the efficiency of the system. Some of the later typical results are given in Table 2.15. Decontamination factors in excess of 10^4 were obtained in the system at air flow rates of 1.5 liters/min or less.

The experimental arrangement shown in Fig. 2.16 has glass bead packing in the upper part of the reactor column. Good results also were obtained at an air flow rate of 1 liter/min without any packing. It is probable that the methyl iodide hydrolytic-oxidation process occurs primarily in the gas phase. We are not certain how or where conversion of free iodine to iodate occurs. The condenser system temperature is apparently quite important in this respect. When the first condenser was operated at 15°C, considerable absorption of nitrogen oxides into the refluxing acid occurred, and this caused some of the iodine to be retained in the volatile I_2 state. There was some indication that the optimum temperature for the first condenser is between 35 and 60°C, the higher temperature possibly being more efficient at air flow rates where nitrogen oxide stripping from the nitric acid is less effective. The upper, or second, condenser was of the spiral type and was operated at 15°C or less to decrease the nitric acid "dew point" to a low value. This, plus the use of a spiral condenser, was found necessary to minimize the carry-over of iodine in aerosol form.

Preliminary results indicate that the iodine concentration in the nitric acid solution can be built up to a relatively high value while still providing efficient iodine trapping. The solubility of HIO_3 in concentrated nitric acid is reported[14] to be 0.114 *M* at 25°C. This is a factor of about 10^3 higher than the I_2 solubility in nitric acid. Initial tests indicate that the iodine can be recovered from the HNO_3-HIO_3 solution by cooling to 60–80°C and adding nitrite to produce an I_2 precipitate, which could then be separated and converted to a form suitable for long-term storage of the ^{129}I.

Catalytic Oxidation of Organic Vapors

We are studying the destruction of organic vapors in process air streams by catalytic oxidation to form carbon dioxide and water.[15,16] The objective is to convert organic iodides to a form (I_2) that can be more readily trapped and also to prevent poisoning of the iodine sorption beds with organic materials. Almost all of the studies thus far have been made with Hopcalite (CuO-MnO_2) catalyst, but we have recently obtained samples of some other, possibly more suitable, catalytic materials for testing. A modified flame-ionization-gage instrument (Beckman) is used to measure the concentration of organic material in the inlet and exit air streams.

In a series of runs with butane-air mixtures at 195, 220, and 255°C, the efficiency of butane oxidation increased as the temperature was increased; however, the oxidation was not highly efficient even at 255°C.

---

14. J. W. Mellor, *Mellor's Comprehensive Treatise on Inorganic and Theoretical Chemistry*, Suppl. II, Part I, Longmans, Green and Co., London, 1956.

15. *Chem. Technol. Div. Annu. Progr. Rep. May 31, 1969*, ORNL-4422, p. 87.

16. *Chem. Technol. Div. Annu. Progr. Rep. May 31, 1970*, ORNL-4572, p. 72.

ORNL DWG 71-122R1

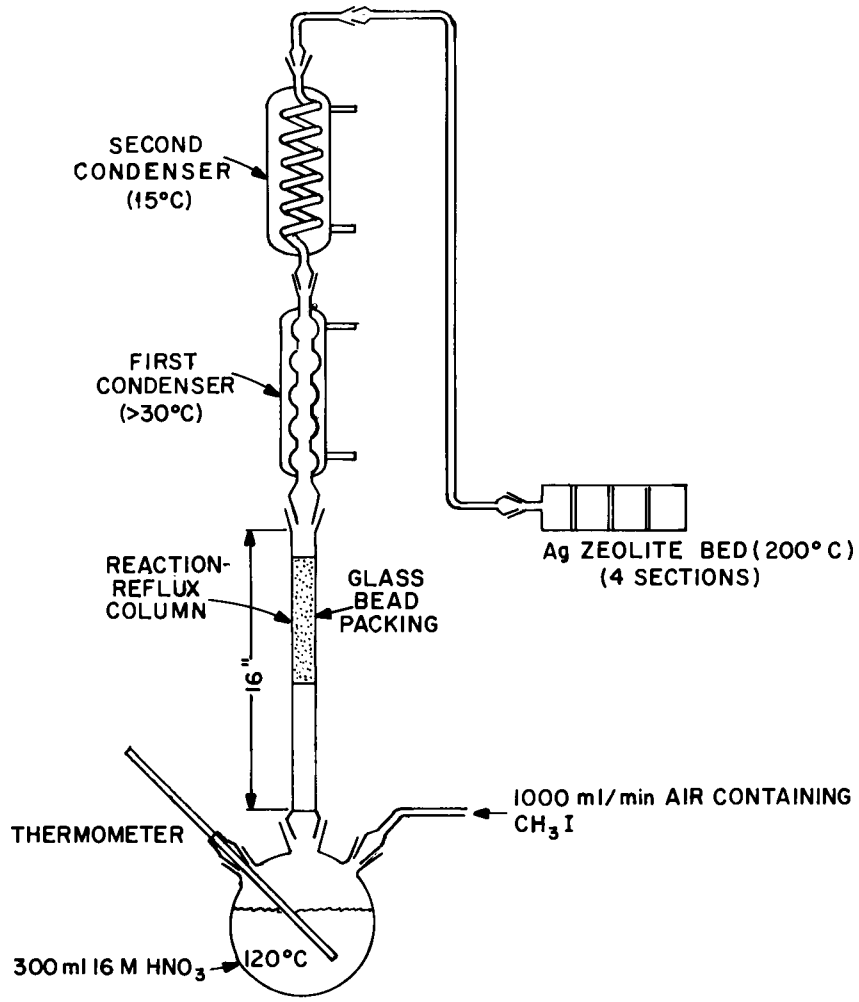

Fig. 2.16. Refluxing concentrated nitric acid system for removing methyl iodide from an air stream.

Table 2.14. Removal of methyl iodide from air with nitric acid solutions

Procedure: Air that contained 20 ppm of ^{131}I-traced CH_3I was dispersed through a glass frit into 100 ml of solution at the rate of 100 cc/min

HNO_3 concentration (*M*)	Temperature (°C)	Iodine decontamination factor
12	90	2
13	90	6
14	90	9
15	90	36
16	25	7
16	50	34
16	75	74
16	90	140
17	90	>500

Table 2.15. Trapping methyl iodide from air with refluxing 16 *M* HNO_3

Procedure: Equipment and conditions as shown in Fig. 2.16; 1-hr runs

Air flow rate (liters/min)	Liquid HNO_3 reflux rate (ml/min)	First condenser temperature (°C)	Iodine decontamination factor[a]
1.0	7.5	55	5.7×10^5
1.5	7.5	45	2.0×10^4
1.5	5.0	45	2.5×10^4
1.5	5.0	60	1.2×10^4
2.0	5.0	55	830
2.0	5.0	35	2.8×10^3

[a]Calculated from the amounts of ^{131}I found in the nitric acid solution and on the silver zeolite bed.

Table 2.16. Oxidation of methane in atmospheric air with Hopcalite catalyst at 350°C

Conditions: 5 cc Hopcalite catalyst; air flow varied from 190 to 1330 ml/min; inlet methane concentration of about 2 ppm

Gas residence time[a] (sec)	Outlet CH_4 concentration (ppm)	Methane oxidized (%)
0.79	0	~100
0.37	0.03	98
0.25	0.27	86
0.19	0.50	75
0.15	0.69	65
0.13	0.90	55
0.11	1.17	40

[a]Calculation of residence time includes correction for temperature but uses bulk volume (5 cc) of catalyst.

For example, with air containing 31 ppm of butane, the amounts oxidized were 12, 91, and 96%, respectively, at 195, 220, and 255°C; with air containing 528 ppm of butane, the amounts oxidized were 56, 79, and 94%. These tests were made with 5 cc of Hopcalite (~1-in.-deep bed) and in air (ambient) flow rate of 1225 cc/min.

Studies of the removal of methane from atmospheric air with Hopcalite catalyst at 350°C showed the importance of gas residence time in the catalyst bed on the methane oxidation efficiency (Table 2.16). Atmospheric air contains about 2 ppm of methane. No methane was detected in the effluent air when the residence time was about 0.8 sec. The amount oxidized decreased to 75% and 40%, respectively, for residence times of about 0.2 and 0.1 sec.

Earlier tests[16] showed that heating Hopcalite at 400°C and higher significantly decreased its surface area, although no impairment of catalytic efficiency was indicated. Additional surface area measurements have since been made. Heating the Hopcalite in air for 1 and 60 hr at 400°C decreased its surface area from an initial value of 132 to 123 and 94 m^2/g respectively. Heating for 1 hr at 500, 600, and 700°C decreased the surface area to 68, 17, and 11 m^2/g respectively.

A series of thermal degradation tests was made in which the Hopcalite catalyst was subjected to three consecutive long-term heat treatments in still air, first at 350°C, then at 450°C, and finally at 500°C. For a short period each day during the heat treatments, a butane-air mixture or atmospheric air (containing methane) was passed through the bed, and the oxidation efficiency was measured. The results show that each of the heat treatments caused a large, although not catastrophic, decrease in the oxidation efficiency (Table 2.17).

Table 2.17. Effect of heat treatments on the efficiency of Hopcalite

Inlet butane concentration (ppm)	Air flow (cc/min)	Decontamination factor[a]		
		First heat treatment (875 hr at 350°C)	Second heat treatment (138 hr at 450°C)	Third heat treatment (154 hr at 500°C)
34	2550	2,900	1700	410
575	2550	100	58	47
34	1225	18,000	5100	3100
575	1225	870	190	107

[a]Ratio of butane concentrations, inlet/outlet, obtained in characterization tests at the end of each heat treatment.

Qualitatively similar results were obtained with respect to oxidation of the methane in atmospheric air (results not shown).

The new catalysts that we are accumulating for testing are reportedly much less subject to thermal degradation.

Trapping of Iodine with Solid Sorbents

Evaluation of the iodine trapping efficiencies of silver-containing solid sorbents was continued. The objective is to find systems that have, and will maintain, a high decontamination capability for iodine species under all conditions expected to be encountered in treating off-gases from LMFBR fuel reprocessing plants.

Prior tests[17] surveyed the CH_3I and C_4H_9I trapping capabilities of several metal zeolites and of a silver-treated alumina (GX-100). None of the materials tested seemed to offer advantages over silver zeolite as an iodine sorber.

Most of the tests reported here were made with silver zeolites,[18] which are prepared by treating Linde molecular sieves with silver nitrate solution. In most cases the 13X molecular sieve was treated to replace either 25% (designated 25% AgX) or 90% of the sodium in the cation sites with silver. Some tests were also made with GX-135, a silver nitrate–treated mixture of alumina and silica that was obtained from North American Carbon, Inc. The silver contents of these materials, in grams per cubic centimeter, are about 0.09 for 25% AgX, 0.31 for 90% AgX, and 0.025 for GX-135.

17. Ibid., pp. 69–71.

18. W. J. Maeck, D. T. Pence, and J. H. Keller, "A Highly Efficient Inorganic Adsorber for Airborne Iodine Species," pp. 185–203 in *Proceedings of Tenth Air Cleaning Conference, New York, August 28, 1968,* CONF-680821.

With each material, several CH_3I trapping tests were done at temperatures ranging from room temperature to 200°C (or higher). In most tests, the CH_3I-laden air stream also contained 3 vol % of water (which corresponds to about 90% relative humidity at room temperature); a few room-temperature tests were done at zero percent relative humidity. I_2 trapping efficiencies at 200°C were measured (again from 3 vol % H_2O atmospheres).

The trapping efficiency results for the three sorbents (90% AgX, 25% AgX, and GX-135) are presented in Figs. 2.17, 2.18, and 2.19, respectively, as plots of DF vs loading of CH_3I or I_2. As can be seen, the 90% AgX provided DFs of about 10^4 or higher at both 100 and 200°C up to loadings of at least 12 mg/cm^3. At 26 to 27°C, CH_3I was trapped efficiently from dry air but not from wet air. At 200°C, I_2 was trapped with a DF higher than 10^5 up to loadings of about 15 mg/cm^3.

The trapping efficiencies of 25% AgX (Fig. 2.18) for CH_3I from 3 vol % water atmospheres tended to show a larger decrease as the loading was increased or the temperature decreased than did the trapping efficiencies of the 90% AgX. Like 90% AgX, the 25% AgX traps CH_3I efficiently at room temperatures from dry air but not from moist air. The I_2 trapping efficiency (at 5 mg/cm^3) was very high. Since this material does perform well near 200°C up to practical loadings (i.e., ~5 mg/cm^3) and since it would be cheaper than material of higher silver content, it is considered to be potentially useful.

The GX-135 (Fig. 2.19) performed best at 200°C; the DFs were smaller at 100°C and at 255°C than at 200°C. The DFs are very high (>10^4) at loadings of probable interest (i.e., ~5 mg/cm^3). Based on these tests, this material is also considered to have high potential for use in the cleanup of off-gas generated during fuel reprocessing.

Results of a series of tests of CH_3I trapping by 90% AgX showed that the presence of CO_2 in the air stream had no effect on trapping efficiency at 100°C and

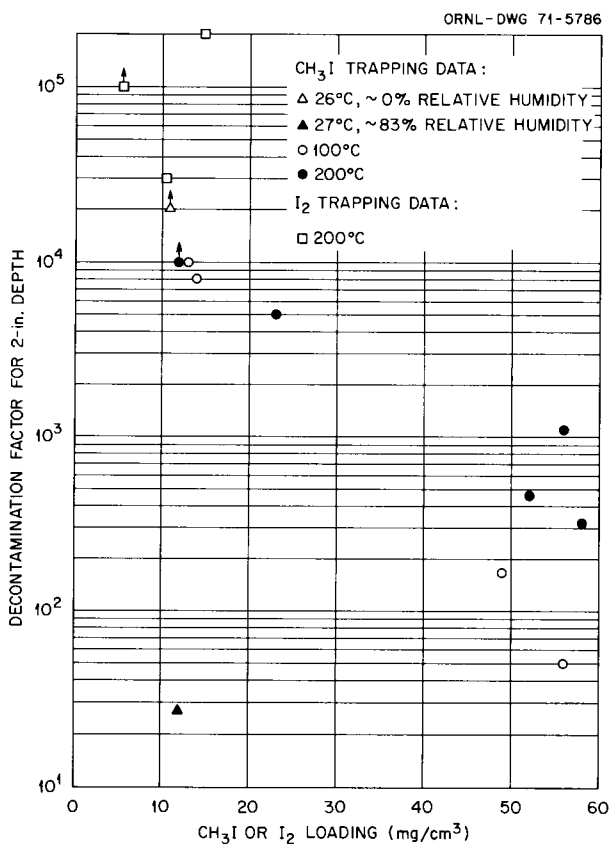

Fig. 2.17. Iodine trapping with 90% AgX.

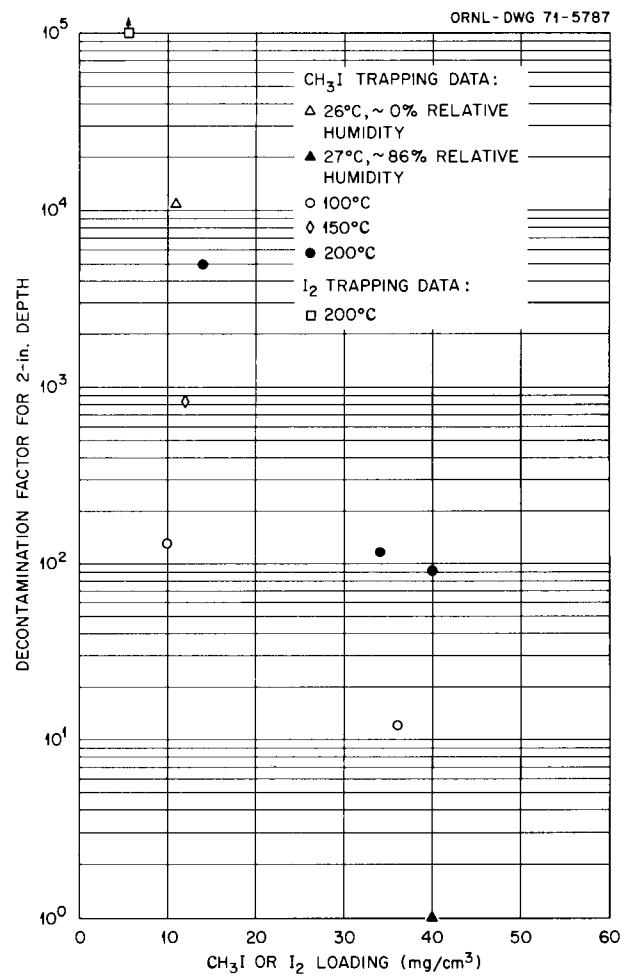

Fig. 2.18. Iodine trapping with 25% AgX.

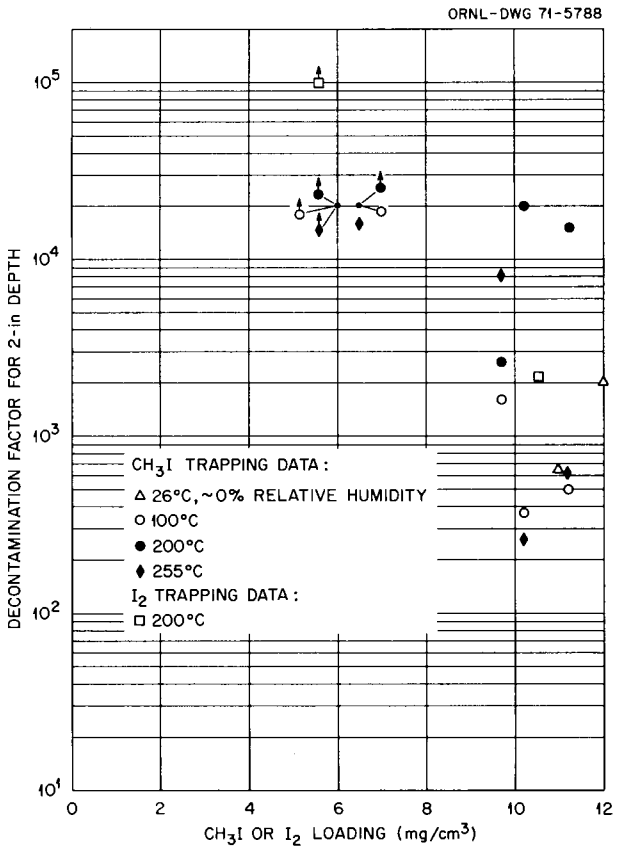

Fig. 2.19. Iodine trapping with GX-135.

200°C. The CO_2 concentration was 10 vol %; 3 vol % H_2O was also included. This CO_2 concentration is greater than that due to decomposition of Ag_2CO_3 at 100°C (but less than the Ag_2CO_3 decomposition pressure at 200°C). The results (i.e., no loss of efficiency) suggest that a substance similar to Ag_2CO_3 probably does not tend to form.

Long-term tests in which sorbents will be subjected to an air stream containing contaminants anticipated in a chemical reprocessing plant off-gas stream are being started in order to determine if the sorber beds will perform satisfactorily after extended use in atmospheres containing potential poisons. In some of the tests, the sorber bed will be preceded by a catalytic oxidation system (containing Hopcalite catalyst at 350°C) to destroy organic vapors and to convert organic iodides to the more readily sorbed I_2 form.

Sorption on porous plastics. Preliminary results of studies of the sorption of iodine by porous polymers showed that all of the Amberlite XAD macroreticular resins (Rohm and Haas Company) were effective in removing iodine from dry air streams.[15] In recent experiments at 25°C with dry air containing 2 to 4 mg of I_2 per liter, one of the more promising resins, Amberlite XAD-12 (an acrylic ester containing a nitrogen-oxygen group), sorbed 1.39 g of I_2 per gram of sorbent with only 0.6% iodine breakthrough. The resin loaded to 995 mg of I_2 per gram at 50°C with 0.015% breakthrough and to 627 mg/g at 100°C with 1% breakthrough. For comparison, at 25°C, iodized charcoal loaded to 2.1 g of I_2 per gram with 0.05% breakthrough and silver zeolite to 126 mg/g with 0.08% breakthrough. The resin was much less effective in removing molecular iodine from wet air; at room temperature, only 430 mg of I_2 was sorbed per gram of Amberlite XAD-12, with 2% I_2 breakthrough. A 5-mm-diam by 10-cm-long column of sorbent and an air flow of 150 ml/min were used in each test.

All of the macroreticular resins sorbed some methyl iodide from dry air at room temperature; two of them, Amberlite XAD-4 (a styrene-DVB polymer) and Amberlite XAD-12, sorbed more than 10 mg of CH_3I per gram of sorbent while still removing more than 99% of the methyl iodide from the air streams. Increasing the temperature decreased the efficiency of the Amberlite XAD-4 but increased the efficiency of Amberlite XAD-12. With the latter resin, increasing the temperature from 25 to 50°C increased the loading (to detectable breakthrough) from 15 mg of CH_3I per gram of sorbent to 93 mg per gram. A further increase in temperature to 110°C decreased the efficiency. In each test, dry air containing 1 to 4 mg of ^{131}I-traced CH_3I was passed through a 5-mm-diam × 10-cm-long column of sorbent at the rate of 150 ml/min.

Batch distribution coefficients for the sorption of iodine from water and nitric acid by macroreticular resins were determined with solutions that had an initial I_2 concentration of about 5×10^{-5} *M*. The distribution coefficients ranged from 10 to 24,000, depending on the resin and the nitric acid concentration (Table 2.18). Sorption of iodine by Amberlite XAD-12 was highly efficient (D = 24,000) from water but much less efficient from nitric acid. Conversely, the coefficient for sorption of iodine from water with XAD-4 was only 25 but increased to a maximum of 14,000 at an HNO_3 concentration of 3 *M*.

Column runs made with Amberlite XAD-12 showed that it was possible to sorb molecular iodine from water, elute the iodine, and reuse the resin in additional sorption-elution cycles with little, if any, deterioration in sorption efficiency. A column subjected to three sorption-elution cycles removed more than 99% of the iodine during each cycle from water containing 5×10^{-4} *M* I_2. The column was loaded to 60 to 130 mg of I_2 per cubic centimeter of sorbent at flow rates that

Table 2.18. Sorption of iodine from water and nitric acid with macroreticular resins

Conditions: 0.1 g of resin contacted for 16 hr with 10 ml of solution that contained 5×10^{-5} *M* I_2

Amberlite sorbent	Iodine distribution coefficient[a]				
	Water	0.1 *M* HNO_3	1 *M* HNO_3	3 *M* HNO_3	7 *M* HNO_3
XAD-2	31	1100	1600	3,100	3300
XAD-4	25	390	2900	14,000	3300
XAD-7	31	750	450	240	180
XAD-8	18	1200	500	300	360
XAD-9	10	650	22	1,100	60
XAD-11	15	1500	470	1,700	310
XAD-12	24,000	720	170	230	130

[a]Calculated from initial and final aqueous iodine concentrations.

ranged from 1 to 4 ml cm^{-2} min^{-1}. Although all of the sorbed iodine could not be eluted from the column, about 90% was easily eluted with either 0.1 *M* Na_2SO_3 + 0.05 *M* HNO_3 or 0.1 *M* $Na_2S_2O_3$ + 0.1 *M* NaOH to yield solutions with an average iodine concentration of 0.02 *M*.

The Amberlite XAD-12 was equally effective in removing iodine from very dilute iodine solutions. Approximately 98% of the iodine was sorbed from 5 liters of 1×10^{-6} *M* I_2 in water as it passed through a 4-mm-diam × 10-cm-long sorbent column at an average flow rate of 1.7 ml cm^{-2} min^{-1}. Column efficiency improved with time, suggesting that the presence of iodine on the plastic enhanced the sorption process. This was verified by the fact that, even at flow rates of 8 ml cm^{-2} min^{-1}, more than 99% of the ^{131}I was removed on passing 1×10^{-6} *M* I_2 (traced with ^{131}I) in water through an Amberlite XAD-12 column that had been preloaded at the top of the column with 2 mg of nonradioactive iodine.

In cyclic sorption-elution tests with Amberlite XAD-4, elution of I_2 from the resin with 0.2 *M* NaOH solution was incomplete, and the efficiency of sorption of the iodine from 0.5 *M* HNO_3 decreased rapidly with cycling.

Chemistry of Uncommon Volatile Iodine Species

As described previously,[16] reaction of I_2 with caustic solutions produces an unstable "active iodine" species (presumably hypoiodite) that is readily extractable (or reacts) with organic solvents. Relatively large amounts (10–40%) of the iodine have been volatilized from these solutions, and it appeared from earlier tests that the active iodine species (HOI has been postulated[19] as a volatile iodine species) itself was being volatilized.

Recent results do not confirm this. It now appears that the highly reactive iodine species rapidly iodinates any organic impurities in the solution or in the sparging air stream and that the iodine volatilized in our tests probably has been mostly in the form of alkyl iodides. By modifying the equipment and paying particular attention to the source and method of preparation of stock reagent solutions in order to avoid organic contaminants, we have decreased the amount of iodine volatilized in a standard test several-fold. Because the iodine concentrations are low (10^{-4} to 10^{-5} *M*), however, even trace concentrations of organic impurities may be important since it may not be possible to reduce these concentrations to the level where their effects can be ignored.

The results suggest that the reaction of hypoiodite with organic materials may be an important factor affecting the operation of caustic scrubbers used to remove radioiodine from gas streams. Also, they may at least partially explain the large differences in iodine removal efficiency that have been observed in the operation of these scrubbers.

Engineering-Scale Application of Solid Sorbents for Iodine Removal

An iodine removal system (Fig. 2.20) consisting of a catalytic oxidation step followed by sorption of iodine on charcoal was installed on the equipment off-gas stream at the Transuranium Processing Plant (TRU). The system was placed in operation in September 1970 and has been on-stream since that time.

19. J. H. Keller et. al., "Hypoiodous Acid: An Airborne Inorganic Iodine Species in Steam-Air Mixtures," pp. 467–81 in *Proceedings of Eleventh Air Cleaning Conference, Richland, Wash., August 31–September 3, 1970,* CONF-700816.

ORNL Dwg 69-11023R1

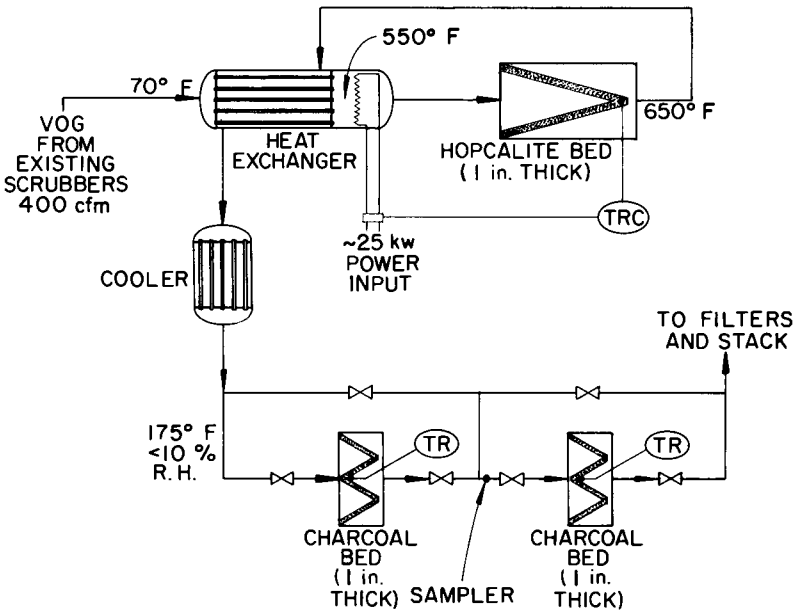

Fig. 2.20. TRU iodine removal system.

Table 2.19. Performance of the primary off-gas removal system at TRU during process campaigns 21 and 22

Campaign No.	Date	Average ^{131}I inventory in TRU (Ci)	Average ^{131}I input to system (mCi/day)	Average ^{131}I release from system (mCi/day)	Decontamination factor		
					First charcoal bed	Second charcoal bed	System
21	11/6–11/11/70	400	12.6	<0.01	30	>20	$>10^3$
	11/22–12/20/70	50	0.5	<0.005			>100
22	1/11–1/23/71	13	1.5	0.018	17	1.6	83

Incoming off-gas (400 cfm) is heated to ~550°F in passing through the tubes of a primary heat exchanger, countercurrently to the exit gas from the catalytic oxidation bed that contains Hopcalite catalyst. Additional electric heat is provided to maintain the Hopcalite bed at 650 ± 25°F. The gases are then cooled to ~225°C in passing through the shell side of the primary exchanger and further cooled to ~175 ± 25°F in a small water-cooled exchanger. The gases then pass through two 1-in.-thick charcoal absorption beds in series for iodine removal. The oxidation step destroys organics in the off-gas, thus improving the efficiency and extending the useful life of the charcoal beds. This system serves as the primary iodine control for the TRU facility and, in addition, will serve as an important test facility to demonstrate the effectiveness and life expectancy of solid sorbents in actual plant application.

Two process campaigns with sufficient iodine input for monitoring have been completed at TRU since installation of the iodine removal system. Performance of the iodine removal equipment is summarized in Table 2.19. During campaign 21, iodine release rates from the system were consistently less than the limit of detection (10 μCi/day) and system DFs approached 10^4. During the period immediately following the active processing in campaign 21, release rates averaged 5 μCi/day, but input rates were too low to permit measurement of realistic DFs. In campaign 22, which began about four months after installation of the iodine removal system, a significant loss in efficiency was evident. Iodine input rates had decreased by a factor of 10 as compared with campaign 21, and release rates averaged 20 μCi/day, more than a factor of 2 higher than previous results. A similar loss of efficiency of

charcoal in similar experimental applications had been observed and is probably due to gradual poisoning of the charcoal.

Future plans for the TRU system include continued measurement of the efficiency of the existing charcoal beds over a period totaling six to eight months. The charcoal beds will then be replaced by silver zeolite beds, and their efficiency will be determined over an extended period of time. Based on laboratory data, the silver zeolite should have both a higher initial efficiency and a longer effective life than charcoal.

2.7 RADIATION, SHIELDING, AND CRITICALITY STUDIES

The objective of this series of studies is to provide basic nuclear data to support the design and development of the LMFBR fuel cycle. The studies of radiation properties and shielding requirements of LMFBR fuels involve correlation of basic nuclear data, including decay schemes, neutron cross sections, energy spectra of radiation sources, and thermal power; development of computer programs for the calculation of transient concentrations of radionuclides; calculation of attenuation kerma of shield materials of interest; and application of these data to LMFBR fuel cycle processes. The criticality studies involve compilation and correlation of basic data, liaison with experimental groups, development and verification of computational techniques, and development of criticality parameters and control techniques for specific process applications.

Radiation and Shielding Studies

During this report period, we evaluated the accuracy of the ORIGEN program and developed parametric data for use in the design of radiation shields.

Development of the ORIGEN program. The thermal power of spent fuels computed by the ORIGEN code[20,21] has been compared with published experimental and calculated afterheat data. Figure 2.21 presents a comparison of the thermal power computed by ORIGEN for thermal-neutron fission of ^{235}U with values obtained from several independent sources of data. The points labeled NSIC-5 are from ref. 22 and represent the combined measurements and calculations of a number of workers, as compiled by Shure.[23] The points labeled PHOEBE were obtained using the PHOEBE code of Arnold,[24] which computes the activity, thermal power, and spectra of ^{235}U fission products. This code uses an empirical fit of experimental data[25] for decay times less than 1550 sec and the calculated afterheats of Perkins and King[26] for decay times greater than 1550 sec. Also shown are the calculated results of Blomeke and Todd.[27] The exposure of the fuel is typical of that which is expected in an advanced LWR converter. All the data agree to within a few percent over the range of decay times from 1000 sec to 100 years. The ORIGEN gamma-ray power falls below the other compilations at postirradiation times of 100 sec or less. This results from uncertainties in fission yields, half-lives, disintegration energies, and decay schemes for nuclides with very short half-lives. For those applications for which the code was developed, decay times of a month or longer are of primary interest.

A comparison has been made of the thermal power of spent fuels as a function of decay time for ^{235}U and ^{239}Pu fission in both thermal and fast reactor spectra. The fuels were assumed to be irradiated at a constant specific power of 250 MW per metric ton of fuel to a burnup of 100,000 MWd per metric ton of fuel in spectra typical of an LMFBR core and of a light-water-moderated research reactor core. The results (Table 2.20) indicate that the differences resulting from different fuel are larger than those from differences in the neutron spectra. At decay times less than 90 days, the ^{235}U afterheats are a few percent higher than those from fission of ^{239}Pu. At long cooling times, the ^{239}Pu thermal power becomes considerably higher as the result of radioactive decay of transplutonium isotopes.

A program has also been initiated to compare the concentrations of individual nuclides in spent fuels

20. *Chem. Technol. Div. Annu. Progr. Rep. May 31, 1969,* ORNL-4422, pp. 88–95.

21. *Chem. Technol. Div. Annu. Progr. Rep. May 31, 1970,* ORNL-4572, pp. 75–77.

22. W. B. Cottrell and A. W. Savolainen (eds.), *U.S. Reactor Containment Technology,* NSIC-5, vol. I, chap. 5 (August 1965).

23. K. Shure, *Bettis Technical Review,* WAPD-BT-24, p. 1 (December 1961).

24. E. D. Arnold, *PHOEBE – a Code for Calculating Beta and Gamma Activity and Spectra for ^{235}U Fission Products,* ORNL-3931 (July 1966).

25. R. W. Peelle, W. Zobel, and T. A. Love, "Measurement of the Spectrum of Short-Lived Fission Product Decay Gamma Rays Emitted from a Rotating Fuel Belt," *Appl. Nucl. Phys. Div. Annu. Progr. Rep. Sept. 10, 1956,* ORNL-2081.

26. J. F. Perkins and R. W. King, *Nucl. Sci. Eng.* 3, 726–46 (1958).

27. J. O. Blomeke and M. F. Todd, *Uranium-235 Fission Products Production as a Function of Thermal Flux, Irradiation Time, and Decay Time,* ORNL-2127 (1957).

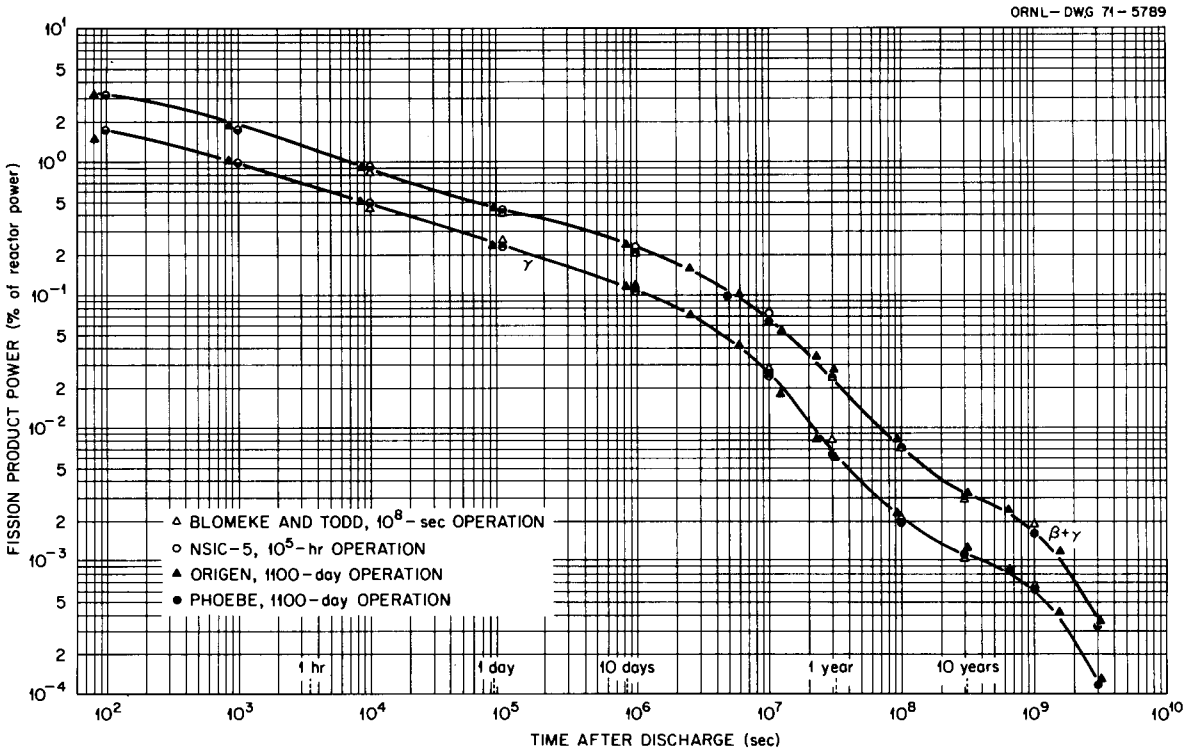

Fig. 2.21. Fission product thermal power as a function of cooling time for thermal-neutron fission of ^{235}U fuel.

Table 2.20. A comparison of the postirradiation thermal power resulting from irradiation of ^{235}U and ^{239}Pu in thermal- and fast-neutron spectra, at a constant specific power of 250 MW/metric ton, to a burnup of 100,000 MWd/metric ton

	^{235}U		^{239}Pu	
	Thermal[a]	Fast[b]	Thermal[a]	Fast[b]
Mass of fission products, g per metric ton of ^{235}U or ^{239}Pu charged to reactor	106,000	105,000	107,000	106,000
Fissions per initial atom, %	10.6	10.6	10.5	10.5
Total neutron flux, neutrons cm^{-2} sec^{-1}				
Initial	1.60×10^{13}	1.51×10^{15}	5.73×10^{12}	1.65×10^{15}
Final	1.81×10^{13}	1.71×10^{15}	6.62×10^{12}	1.86×10^{15}
Time average	1.70×10^{13}	1.61×10^{15}	6.15×10^{12}	1.75×10^{15}
Fission product + actinide thermal power, W per metric ton of ^{235}U or ^{239}Pu charged to reactor, after decay time (days) of:				
1	1,120,000	1,130,000	1,070,000	1,020,000
3	804,000	801,000	770,000	738,000
10	552,000	545,000	511,000	505,000
30	330,000	330,000	304,000	310,000
90	161,000	164,000	158,000	164,000
150	103,000	105,000	110,000	113,000
365	37,000	37,500	49,700	52,200
730	15,900	16,200	23,000	25,200
1096	8,980	9,150	14,300	14,300
3650	3,270	3,080	4,270	4,170

[a]Spectrum is typical of a light-water research reactor (e.g., ORR, ETR, MTR).

[b]Spectrum is typical of an LMFBR core.

predicted by ORIGEN with analyses of actual fuels irradiated in the GETR and EBR-II.

Finally, a series of calculations was performed to determine the isotopic changes to be expected in stainless steels irradiated in fast reactor spectra.[28] The computed concentrations of hydrogen and helium were in good agreement with measured values.[29]

Parametric shielding data. Parametric data for use in the design of neutron shields for LMFBR spent-fuel shipping casks have been developed using the ANISN code[30] in the $S_{16}P_3$ approximation and a $27n$-20γ coupled cross-section set. Cross sections for the attenuation of neutrons and photons and for the production of secondary photons were compiled or calculated using GAM-II, MUG, and POPOP4.[31]

In this investigation, we have determined the neutron shielding properties of iron, lead, and uranium when used alone or with water placed either around the source or around the outside of the shield. The shields were assumed to be spherical shells surrounding a spherical aluminum source having a radius of 1 cm. Two source neutron spectra were used for the calculations: a ^{252}Cf spontaneous fission (SF) spectrum and an (α,n) spectrum typical of that expected from $^{244}Cm_2O_3$.

The results lead to the following general conclusions:

1. The neutron spectrum for the (α,n) source is slightly "harder" than the spectrum for the SF source and results in a higher neutron dose rate.
2. For a given thickness of heavy metal, a 10-cm thickness of water can be three to ten times more effective when placed outside the shield instead of inside.
3. For a given thickness of metal, the effectiveness of the three shield materials in decreasing order is: U, Fe, Pb.
4. For a given slab weight (g/cm^2), the effectiveness in decreasing order is: Fe, U, Pb.
5. Secondary gamma dose rates are only significant in cases where water is placed on the outside of the shield. In such cases, the secondary gamma dose rate can be 20 to 60% of the total dose rate.

The results of the comparative calculations are summarized in Table 2.21. More complete results of these studies will be presented at a topical meeting, "Neutron Sources and Applications," of the American Nuclear Society in April 1971. These results will be published in the proceedings.

Criticality Studies

During this report period, we have been developing parametric data for heterogeneous systems of (U + Pu)O_2 in water and fissile solutions to complement the data for homogeneous systems that were reported previously. Computational techniques used for these parametric calculations were evaluated by comparing results with more exact Monte Carlo techniques and with data from critical experiments.

Computational techniques. A study was made to investigate the adequacy of the resonance treatment in the cross-section preparation code XSDRN for problems with "lumped" absorbers surrounded by moderators containing absorbers. The Monte Carlo code ESP was utilized to determine the reactivity for a (U + Pu)O_2 fuel, at 90% theoretical density, containing 20 wt % PuO_2 and having the isotopic compositions 75 wt % ^{239}Pu, 25 wt % ^{240}Pu, and 0.2 wt % ^{236}U. The code ESP takes basic cross-section data from the ENDF/B tapes and generates an ultrafine energy group structure to be used in the subsequent Monte Carlo calculation. This investigation used 4096 energy groups from version I ENDF/B data and approximated the hydrogen scattering treatment with a free-gas model.

Results of the series of Monte Carlo calculations (standard error, approximately ±1%) are given in Fig. 2.22. These results show that, in the vicinity of optimum moderation for minimum critical volume with a pure H_2O moderator, introduction of dissolved fuel into the moderator causes a decrease in k_∞. Conversely, when the system is highly overmoderated for the pure H_2O moderator, introduction of dissolved fuel into the moderator increases k_∞, since it moves the system nearer to the effective optimum moderation.

We know from previous calculations that the approximate resonance treatment of XSDRN predicts essentially the same results as the more exact Monte Carlo treatment. Therefore, it is concluded that the code XSDRN may be used effectively to estimate the criticality parameters of this type of system.

---

28. H. T. Kerr, M. J. Bell, and E. E. Bloom, "Neutron Cross Section Data Applied to the Materials Irradiation Studies at ORNL," presented at the Third Conference on Neutron Cross Sections and Technology, Knoxville, Tenn., March 15–17, 1971 (to be published in the proceedings).

29. N. D. Dudey, S. D. Harkness, and H. Farrar IV, *Nucl. Appl. Technol.* 1, 700–710 (1970).

30. W. W. Engle, Jr., *A User's Manual for ANISN, a One-Dimensional Discrete Ordinates Transport Code with Anisotropic Scattering*, K-1693 (1967).

31. L. R. Williams and W. E. Ford, Computing Technology Center, Oak Ridge Gaseous Diffusion Plant, unpublished data (November 1969–February 1970).

Table 2.21. Neutron and secondary gamma dose rates at the outer surface of multilayered spherical shells, resulting from an internal spherical neutron source having a radius of 1 cm and spectra typical of those from spontaneous fission of ^{252}Cf and (α,n) reactions in $^{244}Cm_2O_3$

Thickness of shield	$4\pi r^2$·dose rate {cm^2·[(millirems/hr)/(neutrons/sec)]}			
	SF source		(α,n) source	
	Neutron dose rate	Secondary gamma dose rate	Neutron dose rate	Secondary gamma dose rate
10 cm U			6.63×10^{-5}	2.49×10^{-7}
20 cm U			3.53×10^{-5}	1.15×10^{-7}
30 cm U	1.45×10^{-5}	5.04×10^{-8}		
10 cm U + 10 cm H_2O	5.89×10^{-6}	7.31×10^{-6}	8.28×10^{-6}	1.44×10^{-6}
20 cm U + 10 cm H_2O	1.06×10^{-6}	8.49×10^{-7}	1.31×10^{-6}	7.96×10^{-7}
30 cm U + 10 cm H_2O	2.04×10^{-7}	3.59×10^{-7}	2.21×10^{-7}	3.63×10^{-7}
10 cm H_2O + 10 cm U	1.48×10^{-5}	7.77×10^{-8}	2.24×10^{-5}	1.01×10^{-7}
10 cm H_2O + 20 cm U	5.73×10^{-6}	2.07×10^{-8}	8.63×10^{-6}	2.94×10^{-8}
10 cm H_2O + 30 cm U	1.98×10^{-6}	7.53×10^{-9}	2.97×10^{-6}	1.09×10^{-8}
10 cm Fe	1.01×10^{-4}	4.13×10^{-8}	1.12×10^{-4}	3.29×10^{-8}
20 cm Fe	9.17×10^{-5}	9.26×10^{-8}	9.85×10^{-5}	8.53×10^{-8}
30 cm Fe	6.96×10^{-5}	1.49×10^{-7}	7.37×10^{-5}	1.39×10^{-7}
10 cm Fe + 10 cm H_2O	1.23×10^{-5}	2.57×10^{-6}	1.81×10^{-5}	2.37×10^{-6}
20 cm Fe + 10 cm H_2O	4.33×10^{-6}	2.75×10^{-6}	6.01×10^{-6}	2.70×10^{-6}
30 cm Fe + 10 cm H_2O	1.62×10^{-6}	2.61×10^{-6}	2.09×10^{-6}	2.60×10^{-6}
10 cm H_2O + 10 cm Fe	2.47×10^{-5}	5.94×10^{-7}	3.83×10^{-5}	5.41×10^{-7}
10 cm H_2O + 20 cm Fe	1.72×10^{-5}	1.02×10^{-7}	2.65×10^{-5}	1.11×10^{-7}
10 cm H_2O + 30 cm Fe	1.18×10^{-5}	4.72×10^{-8}	1.81×10^{-5}	6.30×10^{-8}
10 cm Pb	1.05×10^{-4}	8.12×10^{-8}	1.12×10^{-4}	1.19×10^{-7}
20 cm Pb	1.10×10^{-4}	4.15×10^{-8}	1.13×10^{-4}	6.42×10^{-8}
30 cm Pb	1.03×10^{-4}	1.90×10^{-8}	1.03×10^{-4}	2.92×10^{-8}
10 cm Pb + 10 cm H_2O	1.76×10^{-5}	2.09×10^{-6}	2.68×10^{-5}	1.88×10^{-6}
20 cm Pb + 10 cm H_2O	9.72×10^{-6}	2.08×10^{-6}	1.40×10^{-5}	2.00×10^{-6}
30 cm Pb + 10 cm H_2O	5.49×10^{-6}	2.16×10^{-6}	7.31×10^{-6}	2.17×10^{-6}
10 cm H_2O + 10 cm Pb	2.77×10^{-5}	8.67×10^{-8}	4.32×10^{-5}	8.00×10^{-8}
10 cm H_2O + 20 cm Pb	2.37×10^{-5}	3.84×10^{-8}	3.69×10^{-5}	3.85×10^{-8}
10 cm H_2O + 30 cm Pb	2.04×10^{-5}	2.29×10^{-8}	3.15×10^{-5}	2.31×10^{-8}

Evaluation of nuclear data. The computational methods and the cross-section data currently in use have been tested by comparison of calculated results with selected experimental results, as reported in the literature. One series of particular interest is the recently reported critical approach and exponential experiments for prototype FFTF fuel.[32] These represent the first reported experiments for $(U + Pu)O_2$ rods in water for which the plutonium weight fraction was in the range of interest for LMFBR core fuels. In this case, the 25.2 wt % PuO_2–UO_2 pellets, at 93% theoretical density, were in 0.20-in.-ID, 0.230-in.-OD, 27.25-in.-long 316 stainless steel rods. The isotopic content of the plutonium was approximately 12 at. % ^{240}Pu and 2 at. % ^{241}Pu. The uranium had the naturally occurring composition. The experimental results and the calculated k_{eff}'s are shown in Table 2.22. The calculated values are all within 1.5% of unity, except the last entry, and are thus considered to be in good agreement. The 2.7% error in the last entry is not thought to be severe since the reported material buckling was only approximate and the moderator-to-fuel volume ratio is beyond the range of interest to LMFBR fuel reprocessing criticality safety.

The calculational procedure for determining the k_{eff}'s employed the code XSDRN to generate 16-group cross sections for the equivalent homogenized cell from a 123-group library of ENDF/B version II data. All resonance nuclides were treated explicitly by the Nordheim integral treatment with appropriate Dancoff correction factors. The 16-group cross sections were then used in one-dimensional diffusion theory calculations with the code CITATION. The second dimension in these calculations was treated by the use of an axial buckling calculated from the fuel height and the measured extrapolation distance.

32. C. L. Brown and C. A. Rogers, "Critical Approach and Exponential Experiments with Prototype FFTF Driver Fuel Pins in Water," *Trans. Amer. Nucl. Soc.* 13, 663 (1970).

Table 2.22. Experimental results and calculated k_{eff}'s for 25.2 wt % PuO_2-UO_2 rods moderated and reflected by water

Lattice pitch (in.)	Water-to-fuel volume ratio	Number of pins for criticality	Effective critical radius (cm)	Material buckling (m^{-2})	Extrapolation distance (cm)	Calculated k_{eff}
0.450	4.26	417 ± 5	12.25	153.8 ± 2.7	8.01	1.0002
0.600	8.60	219.2 ± 0.6	11.85	172.7 ± 2.2	7.25	1.0113
0.779	15.42	156.2 ± 0.8	12.98	160.9 ± 1.0	6.89	1.0121
0.900	21.01	149.8 ± 0.6	14.69	138.5 ± 1.0	6.90	1.0143
1.039	28.45	165.0 ± 0.2	17.80	111.6 ± 0.3	6.61	1.0094
1.200	38.37	232.6 ± 0.1	24.41	77.0 ± 1.0	6.11	1.0004
1.350	48.92	410 ± 10	36.45	~46.8		0.9736

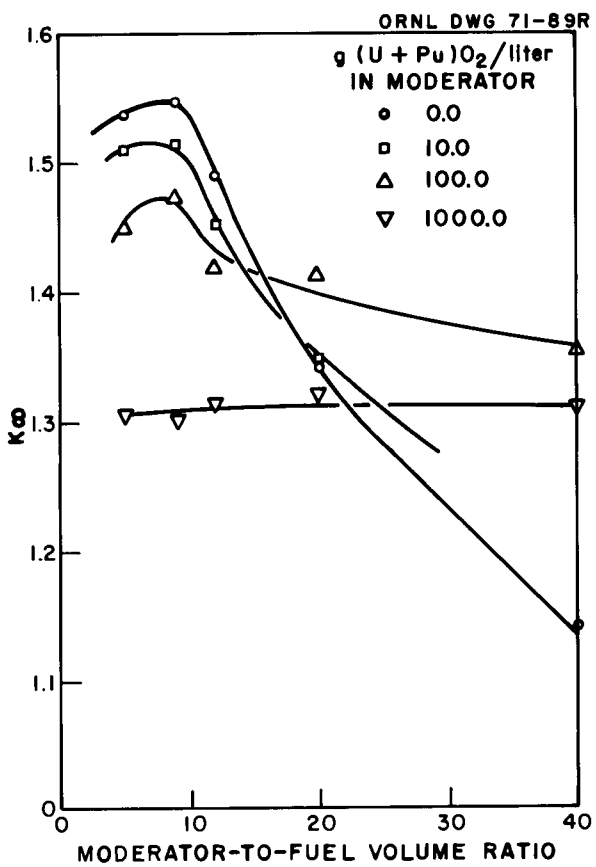

Fig. 2.22. Infinite system multiplication factors for 20 wt % PuO_2-UO_2 rods in fuel moderator solutions.

Parametric criticality data. Calculations are being performed to develop parametric criticality data for (U + Pu)O_2 rods in water, nitric acid, and fissile solutions for isotopic compositions and U/Pu ratios characteristic of those expected from LMFBR discharge fuels. These data are being calculated with the XSDRN and CITATION codes by the method described in the previous section. The complete results will be tabulated and charted in a separate publication for use in safety analyses of preliminary plant component designs.

Typical results for hexagonal arrays of rods of 16 wt % PuO_2-UO_2, at 90% theoretical density, in water are shown in Figs. 2.23 and 2.24. In making these calculations, it was assumed that the plutonium contained 27 wt % ^{240}Pu and the uranium contained 0.2 wt % ^{235}U. The results indicate that "lumping effects" can cause a reduction of as much as a factor of 3 in the plutonium critical mass (at 340 g of Pu per liter) and that the minimum reflected critical cylinder radius is 16% smaller for the 0.10-in.-diam rod system than for the homogeneous system. Thus, in designing process plant components such as dissolvers, which have lumped fuel dispersed in moderating liquids, neglect of the effect of heterogeneities could lead to serious overestimates of allowable masses and dimensions.

2.8 ENGINEERING STUDIES

A study was made of the feasibility of the interim reprocessing of fuels from the Fast Test Reactor (FTR or FFTF) and other conceptual Follow-On LMFBR's in the Nuclear Fuel Services (NFS) plant, West Valley, New York. In general, this study showed:

1. The *present* NFS head-end equipment and facilities (including plant alterations planned for 1973) are inadequate for the reprocessing of LMFBR fuels. The downstream aqueous Purex facilities and equipment are capable of handling LMFBR fuels, although some of the steps (e.g., plutonium isolation and packaging) and waste effluents limit the reprocessing rates to less than half that (≥1 metric ton of U + Pu per day) obtainable in the head end. For fuels decayed less than 200 days, the emission of ^{131}I is restrictive both in gaseous

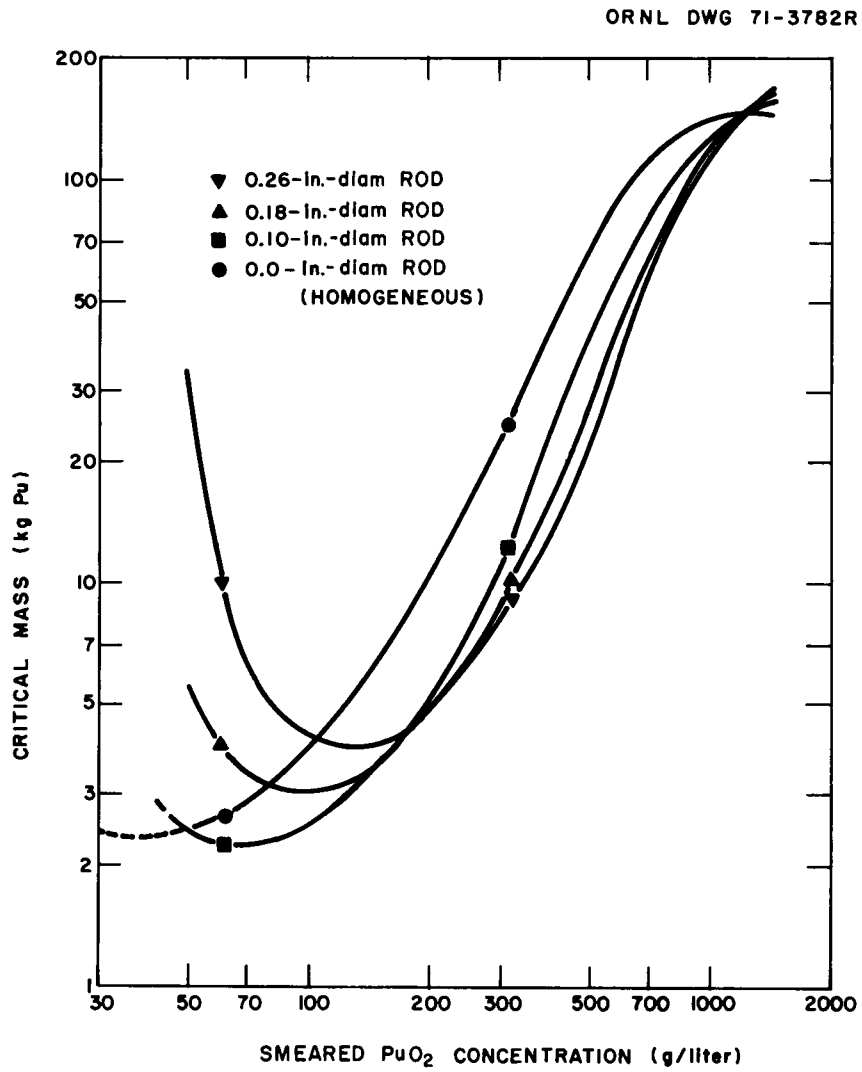

Fig. 2.23. Effect of PuO_2 concentration on the critical mass of plutonium (73% ^{239}Pu–27% ^{240}Pu) in a water-reflected sphere containing rods of 16% PuO_2–84% UO_2 in water.

effluents and in low-level liquid wastes. For postirradiation decay times greater than 200 days, ^{129}I in the low-level wastes restricts the reprocessing rate. At cooling times of less than one year, heat dissipation problems are severe.

Thus, some mechanical modifications and other development work must be accomplished before even long-decayed LMFBR fuels may be reprocessed. The reprocessing of short-decayed fuel in the existing system, even with the most extensive modifications envisioned as being reasonable, would result in excessive radioactive emission as well as cause other problems.

2. LMFBR fuels could be processed in the NFS plant, providing suitable additions or modifications (principally to the head-end equipment and facilities) were made. However, such modifications cannot now be accomplished within the framework of the existing LWR fuel reprocessing technology. A substantial and extensive research and development program to produce the appropriate LMFBR reprocessing technology, particularly for the entire head-end portion of the plant, will be necessary.

The major modifications required for the NFS plant in order to permit the processing of fuel decayed one year or less would include:

a) Addition of a new fuel receiving and cleaning facility.

b) Addition of an off-gas collection and treatment facility for the storage basin, process mechanical cell

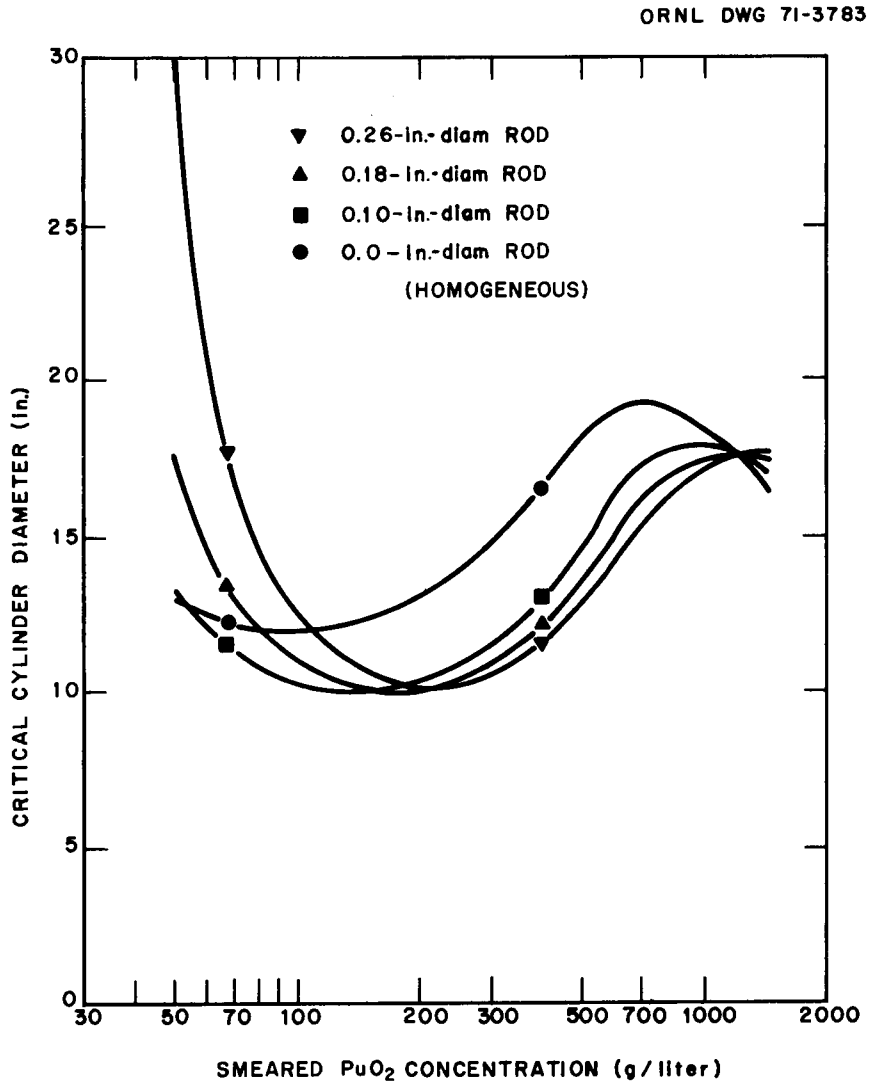

Fig. 2.24. Effect of PuO_2 concentration on the critical mass of plutonium (73% ^{239}Pu–27% ^{240}Pu) in a water-reflected infinitely tall cylinder containing rods of 16% PuO_2–84% UO_2 in water.

(PMC), and general-purpose cell (GPC). If the cleaned fuel is canned for storage in water, an off-gas collection and treatment facility would not necessarily have to be added to the storage basin.

c) Provision for disassembly in the PMC, and alterations to the bundle shear to produce short terminal pieces and small discrete pieces of shroud.

d) A voloxidation and/or internal sodium deactivation[33] capability in the GPC or in the chemical processing cell (CPC).

e) Provision for heat removal in the PMC, GPC, and CPC.

f) Addition of a third dissolver to the CPC if dissolution times of up to 40 hr are found to be necessary.

Items *a*, *c*, *d*, and *f* are independent of decay time and would be required for all LMFBR fuel. Fuels decayed longer than one year would probably not require modifications *b* and *e*.

The NFS facilities would require only minimal modifications if the fuel supplied to the plant could be guaranteed to be free of sodium. For example, a new fuel receiving and cleaning facility would not be required. Sodium-free fuel of a postirradiation time of one year or longer could be processed if a disassembly

33. The self-heating of sheared fuel in storage would promote the evolution of fission gases and burn any sodium present, which is the basic intent of the proposed voloxidation step currently being developed.

capability was added to the PMC or if the bundle shear was suitably altered to ensure that the shroud of each subassembly was cut into small discrete pieces that would pass through the restricted throat of the shear. However, the reprocessing of sodium-deactivated spent fuel after a long decay period would not permit overall demonstration of the technology required for shorter-decayed fuels.

Assuming that a plutonium inventory charge will not be assessed for early LMFBR's, processing of fuel at long decay times would appear to provide for minimal initial reprocessing costs, whereas the development and demonstration of short-cooled processing, using at least a portion of the early fuels, would provide earlier confidence in LMFBR fuel cycle technology and, probably, increased cost benefit to the industry.

Table 2.23 is a comparative chart showing that the development and demonstration of technology for LMFBR fuels decayed longer than one year do not produce all of the technology that is required for the reprocessing of fuels decayed less than one year.

3. Overall, it could be concluded that the processing limitations at NFS and the required modifications are of such a magnitude that, for the shorter-decayed fuels, the addition of a new reprocessing head-end facility (for receiving and cleaning the fuel and for carrying out all the steps through feed adjustment) would probably be more desirable than renovation of the existing facilities.

A more-detailed summary of each of the main sections of the study in the order of their appearance in the final report[34] is given below.

Shipping. Shipping, per se, was not treated in this study. It is being reported separately (*An Engineering Evaluation of LMFBR Fuel Shipment,* ORNL-TM-2723).

Fuel receiving and storage. If the fuel is allowed to decay for about one year and is then cleaned of sodium prior to shipment in gas or water, the existing NFS receiving facilities may be used. If the fuel is shipped by an advanced method using sodium as the primary coolant or if the fuel is not precleaned of sodium, a new NFS receiving facility will be required. This new unit would contain equipment for sodium removal unless an in-shipping-cask sodium removal and deactivation method can be developed and proved feasible.

The existing storage facilities probably could be used for storage of uncanned LMFBR fuel, provided the fuel has been adequately cleaned of sodium. However, if short-decayed material is to be stored in the NFS canal, it will be necessary either to canister it or to establish that in-canal failure of a fuel tube(s) will not result in unacceptable fission product concentrations in the water of the storage canal and the building that houses it.

The heat removal capabilities of the storage canal and the shielding of the various facilities are adequate, and criticality control does not appear to present any unusual challenging problems.

Head-end reprocessing. The principal problems expected to be encountered in the head-end processing of LMFBR fuels are mechanical difficulties, heat dissipation, sodium deactivation, and off-gas collection and treatment. (For summary comments on the head-end off-gas problems, see "Site Effluents" below.)

Mechanical. The longest fuel assembly that can be passed from the storage canal into the PMC is 16 ft; thus AI Reference oxide fuel, which is 17 ft 8 in. long, may have to be cropped. NFS does not now have an underwater cropping capability.

The disassembly (removal of end fittings, deshrouding, gas plenum removal) of LMFBR fuel is desirable to control the heat release rate, by reducing an assembly to a smaller array of rods, and to decrease the amount of non-fuel-bearing material to be handled in the downstream processing steps. The presence of a shroud and gas plenum causes problems in the shearing step, and the gas plenum causes problems in the dissolution step.

Complete disassembly of the fuel into individual fuel rods cannot be accomplished with the present PMC saw. Although the end fittings and gas plenum could be severed by the current method, there is no provision for the collection and disposal of the off-gases and/or sodium released during the operation. The technology for these operations, including shroud removal, would have to be developed, and applicable new equipment would have to be added to the PMC.

The NFS shear is capable of shearing each of the LMFBR fuels, including the shroud and nickel reflector sections of the FTR. However, neither shearing of shrouded fuel in the presence of sodium (fire, galling of shear blades) nor collective shearing of the unfueled gas plenum sections (possible excess wear on shear blades) has been demonstrated. Further, if the shroud is not broken into small discrete pieces by the shearing operation (and this has not been demonstrated), the throat of the shear and discharge chute could become clogged with the sheared product (making the downstream aqueous processing of fuel impossible). Some developmental effort on the shear blade design plus

34. C. D. Watson et al., *A Study of the Reprocessing of Spent Fast Test Reactor Fuel (and Other LMFBR Fuels) in the Nuclear Fuel Services Plant,* ORNL-TM-2906 (in press).

Table 2.23. A comparison of LMFBR fuel reprocessing technology with regard to whether the technology derived with long-decayed fuel is adequate for the reprocessing of short-decayed[a] fuel

Fuel handling or processing step	Fuel decay time	
	Less than one year	More than one year
Shipping		
1. Demonstration of advanced shipping methods, canistered, or uncanistered in sodium, etc.	Yes	No
Receiving and storage		
1. Sodium deactivation and disposal	Yes	No (not shipped in sodium)
2. Off-gas collection and treatment (from ruptured fuel)	Yes	No (^{131}I, Xe); yes (^{85}Kr, Xe, ^{3}H)
Disassembly		
1. Mechanical problems	Yes	Yes
2. Heat dissipation	Yes	No
3. Sodium collection and deactivation	Yes	Yes
4. Off-gas collection and treatment	Yes	No (^{131}I, Xe); yes (^{85}Kr, Xe, ^{3}H)
Shearing		
1. Heat dissipation	Yes	No
2. Shearing in the presence of molten sodium	Yes	Yes; no (if long-decayed)
3. Mechanical (shearing of gas plenums, shredding of shroud, production of short terminal pieces)	Yes	Yes
4. Collection and treatment of off-gases	Yes	No (^{131}I, Xe); yes (^{85}Kr, Xe, ^{3}H)
Voloxidation		
1. Iodine, Kr, Xe, ^{3}H removal	Yes	No (^{131}I, Xe); yes (^{85}Kr, Xe, ^{3}H)
2. Sodium deactivation	Yes	Yes
3. Heat dissipation	Yes	No
Separation of fuel from cladding		
1. Mechanical problems	Yes	Yes
Dissolution		
1. Dissolution of thermally hot fuel	Yes	No
2. Off-gas collection and treatment	Yes	No (^{131}I, Xe); yes (^{85}Kr, Xe, ^{3}H)
3. Fate of noble metals and other insolubles	Yes	Yes
Feed clarification		
1. Centrifugation, filtration, etc.	Yes	Yes
Solvent extraction		
1. Solvent damage	Yes	No
2. Heat dissipation	Yes	No
3. High-level (IAW) waste collection and storage	Yes	No
Product purification and packaging		
1. Quality of Pu product	Yes	No

[a]Heat and iodine tracer cannot be used to simulate short-decayed fuel because the iodine is not in the correct chemical form.

alteration of the shear to increase the cutting stroke to a maximum length might result in an assured capability for producing sheared fuel and shroud in sufficiently small pieces to flow readily through the shear discharge. If this development were not accomplished, the removal of the shroud would be mandatory in the disassembly step. Equipment for this operation does not exist, but it could be developed and installed in the PMC.

Heat dissipation. The NFS head-end facilities lack a means of controlling the temperature of LMFBR fuel (such as by forced circulation of gas) in the PMC, GPC, and CPC, as well as techniques and equipment for handling thermally hot fuel assemblies. Heat (depending on decay time) can cause difficulties throughout the head-end process if the fuel has not been disassembled previously; it becomes a special problem when the fuel is sheared into baskets and stored. For example, AI Follow-On fuel decayed 265 days and collected in a 7.70-in.-ID basket would attain a calculated center-line temperature of 1020°F and an outside wall temperature of 520°F. In comparison, the same fuel decayed 180 days would attain temperatures of 1170°F and 630°F

respectively. Assuming NFS could handle LWR fuel decayed 180 days, the decay time required for LMFBR fuel to roughly equal the temperature of PWR-type LWR fuel would be 385 to 700 days.

Sodium deactivation. The NFS facility is not equipped for the handling and disposal of sodium; thus the presence of this metal would cause problems throughout the receiving and storage, disassembly, shearing, sheared fuel storage, and dissolution steps. For short decay times, the higher the temperature of the LMFBR fuel, the more reactive is the sodium. In this sense, sodium associated with short-decayed fuel is more difficult to deal with than sodium in fuel allowed to decay sufficiently long (two to four years) that the temperature of the sodium is 400°F. If the fuel subassemblies were shipped in sodium or were contaminated with sodium upon arrival at the facility, a new facility for removal of the fuel subassemblies from the shipping cask and for removing the sodium from the external surfaces of the fuel subassemblies would be required. Within the head-end processing system, the possible presence of sodium inside defective fuel rods (internal sodium) causes concern over the potential for fires prior to placing the fuel in the dissolver and for violent reactions within the dissolver. The sodium problem is probably most severe in the dissolver since sodium reacts explosively with the oxides of nitrogen even when blanketed with argon. Either the development of a reliable method for detecting failed fuel rods or the development of a suitable method for reacting sodium harmlessly (voloxidation) after the shearing step is required before LMFBR fuels can be processed at NFS. The development of a proven and feasible sodium deactivation technology will be required to solve the head-end sodium problems, regardless of the fuel decay time used.

Dissolution. The NFS dissolvers appear to be capable of accommodating LMFBR fuel without modification. It is estimated that sheared FTR fuel (including the gas plenums) could be processed in the two existing NFS dissolvers on a 12-hr dissolution cycle at a throughput of 0.6 metric ton of U + Pu per day. If the gas plenums are removed, the rate would be increased to 1.23 metric tons of U + Pu per day. The dissolution times recommended for the NFS dissolvers are 12 hr based on 8 *M* HNO_3 and 8 hr for 13 *M* HNO_3. Actually, NFS may use a 20-hr dissolution time or longer for LWR fuels when terminal pieces of sheared fuel up to 3½ in. long are present. Hopefully, new shearing technology that will resolve the short terminal pieces problem can be developed.

Criticality can be avoided in the dissolver by limiting the fluid level to a point not significantly above the top of the fuel baskets; however, nuclear poisons are required to avoid criticality in the downstream feed adjustment tank. It is proposed that a redundant system be provided to ensure that all solutions fed to the dissolver contain a prespecified concentration of nuclear poison. Such a system could guarantee that no unpoisoned solutions would reach the large-diameter feed adjustment tank.

Solvent extraction. The existing NFS solvent extraction system has the capability for producing the desired decontaminated uranyl and plutonyl nitrate solutions. The basic system would be comprised of a 15 vol % tri-*n*-butyl phosphate–*n*-dodecane coextraction column, a partitioning column, a uranium stripping column (plus two solvent extraction purification columns), and plutonium solvent extraction and stripping (two cycles). The second plutonium cycle would be used for final purification of the plutonium. Flowsheets were developed for each of the LMFBR fuels, using a combination of experimental data and the computer code SEPHIS. The solvent extraction system can easily process 1 metric ton of U + Pu per day, except in the case of the plutonium stripping columns, which limit the throughput to about 0.3 to 0.6 metric ton of U + Pu per day. Nuclear safety in the solvent extraction columns will not be of concern, provided the ^{240}Pu isotopic content is 12% or greater.

Plutonium packaging and shipping. The NFS plutonium packaging and shipping facility can be used to recover plutonium as plutonyl nitrate from LMFBR fuels. However, the plutonium stripping contactor (second plutonium cycle) can supply twice as much feed to the facility as that part of the plant can process. Thus, it becomes a processing bottleneck at the product end of the NFS plant. The estimated maximum processing rates for the bottleneck are 0.3 and 0.6 metric ton of Pu per day for FTR and the AI-GE fuels respectively.

Site effluents. *Gaseous.* A review of the present NFS equipment and operations (including the 1973 alterations) indicates that emissions of gaseous fission products will probably not exceed the quantities permitted by *current* regulations when up to 1 metric ton of U + Pu from LMFBR fuel cooled longer than 200 days is processed per day. The control and the release of iodine govern the selection and restriction of the 200-day decay time. The processing of fuels decayed 200 days or less would probably require the addition of a new off-gas treatment system to the fuel receiving and storage facility, the PMC, the GPC, and the waste storage tanks.

The release of tritium to the environment via the NFS stack would fall within the present limitation on the

routine stack release for up to 5 metric tons of typical LMFBR fuel per day; the ^{85}Kr restraints would allow the processing of 1.1 metric tons per day.

Liquid. With the exception of the discharge of iodine, the present procedures and equipment at NFS for handling low-level liquid waste effluents appear to be adequate for LMFBR fuels.

Assuming that 10% of the tritium produced in the fuel[35] reports to the low-level waste, it is estimated that 1.5 metric tons of typical LMFBR fuel could probably be reprocessed per day without exceeding the current guidelines of 5% of 10 CFR 20 limits in Cattaraugus Creek. If it is assumed that all the tritium produced in the fuel reports to the low-level waste, a throughput of only about 0.14 metric ton per day would be permissible. The estimate of the release of 10% of the tritium to the low-level waste assumes that the bulk of the tritium would diffuse from the fuel during irradiation, since most of the tritium in fuel that is processed reports to the low-level waste.

Experience indicates that the discharge of ^{129}I to the creek would limit LMFBR production rates, regardless of the decay time, while the discharge of ^{131}I would cause an even more severe limitation at short decay times. The ^{129}I concentration (without the addition of new equipment) would possibly limit the throughput of the NFS plant to only ~0.25 metric ton of typical LMFBR fuel per day. However, iodine-removal technology currently under development has the potential of alleviating this problem to the extent that it would no longer appreciably influence the capacity of the plant.

35. Present experience would indicate that about only 5% or less of the tritium produced in the fuel would arrive at the reprocessing plant.

3. Development of Methods for Reprocessing HTGR Fuels

3.1 HEAD-END REPROCESSING STUDIES WITH UNIRRADIATED FUEL

Comminution Studies with Resin-Bonded Fuel

Two unirradiated graphite fuel samples containing resin-bonded TRISO-coated[1] ThC_2 and UC_2 particles were crushed in the hammer mill, using ¾- and ⅜-in. grate spacings, to determine the size distribution and particle coating breakage (Table 3.1).

Fuel particles or pieces of the fuel rod were found in all +60-mesh or larger size fractions from both tests. Particle coating breakage was determined by leaching the product with Thorex dissolvent (13 *M* HNO_3; 0.04 *M* F^-, 0.1 *M* Al^{3+}). Coatings were broken on 1.6% of the fertile and 0.8% of the fissile particles in the −¾-in. hammer mill product and on 17% of the fertile and 3.4% of the fissile particles in the −⅜-in. hammer mill product. In the head-end reprocessing flowsheet, all of the fertile material will be recovered; thus the 17% breakage of fertile particle coatings in the −⅜-in. hammer mill product is not significant. The 3.4% loss (crossover) of fissile material due to broken particle coatings in the −⅜-in. product is well below the 10% crossover allowed for the reprocessing flowsheet.[2]

Table 3.1. Size distribution of the product obtained by crushing HTGR fuel in a hammer mill

Size fraction	Hammer mill product (wt %)	
	¾-in. grate spacing	⅜-in. grate spacing
+¾ in.	0.8	
−¾ +⅜ in.	19.7	0.2
−⅜ in. +4 mesh	27.0	14.6
−4 +12 mesh	14.8	20.1
−12 +30 mesh	19.3	30.6
−30 +45 mesh	9.3	13.0
−45 +60 mesh	2.5	4.7
−60 +80 mesh	1.3	3.3
−80 mesh	5.6	13.6
	100.3	100.1

Comminution and Fluidized-Bed Burning Studies with Pitch-Bonded Fuels

One pitch-bonded fuel rod, containing TRISO-coated[1] fissile and BISO-coated[1] fertile ThC_2 particles, was received from Gulf Energy and Environmental Systems. It was crushed in a hammer mill with the grates set to pass −⅜-in. material. Microscopic examination of the crushed material showed very few, <1%, broken TRISO particles. The crushed fuel rod was then combined with graphite at a 1 to 4 ratio, and the mixture was burned in the fluidized-bed burner (3 psig, 1.25 fps superficial gas velocity, 16.3 kg of carbon per square foot per hour); 90- to 120-mesh alumina was used as the heat transfer medium. No operating problems were encountered, and the buildup of fine particles on the filters, as indicated by the pressure drop, was similar to that obtained when TRISO-TRISO fuel is burned. Microscopic examination of the burner residue indicated that the breakage of TRISO-coated particles was low and that the BISO-coated ThC_2 particles had been converted to a fine ThO_2 powder which was associated with the alumina. Leaching tests of two samples riffled from the burner residue showed 4.0% breakage in one and 1.3% breakage in the other

1. These particles were made and coated by Gulf General Atomic Division, Gulf Energy and Environmental Systems, Inc. The TRISO coatings consist of a porous carbon buffer layer on the fuel kernel, a thin sealer layer, and two outer isotropic pyrocarbon layers separated by a silicon carbide layer; BISO coatings consist of two pyrocarbon layers.

2. *Chem. Technol. Div. Annu. Progr. Rep. May 31, 1970*, ORNL-4572, p. 85.

sample (average, 2.6%) of the TRISO-coated particles broken in the crushing and burning step. Some of this material was also burned with the fluidized-bed burner operating at a much higher carbon burning rate (47.5 kg ft^{-2} hr^{-1}, 22 psig, 1.75 fps superficial velocity). Breakage of the TRISO coatings, based on microscopic examination of the residue, appeared to be similar to that obtained with the lower carbon burning rate.

Fluidized-Bed Burning Rates

Tests were carried out in the 2-in.-diam fluidized-bed burner using crushed graphite (material passing a $^3/_8$-in. grate spacing in the hammer mill) to determine the maximum burning rate as a function of oxygen partial pressure and superficial gas velocity. Norton RR grade alumina (–90 +120 mesh) was used as the heat transfer medium. The reagent gas composition was held constant at 70% oxygen–30% diluent since previous work indicated that, with 100% oxygen, breakage of the fertile particle coatings increased and sintering of the bed occurred.[3] Wall temperature was held at 750 ± 25°C. Increasing the bed overpressure from 3 to 18 psig while holding the superficial gas velocity constant at 1.25 fps increased the carbon burning rate from 16.3 to 30.1 kg ft^{-2} hr^{-1} (see Table 3.2). A further increase in pressure to 22 psig caused a hole to be burned through the side of the burner. Repeating these tests with a superficial velocity of 1.75 fps increased the burning rate from 22.8 to 47.5 kg ft^{-2} hr^{-1} as the bed overpressure increased from 3 to 22 psig. These values can be used to obtain an idea of the size of the primary burner that would be required for a TURF demonstration plant reprocessing 9.7 Fort St. Vrain reactor (FSVR) fuel elements per day (i.e., a burning rate of ~41 kg/hr). The diameter of the burner would decrease from the $22^1/_2$ in. required for a superficial velocity of 1.25 fps at 3 psig to $12^5/_8$ in. for a superficial velocity of 1.75 fps at 22 psig.

TURF Process Flowsheets

Detailed process chemical flowsheets have been prepared for the head-end and Acid-Thorex pilot plants. These flowsheets are presented in simplified form in Figs. 3.1 and 3.2. Calculations were based on the following assumptions: (1) production capacity (three shifts) will be 12 kg of $(Th,U)O_2$ microspheres (Th/U ratio = 4.25) per day, and (2) all of the uranium will be ^{233}U recovered from the fertile particles in spent FSVR fuel. For simplicity, the uranium, thorium, and fission product concentrations and isotopic compositions that were calculated by the ORIGEN code for fertile particles discharged from the FSVR after two years of full-power operation were used as the average values for all fuel reprocessed. Thus, reprocessing approximately ten fuel elements per day will provide sufficient uranium, when combined with the internal uranium recycle stream, to produce 12 kg of microspheres per day.

Table 3.2. Fluidized-bed burning rates

Superficial gas velocity (fps)	Burning pressure (psig)	Oxygen flow rate (std liters/min)	Carbon burning rate (kg ft^{-2} hr^{-1})
1.25	3.0	11.0	16.3
1.25	12.0	17.0	24.5
1.25	18.0	20.4	30.1
1.25	22.0	22.9	*a*
1.75	3.0	15.5	22.8
1.75	12.0	23.5	34.6
1.75	18.0	28.5	42.0
1.75	22.0	32.2	47.5

[a]Hole burned in the reactor wall.

Burner Off-Gas Decontamination Studies

Hot-cell studies[4,5] have shown that the burner off-gas evolved during the head-end reprocessing step will contain 98+% of the tritium, noble gases, and iodine present in spent HTGR fuel elements. The expected analysis for the burner off-gas produced during the head-end reprocessing of FSVR fuel in TURF is given in Table 3.3.

Although it is anticipated that at least 99% of the radioactive contaminants must be removed from the burner off-gas stream, the chemically reactive contaminants should present no special separation problems. Charcoal trapping, Freon absorption, membrane permeation, etc., are effective in separating the noble-gas contaminants from dissolver-type off-gases, but the physical similarity of carbon dioxide (in the burner-type off-gas) and the noble gases with respect to such separations practically precludes the direct use of these procedures for burner off-gas cleanup.

Thus it appears likely that the critical stage in the decontamination of burner off-gas will be the selective

3. *Chem. Technol. Div. Annu. Progr. Rep. May 31, 1970,* ORNL-4572, p. 90.

4. *Chem. Technol. Div. Annu. Progr. Rep. May 31, 1970,* ORNL-4572, p. 92.

5. *Chem. Technol. Div. Annu. Progr. Rep. May 31, 1969,* ORNL-4422, p. 114.

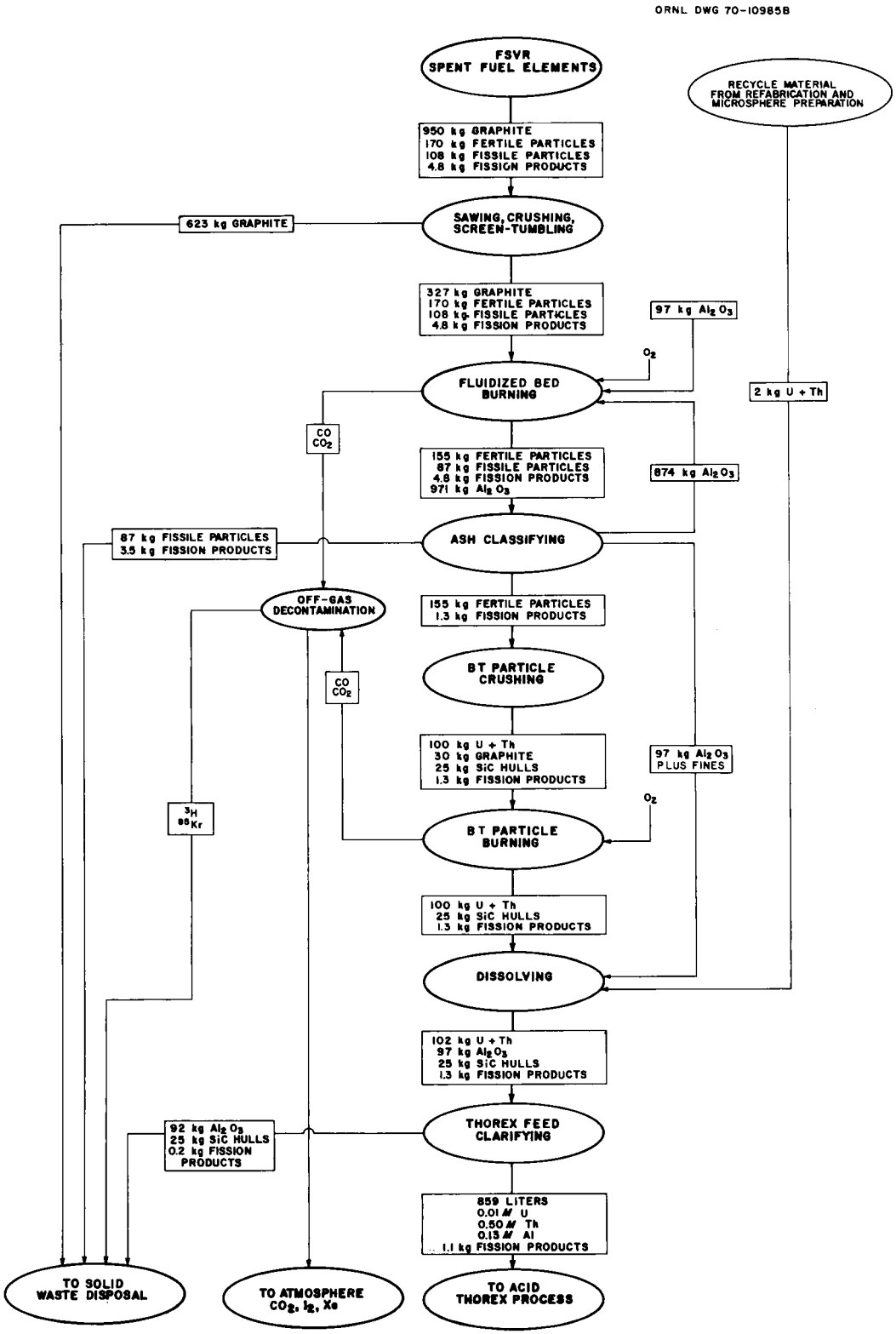

Fig. 3.1. Head-end process chemical flowsheet.

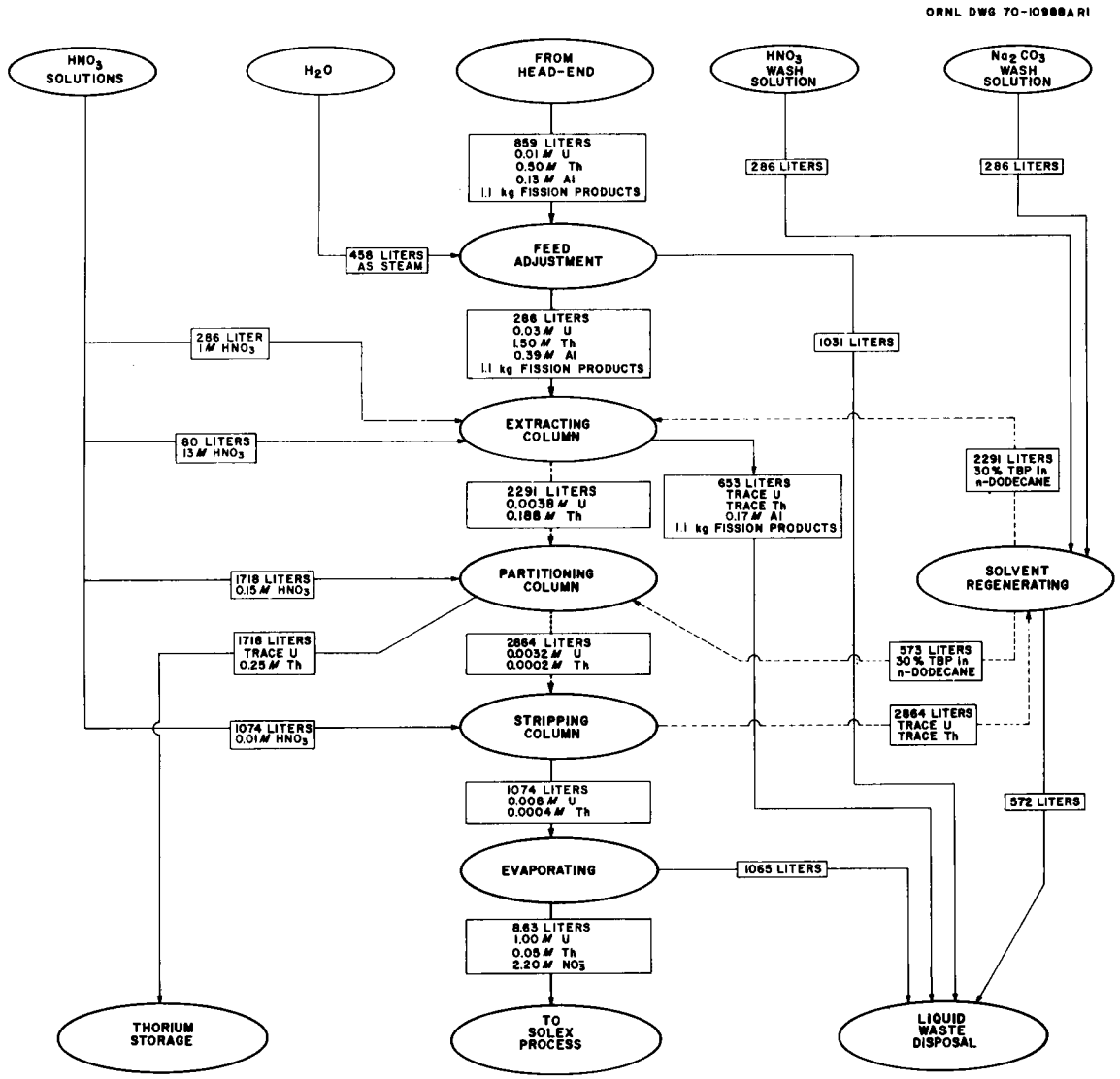

Fig. 3.2. Acid-Thorex process chemical flowsheet.

removal of the bulk of the carbon dioxide. In line with both pretreatment and final cleanup procedures, three carbon dioxide removal processes are presently being investigated. These processes are discussed below.

Liquefaction of the carbon dioxide fraction, coupled with gas rectification. Because the phase characteristics of carbon dioxide differ appreciably from those of other burner off-gas constituents, it is possible that the bulk of the carbon dioxide can be removed by liquefaction. Subsequent gas rectification would be necessary since the solubility of the noble gases in liquid carbon dioxide and the vapor pressure of liquid carbon dioxide will be significant at the probable fractionation conditions.

Catalyzed sorption in hot potassium carbonate. This is a process that typically employs both high temperature and high pressure in a continuous packed-tower operation. The carbonate-bicarbonate sorption-regeneration cycle is generally aided by a catalyst such as arsenious acid.

Solidification of the carbon dioxide. By forming solid carbon dioxide, the remaining off-gas components could be swept away in relatively pure form. Occlusion and interstitial trapping of contaminants in the carbon dioxide snow can hopefully be controlled by properly manufacturing and collecting the dry-ice crystals.

Table 3.3. Expected analysis[a] of burner off-gas evolved during the head-end reprocessing step

Major components	scfm	Mole fraction
CO_2	28.9	0.897
O_2	2.4	0.075
N_2	0.9	0.028
Contaminants	**ppm**	**Ci/day**
^{85}Kr	5×10^{-1}	1024
^{3}H	9×10^{-4}	16
^{131}I	1×10^{-6}	1
Total Xe	23	
Total Kr	6	
Total I	1	

[a]See head-end reprocessing flowsheet (Fig. 3.1); based on ORIGEN code, 9.7 FSVR blocks per day, 2-year exposure, 150-day cooling period.

3.2 HEAD-END REPROCESSING STUDIES WITH IRRADIATED FUELS

Head-end methods are being developed for the reprocessing of HTGR fuel. The reprocessing studies cover both the Fort St. Vrain reactor (FSVR) and the 1100-MW(e) reference reactor fuels. The primary emphasis is on FSVR fuel since it will be the first HTGR fuel to become available for use in recycle studies in the Thorium-Uranium Recycle Facility (TURF). A recent important programmatic change that affects the head-end reprocessing studies is the firm decision by Gulf General Atomic (GGA) to use bonded graphite fuel sticks rather than loose fuel particles in the graphite block. Fuel sticks for the FSVR contain TRISO-coated $(U,Th)C_2$ fissile and ThC_2 fertile particles that are expected to maintain their integrity during exposure in the reactor and through the reprocessing steps. A method is being developed to separate fertile from fissile particles, based on their difference in size after the block graphite, binder graphite, and the outer pyrocarbon (PyC) layer are removed by burning.

The reference 1100-MW(e) reactor fuel uses TRISO-coated $^{235}UC_2$ fissile and BISO-coated ThC_2 and $(^{233}U,Th)O_2$ fertile particles. Burning should convert the ThC_2 particles to a finely powdered oxide, which must be separated from the fissile particles. The $(Th,U)O_2$ fertile particles are expected to maintain their integrity during the burning step. A method is being developed to recover the fertile material by leaching all the fluidized-bed burner ash except the recycle alumina. The bred uranium will be separated from the thorium in the Acid-Thorex solvent extraction process. Although fissile particles will probably be stored, the uranium and thorium can be recovered by a separate crush-burn-leach process, followed by a solvent extraction step. The previously published reprocessing flowsheet has been modified to reflect these changes.

The lowest calculated power cost for an HTGR occurs when only the bred uranium (^{233}U) is recycled. Since cost penalties accrue for crossover of ^{233}U to the discarded ^{235}U fraction, or of ^{235}U to the ^{233}U fraction, emphasis has been placed on determining the efficiency of separation of the fertile (^{233}U) particles from the fissile (^{235}U) particles in both engineering-scale and hot-cell tests. Crossover can occur by particle breakage and/or by inefficient particle separation. For example, the particles cannot be separated by screening if they stick together in small agglomerates after burning.

A second set of irradiated fuel compacts and unirradiated controls was obtained through the courtesy of the Dragon Project. The fuel compacts that were received are listed in Table 3.4. Unirradiated compacts of the following fuel types have been studied: 2M4, 19M, 18M, and 38M. The study of irradiated compacts of fuel types 2M4 and 19M is now in progress.

The processing flowsheets used in these small-scale studies are dependent on the fuel type. As seen in Table 3.4, fuel type 2M4 is a BISO-coated mixed oxide fuel of the reference recycle type; however, it is not sol-gel derived. The reference flowsheet for this fuel is crush-burn-leach. It is of interest to determine if the oxide kernels retain their integrity adequately to be separated from the alumina according to size, because recycle of the alumina to the burner without leaching would be advantageous. In addition, both the fissile and fertile particles of the reference fuel proposed for future HTGR's have BISO coatings. If this fuel is to be recycled in such a way that the ^{236}U is always kept separated from the ^{233}U, the fertile oxide kernel must retain its integrity through the burning step so that it can be separated from the alumina and fissile particle ashes (U_3O_8) by a procedure based on size difference. It is virtually certain that the BISO-coated fissile particles will convert to powdered U_3O_8 because of their high burnup.

Fuel types 18M (TRISO UC_{20}) and 38M [BISO $(U/5Th)C_{2.4}$] were mixed to simulate a reference B block makeup fuel. In this concept, the TRISO coating preserves the fissile (^{235}U) particle through the burning step so that crossover of uranium between the fuel types is minimized.

Table 3.4. Irradiated Dragon compacts[a] received for ORNL head-end studies

Experimental fuel no.	Th/U atom ratio (93% ^{235}U)	Kernel composition	Kernel diameter (μm)	Type of coating	Thickness of coatings (μm)	Comments
2M4	10	$(U,Th)O_2$	500	BISO	130	Simulates ($^{233}U,Th)O_2$ reference (BISO) recycle particle for 1100-Mw (electrical) HTGR. Will be compared with ORNL sol-gel recycle particle.
2M7	10	$(U,Th)O_2$	500	TRISO	160	Simulates ($^{233}U,Th)O_2$ alternate (TRISO) recycle particle for 1100-Mw (electrical) HTGR.
2M10	10	$(U,Th)C_2$	500	TRISO	150	Suitable for comparison of carbides vs oxides in head-end studies. Simulates Ft. St. Vrain fertile-fissile particle.
3M	10	$(U,Th)C_2$	900	TRISO	50/30/80	Large kernel size; can be mixed with other fuels for particle separation studies of TRISO-TRISO and TRISO-BISO mixes (18M and ORNL sol-gel BISO-coated fuels).
18M		UC_{20}	500	TRISO	25/30/70	Simulates fissile (^{235}U) particles. Will be used in particle separation studies.
19M		ThC_2 UC_{10}	900 500	TRISO TRISO	25/30/70 25/30/70	Simulates Ft. St. Vrain fuel particles. Will be used in particle separation studies.
38M	5	$(U,Th)C_2$	500	BISO	40/80	1100-Mw (electrical) HTGR simulated fertile-fissile particle with accelerated burnup. Could be mixed with UC_{10} TRISO-coated particles (which are presently available) for separation studies.
ORNL sol-gel[b]	3, 4.5	$(U,Th)O_2$	290	BISO		1100-Mw (electrical) reference recycle fuel (fertile).

[a]To a burnup of about 7% fissions per initial metal atom and 2.5×10^{21} fast fluence.

[b]12 to 18% fissions per initial metal atom. Not yet received.

Fuel type 19M is analogous to the FSVR fuel; that is, it consists of a mixture of small TRISO-coated UC_{10} and larger TRISO-coated ThC_2. Since both particles are TRISO coated, a postburning particle separation based on size can yield three fractions: fertile, fissile, and alumina (plus broken particle ash). An unirradiated compact of this type has been studied, and results are reported below. Work on the irradiated compact is in progress.

Crushing Studies with Dragon Compacts

In each head-end flowsheet, the preliminary step is size reduction to provide suitable feed for a burner. Typically, one compact of each fuel type was available. For these cases, half a compact (napkin ring) was saved for an archive sample. The remaining half was crushed and sieved to determine the product size distribution for correlation with breakage results.

The half compacts were crushed by the standard procedure (first by the $^5/_8$-in. jaw opening and then by the $\sim^1/_8$-in. jaw opening). Since sawing has been found to break all particles contacted by the saw, the weighed fines were usually combined with the crusher product before sieving. However, the saw fines (a total of 5.9% of the compact) from compact 22365, containing irradiated BISO-coated oxide (2M4), were sieved separately to obtain an estimate of their size distribution. Table 3.5 shows the size distribution of these fines as well as the results for the crusher-product–fines combinations for the other compacts.

Two general observations can be made on examining the early crushing results: (1) The particle loadings are lower (i.e., the burnable carbon content is greater) than was the case in compacts received previously. The results show a steadily decreasing weight with decreasing size (similar to the results of crushing pure graphite), without a large weight of loose whole particles in the +42-mesh size fraction. (2) There is evidence for some differences in crushing behavior due to fuel type (e.g., TRISO vs BISO) and level of irradiation, but these are not excessive. Additional confirmatory experiments are needed to determine the relationship.

Head-End Studies of Unirradiated Dragon Compact 14719, Fuel Type 19M (TRISO UC_{10}–TRISO ThC_2)

Fuel type 19M is an experimental fuel from the Dragon Project Metallurgical Series I. The fissile particle kernel is fully enriched UC_{10}, 60 to 70% of theoretical density, 422 to 600 μm (509 μm, av) in diameter, with PyC/SiC/PyC coatings of 18/31/63 μm respectively. The fertile particle kernel is 850- to 1200-μm-diam ThC_2, 60 to 70% of theoretical density, with PyC/SiC/PyC coatings of 30/29/56 μm respectively.

Compact 14719 was weighed and sawed into two rings. One became an archive sample, while the other was used in further studies (Fig. 3.3). The sawdust was burned and leached to determine particle breakage. (The thorium and uranium carbide kernels exposed by breakage are readily soluble.) One ring was crushed by the standard procedure and sieved (Table 3.5), and then each sieve fraction was divided into duplicate samples. Overall handling losses were <1%. Each sample was mixed with about 2 g of Al_2O_3 per gram of fuel and was burned in a fluidized-bed burner at 750°C using a superficial gas velocity of 1 to 1.5 fps. Burning proceeded over a 4- to 8-hr period with oxygen-nitrogen mixtures. About 90% of the fuel weight charged was

Table 3.5. Crushing and sieving results

Type	Comment	Percent by weight on screens						Total handling loss (%)
		+4	−4 +9	−9 +20	−20 +42	−42 +100	−100	
19M	TRISO-TRISO[a]	3.4	48.7	27.3	11.0	4.4	5.3	0.9
19M	TRISO-TRISO[b]	4.5	58.0	25.3	6.9	3.1	2.2	0.4
2M4	BISO-oxide[a]	0.7	45.6	38.7	9.6	2.6	2.9	0.1
2M4	BISO-oxide[b]	4.7	53.9	26.9	8.7	2.6	3.2	0.5
18M	TRISO UC_{20}[a]	13.8	40.4	18.1	14.1	6.4	7.1	2.2
38M	BISO $(U,Th)C_{2.4}$[a]	0.4	45.5	40.0	8.4	2.7	3.0	0.4
2M4	BISO-oxide sawdust[c]	0	0	0	21.1	34.8	44.1	4.1

[a]Unirradiated; standardized procedure for the laboratory crusher was used.
[b]Irradiated; standardized procedure for the hot-cell crusher was used.
[c]About 6% of compact.

ORNL-DWG 71-6325

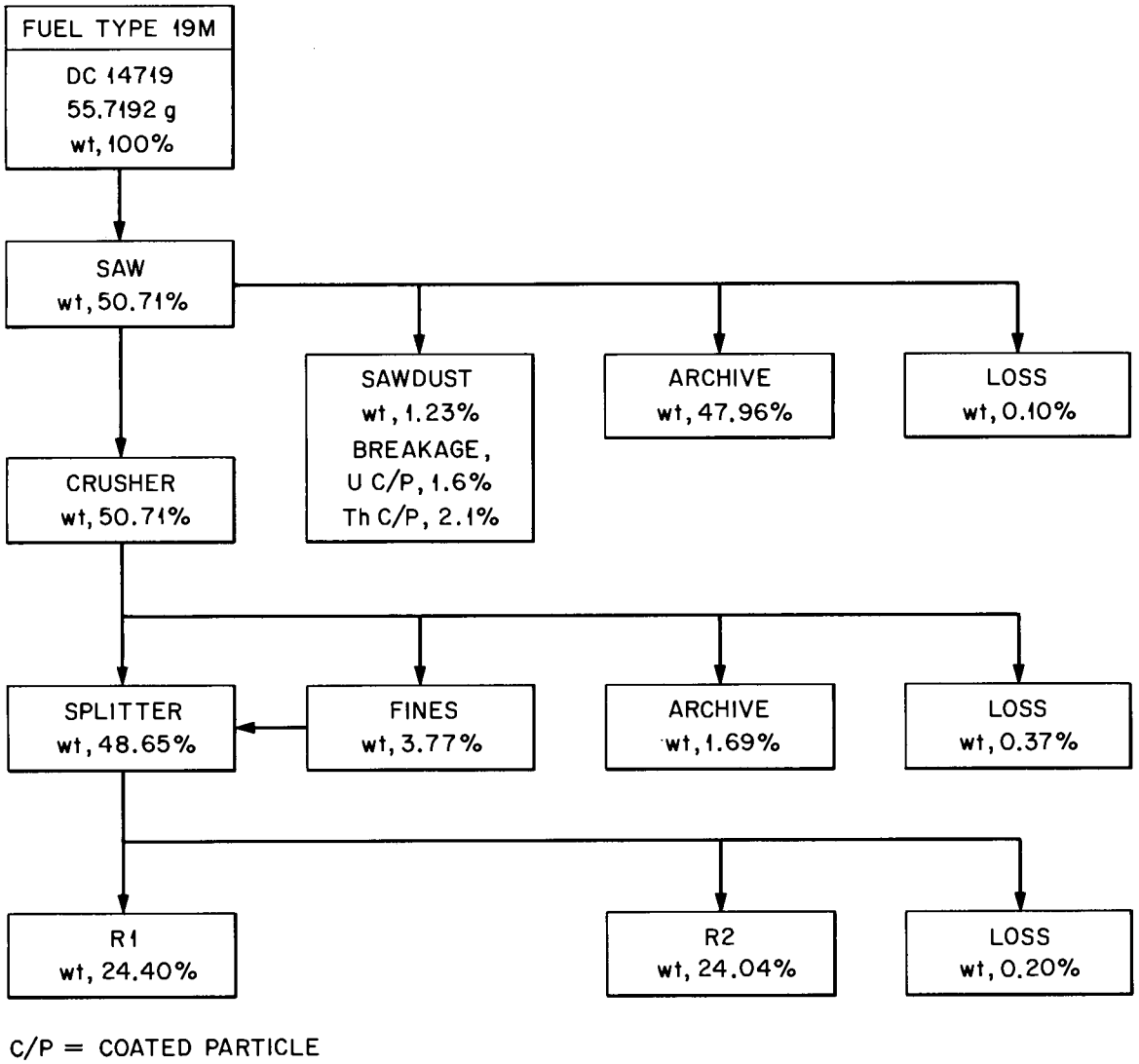

Fig. 3.3. Results of sawing, crushing, and sieving unirradiated Dragon compact 14719, type 19M.

lost during burning. Sample R1 contained some unburned carbon. The burner product was screened, and then the screened fractions were inspected and combined to give three fractions: whole SiC-coated ThC_2 particles, whole SiC-coated UC_{10} particles, and alumina plus broken particles of both kinds. Since there were very few whole SiC-coated particles, only the alumina was processed further. The weights, expressed in grams, of leached uranium and thorium were converted to equivalent weights of SiC-coated particles by dividing by the factors 0.44 and 0.75 respectively.

Particle breakages, based on the calculated total weight of coated particles, are given in Fig. 3.4. Although a small sample burned in a ceramic dish and leached indicated that about 2% of the fissile and about 5% of the fertile particles were broken in the uncrushed fuel, breakages of about 6 to 9% of the fissile particles and about 20 to 24% of the fertile particles were found in crushed fuel.

Head-End Studies on Unirradiated Compact 22396, Type 2M4 (BISO Oxide)

This experimental Dragon fuel is from the Dragon Project Metallurgical Series II. The kernel is $(10Th/U)O_2$, 60 to 70% of theoretical density, 422 to 600 μm in diameter (523 μm, av), and has two pyrolytic carbon coatings (40/80 μm). The density of the outer coating is

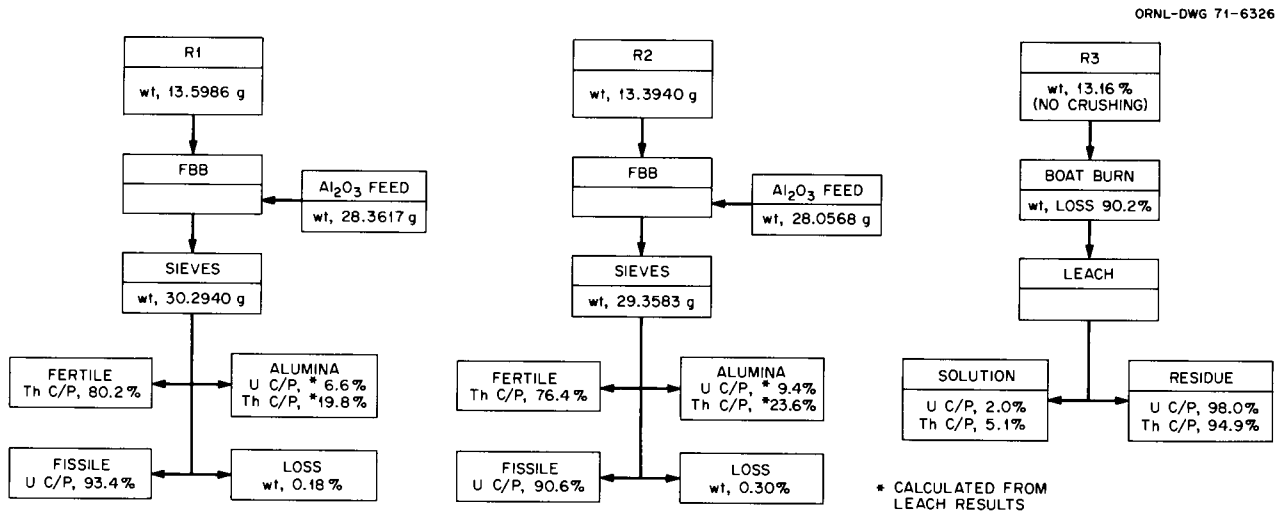

Fig. 3.4. Results of fluidized-bed burning, sieving, and leaching steps with Dragon compact 14719, type 19M.

2.0 g/cc, with a Bacon anisotropy factor of 1.18. The compact contained 14% coated particles by volume.

This type of fuel is similar to the reference recycle fuel proposed for commercial 1100-MW(e) reactors. Although separation of ^{233}U from $^{235(236)}U$ is not required for the recycle fuel blocks, this type of particle might also be used with a TRISO- or a BISO-coated UO_2 fissile particle (which would convert to U_3O_8 powder on burning) in makeup fuel blocks. Consequently, separation by sieving was tested on the burner product before leaching.

The compact was sawed in half. The saw fines were collected, weighed, and added to the crusher product before sieving. One half of the compact was crushed by the standard procedure to give the fractions shown in Table 3.5. The crushed material was sieved, and each sieve fraction ≥42 mesh was divided into two samples (Fig. 3.5). Each of the samples was composited with one sample from the other sieve fractions to produce duplicate samples of crushed fuel. The crusher fines (<42 mesh) were burned and leached. Crusher breakage was about 1.2%. Handling losses were less than 1%.

Each of the duplicate samples was burned in a fluidized bed at 750°C, as before. The burner product was sieved into a series of sizes, inspected, and composited into +60- and −60-mesh fractions (Fig. 3.6). The fractions were leached, and 82 to 85% of the fuel was found in the +60-mesh fraction and 15 to 17.5% in the −60-mesh fraction. This result indicated that more durable oxide kernels than those in this compact would be required if particle separation based on size is required for BISO-coated oxide particles. The burn-leach process is suitable for this unirradiated recycle type fuel if particle separation is not required. Overall losses to insoluble residues were 0.05% of the uranium and 0.21% of the thorium.

Head-End Studies of a Synthetic Mixture – TRISO UC_{20}–BISO $(5Th/U)C_{2.4}$ [a Possible 1100-MW(e) Makeup Fuel Type]

Compact 14397, Dragon Project Metallurgical Series II, containing type 18M fuel, has a kernel of UC_{20} that is 422 to 600 μm in diameter and 60 to 70% of theoretical density. The standard Dragon TRISO coating was used (PyC/SiC/PyC, 25/30/70 μm). Compact 14158 (Metallurgical Series II), containing type 38M fuel, has a kernel of $(5Th/U)C_{2.4}$ that is 600 μm in diameter and 60 to 70% of theoretical density. It has a two-layer PyC coating 121 μm thick.

In a synthetic mixture made up of these two fuel types, the BISO $(U,Th)C_2$ particle represents the ^{233}U recycle particle. Briefly, head-end reprocessing consists of crushing, burning, and leaching. The unbroken TRISO particles are recovered for storage by separation according to size after burning or after leaching. The BISO particles, which should burn to a fine oxide powder, would be recovered from the alumina by leaching.

The flowsheets for the crushing step and the results obtained are given in Figs. 3.7 and 3.8. The three middle-size fractions (+9, +20, +42) were each divided into two samples, which were combined between compacts to give duplicate samples R1 and R2 for burn-leach testing. The fine fractions (−42 mesh) were burned and leached to determine particle breakage

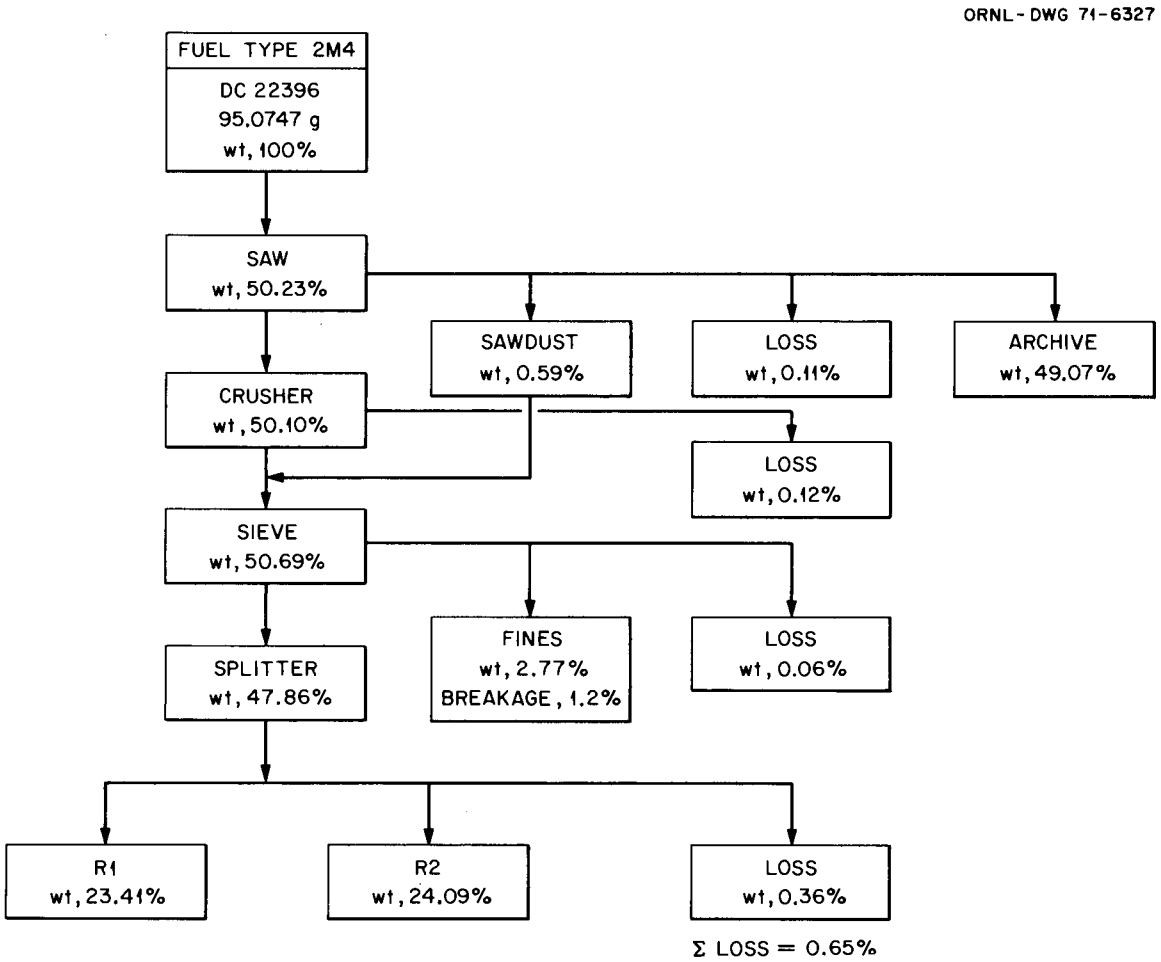

Fig. 3.5. Results of crushing and dividing Dragon compact 22396, type 2M4.

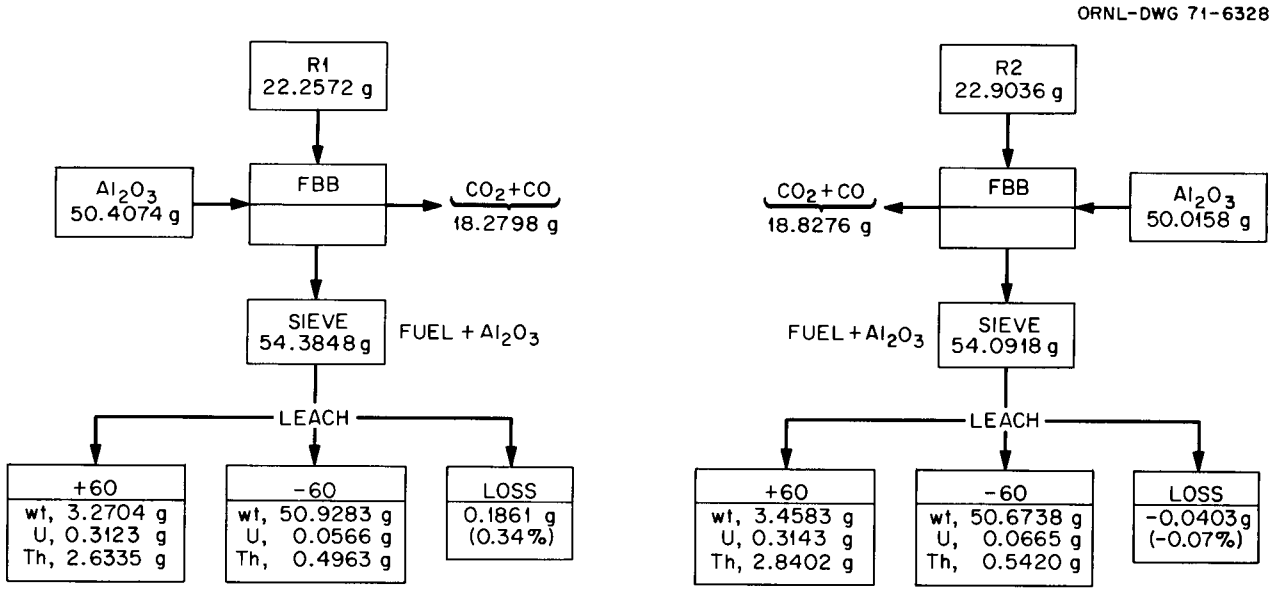

Fig. 3.6. Results of fluidized-bed burning, sieving, and leaching steps with unirradiated Dragon compact 22396, type 2M4.

ORNL-DWG 71-6329

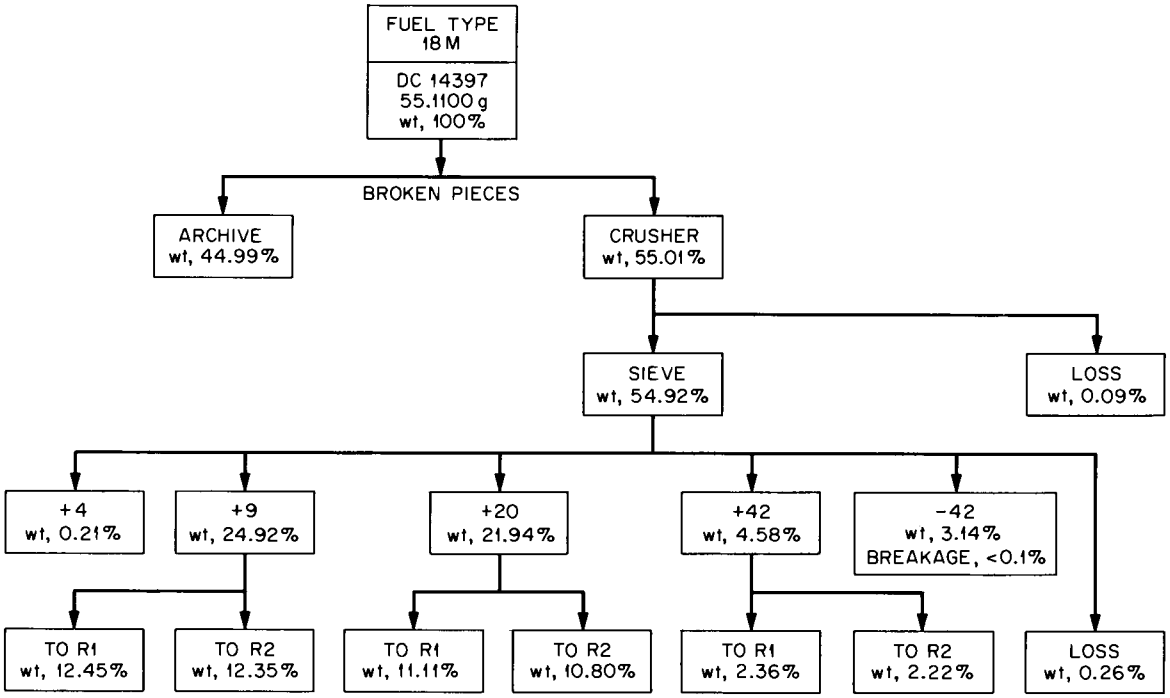

Fig. 3.7. Results of crushing and sieving unirradiated Dragon compact 14397, type 18M.

during comminution operations. Less than 0.1% of the TRISO UC_{20} and 4% of the BISO $(5Th/U)C_{2.4}$ particles were found to be broken.

Samples R1 and R2 were burned in a fluidized bed with about 1 g of Al_2O_3 per gram of fuel (Fig. 3.9). The burner product was sieved to recover a fissile fraction (TRISO particle, +35 mesh), a fertile fraction (–35 +60 mesh), and the alumina fraction (–60 mesh). The three fractions were leached, and 3 to 11% of the leachable oxides (Th + U) were found in the fissile fraction, 52 to 58% in the fertile fraction, and the remaining 32 to 45% in the alumina fraction. Losses to the insoluble residues consisted of <0.1% of the heavy metals.

A rather unexpected result was the finding of 3 to 10% of the oxidized carbide particles in the fissile (+35-mesh) fraction. The oxidation apparently occurred without completely reducing the carbide particle to a fine ash. This occurrence makes leaching of the fissile fraction of this fuel mandatory. It may be necessary to determine whether it was failure of the particles to crumble during oxidation or agglomeration of ash particles in the fluidized bed which led to this result. In experiments[6] with compacts irradiated in the Peach Bottom Reactor, reuse of the alumina fraction was precluded by an accumulation of heavy metals in this fraction when the bed ash was sieved into an alumina (+120-mesh) fraction and a fines (–120-mesh) fraction. This accumulation was attributed to heavy-metal oxide sticking to the alumina particles. In light of the above result, this might have been due to incomplete powdering of the fuel kernel and separation of a third fraction (i.e., +80-mesh oxide). This question can only be answered by alumina recycle tests using irradiated BISO-coated thorium-uranium carbides.

In the experiment as carried out, the sieved burner products were leached in three fractions. However, using the original sieve weight distribution, we calculated that, if the alumina had been screened to the size range of the original alumina (–80 +100 mesh), only about 10 to 15% of the heavy metals would have been found with the alumina. Thus, it may be possible to recover 85 to 90% of the heavy metals by leaching only the small amounts of material present with +80- and –100-mesh fractions. By close-screening (–80 +100 mesh) the alumina, it may be possible to recycle the alumina fraction to the burner without leaching.

6. V. C. A. Vaughen et al., *Hot-Cell Evaluation of the Burn-Leach Method for Reprocessing Irradiated Graphite-Base HTGR Fuels,* ORNL-4120, p. 45 (February 1970).

ORNL-DWG 71-6330

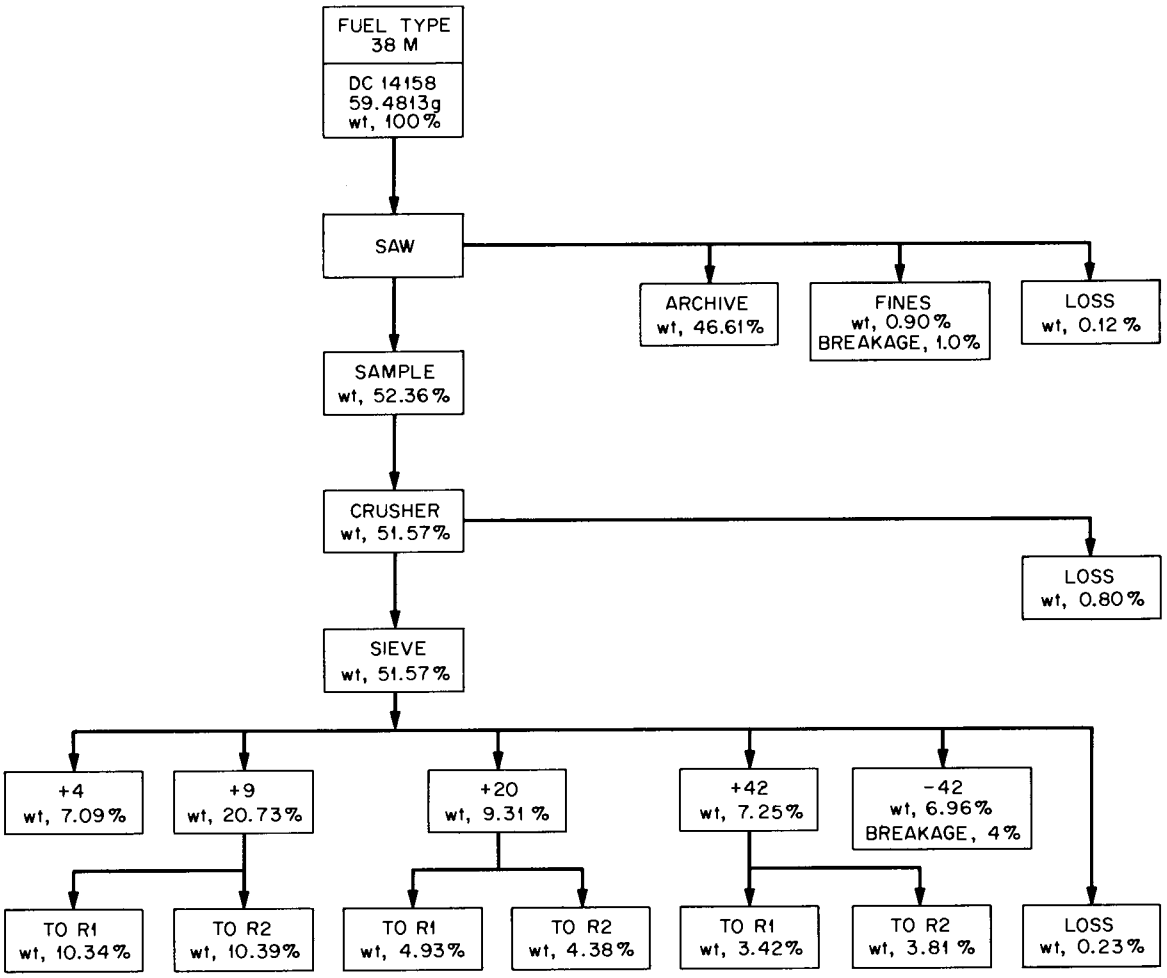

Fig. 3.8. Results of sawing, crushing, and sieving unirradiated Dragon compact 14158, type 38M.

ORNL-DWG 71-6331

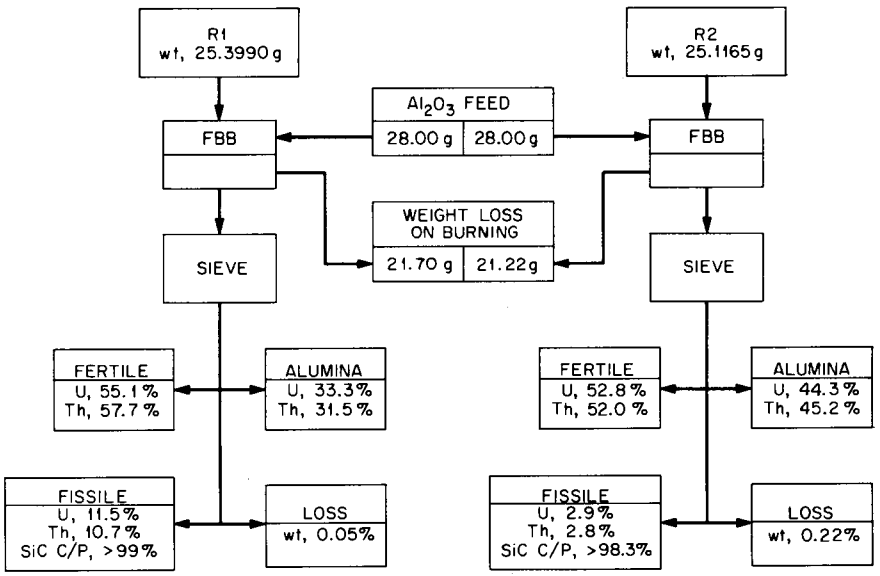

Fig. 3.9. Results of fluidized-bed burning, sieving, and leaching steps with unirradiated Dragon compacts 14397 and 14158, types 18M and 38M.

3.3 PROCUREMENT OF HTGR FUEL FOR HEAD-END STUDIES

Unirradiated Fuel

Gulf General Atomic (GGA) is the only source of unirradiated fuel elements typical of the Ft. St. Vrain reactor (FSVR) first core loading. Since these elements are the same as those that will be processed in TURF, we are negotiating to obtain some rejects for use in head-end small-scale engineering studies.

Irradiated Fuel

A comprehensive study is planned with the following prototype HTGR fuels:

1. ORNL BISO-coated $(Th,U)O_2$ sol-gel microspheres being irradiated as compacts in the Dragon reactor,
2. ORNL test capsules being irradiated in the ETR for combined head-end reprocessing and irradiation performance testing,
3. recycle test elements (RTEs) fabricated jointly by GGA and ORNL, and now being irradiated in the Peach Bottom reactor.

ORNL BISO-Coated $(Th,U)O_2$ Sol-Gel Microsphere Compacts

A number of Dragon compacts were fabricated with BISO-coated ORNL sol-gel $(Th,U)O_2$ microspheres. These compacts will be irradiated to about 12 to 18% FIMA. Samples adequate for use in head-end studies will be made available when these compacts are received at ORNL.

ORNL Test Capsules

The irradiation performance and behavior of small quantities of three types of candidate coated-particle (plus one accelerated reference fuel) 1100-MW(e) HTGR fuels under proposed methods of head-end reprocessing are being studied jointly by the Metals and Ceramics and the Chemical Technology Divisions. The four types of fuel particle combinations, *a, c, g,* and *f* (see Table 3.6), under test in small loose beds and in fuel sticks (~2.5 in. long), are the reference recycle fuel, the accelerated reference recycle fuel, and an alternate recycle fuel (all block A), and the reference recycle (block B) fuel respectively. Only the UC_2 particles have TRISO coatings. The particles in blended beds and in fuel sticks will be irradiated in two capsules at temperatures of 750, 950, 1050, and 1300°C to burnups of approximately (4 to 6) $\times 10^{21}$ fast fluence in the ETR. Although the quantities of fuel are quite small, they will be adequate for an early preliminary determination of the head-end reprocessing behavior of highly irradiated recycle and alternate fuels. Studies will include the separation of fertile and fissile particles (BISO and/or TRISO coated), determination of uranium crossover, estimates of particle breakage, and measurement of the release of volatile fission products such as ^{85}Kr, ^{3}H, ^{90}Sr, and ^{137}Cs in various head-end steps.

The two capsules, designated H-1 and H-2, will be inserted into the ETR in April 1971; they are expected to be discharged in the fall of 1971 after an exposure of approximately 120 equivalent full-power days (~4–6 $\times 10^{21}$ neutrons/cm^2).

Recycle Test Elements

Seven RTEs have been inserted into the Peach Bottom reactor, six in the summer of 1970 and one in the spring of 1971, in a cooperative program between GGA and the Metals and Ceramics and Chemical Technology Divisions. Reference and advanced recycle and makeup fuel particle mixtures in these elements are being tested at operating temperatures (1050 to 2250°F) of interest for use in commercial HTGRs. Bonded beds and some loose particles (blended beds) are being irradiated for one, two, or three years at exposures of 1.4, 2.8, and 4.2 $\times 10^{21}$ fast fluence.

The types of fuel combinations in the RTEs and an indication of the reasons for their inclusion are given in Table 3.6. A more detailed breakdown of the loading combinations and irradiation conditions of the RTEs is given in Table 3.7. Odd-numbered RTEs are the primary source of material for the hot-cell head-end studies. The emphasis is on particle combinations *a, c, f,* and *g,* which are the reference candidates; however, all fuel combinations are covered in each odd-numbered element. The six 15-in. sections of the odd-numbered elements will be quartered lengthwise to obtain one sample (two fuel channels) of each fuel type. RTE 7 will be discharged in April 1971. It contains particle combinations typical of FSVR fuel and will provide the earliest demonstration of the behavior of such fuel during head-end reprocessing.

Even-numbered RTEs will provide larger amounts of the various fuel combinations for additional hot-cell studies as desired and may also be the first irradiated specimens representative of actual 1100-MW(e) reactor fuel that will become available for use in reprocessing studies in TURF.

Table 3.6. Fuel combinations in the RTE program and justifications for each

Particle combination	Particle makeup in combinations		Justification
	Fissile particle (and coating)	Fertile particle (and coating)	
a	(Th, 20% U)O_2 (BISO)		1. Reference recycle fuel 2. Evaluate:[a] Equipment and chemical process checkout Bed sticking Metallic fission product behavior Kernel migration
b	UO_2 (BISO)	ThC_2 (BISO)	1. Backup fuel type if economics indicate that Th should be eliminated from recycle fissile particle
c	(Th, 33% U)O_2 (BISO)	ThO_2 (BISO)	1. Th/U ratio of 2 to obtain reference burnup in 3 years 2. ThO_2 backup if oxide process is adopted for economic reasons 3. Over a period of time, the desired Th/U ratio will move from 4 toward 2
d	(Th, 33% U)O_2 (BISO)	ThC_2 (BISO)	1. Reference-type recycle combination with a Th/U ratio of 2 for accelerated burnup in fissile particle
e	UC_2 (BISO)	ThC_2 (BISO)	1. Reference startup loading
f	UC_2 (TRISO)	ThC_2 (BISO)	1. Reference B block, makeup fuel loading 2. TRISO coating necessary to permit required separation of particles during reprocessing
g	UO_2 (BISO)	ThO_2 (BISO)	1. Backup fertile particle if thorium is eliminated from recycle particle 2. Backup fertile particle if sol-gel process is used
h	UC_2 (BISO)	ThO_2 (BISO)	1. Backup B block loading 2. Possible particle separation by chemical processes (e.g., selective burning or leaching)
i	UC_2 (TRISO)	ThC_2 (TRISO)	1. Needed if cleaner primary heat exchanger circuit becomes requirement 2. Ft. St. Vrain type fuel
k	UO_2 (TRISO)	ThO_2 (BISO)	1. Proposed new reference B block

[a]Applies to tests of all combinations.

Table 3.7. RTE loading combinations[a]

One-year elements will receive a maximum dose of ≅ 1.4×10^{21} neutrons/cm^2
Two-year elements will receive a maximum dose of ≅ 2.8×10^{21} neutrons/cm^2
Three-year elements will receive a maximum dose of ≅ 4.2×10^{21} neutrons/cm^2

Position of fuel body in element	Center-line temperature range (°F)	Discharge after irradiation period of –						
		Nine months	Two years			Three years		
		RTE 7[b]	RTE 2[c]	RTE 4[c]	RTE 1[d]	RTE 5[d]	RTE 6[d]	RTE 8[d]
6[e]	1950–2050	a c f g	f	e[f]	k d e i	b d e i	g	f
5	2050–2250	a c f g	a[f]	d	k d e i	b d e h	f	i
4	2250–2300	b d g h	e	f	a c f g	a c f g	f	d
3	2050–2250	b d g i	f[f]	a[f]	a c f g	a c f g	d	e
2	1650–2050	b d g i	d	f[f]	a c f g	a c f g	f	i
1	1050–1650	b d g i	e[f]	e	a c f g	a c f g	e	f[f]

[a]Loadings are indicated by letters (a, b, c, etc.), which are defined in Table 3.6.
[b]Scheduled to be discharged in April 1971.
[c]Scheduled to be discharged in April 1972.
[d]Scheduled to be discharged in June 1973.
[e]Top of reactor.
[f]Blended beds (unbonded).

3.4 DESIGN SUPPORT FOR HEAD-END STUDIES

The design support for HTGR head-end studies has been limited to three efforts: (1) an evaluation of existing burning technology as related to a 15,000-MW(e) reprocessing plant, (2) the design of a whole-element burner and a CO_2 sorption column for feasibility studies, and (3) planning of work schedules and of manpower requirements to meet the goals of the National HTGR Fuel Recycle Program Plan.

A plant for reprocessing fuel from a 15,000-MW(e) HTGR economy would have to reprocess about 30 FSVR-type fuel elements per operating day (80% load factor). According to our present plan, this would result in the burning of about 3000 kg of carbon and produce about 200,000 ft^3 (STP) of CO_2 per day. Because of the complexity of fluidized-bed burner feed preparation equipment, the complexity of the design of a fluidized-bed burner which would keep the heat flux sufficiently low to ensure a reasonable burner life, and the difficulties anticipated in removing any "clinkers" from a fluidized-bed burner, it is strongly recommended that other types of burners be evaluated. Thus, a burner that is capable of handling whole elements without fluidization is being considered; a test burner in which feasibility studies will be carried out has been designed.

The off-gas from any of the burners under consideration will consist of very large volumes of carbon dioxide containing small quantities of tritium, iodine, krypton, and xenon. The most difficult task in the treatment of off-gas is the separation of CO_2 from krypton and xenon because of the similarity of physical properties. One method being considered is the reversible sorption of CO_2 in hot pressurized K_2CO_3-$KHCO_3$ solution. A 4-in.-diam CO_2 sorption column suitable for use in feasibility studies has been designed.

4. Waste Treatment and Disposal

4.1 RADIOACTIVE WASTE REPOSITORY

We have been involved in a rather substantial effort leading to the establishment of a national repository for radioactive wastes in a bedded salt formation near Lyons, Kansas. While the Chemical Technology Division has participated to some extent in virtually all phases of this project, our major responsibilities have been centered in the conceptual design and safety analysis of the repository, in a survey of the sources and characteristics of transuranium-contaminated solid ("alpha") wastes, and in experimental investigations needed to establish criteria for packaging those alpha wastes to be stored in the repository.

Conceptual Design and Safety Considerations

The conceptual design and preliminary safety analysis were completed in collaboration with Kaiser Engineers, who served as architect-engineers. The principal components of the repository are (Fig. 4.1): (1) the existing salt mine, situated about 1000 ft below the surface, which will be used for storage of the alpha wastes; (2) a building in which the alpha waste packages are received, monitored, and transferred to the existing mined area by direct handling techniques; (3) a building equipped to receive containers of high-level wastes and transfer them remotely from their shipping casks to the mine level; (4) a newly mined area for burial of the high-level wastes; and (5) various support facilities such as operations and office buildings, a warehouse, and those other services and utilities that are required for mining and underground storage operations. All facilities will be designed to ensure that the necessary confinement potential and radiation safety are maintained following exposure to any credible internal and external forces (including tornadoes and earthquakes).

An 18-ft-diam multipurpose "men and materials" shaft with three completely independent compartments will be used for lowering alpha wastes into the mine, for transferring personnel and materials, and for admitting ventilation air into the mine. The alpha waste receiving building will provide earthquake- and tornado-resistant facilities in which waste packages can be removed from returnable cargo containers, assayed, recanned and repaired as necessary, and lowered into the mine. We expect that the alpha waste will be shipped to the repository in gasketed metal drums and in metal crates with outside dimensions no greater than 4 X 6 X 6 ft high and that individual burial units will weigh no more than 5 tons. Initially, shipments of alpha waste will be made only by rail in specially designed ATMX rail cars, but it is probable that provisions will be made later to receive motor freight also.

The high-level waste receiving building will be located about 500 ft from the alpha waste building. Solidified high-level wastes will be sealed in steel containers and transferred by rail to the repository in shipping casks weighing up to 100 tons. The containers will be unloaded here and lowered individually into the mine through a 4-ft-diam shaft. The individual waste containers may vary from 6 to 14 in. in diameter and from 2 to 10 ft in length, may weigh up to 4000 lb, and may possess up to 5000 W of thermal power from radioactive decay.

The presently mined-out area will provide space for storing about 20 million cubic feet of alpha wastes, and the alpha facility will have the capability to store 1 million cubic feet of waste per year. The alpha waste transfer shaft will terminate in an alpha-confinement room at mine level. Here the packages of waste will be unloaded from the hoisting cage by a forklift truck and transported to the disposal rooms where they will be unloaded and stacked. When an area or room has been completely filled, it will be backfilled with salt and sealed with masonry stoppings. The mine will be ventilated with 20,000 cfm of air supplied through the 18-ft-diam multipurpose shaft, directed through the mine with brattices, and combined with the exhaust air from the high-level mine.

The high-level mine will be developed over the life of the repository in a northeasterly direction from the alpha mine, using conventional salt-mining techniques.

ORNL DWG 71-2192R

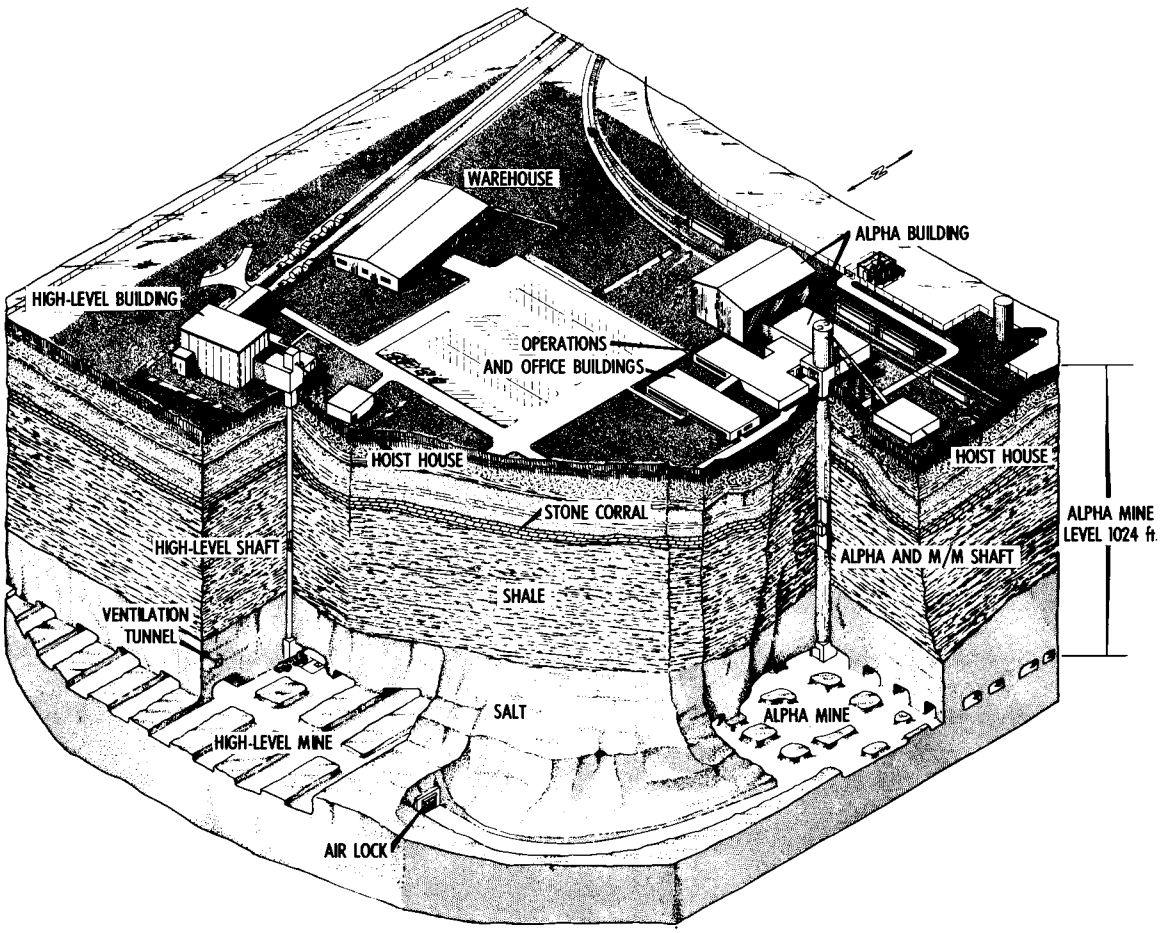

Fig. 4.1. Artist's conception of the demonstration repository.

The facility will ultimately have the capability of handling up to 300 containers of waste per week. The required rate of mining will increase during the life of the facility from about 200,000 tons/year initially to about 1.3 million tons/year during the last several years of operation. About 50% of the salt will be used for backfilling; eventually the remainder will be raised to the surface and offered for sale.

The containers of high-level waste will be transported to rooms mined in the salt formation and buried in holes in the salt. The spacing between containers will be such that the radioactive decay heat will be dissipated without causing excessive temperatures in the salt or in the neighboring geological formations. After the burial area of a room has been utilized, the room will be backfilled with crushed salt and sealed from the remainder of the mine.

Ventilation air leaving the high-level mine will be drawn through ventilation tunnels above the corridors, combined with the air from the alpha mine, and exhausted to the atmosphere through the mine air exhaust shaft, filter station, and stack. The mine exhaust filter station will consist of two banks of roughing filters in series to remove most of the salt particles, followed by two banks of HEPA filters in series to remove practically all the remaining particles.

Assuming FY 1972 funding, Title I design of the alpha facility will begin in October 1971. Title II and some early mine cleanup and shaft work should begin in April 1972. Construction of the alpha facility will begin in May 1973; it should be ready to begin operation as a demonstration facility early in 1975. The high-level facility will proceed apace, with construction starting in 1974 and operations, again on a demonstrational basis, beginning early in 1976.

Repository systems for protection against exposure to radioactive and physiologically hazardous materials are being designed to comply with all federal regulations that apply to radiation safety, mine safety, and industrial safety. The projected waste inventories are given in Table 4.1.

The only significant source of off-site exposure to radioactive or other materials originating from the repository will be from very small quantities of airborne radioactive materials that escape through high-efficiency particulate air (HEPA) filters. It is planned that there will be no discharge of liquid waste from the repository. Solid wastes generated at the repository will be packaged and buried in the mine. Aqueous wastes will be recycled, with any excess water being evaporated to the atmosphere.

Table 4.1. Projected waste inventories at the repository

	Calendar year		
	1980	1990	2000
Number of annual shipments			
High-level waste[a]	23	240	590
Alpha waste[b]	420	1200	0
Accumulated high-level waste[c]			
Volume of waste, ft^3	3170	74,200	319,000
Salt area used, acres	9	200	900
Total thermal power, MW	1.17	24.4	94.9
Total activity, MCi	329	7030	27,700
^{90}Sr	59.0	1310	5290
^{137}Cs	83.1	1850	7500
^{238}Pu	0.102	2.34	9.88
^{239}Pu	0.00157	0.0368	0.158
^{240}Pu	0.00400	0.101	0.470
^{241}Am	0.151	3.54	15.3
^{244}Cm	1.58	34.1	133.3
Accumulated alpha waste[c,d]			
Volume of waste, 10^6 ft^3	2.1	10.3	19.3
Salt area used, acres	20	96	180
Total thermal power, MW	0.0142	0.170	0.476
Total activity, MCi	14.2	151	300
Total mass of actinides, metric tons	1.40	15.8	38.3
Activity, MCi			
^{238}Pu	0.232	2.57	6.02
^{239}Pu	0.0515	0.580	1.41
^{240}Pu	0.0741	0.834	2.02
^{241}Pu	13.8	146	286
^{241}Am	0.0617	1.03	4.74

[a]Each shipment consists of 57.6 ft^3 of waste in thirty-six 6-in.-diam cylinders. Each cubic foot of waste represents 10,000 MWd(t) of reactor operation. Half of the waste is aged five years, and half is aged ten years at the time of its shipment. Last shipments are assumed to be made in the year 2000.

[b]Shipments are made in ATMX rail cars; each shipment contains 832 ft^3 of waste. Last shipments are assumed to be made in the year 1999.

[c]At end of year.

[d]The isotopic composition of Pu at the time of its receipt is 1% ^{238}Pu, 60% ^{239}Pu, 24% ^{240}Pu, 11% ^{241}Pu, and 4% ^{242}Pu.

Table 4.2. Estimated release rates and average annual off-site concentrations of radioactive and other materials resulting from full-scale operation of the repository

Material	Average annual rate of release to atmosphere	Average annual off-site concentrations resulting from repository effluents[a]	Percent of applicable standards for exposure of the public[b]	Percent of estimated present concentration in the atmosphere
High-level waste particles	0.007 Ci/year	2×10^{-15} Ci/m^3	0.02	5.0
Alpha waste particles	0.04 μCi/year	1×10^{-20} Ci/m^3	0.0001	0.02
^{85}Kr (spontaneous fission)	0.014 Ci/year	4×10^{-15} Ci/m^3	0.000004	0.04
^{3}H (spontaneous fission)	0.0009 Ci/year	3×10^{-16} Ci/m^3	0.0000004	0.002
^{222}Rn (natural sources)	0.9 Ci/year	2×10^{-13} Ci/m^3	0.02	0.2
^{220}Rn (natural sources)	0.04 Ci/year	1×10^{-14} Ci/m^3	0.0003	0.2
H_2 (corrosion, radiolysis, electrolysis)	37 scfm	0.2 ppm	0.002	40.
He (alpha decay)	0.001 scfm	0.000004 ppm	4×10^{-8}	0.00008
HCl (brine decomposition)	0.07 scfm	0.0003 ppm	0.006	100.
CO_2 (diesel exhaust)	50 scfm	0.2 ppm	0.004	0.07
CO (diesel exhaust)	0.05 scfm	0.0002 ppm	0.0004	0.2
NO_2 (diesel exhaust)	0.05 scfm	0.0002 ppm	0.004	7
SO_2 (diesel exhaust)	0.03 scfm	0.0001 ppm	0.002	1
CH_2O (diesel exhaust)	0.0007 scfm	0.000003 ppm	0.00003	0.05
Soot (diesel exhaust)	2 lb/year	0.1 μg/m^3	0.0007	0.2
Salt particles	5 lb/year	0.2 μg/m^3	0.001	0.8

[a]These are the maximum concentrations which result at the southern boundary of the site.

[b]Based on one-third of limits in 10 CFR 20, Table II, column 1 for radionuclides and threshold limit values (American Conference of Governmental Industrial Hygienists) for other materials.

Instrument systems will be provided for continuous monitoring of radiation levels and concentrations of airborne materials in work areas, in stack effluents, and at the boundary of the site.

The materials that will escape to the atmosphere in small concentrations include: (1) solid waste particles resulting from resuspension of surface contamination; (2) gases (^{85}Kr, ^{3}H, He) that result from decay of the waste; (3) radon gas that occurs naturally in the mine; (4) nonradioactive gases (H_2, HCl) that result from decomposition of the salt, corrosion, electrolysis, and radiolysis; (5) exhaust fumes from diesel equipment; and (6) salt particles. Concentrations in work areas of the repository will be maintained well below the applicable standards for occupational exposure.

Present estimates of the rate of release of these materials to the atmosphere and the maximum off-site concentrations that will result at the southern boundary of the site are presented in Table 4.2. These maximum concentrations are less than 0.1% of the applicable standards for exposure of the public and, in general, are well below the concentrations of the same materials that exist at present due to natural and man-made sources.

It is estimated that the buildup of off-site surface contamination of various species over the life of the repository will ultimately result in a level that is less than 1% of the level that presently exists for the same species (including such radioisotopes as ^{90}Sr, ^{137}Cs, and ^{239}Pu, which have been deposited by fallout). At these levels of surface contamination, the experience has been that the materials cannot be reconcentrated to hazardous levels in food chains.

Additional experimental work is planned to provide a more precise preoperational background of the radiation environment of the site and surroundings. In addition, continuing studies of the chemical interactions of the waste containers and salt will provide a better definition of the concentrations of the materials that may be released to the atmosphere.

Survey on Sources and Characteristics of Alpha Wastes

Solid wastes containing plutonium and other transuranium elements are routinely produced during operation of nuclear fuel production and spent-fuel reprocessing plants as well as operation of AEC laboratories and production facilities. The major AEC sites

were surveyed during the past year to determine current sources, amounts, characteristics, and practices for the disposal of these alpha-contaminated solid wastes. The wastes consist of a wide assortment of solid materials generated inside glove boxes during work with transuranium elements and outside the boxes during contamination control measures, such as the treatment of liquid waste streams. The transuranium-element content of the wastes ranges from trace amounts to several grams per cubic foot. About 60 vol % are combustible and can be reduced to 2 to 5% of their original volumes by incineration. About 50 vol % are compactable and can be reduced in volume by factors of 2 to 10 by compression. Since they are virtually free of penetrating radiation and evolve only a few hundredths of a watt per cubic foot, they do not require remote handling techniques. Plants in favorable geographic locations bury such wastes on their premises, while those less favorably located ship them to commercial or AEC burial grounds. AEC regulations require that these wastes be packaged and buried in such a fashion that they can be readily retrieved as contamination-free packages for several decades.

Feasibility of Storing Combustible Alpha Wastes

Since about 60% of the alpha wastes are combustible, it is highly desirable to evaluate the feasibility of storing combustible alpha wastes in the repository. We have performed several series of experiments in which simulated wastes contained in both plywood and metal containers were burned under controlled conditions; results of these experiments have led to the tentative conclusion that combustible wastes packaged in metal containers could be accepted, whereas those packaged in combustible containers could not.

To evaluate the possibility that hazardous quantities of noxious fumes may be given off by smoldering or burning waste in combustible containers, several series of experiments were carred out using small plywood boxes, 2 to 6 in. along each dimension, filled with combustible material such as blotter paper, cleaning tissues, cheesecloth, and polyethylene film. In some experiments the combustible mixture was wetted with an equal part (by weight) of an organic solvent. The mixtures were packed in the boxes to give bulk densities ranging from 5 to 10 lb/ft^3. The filled boxes were heated to temperatures representative of those expected from slow oxidation or spontaneous combustion (200 to 1300°F) by electrical resistance heaters distributed throughout the waste. In some tests, the boxes were fully exposed to air; in others, they were covered with about 3 in. of crushed salt. In none of the tests was a flame produced by heating alone. However, the material gave off fumes and gray smoke that could be ignited with an open flame. In those tests in which the boxes were covered with salt, the flame was more difficult to establish. The results indicated that a flame is not easily achieved in these combustibles and that crushed-salt backfill makes the establishment of a flame even more difficult. However, they also show that plywood containers do not ensure against the entrance of air to the package or egression of smoke and fumes from the package in the event that pyrolysis or combustion should occur. We conclude therefore that combustible wastes in combustible containers should not be accepted at the repository.

To evaluate the feasibility of storing combustible wastes in noncombustible containers, the synthetic waste mixture mentioned above and cotton (dry, wetted with small amounts of organic solvents, and also soaked in nitric acid or sodium nitrate solution and dried) were used to simulate typical combustible wastes. Small mild-steel drums with a volume of 0.1 ft^3, an open head, a bolt-ring closure, and a hollow neoprene gasket were used as noncombustible containers. Tests were carried out in these drums in an oven at temperatures ranging from ambient to about 400°F. To ensure uniform temperatures in the systems, the drums were encased in a massive aluminum can. Selected representative results are given in Table 4.3. These results lead to the tentative conclusion that combustible waste in noncombustible containers should be acceptable in the repository, provided they are emplaced so that their temperatures do not exceed about 250°F. If allowed to reach temperatures around 400°F, the gaseous products lead to excessive pressure and breaching of the drum's gasket.

4.2 ENGINEERING, ECONOMIC, AND SAFETY EVALUATIONS

During the past year, we have extended our studies of the economics of high-level waste management to include consideration of fluidized-bed calcination as a method for solidifying the wastes, and we have revised an earlier study on shipment of solidified wastes[1] to include provisions for neutron shielding.[2] Also, a

1. J. J. Perona et al., *Evaluation of Ultimate Disposal Methods for Liquid and Solid Radioactive Wastes. IV. Shipment of Calcined Solids,* ORNL-3356 (October 1962).

2. J. J. Perona, R. S. Dillon, and J. O. Blomeke, *Design and Safety Considerations of Shipping Solidified High-Level Radioactive Wastes,* ORNL-TM-2971 (December 1970).

Table 4.3. Results from the heating of combustible solid wastes in noncombustible containers[a]

Run	Composition	Temperature (°F)	Time at temperature (hr)	Maximum pressure (psig)	Weight loss (g)	Comments
1	Standard[b]	196	42	9.6	None	No obvious change in solids
2	Standard[b]	262	135	14	None	Slight discoloration of solids; incipient melting of plastic
3	Standard[b] wetted with 2 *N* HNO_3 and air dried	257	86	12	1.6	Solids brown in color; incipient melting of plastic
4	Standard[b] wetted with $NaNO_3$ solution[c] and air dried	248	109	9.4	0.5	Solids light tan in color; incipient melting of plastic
5	Standard[b]	401	9	*d*	4.4	Solids dark brown in color; plastic melted; lid bulged and drum leaked
6	Standard[b]	392	105	26	6.7	Solids dark brown in color; plastic melted; lid bulged and drum leaked

[a]Container volume is 0.1 ft^3, and wastes are packed to a density of 5 lb/ft^3.

[b]Standard dry waste is 0.25 wt % blotter paper, 0.25 wt % cheesecloth, 0.25 wt % facial tissue, and 0.25 wt % polyethylene film cut into 1-in. squares.

[c]Final mixture contained 27 wt % $NaNO_3$ and 73 wt % standard dry waste.

[d]Exceeded the range, 0 to 28.8 psig, of pressure recorder being used at the time.

theoretical analysis was made of the leaching of the radionuclides from solid wastes.[3]

Fluidized-Bed Calcination

A tentative procedure was developed for estimating the costs of solidifying high-level aqueous wastes by fluidized-bed calcination, and it has been incorporated in a computer program for calculation of the total costs of waste management. The cost of solidifying the waste from reprocessing 3 tons of fuel per day by fluidized-bed calcination is only 65 to 75% of that for solidification by pot calcination, resulting in a reduction of 10 to 20% in the total cost of high-level waste management. These early estimates are subject to experimental confirmation of the flowsheet upon which they are based, however.

With steam as the atomizing and fluidizing medium, the flowsheet for a fluidized-bed calcination plant is similar to that for pot calcination. The first-cycle solvent extraction raffinate was assumed to be evaporated in the fuel reprocessing plant to the desired composition for feeding to the calciner, as was assumed in the pot calcination study.[4] However, the steam used for atomization and fluidization imposed an additional load on the evaporator, rectifier, and tankage capacity over that needed for pot calcination. According to Schneider,[5] the volume of gas required for atomization and control of bed particle size is 400 to 600 times the volume of the liquid feed, and the fluidizing gas requirements are generally in the range of 0.5 to 1.5 fps. Using a specific volume for steam of 24 ft^3/lb, about 1 lb of steam is required for each pound of concentrated waste solution.

An estimate of the calciner cost was made by adding together cost estimates for (1) the vessel, (2) internal filter elements, (3) heaters, (4) labor cost for fabrication, and (5) instrumentation and insulation. A procedure for estimating the vessel size as a function of throughput was developed. The basic assumptions are that the particle size distribution and residence time are

3. M. J. Bell, *An Analysis of the Diffusion of Radioactivity from Encapsulated Wastes,* ORNL-TM-3232 (February 1971).

4. J. J. Perona et al., *Evaluation of Ultimate Disposal Methods for Liquid and Solid Radioactive Wastes. II. Conversion to Solid by Pot Calcination,* ORNL-3192 (September 1961).

5. K. J. Schneider, *Status of Technology in the United States for Solidification of Highly Radioactive Liquid Wastes,* BNWL-820, p. 32 (October 1968).

independent of vessel size. Therefore, we can assume that the fluidizing velocity is constant; then, if bed temperature and pressure are also constant,

$$\text{throughput} \propto \pi D^2 V$$

and

$$D \propto \sqrt{\text{throughput}} \ ,$$

where D is the calciner diameter and V is the superficial fluidizing velocity. Since D = 8 in. for a 300-ton/year plant, we would predict that D = 16 in. for a 1200-ton/year plant.

A correlation for transport disengaging height (TDH) as a function of calciner diameter and fluidization velocity is given by Kunii and Levenspiel[6] for catalyst in the 20- to 150-μ range. This correlation should be reasonably conservative for waste calciners, which have average particle sizes in the range of 400 to 600 μ. It yields a disengaging height of 60 in. for an 8-in.-diam calciner and can be represented by

$$\frac{\text{TDH}}{D} = 11.8 - 5.3\sqrt{D} \ .$$

We expect to extend these estimates to include interim storage of the fluidized-bed solids in air- or water-cooled bins and to develop costs for solidification by the spray solidification and phosphate glass processes as well.

Shipment of Solidified High-Level Wastes

The high-level waste from processing a ton of spent fuel that has been irradiated to about 30,000 MWd/ton may contain from 20 to 30 g of ^{244}Cm. The neutron flux from spontaneous fission of this isotope is such as to require that a hydrogenous material be included in the shielding of casks to be used for shipment of the solidified wastes. Design calculations were made for a nominal 100-ton cask, which has an internal cavity about 5 ft in diameter and can carry thirty-six 6-in.-diam cans, nine 12-in.-diam cans, or four 24-in.-diam cans. The gamma shield is 24 cm of lead, 40 cm of iron, or 13.5 cm of uranium. Water containing 1% borate was selected for the hydrogenous shield; thicknesses of 11.5 cm are required on the outside of the lead and uranium shields, and 5 cm on the outside of the iron shields, to reduce the neutron dose to 5 millirems/hr at 8.5 ft from the center of the casks.

6. D. Kunii and O. Levenspiel, *Fluidization Engineering*, p. 94, Wiley, New York, 1969.

The outer-surface temperature of the cask is limited to about 380°F by the maximum allowable pressure in the neutron shield. Circular steel fins ½ in. thick and spaced 4 in. apart in lengths of 18 in. for lead and uranium casks and 12 in. for iron casks can dissipate 240,000 to 300,000 Btu/hr, which would allow solidified wastes from reprocessing light-water reactor fuels to be shipped as early as two to three years after the fuel had been removed from the reactor.

A precise calculation of the probability of the release of activity by a shipping accident must await the compilation of accident severity statistics. Until then, we can only point out that the probability of a single accident for the estimated number of shipments which will occur in the year 2000 is 1/77, assuming the accident frequency rate for passenger trains. We cannot estimate the probability that an accident, if it occurs, would be sufficiently severe to breach a cask passing the impact, puncture, fire, and submersion tests specified in current regulations.

As a continuation of this study, we are developing a computer code for use in parametric studies of various design features of waste shipment casks. This will assist in the development of an optimal cask design.

Leaching of Radionuclides from Solid Wastes

In this analysis the movement of radionuclides through the solid matrix was assumed to obey Fick's laws of diffusion. It was found that the loss rates of activity were dependent on a single dimensionless parameter, $L/R^2\lambda$, which can be interpreted as the ratio of a characteristic time for radioactive decay to a characteristic time for diffusion. For small values of this parameter, it is possible to approximate the exact solution to the diffusion equation for a particular geometry by the solution for diffusion in a semi-infinite medium. This asymptotic solution was shown to be valid for all feasible experimental and actual disposal conditions for which the diffusion model applies. Thus the fraction of the initial activity present in the environment at any instant of time is given by diffusion theory as

$$\frac{2F}{V}\sqrt{\frac{Lt}{\pi}}\, e^{-\lambda t} \ ,$$

and the total amount of activity released over all time is given by the simple expression

$$\frac{FA_0}{V}\sqrt{\frac{L}{\lambda}} \ .$$

The time of maximum activity of an isotope of half-life $t_{1/2}$ in the environment occurs at $0.721 t_{1/2}$ after disposal, and the activity present at this time represents 48% of all the activity which will be lost from the matrix by diffusion.

4.3 HIGH-LEVEL RADIOACTIVE WASTE

The shipping, handling, and storage of pots containing solidified high-level waste, each evolving 4 to 5 kW of power, require reliable knowledge of thermal, chemical, and structural integrity of the solidified waste and its container. For more than a decade, ORNL and other national and private laboratories have maintained programs to measure and evaluate the properties of high-level aqueous wastes, the solidified products made from these wastes, and the containers for the products. As a part of its properties evaluation program this year, ORNL continued to study the thermal conductivity of waste solids and the solubility of boron in aqueous waste and initiated studies on energy storage and buildup of electric charges in waste solids. The measured thermal conductivity of a waste product containing 50 wt % oxides from waste and 50 wt % borosilicate glass varied from about 0.75 W m^{-1} $(°C)^{-1}$ at 65°C to 0.94 W m^{-1} $(°C)^{-1}$ at 585°C. These conductivities are about one-fourth of the values which would be expected for this product if it had been a dispersion of macroscopic crystalline waste oxide particles in a glassy matrix. Batch dilutions and evaporations of simulated high-level aqueous waste from the reprocessing of spent LMFBR fuels showed that solutions and slurries of this waste with BO_3^{3-} concentrations of 0.30 to 1.35 *M* could be readily pumped and stored at temperatures above 65 to 70°C. In a new area of investigation (energy storage and buildup of electric charges in waste solids), glass products containing from 25 to 50 wt % waste oxides were irradiated with electrons to doses more than 100 times that which would cause electric discharge in lead glass doped with cerium. No discharge effects were observed.

Thermal Conductivity of Solidified High-Level Waste

Foremost among the properties that determine temperature rise in solidified waste is thermal conductivity. Conductivity measurements were carried out[7] in a radial heat flow apparatus. The specimen (Table 4.4, No. 2) was prepared by incorporating the solids from a high-level aqueous waste from the reprocessing of spent LWR fuel (Table 4.5) in a borosilicate glass composed of 45 wt % B_2O_3, 35 wt % SiO_2, and 20 wt % Na_2O. The final product contained 50 wt % oxides from waste and 50 wt % glass and had a measured conductivity that varied from about 0.75 W m^{-1} $(°C)^{-1}$ at 65°C to about 0.94 W m^{-1} at 585°C, as shown in Fig. 4.2. The results of other investigators with a borosilicate glass[8] and a borosilicate glass incorporating 25 wt % waste oxides[9] are also presented in Fig. 4.2. Although the composition of the borosilicate glass is not the same in each case, comparison of the plots in Fig. 4.2 leads to the

Table 4.4. Composition of glassy waste products used in conductivity and irradiation studies

	Products from LWR (PW-4m[a]) wastes	
	No. 1	No. 2
Composition, wt %		
Corrosion product oxides		
Fe_2O_3	0.99	1.64
Cr_2O_3	0.22	0.37
NiO	0.15	0.25
Al_2O_3	0.01	0.02
Na_2O	0.77	1.28
P_2O_5	0.05	0.09
SiO_2	0.15	0.15
Fission product oxides		
K_2O	1.08	1.80
SrO	0.91	1.52
BaO	1.55	2.59
La_2O_3	11.03	18.38
ZrO_2	4.35	7.26
MoO_3	5.73	9.54
Fe_2O_3	1.61	2.69
CoO	0.25	0.41
NiO	0.79	1.31
CuO	0.08	0.14
SO_3	0.28	0.47
Added oxides		
B_2O_3	31.50	22.50
SiO_2	24.50	17.50
Na_2O	14.00	10.00
Waste oxides	30	50
Density, g/cc	2.52	2.93

[a]Composition of aqueous waste given in Table 4.5.

7. R. J. Dippenaar, Metals and Ceramics Division, personal communication.

8. R. W. Powell, C. Y. Ho, and P. E. Liley, "Thermal Conductivity of Selected Materials," *Nat. Stand. Ref. Data Ser., Nat. Bur. Stand.* 8, 72 (1966).

9. D. B. Auty and J. R. Grover, *Thermal Conductivity of a Borosilicate Glass Suitable for Fission Product Wastes*, AERE-R 4685 (December 1964).

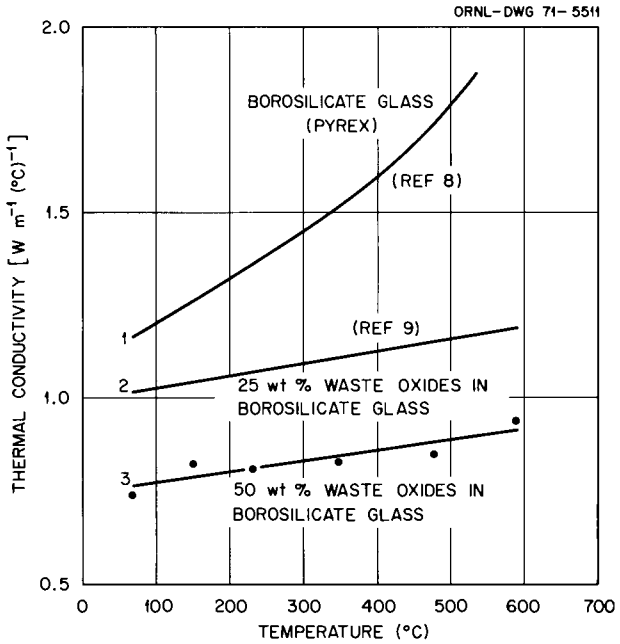

Fig. 4.2. Thermal conductivities of borosilicate glass and borosilicate glasses incorporating waste oxides.

tentative conclusion that incorporating increasing amounts of foreign oxides in borosilicate glass decreases its conductivity. The measured values for the 50% waste oxide–borosilicate glass product are one-third to one-half of those previously reported for waste oxide particles dispersed in a lead silicate glass[10] and in a borosilicate glass[11] and are about one-fourth of those which would be expected for this product if it were composed of macroscopic crystals of waste oxides dispersed in glass. These low values may be explained if most of the waste oxides are dissolved in the glass or if the waste oxide crystallites are so small that they can be considered amorphous.

Solubility of Boron in LMFBR Waste

The use of boron as a neutron absorber during the reprocessing of spent LMFBR fuels is being considered. Thus a series of batch dilutions and evaporations was carried out with a simulated LMFBR waste (Table 4.5) to evaluate difficulties that might arise in handling and storing this type of waste because of the limited solubility of boron in nitric acid solutions. During these tests, the boron concentration was varied from 0.30 to 1.35 *M*, the nitrate from 1.25 to 12.7 *M*, the acid from 1.0 to 12.5 *M*, and the temperature from 25 to 108°C. The general conclusion drawn from the results (Table 4.6) was that all the solutions and slurries obtained with this waste could be readily pumped and stored at reasonable temperatures.

Table 4.5. Chemical compositions of high-level LWR and LMFBR aqueous wastes[a] used for studies on waste properties

Constituent	Substitute chemical	Concentration (*M* at 100 gal/metric ton of U + Pu)	
		LWR fuel (PW-4m)	LMFBR fuel
From fuel processing			
H^+		0.5	0.5
Fe^{3+}		0.050	0.16
Cr^{3+}		0.012	0.046
Ni^{2+}		0.008	0.023
Al^{3+}		0.001	
Na^+		0.10	0.10
NO_3^-		2.4	4.7
PO_4^{3-}		0.003	0.060
SiO_3^{2-}		0.010	
From nuclear fission[b]			
Mo^{6+}		0.130	0.24
Sr^{2+}		0.036	0.040
Ba^{2+}		0.041	0.068
Cs^+	K^+	0.078	0.21
Rb^+	K^+	0.014	0.019
$(Y + RE)^{3+}$	La^{3+}	0.27	0.53
Zr^{4+}		0.14	0.22
Ru^{3+}	Fe^{3+}	0.082	0.22
Rh^{3+}	Co^{2+}	0.013	0.060
Pd^{2+}	Ni^{2+}	0.043	0.16
Ag^+	Cu^{2+}	0.0016	0.019
Cd^{2+}		0.0025	0.010
Sn^{4+}		0.0016	0.010
Sb^{3+}	As^{3+}	0.0004	0.003
Te^{4+}	S^{6+}	0.014	0.034
Se^{4+}	S^{6+}		0.005
Nb^{5+}	Zr^{4+}		0.002
La^{3+}			0.058

[a]More detailed information on these wastes is given in sect. 2 of BNWL-1073, ed. by K. J. Schneider (August 1969).

[b]Burnup of PW-4m fuel: 45,000 MWd/metric ton at a specific power of 30 MW/metric ton; burnup of LMFBR fuel: 100,000 MWd/metric ton at a specific power of 200 MW/metric ton.

10. *Chem. Technol. Div. Annu. Progr. Rept. May 31, 1969*, ORNL-4422, p. 139.

11. *Chem. Technol. Div. Annu. Progr. Rept. May 31, 1970*, ORNL-4572, p. 105.

Table 4.6. Results of studies on the solubility of boron in simulated high-level aqueous waste from the reprocessing of spent LMFBR fuel as a function of nitric acid concentration and temperature

Mix No.	BO_3^{3-} (*M*)	NO_3^- (*M*)	H^+ (*M*)	Temperature (°C)	Conditions and mode of operation	Observations and comments
1A	1.35	1.76	1.0	25	Waste prepared as shown in Table 4.5	10 to 15 vol % precipitate
1B	1.35	1.76	1.0	50	Mix 1A heated and stirred	1 to 2 vol % precipitate
1C	1.35	1.76	1.0	55	Mix 1A heated and stirred	No precipitate
2A	0.45	1.25	1.0	25	Mix 1A diluted with 2 volumes of 1 *N* HNO_3	No precipitate
2B	0.45	4.59	4.3	25	Mix 1A diluted with 2 volumes of 6 *N* HNO_3	No precipitate
2C	0.30	12.7	12.5	25	Mix 1A diluted with 3.5 volumes of 15.8 *N* HNO_3	5 to 10 vol % precipitate
3A	0.69	1.92	1.5	102	Mix 2A volume reduced by a factor of 1.54 in glass evaporator	Hazy mixture, well suspended precipitate (readily pumpable)
3B	0.90	2.50	2.0	102	Mix 2A volume reduced by a factor of 2.0 in glass evaporator	Hazy mixture, well suspended precipitate (readily pumpable)
3C	1.35	3.75	3.0	108	Mix 2A volume reduced by a factor of 3.0 in glass evaporator	Hazy mixture, well suspended precipitate (readily pumpable)
4A	1.35	3.75	3.0	108	Mix 2A volume reduced by a factor of 3.0 in stainless steel evaporator	Hazy mixture, well suspended precipitate (readily pumpable)
4B	1.35	3.75	3.0	60	Mix 4A cooled	Hazy mixture, well suspended precipitate (readily pumpable)
4C	1.35	3.75	3.0	55	Mix 4A cooled	Precipitate begins to settle out

Table 4.7. Charge buildup effects in glassy solids incorporating waste oxides

Sample No.	Type of product	Electron energy (MeV)	Dose ($\mu C/cm^2$)	Results
1	35 wt % HTGR waste oxides[a] dispersed in lead silicate glass	2	70	Darkening but no sparks
		1.2	1200	
2	30 wt % LWR waste oxides[b] incorporated in borosilicate glass	2	70	Nothing
		1.2	1200	Nothing
3	50 wt % LWR waste oxides[c] incorporated in borosilicate glass	2	75	Nothing
		1.2	1200	Nothing
4	25 wt % TBP-25 waste oxides[a] dissolved in aluminophosphate glass	2	75	Nothing
		1.2	1200	Nothing
5	Borosilicate glass (Pyrex)	1	1200	Darkening but no sparks
6	Lead glass doped with cerium	2	6	Sparking
		1.2	18	Sparking

[a]Primarily Al_2O_3.
[b]Table 4.4, No. 1.
[c]Table 4.4, No. 2.

Electric Discharge in Glassy Products

The storage of energy in a wide variety of materials, including silicates, as a result of their irradiation is a familiar phenomenon. Adverse effects, such as very high temperatures and melting, might result from a sudden release of stored energy. Electric discharge of charges built up in some glasses with unidirectional irradiation can be of sufficient magnitude to shatter the glass. Several glassy solids being considered for the long-term storage of solidified waste were irradiated[12] with electrons having energies of 1.2 to 2 MeV (Table 4.7).

12. E. Sonder, Solid State Division, personal communication.

The products incorporating 25 to 50 wt % oxides from waste were prepared with glasses based on the lead silicate, borosilicate, and aluminophosphate systems. Charge buildup and destructive discharge have been observed upon electron irradiation of lead glass doped with cerium (Table 4.7, sample 6). However, the waste products and a commercial borosilicate glass showed no discharge effects after irradiation to doses up to 1200 $\mu C/cm^2$. The glassy product containing HTGR waste oxides and the commercial borosilicate glass showed some darkening as the result of irradiation (Table 4.7, Nos. 1 and 5). This darkening was not observed in the glassy products containing LWR and TBP-25 waste oxides since they are dark prior to irradiation (Table 4.7, Nos. 2 to 4). The doses to which these glassy products containing waste oxides were irradiated are more than 100 times the electron irradiation that would cause discharging in a lead glass doped with cerium.

4.4 COMBUSTION OF PLUTONIUM-BEARING SOLID WASTES

The AEC proposes to construct an underground repository for the storage of solid radioactive wastes in bedded salt formations in central Kansas. In order to minimize underground space requirements, various processes and procedures for reducing the volume of these wastes have been investigated. Because some of the contaminated waste will include combustible material such as paper, cloth, rubber, and plastics, burning of this material prior to shipment would significantly reduce the volume of waste to be stored and eliminate the problem of spontaneous combustion. Pressurized aqueous combustion (PAC), also known as wet oxidation, is being considered for the oxidation of the combustible materials contaminated with long-lived radionuclides (primarily plutonium). PAC offers potential advantages over conventional incineration, including: (1) positive containment of plutonium and other transuranium nuclides, (2) close control of gas input and minimization of off-gas volume, (3) simplified off-gas cleaning, (4) operation at lower temperatures (200 to 260°C), and (5) the use of continuous or semicontinuous systems.

The PAC process consists in heating the waste material in the presence of liquid H_2O and oxygen (e.g., air) in a reactor to a temperature at which oxidation occurs. Carbonaceous material is converted mainly to CO_2, with only a small amount of CO being formed; sulfur is oxidized to sulfate. The required pressure is a function of the operational temperature and of the mode of operation; for continuous or semicontinuous processing, it will amount to the vapor pressure of water plus the pressure required to supply the air for oxidation. At 235°C, for example, a total pressure of about 460 psig should suffice (444 psi for water vapor plus about 16 psi for air). For simple batch oxidation the operational pressure must be higher since all of the oxygen must be introduced into the reactor at one time.

The wet oxidation process was first described by Strehlenert[13] and was later applied to the disposal of paper mill wastes, sewage sludge, etc., by Cederquist[14] in Sweden and by Zimmerman[15] and others in the United States. It has been proposed for use in the disposal of urban waste and for various other applications.[16,17] Controlled wet oxidation is used commercially for the production of vanillin from the lignin-containing waste that is generated in the sulfite process for producing paper pulp.[18]

Laboratory Studies

Previous studies concerning the wet oxidation of municipal waste[19] showed that waste consisting of 85% cellulosic material, 11% gelatin (simulated food waste), and 4% polyethylene was 56% oxidized during a 30-min exposure at 193°C and 89% oxidized during a 1-hr exposure at 222°C.[16] The degree of oxidation obtainable at a given exposure time and temperature can be increased by the addition of heavy metals (Co^{2+}, Fe^{3+}, Cu^{2+}, Zn^{2+}, and Mn^{2+} as nitrates), by the addition of small amounts of HNO_3 (e.g., sufficient to give a final concentration of 0.1 *M*), and particularly by the addition of a silica gel catalyst. Recycle of the effluent, particularly the sludge, is about as effective in

13. R. W. Strehlenert, Swedish Pat. 43,860 (Apr. 13, 1918); R. W. Strehlenert, *Pulp Paper Mag. Can.* 16, 671 (1918); R. W. Strehlenert, *Sv. Papperstidn.* 22, 136 (1919).

14. K. N. Cederquist et al., Swedish Pat. 90,896 (Nov. 23, 1937); K. N. Cederquist et al., U.S. Pat. 2,668,099 (Feb. 2, 1954); K. N. Cederquist et al., *Sv. Papperstidn.* 58, 154–64 (1955).

15. F. J. Zimmerman, U.S. Pat. 2,665,259 (Jan. 5, 1954) and U.S. Pat. 2,824,058 (Feb. 18, 1958) (both assigned to Sterling Drug Co.); F. J. Zimmerman, *Ind. Water Wastes* 6, 102–6 (1961).

16. W. J. Boegly, Jr., W. L. Griffith, and W. E. Clark, *The Development of a Wet Oxidation Process for Municipal Refuse,* ORNL-HUD-15 (February 1971).

17. C. G. Golueke and P. H. McGauhey (eds.), *Comprehensive Studies of Solid Wastes Management. First Annual Report,* SERL report No. 67-7 (May 1967).

18. J. R. Salveson et al., U.S. Pat. 2,434,626 (Jan. 13, 1948).

19. These were carried out at ORNL for the U.S. Dept. of Housing and Urban Development (HUD).

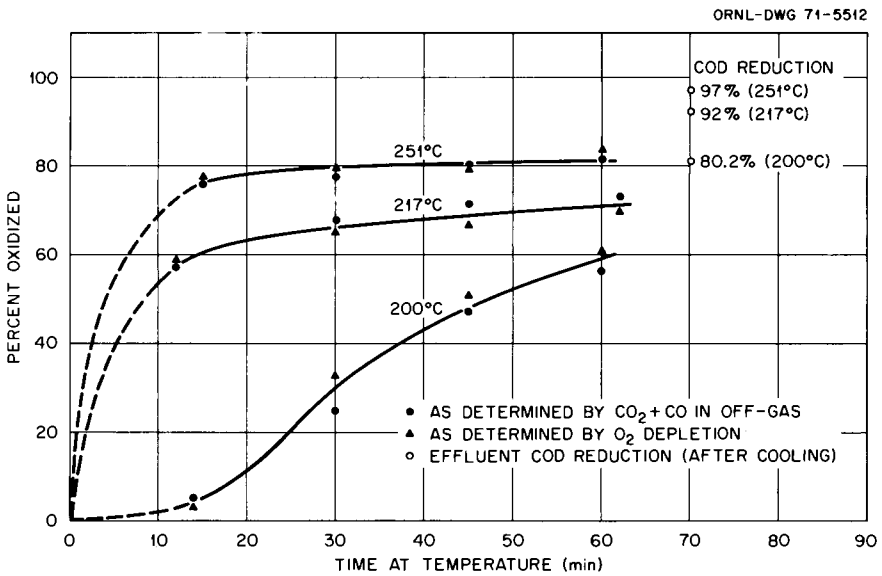

Fig. 4.3. Batch oxidation of pure cellulose at three temperatures.

producing oxidation as any combination of the catalysts tested. The presence of heavy metal ions is of further benefit in hastening the degradation of polyethylene[20] and thus decreasing the tendency of this plastic to melt and stick to the hot wall of the autoclave.

When pure water was used, the effluent resulting from the oxidation of cellulosics and plastics was acidic (pH 2 to 4). The complete oxidation (99%) of waste containing 10% protein produced effluents that were slightly alkaline (pH 8 to 9). In the absence of chloride the acid effluents had a mildly corrosive effect on type 430 stainless steel but did not attack titanium. In the presence of small amounts of chlorinated plastics (e.g., polyvinyl chloride), the acidic solution was increasingly corrosive, although titanium was resistant except when the plastic melted and stuck to the specimen. Nickel was severely corroded by alkaline effluents.

Initial tests, including two recycle runs, were carried out in a 1.4-liter rocking autoclave to test the feasibility of oxidizing various waste constituents. The results (Table 4.8) show that:

1. in the presence of 57 to 76% cellulosics (paper, cloth, wood, etc.), all the materials tested except Teflon are satisfactorily oxidized during a 1-hr exposure at 294°C;
2. rubber, Bakelite, and epoxy are incompletely oxidized at 250°C;
3. the corrosion of stainless steel can be expected to increase upon recycle of acidic effluents even in the absence of appreciable amounts of chloride;[21]
4. titanium is resistant to chloride in strongly oxidizing media.

Experiments were initiated to determine the reaction rates of various components of waste by taking periodic gas samples and determining the rate of oxygen depletion and the rate of CO_2 (plus CO) generation. These data for pure cellulose are plotted as a function of time in Fig. 4.3 at temperatures of 200, 217, and 251°C. There is qualitative agreement between the results obtained from analysis for the two different gases; however, both gaseous monitoring methods give lower total oxidation values than were obtained by chemical oxygen demand (COD) analyses of the liquid effluents. Preliminary data were obtained for epoxy resin, 10 to 20 mesh, at 299 and 319°C. Qualitatively, the oxidation characteristics of the epoxy resin were the same as those of cellulose at 251°C. Since cellulose is one of the most readily oxidizable constituents and epoxy is one of the most difficultly oxidizable constituents expected to be present in contaminated waste, these data effectively bracket the conditions of operation.

Experiments[22] designed to determine the thermal stability of solid residues resulting from the partial

20. H. Alter, *Ind. Eng. Chem.* **52,** 121–24 (1960).

21. Walter E. Clark, *The Status of Pressurized Aqueous Combustion for Burning Solid Wastes Contaminated by Radionuclides,* ORNL-TM-3170 (October 1970).

22. These were run by H. Kubota of the Analytical Chemistry Division using a new technique.

Table 4.8. Pressurized aqueous combustion of simulated contaminated solid wastes

Wastes constituted 9% by weight of slurry. Reaction time at temperature was approximately 1 hr. Run in stainless steel autoclave except as indicated.

Experiment No.	Waste composition		Additives	Concentration of additives	Temperature (°C)	Effluent COD (g of O_2/liter)	Nominal reduction in COD[b] (%)	Apparent corrosion[c] on exposed coupons (mils/month)			Remarks
	Component[a]	Percent by weight						430SS	Ti	Hastelloy C	
					Single Experiments						
1	Cellulosics Polyethylene Latex rubber	60 20 20	Silica gel HNO_3	~5.5 g/liter 0.3 *N*	250	17.4	88	16	0		Rubber remained
2	Cellulosics Polyethylene Latex rubber	60 20 20	Silica gel Cu^{2+} Fe^{3+} Mn^{2+} NO_3^-	~5.5 g/liter 0.038 *M* 0.036 *M* 0.08 *M* 0.344 *M*	246	13.6	91	2.1	0		Rubber remained
3	Cellulosics Polyethylene Latex rubber PVC	56.4 24.9 8.5 10.2	$La(NO_3)_3$	0.02 *M*	294	5.4	96	114	Slight weight gain		No solid remnant; corrosive to autoclave; free acid = 0.13 *N*; pH = 3.9
4	Cellulosics Polyethylene Latex rubber PVC	55.2 27.3 9.0 9.5	$La(NO_3)_3$	0.02 *M*	294	6.3	96		18[d]	Severely pitted	No solid remnant; titanium autoclave; free acid = 0.08 *N*; pH = 4.3
5	Cellulosics Silicone rubber Bakelite	75.6 12.5 12.0	None		252	2.8	98				Silicone partly attacked; Bakelite slightly attacked
6	Cellulosics Silicone rubber Bakelite	75.9 11.6 12.5	None		293	5.7	96				Some black particles and white ash
7	Cellulosics Nalgene Tygon	73.6 13.2 13.3	None		293	4.2	97				No solid remnant; corrosive to autoclave
8	Cellulosics Teflon Epoxy Butyl rubber	72 9 10 9	None		290	3.7	98				Teflon unattacked; epoxy charred

Table 4.8 (continued)

Experiment No.	Waste composition: Component[a]	Waste composition: Percent by weight	Additives	Concentration of additives	Temperature (°C)	Effluent COD (g of O_2/liter)	Nominal reduction in COD[b] (%)	Apparent corrosion[c] on exposed coupons (mils/month): 430SS	Ti	Hastelloy C	Remarks
					Recycle Experiments[e]						
9-1	Cellulosics	50	SiO_2	~4.5 g/liter	303	4.5	97				
	Polyethylene	19	$La(NO_3)_3$	0.02 *M*							
	Butyl rubber	11									
	Bakelite	9						2.2		≤1	Titanium autoclave leaked slightly during these exposures
	Epoxy	9									
	PVC	2									
9-2				None	300	5.4	96				
10-1	Cellulosics	49		None	~300	2.8	98				Temperature control poor on 10-1; residual charred chunks
	Polyethylene	19									
	Butyl rubber	13									
	Bakelite	10									
	Epoxy	9									
10-2				None	320	2.9	98				Some black residue (Bakelite and epoxy)
10-3				None	320	5.6	96				No appreciable remnant solids
10-4				None	318	7.7	95				No appreciable remnant solids; autoclave corroded; pH = 6.7

[a]Cellulosics included cheesecloth, wood chips, and various types of paper. Polyvinyl chloride is abbreviated as PVC. Tygon is polyvinylidene chloride; it yields more chloride on oxidation than does PVC.

[b]Based on effluent only and are therefore high. Not corrected for remnant solids.

[c]Exposure times were so short that the accuracy was low. Corrosion rates ≤ about 5 mils/month may therefore be negligible.

[d]PVC had melted and stuck to this specimen.

[e]91% of the effluent was recycled to the following run in each case and distilled water was added for makeup. Additives [e.g., silica gel, $La(NO_3)_3$] were included only before the first cycle.

oxidation of cellulose indicated that some charring took place below 500°C but that little exothermic reaction occurred. These experiments will be repeated on residues from other waste types.

Results may be summarized as follows:

1. Except for Teflon, the most resistant organic materials included in the tests oxidized almost completely in 1 hr at temperatures between 290 and 300°C. Cellulosic materials with or without polyethylene oxidized sufficiently in 1 hr at temperatures as low as 217°C.
2. Size reduction is not critical for the more common constituents such as the cellulosics and polyethylene; even for polyethylene bottle caps and necks, oxidation is complete in 1 hr at 290°C. Size reduction is particularly helpful with PVC and rubber because it shortens the reaction time and also because it promotes more effective mixing, thus decreasing the chance of melting and sticking to the walls. Residual chunks of relatively inert organics such as Tygon, epoxy, and Bakelite can probably be safely stored without further treatment.
3. Titanium is the most promising containment material tested thus far.

Future studies will be designed to: (1) test the performance of the semicontinuous method of operation (batch charging of solids, with continuous passage of air through the autoclave), (2) determine the degree of oxidation required to produce essentially noncombustible waste residues, and (3) perform more comprehensive corrosion tests on candidate materials of construction.

Design and Engineering Development

Results of a survey[23] of waste generation rates at major AEC sites in the United States were used to estimate the capacities of full-size PAC plants that would be required at each of the sites. It was found that a plant with a capacity of about 1 ton/day would be compatible with the requirements of nearly all of the AEC sites considered; furthermore, it was judged that a pilot plant with a capacity of about 0.1 ton/day would be of a reasonable size to demonstrate the feasibility of the concept and to provide the necessary scaleup information for the full-size plant.[24]

An engineering design survey was made to determine the best mode of operation for the pilot plant.[25] Process flowsheets for semicontinuous and continuous pilot plants were prepared and analyzed. (Simplified versions of the flowsheets are shown in Figs. 4.4 and 4.5.) In the semicontinuous system (Fig. 4.4), shredded waste and water are added to the reactor in batches, the system is heated to operating temperature, and air (or oxygen) is passed through continuously until the reaction has reached the desired state of completion. In the continuous system (Fig. 4.5), both solids (in the form of a slurry) and air (or oxygen) are pumped through the reactor continuously. Results of this survey indicated that it would be more feasible to design and build a semicontinuous pilot plant to determine the basic operating parameters such as temperatures, pressures, and feed concentrations, and to solve problems involving gas cleanup, corrosion, feed and product handling, etc. On the other hand, the results of the survey revealed that a continuous system would be more practical for a full-scale (1-ton/day) plant. The latter decision is largely based on reactor size considerations; that is, the pressurized reaction vessel can be made much smaller in a continuous system at comparable operating temperatures, pressures, and holdup times because turnaround times between batches are eliminated. In the semicontinuous system, the reaction time is only a fraction of the total process cycle time of charging the reactor, heating the system to operating temperature, carrying out the reaction, cooling, and draining the system.

It was recommended that (1) a semicontinuous pilot plant capable of handling 0.1 ton of combustible waste per day be designed, built, and operated; (2) a detailed analysis be made of a full-size plant designed to burn 1 ton of contaminated combustible waste per day; (3) an equipment design and development program be initiated to produce the specialized components (such as the high-pressure slurry pump) and establish the necessary concepts needed for a continuous full-size plant; and (4) consideration be given to the design, construction, and operation at ORNL of a full-size prototype plant based on the results of the pilot plant and development program.

4.5 INCORPORATION OF INTERMEDIATE-LEVEL WASTES IN POLYETHYLENE

Laboratory tests have shown that aqueous intermediate-level wastes can be incorporated in DYDT and DYLT Bakelite polyethylene to produce stable, fire-

23. H. W. Godbee and J. P. Nichols, *Sources of Transuranium Solid Waste and Their Influence on the Proposed National Radioactive Waste Repository,* ORNL-TM-3277 (January 1971). (Official Use Only.)

24. W. C. Ulrich, personal communication, Jan. 18, 1971.

25. W. C. Ulrich, personal communication, March 1971.

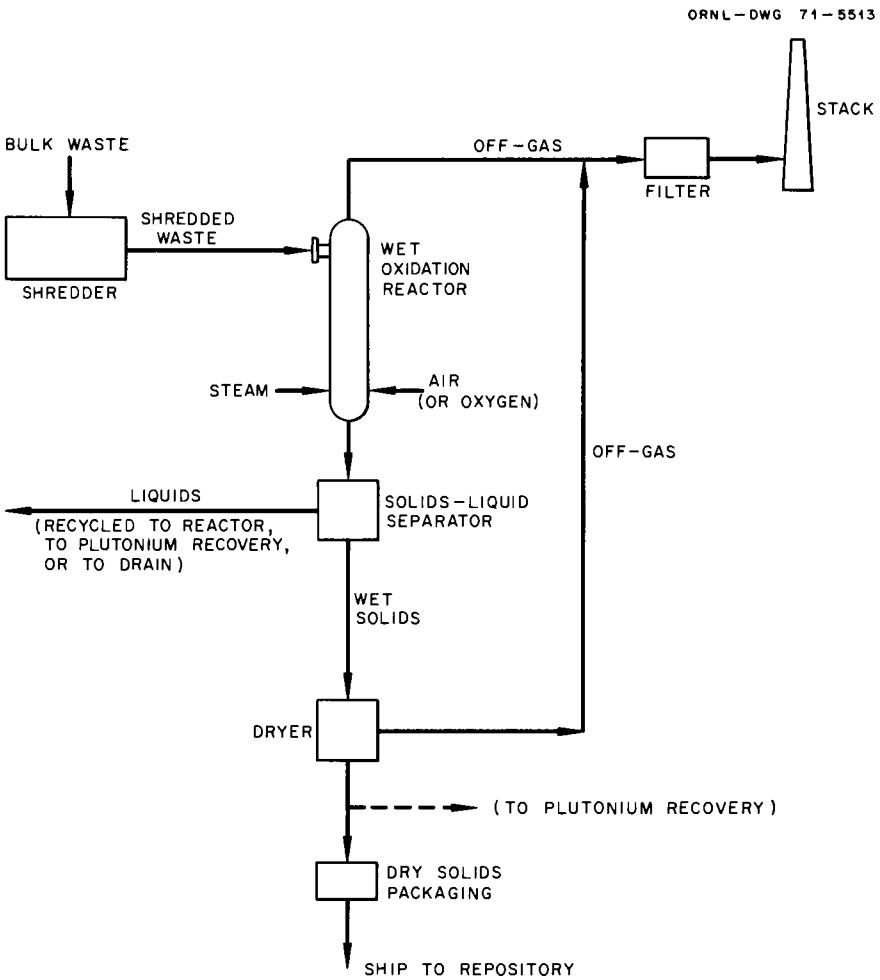

Fig. 4.4. Semicontinuous pilot plant for pressurized aqueous combustion of contaminated solid wastes.

retardant products.[26] The products have low leach rates in water and should be suitable for burial in licensed surface burial grounds. Five ~2-hr tests were made in the existing pilot plant, which had previously been used for incorporating wastes in asphalt,[27,28] to demonstrate the feasibility of the process in large-scale equipment. A 20 wt % sodium borate solution was used to simulate wastes produced at power reactors. DYDT polyethylene was selected because of its lower softening point and viscosity at the proposed operating temperature. The pilot plant was first modified by replacing the liquid asphalt feed system with a system capable of feeding solid polyethylene; also a means of supplying additional heat to the exposed uninsulated sections of the wiped-film evaporator was included.

Contacts with polyethylene manufacturers indicated that it would probably be possible to melt and meter the polyethylene into the evaporator in a single operation by passing it through a polyethylene extruder driven by a variable-speed motor. However, subsequent testing showed that the low-melting DYDT polyethylene had a tendency to soften prematurely, causing plugging of the solids feed nozzle to the extruder. As a compromise, a steam coil was installed in the solids reservoir, and the polyethylene was completely melted and fed to the extruder as a viscous solution. Accuracies of better than 3% were demonstrated with this metering

26. C. L. Fitzgerald et al., "The Feasibility of Incorporating Radioactive Wastes in Asphalt or Polyethylene," *Nucl. Appl. Technol.* 9, 821–29 (1970).

27. *Chem. Technol. Div. Annu. Progr. Rep. May 31, 1969*, ORNL-4422, pp. 147–49.

28. H. W. Godbee, J. H. Goode, and R. E. Blanco, "Development of a Process for Incorporation of Radioactive Waste Solutions and Slurries in Emulsified Asphalt," *Environ. Sci. Technol.* 2, 1034–40 (1968).

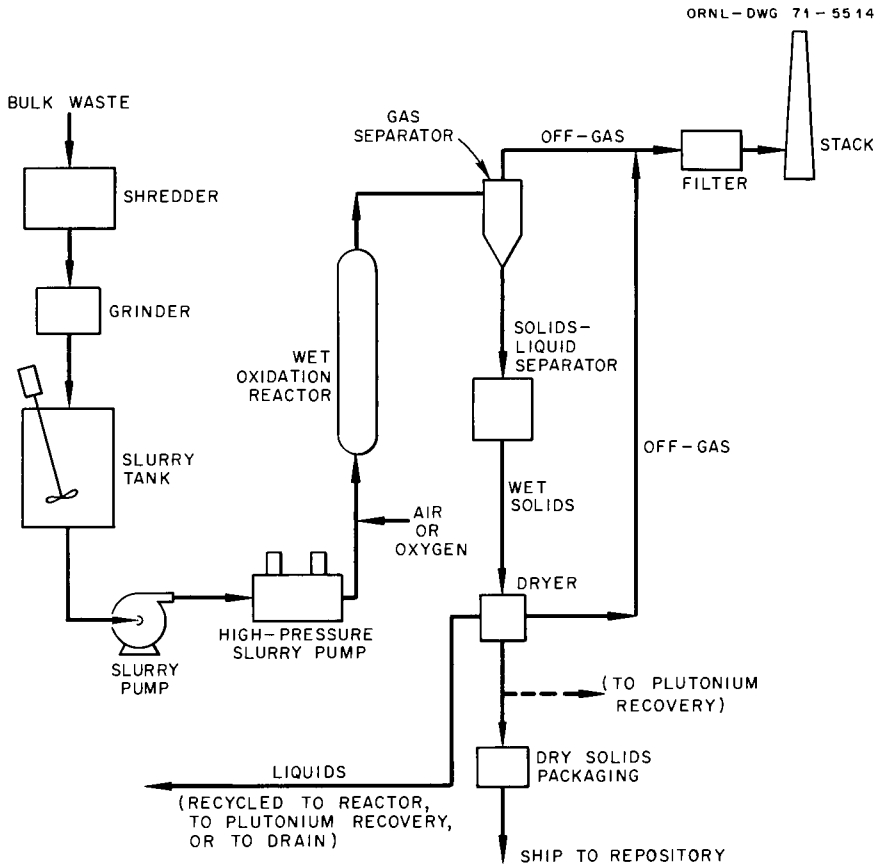

Fig. 4.5. Continuous pilot plant for pressurized aqueous combustion of contaminated solid wastes.

system. Calrod heaters were installed on the wiped-film evaporator head and the product discharge nozzle. This supplementary heat to the evaporator was necessary to compensate for heat loss from the molten polyethylene to the waste solution (ΔT 60°C) at the contact point on the rotor distribution plate and to prevent the polyethylene from solidifying. The additional heat supplied to the product discharge nozzle ensured that all surfaces contacting the product were at a temperature that would maintain fluidity.

The data from the five tests are shown in Table 4.9. In each test, the waste solution and the polyethylene were preheated to 85°C and to approximately 140°C, respectively, before they entered the evaporator. In runs 1 through 3, the evaporator was operated at a wall temperature of 185°C; in runs 4 and 5, it was operated at 200°C. The evaporator rotor speed was nominally 300 rpm in all the runs except run 5, where the speed was reduced to 190 rpm. When the evaporator was disassembled after the completion of run 1, an accumulation of solids was found in the bottom half of the evaporator; the wiper blades were destroyed in this area. However, the waste solids content of the product was near the desired value (30%), and the residual water content and leach rates (over a nine-week period) were nearly as good as those observed in subsequent runs. In order to obtain more effective evaporator performance, runs 2 through 5 were made under conditions selected to give products with a solids content of about 20 wt %. The results showed that neither increased evaporator temperatures nor rotor speed had a marked effect on the quality of the product. However, the amount of sodium entrained in the overhead vapors increased as the operating temperature increased. The water content of the product decreased as the processing rate decreased. This confirms results obtained in tests with asphalt. Graphite wiper blades were used in runs 4 and 5 in place of the standard rotor blades (Teflon-impregnated Fiberglas) used in the asphalt demonstration tests. These blades appeared to suffer less wear

Table 4.9. Incorporation of $NaBO_2$ waste in polyethylene

Run No.	Waste feed rate (lb/hr)	Polyethylene[a] feed rate (lb/hr)	Evaporator boilup rate (lb/hr)	Evaporator sodium decontamination factor	Product rate (lb/hr)	Product solids content (wt %)	Product water content (wt %)	Product temperature (°C)	Product leach rate [fraction sodium leached $(cm^2/g)^{-1}$ day^{-1}]			
									Week 1	Week 2	Week 4	Week 9
1	65.1	31.6	~50.9[b]	~2970	45.9	31.5	3.8	155	7.1×10^{-3}	6.0×10^{-3}	3.1×10^{-3}	1.4×10^{-3}
2	34.6	27.8	24.5	2740	34.9	22.0	1.5	175–180	1.8×10^{-3}	2.0×10^{-3}	1.3×10^{-3}	8.9×10^{-4}
3	62.6	52.6	44.2	2350	72.1	19.3	4.5	175–180	4.2×10^{-3}	4.3×10^{-3}	1.1×10^{-3}	6.1×10^{-4}
4	65.1	52.7	49.9	1470	73.6	19.6	3.6	195–200	3.4×10^{-3}	2.6×10^{-3}	1.4×10^{-3}	9.8×10^{-4}
5	64.3	52.9	45.5	1030	74.9	19.0	5.2	195–200	6.0×10^{-3}	3.0×10^{-3}	1.7×10^{-3}	1.3×10^{-3}

[a]DYDT polyethylene, a product of Union Carbide Corp.
[b]By difference.

than the standard blades. Material balances ranged from 95 to 105%. Product leach rates were acceptable for all of the runs and, based on the nine-week test periods, were comparable with similar products produced in the laboratory equipment.

Although the process demonstration was successful, we do not believe that the full potential of the process will be realized until the process has been demonstrated in equipment that can operate at higher temperatures.

5. Transuranium-Element Processing

The Transuranium Processing Plant (TRU) and the High Flux Isotope Reactor (HFIR) are operated at ORNL as the primary production facilities for the USAEC Heavy Element Program. During this report period, which corresponds to the fifth year of operation of these facilities, efforts at TRU were devoted primarily to the recovery of 200 mg of ^{252}Cf for the commercial sales program sponsored by the Savannah River Plant.

The phases of the program that are under the direction of the Chemical Technology Division, including the operation of TRU, isolation and purification of products, development of chemical processes, and some chemical studies of the actinide elements, are reported here. Target fabrication work, which is directed by the Metals and Ceramics Division, is described in detail in reports issued by that Division.

5.1 TRU OPERATIONS

The functions of TRU are to recover large quantities of the transuranium elements and distribute them to researchers. Since it began operation in 1966, TRU has been the only source of significant quantities of berkelium, californium, einsteinium, and fermium in the United States.

The purpose of this section is to report the production of transuranium materials and to describe recent changes in the processes and equipment being used in TRU. More detailed information is presented in a series of semiannual reports on production, status, and plans.[1,2]

Status and Progress

During the first four years that TRU was in operation, we recovered and shipped to researchers all of the elements from americium through fermium as we demonstrated the process steps that are required to recover transuranium elements from irradiated HFIR targets and to fabricate curium oxide recycle targets. Feed materials were primarily from HFIR irradiations, and about 75 mg of ^{252}Cf was recovered. During the current report period, our major effort was the processing of 164 curium slugs that had been irradiated as part of the Californium-I program at the Savannah River Plant (SRP). This program is designed to evaluate the commercial market for ^{252}Cf. The slugs contained about 430 g of ^{244}Cm (550 g of total curium) and 200 mg of ^{252}Cf. Most of the ^{252}Cf has been returned to SRP. The curium will be purified further, converted to oxide, and then returned to SRP. The other transuranium elements, 25 mg of ^{249}Bk, 400 μg of ^{253}Es, and 3×10^9 atoms of ^{257}Fm, were distributed to researchers through the Transplutonium Committee. Ninety-six shipments were made during this report period. Although the final portions of this campaign will extend a few weeks beyond the end of the report period, total quantities are shown to present the overall picture of this campaign.

The scope of processing operations was increased considerably this year. The slugs contained about three times as much irradiated curium and four times as much californium as were processed in any previous year. The TRU operations group was expanded by about one-third to handle the increased processing load. The expanded group will be retained for about one year in order to process about 20 irradiated ^{242}Pu tubes containing about 400 mg of ^{252}Cf; these are also Californium-I materials. The increased operating costs are being borne by the AEC Division of Production.

Production and Processing

Two processing campaigns were made to produce americium-curium oxide for use in fabricating targets

1. W. D. Burch, J. E. Bigelow, and L. J. King, *Transuranium Processing Plant Semiannual Report of Production, Status, and Plans for Period Ending June 30, 1970,* ORNL-4588 (January 1971).

2. W. D. Burch, J. E. Bigelow, and L. J. King, *Transuranium Processing Plant Semiannual Report of Production, Status, and Plans for Period Ending December 31, 1970,* ORNL-4666 (in press).

Table 5.1. Amounts of materials recovered from the processing of SRP-Californium-I slugs

	Campaign 21	Campaign 22	Campaign 23	Campaign 24[a]	Campaign 25[a]	Total
Number of slugs[b]	35	32	30	32	35	164
^{243}Am, g	0.2	0.2	0.2	0.2	0.2	1.0
^{244}Cm, g	80.8	69.7	96	86	95	428
^{246}Cm, g	32	17	24	21	23	117
^{249}Bk, mg	10	4	4	4	3	25
^{252}Cf, mg	76	43	30	28	27	204
^{253}Es, μg	312	65	18	8	4	407
^{257}Fm, atoms	1×10^9	6×10^8	4×10^8	4×10^8	3×10^8	3×10^9

[a]Calculated quantities; data incomplete at end of report period.
[b]Feed material for the campaigns included various amounts of rework material plus the indicated number of slugs.

for the HFIR, and five campaigns were made to process SRP-reactor slugs. About 22 g of ^{243}Am and 50 g of ^{244}Cm were converted to oxide. The amounts of transuranium materials recovered in the SRP-slug processing campaigns are listed in Table 5.1.

The SRP-Californium-I slugs are similar to HFIR targets in that they contain aluminum-clad pressed compacts of actinide oxides blended with aluminum powder. The processes and equipment used to process the slugs are generally the same as those used to process HFIR targets.

Differences that were noted are as follows:

1. The radioiodine reported almost entirely (94%) to the caustic-nitrate solution used to dissolve the aluminum from the slugs. Only about 50% of the radioiodine reports to the aluminum dissolvent when HFIR targets are processed. During the first slug campaign, we performed a Pubex batch extraction to collect iodine in a small volume so that we could store it to permit decay prior to transfer to the high-level waste tanks. This step was unnecessary in subsequent campaigns because there was much less radioiodine to process and essentially all of it was in the aluminum dissolvent.

2. The acidic dissolver solutions contained large amounts of inactive solids, which hampered solution transfers. Following the first SRP-slug campaign, we installed a larger filter (eight times the solids capacity of the original filter), which reduced the time required for transferring solutions from six days to one day.

3. The decontamination of the actinides from fission products, using the Tramex solvent extraction process, was complicated because of equipment performance problems and chemical problems, all of which are not fully understood. We were unable to establish satisfactory operation of the continuous solvent extraction columns; thus, much of the Tramex processing was done by three-stage batch extractions. Decontamination factors were poor by either method – about a factor of 10 lower than was anticipated.

The other processing steps (dissolving, Cleanex batch extraction, LiCl-based anion exchange, and chromatographic elution using α-hydroxyisobutyrate) were accomplished without significant difficulty. Because of the poor decontamination factors in Tramex, the purity of the curium product is marginal. Specifications are based on gross gamma and neutron dose rates of packaged oxide, and measurements of actual packages must be required in order to determine whether the specifications have been met. If further cleanup is required, it will probably be accomplished by LiCl-based anion exchange.

Equipment and Modifications

Some new equipment was installed, and the existing equipment was modified. These changes were made partly to make it possible to process the SRP-Californium-I materials and partly for general improvement of the TRU facilities. About 100 changes were made in the cell piping.

Several minor plant revisions were required prior to processing the SRP slugs. New 4.75-in.-diam slug chutes were installed in cubicles 1 and 7, which will accommodate the 4.22-in.-diam by 5-ft-long SRP-Californium-I reactor tubes as well as the shipping packages of thirteen 1-in.-diam by 6-in.-long SRP-reactor slugs.

A new equipment rack was installed for use in separating and purifying the transcurium elements, utilizing chromatographic elution from an ion exchange column with α-hydroxyisobutyrate. The equipment employed previously was inadequate for processing the large amount of transcurium elements contained in the SRP slugs.

The liquid wastes that are being generated during the processing of SRP-Californium-I materials contain significantly more radioactivity than wastes being handled routinely in TRU. The high-level wastes from processing the slugs are being segregated and transferred to a stainless steel high-level tank in Building 2531 for storage. Final disposal will be deferred, pending ORNL decisions concerning future waste disposal. A waste loading station was installed in the TRU limited-access area, an unloading station and containment enclosure was installed in Building 2531, and a 450-gal-capacity Isotopes Division shielded transfer tank was modified to effect the transfer of waste solution. Several shipments of waste have been made without difficulty, although some precipitated fission products have remained in the carrier as evidenced by the high level of residual radioactivity when the carrier is emptied.

A cask (DOT-SP-6323) that provides adequate shielding for transporting about 50 mg of ^{252}Cf and about 160,000 Ci (gamma) was designed and built for use in shipping the SRP-Californium-I slugs to ORNL. It weighs 28,800 lb and consists of two 66-in.-diam hemispherical ends joined by a 15-in. cylindrical section. The inner cylindrical cavity is 4.026 in. in diameter by 15 in. long. The shielding consists of a 4-in.-thick cylinder of depleted uranium, which is encased in stainless steel, surrounded by Blackburn limonite concrete. The outer shell of the cask is ½-in.-thick stainless steel. The slugs were shipped in groups of up to 13, packaged in a 4-in.-diam by 13-in.-long aluminum holder having a central hole surrounded by six outer holes. The aluminum holder, which is not reused, may be placed into, or removed from, the carrier through either the top or the bottom. In the latter stages of the fabrication, defects were discovered in the depleted-uranium gamma shield. The defects resulted from swelling due to the reaction of the uranium with water. The water was admitted through the stainless steel encasement surrounding the uranium during drilling operations with water-based coolants. Through oversight, this water was not removed. Repairs involved the remote welding of an insert tube inside an existing housing for a valve-operating rod and machining to remove a bulge in the central cavity. The repairs appear to be adequate; measurements taken after each of the nine shipments that have been made show that no further deformation has occurred.

General improvements to the TRU processing facilities included the installation of (1) four 20-liter-capacity tantalum-lined product storage tanks, (2) an iodine-retention system that is capable of handling the entire 400-cfm vessel off-gas flow, (3) a pneumatically actuated rabbit system for transferring californium between the TURF californium facility and TRU, and (4) a shielded facility for decontaminating targets and sources prior to shipment.

The iodine removal unit, which consists of a catalytic oxidation bed to destroy organic vapors, followed by charcoal beds for adsorbing iodine, has been installed for treating the entire vessel and cubicle off-gas flow. Entering off-gas is heated to about 550°F in passing through the tubes of a regenerative heat exchanger (countercurrent to the exit gas from the catalytic oxidation bed). Additional electric heat (about 20 kW) is provided to maintain the catalyst (Hopcalite) bed at 650 ± 25°F. The gases from the Hopcalite bed are cooled to about 225°F in the shell side of the primary heat exchanger and then cooled further to 175 ± 25°F in a small water-cooled exchanger. The cool gases pass through two 1-in.-thick charcoal beds in series for iodine removal. The oxidation step destroys organic materials in the off-gas and thus improves the efficiency of the charcoal bed for sorption of iodine. (See Sect. 2.6 for detailed results of tests made during the SRP-slug campaigns.)

The pneumatic-rabbit system for transferring ^{252}Cf between TRU and the TURF californium facility has greatly simplified this operation. Previously, our only shipping carrier that can handle more than a milligram of ^{252}Cf had to be used for such transfers. The handling cost was high, and scheduling was inconvenient. Transfer rabbits travel the 700 ft of 1-in.-diam stainless steel line in approximately 12 to 14 sec. During a transfer of 50 mg of ^{252}Cf, doses to personnel would be less than 1 millirem even though the instantaneous dose rate 1 ft from the line is expected to be about 1250 rems/hr.

The rabbit transfer line terminates at TRU in a small portable water-shielded cell located above the target chute at cubicle 1. This cell provides an interface between TRU and TURF, as well as with off-site carriers, where packages may be decontaminated before transfer or shipment. This should eliminate the contamination problem we have created for some of our customers in the past.

Target Fabrication

Seventeen targets containing americium and curium, one special target, and eight rabbits were fabricated during this report period. This work was performed by personnel of the Metals and Ceramics Division and is reported in detail in their reports.

Since our last annual report, three targets have failed during irradiation in the HFIR. One of them was a 90%-dense plutonium target whose failure was antici-

pated by our mathematical model for target failures. However, the other two targets, in which the pellets were pressed to 80% of theoretical density, should not have failed according to the model. Investigation of these failures is incomplete.

5.2 ISOLATION AND PURIFICATION OF TRU PRODUCTS

The final purification of transplutonium elements, the isolation of second-growth isotopes, and the fabrication of actinide shipping packages and neutron sources are accomplished in equipment installed in cell 5 in TRU, the californium facility at TURF, and in supporting shielded-cave facilities. When products reach certain levels of purity, they are moved into these cleaner facilities, which are used only for handling products.

Final Purification and Isolation of Transplutonium Elements

The purified products are obtained from the transcurium fraction (from the LiCl anion exchange process) that is produced routinely in the plant equipment. This processing, which has been previously described,[3,4] consists in the separation of fermium, einsteinium, californium, and berkelium from each other and from residual actinides by selective elution from cation exchange resin with ammonium α-hydroxyisobutyrate; berkelium is further purified from residual actinides by oxidation to Bk^{4+} by $NaBrO_3$ and subsequent extraction from 8 *M* HNO_3 into di(2-ethylhexyl)phosphoric acid (HDEHP).

In recent processing, the use of a small loading column, which can be operated in series with the high-pressure ion exchange column, has greatly increased the amount of ^{252}Cf that can be processed in a single run and has decreased the run time substantially. Using this technique, the actinides can be loaded rapidly onto a small column from dilute acid; and, since only a small volume of resin is used, the resin can be rapidly converted to the ammonium form prior to elution through the regular 4-ft column with ammonium α-hydroxyisobutyrate. Since loading and resin conversion can be accomplished very rapidly, larger amounts of actinides can be processed with less resin degradation.

Using this technique, 69 mg of ^{252}Cf was processed in a single run, and it appears that at least 100 mg of ^{252}Cf can be handled. Prior to the installation of the loading column, it was not possible to process more than 25 mg of ^{252}Cf.

Isolation of Second-Growth Isotopes

Various special separations were made during this report period. These included isolation of 65 μg of ^{253}Es (a daughter of ^{253}Cf) and about 1.3 mg of ^{248}Cm, both of which had grown into highly purified californium during storage. An additional 33 mg of ^{252}Cf, which will be milked to produce about 1.5 mg of ^{248}Cm, was purified. Nine hundred micrograms of ^{249}Cf that had grown into ^{249}Bk was also separated.

Isotopically pure ^{248}Cm is obtained by the alpha decay of ^{252}Cf, which is originally isolated from large amounts of ^{244}Cm. In order to minimize the ^{244}Cm content in ^{248}Cm products, the ^{252}Cf must be highly purified. In the californium TURF facility we have been able to routinely obtain ^{248}Cm containing less than 0.001 at. % ^{244}Cm.

Preparation of ^{252}Cf Shipping Packages

The resin-loading–encapsulation method for ^{252}Cf handling, which has proved to be a versatile technique for the preparation of neutron sources, was utilized to prepare ^{252}Cf shipping capsules. The shipping package is a doubly sealed container which provides for a safe and practical transfer of californium in a small package and permits simple and complete recovery of californium by the customer.

A schematic diagram of the shipping package is shown in Fig. 5.1. The primary container consists of a 3/8-in.-OD by 1-in.-long stainless steel tube that has been platinum-plated and filled with cation exchange resin. Tubes fabricated from a 90% platinum–10% rhodium alloy have also been used. Platinum frits are rolled into each end of the tube to completely encapsulate the resin. The resin is then loaded by passing a solution of californium in dilute nitric acid through the capsule. After being loaded, each capsule is calcined at 650°C for a 3-hr period, during which it is purged with air, at a low flow rate, to decompose the resin. End plugs are then placed on the capsule, and the capsule is welded into a secondary stainless steel container. Essentially complete recoveries are readily obtained from this type of package by passing a small volume of dilute nitric acid through the calcined resin bed.

Resin-loading–encapsulation techniques were used to prepare more than 20 shipping packages and 13 neutron sources. An additional 6 neutron sources were prepared by the quartz bead method.

3. *Chem. Technol. Div. Annu. Progr. Rep. May 31, 1967*, ORNL-4145, pp. 136–51.

4. *Chem. Technol. Div. Annu. Progr. Rep. May 31, 1968*, ORNL-4272, pp. 100–101.

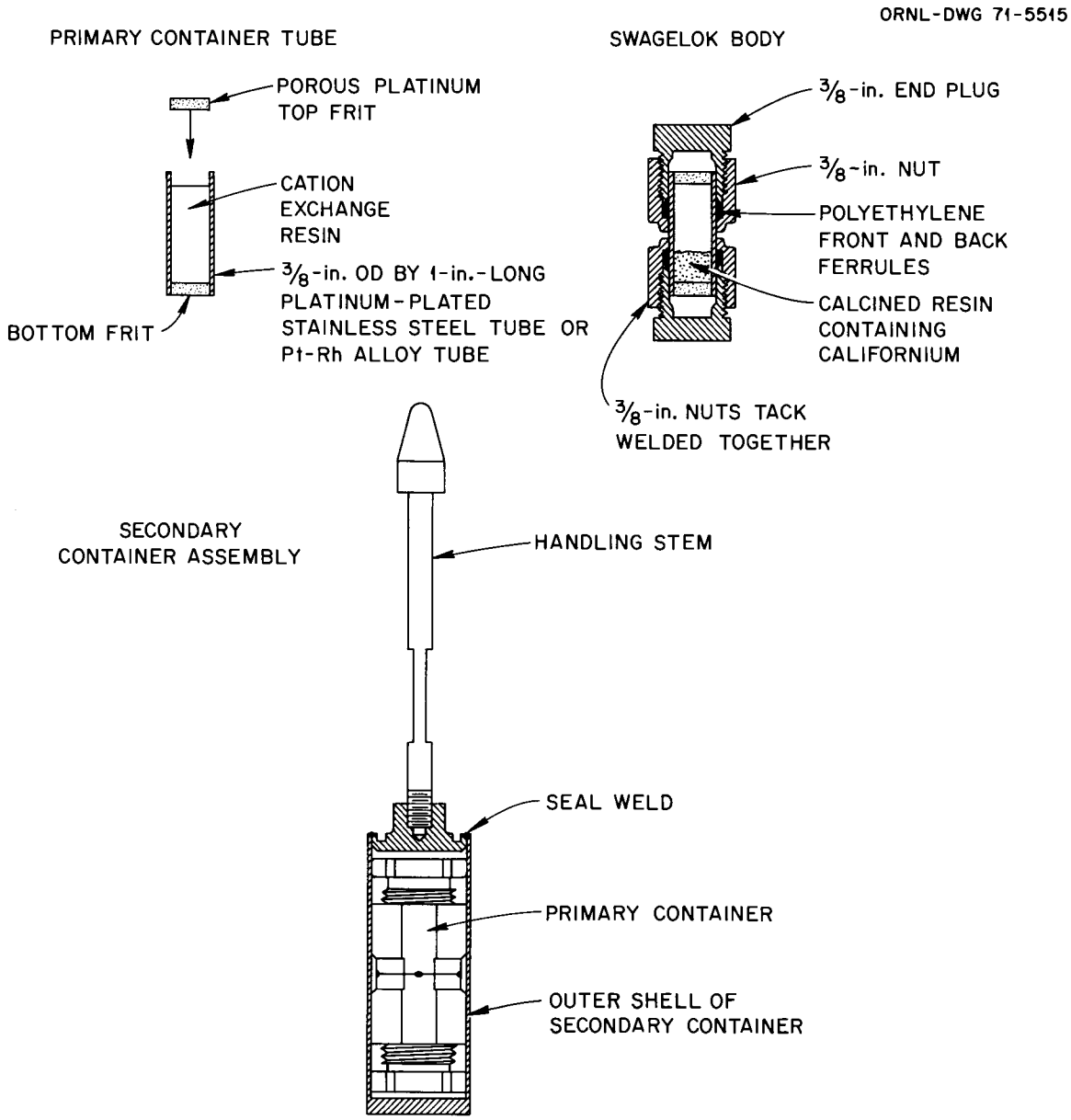

Fig. 5.1. Schematic diagram of ^{252}Cf shipping package.

5.3 SPECIAL PROJECTS

The facilities that are available at TRU are used for a variety of purposes not associated with the main-line production and distribution of transuranium elements. Special projects include nonroutine productions, special preparations, special irradiations in the HFIR, and fabrication of neutron sources using ^{252}Cf.

Fabrication of Neutron Sources Using Californium

Much of the californium recovered at TRU is incorporated into neutron sources, which are subsequently loaned to researchers. Recently, sources have been fabricated from californium that had been highly purified from curium in the new californium facility in TURF. This ultrapurification step makes the cali-

fornium suitable for future reprocessing to recover ^{248}Cm (the alpha decay product of ^{252}Cf) that is free from ^{244}Cm contamination.

Twenty-two sources, containing from 1 μg to 5 mg of ^{252}Cf, were fabricated during this report period. Most of them were encapsulated in type 304L stainless steel in a standard configuration, which was described last year.[5] Three were encapsulated in type 405 stainless steel, a low-nickel alloy, because nickel would interfere with some of the experiments in which they will be used. One, which was doubly encapsulated, was specially fabricated to the same external dimensions as a lower-intensity Pu-Be source which it replaced. A higher-intensity Pu-Be source would have been too large. One source contained 13 μg of ^{252}Cf in a quartz bead coated with two layers of epoxy resin; another, which contained 8 μg of ^{252}Cf in a quartz bead, was encapsulated in a special stainless steel container by the Isotopes Sales Department.

An unusual set of four small sources was prepared for an experimenter who wanted a source containing "exactly" 1 μg of ^{252}Cf. Each of the four sources contained californium incorporated in a quartz bead, which was, in turn, welded into a 0.25-in.-diam by 0.5-in.-long capsule by the Isotopes Sales Department. The sources assayed 1.0, 1.2, 1.35, and 1.75 μg of ^{252}Cf. The experimenter can select the one that best satisfies his current needs, and, as the large sources decay, he can substitute them in his apparatus.

Other Special Projects

Three more in a series of einsteinium rabbits (2–5 μg of ^{253}Es) were fabricated, irradiated, and delivered to H. Diamond at ANL for use in a continuing program to study the energy level structure of the decay product, ^{250}Bk. Two rabbits containing milligram amounts of ^{244}Pu were irradiated at different times to produce ^{246}Pu for two experimenters. Two rabbits, each containing 1 mg of ^{241}Am sorbed on molecular sieves, were irradiated 5 min in tests of a new technique for producing enriched isotopes of the actinide elements (see Sect. 10.5). One rabbit containing 0.3 mg of ^{252}Cf is being irradiated to measure the absorption cross section of ^{252}Cf in the HFIR.

5.4 DEVELOPMENT OF CHEMICAL PROCESSES

Laboratory support was provided to assist the mainline processing in TRU. The investigation of alternative processes for preparing oxides for HFIR targets was continued. In addition, we studied new methods for isolating and partitioning actinides and evaluated ion exchange techniques for removing lithium from curium products.

Status and Progress

Work was continued to develop a resin-loading–calcination technique to produce uniform particles of curium oxide in the desired size range for HFIR targets. Using rare-earth metals as a stand-in for curium, we can now consistently prepare spherical particles of adquate density (50% of the theoretical crystal density) to provide the desired HFIR target loading. Either of two cation exchange resins, Dowex 50W or Amberlite IRC-50, can be used. In each case, curium oxide particles can be produced by loading the resin to saturation with curium from a dilute nitrate solution. After loading, the resin is carefully heated to decompose the resin matrix and then calcined at the appropriate temperature to form the dense oxide.

Laboratory studies were continued in an effort to improve the separation of actinides from fission product lanthanides by displacement elution with aminopolyacetic acids. Displacement elution can potentially accomplish both the actinide-lanthanide separations and actinide partitioning. Promising results were obtained in rare-earth studies with the chelate ethylenediaminetetraacetic acid (EDTA) when diethylenetriaminepentaacetic acid (DTPA) was used as an organic barrier that can be easily removed from the product eluates. (Studies of this system are discussed in Sect. 10.4.)

An alternative process, in which solvent extraction is combined with oxidation by a solid (PbO_2), was developed for the separation and purification of berkelium and californium. This method is convenient for the purification of small amounts of ^{249}Bk and ^{252}Cf, and it may be applicable for processing large quantities of material.

In additional studies, we evaluated cation exchange techniques to remove lithium from americium-curium products obtained from the LiCl-based anion exchange process. This work indicates that the method may be particularly suitable when actinide oxides for HFIR targets are prepared by the resin-loading–calcination process.

Preparation of Actinide Oxides for HFIR Targets

Studies were continued to provide an alternative method for producing curium oxide particles for HFIR

5. *Chem. Technol. Div. Annu. Progr. Rep. May 31, 1970,* ORNL-4572, pp. 115–16.

targets by a resin-loading–calcination technique. In this procedure, cation exchange resin is loaded to saturation from a metal nitrate solution. After being loaded, the resin is dried, heated to decompose the resin, and calcined to form the metal oxide.

Last year we reported[6] that, using rare earths as stand-ins for curium, oxide products consisting of free-flowing uniform particles of the desired size could be prepared. These particles had adequate strength for the required handling operations; however, the densities were generally on the order of 25% of the theoretical crystal density, which was considered to be somewhat low for HFIR target preparation. We can now prepare rare-earth oxide particles that are consistently 50% of the theoretical crystal density with either of two cation resins. Preliminary results from pellet pressing studies indicate that the desired oxide concentration can be readily obtained with oxide prepared from either resin.

The two resins that have produced satisfactory products are Dowex 50W, which contains sulfonic acid exchange groups, and Amberlite IRC-50, which contains carboxylic acid exchange groups. Satisfactory product can be prepared with either resin, and studies with both systems have been continued because each has certain advantages and disadvantages. With Dowex 50W, feed preparation is not critical, but high calcination temperatures (1350–1450°C) are required to obtain high densities and to adequately remove sulfur. Feed adjustment is more critical with Amberlite IRC-50 in that the metal-salt solution must be adjusted to a pH of about 5.5 and a complexing agent such as ammonium acetate must be used to prevent precipitation; however, calcination temperatures of 600 to 1000°C are adequate to provide satisfactory densities.

Several series of experiments were performed with rare earths to evaluate process parameters of interest. In experiments with Dowex 50W the resin was loaded to saturation by passing an excess of dilute rare-earth nitrate solution through the resin bed. Comparable products were obtained using the following range of conditions: a metal concentration of 0.04 to 0.20 *M*, a free acid concentration of <0.01 to 0.70 *M*, a resin cross-linkage of 1 to 16%, and either H^+- or NH_4^+-form resin. After loading, the resin is dried, heated slowly to 600°C to decompose carbon, then rapidly heated to 1450°C and calcined for 4 to 5 hr. At a calcination temperature of 1000°C, these products contain 7 to 9% sulfur (by weight) and have densities varying from 20 to 35% of the theoretical crystal density. Upon further heating to 1450°C the sulfur is removed, and the density is increased to 50–70% of the theoretical crystal density. With temperatures as high as 1450°C, the particles tend to stick together; however, the extent of the problem can only be learned through in-cell experiments with curium.

In comparable experiments made with Amberlite IRC-50, feed metal concentrations of 0.02 *M* provide adequate loading, and much higher concentrations can be used. Acetic acid is added to the metal nitrate solution to provide an acetate/metal mole ratio of 5, and the pH of the feed is adjusted to ~5.5 with NH_4OH. Although the final pH must be in the range of 5 to 6 for adequate loading, a large amount of free acid can be tolerated in the original feed. (Satisfactory resin loading was obtained from feed when acid concentrations as high as 3.75 *M* were neutralized with NH_4OH.) After loading, the resin must be carefully dried at about 120°C. The dried product is then heated to 325°C and held about 2 hr to remove volatile decomposition products. The product can then be heated to 625°C to remove residual carbon and to obtain the oxide product. Oxide calcined at ~650°C has a density about 40% of the theoretical crystal density; this can be increased to about 60% by calcination at 1000°C. Higher calcination temperatures generally tend to fracture the oxide spheres.

Small-scale scouting runs were made with curium with both types of resin. Resin loading was satisfactory in all cases. Equipment was not available to calcine these products at optimum temperatures; however, low-temperature firing produced products whose densities correlated well with those of products obtained in rare-earth experiments. Larger-scale curium experiments employing optimum firing temperatures will be made in the near future.

Purification of Berkelium and Californium

An alternative process, in which solvent extraction is combined with oxidation by a solid, was developed for the separation and purification of berkelium and californium. With this process, berkelium is separated from all impurities except cerium, and californium is separated from berkelium and other highly extractable impurities.

The new process is convenient and effective for preparing small quantities of radiochemically pure ^{249}Bk and ^{252}Cf, and it appears to be adaptable for processing larger quantities of material. Recommended stepwise procedures for processing small quantities are as given below.

6. *Chem. Technol. Div. Annu. Progr. Rep. May 31, 1970,* ORNL-4572, p. 119.

For berkelium-californium separation:

1. Adjust the nitric acid concentration of the solution to 5 *N* in a separatory funnel, add a few milligrams of PbO_2, and mix for 15 min.
2. Contact with 0.1 *M* HDEHP in aromatic-free *n*-dodecane.
3. Let phases separate, preferably without centrifuging. The PbO_2 remains, for the most part, with the organic phase and accelerates phase separation.
4. Drain off the aqueous phase, and subject it to a second extraction in the presence of some PbO_2. Separate phases. The aqueous phase contains the californium.
5. Combine the organic phases, and wash twice with small volumes of 5 *N* HNO_3. The quality of californium may be improved slightly by discarding these washings.

For purification of californium:

1. Filter the aqueous phase, and remove nearly all of the HNO_3 by evaporation.
2. Dilute, and add a drop of concentrated H_2SO_4.
3. Allow the $PbSO_4$ to settle; filter and wash the precipitate with very dilute H_2SO_4.
4. Evaporate the filtrate to dryness, add a very small amount of HNO_3, and dilute to several milliliters.
5. Extract the californium twice with 1 *M* HDEHP in dodecane, combine extracts, and wash with a small volume of 0.1 *N* HNO_3.
6. Dilute the HDEHP to 0.5 *M* or less with a hydrocarbon, and strip the californium with 5 *N* HNO_3.

Various modifications are possible, except that the H_2SO_4 solution must not be evaporated before the lead is removed.

For recovery of berkelium:

1. Filter the original organic phase into another separatory funnel, and wash with a hydrocarbon.
2. Strip the berkelium with 5 *M* HNO_3 – 1 *M* H_2O_2.

Removal of Lithium from Curium Products by Cation Exchange

A study was initiated to determine the feasibility of using ion exchange techniques to convert curium products to feed suitable for actinide oxide preparation. These products, which are obtained from the LiCl-based anion exchange process, are chloride solutions containing substantial amounts of lithium chloride. At the present time, main-line processing flowsheets use a batch Tramex extraction (to remove the bulk of the lithium) followed by an evaporation step (to convert from a chloride to a nitrate form).

A flowsheet for the process, based on a typical batch of curium product, is shown in Fig. 5.2. The actinides are loaded from a dilute HCl-LiCl feed solution which is pumped through the column at a flow rate of 2 ml cm^{-2} min^{-1}. Lithium is eluted from the column with 2 liters of 0.75 *M* HNO_3 or 0.75 *M* NH_4NO_3. During this elution, chloride is washed from the column, and a nitrate product can be obtained by elution with HNO_3. The curium can then be stripped from the column with about 2 liters of 6 *M* HNO_3 or 1 liter of 1.5 *M* ammonium acetate. It should be emphasized that this process has not been optimized for minimum processing time or resin degradation; however, excessive resin damage would not be expected if the indicated feed flow rate was used. With present equipment, up to 25 g of curium might be handled per batch. In comparison, 100-g batches have been handled by the batch extraction technique.

Two washing and product elution procedures are apparently necessary to convert curium in the LiCl solution to oxide. If ammonium nitrate and ammonium acetate are used, the product can be diluted and loaded directly onto Amberlite IRC-50 resin and converted to oxide. This technique has been demonstrated with both neodymium and curium. If the product is eluted with HNO_3, the acid concentration must be adjusted to about 0.5 *M;* then the product can be loaded onto Dowex 50 resin and converted to oxide.

5.5 TRANSPLUTONIUM-ELEMENT RESEARCH

A systematic study of actinide element chemistry and of comparative lanthanide chemistry is being made as significant quantities of new isotopes become available. Such a study materially increases our basic understanding of actinide systems. This part of the USAEC Heavy Element Program includes work on problems involving solution chemistry, with particular emphasis on the formation of complexes and on the preparation of solid actinide compounds that will be characterized by x-ray diffraction, electron microscopy, thermogravimetry, differential thermal analysis, and metallographic examination.

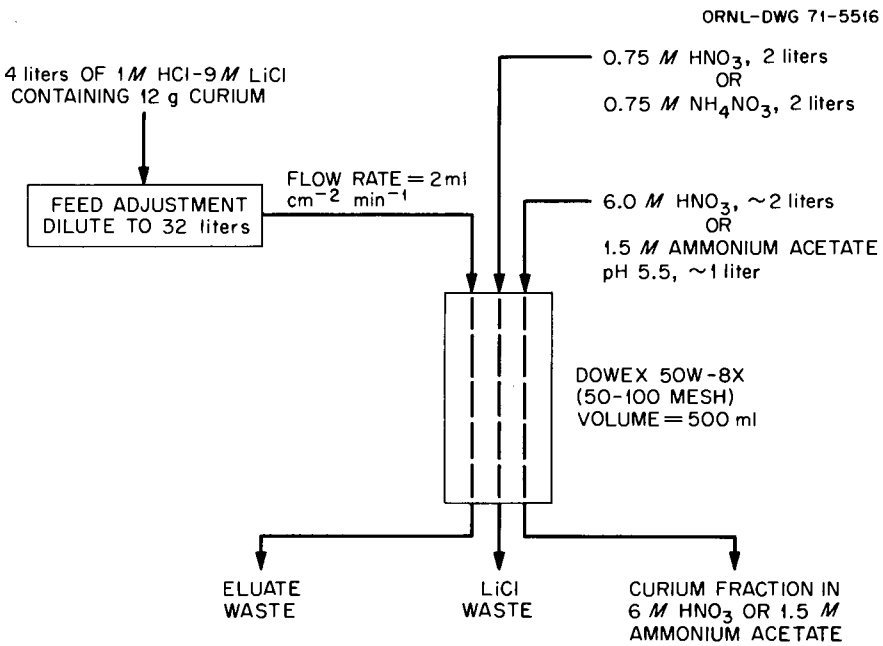

Fig. 5.2. Removal of lithium from Am-Cm product by cation exchange.

Sulfate Complexes of Trivalent Actinides

Studies of the sulfate complexes of europium[7] and the trivalent actinides americium through einsteinium[8] by solvent extraction distribution are essentially complete. A paper was presented at the Combined Southeast-Southwest Regional American Chemical Society Meeting, December 2–4, 1970, at New Orleans, Louisiana. Its abstract follows:

"Sulfate Complexes of the Transplutonium Actinides and Europium," by W. J. McDowell and C. F. Coleman. *Abstract:* The sulfate complexes of the higher actinides, Am, Cm, Bk, Cf, and Es and europium were examined by neutral species distribution between a benzene solution of a long-chain amine sulfate and aqueous acid–sodium sulfate solutions. Sulfate was the only anion present and the ionic strength varied with the ligand concentration. Activity coefficients over the ligand concentration range examined (up to 0.5 *M*) were estimated by a Debye-Hückel expression. The use of the Debye-Hückel equation is justified by the ability to fit the $\gamma\pm_{Na_2SO_4}$ data to 0.5 *M* and even higher concentrations with the same equation. Among the several advantages offered by this method, over the more common procedure of using cation exchange at constant ionic strength, are the ability to refer formation constants to a neutral species of constant activity and the ability to go to higher ligand concentrations, allowing higher complexes to be determined more accurately. Earlier work with thorium and uranium [J. Phys. Chem. **67**, 1138 (1963) and **62**, 777 (1958)] has shown this to be a reliable method for obtaining thermodynamic equilibrium constants in the sulfate system. Evidence for important amounts of the heretofore unreported trisulfate species of these elements was found but no evidence was found for tetrasulfate species. Equilibrium constants for all the actinides are close together but show a smooth periodicity as *Z* varies. The europium equilibrium constants are close to those for the actinides. The overall equilibrium constants K_{0n} (formation of $M(SO_4)_n^{3-2n}$ from M^{3+}) for the actinides tested fall in the following ranges: K_{01}, 4.1×10^3 to 7.3×10^3; K_{02}, 3.7×10^5 to 6.5×10^5; K_{03}, 0.9×10^5 to 2.2×10^5.

Present work is concerned primarily with refined treatment of the data to obtain the best possible values for the equilibrium constants and their error limits. In the best values of the equilibrium constants obtained thus far, a periodic variation called the tetrad effect[9] has been observed (Fig. 5.3). The ability to see such a variation indicates that complexation has a direct effect on the 5*f* electrons[10,11] in these elements and hence implies that the complexes formed are largely of the inner-sphere type.

7. *Chem. Technol. Div. Annu. Progr. Rep. May 31, 1968,* ORNL-4272, p. 116.

8. *Chem. Technol. Div. Annu. Progr. Rep. May 31, 1969,* ORNL-4422, pp. 176–77; *Chem. Technol. Div. Annu. Progr. Rep. May 31, 1970,* ORNL-4572, pp. 125–26.

9. D. F. Peppard, G. W. Mason, and S. Lewey, *J. Inorg. Nucl. Chem.* **31**, 2271 (1969).

10. C. K. Jorgensen, *J. Inorg. Nucl. Chem.* **32**, 3127 (1970).

11. L. J. Nugent, *J. Inorg. Nucl. Chem.* **32**, 3485 (1970).

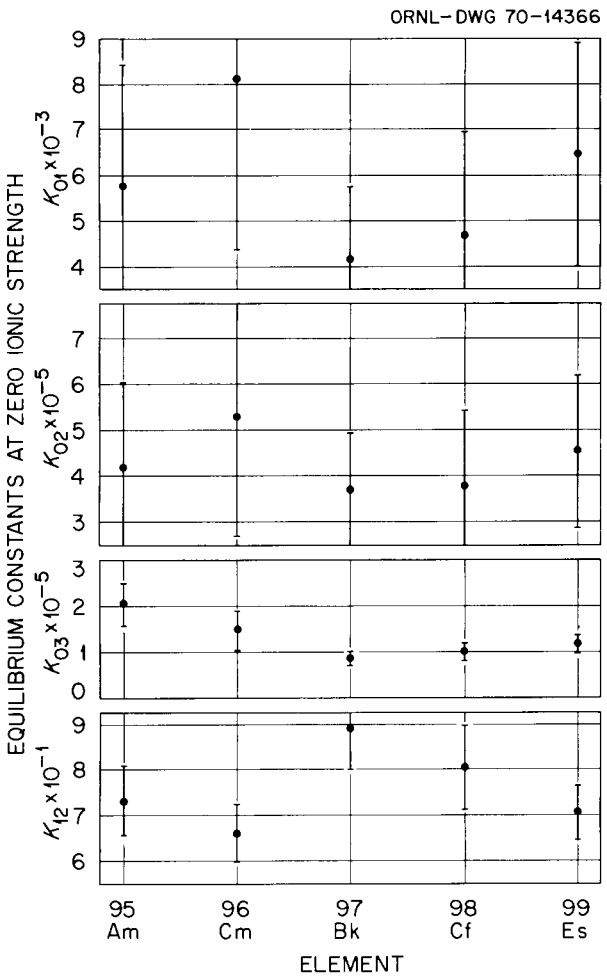

Fig. 5.3. Formation constants for sulfate complexes of the trivalent transplutonium actinides: the "tetrad effect." Subscripts 01, 02, 03, and 12 represent, respectively, the formations $M^{3+} \rightarrow MSO_4^+$, $M^{3+} \rightarrow M(SO_4)_2^-$, $M^{3+} \rightarrow M(SO_4)_3^{3-}$, and $MSO_4^+ \rightarrow M(SO_4)_2^-$. The error bars represent the standard deviation of fitting of each formation constant to the solvent extraction distribution data.

Thiocyanate Complexes of Trivalent Actinides

The study of the aqueous thiocyanate complexes of the trivalent transplutonium actinides[12] was continued by means of distribution equilibria with the cation exchange extractant di(2-ethylhexyl)phosphoric acid (HDEHP). Table 5.2 shows the resulting values of the overall formation constants for the mono-, di-, and trithiocyanate complexes in sodium thiocyanate–sodium perchlorate solution at constant ionic strength ($I = 1$). These formation constants, β_1, β_2, and β_3, are

12. *Chem. Technol. Div. Annu. Progr. Rep. May 31, 1970,* ORNL-4572, p. 187.

Table 5.2. Formation constants for thiocyanate complexes of trivalent actinides

Aqueous $NaSCN$-$NaClO_4$ solution, ionic strength = 1, pH = 2; error limit is the standard deviation of fitting

	β_1	β_2	β_3
Americium	2.3 ± 0.1	1.1 ± 0.4	0.70 ± 0.28
Curium	2.8 ± 0.2	0.9 ± 0.6	0.84 ± 0.47
Berkelium	3.1 ± 0.2	0.3 ± 0.7	2.3 ± 0.56
Californium	3.7 ± 0.2	0.3 ± 0.6	2.6 ± 0.50
Einsteinium	3.6 ± 0.2	0.04 ± 0.7	2.9 ± 0.54

defined by

$$M^{3+} + nSCN^- \rightleftharpoons M(SCN)_n^{(3-n)+} ,$$

$$\beta_n = [M(SCN)_n^{(3-n)+}]/[M^{3+}]\,[SCN^-]^n .$$

Previous workers have not reported formation constants for all three complexes and have not agreed on the species identified. One report gave β_1 and β_2 for Pu, Am, Cm, and Cf,[13] while two others gave β_1 and β_3 for Am[14,15] and Cm.[14] The error limits shown in Table 5.2 are the values obtained by calculating the standard deviation of fitting of each constant to the distribution data. The large error limits for the dithiocyanates make the actual existence of that complex species questionable; at present, our β_2 values can only be considered approximate upper limits.

Plots of β vs Z were examined for the "tetrad effect" (cf. sulfate complexes, above, and refs. 9–11). The tetrad grouping from curium to einsteinium is apparent in β_3 (Fig. 5.4), but not in β_1 or β_2 (Fig. 5.5). This suggests that bonding significantly affecting the $5f$ electrons occurs in the tri- but not the mono- or dithiocyanate complexes. This, in turn, is consistent with the concept that the trithiocyanate complexes are inner-sphere while the mono- and dithiocyanate complexes are outer-sphere.[13]

The apparent values for β_2 (Fig. 5.5) indicate that the formation of the dithiocyanate complex decreases with increasing atomic number from americium to einsteinium, if this species does indeed exist. This might suggest that covalent character increases with Z, causing a relative decrease in the tendency to form outer-sphere complexes. In support of such a suggestion, it may be

13. G. R. Choppin and J. Ketels, *J. Inorg. Nucl. Chem.* **27**, 1335 (1965).

14. T. Sekine, *Acta Chem. Scand.* **19**, 1519 (1965).

15. I. A. Lebedev and G. N. Yakolev, *Radiokhimiya* **4**, 3046 (1962).

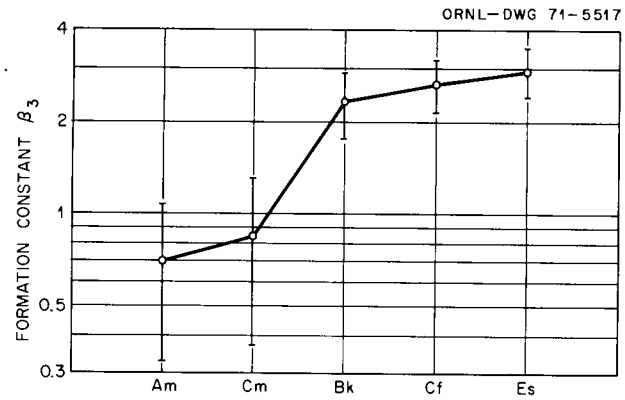

Fig. 5.4. Formation constant β_3 for actinide trithiocyanate complexes, showing "tetrad effect." Ionic strength constant at 1 *M* (NaSCN + $NaClO_4$), pH 2. The error bars represent the standard deviation of fitting of each formation constant to the solvent extraction distribution data.

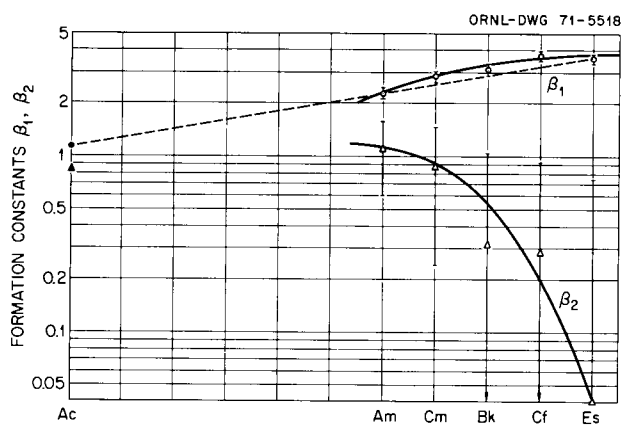

Fig. 5.5. Formation constants β_1 and β_2 for actinide mono- and dithiocyanate complexes (cf. Fig. 5.4). Actinium points taken from ref. 16.

noted that rate constants for the hydration of lanthanides change rapidly in the analogous region Eu-Gd-Tb, and this has been interpreted as a sharp decrease in hydration number.[16]

The values for β_1 increase slightly with *Z*. It is of interest that a straight line through the log β points (Fig. 5.5) can also pass through β_1 for $AcSCN^+$ (ref. 17). This is consistent with the concept that the monothiocyanates are outer-sphere complexes whose stabilities are dependent on electrostatic forces. Extrapolation of the same line for the tentative prediction of β_1 for the monothiocyanates of the actinides above einsteinium appears to be indicated.

16. D. G. Karraker, *J. Chem. Educ.* **47**, 424 (1970).

17. C. L. Rao, C. J. Shahani, and K. A. Mathew, *Inorg. Nucl. Chem. Lett.* **4**, 655 (1968).

Actinide and Lanthanide Hydrides and Metallides

In recent years there has been much discussion and some disagreement concerning the electronic structures of NaCl-type lanthanide and actinide compounds.[18-20] The electronic configurations of these compounds are extremely complex because of variations in the energy state distribution of electrons and the changes in degree of mixed bonding (metallic, covalent, and ionic) that can occur. In most cases the experimental studies of the actinides have been directed toward work with compounds of uranium, with some recent work being done on plutonium and americium. Because of this interest, a program was begun last year[21] to prepare and study such compounds, starting with the metal hydrides. Their stoichiometries are relatively simple to determine, and there are important differences in interpretation of bonding, with some indication of semiconductor properties.

The hydriding equipment, which consists of a hydrogen purification section and a Sieverts reaction section, was described previously.[21] The hydrogen purification section works satisfactorily, but the Sieverts system has required extensive reworking (1) to correct many small leaks, still not completely eliminated, and (2) to decrease the total volume to the design value of $\leqslant 25$ ml. In spite of these difficulties, a series of shakedown runs was completed with the erbium hydride system.

The following equilibrium dissociation pressure-temperature relationship was obtained for the two-phase region of erbium solid solution plus dihydride:

$$\log_{10} P = -\frac{11{,}000 \pm 150}{T} + 10.19 \pm 0.07 ,$$

where *P* is equilibrium hydrogen pressure, torrs, and *T* is absolute temperature, Kelvin. From this equation and the van't Hoff equation, the enthalpy and the entropy of the reaction were evaluated, respectively, as $\Delta H = -50.3$ kcal per mole of H_2 and $\Delta S = -33.4$ cal/deg per mole of H_2. These values represent the heats and entropies of reaction to form the hydride phase from the saturated solid solution. Comparison of these values

18. J. Grunzweig-Genossar, M. Kuznietz, and F. Friedman, *Phys. Rev.* **173**, 562 (1968).

19. H. Adachi and S. Imoto, *J. Nucl. Sci. Technol.* **6**, 371 (1969).

20. L. B. Griffiths, *Nature* **193**, 362 (1962).

21. *Chem. Technol. Div. Annu. Progr. Rep. May 31, 1970*, ORNL-4572, p. 127.

Table 5.3. Enthalpy and entropy of reaction for formation of ErH_2 from Er-H_2 saturated solid solution

ΔH (kcal/mole H_2)	ΔS [cal (°C)$^{-1}$ (mole H_2)$^{-1}$]	Literature reference
-52.6 ± 0.3	-35.2 ± 0.3	22
-48.3	-32.3	23
-55.2	-51.1	24
-53.5	-32.3	25
-50.3 ± 0.7	-33.4 ± 0.3	Present work

with several literature values[22-25] shows reasonably good agreement (Table 5.3). The structure of a compound near the dihydride composition was determined by x-ray diffraction analysis. It exhibited the fcc (CaF_2 type) structure with a lattice parameter of a_0 = 5.218 Å, in excellent agreement with the literature value[22] of 5.126 Å.

Several attempts to determine the equilibrium relationships in the dihydride-trihydride region were unsuccessful because of the extreme slowness of reaction. A small amount of leakage encountered in the apparatus prevented us from using the long equilibration time that would be necessary.

During this period, our studies of the NaCl-type compounds were extended to include the preparation of lanthanide and actinide metallides and chalcogenides. After reviewing several methods,[26-28] we chose the two-step approach. Briefly, the compounds are prepared in granular form by reacting vapor of the group V or group VI element with the desired lanthanide or actinide metal at moderate temperatures (450–950°C). The vapor-solid reactions are carried out in sealed, evacuated quartz tubes, which are designed in such a manner that physical separation of the condensed phases of the reacting elements is maintained. The granular reaction product is then melted down by use of induction heating and cast into an ingot in a tantalum container under argon at a pressure of nearly 1 atm. The first step has been completed for the following reactant pairs:

	Temperature (°C)	Time (hr)	Result
Er-S	400–900	20	Mixture
Er-Se	600–950	24	Mixture
Er-As	450–850	10	Single species
Er-Sb	700–1050[a]	36	Mixture
Am-As	600–950	75	Mixture
Am-Se	600–950	75	Mixture

[a]Heating to 1650°C for 1 hr improved the Er-Sb product.

Only the erbium stibnide has gone through the second step. All products have been examined by x-ray diffraction. Erbium arsenide appeared to be single phase with a lattice parameter of a_0 = 5.743 Å, in excellent agreement with the literature value[28] of 5.745 Å. The other products showed multiple phases. Considerable difficulty is experienced in reading the diffraction powder patterns of the americium products because of fogging of the film by the gamma radiation. Similar problems have been reported by Mitchell and Lam,[29] who recently have reported the crystal structures of Am_3Se_4, Am_3Te_4, and AmSb. The mixture we obtained from reacting Am with Se seems to contain both Am_3Se_4 and a face-centered cubic phase analogous to the 1:1 rare-earth chalcogenides. This suggests that AmSe, not previously reported, may exist. Extensive heat treatment (up to 1650°C) of the ErSb mixture did produce a reduction in the number of extraneous lines in the diffraction pattern, but a single species was still not obtained.

The present facilities for the high-temperature step require the compounds to be exposed to air for several minutes during transfers. A technique for handling radioactive materials in this second treatment step is now being sought.

Preparation and Identification of Californium Dioxide

A study was made to prepare and identify the various compounds formed by californium and oxygen, and especially to prepare californium dioxide. Although strong oxidizing conditions are required to oxidize Cf_2O_3 to CfO_2, two methods were found to give satisfactory results. In one, molecular oxygen at high pressures (~100 atm) was used; the other employed atomic oxygen prepared in an electrical discharge tube.

22. C. E. Lundin, *Trans. Met. Soc. AIME* **242**, 903 (1968).

23. R. L. Beck, report LAR-10, University of Denver, Denver Research Institute (1960).

24. P. M. S. Jones, J. Southall, and K. Goodhead, United Kingdom Atomic Energy Authority, AWRE report No. 0-22/64 (June 1964).

25. R. N. R. Mulford, private communication to K. A. Gschneidner, Jr., in *Rare Earth Alloys*, p. 174, D. Van Nostrand Co., Princeton, N.J., 1961.

26. Y. Baskin and P. D. Shalek, *J. Inorg. Nucl. Chem.* **26**, 1679 (1964).

27. J. F. Miller and R. C. Himes, in *Rare Earth Research*, ed. by E. V. Kleber, p. 232, Macmillan, New York, 1961.

28. A. Iandelli, ibid., p. 135.

29. A. W. Mitchell and D. J. Lam, *J. Nucl. Mater.* **31**, 349 (1970).

In the preparation of each sample, californium was loaded onto a single Dowex 50-4X resin bead from a highly purified solution of $^{249}CfCl_3$. Beads of the proper size to hold from 2 to 4 μg of ^{249}Cf were chosen. The resin beads loaded with californium were ignited in air to burn out the resin matrix and then were heated to 1175°C to decompose the sulfate (sulfur in the sample came from the resin bead) and thus obtain Cf_2O_3. Ignition in air at 1200°C produced californium sesquioxide in a body-centered cubic structure with a somewhat variable lattice parameter of about 10.802 ± 0.006 Å. When this oxide was treated in hydrogen, the lattice parameter increased to 10.828 ± 0.002 Å. The body-centered cubic structure is stable at temperatures up to about 1400°C. Above this temperature the monoclinic crystal structure is stable. Lattice parameters determined for Cf_2O_3 in the monoclinic structure are a_0 = 14.121 ± 0.015 Å, b = 3.592 ± 0.004 Å, c = 8.809 ± 0.007 Å, and β = 100.34° ± 0.08°.

In order to oxidize Cf_2O_3 to CfO_2, a highly reactive form of the sesquioxide is required. Neither the body-centered cubic form produced at high temperatures nor the monoclinic form could be oxidized. It was found that, in the original preparation of oxide from the resin beads, a firing temperature of 1175°C for 2 to 5 min completely removed the sulfur and produced a relatively reactive Cf_2O_3 product.

Oxidation of Cf_2O_3 to CfO_2 with high-pressure molecular oxygen was accomplished in a $^3/_8$-in.-diam Inconel tube. The reactive Cf_2O_3 was transferred into a quartz x-ray capillary and inserted into the Inconel tube. The tube was pressured with 100 atm of oxygen and heated in a clamshell resistance furnace. Preparation of the dioxide was highly dependent upon the reaction temperature, with the optimum temperature of ~300°C resulting in 90% conversion to the dioxide in 100 hr. Heating at either 250 or 350°C produced an oxide of the approximate composition $CfO_{1.8}$. There was apparently no oxidation at either 200 or 400°C. A sample of CfO_2 prepared by heating Cf_2O_3 at 300°C in oxygen at 100 atm for 100 hr was examined by x-ray diffraction over a period of about two months. Immediately after preparation the CfO_2 had a face-centered cubic structure with a_0 = 5.312 ± 0.005 Å. This lattice parameter increased at the rate of about 0.0026 Å/day up to a value of 5.372 Å (see Fig. 5.6) and then remained constant for about 30 days. During this time, some of the diffraction lines of the face-centered cubic structure broadened. By the 53d day, the lines attributed to the 111, 220, 222, and 311 planes had broadened and split into doublets, while lines attributed to the 200 and 400 planes remained as sharp, single lines. Splitting of this nature indicates a distortion of

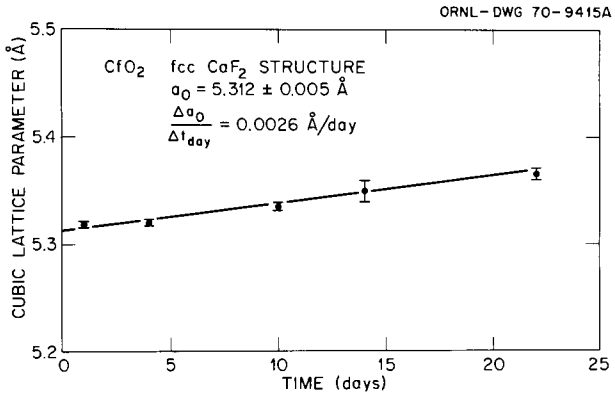

Fig. 5.6. Change of the cubic lattice parameter of CfO_2 with aging.

the face-centered cubic cell along one of the C_3 axes, giving rise to a rhombohedral cell. The pattern at this time could be indexed as a rhombohedral structure with lattice parameters of a_0 = 5.372 ± 0.003 Å and α = 89.92° ± 0.04°.

In order to confirm the lattice parameter for CfO_2, a different method of oxidation was used, and the resultant product was analyzed by x-ray diffraction techniques. The oxidation was accomplished by reacting Cf_2O_3 with atomic oxygen formed in an electrical discharge tube. Since the californium oxide apparently acts as a catalyst for the recombination of atomic oxygen, it was necessary to place the Cf_2O_3 bead in a relatively massive platinum boat to carry away the heat liberated during the recombination. If this was not done and the Cf_2O_3 was heated to ~400°C, the heat of recombination rapidly raised the temperature of the oxide bead to ~1500°C and produced the monoclinic form of the sesquioxide. When the temperature was satisfactorily controlled, the composition of the californium oxide product was a function of the oxygen pressure in the discharge tube, which converted ~15% of the oxygen to the atomic form. At an oxygen pressure of 50 μ, the approximate composition of the product was $CfO_{1.60}$. At 200 μ the approximate composition was $CfO_{1.70}$, and at 400 μ it was $CfO_{1.80}$. The best oxidation conditions for the production of CfO_2 were obtained at oxygen pressures of 800 to 900 μ and at temperatures of 300 to 325°C. Two samples that appeared to be completely in the face-centered cubic form were prepared. The lattice parameter was a_0 = 5.310 ± 0.002 Å, which increased at the rate of ~0.0024 Å/day up to a maximum of 5.375 Å. By this time the samples had converted to a rhombohedral structure, which was essentially the same as that observed for the CfO_2 previously prepared by oxidation with molecular oxygen.

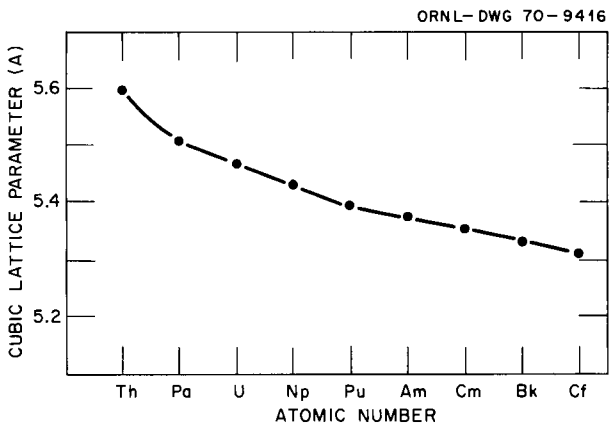

Fig. 5.7. Plot of cubic lattice parameters for the actinide dioxides.

A plot of the cubic lattice parameter of the actinide dioxides vs atomic number is shown in Fig. 5.7. The lattice parameter for the face-centered cubic CfO_2 falls on the smooth extrapolation of the curve for the other actinides. However, the CfO_2 datum point is such that no cusp is evident at the half-filled *5f* subshell of Bk(IV) equivalent to that noted in a similar plot of the sesquioxide parameters of the *4f* elements. The appearance of a cusp has been atrributed to the effect of the half-filled *4f*-electron subshell. The cusp for the tetravalent actinides may be too small to be observed; that is, the magnitude of the effect caused by the half-filled shell may be within the error limits of the cubic lattice parameters. An alternative explanation is that the oxygen/californium ratio in the californium oxide prepared in this work may be slightly below 2.00. At the present scale of study (~2 to 4 μg per sample), it is impossible to determine the metal/oxygen ratio, and the stoichiometry of the oxide can only be inferred from the lattice parameter values.

Thermal Analysis of Lanthanide and Actinide Compounds

Thermogravimetric (TGA) and differential thermal analysis equipment have been used to study several lanthanide and actinide compounds. Some of the materials that have been investigated include the nitrates, chlorides, hydroxides, sulfates, oxalates, carbides, and oxides. Special techniques have been developed to permit the preparation and examination of quantities as small as 0.1 mg. The impetus for the studies was to gain knowledge for process applications, as well as to compare the chemistry of the lanthanides and actinides. The investigations are complemented by additional studies of the materials made by electron microscopy, electron and x-ray diffraction, and gas chromatography.

In thermal decomposition studies of lanthanide hydroxides reported last year,[30] it was found that the amorphous and crystalline forms of the hydroxides had different decomposition patterns but that the decomposition of each form was very similar for all the lanthanides. Thus, there was no observed change in the decomposition pattern to correspond with the change in microstructures or crystal form.[31] Additional work has been done on the trihydroxides of americium, curium, and berkelium. The decomposition of these preparations was found to be very similar to that of the corresponding lanthanide hydroxides. In preparing the hydroxides from nitrate or chloride salts, it was not possible to completely eliminate small amounts of the original anion from the hydroxide products. It was found that in the case of nitrate the decomposition of residual nitrate and the second decomposition step of the hydroxide took place at about the same temperature. To avoid this difficulty, several hydroxide preparations were made from chloride salts. The nitrate and chloride present in the hydroxides decomposed at temperatures assigned to the decomposition of an oxynitrate and the decomposition of oxychloride species respectively. Examination of the hydroxides prepared from chlorides permitted a more accurate determination of the second decomposition step of the hydroxide and will aid the comparison of results for the different elements.

With the availability of larger quantities of the transcurium elements, it is now possible to study compounds of these materials by thermogravimetry and to compare them with other actinides and the lanthanides. In addition to providing knowledge on the decomposition temperatures and possible decomposition products, the data can be used for determining the water of hydration and the coordination number of the actinides. Berkelium is of special interest because it has two well-established oxidation states. Thermal decompositions of several berkelium compounds from approximately 1-mg quantities of highly purified berkelium have been examined. Because of the small amount of material, it was not possible to obtain supporting chemical analyses of these preparations; thus it was

30. *Chem. Technol. Div. Annu. Progr. Rep. May 31, 1970,* ORNL-4572, pp. 127–29.

31. R. G. Haire and T. E. Willmarth, *Trends and Differences in the Crystallization Behavior of Lanthanide Hydroxide Preparations,* ORNL-TM-2387 (October 1968).

necessary to compare the decomposition results with results obtained from lanthanide compounds made by the same techniques and with the same amount of material. The data were then compared with results obtained with well-characterized lanthanide preparations. The decomposition patterns for the nitrates, chlorides, and oxalates of berkelium and three lanthanides are shown in Fig. 5.8. The lanthanides chosen for comparison were cerium, gadolinium, and terbium. Cerium was selected because of its comparable III-IV oxidation states and the similar stabilities of CeO_2 and BkO_2. Gadolinium was used because its ionic radius is nearly the same as berkelium(III) and because it can be considered as possessing a "pure" trivalent state. Terbium was a natural choice since it is the electronic counterpart of berkelium.

The decompositions were studied in air, oxygen, argon, and hydrogen-argon atmospheres. A hydrogen-argon atmosphere was used in an attempt to retain as much of the trivalent character of the elements as possible. There was little hope of success with the nitrates since the decomposition products of nitrate, including oxygen, cause oxidizing conditions to exist. When hydrogen was used with the sulfates (decomposition results not shown in Fig. 5.8), the hydrogen reacted with the anion and lowered the decomposition temperature. Reducing and inert atmospheres were useful for comparing the decomposition of the chlorides and oxalates.

Decomposition of the nitrate salts proceeded by loss of the water of hydration followed by the decomposition of the nitrate. Some of the curves showed inflections indicative of the formation of an oxynitrate intermediate. Cerium and berkelium were each characterized by decomposition of the anhydrous nitrate to the dioxide at temperatures lower than those observed for either the gadolinium or terbium nitrates. Cerium, terbium, and berkelium showed an increased tendency to form an oxynitrate intermediate in hydrogen-argon. With the chlorides, the decompositions were more complex; for example, there are level portions in the decomposition curves which indicate the possible formation of compounds of the type $MOCl \cdot 2MCl_3$. An oxychloride that decomposed above 600°C was also frequently formed. The cerium chloride again showed a strong tendency to form the dioxide when decomposed in air, but berkelium chloride behaved more like terbium chloride. In hydrogen-argon the decomposition curve for berkelium chloride was even more like the curves for the gadolinium and terbium chlorides. Cerium and berkelium oxalates decomposed in air at lower temperatures than gadolinium or terbium oxalates, and only a small cusp (indicating the formation of a subcarbonate) is seen in the cerium or berkelium curves. In hydrogen-argon, the decomposition curves for the four elements are more similar due to the absence of oxidizing conditions. The results of the decompositions shown in Fig. 5.8 can be summarized by stating that, as expected, berkelium behaves very similarly to cerium when oxygen is present or when oxygen can be provided by the anion (i.e., nitrate salts). In an inert or reducing atmosphere, berkelium tends to behave more like terbium. From the decomposition curves, there is no question that the dioxides of cerium and berkelium are very stable and that their stability influences the thermal decomposition of the different compounds.

Calculations made from the decomposition curves indicated that the berkelium(III) oxalates and nitrates were obtained as tetrahydrates and that the berkelium(III) chloride studied was the hexahydrate.

Investigation of Lanthanide and Actinide Compounds by Electron Microscopy

Electron microscopy and electron diffraction have been used to investigate the oxides, hydrous oxides, and hydroxides of the lanthanides and actinides. The investigations are not only intended as a basic study of the chemistry of these materials but also provide information for process development. Previous work on the hydroxides of the lanthanides and actinides has been reported.[32] When lanthanide or actinide hydroxides are first formed, they are generally composed of amorphous-like particles (20 to 50 Å in diameter). These particles are converted to larger, well-defined crystalline microstructures upon aging in aqueous media. For the lanthanides, La through Dy, the crystalline forms are rodlike microstructures, but the heavier lanthanides prepared under similar conditions have a different type of microstructure.[32] On the basis of ionic radii, the trivalent actinides through einsteinium were also expected to form trihydroxides with a rodlike microstructure. However, the crystallization behavior of the transplutonium elements is complicated by the effects of heat and radiolysis resulting from radioactive decay. In earlier work the supply of the transcurium elements was limited; and, since only nanogram quantities of material are needed for electron microscopy, attempts were made to prepare the hy-

32. *Chem. Technol. Div. Annu. Progr. Rep. May 31, 1969,* ORNL-4422, pp. 178–80; *Chem. Technol. Div. Annu. Progr. Rep. May 31, 1970,* ORNL-4572, pp. 128–31.

ORNL-DWG 71-5519

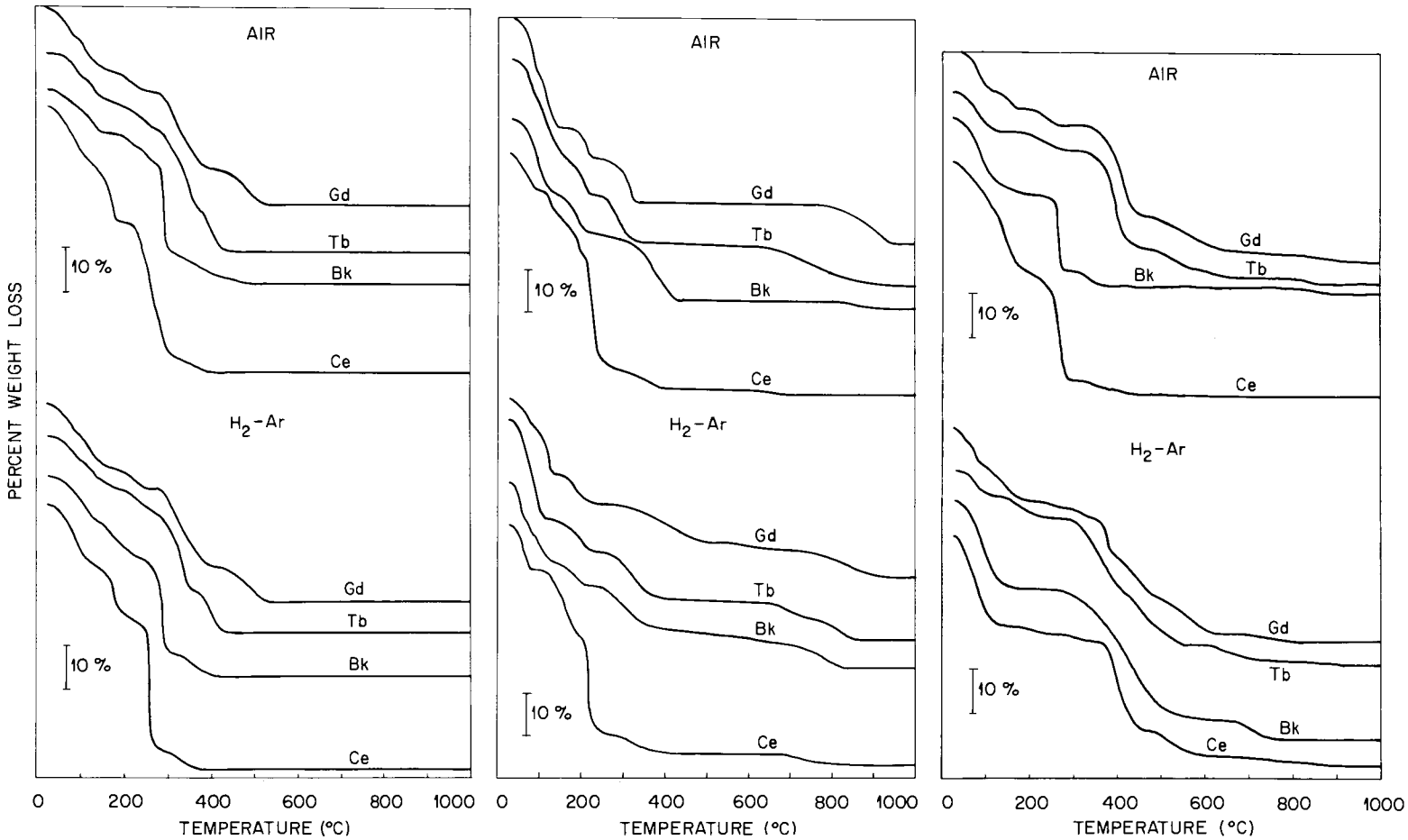

Fig. 5.8. Thermal decomposition of berkelium, cerium, gadolinium, and terbium salts in air and hydrogen-argon.

droxides on a micro scale. Unfortunately, when preparations were made on the microgram scale, the microstructures were different and the crystallization times were increased. The net results were that differentiation between the microstructures and small amounts of foreign substances (inorganic salts, impurities) was difficult and that amorphous-like diffraction patterns were obtained. With ^{253}Es the rate of destruction was probably greater than the rate of conversion to the crystalline state. After several experiments made with both the lanthanides and actinides, it has been concluded that about 1 mg of a metal ion is needed to ensure a reasonable degree of success in preparing the crystalline microstructures.

Recent work has centered on preparing the berkelium hydroxides from 1-mg quantities of berkelium. The preparation of berkelium trihydroxide presents a special problem because of the ease of oxidation of the metal ion in a basic medium. In earlier work with cerium, several preparative methods were tried before crystalline cerium trihydroxide was obtained. With each element, it was necessary to use oxygen-free atmospheres and deoxygenated reagents and to maintain a low concentration of a reducing agent in the solutions during the preparations. When the tetravalent metal ion was used or when extensive oxidation of the trivalent ion occurred, the hydrous dioxide was obtained. The familiar rodlike microstructures of cerium trihydroxide and berkelium trihydroxide are shown in Fig. 5.9*A* and *C*. In Fig. 5.9*D*, the fiber-like structures obtained with 10 μg of berkelium are shown. The small symmetrical particles in Fig. 5.9*B* are hydrous cerium dioxide; particles similar to these were obtained with tetravalent berkelium.

The length of the trihydroxide rods ranged from about 1500 Å for cerium to 0.5 μ for berkelium, whereas the long fibers for berkelium were several microns in length. The cerium dioxide particles were about 15 to 25 Å when first obtained but could be grown to 100 Å under special conditions (particles in Fig. 5.9*B* are ~90 Å in diameter). The diffraction patterns obtained from the fibers shown in Fig. 5.9*D* were amorphous-like in nature even though the material was aged considerably longer than the rods shown in Fig. 5.9*C*. The diffraction patterns obtained from the rodlike berkelium microstructures were isomorphous with those obtained for the other trivalent lanthanide and actinide hydroxides.

Work has also been done on developing techniques for studying other actinide materials by electron microscopy and electron diffraction. Several experiments have been carried out on oxide systems. One result of these studies was the identification of einsteinium sesquioxide by electron diffraction. The high specific activity of the most readily available isotope, ^{253}Es, created special problems. The fact that electron diffraction patterns could be rapidly obtained from very small samples (<200 ng) made this method of analysis attractive. However, it was necessary to control the size of the oxide particles to obtain satisfactory electron diffraction patterns. The particles had to be large enough to be sufficiently crystalline but not large enough to prevent penetration of the sample by the electron beam. An ideal particle size for electron diffraction was found to be 100 to 400 Å in diameter. The conditions for preparing particles of this size were determined empirically. A diffraction pattern for Es_2O_3 and the particles from which it was obtained are shown in Fig. 5.10. An electron diffraction pattern for Gd_2O_3 prepared by the same technique is included for comparative purposes.

As a result of the rapid decay of ^{253}Es (~3%/day), it was impossible to prevent the berkelium daughter from growing in. To determine the effects of berkelium and the radioactive decay process on the einsteinium oxide lattice, data were collected under various experimental conditions. The experiments were performed on several different sources of highly purified einsteinium. Analysis of the data is in progress, but a tentative value for the body-centered lattice parameter of Es_2O_3 is 10.72 Å. The correlation of the Es_2O_3 lattice parameter with published values[33] for the other actinide sesquioxides is shown in Fig. 5.11. The ionic radius of Es^{3+} calculated from the lattice parameter of Es_2O_3 has a value of 0.918 Å, which compares closely with the radius of Tb^{3+} (0.920 Å). Additional electron diffraction studies of the actinide oxides are in progress.

5.6 COLLABORATIVE RESEARCH WITH THE TRANSURANIUM RESEARCH LABORATORY

Several research projects are being carried out in collaboration with personnel at the Transuranium Research Laboratory (TRL). This work is summarized briefly here. More detailed information can be obtained in annual reports published by the Chemistry Division and in papers published in the open literature.

The absolute quantity of curium in a very pure solution can be determined by a newly developed analytical procedure. The procedure is based on a

33. J. R. Peterson, Ph.D. thesis, University of California, Lawrence Radiation Laboratory report UCRL-17576.

PHOTO 0624-71

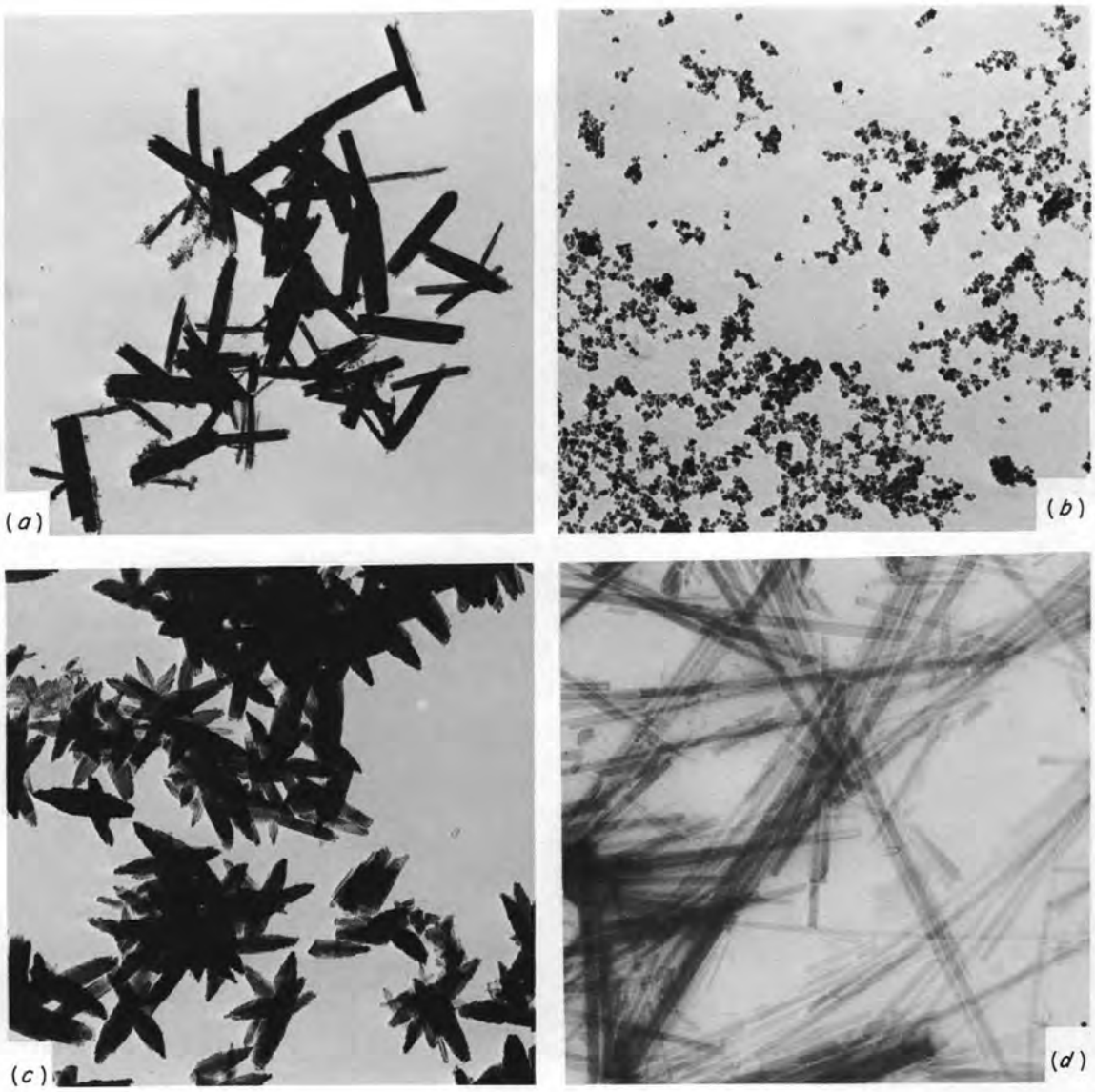

Fig. 5.9. Electron micrographs of cerium and berkelium hydroxides. (*A*) $Ce(OH)_3$; (*B*) $CeO_2 \cdot XH_2O$; (*C*) crystalline $Bk(OH)_3$; (*D*) poorly crystalline $Bk(OH)_3$.

complexametric titration of curium with ethylenediaminetetraacetic acid (EDTA). A known amount of EDTA, which exceeds that needed to completely complex the curium, is added to a very pure solution of curium. The excess EDTA is determined by complexametric titration with mercury(II) that is generated coulometrically. This method was used to determine absolute amounts of ^{246}Cm and ^{248}Cm prepared for use in measurement of half-lives. The measured value for the half-life of ^{246}Cm by alpha decay is $(4.655 \pm 0.40) \times 10^3$ years. The values for the partial half-lives of ^{248}Cm by alpha decay and by spontaneous fission are $(3.703 \pm 0.032) \times 10^5$ years and $(4.115 \pm 0.034) \times 10^6$ years respectively.[34]

The ultraviolet-light-excited energy transfer and sensitized luminescence for $^{253}Es^{3+}$ doped into a cesium-gadolinium hexafluoroacetylacetonate chelate were induced and measured. The measurements and calculations show that the first excited ($J = 7$) energy level in

34. J. E. McCracken, J. R. Stokely, R. D. Baybarz, C. E. Bemis, Jr., and R. Eby, "Determination of the Half-Lives of ^{246}Cm and ^{248}Cm by Absolute Specific Activity Techniques," to be published in *J. Inorg. Nucl. Chem.*

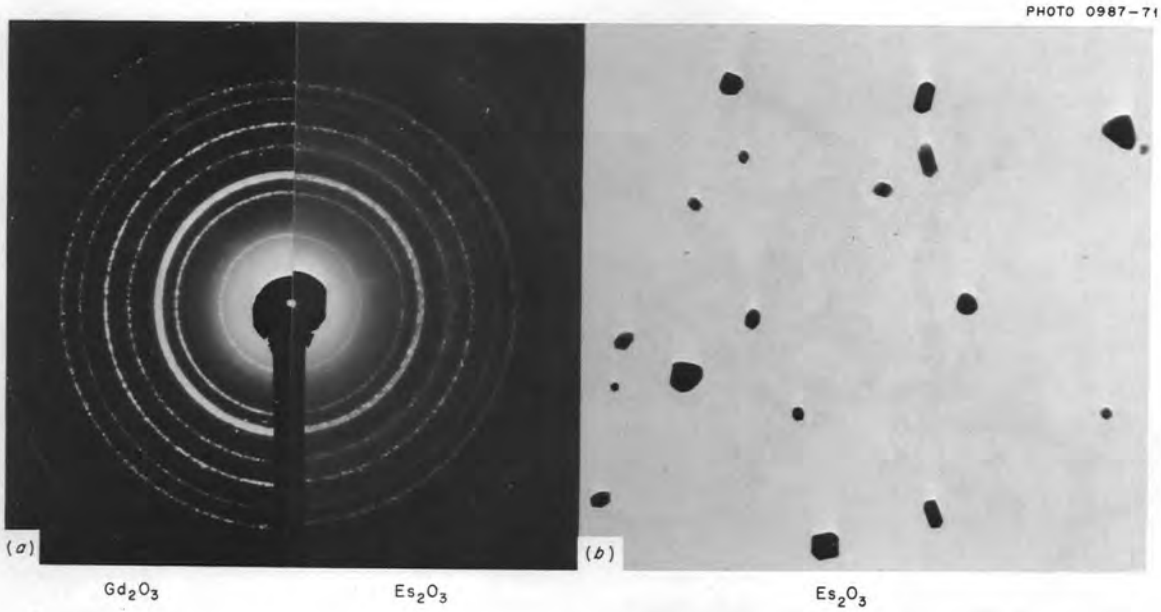

Fig. 5.10. The sesquioxides of gadolinium and einsteinium. (*A*) Electron diffraction patterns; (*B*) Es_2O_3 particles, 100–400 Å in diameter.

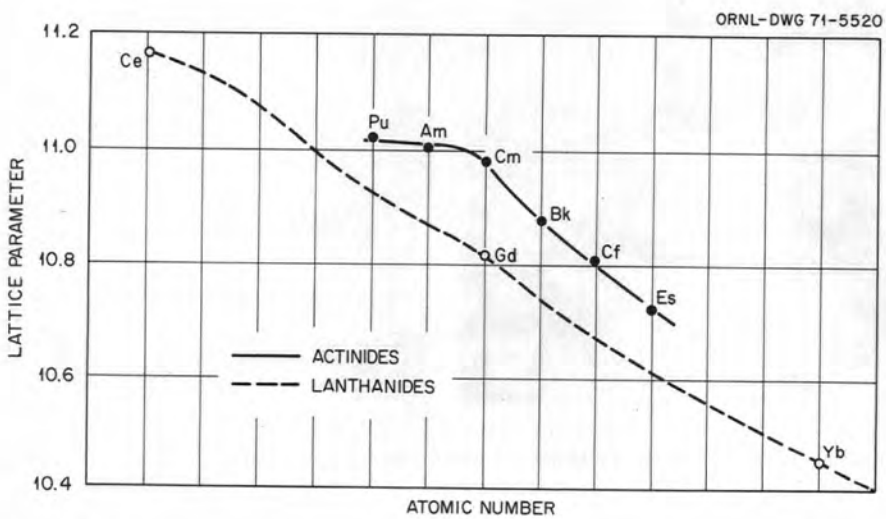

Fig. 5.11. Variation of the actinide and lanthanide M_2O_3 lattice parameter with atomic number.

the $5f^{10}$ electronic configuration of Es^{3+} in aqueous 1 *M* $HClO_4$ is at 9600 cm^{-1}. The lower-lying energy levels of Es^{3+}(aq) were also determined by absorption spectrophotometric methods and have been reported.[35]

An investigation is being carried out to determine the coordination numbers of the lanthanide and actinide elements. Solid compounds of elements from the two groups are being prepared, and the coordination number is being determined by single-crystal x-ray diffraction. Single-crystal absorption spectrophotometry and thermogravimetric analysis are also being used. Solid single crystals of $Am_2(SO_4)_3 \cdot 8H_2O$, $Am(ClO_4)_3 \cdot XH_2O$, and $Pr(ClO_4)_3 \cdot XH_2O$ have been prepared and are being analyzed. The effect of temperature on the $f \rightarrow d$ bands of the lanthanides and actinides in aqueous solutions is also being investigated in an effort to determine the changes in coordination number across the two series.

35. L. J. Nugent et al., *Chem. Phys. Lett.* 7, 179 (1970).

6. Development of the Thorium Fuel Cycle

Development of the thorium fuel cycle as described in this chapter is based on the timely introduction of high-temperature gas-cooled reactors (HTGR's) using Th and ^{233}U as fuel. This type of reactor is typified by the Fort St. Vrain Reactor, which is being constructed by Gulf General Atomic. These reactors will use small spheres of carbide or oxide fuel encased in pyrolytic carbon coatings. Sol-gel processes, which are well suited to the preparation of oxide fuel spheres, are being developed as an integral part of the fuel cycle. They can be adapted readily to remote operation to give high-density oxide spheres by use of the following three principal operations:

1. preparing an aqueous oxide sol;
2. dispersing the sol, as drops, into an organic fluid and then removing the water from these drops to give solid gel particles;
3. firing at controlled conditions to remove volatiles, sintering to a high fuel density, and performing any necessary reductions or chemical conversions.

This program has been in progress for several years, and development is well advanced. Using processes we have developed, spheres of ThO_2, UO_2, and ThO_2-UO_2 were produced for a variety of HTGR fuel tests elements. Process and equipment development and design are in progress for refabrication of ThO_2-$^{233}UO_2$ spheres in the Thorium-Uranium Recycle Facility (TURF).

During the year we continued our function as a ^{233}U storage, purification, and distribution center.

6.1 RECYCLE OF THE ALCOHOL USED IN THE MICROSPHERE-FORMING COLUMN

The successful continuous formation of gel spheres requires control of the composition of the 2-ethyl-1-hexanol (2EH) fluidizing medium. The desired concentrations for surfactants, water, and nitrate fall in ranges having maximum and minimum values. Materials extracted from the sol or formed by degradation of surfactants or 2EH probably only have maximum limits, with zero as the desired lower limit. The water content can easily be controlled by simple distillation to remove water as vapor. The surfactants can be added to replace losses, although the control of the concentrations of these substances is difficult because of the lack of convenient methods for their measurement. Most of our development studies involving large columns during this report period were concerned with procedures for recycling the 2EH without excessive accumulation of impurities. The studies with CUSP-type UO_2 sols are reported in Sect. 7.3.

Application of Ion Exchange to the Recycle of 2EH

The 2EH entering the still contains surfactants (Span 80, Ethomeen S/15), nitric acid, and perhaps formic acid. The nitric acid may be extracted from any of our sol droplets by the 2EH; formic acid is extracted from UO_2 sols.

Water accumulating in the 2EH during sol droplet gelation must be removed by distillation. As the distillation operation takes place, the nitric acid reacts with the surfactants (and perhaps the alcohol), and degradation products are formed. These degradation products and the formic acid prevent continuous long-term operation of the sphere-forming column. Small amounts of formic acid, for example, a concentration of only 0.005 *M*, cause clustering and coalescence and thus make fluidization impossible. The application of ion exchange to remove these acidic materials from 2EH before the feed stream of 2EH enters the distillation operation was investigated and reported.[1] Conditions were determined for using Amberlite IRA-93 or Amberlyst A-21 anion exchange resins to remove the formic and nitric acids. Complete operating cycles were demonstrated in 1-in.-ID and

1. A. P. Luina, P. A. Haas, and C. C. Haws, Jr., *Application of Ion Exchange for Recycle of 2-Ethyl-1-hexanol to Sol-Gel Preparation of Spheres*, ORNL-TM-3226 (February 1971).

4-in.-ID ion exchange columns of 24-in. lengths. Breakthrough of the formic acid was determined by measuring the pH of the 2EH effluent. The regeneration cycle was controlled by use of preset solution volumes. Detailed results and recommended operating cycles were reported.[1]

The application of ion exchange to remove nitric acid from the 2EH before it enters the still to remove H_2O is a significant process improvement. Starting with pure 2EH, excellent ThO_2 spheres are easily prepared with Ethomeen S/15 as the only surfactant. The nitric acid extracted from the ThO_2 sol into the 2EH has two deleterious effects. First, the Ethomeen S/15 is less effective for preventing doublets and clustering as the pH of the 2EH decreases, and for this reason the addition of Span 80 may be necessary to prevent doublets and clustering. Second, the nitric acid reacts with both Ethomeen S/15 and Span 80 at 150°C in the still and destroys them; thus surfactant additions are necessary. By using ion exchange to remove the nitric acid, we eliminate the need for Span 80 and reduce the loss of Ethomeen S/15.

Formation of ThO_2-UO_3 Spheres

The ThO_2-UO_3 sol prepared in recent runs (see Sect. 6.4) can be formed and fired into dense ThO_2-UO_3 spheres, using a combination of Ethomeen S/15 and Span 80 as the surfactant and ion exchange in the 2EH recycle as a means of preventing degradation reactions in the still. This sol (Th/U ratio of 3.0) was prepared by the solvent extraction process. The pH of the 2EH remains at about 6.5 as compared with the steady-state pH of 5 reached without ion exchange.

We had hoped to be able to use Ethomeen S/15 alone as the surfactant (as in the case of ThO_2 sols) so that ion exchange would eliminate or greatly reduce the need for surfactant additions. However, although Ethomeen S/15 gave very good product for small test samples, it gave approximately 1% doublets at the beginning of normal column operation. Coalescence and clustering increased with operating time until they became intolerable after about 4 hr. The addition of 0.05 vol % Span 80 gave excellent operation for the following 4 hr; however, at this time, clustering was again observed. Two more additions of 0.05 vol % Span 80 gave the same results. The concentration of Span 80 must be lower than the concentration of Ethomeen S/15 since Span/Ethomeen ratios greater than 1 result in distortions of the "wrinkle" or the "raisin" type.

The use of ion exchange does not prevent the loss of Span 80. Although the reactions with nitric acid in the still are eliminated, the Span 80 is inactivated, probably by hydrolysis in the ion exchange column. Results of our initial tests of ion exchange for the recycle of 2EH were difficult to interpret because of this reaction. Span 80 concentrations, based on measurements of infrared absorption or determinations of the high-boiling residues, showed no change on passing through the ion exchange column. On the other hand, the clustering and coalescence behavior in the sphere-forming column indicated rapid losses of Span 80. Span 80 additions must be made during operation. In long-term operations, in which the presence of Span 80 is necessary to achieve satisfactory results, the used 2EH will have to be replaced by pure 2EH, and fresh additions of surfactants will have to be made at specified intervals. Studies of distillation to recover pure 2EH from the used 2EH containing surfactants and impurities are reported in Sect. 7.3.

6.2 DEVELOPMENT OF PROTOTYPE EQUIPMENT FOR TURF

The Thorium-Uranium Recycle Facility (TURF) will contain equipment to convert thorium nitrate and uranyl nitrate (^{233}U) solutions to ThO_2-UO_3 sols by solvent extraction, form them into ThO_2-UO_3 gel spheres, and dry and fire them to produce ThO_2-$^{233}UO_2$ for subsequent fuel fabrication. The process and equipment for these operations have been demonstrated under conditions of direct operation at 10 kg of oxide (ThO_2 + UO_2) per day,[2] the design capacity of the TURF. Additional development work is needed to demonstrate the capability for remote operation and provide design information for prototype equipment.

Design of Equipment for TURF

Sol is to be prepared by the Solex process,[3-5] and 350-μ-diam microspheres are to be prepared as dense oxide particles using microsphere-forming techniques

2. C. C. Haws, Jr., B. C. Finney, and W. D. Bond, *Engineering-Scale Demonstration of the Sol-Gel Process: Preparation of 100 kg of ThO_2-UO_2 Microspheres at the Rate of 10 kg/day*, ORNL-4544 (June 1971).

3. *Chem. Technol. Div. Annu. Progr. Rep. May 31, 1968*, ORNL-4272, pp. 129–34.

4. *Chem. Technol. Div. Annu. Progr. Rep. May 31, 1967*, ORNL-4145, pp. 154–59.

5. *Chem. Technol. Div. Annu. Progr. Rep. May 31, 1969*. ORNL-4422, pp. 183–90.

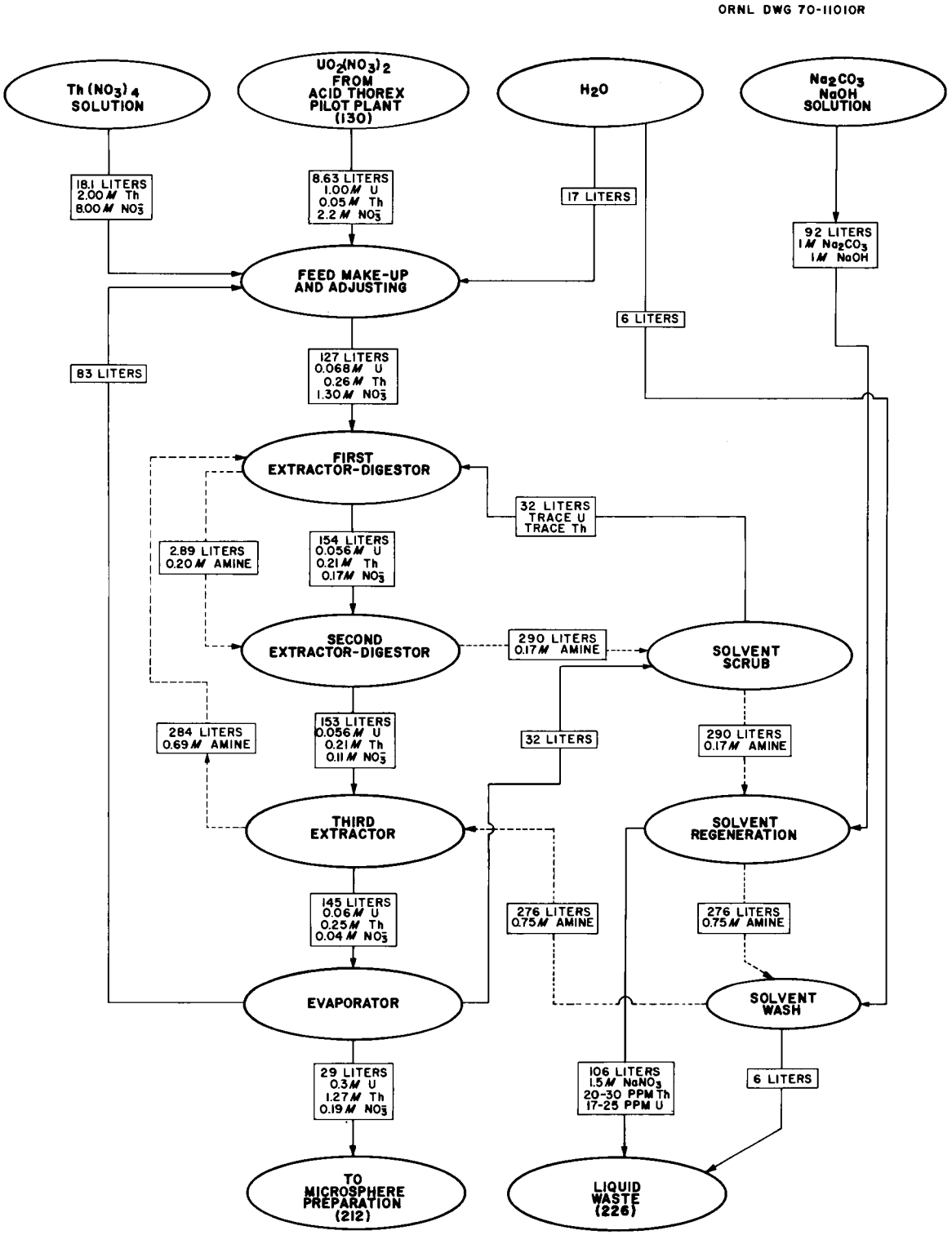

Fig. 6.1. Proposed chemical flowsheet for the preparation of sol for forming 10 kg of microspheres (Th/U ratio of 4.25) per day by the Solex process.

ORNL DWG 70-10989

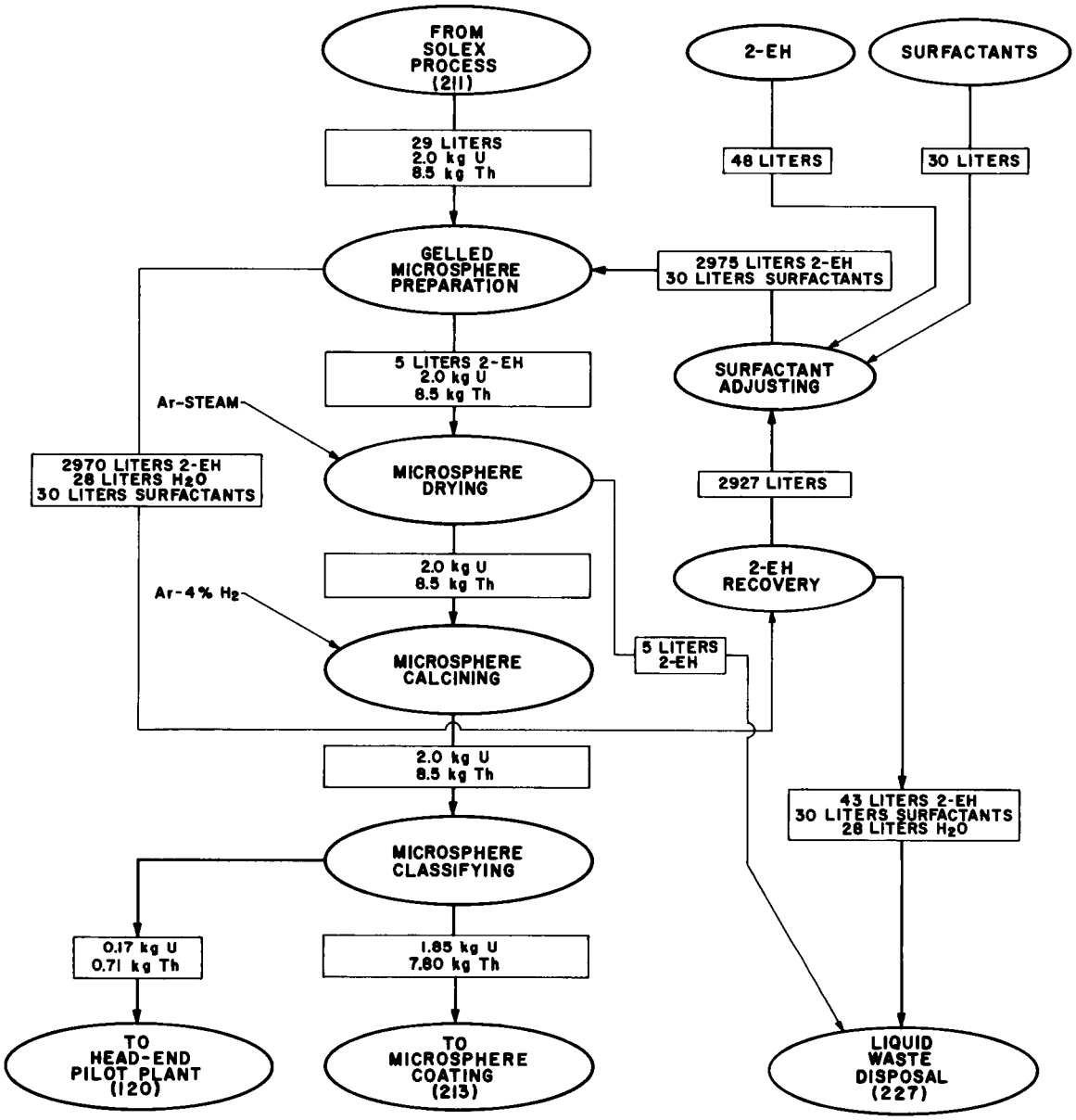

Fig. 6.2. Proposed chemical flowsheet for the preparation of 10 kg of ThO_2-UO_2 microspheres (Th/U ratio of 4.25) per day.

discussed in previous years.[6–9] Flowsheets of the Solex (Fig. 6.1) and microsphere-forming (Fig. 6.2) processes based on TURF design throughput were prepared to determine the materials and waste handling problems to be expected in the TURF.

Development of this equipment has now reached the point where the design of TURF prototypes can begin as soon as it appears to be appropriate.

6. *Chem. Technol. Div. Annu. Progr. Rep. May 31, 1970,* ORNL-4572, pp. 135–44.

7. *Chem. Technol. Div. Annu. Progr. Rep. May 31, 1968,* ORNL-4272, pp. 129–37.

8. *Chem. Technol. Div. Annu. Progr. Rep. May 31, 1967,* ORNL-4145, pp. 169–75.

9. *Chem. Technol. Div. Annu. Progr. Rep. May 31, 1966,* ORNL-3945, pp. 146–52.

Studies Related to the Development of Experimental Equipment

The solvent extraction equipment for preparing ThO_2-UO_3 sol was demonstrated at capacities up to three times the capacity of TURF (see Sect. 6.4).[2] The additional requirement that the equipment be remotely operable does not appear to pose difficulties. The equipment and processes are similar to those which have been repeatedly and successfully met for other applications of solvent extraction processes.

Demonstration of sphere-forming equipment for the formation of ThO_2-UO_3 gel spheres was carried out at TURF design capacity with natural uranium.[2] Visual observations were used for control of the sphere-forming column. A periscope (Fig. 6.3) that can be used in-cell with simple extension sections to accommodate hot-cell walls is being tested. Demonstration of two observations critical to the operation of the in-cell system will be made by the use of the periscope.

Demonstration of drying and firing the gel beads will require additional equipment development. Drying is carried out with a flowing stream of gas in a heated container. Critical requirements are (1) good contact between the gel spheres and the flowing gas and (2) smooth temperature changes carried out on a reasonable schedule without excessive temperature gradients. We have successfully met these requirements in rather primitive equipment. The need for remote operation, for conservation of cell space, and for criticality control imposes severe limitations on the design of equipment for use in TURF. We are in the process of selecting prototype designs.

6.3 PREPARATION OF MICROSPHERES IN NONFLUIDIZED-BED COLUMNS

Uranium dioxide microspheres smaller than 200 μ in diameter may find application as fuel for future HTGR's. Thus it is of interest to find improved ways to

ORNL PHOTO 0579-71A

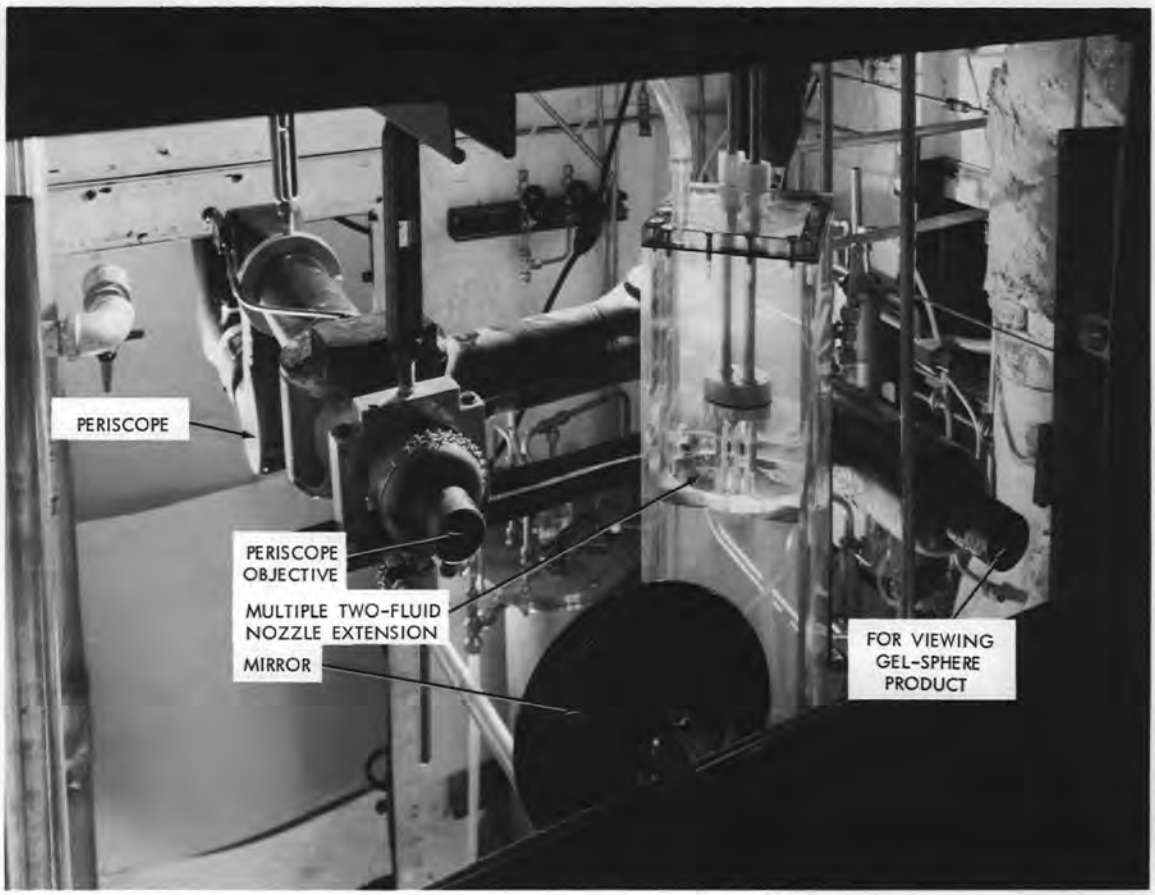

Fig. 6.3. Periscope installed in CPDL microsphere preparation cubicle.

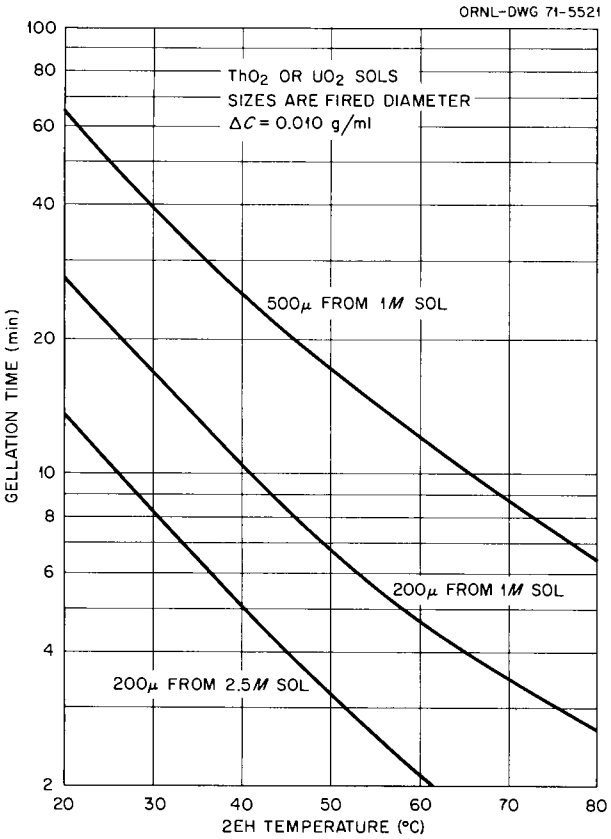

Fig. 6.4. Calculated gelation times vs 2EH temperature.

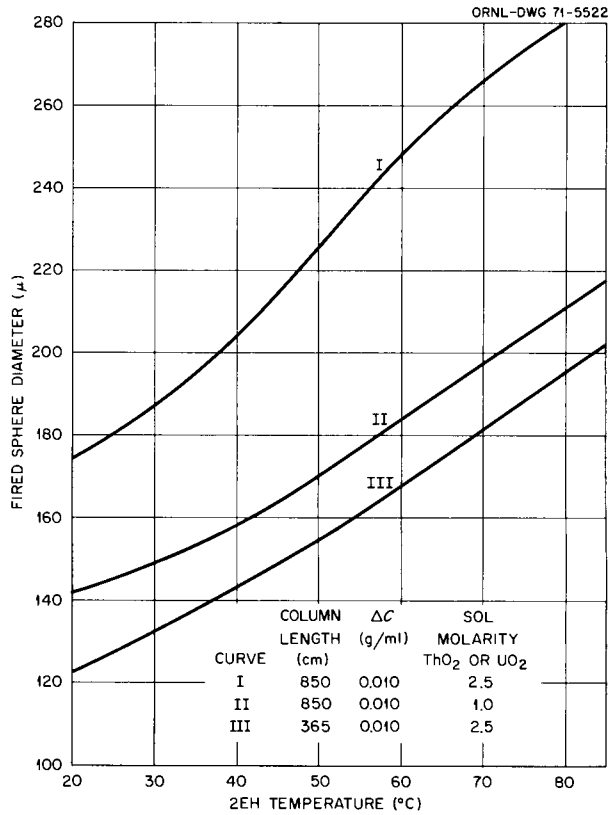

Fig. 6.5. Calculated fired sphere sizes for nonfluidized columns.

produce spheres in this size range. The preparation of sol-gel spheres by extraction of water into alcohols is simpler for nonfluidized- than for fluidized-bed operation. This mode of operation is practiced for spheres smaller than about 200 μ. The principal limitation on the nonfluidized preparation of spheres is that the sol drops introduced into a nonfluidized column must be small enough to gel before they settle to the bottom. The maximum sphere diameter that can be produced is typically 200 μ or less. The column heights required are dependent on mass transfer and the settling velocity. Mass transfer as a function of sol drop and organic liquid variables was investigated and correlated by Clinton.[10] The settling velocities may be calculated using Stokes' equation or a drag coefficient. Both the sol-drop size and the density vary with time. Thus, mass transfer and the settling velocity also vary with time, and analytical solutions are not possible. However, the time and free-fall distance as a function of sol drop variables and alcohol variables can be conveniently calculated using a computer program. These and other general considerations and some results of nonfluidized column operation have been reported.[11]

Additional calculations were made with a computer program for mass transfer to determine the effects of varying the temperature of the 2EH. The conditions were selected to apply to a new 28-ft-high nonfluidized column with our usual UO_2 or ThO_2 sols. The calculated values are for a water concentration driving force, ΔC, of 0.010 g/ml or 1.0 vol % water (i.e., the water concentration in the 2EH is 1 vol % less than saturation). The gelation times (Fig. 6.4) or the free-fall distances (Fig. 6.5) are inversely proportional to ΔC; therefore the values for other water concentrations can be easily calculated. For example, the times or distances for 1.8 vol % H_2O in the 2EH at 28°C ($\Delta C = 0.005$) would be twice those shown for 1.3 vol % H_2O in the 2EH at 28°C (ΔC = 0.010). For the 28-ft (850-cm)

10. S. D. Clinton, *Mass Transfer of Water from Single Thoria Sol Droplets Fluidized in 2-Ethyl-1-hexanol,* M.S. thesis, University of Tennessee, Knoxville (1968); also issued as ORNL-TM-2163 (June 1968).

11. P. A. Haas, "Preparation of Sol-Gel Spheres Smaller than 200 Microns without Fluidization," *Nucl. Technol.* **10**(3), 283–92 (1971).

ORNL PHOTO 0578-71A

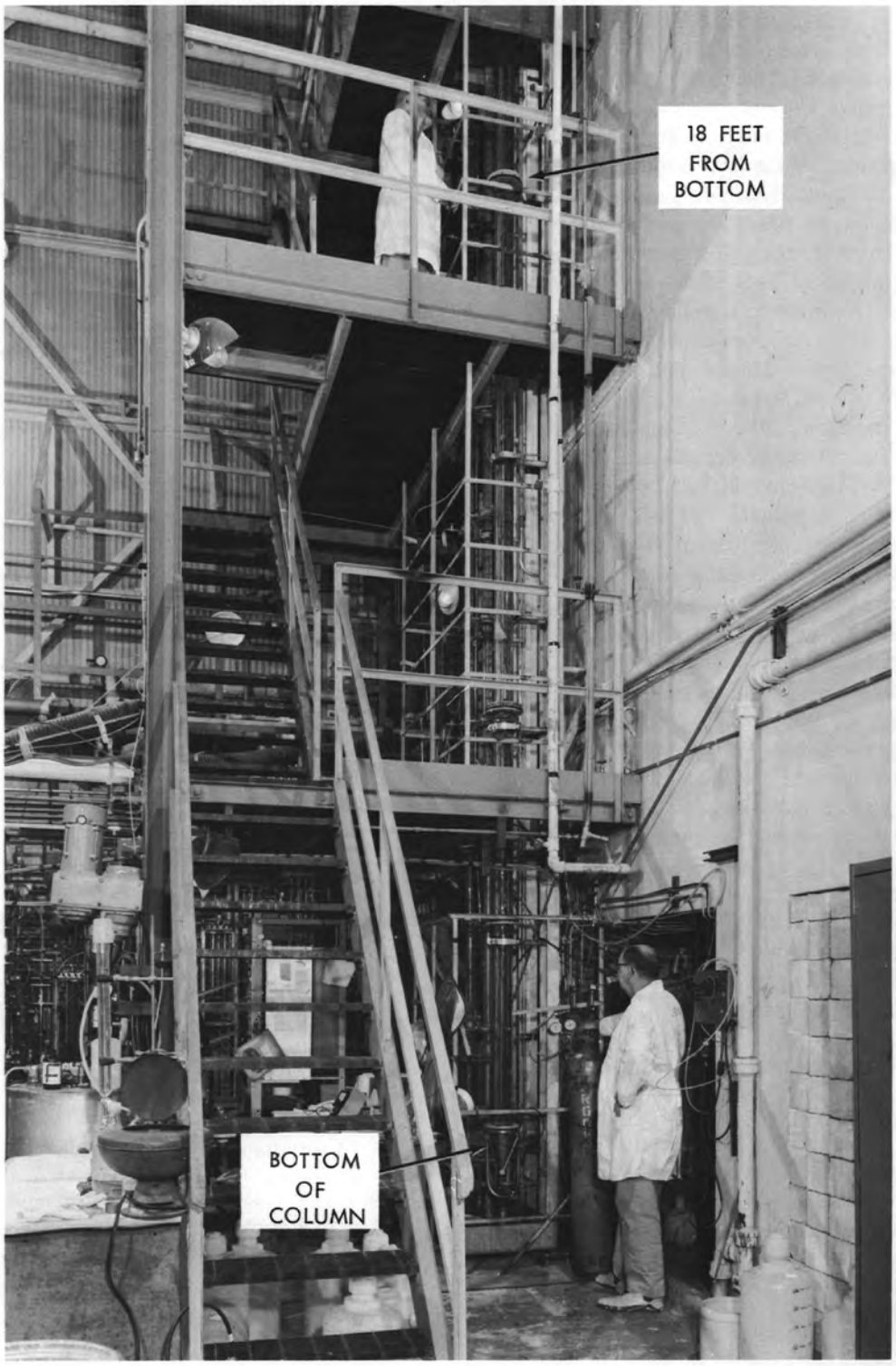

Fig. 6.6. Bottom 20 ft of 28-ft-high nonfluidized column for formation of sol-gel spheres.

column (Fig. 6.6), the sizes of the fired spheres shown increase from 180 to 280 μ for 2.5 M ThO_2 sol and from 145 to 210 μ for 1.0 M UO_2 sol as the 2EH temperature increases from 25 to 80°C. While the rate of water extraction increases by a factor of 7 or 8, the allowable sphere size only increases by about 50% as the 2EH temperature increases from 25 to 80°C. This can be explained by the increase in settling velocity as the temperature increases. For the same column conditions the allowable initial sol drop sizes are generally about 5% larger for the 1 M UO_2 sol as compared with those for the 2.5 M ThO_2; however, the drops of the more dilute sol shrink to a smaller final size. While the thoria sol, which is more concentrated, is closer to gelation, the higher density and the higher settling velocity for a ThO_2 sol drop, as compared with those for a UO_2 sol drop of the same initial size, result in a larger free-fall distance before gelation.

A new 28-ft-high nonfluidized column was operated with 2.5 M ThO_2 sol and 1 M UO_2 sol feed. Heated 2EH is supplied to the top of the column, and the temperature down the column decreases as heat is lost to the surroundings. This temperature gradient is favorable since it gives rapid extraction of water at the top, where the sol is fluid, and slower extraction at the bottom, where gelation occurs. Operation was satisfactory with sol drops having an initial diameter of 470 μ (yielding 190-μ-diam ThO_2 spheres after firing). This result agrees with the calculated allowable sol drop size (480 μ) for these conditions and a 2EH temperature of 35°C. For sol drops with an initial diameter of 520 μ, gelation was incomplete in 2EH at about 30°C, and the drops clumped in the transfer line. For an average 2EH temperature of about 45°C, the 520-μ drops were gelled without difficulty. Results with the 1 M UO_2 sol also confirmed the allowable sol drop diameters predicted by mass transfer calculations.

6.4 PREPARATION OF TEST MATERIALS

As in previous years, sol-gel oxide spheres were prepared for a number of National HTGR Recycle Program needs. In some cases, these needs have been satisfied by material produced as part of the sphere preparation development studies; for the most part, however, special preparations were necessary. Special preparations during this report period have included:

1. Additional (100 ± 30)-μ-diam UO_2 from UO_2 (93% ^{235}U) sol. This was additional material for the recycle test elements described previously.[12]
2. Six kilograms of 400-μ-diam ThO_2 spheres for near-term test elements and capsules.
3. About 1600 g of 200-μ-diam UO_2 spheres from UO_2 (93% ^{235}U) sol for near-term test elements and capsules.
4. About 5000 g of 350-μ-diam ThO_2-UO_2 spheres from a blend of UO_2 (93% ^{235}U) and ThO_2 sols (to give a sol having a Th/U atom ratio of 2.75) for use in near-term test elements and capsules.
5. About 100 kg of ThO_2-UO_3 as sol (Th/U atom ratio = 3.0) from ^{238}U. This sol will be formed into 350-μ-diam spheres for fabrication development and for test elements to be used in head-end processing development.
6. About 40 kg of 400-μ-diam ThO_2 spheres for fabrication development and for test elements to be used in head-end processing development.

The preparation of additional UO_2 spheres for recycle test elements (item 1) was identical to that previously reported.[12] The ThO_2 spheres (items 2 and 6) were prepared with an improved 2EH recycle system, as described in Sect. 6.1.

Formation of UO_2 Spheres (Item 3)

Five batches of UO_2 sol (93% ^{235}U) prepared by the precipitation-peptization process were formed into 200-μ-diam UO_2 spheres for near-term test elements and capsules. Operation of the sphere-forming system was satisfactory with 2EH containing 0.4 vol % Span 80–0.1 vol % Ethomeen S/15. Ion exchange was used to remove nitric and formic acids, and distillation was used to remove H_2O; addition of Span 80 was necessary for recycle of the 2EH. During previous operations with UO_2 sols prepared from enriched uranium, in which ion exchange was not used, the 2EH had to be replaced more frequently to avoid clustering that is caused by accumulation of formate in the 2EH.

Formation of ThO_2-UO_2 Spheres (Item 4)

The 350-μ-diam ThO_2-UO_2 spheres required for near-term test elements and capsules were prepared by mixing ThO_2 sol with UO_2 (93% ^{235}U) sol prepared by the precipitation-peptization process. The target Th/U atom ratio was 2.77. The analytical results for the first three products were 2.74, 2.77, and 2.78.

The sphere-forming behavior was similar to that of pure UO_2, despite the high ThO_2 content. The initial surfactant concentrations were 0.35 vol % Span 80 and 0.1 vol % Ethomeen S/15 in the 2EH. Additions of

12. *Chem. Technol. Div. Annu. Progr. Rep. May 31, 1970*, ORNL-4572, pp. 142–44.

Span 80 were required when the ion exchange system and the still were used to remove nitric acid and water from the 2EH.

Preparation of ThO_2-UO_3 Sol (Item 5)

The amine solvent extraction system[13] was operated in continuing engineering demonstrations to prepare 100 kg of ThO_2-UO_3 sol that will be used in fuel fabrication studies and to fabricate prototype HTGR fuel elements for use in studies of spent power reactor fuel reprocessing. The sol was prepared by extraction of the nitrate from a 0.27 *M* $Th(NO_3)_4$–0.09 *M* $UO_2(NO_3)_2$–1.3 *M* NO_3^- feed (Th/U atom ratio of 3) using 35% excess 0.75 *M* Amberlite LA-2 in *n*-paraffin as the extractant and a countercurrent extraction flowsheet similar to the continuous demonstration previously described.[2] In contrast to the earlier continuous operation demonstration, the equipment was operated for 6 to 7 hr each day at the rate of 1.0 kg of oxide per hour; no difficulty was encountered with the frequent startups and shutdowns.

Prior to this campaign, the volume of the digester that is located between the first and second extraction contactors was doubled; otherwise, the equipment was the same as that operated for 200 hr at a production rate of 0.5 kg of oxide per hour.[2] An attempt to start up at a rate of 2.0 kg of oxide per hour was unsuccessful due to excessive interfacial crud and emulsions. Therefore the equipment was started up at a 0.5-kg/hr rate; then, when steady state was attained, the rate was increased to 1.0 kg/hr. Operation was very satisfactory at the latter rate. After approximately 100 kg of sol had been prepared at the 1.0-kg/hr rate, rates of 1.5 and 2.0 kg/hr were tested for short periods. Operation was normal at 1.5 kg/hr but became unsteady at the 2.0-kg/hr rate, as indicated by fluctuations in the conductivity of the product sol leaving the third extraction contactor. Analyses of typical ThO_2-UO_3 sols prepared by continuous amine solvent extraction in the engineering-scale equipment, using a countercurrent flowsheet, are presented in Table 6.1. The data indicate that the engineering-scale equipment designed for a rate of 10 kg of oxide per day can be successfully operated at 1.5 kg/hr (or 36 kg/day), but it would be necessary to carry out continuous operations for prolonged periods to verify this.

The sol prepared at the 1.0-kg/hr rate was divided into 40-liter batches and concentrated to 1.5 *M* (Th + U) in the forced-circulation evaporator without difficulty.

13. *Chem. Technol. Div. Annu. Progr. Rep. May 31, 1969*, ORNL-4422, pp. 156–59.

Table 6.1. Analyses of ThO_2-UO_3 sols prepared by amine solvent extraction using a countercurrent flowsheet

	Sol production rate (kg of oxide per hour)				
	0.5	1.0	1.5	2.0[a]	0.5[b]
Th, *M*	0.223	0.227	0.225	0.227	0.253
U, *M*	0.075	0.076	0.076	0.076	0.059
Th/U atom ratio	2.97	2.95	2.98	2.99	4.28
NO_3^-, *M*	0.026	0.029	0.031	0.036	0.038
NO_3^-/metal mole ratio	0.087	0.096	0.10	0.12	0.12
Conductivity, micromhos/cm at 18°C	518	559	578	853	546

[a]Operation at this ratio was not satisfactory, and the product was not considered to be acceptable.

[b]Data obtained in previous operation (see ref. 2).

The engineering-scale sol preparation equipment is located adjacent to the wall in a sheet-metal building that is inadequately heated. Two abnormal upsets in operation were encountered during the campaign due to severe cold weather that caused the solvent to separate into two phases in the contactors and surge tank.

Immediately following an equipment malfunction caused by excessive cooling of the building in which the sol preparation equipment was located, off-specification sol was produced. Because of this, the two batches of sol involved were collected separately. Analyses of them are presented in Table 6.2. When attempts were made to concentrate the sols in the forced-circulation evaporator, both sols became very thick at ~1 *M* (Th + U) and gelled within three days. In comparing the first three sols in Table 6.1 with the off-specification sols, it can be noted that the acceptable sols have a NO_3^-/metal mole ratio of $\leq$0.1 and conductivities that fall in the range 500 to 600 micromhos/cm at 18°C; conductivities of the off-specification sols fall in the range 900 to 1100 micromhos/cm at 18°C. It can also be noted that the last sol in Table 6.1 (Th/U ratio of 4.28) has a conductivity in the range for acceptable sols. This would indicate that, in order for a dilute ThO_2-UO_3 sol

Table 6.2. Analyses of off-specification dilute ThO_2-UO_3 sol

	Batch EV-43-25	Batch EV-43-26
Th, *M*	0.226	0.225
U, *M*	0.078	0.076
Th/U atom ratio	2.90	2.96
NO_3^-/metal mole ratio	0.082	0.077
Conductivity, micromhos/cm at 18°C	925	1040

(Th/U atom ratio of 3 or 4.25) prepared by the countercurrent flowsheet to be concentrated and remain stable, it should have a conductivity in the range of 500 to 600 micromhos/cm at 18°C.

6.5 ^{233}U STORAGE, PURIFICATION, AND DISTRIBUTION

Oak Ridge National Laboratory serves as a national distribution center for ^{233}U. The facility includes shielded wells for storing up to 454 kg of ^{233}U in solid form (density = 1 g/cm^3) and tanks (containing borosilicate glass for neutron poisoning) that can store 900 kg of ^{233}U in uranyl nitrate solutions at ^{233}U concentrations up to 250 g/liter. Also, a shielded interim storage vault (located in Building 3100) can hold up to 70 kg of ^{233}U or ^{239}Pu in shipping containers. The above capacities include the new facilities, nine dry wells and five storage tanks, needed for the storage of feed material for the Light Water Breeder Reactor (LWBR) support program; later, the solids storage facility will be required for storing 200 kg of ^{233}U from the Elk River reactor. (However, the material must first be recovered and converted to oxide at the Italian CNEN Plant.)

The storage facility accepts ^{233}U in the form of uranyl nitrate solution or as properly packaged solids. The solids may consist of uranium metal or uranium compounds that can be readily and safely dissolved in stainless steel equipment.

The purification facilities include a single-cycle solvent extraction system that is capable of purifying ^{233}U at the rate of 25 kg/week. At present, all the ^{233}U that is processed in the facility is shipped as nitrate solution. The system is presently being modified to increase its reliability and flexibility, and a complete nitrate-to-oxide conversion line with a capacity of 22 kg of ^{233}U per week is being installed for the LWBR support program (see Sect. 9).

Summary of Distribution Activities

During the past year 27 shipments, containing 831 kg of ^{233}U, were received by the facility. Twenty-one shipments, amounting to 15 kg of ^{233}U, were made from the facility. The largest single shipment received was 111 kg of ^{233}U nitrate (from Atlantic Richfield at Hanford) for use in the LWBR support program. The activity of the facility for each calendar year from 1960 through 1970 is shown in Fig. 6.7. Table 6.3 shows the inventory of ^{233}U (exclusive of Consolidated Edison

Table 6.3. ^{233}U inventory as of March 31, 1971

Form	Isotopic purity (wt %)	^{232}U content (ppm)	Quantity (kg)
Nitrate	92	22	58.5
	98	7	189.3
	98	8–9	563.6
Oxide	98	6–7	186.2
	96	50	11.0
	91	250	61.7
	98	6	2.3
	97	35	0.6
Fluoride	91	250	2.9
Metal	97	42	5.1
Total			1081.2

Table 6.4. Analyses of solution in TRUST tank

Date sampled	Solution volume (liters)	U (kg)	HNO_3 (*M*)	Soluble poison content			
				Cd		Gd	
				kg	moles/mole U	kg	moles/mole U
9/11/68	1110	0	0.11	164.2		21.4	
2/20/69	6970	1040	2.72	164.2	0.33	16.2	0.023
3/28/69	7100	1036	2.57	142.4	0.29	14.8	0.021
4/17/69	7240	1039	2.66	144.8	0.29	15.1	0.022
7/29/69	7300	1053	2.59	142.4	0.28	14.6	0.021
10/10/69	7280	1055	2.46	143.4[a]	0.28[a]	15.3[a]	0.021[a]
11/11/69	7030	1041	2.51	152.9	0.31	17.8	0.025
4/6/70	7085	1020	2.65	145.3	0.30	16.6	0.024
12/4/70	7010	1031	2.73	140.9	0.29	18.5	0.027
3/9/71	7040	1015[b]	1.82[b]	154.2	0.31	20.7	0.030

[a]A total of 14.2 kg of cadmium and 3.8 kg of gadolinium was added to the tank on Oct. 3, 1969.

[b]Possible dilution of sample.

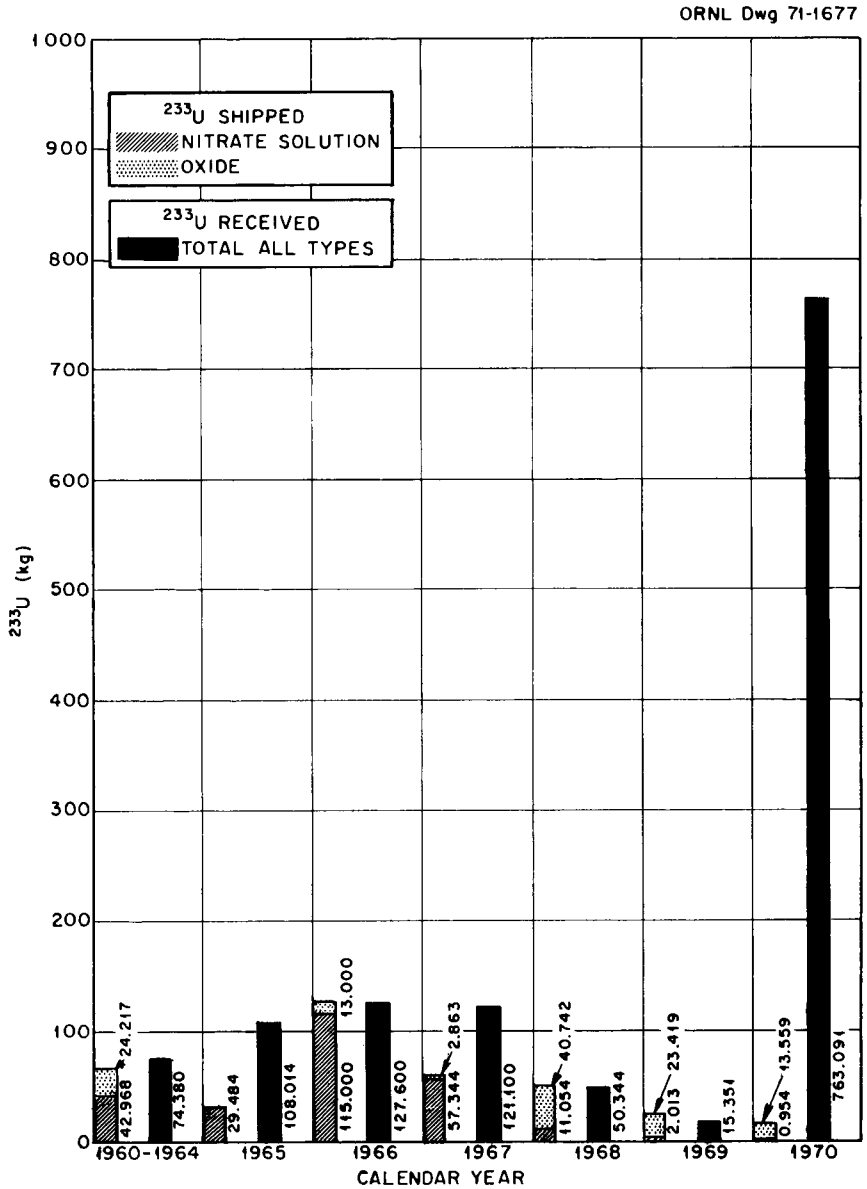

Fig. 6.7. ^{233}U receipts and shipments, Building 3019 dispensing facility.

fuel) in the facility as of March 31, 1971; the form, isotopic purity, and ^{232}U content are also given.

The TRUST (Thorium Reactor Uranium Storage Tank) facility, described previously,[14,15] was placed in operation in 1969.

Analyses of samples of the solution withdrawn at intervals during the past 25 months are presented in Table 6.4. The uranium determination varied from 1015 to 1055 kg, as compared with 1047 kg determined by analysis of the individual shipments received. Discrepancies in the soluble poison content are probably due to inadequate mixing of the solution prior to sampling; however, the possibility of analytical error or deposition of the poisons should not be overlooked. Initial efforts to sparge the solution for a long period of time resulted in excessive radiation exposures from the off-gas piping and filter. This condition was improved by the addition of a shielded de-entrainment separator and a small absolute filter.

14. *Chem. Technol. Div. Annu. Progr. Rep. May 31, 1969,* ORNL-4422, pp. 199, 202.

15. J. R. Parrott, R. G. Nicol, and J. P. Nichols, *Receipt and Analysis of the Consolidated Edison Uranium Product Solution, and Subsequent Storage Utilizing Soluble Neutron Absorbers,* ORNL-TM-3348 (June 1971).

7. Sol-Gel Processes for the Uranium Fuel Cycle

Sol-gel processes are ideally suited for the preparation of LMFBR fuel since they can be readily adapted to continuous and remote operations for processing materials behind shielding. In the processes under development, sols are prepared by the controlled extraction of nitrate from uranium nitrate and plutonium nitrate solutions, which are the products from fuel reprocessing plants. The sols are then converted into the desired form required for subsequent fabrication into recycle fuel elements; this form usually consists of high-density oxide microspheres for use in Sphere-Pac operations.

Most of the development work on the CUSP process during the last year has been directed at the evaluation of various types of contactors used for extracting nitrate and at the characterization of sols produced in engineering-scale equipment. There has been no need to make any appreciable changes in the process, since it continues to produce satisfactory urania sols. The preparation of sols by this process is one step in the production of UO_2-PuO_2 for spheres and pellets. In addition, the UO_2 sols are used in sphere-forming studies that serve as a base line for evaluating the behavior of mixed sols. The CUSP process is amenable to scaleup and remote operation. It has been operated throughout the past year in engineering-scale equipment.

Continued development of the APEX process has resulted in significant changes in the flowsheet and in the quality of the plutonia sols produced. It is now possible to prepare sols with lower nitrate-to-plutonium ratios and with larger plutonia crystallites. When these sols are combined with CUSP urania sols, the resulting mixed sols are quite stable, with shelf lives up to about a week; and high-quality $(U,Pu)O_2$ microspheres can be prepared from the mixed sols. The improved APEX sols can also be used to prepare high-quality PuO_2 microspheres. So far, all of these studies have been made on a laboratory scale. Additional investigation and scaleup of the APEX process and preparation of $(U,Pu)O_2$ microspheres are required.

Much of the mixed $(U,Pu)O_2$ for irradiation testing is still prepared by precipitation-peptization processes since equipment is not yet available for the production of enriched urania sols by the CUSP process or for plutonia sols by the APEX process.

7.1 PREPARATION OF UO_2 SOL BY THE CUSP PROCESS

The CUSP process for preparing concentrated ($\geqslant 1\ M$) urania sols directly by solvent extraction[1,2] continues to be a reliable and easily controlled method for the routine preparation of urania sol. The process is being operated to produce 1 M urania sol at two levels, 1 and 4 kg of UO_2 per batch.

During the past year (1) laboratory support was provided for the engineering operations, (2) characterization and aging studies of CUSP sols prepared in engineering-scale equipment were made, (3) several types of contactors for extracting nitrate were tested, and (4) engineering equipment was operated at 1 and 4 kg of UO_2 per batch to prepare sol as required for microsphere-forming studies.

Laboratory Development

Laboratory-scale equipment for the preparation of urania sol. The equipment for preparing urania sol at a 1-kg-per-batch level, which was described last year,[2] has been modified to include a multichambered J-column contactor and phase separator, a 4-in.-diam surge tank mounted directly below a T section at the end of the J column, and a 2-in.-diam riser above the T. The changes permit the extraction column to be operated with the organic phase continuous, as in the engineering-scale

1. *Chem. Technol. Div. Annu. Progr. Rep. May 31, 1969,* ORNL-4422, pp. 203–10.

2. *Chem. Technol. Div. Annu. Progr. Rep. May 31, 1970,* ORNL-4572, pp. 149–55.

equipment, and raise the sol capacity to 1.25 kg of U as 1 *M* urania sol. The equipment will be used to study chemical and operating changes in urania sol preparation by the CUSP process.

Two 5-liter batches of 1 *M* UO_2 sol were prepared to check out the equipment: one (LS-10) was made with a solution of 0.25 *M* Amberlite LA-2 in pure diethylbenzene diluent and the other (LS-11) with a solution of 0.25 *M* Amberlite LA-2 in a diluent composed of 75% diethylbenzene–25% *n*-paraffin (average carbon chain length of 12). As in the initial laboratory development work, better operation was achieved with the mixed diluent; therefore the mixed diluent will continue to be used in future process studies and sol production.

Characterization and aging studies of CUSP UO_2 sols. During engineering-scale development of the CUSP process, characterization and aging-effects studies were a routine part of the laboratory support work. These studies include chemical analyses, periodic measurement of the conductivity of the sols, some viscosity and gelation concentration (i.e., highest concentration to which the sol may be concentrated and still remain fluid) measurements, and a recording of the time required for the sols to gel. The results of any of these measurements, with the possible exception of gelation concentration, are not sufficient in themselves to assure that a given sol is of high quality. Taken together, however, the results can distinguish the better-quality sols from the poorer-quality sols and can establish within reasonable limits whether or not the process is being operated in a manner that will prepare sols with reproducible properties.

The studies included 52 sols produced in a mechanically stirred J-column contactor, 45 sols produced in a spray-column contactor, 8 sols produced in a packed-column contactor containing ceramic Berl saddles, which are aqueous wettable, and 10 sols produced in a packed-column contactor containing non-aqueous-wettable Teflon rods.

The time-temperature-conductivity flow path of the CUSP process was optimized for the J-column contactor, but this path is not necessarily ideal for the other types of contactors used. Throughout these runs, some of the chemical conditions of the CUSP flowsheet were varied slightly in order to evaluate their effect upon the process behavior in the engineering equipment. The sols, therefore, were produced under similar but not identical conditions.

The mechanically stirred J-column contactor produced 1 *M* urania sols with the longest shelf lives. The time required for gelation ranged from 1.5 to 19 months, with an overall average of 5.75 months. The spray-column contactor produced sols of slightly shorter shelf lives, with an average of 3.5 months. The average shelf life of sols prepared in the packed-column contactor with aqueous-wettable packing was 1.9 months. Shelf lives were the same or somewhat less for sols prepared in the packed-column contactor with non-aqueous-wettable packing.

As produced, all of the sols had conductivities very close to the specified 4000 ± 500 micromhos/cm at 25°C, but the initial rates of rise in conductivity were quite variable. Generally, the J-column sols were most stable, with initial rise rates that varied from 100 to 200 micromhos/cm during the first 24-hr period of storage. The sols with the longest shelf lives were usually those with low initial rates of change in conductivity. During the first 24 hr, the spray-column sols had initial conductivity rise rates of 100 to 600 micromhos/cm; the rates for the packed-column sols were 150 to 1500 micromhos/cm. Conductivities and aging times to gelation are reported in Table 7.1 for some typical sols prepared in engineering-scale equipment.[2]

The conductivities of two of the 1 *M* urania sols as prepared and of 2 and 3 *M* urania sols prepared by concentrating the 1 *M* sols are given in Table 7.2. When the sol concentration was increased by a factor of 3, the conductivity (or free acid content) was increased by only 30 to 40%. This is indicative of enhanced nitric acid adsorption by the sol particles as the free acid concentration is increased.

Table 7.3 shows viscosity data obtained for CUSP-ES-55 UO_2 sol and for 2 *M* CUSP-ES-55C-2 and 3 *M* CUSP-ES-55C-3 urania sols prepared by concentrating CUSP-ES-55 sol. The 1 *M* urania sol, with a viscosity of 1.3 cP, and the 2 *M* urania sol, with a viscosity of 2.0 cP, were Newtonian in their behavior (i.e., the viscosity remained constant as the rate of shear was increased). The freshly prepared 3 *M* urania sol had a considerably higher viscosity (~7 cP), and it showed dilatant behavior (i.e., the viscosity increased with increasing rate of shear). After aging a week (or 12 days after the 1 *M* CUSP-ES-55 sol was prepared), the viscosity of the 3 *M* urania sol had increased by a factor of 2 to 16 cP and showed thixotropic behavior (i.e., there was a time-dependent decrease of viscosity with shear). After an additional week's aging, the sol had a viscosity greater than 1000 cP.

The viscosities of the 1 and 2 *M* urania sols were measured on a Brookfield model LVT viscometer equipped with the UL adapter, which consists of a special cup and bob having a 1-mm annulus. The viscosity of the 3 *M* urania sol was measured with the No. 1 bob. When an attempt was made to run the 3 *M* urania sol in the UL adapter, the needle went off scale,

Table 7.1. Conductivities and aging times to gelation for some typical 1 *M* UO_2 sols prepared in engineering-scale equipment by the CUSP process

Run No.	U(IV) (% of total U)	NO_3^-/U mole ratio	Conductivity at 25°C (micromhos/cm)			Aging time to gelation (months)
			As prepared	After aging one month	At the time of gelation	
			J-column contactor			
CUSP-ES-7	88	0.12	3250	6750	7,300	12
CUSP-ES-8	85	0.11	3730		8,500	2
CUSP-ES-45	86	0.11	3560		7,600	6
CUSP-ES-47	86	0.10	3310		8,400	6
CUSP-ES-53	84	0.11	3650	6000	8,030	4
CUSP-ES-55	84	0.11	3990	6110	8,650	6
CUSP-ES-57	83	0.11	3980	6250	9,150	8
			Spray-column contactor			
SCL HB-9	86	0.12	3880	7041	8,600	4.5
SCL HB-13	86	0.13	3060	6430	7,780	2
SCL HB-32	87	0.13	3480	6060	10,100	4.5
SCS HB-43	82	0.18	3751	8500	10,950	1.8
			Aqueous-wettable packed-column contactor			
PC HB-2	86	0.15	5600	9000	9,700	1.5
PC HB-3	83	0.14	2420	6500	9,900	3.5
PC HB-4	85	0.14	5000	9300	10,600	1.3
PC HB-5	88	0.13	7690	7440	9,100	3
			Non-aqueous-wettable packed-column contactor			
PCL HB-55	88	0.12	4440	7090	8,690	3
PCL HB-57	84	0.14	3860	8180		>2

Table 7.2. Comparison of CUSP sol conductivities at concentrations of 1, 2, and 3 *M* UO_2

Sol	Uranium concentration (*M*)	Conductivity at 25°C (micromhos/cm)			
CUSP-ES-55	1	5825	at 17 days[c]	6890	at 38 days[c]
CUSP-ES-55C-2[a]	2	6945		8750	
CUSP-ES-55C-3[b]	3	8065		Gelled	
CUSP-ES-57	1	5285	at 9 days[c]	6270	at 30 days[c]
CUSP-ES-57C-2[d]	2	6420		7780	
CUSP-ES-57C-3[e]	3	7080		8645	

[a]Concentrated two days after preparation of ES-55.

[b]Concentrated seven days after preparation of ES-55.

[c]Time elapsed since preparation of parent sol.

[d]Concentrated one day after preparation of ES-57.

[e]Concentrated five days after preparation of ES-57.

Table 7.3. Comparison of CUSP sol viscosities at concentrations of 1, 2, and 3 *M* UO_2

Sol	Speed of viscometer rotor (rpm)	Viscosity[a] (cP at 26–27°C)				
		As prepared	After aging[b]			
			8 days	12 days	19 days	29 days
CUSP-ES-55	12	1.3	1.4	1.4	1.3	
(1 *M*)	30	1.3	1.4	1.4	1.3	
	60	1.3	1.4	1.4	1.3	
CUSP-ES-55C-2[c]	12	2.0	2.1	2.1	2.3	2.6
(2 *M*)	30	2.0	2.2	2.1	2.3	2.5
	60	2.1	2.2	2.1	2.4	2.6
CUSP-ES-55C-3[d]	12	7.3	16	14[e]	>1000	
(3 *M*)	30	8.4	16	14[e]	>1000	
	60	9.1	15	15[e]	>1000	

[a]Measured on Brookfield model LVT viscometer: No. 1 bob used for 3 *M* sols and the UL adapter used with 1 and 2 *M* sols.

[b]Age from date of preparation of CUSP-ES-55 sol.

[c]CUSP-ES-55 concentrated to 2 *M* two days after the date of its preparation.

[d]CUSP-ES-55 concentrated to 3 *M* seven days after the date of its preparation.

[e]Values obtained after shearing at 60 rpm.

indicating an apparent viscosity of over 100 cP. This is probably the result of "structuring," or secondary flocculation at this concentration.

Removal of extraneous material from urania sols prepared in engineering-scale equipment. The possibility of using *n*-hexanol to separate extraneous materials (crud) from 1 *M* urania sols was examined qualitatively in laboratory experiments. Concurrently, tests were made to determine the effect of such treatment on sol stability. The results indicated that the effectiveness of the *n*-hexanol treatment in separating crud from urania sols depended upon the nature and quantity of crud in the sol. The treatment was less effective for sols containing a white emulsion-like layer on the surface than for sols containing bulky gray material distributed on the surface and throughout the body of the sol. In the latter case, treatment with *n*-hexanol converted dull gray-colored sols to shiny black sols. Furthermore, sols treated in this way showed no indication of formation of an immiscible organic residue when they were dissolved in nitric acid, whereas sols from which all visible crud was removed mechanically produced visible amounts of organic matter on dissolution. The separation of the bulky gray material from an aqueous sol by treatment with *n*-hexanol appeared to be due principally to the differences in densities of the sol, the crud, and the *n*-hexanol. The sol, being the most dense phase, separated rapidly from the *n*-hexanol, whereas the crud, being intermediate in density, settled more slowly and accumulated at the interface.

Possible effects on sol stability due to the extraction of formic acid by the *n*-hexanol treatment were evaluated by determining the concentration at which the sol gelled, since it had been found that the gelling concentration of UO_2 sols is related to the stability of the sol. No marked differences were noted between treated and untreated sols; therefore it appears that the *n*-hexanol treatment has no deleterious effect on sol stability.

The sols used in these studies were prepared in engineering equipment with either spray- or packed-column contactors. The laboratory tests were carried out in an inert-atmosphere glove box to minimize U(IV) oxidation. Equal volumes of well-mixed sol and *n*-hexanol were equilibrated for 5 min in separatory funnels and then allowed to stand 24 hr before the aqueous phase was carefully withdrawn. The removal of all visible crud from untreated sols by allowing them to stand in separatory funnels and then carefully withdrawing the aqueous phase was not as effective. The use of diethylbenzene for crud separation appeared to be less efficient that the use of *n*-hexanol but better than the simple mechanical method.

Engineering Development

Equipment development and evaluation. Development studies were continued to evaluate various types of nitrate extraction contactors in addition to the multichambered J column, which was originally in-

stalled for use in the engineering development of the CUSP process.[2] In each case the contactor and its associated recirculation system for the aqueous phase were simply substituted for the original J column and recirculation system; the remainder of the original equipment was used for continuous solvent regeneration.

A second extraction system, which included a 15-liter surge tank for the aqueous phase, a nitrate extraction column, and a solvent reservoir located directly over the surge tank, was added to an existing extraction unit which has a sol capacity of 4 liters (see Fig. 7.6, p. 155 in ref. 2). Appropriate piping and valves were installed so that the two systems for sol preparation could use the same conductivity probe, heat exchanger, circulating pump, and differential pressure cell. One system has a 4-liter sol capacity (~1 kg UO_2) and the other a 15-liter capacity (~4 kg UO_2). The nitrate extraction columns can be operated as either spray or packed columns. Conversion of the spray column, which is a glass pipe 2 in. ID by 36 in. long, to a packed column was accomplished by simply removing the spray header and filling the column with either aqueous-wettable Berl saddles or Teflon cylinders (¾ in. diam × ¾ in. long) which are not wetted by aqueous solution.

One of the reasons for investigating various types of contactors stems from the fact that a small amount of crud is formed during the operation of the CUSP process (see previous section); also, various modes of operation have been evaluated in attempts to minimize its formation. Possible causes of the formation of the emulsified crud are: (1) overextraction at the surface of the small droplets formed in the spray column, (2) pickup of acetate by the solvent from the HNO_3-$HC_2H_3O_2$ scrub used for solvent cleanup, (3) impurities originally present in the solvent, and (4) emulsification of solvent entrained in the aqueous phase by the centrifugal pump used to circulate the aqueous phase. While good-quality sols were prepared using either the spray or packed columns, no apparent differences were observed in the amount of crud formed. Sol yields based on the amount of uranium in the feed are consistently greater than 90%, but efforts are continuing in both laboratory and engineering studies to minimize crud formation and thus increase the yield.

During the preparation of one sol, a 1 *M* HNO_3–0.4 *M* HCOOH scrub was substituted for the 1 *M* HNO_3–0.4 *M* $HC_2H_3O_2$ scrub that is generally used for solvent cleanup. The sol appeared to be fluid when removed from the equipment, but it gelled in 3 hr. Two operational anomalies were observed during the sol preparation: gas evolution during crystallization was more vigorous than that usually observed, and the conductivity tended to level off at 3900 micromhos/cm during the final nitrate extraction step. An infrared spectrophotometric examination showed no significant differences between the solvent used during the run and the fresh, unused solvent. Chemical analysis of the aqueous and organic samples taken during the run provided no clue as to what caused the rapid gelation of the sol.

A Vanton Flexi-Liner pump with a Viton Flexi-Liner and Teflon body is being evaluated as a possible replacement for the centrifugal pump used to circulate the aqueous phase. Pumping is accomplished by a rotor mounted on an eccentric shaft that rotates within the liner, thus creating a progressive squeegee on the fluid trapped between the liner and the body block. The pump will circulate gas-liquid mixtures without cavitation and will not emulsify mixtures of immiscible liquids. A pump of this type has been installed in a loop and has been operated intermittently to pump UO_2 sol for a total of 177 hr at 60°C with no operational difficulties. Evaluation of the pump in the sol preparation equipment will be continued.

Solvent evaluation. Several compositions of solvent used to extract nitrate in the CUSP process were investigated. It was found that the use of 0.5 *M* Amberlite LA-2 promotes the formation of emulsion and that the solvent becomes much darker and in less time than when 0.25 *M* Amberlite LA-2 is used. The use of pure diethylbenzene as the diluent instead of 75 vol % diethylbenzene–25 vol % *n*-paraffin also tends to promote emulsions. It is concluded that the most satisfactory solvent is Amberlite LA-2 at a maximum concentration of 0.3 *M* in 75 vol % diethylbenzene–25 vol % *n*-paraffin.

When 0.3 *M* Amberlite LA-2 in 75 vol % diethylbenzene–25 vol % *n*-paraffin is used as the extractant and the regeneration cycle consists of a 1 *M* HNO_3–0.4 *M* $HC_2H_3O_2$ scrub, water wash, and 1 *M* Na_2CO_3–1 *M* NaOH scrub, the average loss of amine is 0.06 to 0.10 mole per kilogram of UO_2 prepared as 1 *M* sol. The amine concentration can be satisfactorily maintained at an essentially constant value by periodic additions of Amberlite LA-2 to the solvent storage tank.

The loss or uranium to the HNO_3-$HC_2H_3O_2$, water, and carbonate-caustic effluent streams has been 0.5–1.0%, 0.03–0.06%, and 0.03–0.4% respectively. The HNO_3-$HC_2H_3O_2$ scrub effluent (0.85 *M* HNO_3, 0.3 *M* $HC_2H_3O_2$, 0.5–1.0 g $\bar{U}$ per liter) can be used to clean out the spray-column equipment after the solvent and sol have been drained. This will minimize the volume of aqueous waste generated when preparing UO_2 sol containing enriched uranium.

Preparation of 1.8 *M* UO_2 sol by the CUSP process. The preparation of urania sols at concentrations greater than 1 *M* would greatly increase the capacity not only of the sol-making equipment but also of the microsphere-forming column. In a preliminary investigation, 8 liters of a solution that was 1.8 *M* in U(IV), 3.83 *M* in NO_3^-, 1.08 *M* in $COOH^-$, and 0.1 *M* in urea was prepared in the engineering-scale batch slurry reductor without difficulty in 3 hr. A small amount of whitish-green precipitate, which prevented draining the solution through the 10-μ-pore stainless steel filter, was produced and made it necessary to siphon the solution out of the reductor.

The U(IV) feed solution was divided into two 4-liter batches, and sols were prepared on successive days in the spray-column extraction equipment by a modified CUSP process. The first nitrate extraction was carried out at 40°C and continued until a conductivity of ~40,000 micromhos/cm was attained; at this time, the aqueous phase was heated while the nitrate extraction was continued. Crystallization commenced at 58 to 60°C, as evidenced by gas evolution and a color change from dark green to black. The solvent flow was regulated during crystallization to maintain the conductivity at 30,000 to 40,000 micromhos/cm for the first run and at 35,000 to 45,000 micromhos/cm for the second run. After crystallization was complete, nitrate extraction was continued until the conductivity was decreased to ~20,000 micromhos/cm for both preparations. Nitrate extraction was then stopped by turning off the solvent flow. The third nitrate extraction was carried out at 25°C, and nitrate was extracted until a conductivity of 5905 micromhos/cm was attained for the first run and 3830 micromhos/cm for the second. The NO_3^-/U mole ratios were 0.18 and 0.12 for the first and second sols respectively; the U(IV)/U ratios were 0.84 and 0.87 respectively. Both sols were very fluid, had long shelf lives (1.5 months for the first and 1.0 month for the second), and produced good spheres in the forming column. Additional work is required, especially to optimize the feed preparation step.

7.2 DEVELOPMENT OF THE UO_2-PuO_2 SOL-GEL PROCESS

During the past year, laboratory work to develop a solvent extraction process for the preparation of mixed UO_2-PuO_2 sol was continued. Emphasis was centered on solvent extraction, since this type of process should be readily amenable to scaleup and to the remote operations necessary for fabricating LMFBR recycle plutonium into reactor fuel. In the process selected for study, CUSP-prepared urania sol is pretreated to remove excess formate and is then mixed in the proper proportions with a plutonia sol prepared by an alcohol extraction process (i.e., APEX). During this report period, development efforts were concentrated on (1) modifications of the APEX process to produce low-nitrate sol, (2) laboratory experiments to prepare UO_2-PuO_2 microspheres by the CUSP-APEX mixed-sol process, and (3) mixed-sol compatibility studies.

The results of these studies have been very encouraging in that we have discovered that the primary crystallites in APEX sols can be arranged in aggregated micelle structures, which result in rapid denitration and crystallite growth when the sols are taken to dryness and heated. The resulting low-nitrate sols can be used to prepare mixed UO_2-PuO_2 sols with greatly improved shelf lives or to prepare pure plutonia microspheres.

Evaluation and Modification of the APEX Process

In continued studies of the APEX process, we evaluated two process modifications that have resulted in improved sol characteristics. The first modification results in high-nitrate sol that exhibits increased sol stability; however, the second modification produces low-nitrate sol by virtue of a substantial increase in the PuO_2 crystallite size. Sols of this type mixed with urania sols produce mixed UO_2-PuO_2 sols with greatly improved shelf lives. These low-nitrate plutonia sols can also be used to prepare pure plutonia microspheres, which has not been possible with high-nitrate plutonia sols.

The first modification differs from the APEX process described last year[3] in that the feed solution is extracted continuously at room temperature to a NO_3^-/Pu mole ratio of ~0.8, whereas the previous procedure consisted of an initial extraction to a NO_3^-/Pu mole ratio ≃2.5, digestion at 100°C, and then a second extraction to a NO_3^-/Pu mole ratio ≃1.0. In both cases, the dilute sols are concentrated by evaporation to a plutonia concentration of about 1 *M*. The primary advantage of this modification is that the sol shelf life is greatly improved. Regular APEX sols gel in ~33 days, but sols prepared by continuous extraction remain fluid for ~120 days. The shelf life of mixed UO_2-PuO_2 sols prepared with this type of sol was also noticeably improved (see next section).

The second, and principal, modification studied was the effect of seeding, in which a portion of a normally prepared APEX sol is added to feed solution during the

3. *Chem. Technol. Div. Annu. Progr. Rep. May 31, 1970*, ORNL-4572, p. 157.

initial extraction of a subsequent sol preparation. We discovered that this technique can produce sol in which the primary crystallites are arranged in aggregated micelle structures and that these structures result in rapid denitration and crystallite growth when the sols are taken to dryness and heated.

In initial experiments, it was demonstrated that low-nitrate sols can be prepared (NO_3^-/Pu mole ratio $\cong 0.2$) with average crystallite diameters of ~60 Å when a sol with the appropriate aggregate structure is taken to dryness and heated for 30 to 90 min at temperatures in the range of 180 to 230°C. This is in direct contrast to the behavior of regular APEX sols or high-nitrate sols prepared by the precipitation process; these sols show no detectable change in crystallite size or any significant reduction in NO_3^-/Pu mole ratio when heated at the above temperatures for much longer times. It was also shown that the size of the PuO_2 crystallites obtained is related to the micelle size and the completeness of micelle formation. These factors also appear to relate to the time and temperature required for crystallite growth. Single seeding experiments produce sol in which a micelle size of 50 to 75 Å converts to crystallites 35 to 40 Å in diameter; however, sol crystallites as large as 50 to 60 Å have been obtained by several techniques. It was found that larger micelles (which form larger crystallites) can be obtained by double seeding, in which the product sol from a first seeding experiment is used as seed in a subsequent sol preparation. It was also demonstrated that the effect of multiple seeding can be accomplished in a single run by incremental addition of the feed solution during continuous extraction. A multiple seeding effect is obtained because extraction is continued after each feed addition until plutonium polymerization occurs before the next feed addition is made. There was no penalty in total extraction time as a result of this technique, and an excellent sol was obtained in which the average crystallite size appeared to be greater than 60 Å.

Electron micrographs and electron diffraction patterns were obtained for all sols before and after thermal denitration, and it was apparent from these data that several process variables are significant in the development of an optimum micelle structure. The principal variation in micelle structure was the degree of micelle formation, that is, the presence of both aggregated micelles and unaggregated plutonia crystallites as opposed to complete aggregation of crystallites. It is of interest to note that sol which is only partially aggregated generally exhibits crystallite growth and rapid denitration similar to fully aggregated sol; however, comparative rates for the various types of material have not as yet been determined. Because of this variation, studies to date have been primarily concerned with the effect of process variables on micelle structure. Although additional work will be required to completely optimize key variables, we can now prepare sols with partially or fully aggregated micelles in single and double seeded experiments by the appropriate selection of process parameters.

Two principal variables which relate to the degree of aggregation are the amount of seed polymer used and the extraction rate. Minimum seed concentrations of 20% for single-seeding and 25 to 30% for double-seeding experiments are required for complete crystallite aggregation. The effect of higher seed concentrations has not been extensively investigated; however, it might be anticipated that an excessive seed concentration would result in smaller micelles. The rate of nitrate extraction also appears to be critical. This was evaluated by using batch sizes of 250 and 500 ml, which required different times to extract to the same end point. Since the concentration of plutonium and HNO_3 in the feed solution would also affect the extraction rate, these were kept nearly constant in all experiments. The plutonium feed concentration varied from 26.5 to 28.0 mg/ml, and the HNO_3 concentration was about 0.6 to 0.7 *M*. Feed of this composition had an initial conductivity of about 100 millimhos/cm. In the APEX extraction equipment used, about 4 hr of continuous extraction was required to reduce the conductivity of a 250-ml batch from 100 to 14; about 6 hr was required for a 500-ml batch. Complete crystallite aggregation has been obtained only when the 500-ml batch size was used. Slower extraction rates have not been investigated.

Most of the other variables investigated do not appear to be highly critical. The seed polymer can be added to the feed solution prior to extraction or during extraction, before the conductivity of the feed has been reduced much below 70 millimhos/cm. Poor results were obtained when seed was added to feed that had already been extracted to a conductivity of 60 millimhos/cm. The NO_3^-/Pu mole ratio of the seed polymer can vary from 0.7 to 1.2, and the age of the seed polymer is not critical, providing that gelation has not occurred. There were no appreciable differences in seeded sols prepared by continuous extraction at room temperature and seeded sols prepared by a procedure which incorporates a digestion step after extraction to a NO_3^-/Pu ratio of 2.5; we have now standardized on the continuous extraction process because it is simpler. Plutonium feed concentration is not highly critical in that the plutonium concentration can be decreased from 28 to about 15 g/liter. Somewhat higher concen-

trations can also be used if an appropriate batch size is selected; however, plutonium extraction becomes excessive when the concentration exceeds about 30 g/liter.

Thermal denitration and crystallite growth studies as a function of micelle structure and baking temperature have not been completed; however, several significant characteristics have been demonstrated. The NO_3^-/Pu mole ratio of the sol prior to evaporation to dryness is important. The optimum ratio is in the range of 0.7 to 0.9. Higher ratios appear to decrease the denitration rate, and values around 0.6 or less result in plutonia solids that will not resuspend in water after thermal denitration.

As previously mentioned, the aggregated micelle structure promotes rapid denitration during baking. For example, a completely aggregated sol prepared by double seeding will denitrate to a NO_3^-/Pu mole ratio of ~0.3 in 15 min at 230°C, and the sol will denitrate to its minimum value (NO_3^-/Pu mole ratio = 0.18–0.20) in 90 min. By comparison, the NO_3^-/Pu ratio of regular (unaggregated) APEX sol is still 0.4 after 4 hr of baking at this temperature. Aggregated sols can also be denitrated at lower temperatures. Minimum nitrate-to-plutonium mole ratios were obtained in about 2 and 5 hr at baking temperatures of 210 and 195°C respectively. Unaggregated sol requires at least 24 hr of baking time at 195°C, and it is doubtful that useful sol could be prepared at all at this denitration rate.

One very important feature of obtaining large crystallites by this method and at these temperatures is that the dried sols are quite insensitive to overheating. In general, the sols can be baked at least twice as long as required without adversely affecting the final sol characteristics or changing the NO_3^-/Pu mole ratio significantly. This represents a significant processing advantage as compared with the standard baking procedure for unaggregated sols where baking time is critical, since overbaking results in solids that will not resuspend.

CUSP-APEX Mixed-Sol Stability Tests and Microsphere-Forming Experiments

A series of tests was made with various products prepared by the modified APEX process to evaluate the effects of low-nitrate concentration and larger crystallite sizes on the stability of mixed UO_2-PuO_2 sol. The shelf life of mixed sol prepared from low-nitrate APEX sol (NO_3^-/Pu mole ratio = 0.2–0.4) and CUSP sol was five to eight days at 25°C. This compares with a shelf life of only 30 min for mixed sols prepared with regular APEX sol (NO_3^-/Pu ≅ 0.7). Because of the improved shelf life, a series of mixed CUSP-APEX (low-nitrate) microsphere-forming runs was made in which the sols were not cooled to 5°C, as is required when regular APEX sol is used. High yields (90–95%) of calcined microspheres were consistently obtained in these experiments. Pure plutonia microspheres were also readily prepared from low-nitrate APEX sols. This has not been possible with high-nitrate plutonia sols, including regular APEX sols, because of extensive cracking and disintegration of the spheres during calcination.

Mixed-sol stability tests. The effects of APEX sol characteristics on mixed UO_2-PuO_2 sol shelf life is shown in Table 7.4. When sols were baked at high temperatures, they were evaporated to dryness slowly at temperatures below 100°C. The dry solids were then rapidly heated to the desired temperature, held at this temperature for 30 min, removed from the heat, and allowed to cool. Sols which were not dried were concentrated to ~1 *M* PuO_2 by evaporation and

Table 7.4. Effects of APEX sol characteristics on mixed (UO_2-PuO_2) sol shelf life

APEX sol			Mixed UO_2-PuO_2 sol shelf life at 25°C
Preparation	Denitration temperature (°C)	NO_3^-/Pu mole ratio	
Regular APEX	Not dried	0.71	30 min
Continuous extraction APEX	Not dried	0.67	1 hr 50 min
Single seeding, continuous extraction	~230	0.39	132 hr (5½ days)
Double seeding, continuous extraction	Not dried	0.64	1 hr
Double seeding, continuous extraction	~160	0.63	2 hr 30 min
Double seeding, continuous extraction	~180	0.50	10 hr
Double seeding, continuous extraction	~200	0.41	48 hr
Double seeding, continuous extraction	~220	0.20	138 hr (5¾ days)
Seeding by multiple feed addition	~230	0.19	192 hr (8 days)

extracted three times with *n*-hexanol. Ten volumes of *n*-hexanol were contacted with one volume of sol during each extraction. This procedure was expected to remove nearly all of the extractable HNO_3. Mixed-sol stability tests were made by mixing sufficient PuO_2 sol with CUSP sol (which had been freshly contacted with an equal volume of water-saturated *n*-hexanol) to provide a total metal concentration of 0.95 *M* (80% UO_2, 20% PuO_2), and the sols were aged at 25°C until gelation occurred.

There appears to be some advantage in preparing high-nitrate APEX sol by continuous extraction instead of by the regular procedure (which includes a digestion step at 100°C) since the shelf life of the mixed sol is increased. However, this improvement is minor compared with the improvement attainable with seeded APEX sols that have been denitrated by baking at ~220°C.

It is significant that mixed-sol stability is comparable for single- and double-seeding experiments even though the NO_3^-/Pu mole ratio is about twice as high, and the crystallite size is smaller, for sol prepared by single seeding. The data also demonstrate that there is no particular advantage in preparing seeded sols unless they are baked; however, it is interesting that a marked improvement in mixed-sol stability occurs at relatively low baking temperatures even though only partial conversion to large crystallites occurred at temperatures below 220°C. The excellent results obtained with sol prepared by multiple feed addition is especially significant because it affords a simple method for preparing this type of sol.

Microsphere forming. A series of laboratory tests was made to demonstrate the formation of microspheres from mixed UO_2-PuO_2 sols prepared from low-nitrate APEX sols. A number of mixed sols containing 80% UO_2 and 20% PuO_2 were prepared from two APEX sols and two CUSP sols. Good calcined microspheres were obtained in yields of 90 to 95% in eight consecutive experiments from mixed sols prepared from one of the CUSP sols (SCLHB-40) and either of the APEX sols; however, we were unable to prepare acceptable microspheres from mixed sols prepared from the other CUSP sol (SCSHB-45).

The NO_3^-/Pu mole ratios of the APEX sols were 0.19 and 0.20. All experimental conditions were the same as those described last year,[4] except that the sols were not cooled but were kept at room temperature. The urania sols were extracted with an equal volume of water-saturated *n*-hexanol to remove extractable HCOOH just prior to mixing the sols.

Two APEX sols were also used to prepare pure plutonia microspheres. The NO_3^-/Pu mole ratios were also 0.19 and 0.20. High yields of calcined microspheres were obtained in these experiments, and all products were completely crack free. Surfactant concentrations in the drying alcohol were the same as those used in the mixed-sol experiments, namely, 0.15 vol % Span 80 and 0.40 vol % Pluronic L-92.

Mixed-Sol Compatibility Studies

Studies were continued in an effort to understand the variables that affect the shelf life of mixed CUSP-APEX sols and the mechanisms responsible for gelation. In data reported last year,[5] we demonstrated that mixed-sol instability is a function of formic acid concentration, and various tests indicated that the instability is related to a redistribution of the nitrate and formate anions when the urania and plutonia sols are mixed. The initiating step appeared to involve a preferential association of $HCOO^-$ (or HCOOH) with PuO_2 crystallites and a release of NO_3^-. During this report period, a study of colloidal charge was initiated. The results obtained correlate well with previous work and tend to substantiate that anion redistribution and imbalance are related to mixed-sol gelation.

The instrument used for this work is a Streaming Current Detector manufactured by Waters Association, Inc. The readout for the instrument is a microammeter which is calibrated in arbitrary units. The exact relationship between the readout and colloidal charge or zeta potential is at present undetermined. However, the charge sign and magnitude are indicated, and changes in charge can be determined. Successful applications of the instrument have involved the titration of sols with charge-influencing materials. Titrations are carried out in the same fashion as acid-base titrations in that continuous readings are obtained while the charge-influencing material is being added to the sol.

It was determined that each of the CUSP, APEX, and mixed CUSP-APEX sols has a positive charge, and the Streaming Current Detector was used in a series of experiments in which APEX and CUSP sols were titrated with HNO_3 or HCOOH. When HNO_3 was added to either an APEX or a CUSP sol, a decrease in charge was obtained. Similarly, a decrease was obtained when CUSP sol was titrated with HCOOH. However, in

4. *Chem. Technol. Div. Annu. Progr. Rep. May 31, 1970,* ORNL-4572, pp. 164–66.

5. *Chem. Technol. Div. Annu. Progr. Rep. May 31, 1970,* ORNL-4572, pp. 158–64.

contrast to this behavior, an increase was obtained when APEX sol was titrated with HCOOH. It was shown that these changes were caused primarily by the HNO_3 or HCOOH added since simple dilution of the sols with water results in a small increase in the streaming-current reading.

Streaming-current readings were obtained for mixed CUSP-APEX sol [80% UO_2–20% PuO_2] as a function of time after mixing. The results of a typical experiment are given in Fig. 7.1. Immediately after mixing, there is a rapid increase in streaming-current reading, followed by a brief period during which the reading decreases and then a final increase until the sol gels (about 30 min after mixing). After gelation, there is essentially no change in the reading. The change in streaming-current reading is accompanied by a continuous increase in apparent pH until the sol gels (Fig. 7.1, lower curve).

The increase in streaming-current reading when the sols are first mixed again indicates that sorption of HCOOH by PuO_2 is the initiating reaction involved in mixed-sol gelation, since an increase in reading was obtained only when plutonia sol was titrated with HCOOH. It was shown previously[5] that the addition of HCOOH to plutonia sol results in the release of nitrate; however, since the apparent pH of the mixed sol increases, it appears that nitrate is being sorbed by the urania crystallites more rapidly than it is being released from the plutonia.

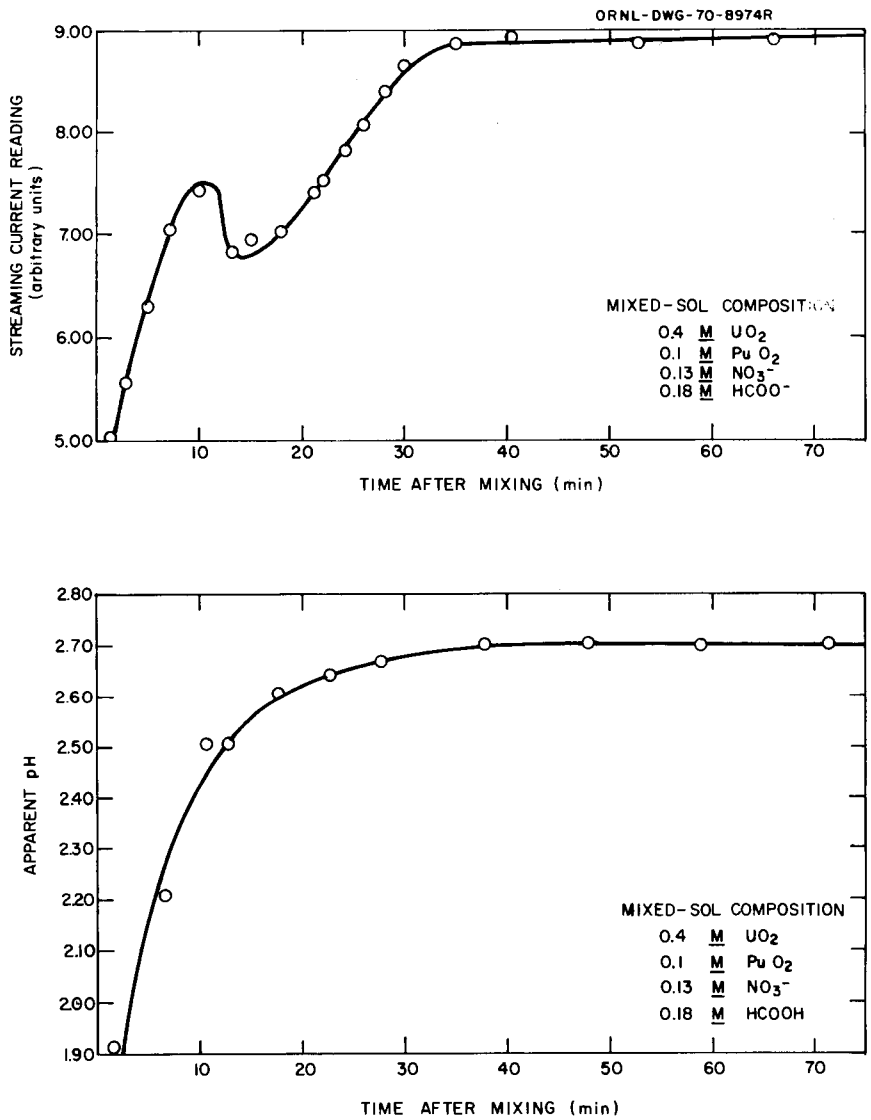

Fig. 7.1. Streaming current detector reading and apparent pH of mixed CUSP-APEX sol as a function of time after mixing.

The shape of the Streaming Current Detector reading curve is characteristic of mixed UO_2-PuO_2 sols and appears to reflect changes in sorption rates which result from accompanying changes of anion concentrations in the aqueous phase. After the initial rise in the Streaming Current Detector reading, the curve goes through a minimum. This suggests that nitrate sorption by the UO_2 component may be the predominant mechanism for a short period of time. The subsequent increase in the reading again reflects continued HCOOH sorption by the PuO_2. The continuous increase in the apparent pH curve indicates that HNO_3 is being continuously depleted from the aqueous phase of the sol until gelation of the sol occurs.

If the indicated anion rearrangement occurs, sol gelation could be expected from at least two mechanisms. The plutonia component could gel, since it has been demonstrated that the addition of HCOOH to APEX sol, followed by extraction of HNO_3 from the aqueous phase, results in sol gelation.[6] (In the mixed sol, the HNO_3 is apparently removed by sorption on the urania crystallites.) Similarly, the urania component could gel due to an anion deficiency or HCOOH depletion since previously obtained data indicate that PuO_2 can sorb more than twice as much $HCOO^-$ as NO_3^- and that CUSP sol will gel as a result of extracting excessive amounts of HCOOH.[7] If the plutonia component in a mixed (20% PuO_2–80% UO_2) sol sorbed the maximum possible amount of HCOOH, the anion-to-urania mole ratio would be decreased from ~0.55 to <0.37.

Several techniques have been evaluated to analyze streaming-current data obtained by titrating PuO_2 sols with HNO_3. The relationships found are of interest because they indicate that there is an equilibrium between nitrate in the aqueous phase and nitrate sorbed on plutonia crystallites and that the equilibrium is a function of the total nitrate concentration. Based on one interpretation of the data, it appears that it should be possible to determine nitrate distribution and equilibrium constants; however, since the exact relationship between Streaming Current Detector readout and colloidal charge is not known, the validity of a given interpretation is difficult to substantiate. Conductivity and pH studies were also made as an aid in the interpretation of streaming-current data. Several experimental techniques were evaluated, and the results obtained indicate that conductometric titrations of PuO_2 sols may be particularly useful.

The analysis of conductometric titration data and their correlation with streaming-current data has not been completed, but it is significant that this work also indicates a nitrate equilibrium which can be plotted in the form of linear Langmuir adsorption isotherms. A preliminary interpretation of the titration curves obtained indicates that this technique can be used to determine the HNO_3 concentration in PuO_2 sols and the equilibrium between NO_3^- in the aqueous phase and NO_3^- sorbed on the plutonia.

7.3 MICROSPHERE-FORMING STUDIES

The optimum conditions for forming a sol into gel microspheres change in a complex manner as the properties of the sol vary. When a sol with specified properties is formed into gel spheres, the composition of the organic drying medium is the principal operating variable. The successful continuous operation of a sphere-forming column requires that the alcohol composition be controlled within satisfactory ranges. This is largely empirical and requires demonstration in three stages: (1) satisfactory initial operation, (2) control of surfactant depletion, and (3) control of excessive accumulations of surfactant degradation products or impurities. Tests to develop and demonstrate these stages were continued for the UO_2 sols prepared by the CUSP process. Investigations involving the first stage were made primarily in small laboratory columns. Large-column studies were primarily concerned with investigations of the second and third stages.

The formation of a good sphere requires that the sol drop be suspended until enough water is extracted to cause gelation. Nearly all of our successful operations with CUSP UO_2 sols have been with 2-ethyl-1-hexanol (2EH) containing Span 80 and Ethomeen S/15 as surfactants. The times required for gelation can be calculated from mass transfer considerations (see Sect. 6.3). For CUSP sols, from 4 to 40 min is required to form gel spheres that will calcine to high-density UO_2 spheres 200 μ in diameter, and from 10 to 100 min is required to form gel spheres that will calcine to 500-μ-diam UO_2 spheres. The principal variables affecting the gelation time for a given sol are the sphere diameter, temperature of the 2EH, and water content of the 2EH. The higher 2EH temperatures greatly reduce the gelation times and often improve the surface appearance of the gel spheres but may increase the amount of clustering or cracking.

6. *LMFBR Fuel Cycle Studies Progress Report for May 1970, No. 15*, ORNL-TM-3018, pp. 38–39.

7. *LMFBR Fuel Cycle Studies Progress Report for August 1969, No. 5*, ORNL-TM-2671, pp. 65–66.

Of the four principal operating problems discussed previously,[8] the two most troublesome ones for preparation of UO_2 spheres from CUSP sols are:

1. Increasing amounts of sticking, clustering, or coalescence as column operation is continued, owing to a combination of loss of Span 80, extraction of formic acid from the UO_2 sol into the 2EH, and accumulation of surfactant degradation products.
2. Excessive cracking during drying and firing, even though the cracking is not noticeable in the gel. This cracking is dependent upon the size of the microspheres produced and does not present any significant problem in the production of UO_2 spheres 250 μ or less in diameter.

Cracking of the spheres can be due to a number of causes, and interactions between two or more causes can give confusing results. Principal factors that we have found to favor cracking include:

1. large particle diameters;
2. high surfactant concentrations in the 2EH;
3. high rates of water extraction resulting from the use of dry 2EH or high temperatures in the sphere-forming column;
4. oxidized, thixotropic, aged, or otherwise inferior sols;
5. formation and subsequent breakup of clusters of sol or gel particles in the forming column;
6. excessive oxidation or thermal shocks during drying and firing of the gel microspheres;
7. incomplete extraction of H_2O due to inadequate time of fluidization in the forming column;
8. excessive impurities in the 2EH, such as degradation products.

The size of the microspheres is generally specified as a product requirement, but the other factors can be varied within limits to optimize the production of high-quality product. Surfactant concentrations are limited to those which will satisfactorily control the sticking-clustering-coalescence problems.

Small-Column Studies

Laboratory-scale studies of microsphere forming in small columns were continued. Several factorial experiments, in which a limited number of variables were examined in all possible combinations, were completed. Experiments involving other variables individually were also carried out, and these investigations demonstrated benefits derived from higher column operating temperature and longer holding times in the column.

Factorial experiments have been used in order to obtain systematic coverage over a given set of variables once the approximate ranges have been established. Data from the factorial experiments are readily amenable to statistical evaluation and can be used to determine the presence of cross effects (interactions between variables). The first factorial experiment was carried out under the Thorium Fuel Cycle Program and was performed with ThO_2-UO_3 sols.[9,10] The second factorial experiment pertained to both the thorium and the uranium fuel cycles and involved ThO_2 and ThO_2-UO_3 sols and included a partial coverage of a CUSP urania sol. The early results have been reported elsewhere,[11] and a full report will be available soon;[12] therefore, only a brief summary is given here. Concentrations of four components in the 2EH were investigated, three of them at two levels and the fourth at three levels:

Ethomeen S/15 concentration	0.05 and 0.5 vol %
HNO_3 concentration	0.001 and 0.01 *M*
H_2O concentration	0.5 and 1.7 vol %
Span 80 concentration	0, 0.05, and 0.5 vol %

Used in all possible combinations, this gives a total of 24 different compositions ($2^3 \times 3^1$). The uranium-containing sols produced deformed or cracked microspheres to a far greater extent than did the thoria sol. For ThO_2-UO_3 sols, the best results were obtained with a low Ethomeen S/15 content, complete exclusion of Span 80, and within a pH range of about 3 to 4 (0.001 *M* HNO_3); the two water content levels were equally satisfactory. For the UO_2 sol, some Span 80 was necessary to prevent clustering, and the undesirable side effects of the Span 80 relative to sphere deformation were counteracted by Ethomeen S/15. Statistically,

8. *Chem. Technol. Div. Annu. Progr. Rep. May 31, 1970,* ORNL-4572, pp. 166–68.

9. *Chem. Technol. Div. Annu. Progr. Rep. May 31, 1969,* ORNL-4422, pp. 192–97.

10. K. J. Notz and A. B. Meservey, *Microsphere Forming Conditions for ThO_2-UO_3 Sols: A Factorial Experiment,* ORNL-TM-2516 (August 1969).

11. R. G. Wymer and A. L. Lotts, *Status and Progress Report for Thorium Fuel Cycle Development for January 1, 1969 through March 31, 1970,* ORNL-4629, pp. 43–49 (February 1971).

12. Albert B. Meservey and Karl J. Notz, *Conditions for the Formation of Sol-Gel Microspheres: Further Factorial Experiments on ThO_2-UO_3, ThO_2, and UO_2 Sols,* ORNL-TM-2957 (February 1971).

significant primary effects were found for Span 80, Ethomeen S/15, and HNO_3. First-order cross effects (two factors) were found for Span 80–Ethomeen S/15, Span 80–HNO_3, and Ethomeen S/15–HNO_3.

It was established in several factorial experiments that microspheres can be formed from CUSP UO_2 sols in 2EH which has a pH within the range of 2 to 6, a temperature of 30 to 55°C, and contains ~0.3 vol % Span 80 to prevent clustering, ~0.1 vol % Ethomeen S/15 to smooth the surfaces and prevent distortions caused by Span 80, and 0.5 to 1.5 vol % H_2O. Experimental changes in sol manufacturing methods resulted in changes in microsphere appearance and behavior. Raising the temperature of the 2EH to 55°C greatly increased production rates, without damage, by shortening the drying time required in the column. The higher temperature also eliminated Span-caused pits at low pH, thus making the pH dependence less critical. Urania microspheres formed at 55°C were fired successfully to 1200°C.

An important cause of cracking in unfired UO_2 microspheres and of cracking in the early stage of firing was found to be inadequate residence time in the forming column. This resulted in residual moisture in the gel and made it susceptible to rapid oxidation on slight exposure to air. Oxidation and cracking did not occur when the gel spheres were more thoroughly dried in the column, either by longer residence times or by higher column temperatures. Cracking also occurred when the gel microspheres from the sphere-forming column were dried too rapidly in argon. This type of cracking was a gel-layer breakage along a toroidal path, as described earlier for ThO_2-UO_3 sols.[10]

By saturating the 2EH with air, smooth-surfaced UO_2 microspheres were produced from some sols which normally yielded badly chipped microsphere surfaces. This was accomplished by bubbling air through the recirculating stream of 2EH in a vessel remote from the forming column and returning the air-saturated but bubble-free 2EH to the forming column. Enough oxygen was thus present in the 2EH (at 55°C) to produce a chip-resistant gel coating but not enough to penetrate the spheres and cause them to crack. These microspheres were successfully fired without breakage.

The shelf life of UO_2 sols can be greatly increased by storing them at a low temperature (e.g., 3°C), and it was demonstrated in a controlled set of experiments that storage in this fashion had no effect on sphere-forming properties.

Alcohol Recycle and Large-Column Studies

The large-column studies of the formation of microspheres from CUSP UO_2 sols have been concerned primarily with development and testing of procedures for treating the 2EH so it may be continuously reused. At the beginning of most of these tests, the 2EH was adjusted to contain 0.3 or 0.4 vol % Span 80, 0.1 vol % Ethomeen S/15, and about 1.2 vol % water. New 2EH containing these amounts of additives gave good UO_2 gel spheres when the pH of the 2EH was in the range from 3 to 5.7 and for 2EH temperatures up to 55°C. However, gel spheres large enough to produce high-density UO_2 spheres with diameters of 550 μ are difficult to dry and fire without cracking. If 2EH from the sphere-forming column is treated only by distillation to remove the water, it can be recycled only a short time because of the following changes in composition:

1. buildup of formic acid in the 2EH by extraction from the UO_2 sol, which results in coalescence, clustering, and sticking;
2. loss of Span 80 and Ethomeen S/15 by reactions with nitrate in the still;
3. accumulation of surfactant degradation products, which contribute to cracking problems and to increased coalescence, clustering, and sticking.

It has been found that formic acid and nitric acid can be removed from 2EH by ion exchange. During the large-column studies with CUSP sols, 2EH from the forming column was passed through a column of ion exchange resin before it was distilled to remove water. This technique prevents the accumulation of excessive amounts of formic acid in the 2EH and eliminates the degradation of Ethomeen S/15 which takes place if nitric acid is allowed to remain in the 2EH during distillation. Continuous recycle of 2EH for more than 100 hr was demonstrated without difficulty from accumulations of formic acid or from loss of Ethomeen S/15. Unfortunately, Span 80 is lost during this treatment, probably by hydrolysis in the ion exchange column. Periodic additions can be made to replace the Span 80, but its degradation products accumulate in the 2EH. We now plan to limit the accumulation of Span 80 degradation products to tolerable levels by continuously bleeding off a small stream of the 2EH and replacing it with purified 2EH containing the appropriate amounts of surfactants. For each volume of sol feed, it is necessary to circulate about 100 volumes of 2EH through the ion exchange–distillation loop in order to control the water concentration in the 2EH, but we expect that a much lower rate of continuous replacement of 2EH is required to control the concentrations of surfactants and surfactant degradation products. However, the waste stream will be large

enough to warrant recovery and purification of 2EH for reuse.

Distillation is being considered for purifying waste 2EH so it may be recycled to the sphere-forming column. When waste 2EH is distilled at temperatures ranging from 100 to 180°C (depending upon the water content), both the 2EH and water can be recovered in the distillate while the surfactants and many of the degradation products remain in the still bottoms. By means of the azeotropic distillation method normally used, water can then be removed from the 2EH. It has been shown that 2EH recovered by this method contains essentially no surface-active materials. However, analyses by gas chromatography show that the recovered 2EH is only 99.4% pure compared to 99.93% purity for the 2EH as received from the manufacturer. This amount of impurity is comparable to, or larger than, the amounts of surfactants which we add. Thus, it may have an important effect on sphere forming. The boiling point of the impurity is somewhat lower than the boiling point of 2EH, and experiments are in progress to remove the impurity by further distillation. Some of the 2EH recovered by this double distillation method was used to form spheres from CUSP sols. Column operation was satisfactory, and good gel spheres were formed. These spheres cracked when they were fired, but this is not necessarily an indication that the purified 2EH was unsatisfactory since comparable samples prepared with new 2EH also showed excessive cracking. Continued development is required to perfect the distillation method of purification and to test the quality of the purified 2EH.

Urania spheres have been prepared from about a hundred different CUSP sols. We have been able to correlate the behavior of gel-sphere formation with changes in the method of sol preparation and with sol properties. However, drying and firing procedures have not been sufficiently controllable or reproducible to correlate sphere cracking with sol preparation methods and properties. The standard CUSP process consistently forms reproducible sols, so that the variations from sol to sol do not appreciably affect the sphere-forming behavior. If the sol viscosity, conductivity, U(IV)/U ratio, and the amount of entrained organic material, or crud, are within normal ranges, sphere-forming behavior is almost always normal. Difficulties are usually encountered with thixotropic sols; therefore, sols should have sufficiently long shelf lives to remain fluid until they are formed into spheres. Sols with large amounts of entrained organic material, or crud, high or low conductivities, or low U(IV)/U ratios almost always caused difficulties in sphere forming; thus these variations in sol properties should be avoided.

Preparation of Microspheres in Nonfluidized-Bed Columns

Fewer problems are usually encountered if gel spheres are not fluidized in the forming column. Coalescence, sticking, and clustering are much less troublesome, owing to the much lower particle concentrations and the absence of particle-to-particle interactions. However, the nonfluidized operation is only practical for smaller spheres, and small spheres are generally less prone to cracking.

Urania spheres up to 200 μ in diameter were formed in nonfluidized columns, as described in Sect. 6.3. The maximum practical diameter of spheres that can be formed in the 28-ft-high column from 1 M UO_2 sol increases from about 145 μ if the 2EH temperature is 25°C to 200 μ if the temperature is 70°C (Fig. 6.5). Satisfactory operation was maintained by using Ethomeen S/15 as the only surfactant and by using ion exchange to remove formic and nitric acids, followed by distillation to remove H_2O from the 2EH. The nonfluidized columns are much simpler to operate than the fluidized-bed column and are therefore preferred if the allowable column height is adequate for the sphere size required.

Formation of Microspheres from Sols Containing PuO_2

Approximately 7 kg of dense microspheres of plutonium and plutonia-urania were formed in the alpha facility located in Building 3019. Plutonia sol or blends of plutonia sol with urania sols served as feed material. The sphere-forming column had a $^5/_8$-in.-diam throat, a taper of 1:18, and was equipped with a sol feed system having a capacity of 1 cc/min. A side stream of the 2EH used in the sphere-forming column was sent through an electrically heated still to remove H_2O. The pH, temperature, and water content of the recirculating 2EH were continuously monitored. The pH of the 2EH was controlled by periodic additions of dilute HNO_3, and the moisture content was controlled by regulating the still pot temperature. Surfactants (~5% solutions in 2EH) were added to the recirculating 2EH as required to control coalescence or clustering of the partially dried sol droplets and gel beads.

Trouble-free operation of the forming operation and high yields of good-quality spheres were routinely achieved with PuO_2 sols formed at 40 to 45°C in 2EH containing 0.2 to 0.3 vol % Ethomeen S/15, 0 to 0.5 vol % Span 80, and 0.5 to 1.5 vol % H_2O. After drying and firing to 1200°C, these microspheres were lustrous and free of surface cracks and irregularities.

When PuO_2-UO_2 mixed-sol feeds were formed into spheres, coalescence, clustering, and sticking to the column walls were always encountered to some degree. It is difficult to isolate and assign the sources of these problems to either the sol mixture or the 2EH. The UO_2 sols were generally contacted with *n*-hexanol to remove the extractable formic acid before mixing with PuO_2 sols. When UO_2 sol prepared by the precipitation-peptization method was blended with PuO_2 sol to obtain mixed sols with Pu/(Pu + U) ratios of 0.20 or 0.25, we were able to form acceptable microspheres in about 80% yield. The initial conditions for forming spheres >100 μ in diameter were as follows:

2EH temperature to the column	40–42°C
Ethomeen S/15 concentration in 2EH	0.2 vol %
Span 80 concentration in 2EH	0.4 vol %
H_2O concentration in 2EH	1.0 vol %
pH of 2EH	3 to 5
Still pot temperature	145°C
Average retention time of spheres in column	45 min

Spheres less than 44 μ in diameter were formed at similar conditions, except that the 2EH temperature was 55°C and the 2EH contained 0.5 vol % H_2O. In order to produce satisfactory microspheres over an extended period of time, it was necessary to make periodic additions of Ethomeen S/15 and Span 80 and to occasionally lower the pH of the 2EH by the addition of dilute nitric acid. When the cumulative additions reached 0.4 vol % Ethomeen S/15 or 2 vol % Span 80, further additions resulted in the production of malformed (dimpled and nonspherical) gel beads. A batch of 2EH could be used about 100 hr before this occurred. The 2EH at this time was a dark yellowish-brown. It was also found that the surface quality of the microspheres became poorer as the 2EH was used for longer periods of time. Initially, the microspheres produced had very glossy surfaces, and there was little cracked material in the product; the surface quality varied as the surfactant adjustments were made. When the moisture content was increased to about 1.5 vol %, larger increments of surfactants (mainly Span 80) were required to control clustering, but more lustrous gel beads were obtained.

Evidence of cracking in some of the gel spheres was almost always detectable. When the gel beads were steam dried, the cracks were widened; during the firing step, the cracks appeared to deepen. Despite the presence of the cracked microspheres, the composite fraction could be packed (tapped) to a density of 6.5 g/cc, which indicates that the density of the spheres is about 95% of theoretical density.

7.4 PREPARATION OF UO_2-PuO_2 MATERIALS

Preparation of sol-gel materials for use in the LMFBR fuel cycle program is reported here. This includes the preparation of materials for irradiation capsules and development of fuel fabrication techniques such as Sphere-Pac or pellet formation. Some material prepared for other programs is also discussed here since the preparation methods are the same as those developed for the uranium fuel cycle.

Preparation of Plutonia Sols

Approximately 7 kg of plutonium was converted into PuO_2 sol by a slightly modified version of the standard precipitation-peptization-baking process.[13] The modifications consisted in increasing the plutonium nitrate concentration in the feed solution and the NH_4OH concentration in the solution used to precipitate the plutonium hydroxide. These modifications permitted us to increase the batch size to 225 g of Pu (from 150 g) without any noticeable effect on the properties of the sol product.

All of the sols were stable and of high quality. They were used in the preparation of PuO_2 and $(U,Pu)O_2$ microspheres and in the preparation of $(U,Pu)O_2$ powder which was pressed into pellets.

Preparation of Urania Sols

Thirty-three urania sols (each containing ~300 g of U) were prepared by the standard precipitation-peptization process;[14] 31 of these were prepared from 93% enriched uranium, and the other 2 were made from natural uranium. These sols were used in the preparation of UO_2 and $(U,Pu)O_2$ microspheres and in the preparation of $(U,Pu)O_2$ powder which was pressed into pellets.

Preparation of Microspheres

During this report period, we prepared about 7 kg of high-density PuO_2 and $(U,Pu)O_2$ microspheres. Standard sphere-forming techniques were used (see Sect. 7.3). The gel microspheres were dried in a stream of argon-steam up to 170°C and were then fired to 1200°C in a controlled atmosphere. The atmosphere

13. J. P. McBride, *Laboratory Studies of Sol-Gel Processes at the Oak Ridge National Laboratory*, ORNL-TM-1980, pp. 51–53 (September 1967).

14. J. P. McBride, *Laboratory Studies of Sol-Gel Processes at the Oak Ridge National Laboratory*, ORNL-TM-1980, pp. 29–28 (September 1967).

maintained in the furnace was argon when pure PuO_2 was fired. When PuO_2-UO_2 microspheres were fired, the atmosphere was argon-steam up to 500°C and then argon–4% H_2 up to 1200°C. In all cases, the atmosphere was changed to pure argon as the material was cooled from 1200°C to room temperature. Fired products were sieved to select material of the desired size and were passed over a shape separator (Roundometer) to remove distorted or cracked spheres.

About 2.5 kg of $(U,Pu)O_2$ microspheres were prepared for use by Argonne National Laboratory. The material was made from 93% enriched uranium and had a Pu-to-(Pu + U) ratio of 0.25. Since the microspheres were intended for use in preparing irradiation specimens by the Sphere-Pac process, about one-third of the material was <44-μ-diam microspheres and the rest was 350- to 595-μ-diam microspheres.

About 550 g of $(U,Pu)O_2$ microspheres were prepared for use by the Metals and Ceramics Division in the investigation of the U-Fines method for fuel fabrication. This material was made from natural uranium and had a Pu-to-(Pu + U) ratio of 0.27. Only large microspheres (400 to 595 μ in diameter) were prepared since the <44-μ-diam microspheres used were pure UO_2.

About 4 kg of the plutonium that was formed into sol had a special isotopic content, ~23% ^{240}Pu and ~3.5% ^{241}Pu. This material was formed into high-density PuO_2 microspheres (~200 μ in diameter), coated with pyrolytic carbon by the Metals and Ceramics Division, and sent to Pacific Northwest Laboratory for use in the High Temperature Lattice Test Reactor. Despite the high level of gamma activity associated with this material, none of the personnel preparing this material received overexposures.

8. Conversion Studies in the LMFBR Fuel Cycle

8.1 TECHNICAL AND ECONOMIC EVALUATION

An analysis is being made of the interrelations of LMFBR fuel conversion processes with the fuel reprocessing and refabrication processes. Although the study is still in progress, it is apparent that geographical relations are important. The situation in which the reprocessor and the refabricator are located at the same site is very different from the situation in which the reprocessor and refabricator are separated by hundreds of miles. In the former situation the important question of whether to ship liquid or solid forms of plutonium does not arise. In the latter situation it becomes a matter of considerable importance, both from the point of view of safety and of cost. In addition, if solid forms of plutonium are to be shipped, it appears superficially that the reprocessor should ship a solid which can be used directly in fuel fabrication; however, a detailed economic analysis may show that a very simple solids conversion process at the reprocessing plant, followed by a conversion process at the refabrication plant to make the desired pelletizable material, is better.

Considerations such as the above are being made as part of the overall analysis of this complex group of factors. It is hoped that this analysis will provide a basis for future experimental work. A report on this work is in preparation.

8.2 CONVERSION BY HOMOGENEOUS REDUCTION

The chemical reduction of metal nitrates in pressurized solutions is a possible improved process for converting uranyl and plutonium nitrates into UO_2-PuO_2 powders suitable for use in making pellet fuels. Studies have been made to demonstrate the feasibility of chemical reduction at elevated temperatures and pressures to produce uranium dioxide from uranyl solution in a single process step. When a uranyl nitrate solution containing ethylene glycol was reacted at 260°C, >99.9% of the uranium precipitated. The uranium oxide powder produced by filtering this precipitate and drying it at 200°C in argon contained 0.62 wt % carbon, was 90% U(IV), and had a specific surface area of 5.51 m^2/g. With the proper choice of reductants (such as alcohols, ethylene glycol, sugars, or hydrazine), the uranium is reduced to the tetravalent state, and, at the same time, the nitrate is reduced, with the resultant formation of water, carbon dioxide, nitrogen, and nitrogen oxides.

Tests are planned, but have not yet been made, with plutonium nitrate solutions; however, this technique offers the promise of a process in which the problems normally encountered with plutonium polymer, gelatinous precipitates, and U-Pu valence incompatibility may be eliminated. Tests with cerium as a chemical stand-in for plutonium have given promising product properties (Table 8.1).

In addition to chemical analyses, x-ray analyses were performed on the reduction products. Table 8.2 shows results of x-ray analyses of five oxide products selected as representative of the results that are obtained when the feed is uranyl nitrate, uranyl nitrate–cerium(IV) nitrate, or uranyl nitrate–thorium nitrate.

Results with Semicontinuous Equipment

A system that allows continuous feed introduction and control of temperature and pressure has been developed. The product is removed batchwise. A series of experiments was carried out using uranyl nitrate or uranyl nitrate mixed with cerium or thorium nitrate as feed. The principal variables studied were chemical reductant and temperature. Properties of the product oxide and the completeness of nitrate reduction were about the same with this equipment as with similar experiments carried out in an autoclave.

Ethylene glycol, ethyl alcohol, and hydrazine were employed as reductants. When ethylene glycol and ethyl alcohol were used, pressures of 250 psig were required to satisfactorily precipitate uranium and cerium oxide mixtures. Hydrazine was found to be a more

Table 8.1. Analyses of homogeneous reduction-precipitation products

Feed solution:[a] 0.6 *M* UO_2^{2+}, 0.15 *M* Ce^{4+}, 2.1 *M* NO_3^-
Run conditions: 2 to 3 hr at 250 to 264°C

Reducing compound		Product solution			Precipitate dried to 225 or 250°C in Ar					
Name	Moles	pH	Percent of feed U	Percent of feed Ce	U (g/g ppt)	Ce (g/g ppt)	U(IV)/U ratio	Surface area (m^2/g)	Bulk density (g/cc)	C (g/g ppt)
Ethanol	6.4	4.88	0.1	~0	0.705	0.102	0.61	16.3	1.26	0.0115
n-Propanol	5.7	4.18	0.4	0.1	0.698	0.108	0.52	4.33	1.72	0.0055
Ethylene glycol	5.2	5.96	0.01	~0	0.693	0.102	0.96	12.4	1.69	0.0178
Hydrazine	4.6	8.82	0.3	0	0.733	0.090[a]	0.48	24.3	1.41	0

[a]Feed was 0.123 *M* Ce^{4+} for run with hydrazine.

Table 8.2. Results of x-ray analyses of selected products

Sample No.	Metals in nitrate feed	Oxygen/metal mole ratio	Found by examination of characteristic x-ray lines
A130	U	2.61	Primarily U_3O_8
A135	U-Ce	2.30	Probably UO_2-CeO_2 solid solution
PAR-7	U-Ce	2.36	Both UO_2 and CeO_2 present
PAR-17	U-Th	2.33	Both primarily UO_2, but lattice is shifted and smaller than UO_2 lattice
PAR-18	U-Th	2.26	

Table 8.3. Properties of oxide powder samples

Firing conditions: Samples analyzed after drying and firing to varying temperatures of 200°C to 400°C; all samples refired to 460°C for 3 hr

Sample No.[a]	Run conditions: Composition of feed (mole %)			Reducing agent	Powder analyses before refiring at 460°C			
	U	Ce	Th		Oxygen to metal mole ratio	Surface area (m^2/g)	Cerium or thorium to metal[b] mole ratio	C (wt %)
PAR-13	100	0	0	Hydrazine	2.44	23.1		
PAR-7	80	20	0	Hydrazine	2.36	28.2	0.209	0.036
A135	80	20	0	Ethylene glycol	2.30	41.1	0.214	0.43
PAR-18	80	0	20	Hydrazine	2.33	42.7		0.054
PAR-17	80	0	20	Ethylene glycol	2.33	48.9	0.221	0.34

[a]Sample A135 from batch autoclave run; PAR samples from semicontinuous runs.
[b]Uranium plus cerium or thorium.

effective reductant and yielded a product with less tendency to cake in this equipment than in the autoclave operated at temperatures of both 150 and 210°C.

Temperatures ranged from about 100 to 210°C; most runs were made at 160 or 205°C.

Equipment will be installed in an alpha-contained glove box to allow preparation of PuO_2 or UO_2-PuO_2 powders from nitrate solutions by pressurized aqueous reduction. With this new glove box, preliminary testing without plutonium can be done outside a high-alpha-level area.

Evaluation of Products

Six oxide samples (one UO_2, two UO_2-CeO_x, and three UO_2-ThO_2 samples) were fabricated into pellets, and the pellet characteristics were determined to provide a direct comparison of the six powders and to obtain an early evaluation of their suitability for use in making pellet fuels. We do not intend to optimize the pellet fabrication procedures for any of the powders at this stage of the study. Although the results of pelletizing tests are not complete, the densities of the pellets after being fired to 1650°C in H_2 indicate that the oxides prepared with hydrazine have much more desirable sintering characteristics than those prepared using ethylene glycol.

The UO_2 and UO_2-CeO_x products prepared by hydrazine reduction sintered as well as a reference, or standard, UO_2 powder (i.e., 94 to 95% of theoretical density for pellets prepared at 10,000 and 15,000 psi pressures). The UO_2-ThO_2 powder prepared by hydrazine reduction and pelletized at 10,000 to 15,000 psi sintered to 87 to 89% of theoretical density.

The UO_2-CeO_x and UO_2-ThO_2 powders prepared with ethylene glycol sintered to 61–64 and 74–78% of theoretical density respectively. A UO_2 powder prepared using ethylene glycol reduction sintered to 69% of theoretical density during a previous sinterability test with similar, but not identical, conditions.

Table 8.3 lists some of the properties of the oxide samples studied, and Table 8.4 gives some of the pellet pressing results obtained with them. Overall, the handling properties and behavior of the powder and the final appearance of the pellets were acceptable. Unless some unexpected negative results are obtained from the remaining determinations (microstructure, O/U ratios, crystal lattice parameters), the prospects for preparing usable UO_2-PuO_2 or PuO_2 products are very good.

Table 8.4. Densities of fired pellets examined in the study made to evaluate homogeneous reduction products[a]

Sample No.	Source	Pelletizing pressure (10^3 psi)	Pellet density (% of theoretical)[b] 1650°C firing	1750°C firing
215	Reference ceramic-grade UO_2	7	93.5	94.5
			92.0	94.3
			92.9	
		10	94.2	95.8
			94.3	95.9
			94.7	
		15	95.1	96.3
			94.9	96.0
			94.9	
PAR-13	UO_2, using hydrazine	7	91.9	91.6
			91.2	92.2
			91.7	
		10	93.8	94.1
			93.3	93.7
			93.4	
		15	94.0	94.5
			93.4	94.9
			94.5	
PAR-7	UO_2-CeO_x, using hydrazine	7	94.1	94.4
			94.2	94.6
			94.2	
		10	93.4	95.0
			94.8	94.8
			95.0	
		15	95.0	95.5
			94.9	95.4
			94.5	
PAR-18	UO_2-ThO_2, using hydrazine	7	85.2	87.0
		10	87.3	89.6
		15	89.7	91.5
A135	UO_2-CeO_x, using ethylene glycol	7	60.7	64.9
		10	61.5	65.3
		15	63.6	67.3
PAR-17	UO_2-ThO_2, using ethylene glycol	7	71.4	75.3
		10	74.6	78.5
		15	78.5	82.6

[a]Personal communication with R. A. Potter, ORNL, March 1971.

[b]All tests with three pellets at 1650°C and two at 1750°C; single values are averages.

9. Preparation of $^{233}UO_2$ for Light-Water Breeder Reactors

ORNL participation in the Light Water Breeder Reactor (LWBR) Program, under contract with Bettis Atomic Power Laboratory (BAPL), involves (1) the receipt and storage of approximately 750 kg of ^{233}U (475 kg as UNH and 275 kg as UO_2), (2) the purification of this material in small batches (~20 kg of ^{233}U per week) to remove ^{232}U daughters, (3) the conversion of the UNH to ceramic-grade UO_2 powder at the rate of about 20 kg of ^{233}U per week, (4) the packaging and shipping of the UO_2 to BAPL for blending with thoria and pressing into pellets, and (5) the recovery of ^{233}U from the $^{233}UO_2$ scrap generated at ORNL and the $^{233}UO_2$-ThO_2 scrap generated at BAPL.

During the past year, additional storage facilities, which were described previously,[1] were constructed, and all the feed material (750 kg of ^{233}U) was received and stored. A dissolver capable of dissolving 50 kg of ThO_2-UO_2 in a 12-hr cycle was constructed and is presently being installed in the processing cell. Modifications to the existing solvent extraction purification equipment and installation of an ion exchange system will be completed in the early part of April 1971. Construction of the oxide conversion equipment will be completed by July 1, 1971. The facility is scheduled to begin qualifying runs in July 1971, and production will begin in December 1971.

9.1 PROCESS DEVELOPMENT AND FLOWSHEETS

Process development work consisted primarily in (1) determining the optimum conditions for dissolving sintered ThO_2-UO_2 scrap from BAPL; (2) developing a solvent extraction flowsheet for purification of this scrap, which will have a UO_2 content varying from 1.0% to 6.0% UO_2; (3) providing a thorium removal system capable of reducing the thorium concentration in the UO_2 product to less than 500 ppm; and (4) developing the chemical flowsheet and testing the equipment that will convert the nitrate solution to a ceramic-grade UO_2 powder having the desired characteristics to permit uniform blending with the ThO_2 powder and pressing into high-density homogeneous pellets.

Suitable dissolution rates (~50 kg of UO_2-ThO_2 in 12 hr) for high-fired pellets were obtained in laboratory-scale equipment by first crushing the pellets and dissolving in 13.6 *M* HNO_3 that was 0.04 *M* in F^- and 0.1 *M* in $Al(NO_3)_3$, maintaining a 100% heel (e.g., 100 kg of UO_2-ThO_2 was charged, but only 50 kg was dissolved).

A solvent extraction flowsheet similar to that used to purify ^{233}U for the Kilorod Program[2] will be used to recover ^{233}U from the dissolved $^{233}UO_2$-ThO_2 scrap pellets from BAPL and to remove ionic impurities from feed material that does not meet specifications and thus cannot be fed directly to the thorium removal system. However, the di-*sec*-butyl phenylphosphonate concentration will be 5.0 vol %, which will increase the plant throughput by a factor of about 3. The flow ratios to the columns will depend upon the uranium/thorium ratio in the feed solutions.

The thorium removal process, described previously,[1] was modified slightly during the past year. The ion exchange resin, Dowex 50W-X12, is now contained in two separate columns; the first contains 2 liters of resin, and the second contains 3 liters. The first column is equipped with a monitor that will precisely locate the thorium band on the column, thereby ensuring that thorium will not be present in the second column. The second column is used primarily to remove ^{224}Ra. The direction of flow through the first column is up during loading and down during elution as a further attempt to keep the thorium from breaking through to the second column. Our finalized chemical flowsheet is shown in Fig. 9.1. The fabricated system (see Sect. 9.2) was

1. *Chem. Technol. Div. Annu. Progr. Rep. May 31, 1970,* ORNL-4572, pp. 174–75.

2. R. H. Rainey, *Recovery of ^{233}U for the Kilorod Program,* ORNL-TM-403, p. 19 (September 1962).

ORNL DWG NO. 70-12415R1

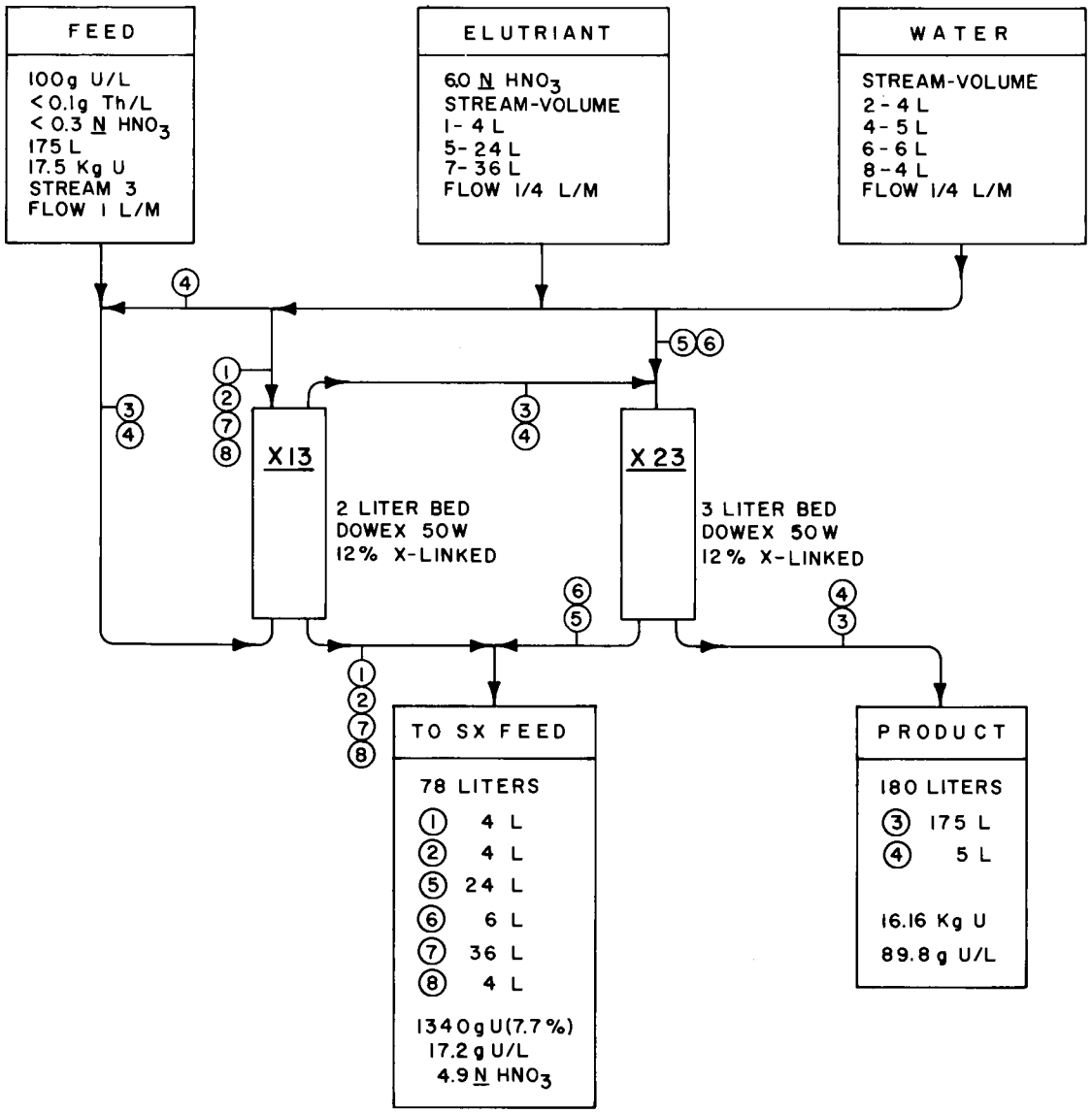

Fig. 9.1. Chemical flowsheet for thorium removal.

tested prior to installation in the cell and gave satisfactory results during hydraulic operation. Several test runs with ^{233}U will be made during the next two months.

Flowsheet development work on the operating parameters for converting nitrate solution to a ceramic-grade UO_2 powder dictated that several alterations be made in our previous flowsheet.[1] This work, performed by the Metals and Ceramics Division, resulted in the following changes:

1. Precipitation is carried out at 60°C rather than at room temperature, in order to control the particle size of the precipitate.
2. The ammonium diuranate powder is heated to 500°C in argon before being exposed to hydrogen; this will reduce the surface area of the calcined powder to the desired value of 6 m^2/g.
3. The calcined powder is stabilized at a temperature of 25°C rather than at 10°C, as originally planned, since the lower temperature is not essential.
4. Grinding and sizing are performed after instead of before stabilization.

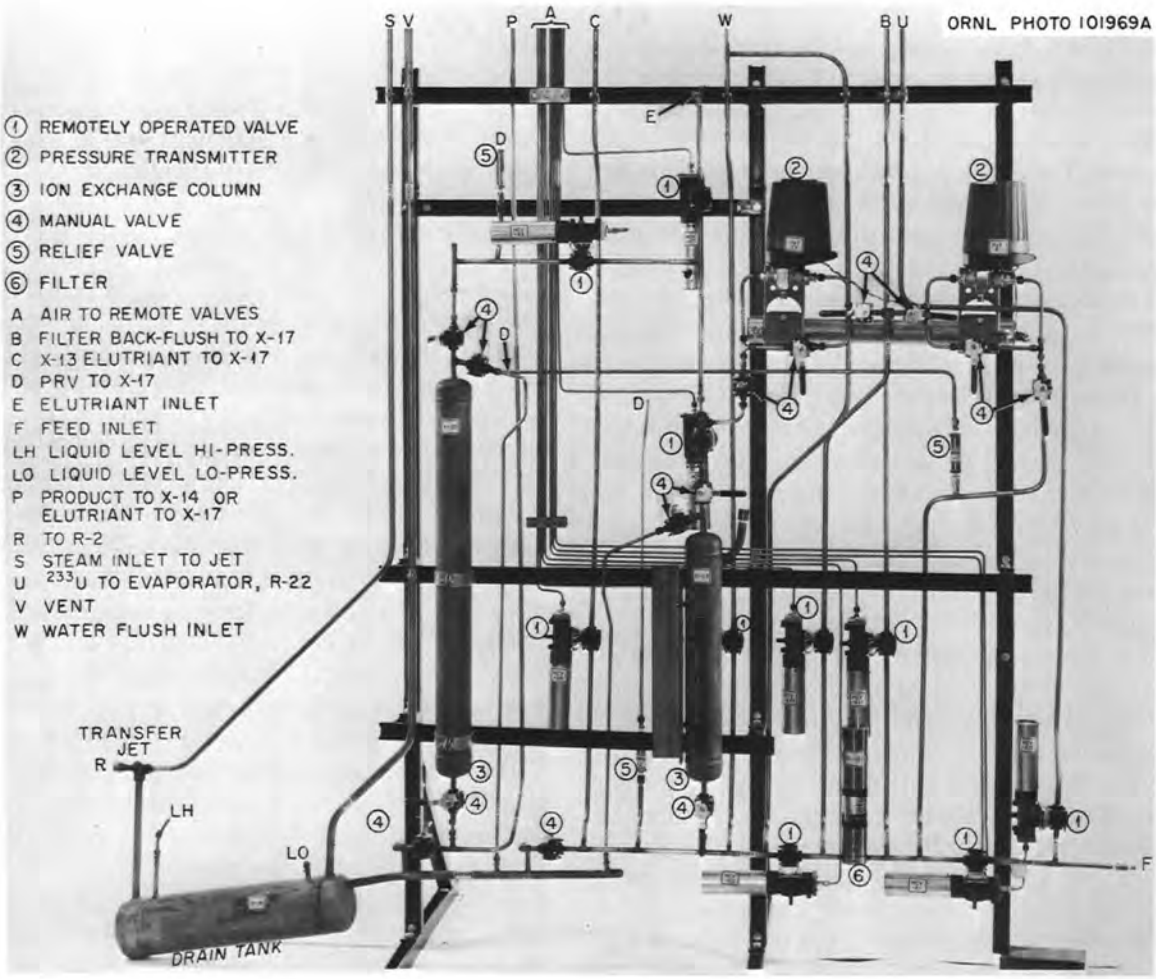

Fig. 9.2. Ion exchange equipment.

9.2 PLANT MODIFICATIONS

Modifications to the existing solvent extraction plant included:

1. fabrication and installation of a thermo-siphon dissolver to dissolve the ThO_2-UO_2 scrap from BAPL,
2. design, fabrication, and installation of an ion exchange system (Fig. 9.2) to remove thorium from the uranium product,
3. changes in the existing solvent wash system to provide a more efficient, more easily operated system,
4. the overhaul, or replacement, of pumps and instrumentation,
5. the installation of necessary tanks and piping to connect the purification system to the oxide conversion equipment.

These modifications are 95% complete. The entire system will be operated with ^{233}U in May 1971.

9.3 DESIGN OF EQUIPMENT FOR THE UO_2 CONVERSION LINE

The UO_2 conversion equipment will be enclosed in seven alpha enclosures. The following provides a brief description and discusses the present status of each of these enclosures and its associated equipment:

1. Liquid waste handling enclosure. This enclosure contains the vessels for metering the uranyl nitrate (^{233}U) from the purification system to the precipitator, for metering nitric acid and demineralized water

to the process, for collecting and metering the supernate obtained by centrifuging, and for collecting all washdown solutions from the other enclosures. This enclosure and its associated equipment have been fabricated. The piping is scheduled for completion in March 1971.

2. Precipitation enclosure. This enclosure contains the precipitator and the centrifuge. Fabrication of the enclosure and its associated equipment is scheduled for completion in March 1971; also, the centrifuge is scheduled to be delivered during March. The centrifuge has a Teflon bowl, which will eliminate the undesirable transfer of ammonium diuranate. After centrifugation, the Teflon bowl with the ammonium diuranate cake will be transferred as a unit to the microwave dryer.

3. Microwave dryer enclosure. This enclosure contains the microwave oven, which is already on hand. The designs of the auxiliary equipment and the enclosure are 90% complete.

4. Furnace tray loading enclosure. This enclosure is divided into two sections: (1) an air-filled compartment in which the granulator and the furnace boat loading station are located and (2) an argon-filled compartment enclosing the entrance end of the furnace. The continuous furnace is of the belt type and contains internal gas barriers to prevent H_2 from escaping. The use of argon at the ends of the furnace provides additional safety. The design of the equipment for this enclosure is 75% complete, and the design of the enclosure itself is 50% complete. The granulator is scheduled for delivery by April 15, 1971.

5. Furnace tray unloading and powder stabilization enclosure. This enclosure, which is maintained under argon, contains the furnace tray unloading mechanism and the reduced powder stabilizer. The stabilizer consists of a vibratory trough in which a very thin layer of powder is contacted with air at room temperature. The stabilizer has been fabricated and shipped to the vibrator manufacturer for mounting and timing. Conceptual drawings of the tray unloading mechanism have been prepared.

6. Powder inventory and packaging enclosure. This enclosure contains a shielded (2 in. of lead) 20-kg batch powder blender and the product weighing system. The blender and the powder weighing system are scheduled for delivery by May 15 and by April 15, 1971, respectively. Preliminary conceptual drawings have been prepared for this enclosure.

7. Isotopic dilution enclosure. All liquid waste being sent to the ORNL tank farm from the UO_2 conversion line must first go through this enclosure. The waste is routed to a mixing vessel in which ^{238}U is added at the ratio of 100 parts ^{238}U per part ^{233}U. Solutions from this enclosure cannot be transferred into the 3019 complex because of the possibility of contaminating the system with ^{238}U. This enclosure and its associated equipment have already been fabricated.

9.4 RECEIPT AND STORAGE OF ^{233}U FEED MATERIAL

During the past year, construction of the necessary additional storage systems was completed, and all the feed material was received. A total of 274 kg of ^{233}U (as UO_3) was received in 11 shipments from the Savannah River Plant, and 474 kg of ^{233}U [as $^{233}UO_2(NO_3)_2$] was received in 10 shipments from the Hanford Plant. The oxide was stored in the solids storage facility; however, several runs were made to demonstrate our ability to dissolve this material in nitric acid of sufficiently low concentration (<0.5 *N* HNO_3) to be suitable for feed to the ion exchange system. As a result, 87.5 kg of the Savannah River material has been converted to nitrate and is now stored in the solution storage facility.

The nitrate solution was weighed, sampled, and charged directly to the solution storage facility. The total quantity of ^{233}U, as measured at ORNL, agreed within 0.6% of the shipper's values. All of the ^{233}U received from Hanford and Savannah River meets LWBR powder specifications with two exceptions: both the iron content of the material from Savannah River (525 ppm vs 400 ppm specified) and the ^{232}U content of the Hanford material (9 ppm vs 8 ppm specified) are too high.

9.5 PLANT SAFETY

The presence of multikilogram quantities of the fissile isotope ^{233}U necessitates careful control of storage, handling, and processing operations in order to avoid a nuclear excursion. The following operations have been examined for conformity to good practice based on data from published literature:[3,4]

1. uranium oxide storage wells,
2. ^{233}U nitrate solution storage facility,
3. dilution and storage of the ^{233}U solution from Hanford,

3. Subcommittee 8 of ASA Sec. Comm. N6, Project 8, ANS Standards Committee, *Nuclear Safety Guide,* TID-7016, Rev. 1 (1961).

4. H. C. Paxton et al., *Critical Dimensions of Systems Containing* ^{235}U, ^{239}Pu, ^{233}U, TID-7028 (June 1964).

4. operation of the $^{233}UO_2$-ThO_2 scrap dissolver,
5. operation of the ion exchange system,
6. operation of the solvent extraction system.

Specified data for this program were developed by D. W. Magnuson of the Y-12 Critical Experiment Facility. Nuclear calculations based on the oxide storage wells resulted in subcritical values for oxide that has a density of less than 3.5 g/cm^3 and is stored in a dry system in cans with diameters less than 3.25 in.

Criticality calculations were made for the solution storage system, which consists of ten 36-in.-diam tanks containing uranyl nitrate solution at a ^{233}U concentration of 250 g/liter. The ANISN transport code[5] in the S_8 approximation was used to calculate k_∞ and to generate flux-averaged (homogenized) cross sections from fissile solution containing Raschig rings. The cylindrical tube model, which was devised as a model to evaluate[6] some exponential experiments with these materials, and Hansen-Roach 16-group cross sections[7] were used. Finite-geometry calculations for a cylindrical unreflected tank and for the ten-tank arrangement were made with the KENO-II Monte Carlo code, using the flux-averaged cross sections for the solution-glass mixture. The results of these calculations are summarized in Table 9.1.

Certain approximations were made in order to simplify the calculation for the tank arrangements. Each cylindrical tank was assumed to have an inside diameter of 36 in. and a height of 63.4 in. The walls of the stainless steel tanks were assumed to be $^3/_{16}$ in. thick (although some are $^1/_4$ in. thick). All center-to-center distances between the tanks were assumed to be the smallest dimension (38 in.). The lead shielding partitions between some of the tanks were ignored. The 4-in. lead shield on two sides of the ten-tank arrangement, as well as the concrete reflector on all sides, was included. For conservatism, the boron content of the glass Raschig rings was reduced to 90% of the actual value.

Table 9.1. Calculated multiplication factors for the ^{233}U solution storage facility

Code	System[a]	Value of k
ANISN	Infinite	$k_\infty = 0.9050$
KENO-II	1 tank	$k_{eff} = 0.8066 \pm 0.0018$
KENO-II	10 tanks	$k_{eff} = 0.8442 \pm 0.0017$

[a]Each tank was assumed to contain uranyl nitrate solution at a ^{233}U concentration of 250 g/liter.

Calculations of reactivity in the scrap dissolver, fabricated from 8-in. pipe with a side arm and installed in a concrete cell, gave a k_{eff} of 0.802 at the most reactive composition (102.7 g of ^{233}U per liter). Reject pellets with the highest UO_2 concentration expected during the program (i.e., 6% UO_2–94% ThO_2) were used for the calculations.

9.6 SITE PREPARATION

The UO_2 conversion line will be located in an area adjacent to the purification system in Building 3019. A plutonium fuels fabrication glove-box facility, which previously occupied this space, was moved to a newly constructed area in Building 4508. Construction of a three-level storage vault, removal of the dividing walls, and installation of a glove-box header in the Building 3019 laboratory have been completed. The design of a new glove-box-ventilation system, which will include three fans, a motor-generator set for emergency operation, and a filter system and ducting to service all glove boxes in Building 3019, is complete; construction will begin in April 1971.

The facility is scheduled for completion by June 1, 1971, and glove boxes will be moved in and connected by July 1, 1971.

5. W. W. Engle, Jr., *A User's Manual for ANISN, a One Dimensional Discrete Ordinates Transport Code with Anisotropic Scattering,* K-1693, Oak Ridge Gaseous Diffusion Plant (1967).

6. J. P. Nichols, C. L. Schuske, and D. W. Magnuson, *Use of Borosilicate Glass Raschig Rings as a Fixed Neutron Absorber in Solutions of Fissile Material,* Y-CDC-8, Y-12 Plant Criticality Data Center (to be published).

7. G. E. Hansen and W. H. Roach, *Six and Sixteen Group Cross Sections for Fast and Intermediate Critical Assemblies,* LAMS-2543, Los Alamos Scientific Laboratory (1961).

10. Separations Chemistry Research

10.1 NEW SEPARATIONS AGENTS

Quaternaryalkylphosphonium Salts

The properties of the dimethylphosphate salt of methyltrioctylphosphonium, its ready conversion to other salts, and its extraction characteristics compared with those of Adogen 464 for uranium(VI) and plutonium(IV) were reported previously.[1,2] Data for the extraction of iron(III) and technetium(VII) chloride, nitrate, and sulfate by 0.1 *N* solutions of the corresponding methyltrioctylphosphonium (MTOP) and dodecylbenzyltrioctylphosphonium (DDBTOP) salts in 95% DEB–5% TDA and vanadium(IV) chloride and sulfate by the corresponding MTOP salts are shown in Fig. 10.1. Extractions with the quaternaryalkylphosphonium salts were qualitatively similar to those of the corresponding Adogen 464 (quaternaryalkylammonium) salts. Coefficients for the extraction of Fe(III) from $LiNO_3$–0.2 *N* HNO_3 solutions were 2 to 2.5 orders of magnitude lower than those with MTOP or DDBTOP, whereas for the other systems reported in Fig. 10.1 the differences in extraction power were much less. There appears to be some loss of both the phosphonium compounds to the aqueous; however, it has not been determined if this is an initial loss due to low-molecular-weight impurity, or a steady-state loss.

Extraction of Lithium from Salt Solutions

Lithium extraction from salt solutions with the synergistic extraction combination of a β-diketone and trioctylphosphine oxide (TOPO) has been reported previously.[3,4] Practicable extraction levels, however, were not obtained at pH values below 11. We have recently found that fluorinated β-diketones are sufficiently acidic to allow efficient extraction of lithium from near-neutral salt solutions, for example, salt brines.

A comparison of lithium extractions with 0.2 *M* solutions of several β-diketones (in 0.1 *M* TOPO–benzene) from 1 *M* KCl in the pH range of 4 to 9 is shown in Fig. 10.2. The lithium extraction power increased as the number of fluorine atoms on the β-diketone was increased from 3 to 7. Extraction coefficients with heptafluorodimethyloctanedione (HFDMOD) were about 1 at pH 6 and 10 at pH 7. The nearest nonfluorinated analog to the three fluorinated β-diketones tested was dipivaloylmethane. Lithium extraction coefficients with this compound in the pH range of 6 to 8 were several orders of magnitude lower than those obtained with the fluorinated β-diketones.

In the extraction of lithium from 1 *M* KCl solution at pH 8.3 with 0.2 *M* HFDMOD in TOPO-benzene, the slope of a plot of log E_a^o vs log TOPO concentration was approximately 2 for TOPO concentrations below 0.1 *M* but tended to approach a slope of 1 in the TOPO concentration range of 0.1 to 0.5.

The dependence of lithium extraction coefficients on the concentration of HFDMOD, determined at a constant pH of 8.0 and an HFDMOD/TOPO mole ratio of 2/1, was about third power. However, saturation loading tests indicated combining ratios of 1 mole of HFDMOD per mole of extracted lithium in extractions from lithium or sodium chloride solutions and 2 moles of HFDMOD per mole of extracted lithium in extractions from potassium, rubidium, or cesium chloride solutions.

Investigation of the effect of diluent choice showed lithium extraction coefficients for HFDMOD-TOPO in dodecane diluent were higher by factors of 3 to 20 than the coefficients obtained using aromatic hydrocarbon or carbon tetrachloride.

Selectivity. The separation factors for lithium over the other alkali chlorides that were measured using

1. *Chem. Technol. Div. Annu. Progr. Rep. May 31, 1969,* ORNL-4422, p. 252.

2. *Chem. Technol. Div. Annu. Progr. Rep. May 31, 1970,* ORNL-4572, p. 181.

3. T. V. Healy, *Chem. Div. Progr. Rep. November 1964–April 1965,* AERE PR/Chemistry 8, Harwell, Berks. (1965).

4. D. A. Lee et al., *J. Inorg. Nucl. Chem.* **30,** 2807–21 (1968).

ORNL-DWG 71-5084

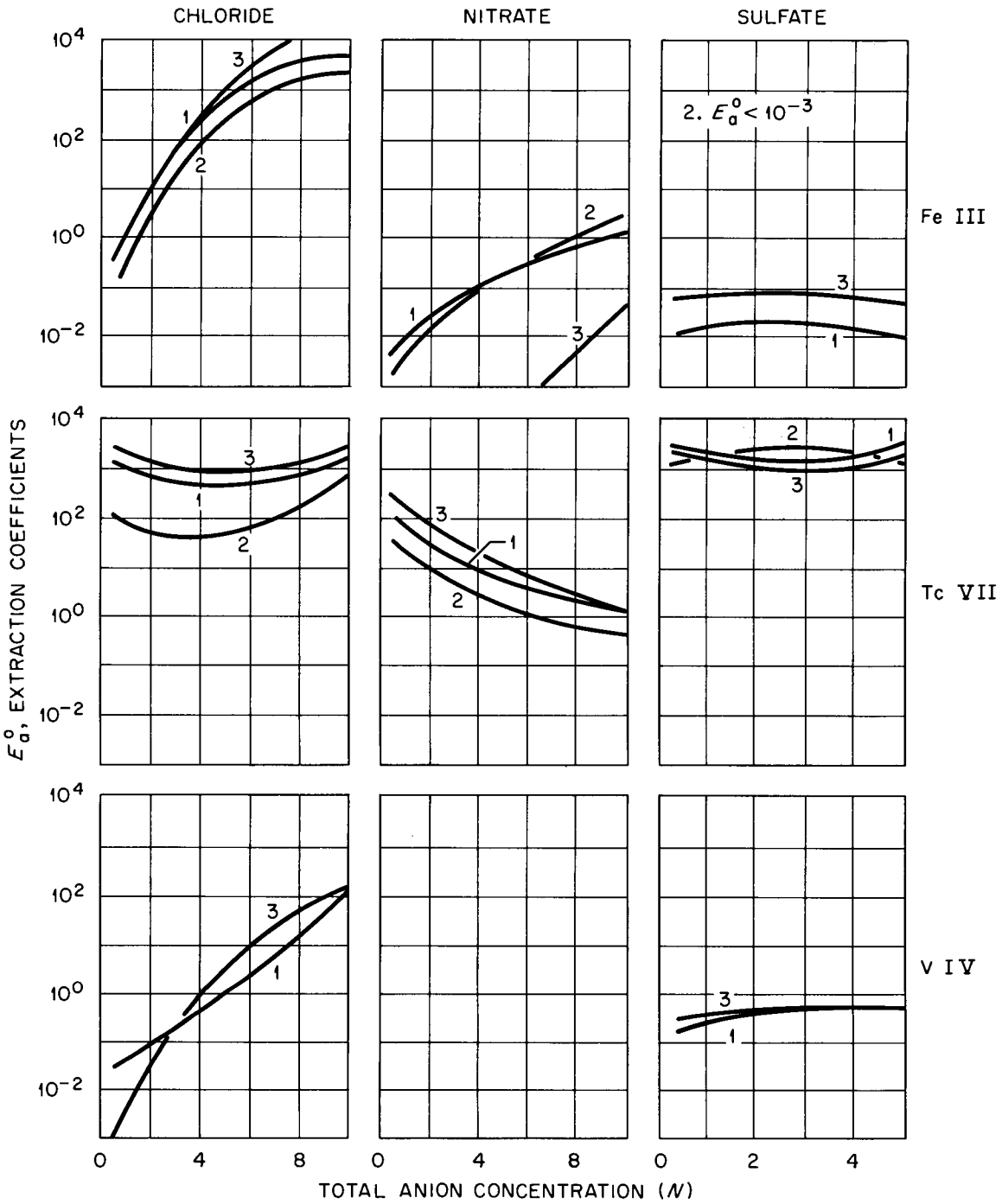

Fig. 10.1. Extraction of selected metals with quaternaryalkylphosphonium compounds. Organic phase: chloride, nitrate, or sulfate salts of (1) methyltrioctylphosphonium, (2) dodecylbenzyltrioctylphosphonium, or (3) Adogen 464 (methyltrialkylammonium) in 95% DEB–5% TDA diluent. Aqueous phase: LiCl–0.2 *N* HCl, $LiNO_3$–0.2 *N* HNO_3, or Li_2SO_4–0.2 *N* H_2SO_4 solutions containing 0.01 *M* metal ion [Fe(III) and V(IV)] or trace quantities in the case of Tc(VII).

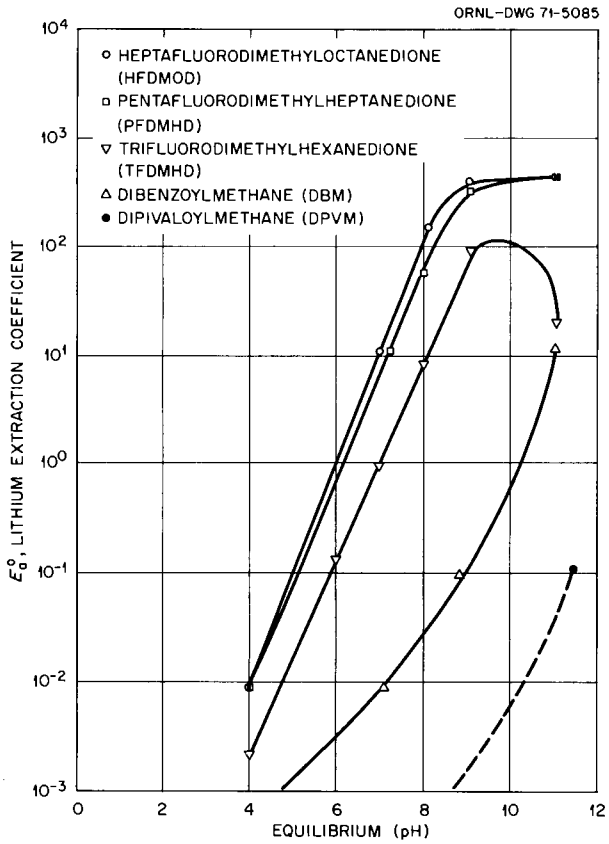

Fig. 10.2. Dependence of lithium extraction coefficients on pH for various β-diketones. Organic phase: 0.2 *M* β-diketone–0.1 *M* trioctylphosphine oxide in benzene. Aqueous phase: 1 *M* KCl–0.01 *M* LiCl. Phase ratio of 1/1. Mixed phases titrated to the desired pH with KOH.

Table 10.1. Separation of lithium from other alkali chlorides with 0.2 *M* HFDMOD–0.1 *M* TOPO in benzene

Alkali	Separation factor
Sodium	1300
Potassium	3800
Rubidium	3700
Cesium	2500

HFDMOD were in excess of 10^3 (Table 10.1). These data were obtained under conditions of high lithium loading.

Solvent Extraction and Ion Exchange Behavior with 1,2-Diaminopropanetetraacetic Acid

The polyaminoacetic acids represent a class of chelating agents finding widespread applications in the separation of the rare earths and the transplutonium elements. Various derivatives of ethylenediaminetetraacetic acid (EDTA) are being investigated for possible use in transplutonium element separations. A relatively new commercially available complexing agent, 1,2-diaminopropanetetraacetic acid (PDTA, mol. wt 306.27) is now being investigated to determine what effect a methyl group connected to a carbon atom in the C-C linkage (which will restrict the rotation about the ethylene bridge) has on the distribution coefficients and the separation factors of the rare earths and the transplutonium elements.

The complexing agent was evaluated by solvent extraction and by ion exchange resin techniques. Solutions containing 0.5 *M* lactic acid–0.01 *M* PDTA at a pH of 4.0 were contacted with 0.3 *M* di(2-ethylhexyl)phosphoric acid (HDEHP) in xylene. The separation factors obtained were Cm/Am = 1.1, Cf/Cm = 4.4, Cf/Es = 1.5, and Eu/Am = 63. Solutions containing 1.0 *M* NH_4NO_3–0.01 *M* PDTA at pH 4.0 gave similar separation factors with better phase separation characteristics. The kinetics of both systems are slow, requiring several minutes to reach equilibrium.

The ion exchange behavior of PDTA was evaluated using the ammonium form of Dowex 50-X8 resin (25–40 μ size) at a temperature of 80°C. The transplutonium elements were separated by chromatographic elution with 0.01 *M* PDTA–0.1 *M* NH_4NO_3 at a pH of 1.85 to 2.2. The normalized separation factors obtained were Fm/Es ~ 2.5, Es/Cf = 1.85, Cf/Cm = 62, and Cm/Am = 1.53. Some problems were encountered with a double elution band coming down the column.

The initial studies with 1,2-diaminopropanetetraacetic acid have been promising, and the results indicate that it is a strong complexing agent, giving enhanced separation factors for the trivalent actinides. Work is continuing on the problems pertaining to PDTA solubility at low pH values and to the occurrence of double elution peaks for individual transplutonium elements.

10.2 RECOVERY OF URANIUM FROM COMMERCIAL PHOSPHORIC ACID

Results continued highly favorable in development of a solvent extraction process[5,6] for recovering uranium from wet-process phosphoric acid. Commercial phosphoric acid that is produced from Florida phosphate rock contains about 1.5 lb of uranium per 1000 gal of

5. F. J. Hurst, D. J. Crouse, and K. B. Brown, "Recovery of Uranium from Wet-Process Phosphoric Acid," submitted to *Ind. Eng. Chem., Proc. Des. Develop.* (1971).

6. *Chem. Technol. Div. Annu. Progr. Rep. May 31, 1970,* ORNL-4572, pp. 184–86.

ORNL DWG 71-161R1

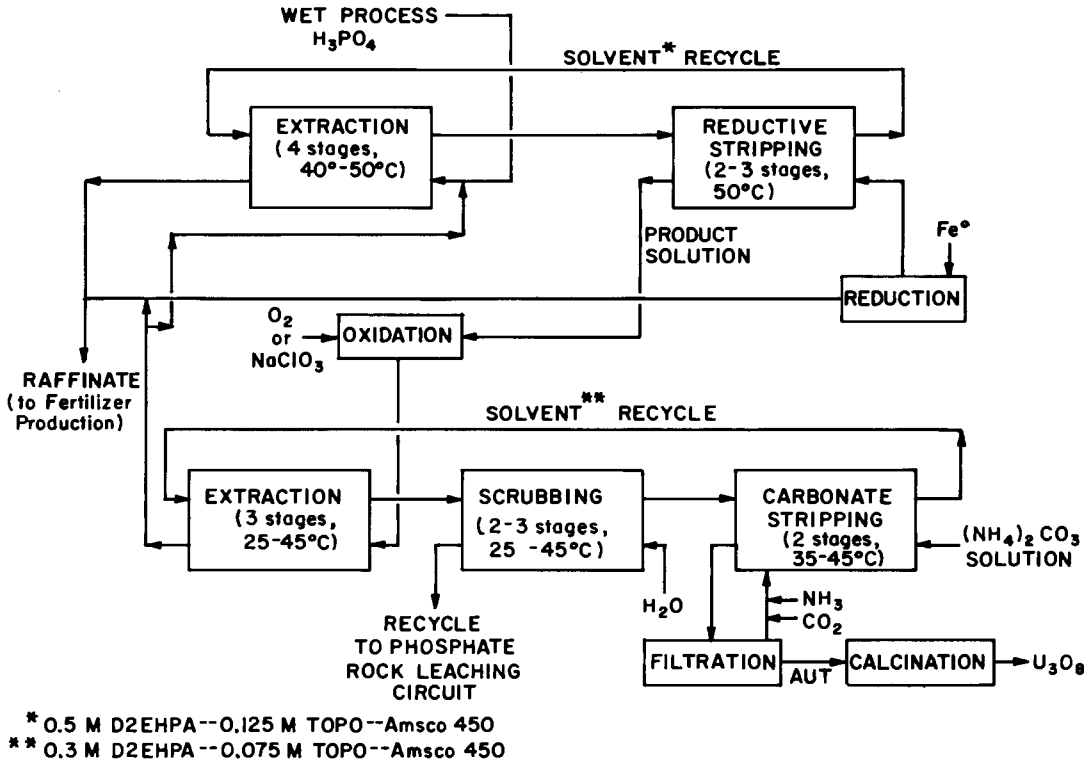

Fig. 10.3. Process flowsheet for recovery of uranium from wet-process phosphoric acid.

acid and represents a potential source of about 2000 tons of U_3O_8 per year.

The process (Fig. 10.3) consists of two cycles and uses as extractant the synergistic combination of di(2-ethylhexyl)phosphoric acid (D2EHPA) plus trioctylphosphine oxide (TOPO). In the first cycle, uranium is extracted with 0.5 *M* D2EHPA–0.125 *M* TOPO in an aliphatic diluent and recovered from the solvent by contacting it with a phosphoric acid solution that contains ferrous iron (Fig. 10.3). The ferrous iron reduces the uranium to the less-extractable tetravalent state and effects its transfer to the aqueous phase. A small volume of raffinate from the extraction system is used for this purpose. Under the proper conditions, uranium strip solutions containing about 12 g of uranium per liter (about a factor of 70 richer in uranium than the original acid) are readily obtained. These solutions are highly amenable to treatment in a second cycle using the same extractant.

In the second cycle, the uranium in the first-cycle strip solution is oxidized to the hexavalent state and then extracted with 0.3 *M* D2EHPA–0.075 *M* TOPO. The extract is scrubbed with water to remove extracted phosphoric acid and is then stripped with an ammonium carbonate solution under conditions that result in direct precipitation in the stripping system of the uranium as rapid-filtering ammonium uranyl tricarbonate (AUT), which is then calcined to U_3O_8.

Status and Progress

Good results were obtained in bench-scale continuous tests of the first cycle of the process.[5,6] No significant change in performance was detected for periods of operation equivalent to about 40 complete cycles of solvent through the extraction-stripping system. The magnitude of mechanical losses of the relatively expensive solvent, which is an item of prime concern, were encouragingly low. Concentrated uranium strip solutions obtained in the first-cycle demonstration tests have now been successfully processed in the second cycle to give a high-grade U_3O_8 product. Chemical reagent costs for the process, including allowance for solvent loss, are estimated at about $0.85 per pound of recovered U_3O_8. On the basis of the favorable results obtained, pilot-scale testing of the process at a phosphoric acid plant is merited.

Demonstration of the Second Cycle

The first-cycle strip solution, which typically contains about 12 g of U(IV), 6 to 10 g of Fe(II), and 10 to 12 g of Fe(III) per liter, is oxidized prior to the second extraction cycle. Essentially all of the Fe(II) must be oxidized before the uranium is oxidized by the Fe(III) in the solution. The oxidation was accomplished by bubbling oxygen or air through the solution at 70 to 90°C, but the oxidation was relatively slow, requiring (in the case of O_2) 1 to 2 hr for completion. Rapid oxidation was obtained by adding sodium chlorate to the solution. Oxidation was complete within a few minutes at 50°C, using only a small excess over the stoichiometric requirement of $\frac{1}{6}$ mole per mole of Fe(II) plus $\frac{1}{3}$ mole per mole of U(IV).

A continuous demonstration of the second cycle was made in a small mixer-settler test array with 0.3 *M* D2EHPA–0.075 *M* TOPO in a high-boiling aliphatic diluent. More than 99% of the uranium was extracted in three stages to give an extract that contained more than 9 g of uranium per liter (Fig. 10.4). In addition to uranium, the extract contained 1.8 g of phosphate and 0.13 g of iron per liter. Three water scrub stages, operated at an organic/aqueous ratio of 5/1, removed more than 98% of the phosphate but very little iron; most of the iron precipitates in the stripping unit along with the AUT product.

Almost all of the uranium was removed from the extract with ammonium carbonate solution in the first of two stripping stages. The first stripping unit was designed to facilitate continuous precipitation and discharge of the AUT precipitate. Intrastage recycle of the slurry from the settler through a filter and back to the mixer was provided for continuous removal of AUT. Makeup ammonia and carbon dioxide were bubbled directly into the aqueous phase of the first-stage settler in order to maintain the ammonium carbonate concentration at about 2 *M*. The concentration of uranium in the recycle solution was about 4 g/liter. Dilute (~0.5 *M*) ammonium carbonate solution was fed at a very low flow rate to the second stripping stage, the function of which is primarily to scrub entrained uranium from the solvent stream. The flow rate of this solution was set to balance the loss of water from the stripping system, which occurs on conversion of the D2EHPA to the hydrated ammonium salt. There was no precipitation in the second stage.

Physical operation in both the extraction and stripping systems was satisfactory.

The AUT precipitate, after being washed with a small volume of 1 *M* NH_4OH and Amsco 450 diluent (to remove entrained solvent) and air-dried, analyzed 12.7% NH_3, 44.9% U, and 34% CO_3. Calcination of the air-dried precipitate for 2 hr at 600°C yielded a product

ORNL DWG 71-162R1

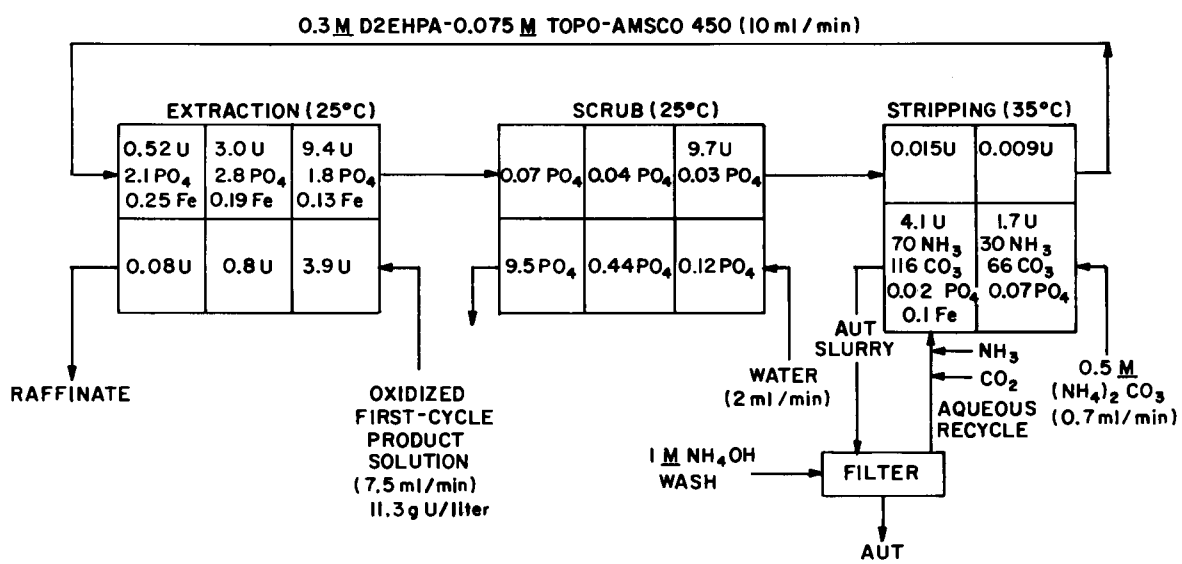

Fig. 10.4. Demonstration of second-cycle flowsheet. Numbers in blocks show concentration in grams per liter at steady state.

that analyzed 97.5% U_3O_8, 0.5% Fe, 0.06% PO_4, and 0.5% CO_3, 25 ppm Ti, 40 ppm V, and 0.7 ppm Mo.

10.3 HIGH-RESOLUTION RARE-EARTH SEPARATIONS

The pressurized ion exchange technique was successfully applied to the rapid simultaneous separation of all the rare earths. There are applications in AEC programs elsewhere that require the quantitative separation of most or all of the lanthanides from a single sample, on a scale of several milligrams of each element, and present methods are rather time consuming and expensive. We have demonstrated that the time required for a separation can be reduced from about a week, as presently done, to less than 2 hr.

A typical elution curve (Fig. 10.5) shows that each element was obtained in greater than 99% yield and purity. An increasing-concentration step gradient of eluent (α-hydroxyisobutyrate) was used in order to space the successive bands at approximately equal intervals. Experiments with columns three times longer but with the same resin volume gave identical results. Increasing the flow rate from 6 to 16 ml cm^{-2} min^{-1} caused possibly a very slight broadening of the bands. Pressures required were on the order of 500 psi. The resin size used, 25 to 60 μ, was larger than optimum. Thus these results indicate that equally good separations should be practicable in substantially less time by using a smaller sized resin, a shorter column, and higher flow rates. They also show that rather short columns – certainly less than 1 ft long – are adequate for these separations, although the general practice has been to use columns several times longer.

A similar experiment with a fourfold greater loading (20 mg of each natural rare earth) gave a poorer separation, with appreciable overlap of about half of the pairs of adjacent bands. Yields of better than 99% pure product varied from a low of 50% for dysprosium to greater than 99% for samarium, promethium, cerium,

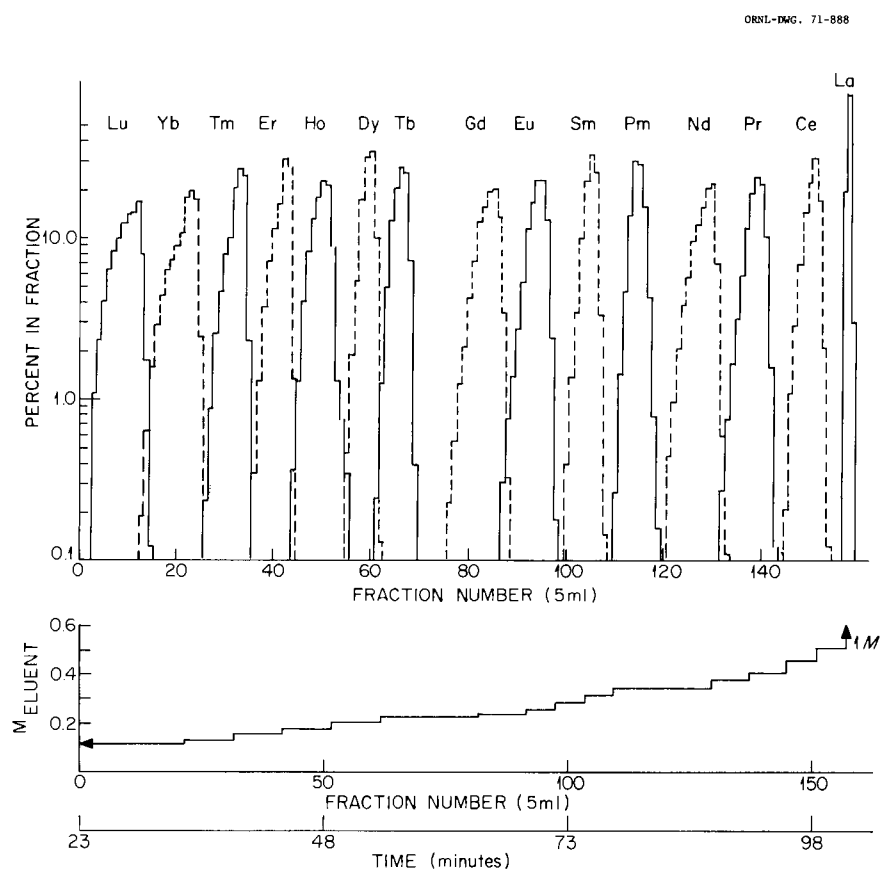

Fig. 10.5. Rapid and quantitative separation of the 15 rare earths by pressurized ion exchange. Dowex 50-X8 resin, 25–60 μ size, was used in a column 0.64 cm^2 by 33 cm long. The column was loaded with 5 mg of each rare earth except for tracer Pm, and elution was done with α-hydroxyisobutyric acid partially neutralized with ammonium hydroxide to pH 4.4, using an increasing concentration gradient. The flow rate was 10 ml/min, and 5-ml fractions were collected.

and lanthanum. Better results could be obtained by using a less concentrated eluent or a flatter gradient. In this experiment about 18% of the resin was loaded with rare earths.

10.4 DISPLACEMENT ELUTION WITH AMINOPOLYACETIC ACIDS

In an effort to find a better ion exchange method for separation of macro quantities of the heavy actinides, some work has been done again this year using the rare-earth elements between erbium and samarium as stand-ins.

A system was sought that could use H^+ ions or other nonmetallic barrier ions which would not complicate the subsequent processing of individual eluted fractions. The first actinide fraction eluted from the column contains not only the wanted element but also the tail of the barrier ion used in the system.

Since ethylenediaminetetraacetic acid (EDTA) is a chelating agent that gives some of the largest spreads in stability constants for these particular rare earths, and is also good in the actinide group, it was desired in this work. However, because of the insolubility of the acid form of EDTA, a barrier ion other than H^+ must be used. An organic barrier which could be easily destroyed or otherwise removed would be ideal for the separation of the actinides. Diethylenetriaminepentaacetic acid (DTPA), which is amphoteric in nature, is sorbed on resin through the basic nitrogen group,[7] and has possibilities as an organic barrier ion. However, to be able to load DTPA on a column, it must be put into solution with NH_4OH or some other base. As this basic solution of DTPA is loaded, the NH_4^+ ions load tighter than the $DTPA^+$, so that the $DTPA^+$ moves ahead of the NH_4^+.

Three high-pressure ion exchange columns were set up in series. Column 1 was 4 ft by 1 in., column 2 was 3½ ft by 1 in., and column 3 was 3½ ft by ½ in. Using the loading characteristics of the $DTPA^+$–NH_4^+ ions, a 30-g/liter pH 3.3 DTPA solution was made up and pumped through the three columns in series. The NH_4^+ ions loaded tighter than the $DTPA^+$, and all of the NH_4^+ remained in column 1. Only the $DTPA^+$ was loaded on columns 2 and 3. Afterward, column 1 was disconnected from the system, stripped with acid, and loaded to breakthrough with the rare-earth mixture for elution tests. Various concentrations and pH ranges of EDTA were used, with 10 g/liter and pH 6.0 possibly being the best tried. Good separation of the individual rare earths was obtained.

$DTPA^+$ was compared with Cu^{2+} as a barrier ion. The $DTPA^+$ barrier runs began elution of the first rare earth in a little more than half the time which was required in the CU^{2+} barrier run, and about half the volume of EDTA solution was used up to that point. No difference was noted in the elution times after the rare earths started off.

Two of eight $DTPA^+$ barrier runs gave some slight problems. In one of these, plugging occurred in a ⅛-in. line between columns 2 and 3. New ¼-in. lines were installed. In the other, plugging occurred below column 3. This appeared to be due to EDTA precipitating out of solution, in spite of the fact that all elutions were done at about 80°C. None of the other runs showed any tendency toward plugging. It is possible that once elution is started it should not be stopped until the separation is complete.

When time is available, this $DTPA^+$ barrier process will be tried in cubicle 5 at TRU to determine its feasibility in the separation of the actinides, particularly americium and curium.

10.5 ISOTOPE ENRICHMENT BY (n,γ) REACTIONS IN MOLECULAR SIEVES

Additional study of the isotopic enrichment resulting from irradiation of lanthanide-exchanged zeolites[8] has shown that product yields as high as 70% can be obtained consistently, with enrichment factors of about 100. It was also shown that Linde X and Y give essentially identical results. Linde Y has the same geometrical structure as Linde X but contains relatively more silicon and less aluminum and therefore has a lower exchange capacity. Similar product yields are obtained with actinides, provided the total loading is sufficiently high, but enrichment factors are lower. With type L zeolite, which has a different although related structure, both the yields and enrichment factors were substantially lower.

In order to obtain appreciable production of isotopes of interest, it is necessary either that comparable results be obtained after much greater neutron exposures (greater by factors of 10^3 to 10^5) or that greater enrichment factors be achieved if such long irradiations cannot be tolerated. Study of the effects of radiation damage has been delayed by the lack of suitable irradiation facilities for this work, but such experiments are now started.

7. D. R. Asher et al., *Ind. Eng. Chem., Proc. Des. Develop.* **1**, 52 (1962).

8. *Chem. Technol. Div. Annu. Progr. Rep. May 31, 1970*, ORNL-4572, p. 225.

Attempts to obtain greater enrichment factors have met with little success. The isotopic enrichment obtained depends directly on the product yield and inversely on the amount of target material that is eluted from the zeolite along with the product. Since yields are generally greater than 50%, any increase in yield can have only a small effect on the enrichment factor. Thus a major improvement in the enrichment factor can result only from a marked decrease in the amount of target material that is eluted. This problem of target elution is several times more severe for americium (3 to 5%) than for lanthanides (usually less than 1%), and this causes lower enrichment factors with actinides.

A series of tests was made with Linde 13X exchanged with ^{241}Am to investigate the effect of various manipulations on subsequent elution with lithium chloride solution. The standard procedure is to wash the exchanged zeolite, after ignition to $\geqslant 500°C$, with LiCl solution to remove the exchangeable americium, with $Ca(NO_3)_2$ solution to remove the lithium, and finally with water, and then to ignite the zeolite again to 500°C to produce a dry product for irradiation. Subsequent elution of the neutron capture product removes generally 3 to 5% of the americium target. The amount of americium removed decreases with successive elutions; for example, four elutions removed successively 4.7, 1.2, 0.53, and 0.18% of the americium. The time of equilibration, up to a day, had little effect on these percentages, and in all cases very little americium was removed after two or three elutions. However, if the zeolite was then washed and reignited, as it usually is before irradiation, then a subsequent series of elutions removed essentially the same fractions of americium as stated above. Several milder treatments were tested, with varying results. Drying at 110°C, which does not remove all the water from a zeolite, resulted in removal of about 2% of the americium when the zeolite was subsequently eluted; superficially drying in air at 90°C caused a smaller removal, around 1% of the americium. Even after ten cycles of drying and eluting, ignition to 500°C gave a product from which more than 3% of the americium was eluted. Thus, it is apparent that drying the zeolite, even under rather mild conditions, causes a migration of some of the americium from nonexchangeable to exchangeable sites, which results in reduced enrichment of the product. For the practical purpose of minimizing target elution following irradiation, it may be desirable to irradiate the zeolite in water, although this has obvious disadvantages. This area, the effect of the experimental conditions on the elution of exchanged metal ions, needs additional study since the mechanisms involved in ion exchange on zeolites are not adequately understood.

It was reported last year that it was more difficult to load Linde 13X zeolite with actinides than with lanthanides; and, in most early work, procedures which gave nearly quantitative exchange with lanthanides gave only 30 to 50% exchange with americium or curium. It was known that lower ionic concentrations in the aqueous phase favor the natural selectivity of Linde X for polyvalent ions over monovalent (sodium) ions and also that temperature sometimes has a remarkable effect on exchange kinetics. When more-dilute americium solutions were used at elevated temperatures, essentially complete exchange of americium into Linde X was achieved. However, it does appear that the zeolite shows less selectivity for americium than for lanthanide ions like praseodymium.

10.6 DISTRIBUTION EQUILIBRIA AND MECHANISMS

Comparison of Organophosphorus Extractants

A comparative study was completed of di(2-ethylhexyl)phosphoric acid and two related phenylphosphonic ester acids, and a paper is in press in *J. Inorg. Nucl. Chem.* Its abstract follows:

"Comparison of Some Monoacidic Organophosphorus Esters as Lanthanide-Actinide Extractors and Separators," by Boyd Weaver and R. R. Shoun. *Abstract:* Comparison of di(2-ethylhexyl)phosphoric acid (HDEHP), 2-ethylhexyl phenylphosphonic acid (HEH[ΦP]), and 1-methylheptyl phenylphosphonic acid (HMeH[ΦP]) in an aliphatic and an aromatic diluent as intragroup separating agents for trivalent lanthanides and actinides shows some important advantages of HMeH[ΦP]. In extractive power, HMeH[ΦP] is intermediate to the other compounds. In several separations systems HMeH[ΦP] is at least twice as effective as HDEHP and significantly better than HEH[ΦP] for separation of tracer-level Eu from Ce, and its advantage for separating Cf from Cm is nearly as great. Neither of the phosphonic acids is suitable for separating natural lanthanides at the usual high concentrations because of solubility limitations.

Extractions of these elements frequently deviate from the theoretical third-power dependence on extractant concentration and inverse third-power dependence on acid concentration. Extractant concentration dependence varies with extractant and diluent. Acid concentration dependence varies somewhat with extractant and diluent, and much more with element and aqueous acid.

A process which has been used successfully for separating Cf from Cm is based on extraction by an aliphatic solution of HDEHP from HCl. More effective separation can be obtained with HMeH[ΦP]. With HEH[ΦP] or HMeH[ΦP], HNO_3 can be substituted for HCl, giving a separation superior to that with the HDEHP-HCl system, provided that solubility limitations are not exceeded.

Studies of Metal Complex Formation at High Ionic Strength

We are studying several different methods for investigating the formation of weak metal-ion complexes, that is, those that are formed to an important extent only in the presence of moderate to high ligand concentrations. These methods include phase distribution equilibria with fixed ionic strength and with varying ionic strength, electromigration, spectrophotometry, and "tagged-ligand transfer" (defined below).

The weak complexes are of great practical interest. High concentrations of the common mineral acid anions are frequently encountered in processing, and appreciable complexing of various metal ions occurs. An appropriate example is the TRAMEX process, in which actinides and lanthanides are separated by amine extraction from 10 to 12 *M* lithium chloride solution. The role of the high chloride concentration in this process is not well understood but is usually attributed to differences in chloride complexing between lanthanides and actinides.

Thermodynamic methods alone (distribution, potentiometry, solubility, etc.) usually cannot be applied at high ligand concentrations because activity coefficient information is lacking and cannot be sufficiently well estimated. The usual procedure for circumventing activity coefficient problems, measurement at constant ionic strength, does not really avoid these problems. The possibility of changing medium effects and unknown salting effects makes questionable the equilibrium constants obtained by such measurements at ionic strengths greater than 1 or 2 *M*. Furthermore, such constants can be related only to the particular ionic medium in which they were determined.

Our attempts to understand weak complexes have been successful with several metals in sulfate systems at moderate concentrations, by the use of amine extraction of neutral and anionic species. It was possible to use varying ionic strength in the aqueous phase and estimate activity coefficient ratios by means of a Debye-Hückel type equation (cf. Sect. 5.5).[9] However, the same approach failed with lanthanide ions in chloride and thiocyanate systems, apparently because of nonnegligible variation of neutral-species extraction with ionic strength. (Cation exchange extraction at constant ionic strength and spectrophotometry[10] have been successful with trivalent actinides at thiocyanate concentrations up to 1 *M*; cf. Sect. 5.5.)

Some preliminary electromigration experiments have been made in the sulfate, thiocyanate, and chloride systems, in a cell with three compartments separated by medium-porosity frits. Electrolysis was from 10 to 30 min at 10 to 15 mA, 10 to 12 V. Although these measurements could not be made quantitative because we lack the individual ionic mobilities, they give qualitative evidence for existence of anionic complexes in significant amounts. Tests with tracer levels of ^{241}Am in the sulfate system showed amounts of americium migrating to each electrode in qualitative agreement with the known anion-cation composition of the solutions. Tests of the same type indicated large amounts of anionic americium thiocyanate complexes at concentrations above 1.0 *M* SCN^- and appreciable amounts of anionic americium chloride complexes at 10 *M* Cl^-.

Currently the most interesting and perhaps the most promising method of examining complexes at high ionic strength is a method we call *tagged-ligand transfer.* (It was previously found by this method that the uranium species transferring across the interface from sulfate solution to an amine sulfate extractant could be either neutral or anionic, depending on the composition of the aqueous phase.[11]) The ligand in the aqueous phase of a solvent extraction system is tagged radioactively, and its appearance in the organic extractant phase through a limited interface is followed as a function of time. Ligand transferring to the organic phase in other ways than as a part of the metal complex can be determined by appropriate analyses and subtracted from the total. The resulting net ligand concentration transferred, divided by the metal concentration transferred, gives the ratio, moles of ligand/mole of metal, as a function of time. This ratio extrapolated back to zero time should be the average ligand/metal association number in the species that cross the interface before any disruption caused by the progress of the extraction has occurred.

The tagged-ligand method has been tested with iron(III) complexes in the chloride system. It indicated an average of three chlorides per iron at 4 *M* aqueous chloride, in agreement with the complex composition found spectrophotometrically.[12] Tests made with europium to date indicate surprisingly large chloride to

9. K. A. Allen and W. J. McDowell, *J. Phys. Chem.* **67,** 1138 (1963); *Chem. Technol. Div. Annu. Progr. Rep. May 31, 1968,* ORNL-4272, p. 116.

10. *Chem. Technol. Div. Annu. Progr. Rep. May 31, 1970,* ORNL-4572, p. 188.

11. W. J. McDowell and C. F. Coleman, *J. Inorg. Nucl. Chem.* **29,** 1325 (1967).

12. G. A. Gamlin and D. O. Jordan, *J. Chem. Soc. (London)* **1953,** 1435.

europium ratios. With chloride concentrations of 5 to 9 *M*, between six and eight chlorides per europium are indicated as crossing the interface into the organic phase. Since no other measurements have indicated such high numbers for aqueous-phase chloro complexes of the lanthanides, there is some concern as to their meaning. Coordination numbers of 9 have been quoted for the lanthanides with chloride,[13] but only in nonaqueous systems. Although concentrated lithium chloride solutions are not strictly aqueous systems, it is difficult to think of them as sufficiently nonaqueous to have so much water of hydration replaced by chloride. Further, if so many chloride ligands were inner-sphere association, that should be discernible by spectrophotometry. In any case, however, these numbers represent chlorides crossing the interface with europium and indicate the existence of some aqueous-phase europium-chloride grouping of sufficient integrity to remain together while transferring to the organic phase.

Liquid Scintillation Analysis of Heavy Actinides

Liquid scintillation counting using the extractive scintillator technique[10] is being used for the determination of transplutonium actinide concentrations in aqueous thiocyanate-perchlorate solutions (cf. Sect. 5.5). The extractive scintillator composition in this case is 7 g PPO, 0.5 g Me_2POPOP, and 161 g HDEHP extractant diluted to 1 liter with toluene.[14] The aqueous samples (usually 1 ml) were added directly to the scintillator vial, as previously described. A trace of iron contaminant in the HDEHP caused some quenching by forming the deeply colored ferric thiocyanate complex; this quenching was suppressed by addition of a small amount of ethylenediamine. Counting efficiency was 100%. Americium-241 was determined by both liquid scintillation alpha counting and gamma counting, with excellent agreement. Resolution in the liquid scintillation counting was sufficiently good for the simultaneous determination (in one vial) of ^{244}Bk by means of its 0.125-MeV beta and ^{253}Es by means of its 6.6-MeV alpha group.

10.7 RELATIVE POTENTIALS OF THE Bk(IV)-Bk(III) AND Ce(IV)-Ce(III) COUPLES

Measurements of the difference between berkelium and cerium oxidation potentials by means of solvent extraction[15] were completed, and a paper is in press in *J. Inorg. Nucl. Chem.* Its abstract follows:

"Relative Oxidation Potentials of the Bk(IV)-Bk(III) and Ce(IV)-Ce(III) Couples in Acid Solutions," by Boyd Weaver and J. N. Stevenson.[16] *Abstract:* The differences in formal oxidation potentials of the Bk(IV)-Bk(III) and Ce(IV)-Ce(III) couples in a wide range of concentrations of nitric and perchloric acids have been measured by a solvent extraction method which separates the Bk(IV) from the Bk(III) present in equilibrium with a Ce(IV)-Ce(III) mixture of predetermined composition in an aqueous solution. The differences in potential are then calculated from a form of the Nernst equation. In nitric acid Ce(IV) was the stronger oxidant in all concentrations of acid below about 7.5 *N* HNO_3, with a maximum difference of ~0.08 v in 2 *N* HNO_3. In perchloric acid the maximum difference was ~0.11 v in 4 *N* $HClO_4$ with differences of ~0.08 v in 1 *N* and 8 *N* $HClO_4$. Attempts to measure potential differences in sulfuric and phosphoric acids by this method were unsuccessful because of strong complexing in the aqueous solutions.

10.8 LANTHANIDE AND ACTINIDE HYDROXIDES

Previously[15] we reported a comparison of the basicities of americium and curium with those of the lanthanides by titration of very dilute (~0.002 *M*) solutions of their nitrates with dilute sodium hydroxide solutions. We repeated part of this work with chloride solutions, obtaining essentially identical results. We also included titrations of yttrium solutions and titrations of some of the elements at considerably higher concentrations in order to make possible comparisons with previous work of others.[17,18]

Data in the form of pH values at given ratios of added NaOH to metal present may be used to calculate solubility products and solubilities. Figure 10.6 shows the titration curves for americium, curium, and some of the lanthanides at low concentration. From the titration curves, americium can be seen to be between neodymium and samarium. Curium, however, cannot be placed so definitely. It begins to use NaOH at a much lower pH than any of the lanthanides, but there is no flat region in its titration curve, which eventually crosses all the others. Curium also requires less NaOH for complete titration than any of the other elements, only about 2.1

13. D. G. Karraker, *J. Chem. Educ.* **47**, 424 (1970).

14. PPO = 2,5-diphenyloxazole; Me_2POPOP = 1,4-bis(4-methyl-5-phenyloxazolyl)benzene; HDEHP = di(2-ethylhexyl)-phosphoric acid.

15. *Chem. Technol. Div. Annu. Progr. Rep. May 31, 1970,* ORNL-4572, p. 192.

16. University of Tennessee, Knoxville.

17. K. A. Kraus and J. R. Dam, "Hydrolytic Behavior of Plutonium(III)," pp. 466–77 in *The Transuranium Elements* (ed. by Glenn T. Seaborg et al.), National Nuclear Energy Series, vol. 14B, McGraw-Hill, New York, 1949.

18. Therald Moeller and H. E. Kremers, *J. Phys. Chem.* **48**, 395 (1944).

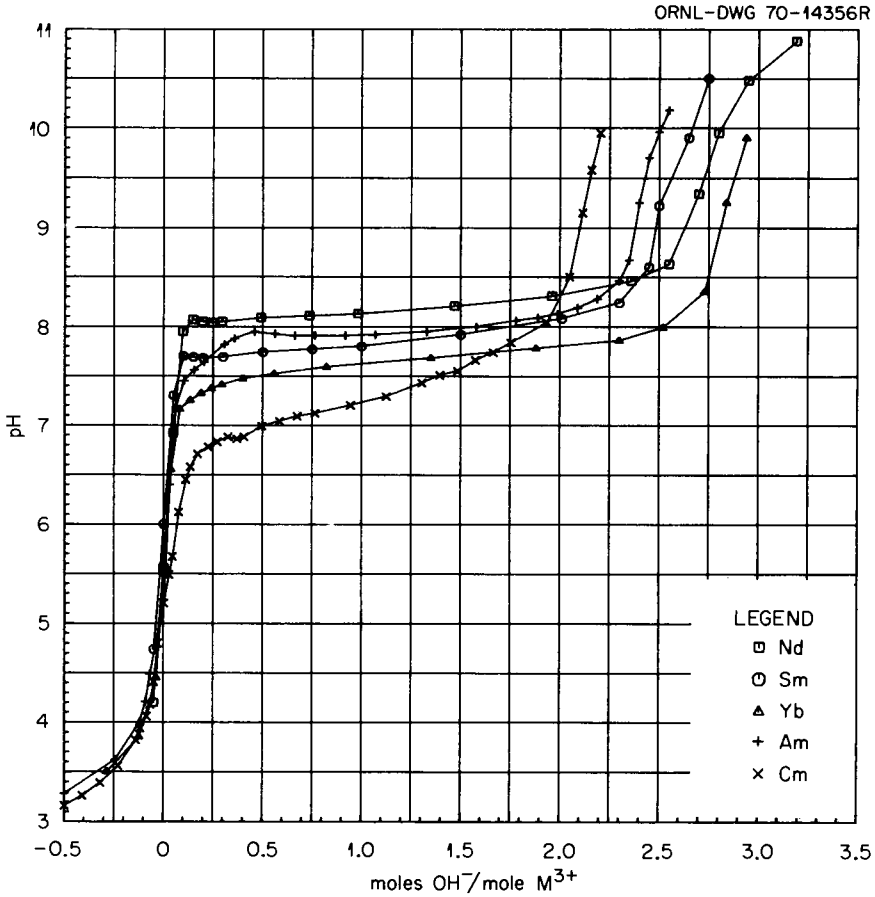

Fig. 10.6. Titration of 0.002 *M* solutions of Am, Cm, and selected lanthanides with 0.050 *N* NaOH.

equiv/mole. The other elements vary in stoichiometry, but none of them reaches 3.0 equiv/mole.

The basicities of the lanthanides have often been compared with their ionic radii. In Fig. 10.7, one set of curves is a plot of the ionic radii of lanthanides and trivalent actinides arranged so as to maximize their correspondence. The other set of curves shows, for each element, the pH at the point at which 0.5 equiv per mole of metal has been added. The pH value does not necessarily apply to Pu, which is placed with Pr because they had previously been found alike.[17] The difference between consecutive lanthanides decreases as the ionic radii decrease, while the opposite appears to occur in the case of the actinides. While yttrium has an ionic radius equal to that of erbium, its basicity is near that of samarium at the low concentration used here.

Solubility products of the hydroxides of trivalent metals are usually calculated from the equation $K_{SP} = [M^{3+}][OH^-]^3$. Moeller and Kremers[18] calculated solubility products of most of the lanthanides in this manner from their titrations at ~25 times higher concentrations, though they also observed anomalous stoichiometries. We believe that true solubility products can be obtained only from actual stoichiometries. In Table 10.2, average values of solubility products from our data at NaOH/M values of 1.0, 1.2, and 1.5 are compared with the data of Moeller and Kremers.

Solubilities of the hydroxides in pure water may be calculated, at least theoretically, from the solubility products. The equation is $S = (K_{SP}/n^n)^{1/(n+1)}$ for $M(OH)_n$ hydroxides. Table 10.2 also compares our values for solubilities with those of Moeller and Kremers. All of our solubility products are much larger than theirs, and the differences increase by magnitudes as the series progresses. The solubilities show much smaller differences.

The factor of 25 in concentration between the two sets of experiments should make a difference of around 0.5 pH unit at corresponding points in the titrations, if the stoichiometries were exactly $M(OH)_3$. Figure 10.8 compares pH values for NaOH/M = 0.4. Our values are about 0.6 to 0.8 pH unit higher than theirs. Figure 10.8

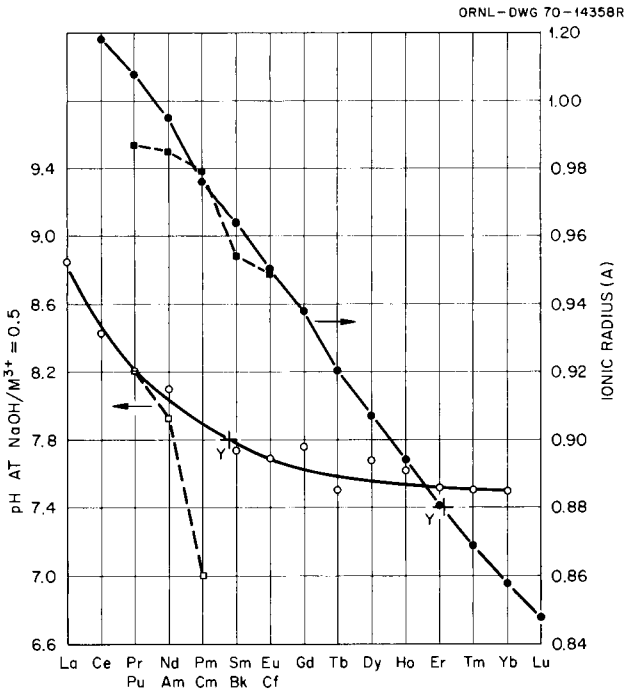

Fig. 10.7. Ionic radii and comparative pH values at NaOH/M = 0.5 for actinides, lanthanides, and yttrium. ● –, ionic radii of lanthanides; ■ ––, ionic radii of actinides; ○ –, pH values of lanthanides; □ ––, pH values of actinides.

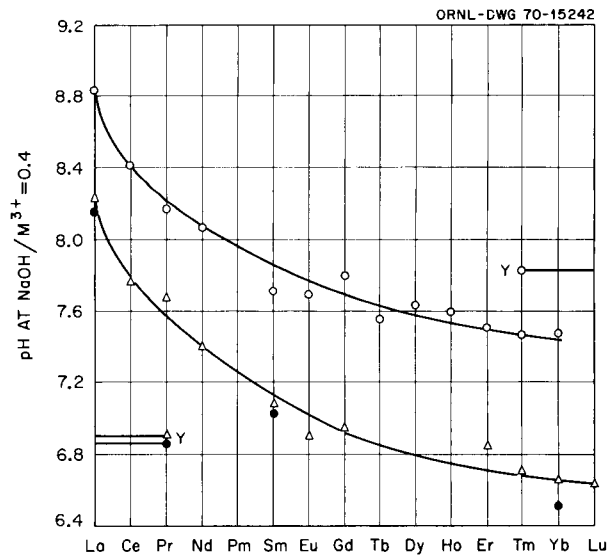

Fig. 10.8. Comparison of lanthanide pH values at NaOH/M = 0.4 with data of Moeller and Kremers (ref. 18). ○, our data for 0.002 *M* solutions; ●, our data for 0.05 *M* solutions; Δ, data of Moeller and Kremers for 0.05 *M* solutions.

Table 10.2. Solubilities and solubility products of lanthanide and actinide hydroxides

M	Stoichiometry[a]	$K_{SP} \times 10^{20}$		$S \times 10^6$ (moles/liter)	
		Our values[b]	M and K[c]	Our values[b]	M and K[c]
La	2.88	250	11	13.2	8.0
Ce	2.65	500	0.70	3.1	4.0
Pr	2.70	50	0.84	5.5	4.2
Nd	2.48	410	0.031	5.3	1.8
Sm	2.52	37	0.0046	3.0	1.1
Eu	2.62	8.6	0.0013	2.7	0.8
Gd	2.65	6.9	0.0018	2.8	0.9
Tb	2.65	1.7		1.9	
Dy	2.55	21		2.8	
Ho	2.65	5.4		2.6	
Er	2.83	0.24	0.00075	1.9	0.7
Tm	2.65	2.5	0.00030	2.1	0.6
Yb	2.85	0.097	0.00022	1.6	0.5
Y	2.53	37	0.0014	3.1	0.9
Am	2.40	340		3.9	
Cm	2.10	1700		2.3	

[a]Number of hydroxyls per metal ion in the solid phase.

[b]Average of values obtained at NaOH/M = 1.0, 1.2, and 1.5.

[c]Moeller and Kremers, ref. 18.

also includes results from our duplication of some of their experiments; we obtained remarkably close checks.

10.9 KINETICS OF METAL-ION EXTRACTIONS BY ORGANOPHOSPHORUS ACIDS

A review article on this subject, covering the literature through 1969, is in press for publication in the first issue of a new journal, *Solvent Extraction Reviews.*[19]

Iron Extraction by HDEHP

The current study of iron extraction kinetics was completed and reported in a paper submitted to the *Journal of Inorganic and Nuclear Chemistry* (in press). Its abstract follows:

"Mechanism of the Slow Extraction of Iron(III) from Acid Perchlorate Solutions by Di(2-ethylhexyl)phosphoric Acid in *n*-Octane," by J. W. Roddy, C. F. Coleman, and Sumio Arai. *Abstract:* The rate of iron(III) extraction by di(2-ethylhexyl)-phosphoric acid (HDEHP, HA) in *n*-octane from acid perchlorate solutions, as $FeA_3 \cdot 3HA$, is controlled by series and parallel reactions in the introduction of the first and second anion ligands, all occurring at the interface. (In the following subscripts, 1 and 2 refer to first and second anion ligands, *m* to extractant monomer, *d* and *df* to extractant dimer, *s* to interface saturation.) The measured rate/[Fe],

19. C. F. Coleman and J. W. Roddy, "Kinetics of Metal Extraction by Organophosphorus Acids," *Solvent Extraction Reviews* (in press).

$$r \equiv -d[Fe]/[Fe]\,dt\,,$$

is well fitted by the step rates (25°C)

$$r_{1m} = 5.5 \times 10^{-4}\ [\Sigma HA]^{0.5}/[H^+]$$

$$r_{1d} = 1.8 \times 10^{-3}\ [\Sigma HA]/[H^+]$$

for parallel reactions introducing the first anion ligand, in series with

$$r_2 \approx 4 \times 10^{-4}/[H^+]^2$$

$$r_{2s} = 1.5 \times 10^{-7}/[H^+]\,[Fe]$$

$$r_{2d} = 9.0 \times 10^{-6}\ [\Sigma HA]^{1.5}/[H^+]^2$$

$$r_{2df} = 1.2 \times 10^{-5}\ [\Sigma HA]^2/[H^+]^2$$

for parallel reactions introducing the second anion ligand. Step 2*s* is zero order, while all the other steps are first order, with respect to the aqueous iron concentration. In extractions through a quiescent interface these step rates combine so that

$$r = (r_{1m} + r_{1d})(r_{2s} + r_{2d} + r_{2df})/\Sigma r_i\,,$$

and in extractions with dispersion mixing so that

$$r = (r_{1m} + r_{1d})r_2/(r_{1m} + r_{1d} + r_2)\,.$$

The rate decreases slightly with increasing ionic strength, increases with increasing temperature (heat of activation ≈ 10–15 kcal/mole) and with conditions that increase the ionization of HA, and increases sometimes markedly with addition of proton-accepting complexers that can bypass the interface steps 1*m* and 1*d* with analogous reactions homogeneous in the aqueous phase.

After the reaction steps and their rate parameters were determined in a quiescent-interface cell as previously described,[20] key points were cross-checked by dispersion mixing with a flat-blade turbine in a baffled cell under conditions that have been standardized for scaleup.[21-23] The results (Fig. 10.9) showed only a small shift of the observed rate *ra* with changing initial iron concentration, that is, a much smaller contribution from a zero-order step in the rate control than there is with the quiescent interface. This is not surprising, as the changing interfaces of the rapidly forming and

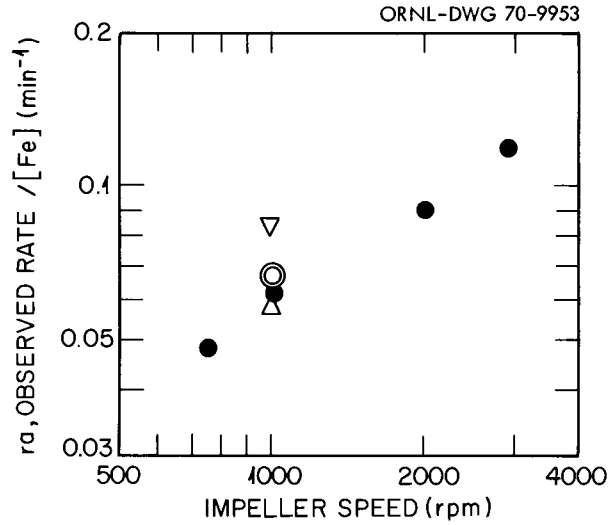

Fig. 10.9. Rate of iron extraction by HDEHP in dispersion mixing. Effects of impeller speed, iron concentration, and ionic strength. Molarities: [HA] = 0.05; [$HClO_4$] = 1. I = 1: Δ; 2: ○, ●; 3: ∇. [Fe] = 0.0001: ○; 0.002: ●.

recoalescing droplets may not have time to reach saturation. The observed rate *ra* increased slightly with increasing ionic strength. However, calculation of the specific interfacial area *a* (see below) showed that this reflects an increase in *a* at constant rpm due to increased aqueous-phase density. The resulting values of the rate *r* are nearly constant at ionic strengths from 1 to 3 *M*. As the HDEHP concentration was increased from 0.005 to 1 *M*, the power dependence of *r* on [HDEHP] decreased from ~0.4 to ~0.1, and that on [H^+] increased from ~1 to ~1.7. This shows that some step in the introduction of the second anion ligand is becoming important with increasing HDEHP concentration. The overall rate data are usefully well fitted when this step rate is represented by the approximate equation listed in the foregoing abstract, $r_2 \approx 4 \times 10^{-4}/[H^+]^2$.

Interfacial Area in Dispersions. In the quiescent-interface cells both interfacial area and volume are measured directly. In dispersion mixing the interfacial area varies with power input and must be measured by special techniques or estimated by correlation with such measurements. In a mixer suitably baffled to prevent swirling and vortex formation, the specific interfacial area *a* is proportional[23] to the cube root of the specific power input, $(P/V)^{1/3}$, where the total power input[21] is $P = N^3D^5K\rho/g$. N is the impeller speed, D is the impeller diameter, K is a constant for the type of impeller,[21] ρ is the mean density of the two phases,

20. *Chem. Technol. Div. Annu. Progr. Rep. May 31, 1968,* ORNL-4272, p. 182, and references therein.

21. J. H. Rushton and J. Y. Oldshue, *Chem. Eng. Progr.* 49, 161 (1953).

22. W. A. Rodger, V. G. Trice, Jr., and J. H. Rushton, *Chem. Eng. Progr.* **52,** 515 (1956).

23. A. D. Ryon, F. L. Daley, and R. S. Lowrie, *Chem. Eng. Progr.* **55**(10), 70 (1959); more fully in ORNL-2951 (Sept. 15, 1960).

and g is the gravity constant. From this,

$$a = A/V_{aq} = kN(D^5 K\rho/V)^{1/3} , \quad (1)$$

where k is a proportionality constant for similar systems in geometrically similar mixers. Its relative values in different systems can be estimated from published correlations of the effects of density, kinematic viscosity, interfacial tension, and settling time,[22]

$$k \propto A/V \propto (\exp \Delta\rho/\rho_{cont}) \times (\nu_{disp}/\nu_{cont})^{1/5} (\sigma_i^{-0.36})(t_s^{1/6}) . \quad (2)$$

Fitting Eq. (1) to the specific areas calculated in ref. 23 gave k = 14.6 (cgs units), and adjustment by proportionality (2) led to k values in the range of 16 to 24 for the various conditions used here. The self-consistency of the calculated a values over the range of mixing conditions and the agreement of the resulting r values with those from the quiescent-interface measurements at HDEHP concentrations below 0.1 M were both surprisingly good and support confidence in the general validity of the published correlations.

Beryllium Extraction by HDEHP

In spite of the elimination of several sources of experimental error,[24] the reproducibility of the beryllium extraction kinetics measurements continues to be much poorer than that typical of the iron extraction kinetics. Thus repeated runs continue to confirm that the power dependence of rate (expressed as first-order rate constant with respect to beryllium) on the HDEHP concentration is near ¾ below and ⅝ above about 0.2 M HDEHP, but they still fail to distinguish between alternative possible mechanisms for the extraction reaction. Work continues on trying to identify and eliminate the causes of poor precision, including as possibilities (1) unexpectedly early reverse reaction, (2) interface blocking, and (3) variable catalytic effects beyond those already identified and eliminated.

24. *Chem. Technol. Div. Annu. Progr. Rep. May 31, 1970,* ORNL-4572, p. 194.

11. Chemical Applications of Nuclear Explosives

The purpose of this program is to provide research and development in selected areas of the Plowshare Program. Research was performed during the past year in areas of study associated with evaluation of proposed underground engineering applications of nuclear explosives. The studies included determination of the behavior of radionuclides (1) in the recovery of copper from ore deposits that have been fractured with nuclear explosives, (2) in the recovery of oil from shales, and (3) in natural-gas storage reservoirs.

11.1 COPPER ORES

Fracturing of copper ore deposits with nuclear explosives, followed by leaching in place, is being studied by the Division of Peaceful Nuclear Explosives of the U.S. Atomic Energy Commission and by associated contractors. We are cooperating in this program by studying potential problems that might arise from the presence of radioactive contaminants in the processing cycle. The recovery flowsheet involves percolating dilute sulfuric acid down through the broken ore to dissolve the copper, collection of leach liquor at the bottom of the chimney and pumping it to the surface, recovery of a copper concentrate from the solution by cementation or solvent extraction, upgrading the copper concentrate to pure copper metal, and recycling of the copper-barren solution to leaching after fortifying it with acid.

Our laboratory studies on this project are now complete, and a final summary report[1] has been written. In the most recent studies, a bench-scale demonstration was made of solvent extraction recovery of copper (as an alternative to cementation) from the leach liquor. The tests indicated that solvent extraction would yield a copper product free of radionuclides. It is the recommended process route for recovering copper from ores that have been fractured with nuclear explosives.

Solvent Extraction of Copper

A bench-scale cyclic column leaching–solvent extraction–electrowinning circuit was operated to measure the separation of copper from radioactive contaminants by this process. Although the column of ore was dosed with relatively large amounts of several radionuclides in soluble form, the radioactive contamination of the copper metal products was extremely low, being detectable only in a special low-level counting facility.

A flow diagram for the test is shown in Fig. 11.1. The 4-in.-ID column contained 4500 g of –0.5-in. Safford ore (1.3% Cu) that was spiked with a small volume of solution of ^{85}Sr, ^{95}Zr-Nb, ^{106}Ru, ^{125}Sb, and ^{134}Cs. The ore was leached with dilute sulfuric acid (pH 2.0) at a flow rate of 0.5 ml/min. Copper was recovered from the effluent by batch countercurrent extraction with 10 w/v % LIX-64 in Varsol, and the copper-barren liquor was recycled to leaching. The solvent extract was scrubbed with water to remove entrained liquor, stripped with about 4 N H_2SO_4, and recycled to extraction. The strip solution was treated in a small electrolytic cell to deposit part of the copper and then recycled to the stripping system.

The copper concentrations in solutions in the process circuits during the run are shown in Fig. 11.2. About 65% of the copper was leached from the ore in 24.6 liters of effluent; most of the copper was leached at an effluent pH of about 3.5. Only minor fractions of the radionuclides reported to the column effluent, due to effective ion exchange retention of the radionuclides by the ore. Strontium-85 was the dominant radionuclide in the initial effluent, and ^{106}Ru was dominant in the final effluent (Fig. 11.3). About 20% of the ^{85}Sr was in solution in the first half of the test; about 4% of it was in solution at the end. The amount of ^{106}Ru in solution increased from less than 1% in the early part of

1. W. D. Arnold and D. J. Crouse, *Radioactive Contamination of Copper Recovered from Ore Fractured with Nuclear Explosives*, ORNL-4677 (in press).

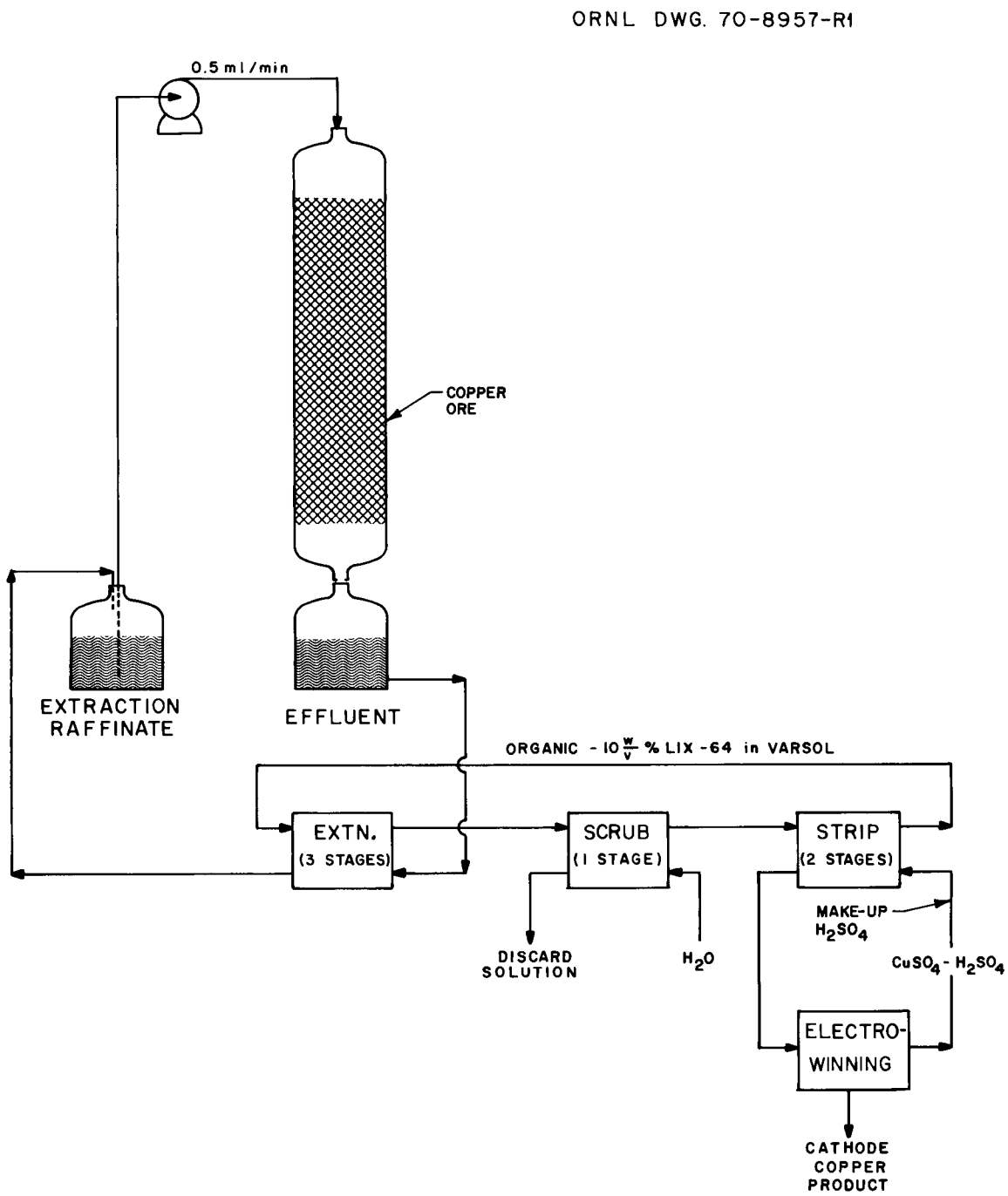

Fig. 11.1. Flowsheet for column-leaching–solvent-extraction–electrowinning circuit.

ORNL DWG. 70-8958

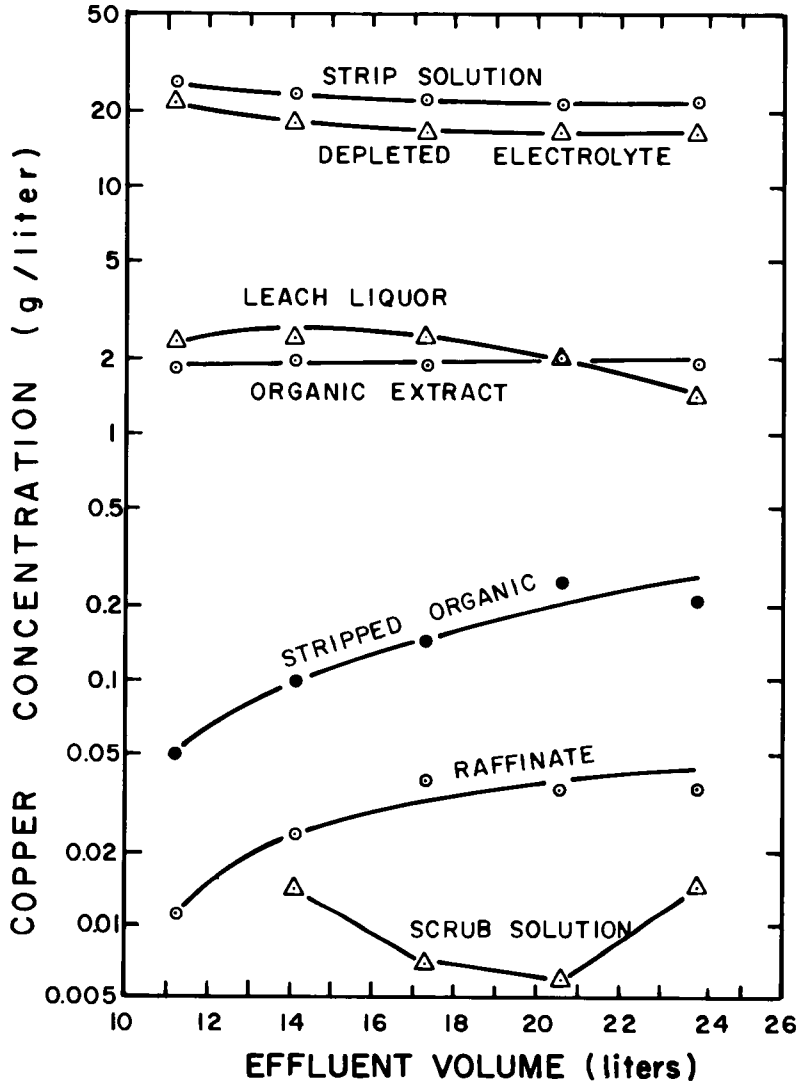

Fig. 11.2. Profile of copper concentrations in the copper recovery system.

the test to about 16% at the end. Less than 1% of the ^{125}Sb or ^{134}Cs was in solution at any time, and ^{95}Zr-Nb was not detected in any of the effluent samples.

Copper was separated efficiently from the radioactive contaminants in the three-stage extraction step. More than 98% of the copper was extracted. The highest gross gamma count rate for any solvent extract sample was only 8% above background.

Copper was stripped with about 4 N H_2SO_4 in a two-stage batch countercurrent stripping system. The strip solution had a gross gamma count rate that was less than 5% above background.

Copper was deposited from the strip solutions in a small electrolytic cell. Radioactivity of the cathode copper products was undetectable by our usual procedures. However, tiny concentrations of ^{106}Ru, but no other radionuclides, were detected in a special

ORNL DWG. 70-8960

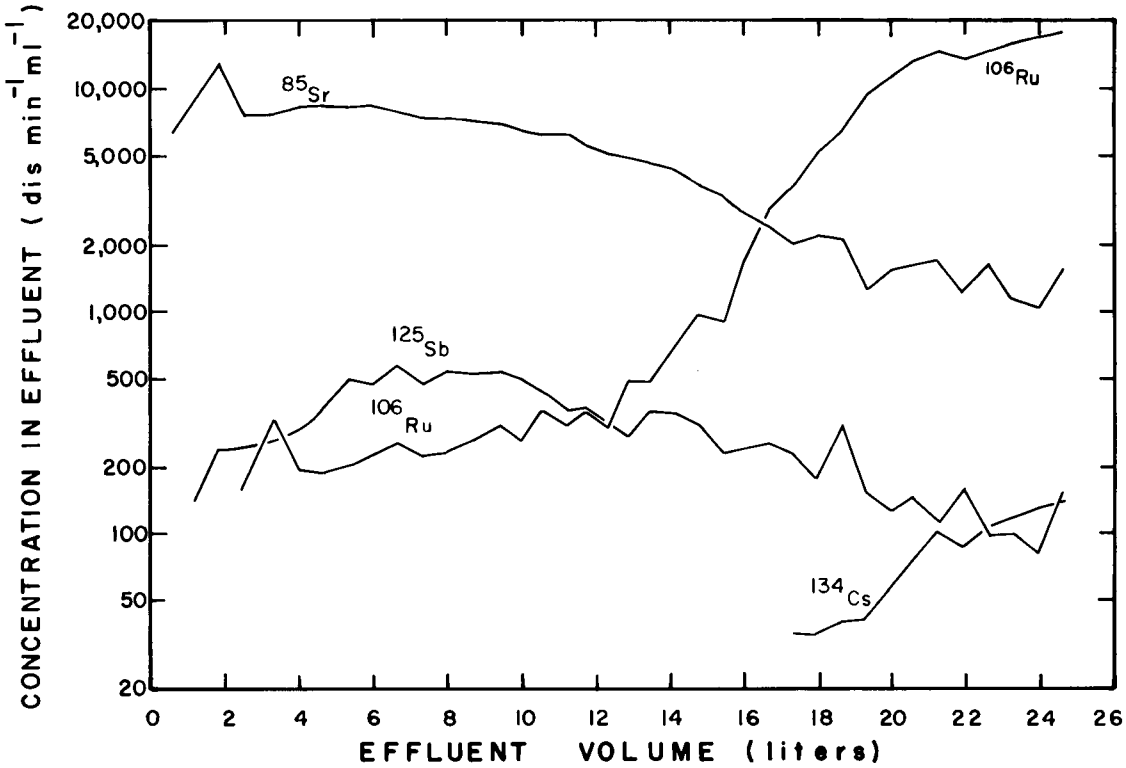

Fig. 11.3. Concentration of radionuclides in the column effluent. The ^{95}Zr-Nb concentration was less than 20 dis min^{-1} ml^{-1} in all samples.

low-level counting facility at ORNL. The activities of copper products obtained early and late in the run, respectively, were measured to be 9×10^{-6} and 1.9×10^{-5} μCi of ^{106}Ru per gram.

Copper cementation products prepared (from small leach liquor samples) during the run for comparison purposes were appreciably contaminated with ^{106}Ru; the ^{106}Ru concentration increased from 0.02 to 1.0 μCi per gram of copper as the ^{106}Ru/Cu ratio in the leach liquor increased during the run. Much lower, although significant, amounts of ^{125}Sb also contaminated the cement copper products. Assuming a decontamination factor of 100 from ^{106}Ru during electrorefining of the cement copper, the activity of the final copper products would be one to three orders of magnitude higher than the activity of the products that were obtained by the solvent extraction–electrowinning process.

11.2 RECOVERY OF OIL FROM SHALE

The feasibility of recovering oil from Green River oil shales by using a nuclear device to fracture the shale and then retorting the oil in place is being investigated by several governmental agencies and commercial companies. We are participating in this program by examining the oil recovery system with regard to the behavior of the radioactive contaminants that would be formed in a nuclear detonation. Studies of tritium behavior were continued this year in small-scale tests. Samples of oil shale were heated at 85°C and 560 psig in small pressure vessels with tritiated compounds, using about 1 μCi of tritium per gram of shale. Oil was then retorted from the shale after washing it with water and drying with warm air.

The oil retorted from shale that had been exposed for 85 days to tritiated hydrogen contained 0.46 μCi of

tritium per gram, about the same concentration that was found in the oil obtained from shale exposed 44 days. The contamination of the oil had increased with increasing exposure time to 44 days. Similar behavior was measured earlier[2] on exposure of the shale to tritiated water. In this case, the tritium contamination increased with exposure time to 29 days and then did not change significantly as the exposure was increased to one year. Contamination from tritiated methane or tritiated ethane, which was more than an order of magnitude less than from tritiated hydrogen, was not affected by increasing the exposure time from 7 to 25 days. Adding water equivalent to 1% of the shale weight to the pressure vessel during exposure to tritiated hydrogen or tritiated methane reduced the tritium contamination of the retorted oil by about one-fourth.

At the request of the Division of Peaceful Nuclear Explosives of the U.S. Atomic Energy Commission, our studies on this project have been suspended, and a terminal report is being written.

11.3 NATURAL-GAS STORAGE

The use of nuclear explosives has been proposed to create storage reservoirs for natural gas. The natural gas would be stored in chimneys formed by contained nuclear detonations in tight rock formations and removed for use as needed. We are investigating the potential contamination of the stored natural gas by radionuclides released in the detonation and are studying methods of decontaminating the chimney before gas storage.

In our initial tests, we studied the behavior of tritiated water in contact with Lewis shale. Lewis shale is the dense, relatively impermeable shale that underlies the gas-bearing sandstone in the San Juan Basin (where the Gasbuggy test was made). The shale sample used is from a core sample taken 300 ft from the Gasbuggy shot point at a depth of 4210 ft. The porosity of the shale sample was measured to be about 2.0%. More than 65% of the pore volume is due to pores less than 0.1 μ in diameter, and more than 85% is due to pores less than 1 μ.

When Lewis shale is exposed to tritiated water at elevated temperature, some of the tritiated water enters the pores and fractures of the shale and is not easily removed by flushing with moist air. In one test, only about 65% of the tritiated water was removed from a contaminated shale sample in eleven 24-hr treatments at 50°C. The total air flow was more than 100 times the bulk volume of the shale.

The potential contamination of natural gas in a storage cavity is being studied by measuring the tritium concentration of methane that has been held in contact with contaminated shale in a small pressure vessel for various periods of time. Several tests are made with the same shale sample by pressurizing with fresh methane. The amounts of tritium found in the methane (after elaborate treatment to remove tritiated water from the gas stream) were extremely low (Table 11.1). The highest concentration measured, 0.0020 μCi/liter, is more than 100 times lower than the tritium concentration in the initial gas removed from the Rulison chimney. The concentration in the methane, which was measured by burning the methane to form carbon dioxide and water and measuring the tritium in the water, was near the detection limit in the last three releases.

Table 11.1. Contamination of methane during storage

Procedure: 100 g of Lewis shale (0.1- to 0.5-in.-diam pieces) was contaminated by heating at 50°C for 33 days with 1 ml of water containing about 92 μCi of tritiated water. After removal of about 23 μCi of tritiated water by purging with air, the shale was transferred to a pressure vessel for storage with methane. The vessel was repressurized with fresh methane after each release.

Methane release	Methane storage time (days)	Pressure (psig)	Tritium distribution (μCi)		Tritium in methane (μCi/liter)
			In water	In methane	
1	2	900	0.14	0.0278	0.0020
2	39	900	0.68	0.0181	0.0013
3	34	850	0.45	0.0008	<0.0001
4	40	725	0.44	0.0038	0.0003
5	29	790	0.39	0.0005	<0.0001

2. *Chem. Technol. Div. Annu. Progr. Rep. May 31, 1970,* ORNL-4572, p. 196.

12. Biochemical Technology

MACROMOLECULAR SEPARATIONS

12.1 PREPARATION OF CRUDE BOVINE LIVER TRANSFER RIBONUCLEIC ACID

Livers from large beeves (weighing more than 1000 lb) were used in our initial experimental work for the preparation of mammalian crude tRNA. Numerous tRNA preparations were made by following different isolation procedures. The resulting samples of crude tRNA were less active than typical crude tRNA preparations obtained from *E. coli.* The total amino acid acceptance was only 500 to 700 picomoles per A_{260} unit, and the terminal 3′-nucleoside assay indicated 500 to 700 picomoles of adenosine per A_{260} unit, 500 to 600 picomoles of cytidine per A_{260} unit, and small amounts of guanosine. It was obvious that these beef liver preparations contained appreciable quantities of degraded tRNAs. The use of reagents such as bentonite or diethyl pyrocarbonate to inhibit nuclease attack during recovery did not improve the product. The low terminal adenosine content and the low amino acid acceptance appeared to be characteristic of liver tRNA from mature beeves.

When calf liver, instead of beef liver, was used as the mammalian tRNA source, a more active crude tRNA was obtained. The livers used in these tests came from young animals weighing less than 500 lb. The best calf liver tRNA preparations had a total amino acid acceptance of 1050 picomoles per A_{260} unit and a 3′-terminal adenosine content of 1410 picomoles per A_{260} unit (Table 12.1). These values compare favorably with the values of total amino acid acceptance and 3′-terminal nucleoside content for typical *E. coli* tRNA preparations.

To date, the highest yield of calf liver tRNA has been 4.5×10^6 picomoles of tRNA per kilogram of liver. Comparison of this value with the typical yield of tRNA from *E. coli.* cells (i.e., 72×10^6 picomoles of tRNA per kilogram of cells) indicates that the recovery from calf liver is only about 6% of that from *E. coli.* This low yield appears to be typical of that to be expected from tissue sources and will restrict the quantity of purified mammalian tRNAs that can easily be recovered.

A simplified flowsheet of the procedure is shown in Fig. 12.1. After the animal had been slaughtered, the

Table 12.1. Summary of crude tRNA preparation from bovine liver

Run No.	Source	Sum of 20 tRNAs		3′-Terminal nucleoside (picomoles per A_{260} unit)			
		Yield (micromoles per kilogram of liver)	Acceptance[a] (picomoles per A_{260} unit)	Adenosine	Cytidine	Guanosine	Total
14	Beef	0.9	540	700	830	450	1980
23	Beef	4.0	790	1080	480	300	1860
15A	Calf	0.6	800	1410	150	170	1730
15B	Calf	1.7	870	1080	150	110	1340
16	Calf	2.7	1050				
17	Calf	1.9	730				
18	Calf	1.3	440				
20	Calf	3.2	690	1200	300	<150	~1650
21	Calf	3.5	730	860	150	<150	~1160
22	Calf	4.5	530	740	840	<100	~1680

[a]Total acceptance for 20 amino acids.

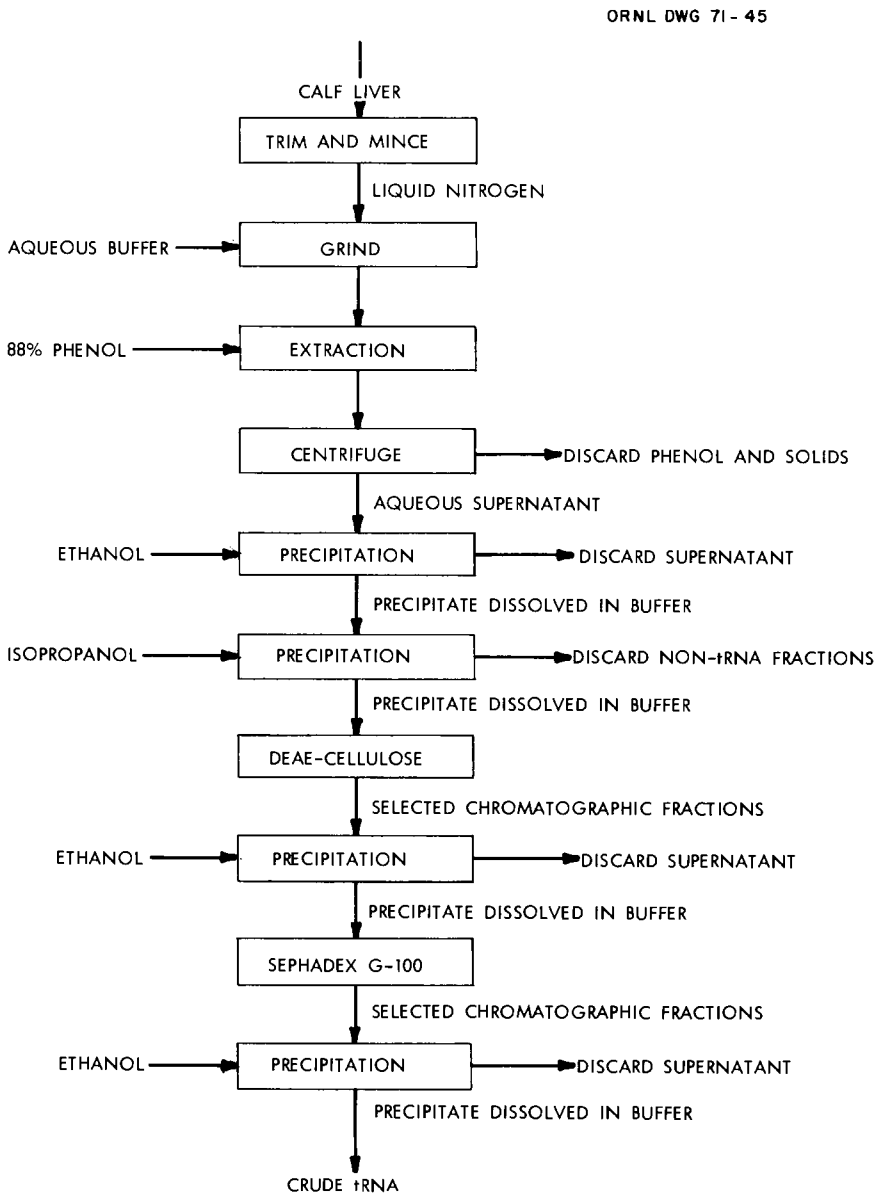

Fig. 12.1. Flowsheet for the recovery of crude tRNA from calf liver.

liver was removed promptly, and the bile sac was carefully cut off. The liver was washed with warm water, the connective tissue was removed, and the liver was sliced into 1-in. strips and frozen immediately in liquid nitrogen. The frozen product was transported to ORNL in a container of liquid nitrogen and then broken into small cubes and stored at −20°C.

In order to recover the tRNAs, the frozen chunks of liver were ground for about 5 min in an Eppenbach colloid mill with a buffer of the following composition: 0.005 *M* EDTA, 0.001 *M* $Na_2S_2O_3$, 1% w/v bentonite, and 0.1 *M* Tris-HCl (pH 8.0). Two liters of buffer was used per kilogram of liver. The resulting suspension was filtered through sterile cheesecloth. The mill was cleaned of remaining connective tissue, and the filtrate was reintroduced into the mill. Then 1 liter of 88% phenol was added per liter of filtrate, and the solution was made 1% in *n*-octyl alcohol. The phenol and the aqueous filtrate were mixed for a period of 30 min, during which the temperature increased to 20°C. The phenol–aqueous buffer suspension was centrifuged to recover the aqueous solution containing the nucleic acids. In some of the runs, the centrifugate was not clear and had to be filtered through a 5-μ Millipore

filter. Solid NaCl was added to make the centrifugate (or filtrate) 0.5 *M* in NaCl; then two volumes of ethanol were added to precipitate the RNA product. After standing for 16 hr at 4°C, the precipitate was recovered by centrifugation.

In order to remove high-molecular-weight RNA and other contaminants, the precipitate was redissolved in a volume of buffer (0.3 *M* NaCl; 0.001 *M* $Na_2S_2O_3$; 1% bentonite; 0.1 *M* Tris-HCl, pH 7.0) equal to the previous volume. Isopropyl alcohol was added slowly to achieve a final concentration of 25%, and the resulting precipitate was removed by centrifugation and discarded. The tRNA was then precipitated by the addition of an equal volume of isopropanol. After standing for 16 hr at 4°C, the precipitate was recovered by centrifugation.

Additional purification was achieved by DEAE-cellulose chromatography. The solid product was dissolved in buffer (0.1 *M* Tris-HCl, pH 7.5; 0.01 *M* $Na_2S_2O_3$) at a concentration of 50 A_{260} units/ml. The feed solution was loaded onto a DEAE-cellulose column (Schleicher and Schuell), which was subsequently washed with a buffered 0.2 *M* NaCl solution to remove low-molecular-weight RNAs. The desired tRNAs were then eluted from the column using a buffered 1.0 *M* NaCl solution and were recovered by precipitation with ethanol.

Final purification of the crude calf liver tRNA was accomplished by means of Sephadex G-100 gel permeation chromatography. The crude tRNA was dissolved in buffer (0.4 *M* NaCl; 0.01 *M* $MgCl_2$; 0.01 *M* Tris-HCl, pH 7.0; 0.002 *M* $Na_2S_2O_3$) and loaded onto the column. The tRNAs were eluted after two peaks containing higher-molecular-weight material. They were recovered by precipitation with ethanol, redissolved in buffer, and stored frozen (−20°C).

12.2 NEW CHROMATOGRAPHIC SYSTEMS FOR THE SEPARATION OF TRANSFER RIBONUCLEIC ACIDS

A substantial improvement in the chromatographic resolution of tRNAs by reversed-phase chromatographic (RPC) columns was achieved by the replacement of the diatomaceous earth support with a plastic support material. The new material is polychlorotrifluoroethylene (Plaskon CTFE, 2300 grade, powder), which is marketed by Allied Chemical Corporation as a molding and extrusion resin. As received, the material contains lightly bonded aggregates of particles. These are easily reduced to the 10-μ primary particles.

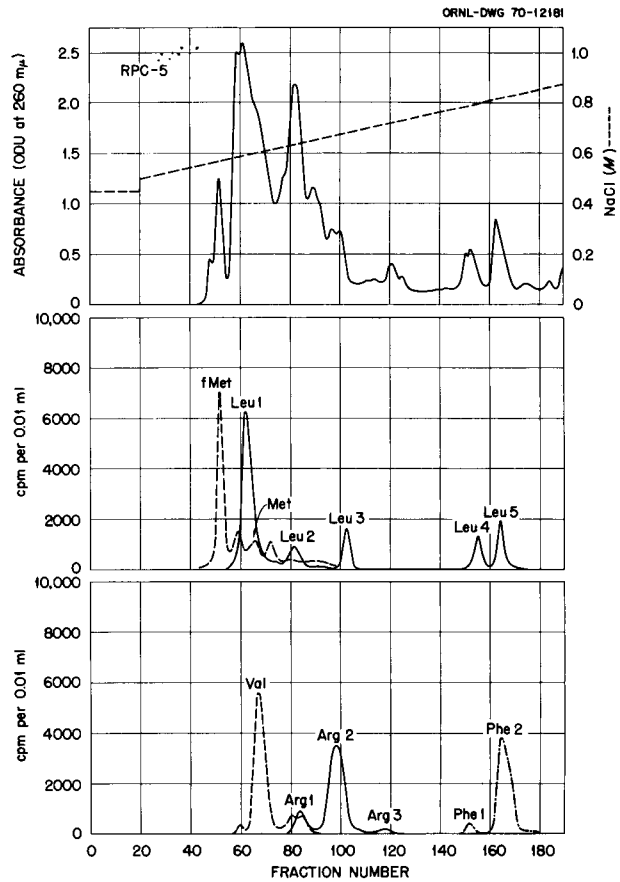

Fig. 12.2. RPC-5 chromatogram of *E. coli* tRNAs. Packing: 4% Adogen 464 on Plaskon CTFE; equilibrating solution: 0.45 *M* NaCl, 0.01 *M* $MgCl_2$, 0.01 *M* Tris buffer at pH 7, 0.001 *M* β-mercaptoethanol; gradient: 2 liters of 0.50 to 0.90 *M* NaCl plus other constituents.

Two new RPC systems were developed using the Plaskon support. These were designated RPC-5 [4% tricaprylylmethylammonium chloride (Adogen 464) on Plaskon] and RPC-6 (5% trioctylpropylammonium bromide on Plaskon). The chromatographic peaks (Figs. 12.2 and 12.3) were much sharper than those obtained with RPC-2 and RPC-3 chromatography (the corresponding quaternary ammonium salts supported on diatomaceous earth); also, more effective resolution of isoaccepting tRNAs was achieved. For example, the five leucine tRNAs were sharply defined by either RPC-5 or RPC-6 chromatography; in contrast, under corresponding conditions, they were more poorly resolved in RPC-2 runs, and they were broad and very ill-defined in RPC-3 runs. No solvent was employed in RPC-5, whereas tetrachlorotetrafluoropropane, which is expensive and difficult to obtain, was used in the RPC-2 system. Recoveries of the tRNAs, based on acceptance

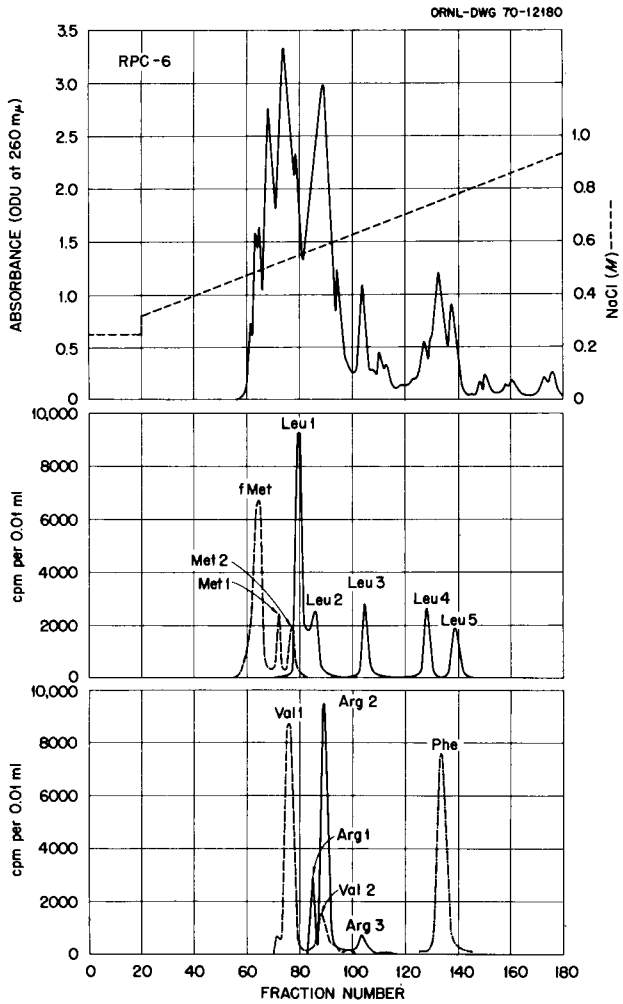

Fig. 12.3. RPC-6 chromatogram of *E. coli* tRNAs. Packing: 5% trioctylpropylammonium bromide on Plaskon CTFE; equilibrating solution: 0.25 *M* NaCl, 0.01 *M* $Mg(C_2H_3O_2)_2$, 0.01 *M* $NaC_2H_3O_2$ buffer at pH 4.5, 0.002 *M* $Na_2S_2O_3$; gradient: 2 liters of 0.32 to 1.0 *M* NaCl plus other constituents.

activity, averaged 90%. The RPC-5 columns can be used repeatedly; as many as 30 runs have been made on smaller columns with no loss in resolution. Because the trioctylpropylammonium bromide used in the RPC-6 system has a slight aqueous solubility, RPC-6 columns probably can be used for only three to six runs.

The increased chromatographic resolution of the RPC-5 and -6 systems greatly simplifies the preparatory-scale purification of individual tRNAs by reducing the overlap of adjacent tRNA peaks. Also, the multiple isoaccepting peaks for certain tRNAs can be more readily observed. The improved resolution probably results from the uniform small size (approximately 10 μ) of the coated particles and the chemically inert nature of polychlorotrifluoroethylene.

12.3 MINIATURE CHROMATOGRAPHIC SYSTEMS FOR TRACER-LABELED TRANSFER RIBONUCLEIC ACIDS

Our reversed-phase chromatographic systems are essentially anion exchange columns, constructed in such a manner that the active exchange sites are present as a thin film on the surface of an inert support. Hydrophobic diatomaceous earth is employed as the inert support in the RPC-2, -3, and -4 systems. These systems are useful for the large-scale purification of individual tRNAs as well as for the resolution of tracer-labeled isoaccepting tRNAs. However, since satisfactory small columns of this type could not be constructed for the tracer-labeled experiments, relatively large (1-cm-diam by 240-cm-high) columns and 2- to 3-liter elution volumes were used. Thus, a period of one to two days was required to complete a chromatographic run. Recently, we have developed two new systems, RPC-5 and -6 (see Sect. 12.2), which employ 10-μ particles of Plaskon as the inert support.

Small (0.6-cm-diam by 30-cm-long) chromatographic columns and correspondingly small (100-ml) elution volumes proved to be practical for the separation of $[^3H]$- or $[^{14}C]$aminoacyl-tRNAs. Further, by utilizing commercially available high-pressure columns and fittings (Chromatronic, Inc.) and a positive displacement pump to force the eluent through the column at 300 to 500 psi, the time required to complete the chromatographic run was shortened to 30–60 min. Typical results with tracer-labeled calf liver tRNAs are shown in Fig. 12.4. Sharp resolution of the multiple peaks for isoacceptors of methionyl-, leucyl-, and seryl-tRNAs is shown. Recoveries of these calf liver tRNAs averaged 99%.

Experiments were carried out with *E. coli* phenylalanyl-tRNA to determine the minimum amount of tRNA that could be resolved. Figure 12.5 shows the chromatogram of a sample of $[^{14}C]$phenylalanyl-tRNA having a radioactivity level of 44 counts/min. A total of 24.8 counts/min (56% of the initial activity) was detected in the chromatographic peak. This chromatographic peak represents 3.5×10^{-9} g, or 60×10^{-6} A_{260} unit, of phenylalanyl-tRNA.

The advantages of this miniature chromatographic system are (1) the speed with which chromatographic runs can be carried out, (2) the very small quantity of tRNAs required, and (3) the superior resolution of isoaccepting tRNAs. The ability to detect and compare such small quantities of tRNAs makes possible the investigation of differences using small quantities of cells (e.g., in biopsy samples).

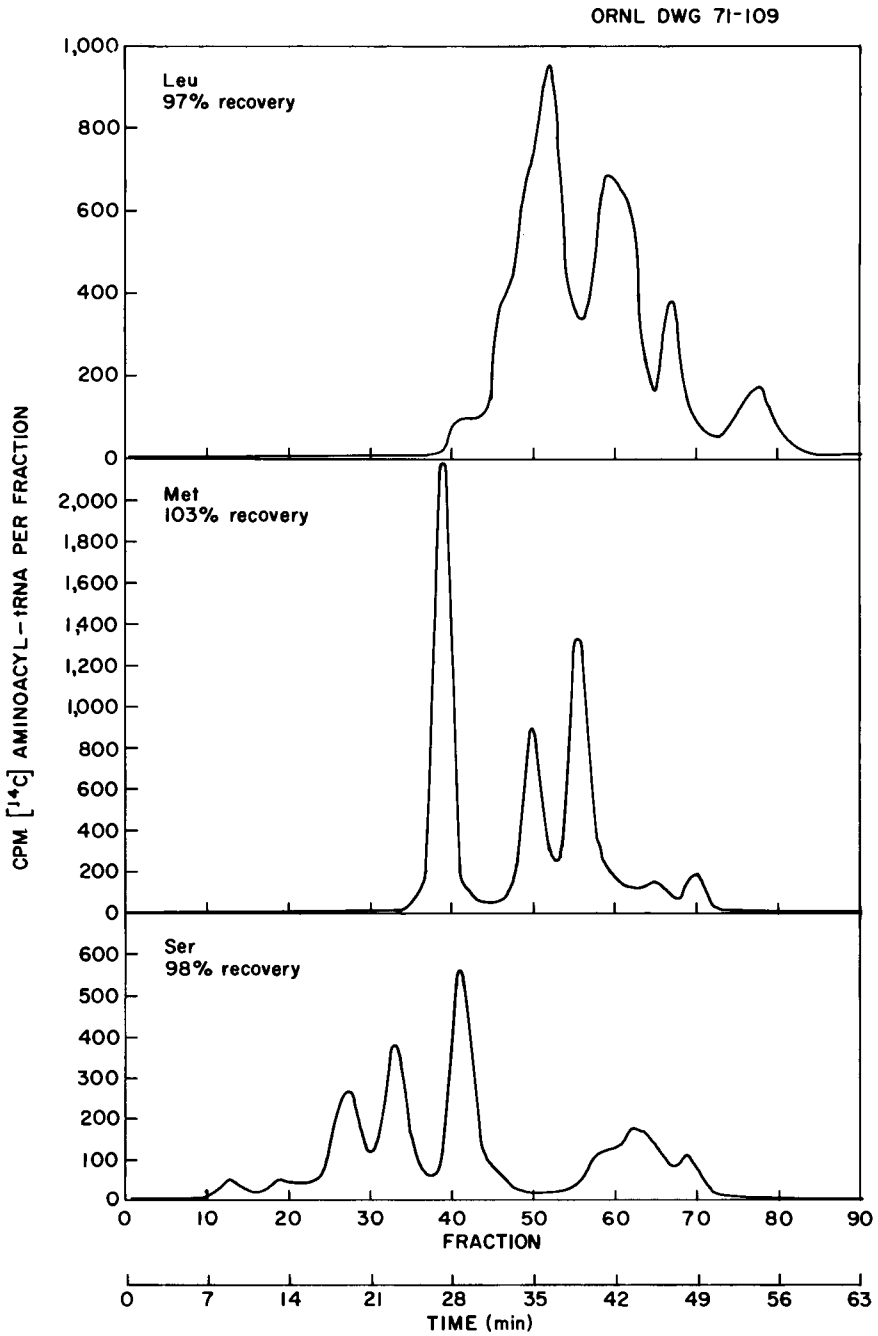

Fig. 12.4. Separation of calf liver tRNAs.

12.4. SEPARATION OF RIBOSOMAL RIBONUCLEIC ACIDS

A reversed-phase chromatographic system employing a column consisting of methyltrialkylammonium chloride dissolved in chloroform and supported on Plaskon CTFE, used previously for separating tRNAs and higher-molecular-weight ribosomal RNAs (i.e., 16S and 23S rRNAs), has been applied to the isolation of 5S rRNA from *E. coli.* Total ribosomal RNA was prepared from *E. coli* Q13 ribosomes by a phenol extraction procedure. The 16S and 23S rRNAs were precipitated from a 2 *M* sodium acetate solution, leaving most of the lower-molecular-weight material (primarily tRNAs and 5S rRNA) in solution. The tRNAs and 5S rRNA were then precipitated with cold ethanol. The precipitate was

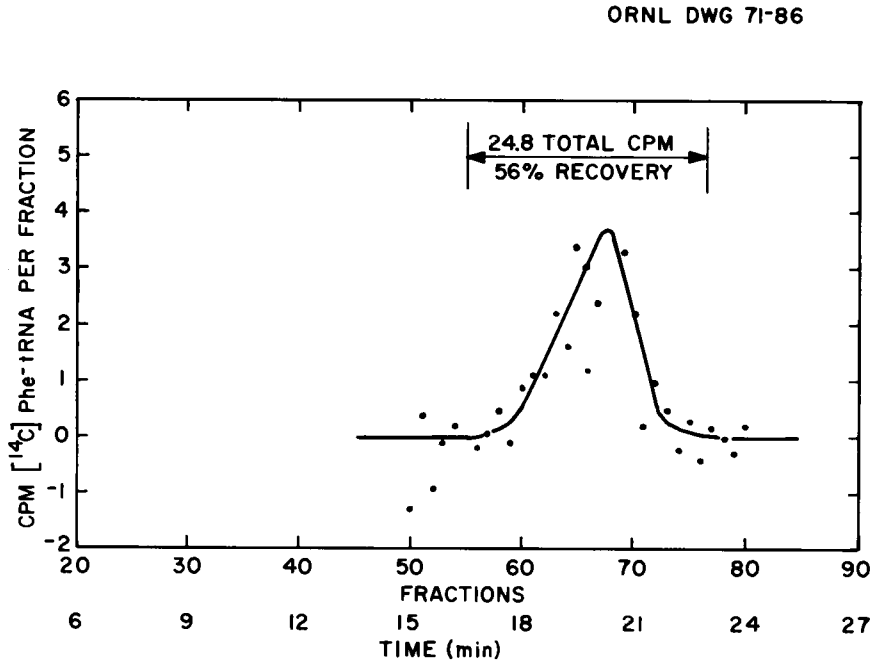

Fig. 12.5. Chromatogram of a sample of [^{14}C] phenylalanyl-tRNA with a radioactivity level of 44 counts/min.

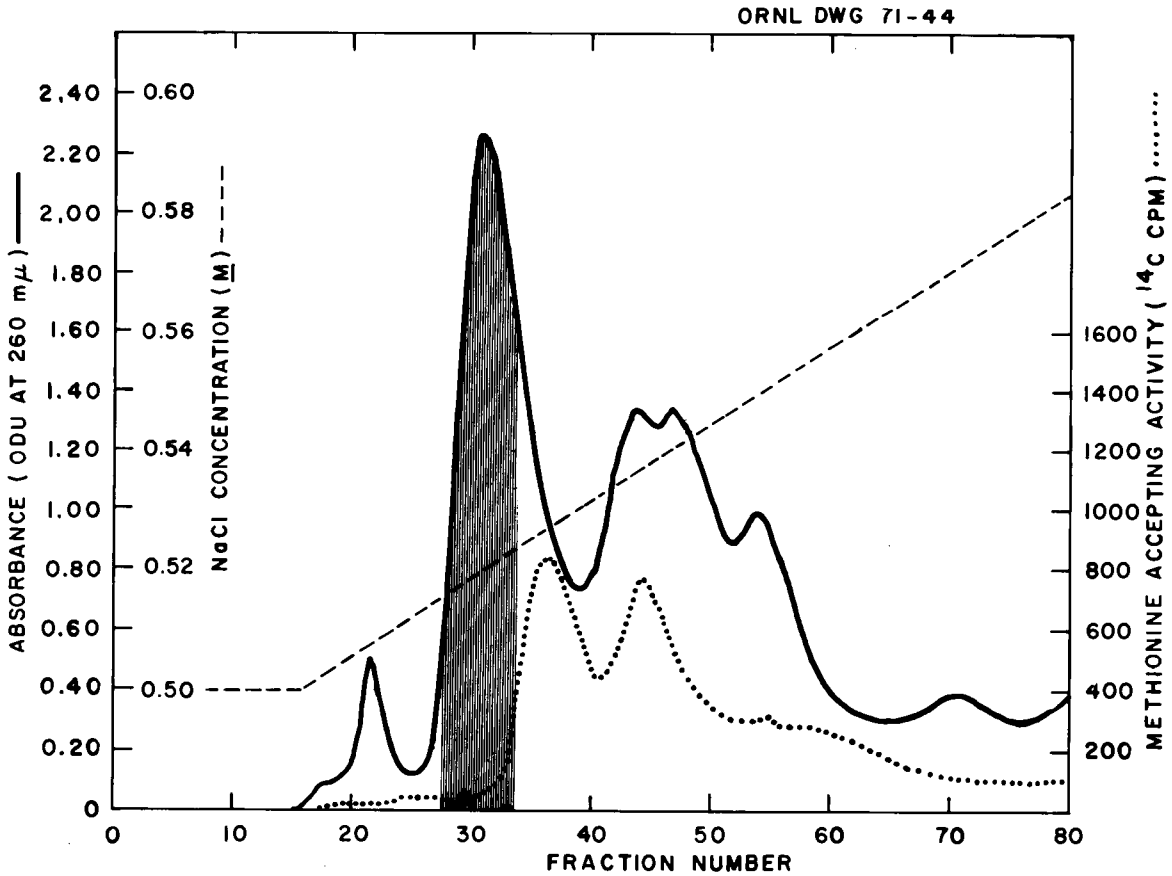

Fig. 12.6. Reversed-phase chromatogram of 4-5S RNA from *E. coli* Q13. Column: 1 cm in diameter by 60 cm high; temperature: 25°C; flow rate: 1.25 ml/min; eluent: 0.01 *M* $MgCl_2$, 0.05 *M* Tris-HCl (pH 7.3), NaCl as shown. The shaded peak contains 5S rRNA.

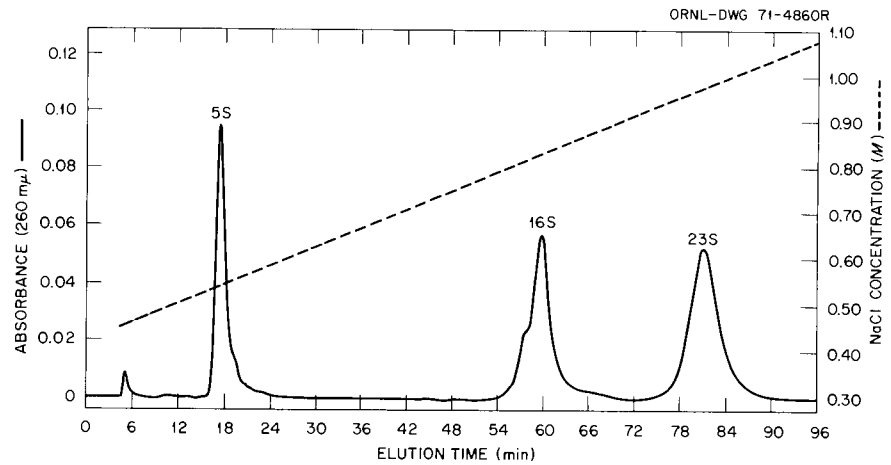

Fig. 12.7. Reversed-phase chromatogram of a mixture of 5S, 16S, and 23S rRNA from *E. coli*. Column: 0.63 cm in diameter by 30 cm high; temperature: 25°C; flow rate: 1.0 ml/min; eluent: 0.01 *M* $MgCl_2$, 0.05 *M* Tris-HCl (pH 7.25), NaCl as shown.

redissolved, and 30 to 150 A_{260} units were chromatographed on a 1-cm-diam by 60-cm-high column at room temperature. Elution was achieved with a solution of the following composition: 0.01 *M* $MgCl_2$, 0.05 *M* Tris-HCl (pH 7.3), and a NaCl gradient ranging from 0.50 to 0.60 *M*. The tRNA peaks were located by assaying the fractions for amino acid acceptance. A major non-tRNA peak was eluted ahead of the tRNAs and was characterized by base composition and electrophoresis; it was identified as 5S rRNA. On electrophoresis on 10% polyacrylamide gels, the 5S rRNA (shown as the shaded area in Fig. 12.6) gave a single band with a lower mobility than tRNAs. The hydrolysates obtained by hydrolysis of the 5S rRNA with 0.33 *M* KOH at 37°C for 18 hr were separated by anion exchange chromatography. The unusual bases present in tRNAs were not found in the 5S rRNA, and uridine-3′-phosphate was obtained as the terminal nucleoside. (Adenosine-3′-phosphate is the terminal nucleoside of tRNAs.)

Small (0.63-cm-diam by 30-cm-long) reversed-phase chromatographic columns have been utilized for the rapid separation of 5S, 16S, and 23S rRNAs from *E. coli* in a single chromatographic run. Figure 12.7 shows a chromatogram obtained from a sample containing about 1.2 total A_{260} units of a mixture of 5S, 16S, and 23S rRNAs. The time required for a chromatographic run can be shortened by using a smaller volume of eluent or a faster flow rate. Good separation of 16S and 23S rRNAs has been obtained with only 0.1 A_{260} unit in about 30 min. Compared with other techniques, this method gives better resolution and is faster and more reproducible; in addition, it uses only small amounts of material, which can be recovered.

12.5 PURIFICATION OF FIVE LEUCINE TRANSFER RIBONUCLEIC ACIDS FROM *E. COLI*

A general method for the purification of isoaccepting transfer ribonucleic acids (tRNAs) has been developed. To demonstrate the procedure, the five chromatographically resolvable leucine tRNAs were separated and purified by aminoacylation, chemical derivatization, BD-cellulose chromatography, basic hydrolysis, reversed-phase chromatography, and DEAE-Sephadex chromatography.

Figure 12.8 shows the BD-cellulose chromatogram of 75,300 A_{260} units of crude tRNA that had been aminoacylated with leucine and derivatized with the *N*-2-naphthoxyacetic acid ester of *N*-hydroxysuccinamide. The combined product pools *E*, *F*, and *G* had a specific activity of 1140 picomoles of leucine accepted per A_{260} unit, representing an 8.5-fold purification of the feed.

Figure 12.9 shows the separation on a reversed-phase column (RPC-5) of 500 A_{260} units of the leucine product into the individual leucine tRNAs. The five leucine tRNA pools were further concentrated and purified by DEAE-Sephadex chromatography. The leucine-accepting activities of $tRNA_1^{Leu}$, $tRNA_3^{Leu}$, $tRNA_4^{Leu}$, and $tRNA_5^{Leu}$ were increased to 1350–1600 picomoles per A_{260} unit, and the activity (leucine acceptance per terminal adenosine) varied from 80 to 103%. The sample of $tRNA_2^{Leu}$, which was present in only small quantities, was less pure, accepting only 905 picomoles of leucine per A_{260} unit.

Overall recovery of the isoaccepting leucine tRNAs for the total process, based on aminoacylation of small

ORNL DWG 70-14729

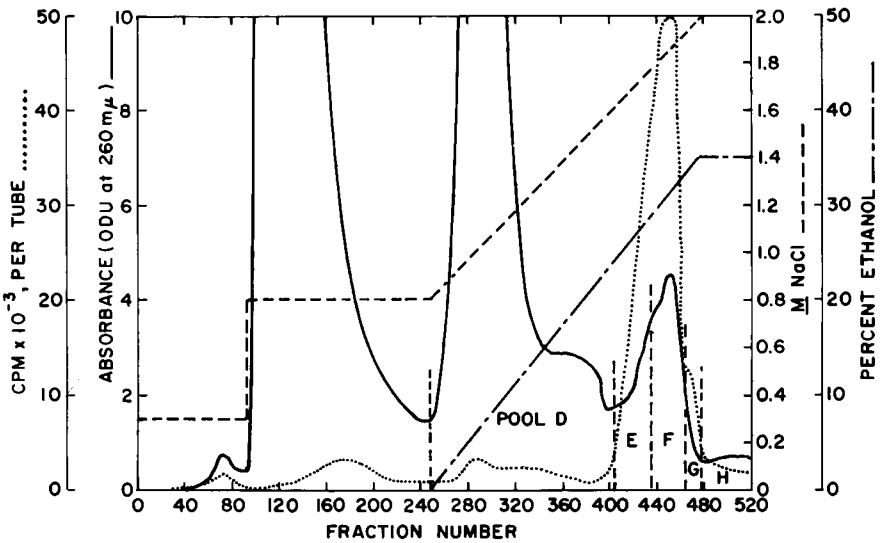

Fig. 12.8. BD-cellulose chromatogram of aminoacylated and derivatized crude tRNA.

ORNL DWG 70-15136

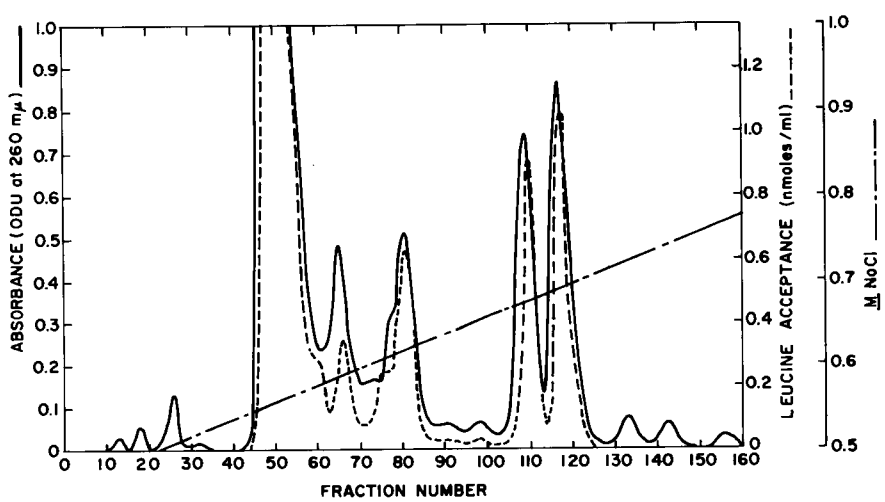

Fig. 12.9. Separation of leucine tRNAs by RPC-5 chromatography.

aliquots of the DEAE-Sephadex products, varied between 10 and 20%. The method is amenable to scaleup and could be used to prepare large quantities of purified leucine tRNAs.

In ribosome binding experiments, $tRNA_1^{Leu}$ and $tRNA_2^{Leu}$ recognized the codon CUG, and $tRNA_5^{Leu}$ recognized UUG. The $tRNA_3^{Leu}$ and $tRNA_4^{Leu}$ did not recognize any of the known leucine codons.

The four arginine tRNAs from *E. coli* were also recovered by this method; however, they were less pure, possibly due to chemical damage in the derivatization step.

12.6 FLOWSHEET DEVELOPMENT AND LARGE-SCALE PURIFICATION OF *E. COLI* TRANSFER RIBONUCLEIC ACIDS

A new process was developed for separating and purifying the tRNAs that are usually situated in the middle of the chromatogram. This process is a modified

ORNL-DWG 71-5372

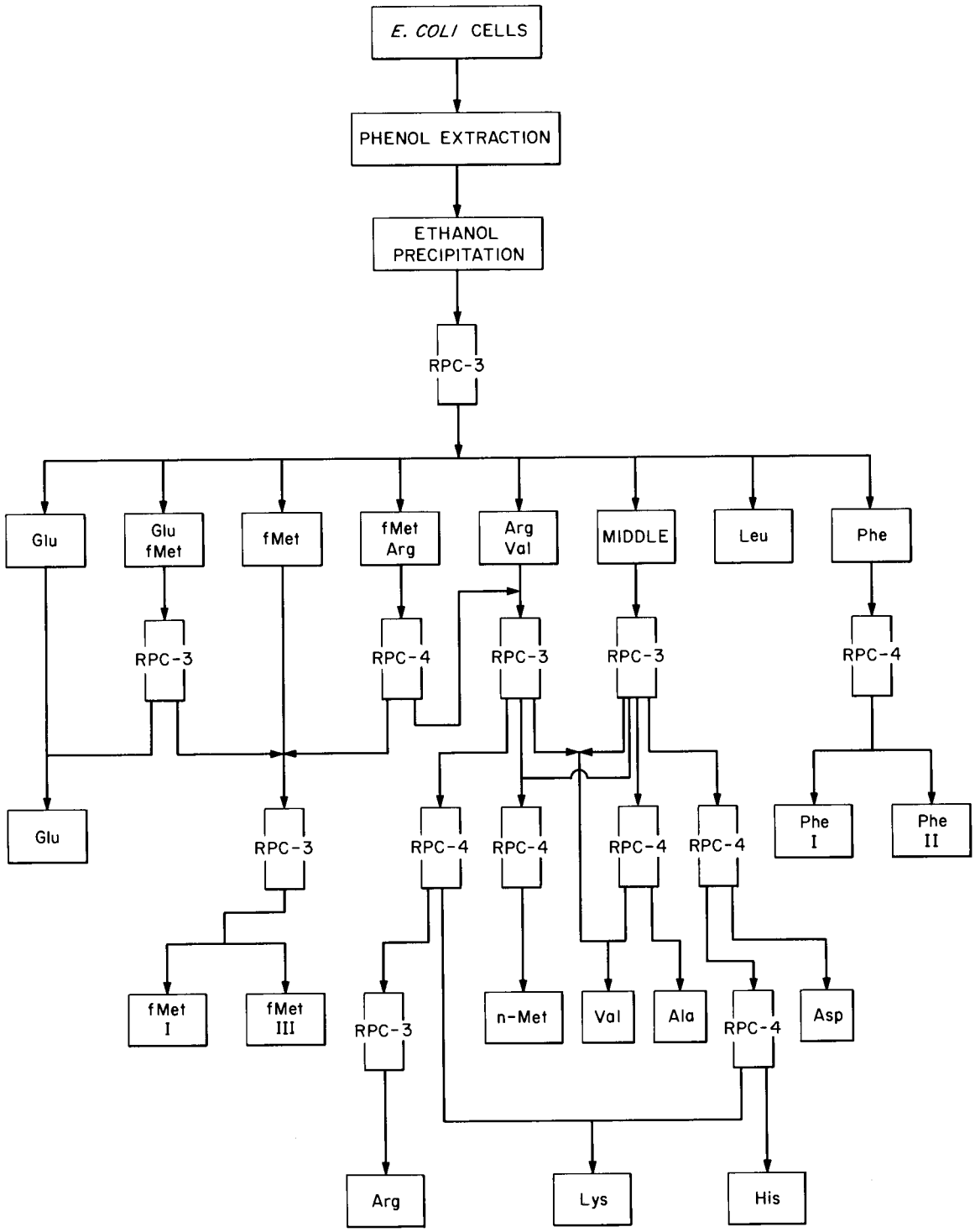

Fig. 12.10. Improved flowsheet for the purification of *E. coli* tRNA.

Table 12.2. Purified tRNAs obtained by the improved flowsheet

tRNA	Quantity (g)	Amino acid accepting activity (picomoles per A_{260} unit)	3′-Terminal adenosine content (picomoles per A_{260} unit)
Formylmethionine	3.5	1615 ± 77[a]	1610 ± 43
Glutamic acid	6.2	1210 ± 34	1555 ± 23
Phenylalanine-1	0.4	1152 ± 44	1680 ± 70
Phenylalanine-2	0.4	1400	

[a]Formyl acceptance, 1690 ± 62 picomoles per A_{260} unit.

version of the method previously used for preparing large quantities of tRNAs from *E. coli.* The earlier method consisted of a primary separation of a crude mixture of tRNAs on a DEAE-cellulose column into two pools – one enriched in formylmethionine tRNA and the other enriched in phenylalanine tRNA. These pools were further processed on reversed-phase columns (RPC-3 and -4) to yield purified tRNAs at the ends of the chromatograms. However, it was found that the method could be improved considerably by the substitution of RPC-3 for DEAE-cellulose in the primary separation of the crude mixture. With this modification, several tRNAs were eluted as sharply defined peaks well separated from most of the other tRNAs. A simplified version of the improved flowsheet, as developed for small columns, is shown in Fig. 12.10. The fractions from the RPC-3 column are divided into eight pools: glutamic acid tRNA, glutamic acid–formylmethionine tRNA mixture, formylmethionine tRNA, formylmethionine-arginine tRNA mixture, arginine tRNA, a "middle" pool containing many tRNAs, leucine tRNA, and phenylalanine tRNA. These pools are then rechromatographed under different conditions to separate specific tRNAs. Advantage is taken of the fact that the tRNA elution sequence varies with the RPC system used, the pH of the eluent, and the presence or the absence of divalent metal ions (usually magnesium). Certain pools of tRNA fractions from the RPC-3 chromatographic separation are rechromatographed under a set of conditions selected to maximize the separation of the desired tRNA. The effluent fractions are pooled, concentrated, and, if necessary, rechromatographed again under a different set of column conditions to effect further purification.

The new flowsheet was developed on a small scale, using crude tRNA from two different batches of *E. coli* K-12 MO. Small quantities of glutamic acid, formylmethionine, arginine, normal methionine, lysine, valine, alanine, histidine, aspartic acid, and phenylalanine tRNAs were purified, while several other tRNAs were partially separated. This successful separation of tRNAs from the middle of the chromatogram confirmed the practicability of the flowsheet. The tRNA recovery varied with the number of rechromatography steps required and averaged about 70% per column run. The amino acid acceptance of each product was generally greater than 1200 picomoles per A_{260} unit.

Preparatory to a large-scale test of the new flowsheet, four batches of *E. coli* K-12 MO cells were grown and processed by phenol treatment and successive ethanol precipitations; they yielded a total of 5.5×10^6 A_{260} units of crude tRNA. The crude tRNAs were separated in a series of runs on RPC-3 columns and combined in eight pools, as described above. These pools were concentrated on small DEAE-cellulose columns and stored at −20°C. Then the formylmethionine, glutamic acid, and phenylalanine tRNA pools were rechromatographed, as shown in Fig. 12.10. The quantities of purified tRNAs obtained and the results of the analyses are shown in Table 12.2. About 3.5 g of formylmethionine tRNA at 100% activity (amino acid acceptance per terminal nucleoside), 6.2 g of glutamic acid at 78% activity, and 0.4 g each of $tRNA_1^{Phe}$ and $tRNA_2^{Phe}$ were obtained. Other tRNAs could have been recovered from the pools on hand by following the flowsheet shown in Fig. 12.10; however, a decision was made to terminate the large-scale work at this point because of reduced funds.

12.7 DISTRIBUTION OF PURIFIED TRANSFER RIBONUCLEIC ACIDS

The distribution of purified samples of *E. coli* tRNAs was continued in accordance with the recommendations of the National Institute of General Medical Sciences committee that reviews all requests. Samples of arginine, formylmethionine, glutamic acid, phenylalanine, and valine tRNAs were distributed in 162 shipments containing a total of 5.5 g of purified tRNAs. These shipments went to investigators working in fields such as x-ray crystallography, nucleotide sequence, solution conformation, codon response, etc. During the year, additional quantities of formylmethionine, glutamic

acid, and phenylalanine tRNAs were added to the inventory upon completion of the large-scale evaluation tests (Sect. 12.6). All large-scale work with *E. coli* tRNAs has now been terminated, and no future additions will be made to the inventory. The supply of arginine, phenylalanine, and valine tRNAs has been exhausted; thus only formylmethionine and glutamic acid tRNAs will be distributed. Currently, we have a total of about 10 g of these two tRNAs on hand.

BODY FLUIDS ANALYSES PROGRAM

The goal of the Body Fluids Analyses Program is to develop separation methods and automated systems for use in the clinical laboratory for analysis of the molecular constituents of body fluids. The third-generation prototype analyzers for the high-resolution analyses of the UV-absorbing and carbohydrate constituents in body fluids have been designed and built. Several additional separated body fluid constituents have been isolated and identified, and new separation systems are being developed for the analysis of trace organic compounds in body fluids, for the 5-hydroxyindoles in whole blood, and for ninhydrin-positive compounds in body fluids.

12.8 PROTOTYPE ANALYZERS

Eleven high-resolution analytical prototype systems have been fabricated from ORNL construction plans and have been placed in laboratories other than those of the Body Fluids Analyses Program (Table 12.3). Three additional UV-analyzer prototype systems are being fabricated for installation at three other laboratories for continuing evaluation. The principal investigators of these prototype systems will be as follows: Dr. J. Edwin Seegmiller, Director of Department of Medicine, University of California, La Jolla; Dr. Stanton Segal, Department of Pediatrics, The University of Pennsylvania; and Dr. Lloyd H. Smith, Jr., Chairman, Department of Medicine, San Francisco Medical Center, University of California. During fiscal year 1972, an intensive evaluation program will be initiated at these three laboratories, as well as at the three laboratories where UV-analyzer prototype systems have already been placed.

The concepts of the Mark III miniaturized carbohydrate analyzer (Fig. 12.11) were discussed in the last annual report.[1] Development of this analyzer has now been completed, and two prototypes have been built for evaluation by other laboratories. One of them has been installed in the Clinical Center of the NIH, where it will be used by Dr. Donald Young for in-depth analyses of body fluids from general hospital patients; the other will be installed in the Department of Pediatrics at Johns Hopkins Medical Center, where Dr. R. Rodney Howell will use it to investigate abnormal infants and children.

12.9 SEPARATION SYSTEMS

The use of an anion exchange column and a cation exchange column in series, with concurrent elution of both columns after the initial loading phase, is being evaluated with the UV-analyzer. Preliminary results show that the system gives increased resolution and a significant decrease in analysis time. Neutral resins manufactured by the Rohm and Haas Company have been found useful in concentrating the trace organic compounds in urine so that an additional 50 to 60 chromatographic peaks can be resolved in a separate

1. *Chem. Technol. Div. Annu. Progr. Rep. May 31, 1970,* ORNL-4572, pp. 213–24.

Table 12.3. High-resolution analytical prototype systems in other laboratories

Laboratory	Principal investigator	Type of prototype system
Clinical Center, NIH	Dr. Donald S. Young	UV-analyzer, Mark II[a]
		UV-analyzer, Mark II-A
		Carbohydrate analyzer, Mark II
		Carbohydrate analyzer, Mark III
Johns Hopkins University Medical Center	Dr. R. Rodney Howell	UV-analyzer, Mark II
		Carbohydrate analyzer, Mark III
Duke University Medical Center	Dr. James Wyngaarden	UV-analyzer, Mark II-A
Eli Lilly Clinical Laboratory	Dr. Robert Wolen	UV-analyzer, Mark II-A
University of Salford	Dr. R. W. A. Oliver	UV-analyzer, Mark II-A[a]
Analytical Chemistry Division, ORNL	Dr. Gerald Goldstein	UV-analyzer, Mark II
Biology Division, ORNL	Dr. James Epler	UV-analyzer, Mark II-A

[a]Fabricated by the other facility, using ORNL construction plans.

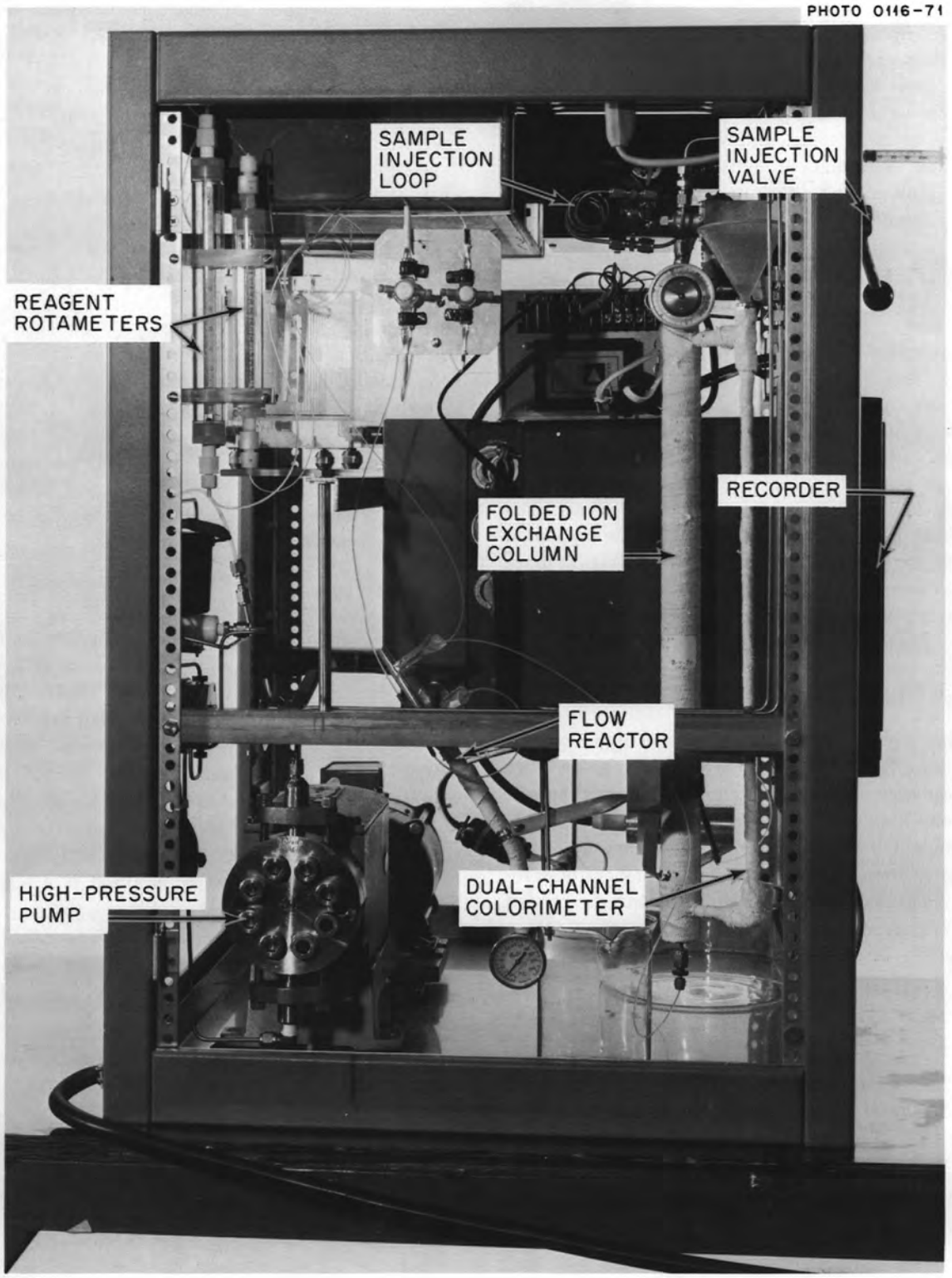

Fig. 12.11. Mark III miniaturized carbohydrate analyzer.

elution. A new concept in which multiple columns are operated at the same time in a single analyzer system will allow many samples to be run simultaneously, thereby increasing the sample throughput rate of such systems.

Ion Exchange Columns in Series

The use of two or more ion exchange columns that are connected in series and contain different types of resin offers the potential of a high-resolution system for the separation of complex mixtures. Preliminary tests make this concept look very promising. An anion exchange column (0.22 cm in diameter and 100 cm long) and a cation exchange column (0.22 cm in diameter and 50 cm long) were connected in series during analysis of a reference urine sample, using an ammonium acetate–acetic acid buffer concentration gradient similar to that employed with the Mark III UV-analyzer. The results of this analysis were acceptable from the standpoint of resolution; that is, the resolution for the initial portion of the chromatogram was somewhat superior, while the resolution for the middle portion was somewhat inferior, to that obtained with the standard 150-cm anion exchange column (Fig. 12.12).

A second run was then made in which the urine sample was again loaded onto the coupled columns; then, after 2 hr of elution with dilute buffer, the two columns were uncoupled and eluted separately with the usual ammonium acetate–acetic acid buffer concentration gradient. The results of this analysis showed about a 15% increase in the number of peaks over that obtained with elution in series; and, since the two columns could have been eluted simultaneously, there was a potential for reducing the analysis time from more than 23 hr to about 18 hr.

This second type of run, in which the columns are loaded sequentially and then eluted separately, looks very promising; hence it will be investigated further. It is interesting to note that, after only a slight modification, the previously developed sample injection valve[2] can be used as an automated switching valve for this type of analysis.

Neutral Resins

A study has been initiated to determine the feasibility of using a family of neutral resins as separations media. These resins, the XAD series marketed by Rohm and Haas Company, are potentially useful for concentrating trace organic constituents in body fluids. Their characteristics are briefly outlined in Table 12.4. The polarities of these resins differ widely, ranging from nonpolar (XAD-2 and XAD-4) to highly polar (XE-284).

A procedure developed for evaluation of the neutral resins was used to determine, qualitatively, the relative number of urinary constituents held up by the resin. About 25 cc of wet resin was packed, as a slurry, into a column and backwashed with water to remove small resin particulates. The column consisted of a 50-ml buret containing a small plug of glass wool to hold the resin. A 50-ml aliquot of urine was percolated through the column; then the resin was washed with about two bed volumes of 0.18 *M* ammonium acetate–acetic acid

2. C. D. Scott, W. F. Johnson, and V. E. Walker, *Anal. Biochem.* **32,** 182 (1969).

Table 12.4. Typical properties of Amberlite polymeric adsorbents[a]

Resin	Chemical nature	Surface area (m^2/g)	Average pore diameter (Å)	Skeletal density (g/cc)	Nominal mesh size	Dipole moment
		Nonpolar				
XAD-2	Polystyrene	330	90	1.08	20–50	0.3
XAD-4	Polystyrene	750	50	1.09	20–50	0.3
		Intermediate polarity				
XAD-7	Acrylic ester	450	80	1.25	20–50	1.8
XAD-8	Acrylic ester	140	250	1.26	25–50	1.8
		Polar				
XAD-12	Very polar; nitrogen-oxygen group	25	1300	1.17	20–50	4.5
XE-284	Sulfonic acid	600	40	1.44	20–50	>5.0

[a]Taken from "Amberlite XAD Macroreticular Adsorbents" (bulletin), Rohm and Haas Co., 1970.

ORNL DWG 70-12446

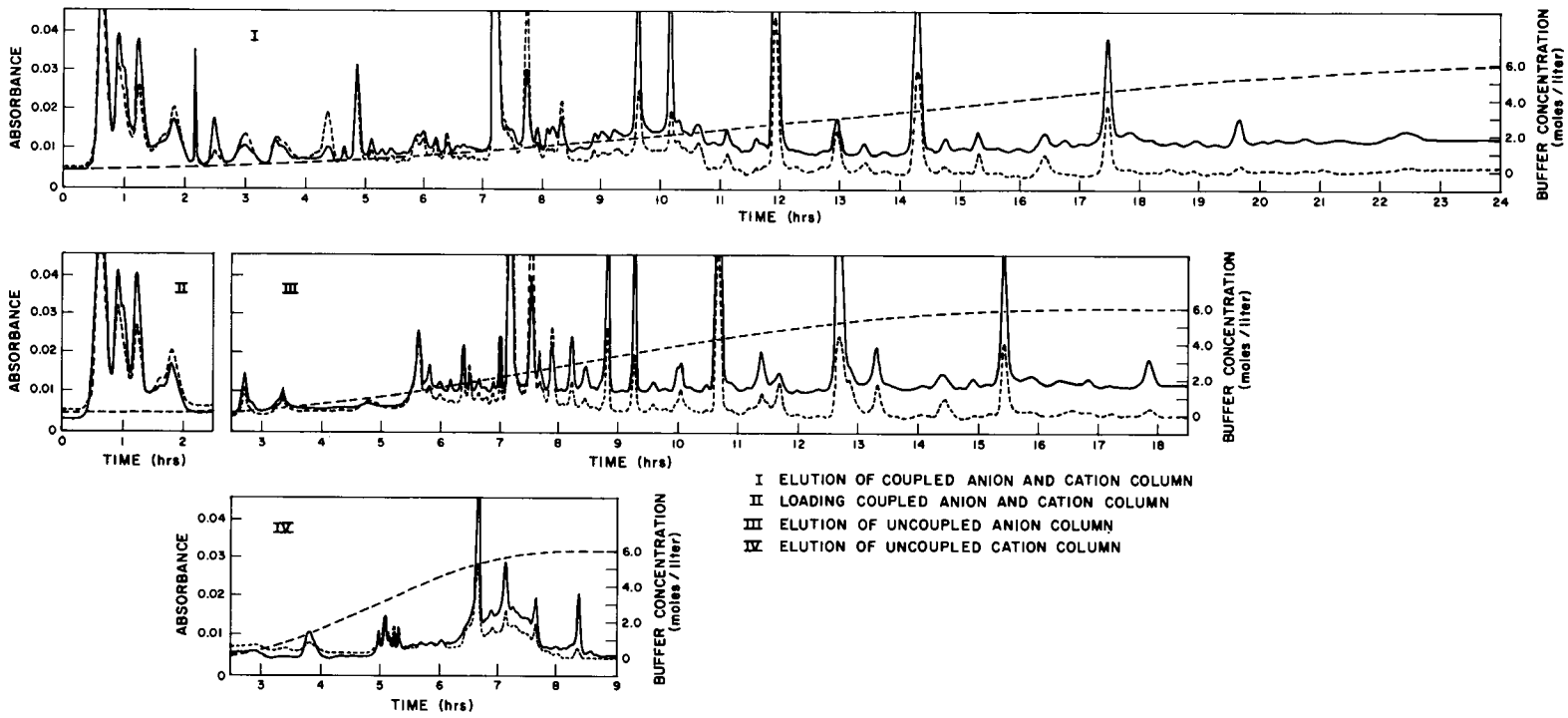

Fig. 12.12. Analysis of urine for its UV-absorbing constituents using coupled anion exchange and cation exchange columns with both coupled and simultaneous elution.

buffer (pH 4.4). Methanol was found to elute most sorbed species, and a 50-ml methanol wash was collected in a round-bottomed flask and evaporated to dryness in a rotary evaporator. The residue was dissolved in 1 ml of 0.015 *M* ammonium acetate–acetic acid buffer and stored at −70°C.

During the loading of the urine on the column and the subsequent wash with dilute buffer, eluate fractions of 8 ml each were collected in sequence. These samples were analyzed by the UV-analyzer, and the resulting chromatograms were compared with a reference chromatogram obtained for the urine sample prior to treatment. With each neutral resin tested, the early effluent fractions showed a striking absence of urinary constituents. However, the effectiveness of removal of the total UV-absorbing compounds from urine increased with the polarity of the resin. Thus, the XAD-2 resin tended to remove only the less-polar compounds usually found as trace urinary constituents. This increased removal of UV-absorbing material as the polarity of the resin increases appears to stem from the ability of the more polar resins to remove the polar, as well as the more nonpolar, urinary compounds. It follows, then, that the XAD-2 resin removes the methylated xanthines but not xanthine, hypoxanthine, or uric acid. Although the concentration of uric acid in the effluent remains high in the case of XAD-4, it is significantly reduced by XAD-7 and virtually eliminated by XAD-12. Although methanol was used to elute the bulk of the urinary compounds from the resins, formic acid was found to be effective in eluting colored compounds from the XAD-12 and XE-284.

The above results indicate that the family of XAD resins should prove to be very useful as concentration media for the chemical constituents of urine. At present, they do not appear to have utility for separating individual constituents from one another, although such potential has not yet been explored. The resins are capable of concentrating certain urinary constituents, retarding various compounds, and passing others. Some compounds are eluted with water, and others are eluted with methanol; a few are not removed unless formic acid is used. This indicates that certain solvents can be used to elute certain groups of compounds. Thus, it may be possible to remove and concentrate trace components and various drugs and drug metabolites from urine by passing urine through a column containing neutral resin. These compounds can then be recovered with a solvent system, and the usual chromatographic analysis can be made.

High-Resolution Amino Acid Analysis

A high-resolution analyzer for ninhydrin-positive compounds (amino acids and related compounds) is being developed. A single-column cation exchange separation system patterned after the work of Hamilton[3] is being used. The system is aimed at separation of the constituents of urine, using all of the automated features of our other systems. Initial results show that a 0.45-cm-diam by 100-cm-long cation column operating with 12- to 15-μ-diam particles can separate up to 100 chromatographic peaks from a single urine sample. Longer columns will be used to increase this resolution.

Parametric Studies

The study of the effects of operating parameters on the pressure drop, void fraction, and peak dispersion in a packed bed of small spheres was continued as an aid in determining the optimum design for a chromatographic system. In this technique, distilled water was used as the eluent, and a small quantity of NaCl solution was injected into the flowing streams just ahead of the packed bed. The electrical conductivity of the column effluent was then measured as a function of time. The void volume was obtained by determining the elution volume required between the injection of NaCl and the arrival of the peak maximum at the detector. It was, of course, necessary to subtract the dead volume of the system (i.e., fittings and tubing between the column and the electrical conductivity cell) from the elution volume. Experimental data were taken, using a single 0.45-cm-diam by 50-cm-long column, at temperatures from 30 to 60°C, flow rates from 80 to 800 cm^3 cm^{-2} h^{-1}, and particle sizes from 3.6 to 34.1 μm.

The pressure drop through a packed bed of small spherical particles has been previously shown to be linearly dependent on column length and flow rate and inversely dependent on the square of the particle diameter; the more recent work confirms these relationships. However, a more general correlation would be useful. Such general correlations have been derived in engineering studies of pressure drop in fixed beds of larger particles. Typical of these is the work of Ergun,[4] who followed earlier workers in correlating a dimensionless pressure drop in the form of a friction factor f with a dimensionless flow parameter called the modi-

3. P. B. Hamilton, *Anal. Chem.* **32**, 1779 (1960).
4. S. Ergun, *Chem. Eng. Progr.* **48**(2), 89 (1952).

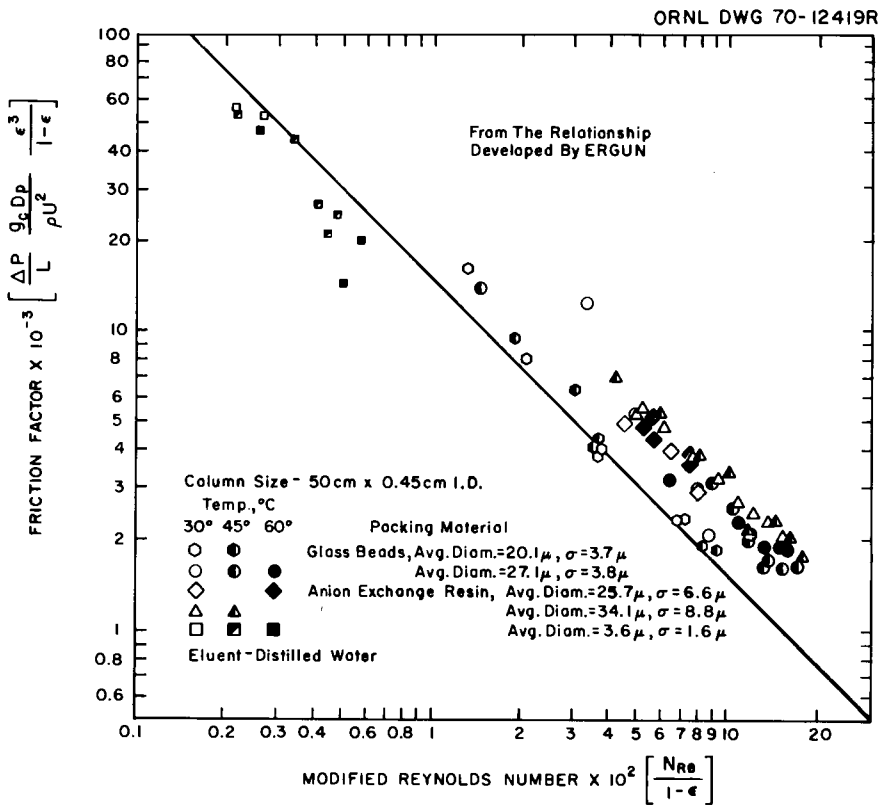

Fig. 12.13. Pressure drop across packed beds of small particles as a function of operating parameters in a generalized correlation of friction factor vs modified Reynolds number.

fied Reynolds number, N_{Re}:

$$f = 150\,\frac{1-\epsilon}{N_{Re}} + 1.75\,, \qquad (1)$$

where

$$f = \frac{\Delta P}{L}\,\frac{g_c D_p}{\rho U^2}\,\frac{\epsilon^3}{1-\epsilon}\,,$$

$$N_{Re} = \frac{D_p \rho U}{\mu}\,,$$

ΔP = pressure drop across the column,

L = length of the column,

g_c = gravitational constant,

D_p = average diameter of the spheres in the column,

ρ = density of the mobile phase,

U = superficial fluid velocity based on an empty column and average conditions,

ϵ = void fraction = void volume/geometric volume,

μ = viscosity of the eluent.

Figure 12.13 shows the correlation of the experimental data obtained with five different column packings, as compared with the semiempirical relationship developed by Ergun for beds packed with much larger particles. The correlations are consistent within the same packed bed, and the resulting f-vs-N_{Re} plot on log-log paper gives a relatively straight line with a slope similar to that of the extrapolated Ergun relationship. However, particle size seems to have some effect on the absolute values of the friction factor. Perhaps, in the case of these smaller particles, the particle size must also be considered in the correlation. This will be investigated further.

12.10 SYSTEM COMPONENTS

The primary developmental emphasis with regard to system components has been centered on new detection systems. Work is progressing on two flow detectors: a multiple-channel photometer and a flow fluorimeter–photometer.

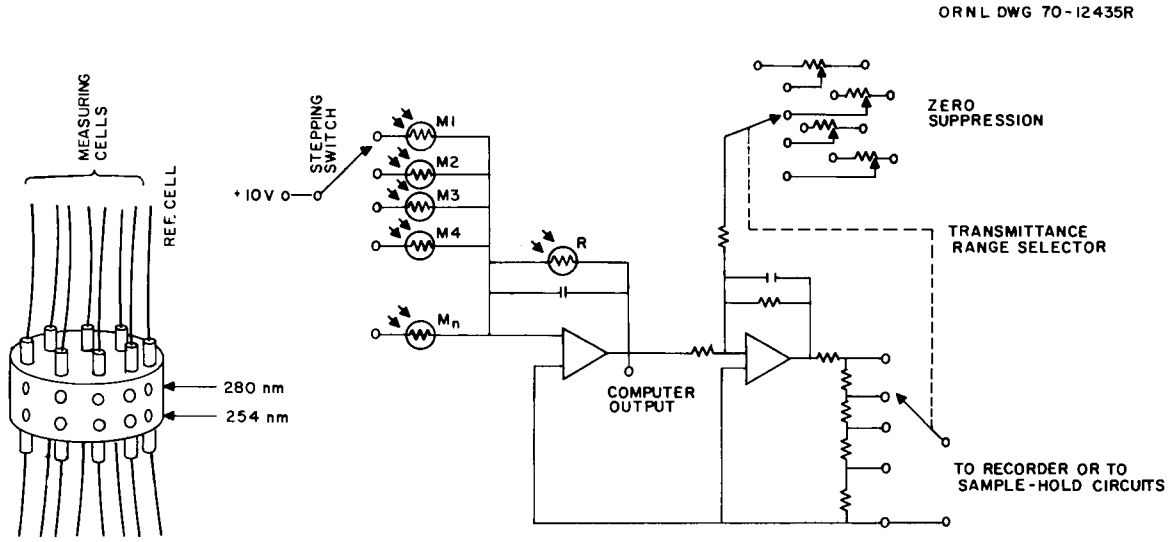

Fig. 12.14. Schematic of the design for a multichannel dual-beam, dual-wavelength UV photometer.

Multiple-Channel Photometer

In order to reduce the cost of a parallel-column analyzer, it would be desirable to replace the several individual detectors with a single detector capable of monitoring multiple streams. We have completed the conceptual design of a multichannel two-wavelength UV photometer that will simultaneously measure the transmittance of UV-absorbing constituents eluted from, perhaps, as many as eight chromatographic columns. The instrument would make use of a single light source, a single reference flow cell, and a single electronics channel with electronic switching of the measuring photocells (Fig. 12.14). The photometer outputs can be recorded on a multipoint recorder that is synchronized with the photometer channel stepping switch, or the outputs of the individual channels can be stored in a sample-and-hold circuit that would permit either unsynchronized multipoint recording or the use of a continuous pen trace recording on specific channels. Obviously, the ideal mode of operation would involve the use of an on-line computer. A two-channel photometer is now being fabricated to prove the feasibility of the concept.

Flow Fluorimeter–Photometer

A new detection system combining a fluorimeter and a photometer in a single miniaturized detector head (Fig. 12.15) has been designed and fabricated, and a prototype system is being tested. Both the fluorimetric and the photometric measurements are made at an excitation wavelength of 254 nm. The instrument uses photoconductors as detectors for the UV photometer and a photomultiplier for the fluorescence detector. The flow cells, of "U" configuration, are embedded in a small cylinder of solid acrylic plastic and have a quartz window at each end. The design of the flow cell provides essentially 100% collection of emitted fluorescent light at wavelengths about 350 nm; cutoff occurs at about 310 nm. The 254-nm light from the excitation lamp is very effectively blocked by the acrylic transmission characteristics. Preliminary tests are encouraging, and modifications to improve the response of the instrument are being designed.

12.11 IDENTIFICATION OF BODY FLUID CONSTITUENTS

Major progress has been made in identifying constituents separated from human urine by the UV-analyzer. The number of positively identified compounds has increased from 35 (at the end of the last report period) to 69. Included among these new compounds are several that have little UV absorbance. No new identifications were made with the carbohydrate analyzer. Positive identification requires corroborative evidence by at least two of the following methods: UV spectrophotometry, gas chromatography, UV chromatography (with standards), and mass spectrometry. The last method is almost always used to obtain a confirmation.

Several compounds that show weak or no UV absorbance have been identified in urinary fractions

ORNL DWG. 70-12463

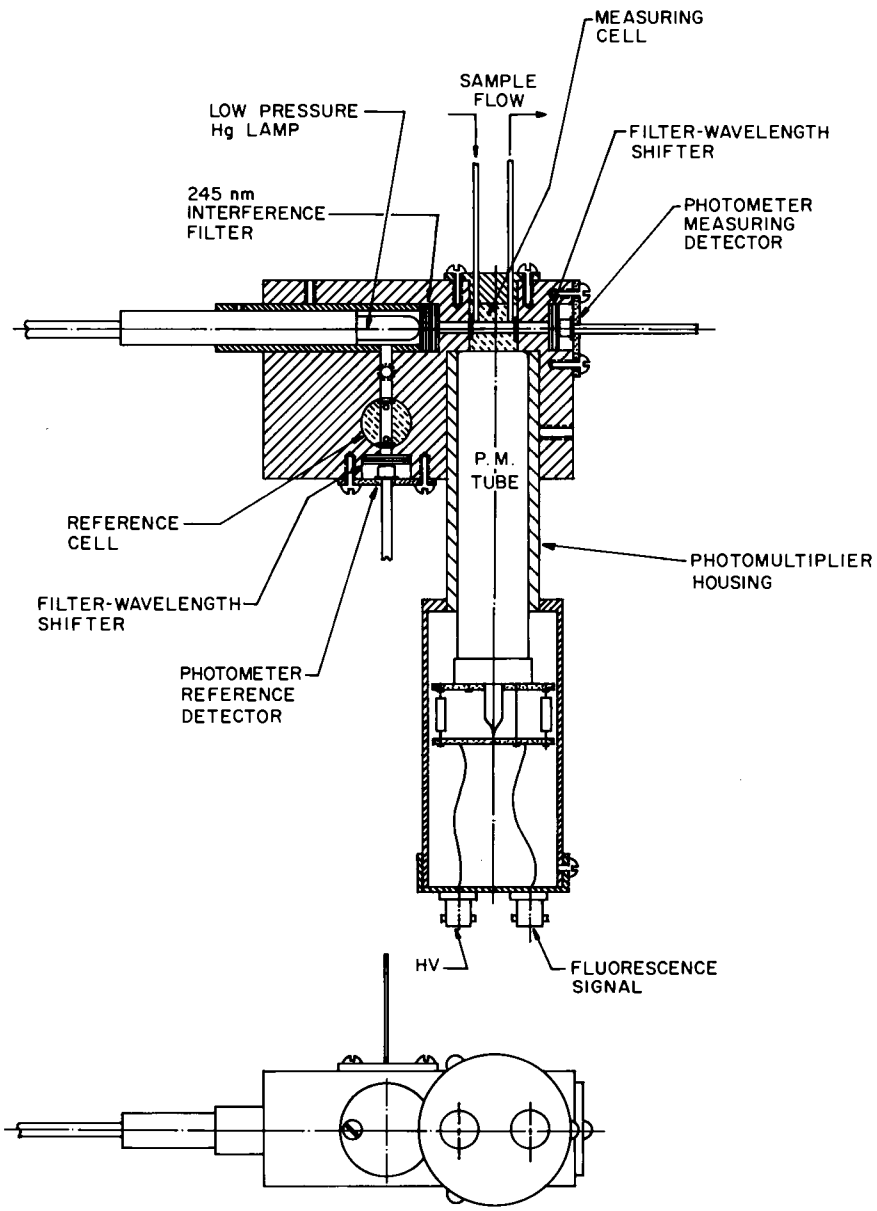

Fig. 12.15. Dual-beam flow monitor incorporating UV absorbance and fluorescence detection.

from the UV-analyzer. These compounds include urea, citric acid, glyoxylic acid, inorganic phosphate, and mannoheptulose. Although many other carbohydrates have been found in early fractions from the UV-analyzer, mannoheptulose is currently of some interest since it is reported to be an inhibitor of insulin release and glucose oxidation.[5] The compound was found in appreciable quantities in the urine of a 21-year-old institutionalized patient afflicted with phenylketonuria. (The only dietary source of mannoheptulose is reported to be avocado pears, and it is difficult to believe that an institutionalized patient had ingested a large amount of this fruit.)

5. *Carbohydrate Metabolism and Its Disorders* (ed. by F. Kiclens, R. J. Randle, and W. J. Whelan), Academic, New York, 1968.

12.12 APPLICATIONS AND EXPERIMENTAL RESULTS

Several interesting analytical results were obtained from pathologic urine samples. For example, a new metabolite of nicotinamide, nicotinamide-N^1-oxide, was found in the urine of two schizophrenic patients and a mentally retarded child; large quantities of uracil and uridine were found in the urine of a three-year-old boy afflicted with orotic aciduria; and large amounts of sucrose were found to be excreted by an infant who lacked the enzyme galactokinase.

Chromatographic peak areas were shown to be linear over a fourfold change in urinary concentration, elution volumes were reproduced within ±2%, and absorbance ratios (254 nm/280 nm) coupled with elution volumes were shown to be useful data for peak identification by the computer.

Metabolism of Nicotinamide and Nicotinic Acid

The metabolic pathways involved in the metabolism of nicotinic acid (niacin) and nicotinamide (niacinamide) were investigated using the UV-analyzer. Samples of 24-hr urine composites were collected from a clinically normal subject who had ingested different dosages of nicotinic acid and nicotinamide; and urine samples from two patients diagnosed as schizophrenics and one mentally retarded patient, who were being tested with these drugs, were also analyzed.

The principal metabolite of nicotinamide in humans is reported to be N^1-methyl-2-pyridone-5-carboxamide; up to 60% of an ingested dose of nicotinamide is excreted in the urine as this pyridone.[6] The compound N^1-methyl-4-pyridone-3-carboxamide has been identified as a metabolic product of nicotinamide in human plasma, and about 38% of an ingested dose of nicotinamide has been reported to be present in body fluids in the form of this metabolite.[7] Another major metabolite of nicotinic acid or nicotinamide is reported to be N^1-methylnicotinamide; however, we have been unable to identify it in the studies we have made thus far. The compound nicotinamide-N^1-oxide has been reported to be a metabolite of nicotinamide in mice but has not, to our knowledge, been reported in humans.[8]

The significant feature of the analyses of excreted nicotinic acid metabolites is the confirmation of the presence of significant quantities of the metabolite nicotinamide-N^1-oxide in the urine of the three subjects with two different pathologies. (This compound is absent in a normal subject.) The appearance of this new metabolite could be either dose- or threshold-related. However, it is equally possible that its appearance may be related to the pathologic condition of the patient. In either case, it would seem to be important to determine any possible secondary effects of this compound on the human body. Studies will be continued in order to determine whether the appearance of this new metabolite is dose- or history-related, or whether it is connected with a particular pathology.

Orotic Aciduria

Hereditary orotic aciduria is a rare genetic disorder of pyrimidine metabolism characterized by excessive excretion of orotic acid in the urine. The metabolic defect is apparently caused by the absence, or very low activity, of the enzymes orotidylic pyrophosphorylase and orotidylic decarboxylase. The absence (low activity) of these enzymes causes a blockage in the metabolic pathway leading from orotic acid to uridine-5-phosphate. Drug therapy, utilizing uridine or uracil to inhibit orotic acid synthesis by means of a feedback mechanism via end-product repression of enzyme synthesis, is employed to control orotic acid synthesis.[9]

Urine samples from two children afflicted with orotic aciduria were analyzed on the UV-analyzer.[10] One of the children was being treated with uridine, while the other was not receiving drugs. Both sets of chromatograms showed the excretion of massive amounts of orotic acid and the absence of orotidine, which suggest a blockage of the normal enzyme. Uracil excretion for the child undergoing uridine therapy was about normal; however, large amounts of both uracil and uridine were excreted by the other child. These results may indicate an in vivo synthesis of uridine monophosphate (UMP) from uracil. UMP may be formed by a reversible pyrophosphorolysis between uracil and 5-phosphoribosyl pyrophosphate, a reaction analogous to the

6. W. A. Perlzweig, F. Rosen, and P. B. Pearson, *J. Nutr.* **40**, 453 (1949).

7. D. M. Abelson and A. Boyle, *Clin. Chim. Acta* **14**, 483 (1966).

8. V. Bonavita, S. A. Narrod, and N. O. Kaplan, *J. Biol. Chem.* **236**, 936 (1961).

9. *The Metabolic Basis of Inherited Disease*, 2d ed. (ed. by J. B. Stanburg, J. B. Wyngaarden, and D. S. Fredrickson), McGraw-Hill, New York, 1966.

10. Samples obtained through the courtesy of Dr. P. Rowe, Royal Alexandra Hospital for Children, Australia, and Dr. R. Howell, Johns Hopkins Medical Center, Baltimore.

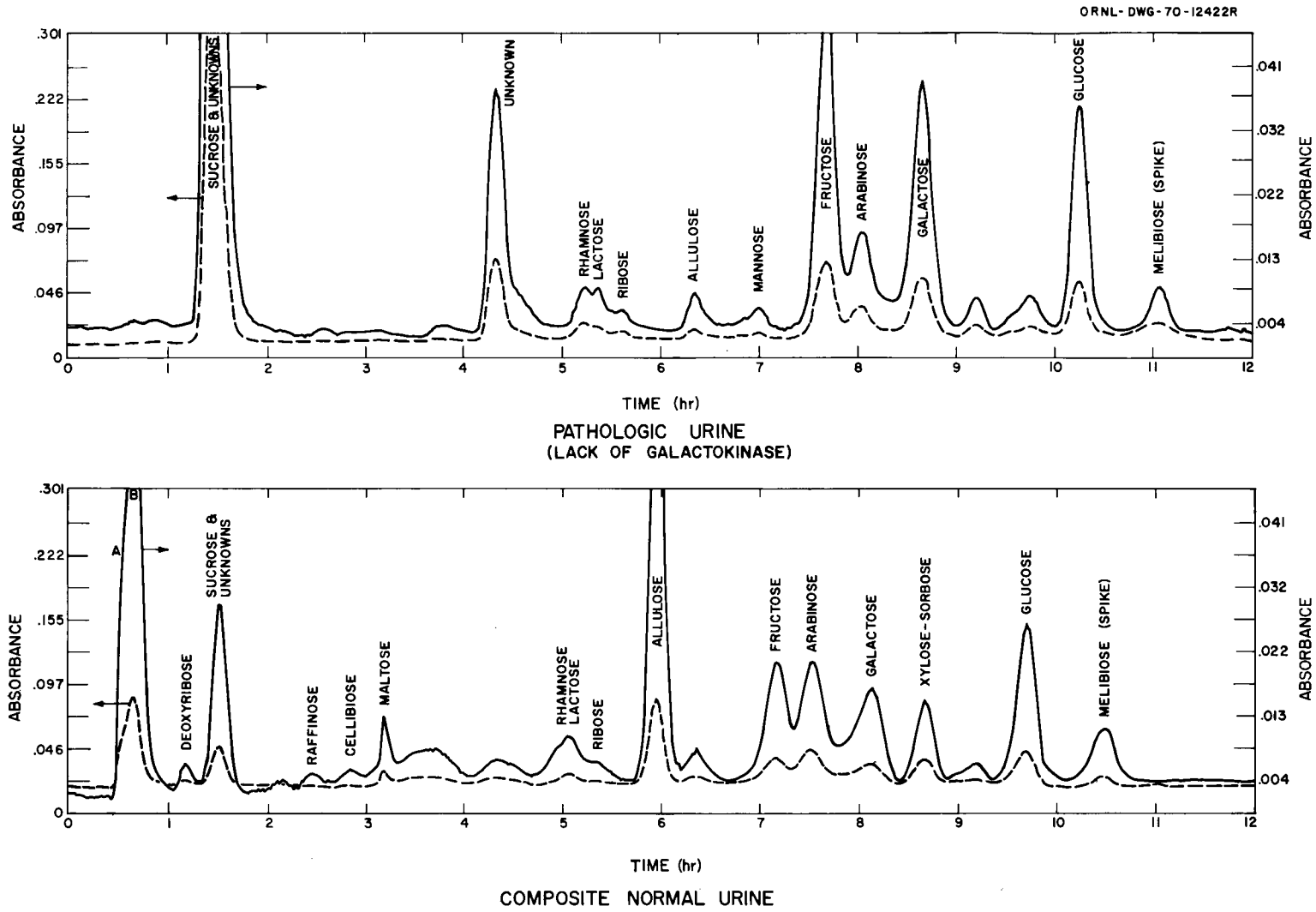

Fig. 12.16. Comparison of the urinary carbohydrate chromatogram of an individual lacking the enzyme galactokinase with the urinary chromatogram of a clinically normal subject.

reaction of orotic acid with orotidylic pyrophosphorylase to give orotidine-5-phosphate.[11] UMP has been synthesized from uracil in rat tissue, both in vivo and in vitro, but the reaction has not been demonstrated in mammalian tissues. The reaction in rat tissues is less effective than the reaction with orotic acid except under conditions of very high concentration.[12,13]

The presence of a relatively large amount of uracil may indicate the existence of a "shunt" synthetic pathway that does not involve orotic acid. The possible existence of such a pathway was suggested by Stanburg, Wyngaarden, and Fredrickson;[9] however, Reichard has reviewed evidence which appears to show that the pathway does not normally operate in mammalian tissues.[14] This brief chromatographic study demonstrates the utility of the UV-analyzer in basic studies of some inborn errors of metabolism.

Infant Who Lacked Galactokinase

The miniaturized carbohydrate analyzer has been demonstrated to have improved sensitivity, which makes possible the analysis of urinary samples without prior concentration. An interesting chromatogram was obtained from a urine sample from a child afflicted with a rare carbohydrate disorder characterized by the lack of galactokinase. The chromatograms of the pathologic sample and a typical normal sample are shown in Fig. 12.16. Note the absence of peaks *A* and *B* (i.e., the first two peaks in the normal urine) in the pathologic sample and the appearance of a new peak at 4.3 hr.

Feeding the child a diet low in galactose content appeared to control the galactose level of the body quite satisfactorily. The abnormally large sucrose peak would indicate that increased amounts of glucose and fructose should also be observed, assuming that the bodily hydrolytic degradation was functioning properly. However, concentrations of both of the latter sugars appeared to be approximately normal, leading one to conclude that the normal degradation process was impaired by the pathologic state.

Analytical Reproducibility and Linearity

UV analyses of a series of samples of the same reference urine were made at different dilutions in order to determine the reproducibility of elution volumes, elution times, and absorbance ratios (254 nm/280 nm) of the chromatographic peaks, as well as to determine the linearity of peak areas with concentration. Four analyses were made using 0.25, 0.50, 0.75, and 1.0 ml of a standard reference urine on a UV-analyzer comparable to a Mark II prototype. An on-line computer evaluated the resulting chromatograms. The data were examined for relationship between chromatographic peak area and sample size. The areas of most of the larger peaks and of peaks that were known to represent relatively pure compounds varied almost linearly with sample volume. The data for creatinine, whose absorbance is highly dependent on pH, and for some of the smaller peaks (e.g., orotic acid) were scattered (see Fig. 12.17).

Elution volumes and elution times for most of the chromatographic peaks were reproducible within a 2% relative standard deviation. The highest deviations in elution position were observed for creatinine and for those peaks occurring at elution times from 6 through 9 hr. This area of the chromatogram corresponds to a region in which chromatographic peak positions are somewhat more uncertain because of an acetate front moving through the column.[15] The reproducibility of elution positions is satisfactory for computer analysis and for the assignment of peak identity when coupled with the absorbance ratio data (A_{254}/A_{280}). No attempt was made to determine whether the reproducibility is improved for this series of runs by normalizing to one or several reference peaks.

12.13 DATA ACQUISITION AND ANALYSIS

The routine use of an on-line model PDP-8/1 computer has significantly increased the speed and flexibility with which data from the high-pressure anion exchange chromatographic system can be analyzed. The data analysis program previously described[16] has been in a continual state of refinement and is now capable of delivering precise quantitative results. Various improvements have been added to the chromatographic analysis computer program.

Extra Area

A chromatographic run often yields a chromatogram with overlapping peaks that do not interfere severely enough to eliminate the minimum absorbance value or

11. E. S. Canellakis, *J. Biol. Chem.* **227**, 329 (1957).
12. E. S. Canellakis, *J. Biol. Chem.* **227**, 701 (1957).
13. O. Skold, *Biochim. Biophys. Acta* **44**, 1 (1960).
14. P. Reichard, *Advan. Enzymol.* **21**, 263 (1969).
15. S. Katz, *J. Chromatogr.* **53**, 415 (1970).
16. C. D. Scott and D. D. Chilcote, *Clin. Chem.* **16**, 637 (1970).

ORNL DWG 70-12427R

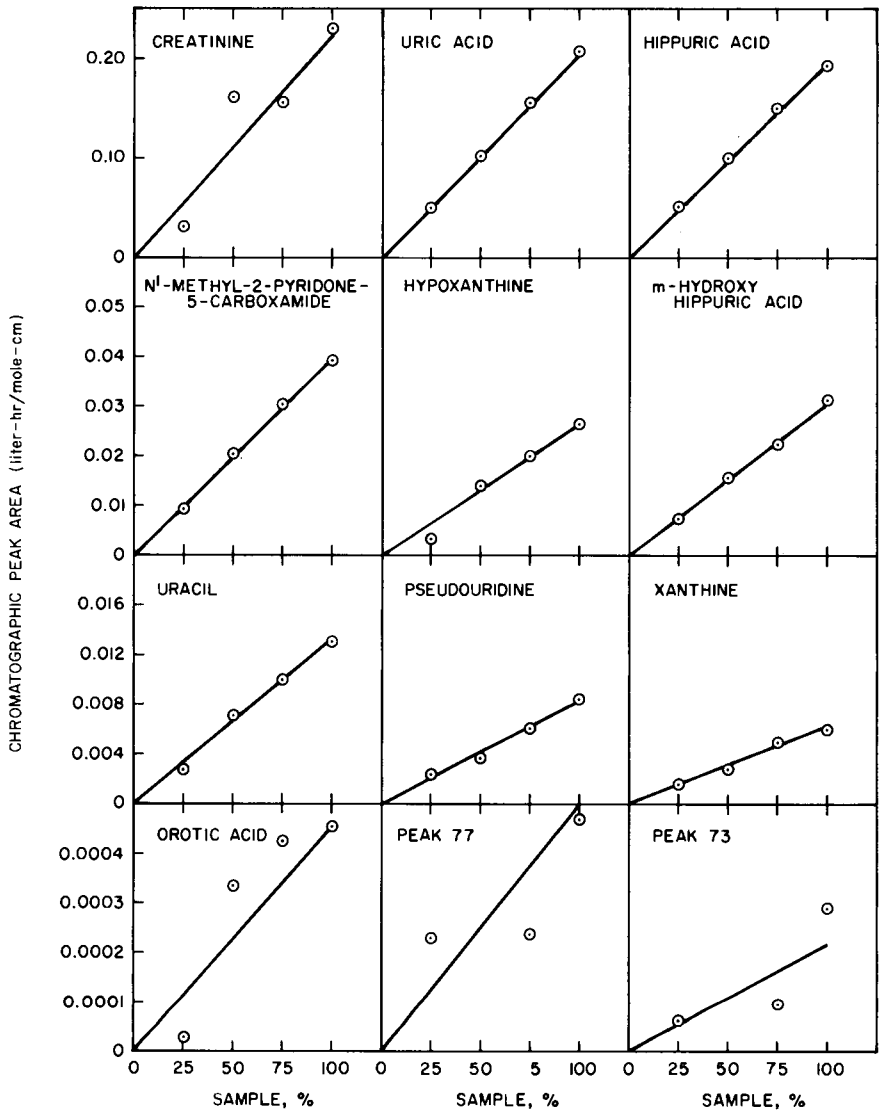

Fig. 12.17. Linearity of computer-determined chromatographic peak areas using 1-cc samples and urine concentrations from 25 to 100%.

"valley" between the two peak maxima. Since the program demands a second verification of this minimum before the first peak is considered to be ended, it will have already examined and included data for the second peak in the analysis of the first peak. To alleviate this situation, the program was modified so that the computer is instructed to search for an absolute minimum after the peak maximum is found. A separate routine is used to determine the area under the curve from this minimum to the point where the end of the first peak is verified. The resulting area is subtracted from the determined area of the first peak in order to yield the true area. After the termination of the first peak, the computation of this extra area continues until either the beginning of a new peak is found or the absorbance value begins to decrease.

Tailing Peak

Occasionally, a peak does not return to the base line in a symmetrical manner but, instead, "tails" severely. It is difficult to detect the end of such a peak by using a

first derivative limit since this would stop the analysis prior to the end of the peak. The program is now written so that, once the base-line limit is exceeded, an absolute minimum must be found before the analysis stops. If no minimum is found before the base line is reached, the program allows analysis of the "tail."

Verification of the Beginning of a Peak

Large peaks that rise sharply from the base line are easy to recognize, whereas small, slowly rising peaks present a considerable problem. The first derivative is used to determine the beginning of a peak. Because base-line noise is an ever-present problem, it is necessary to use a first derivative limit that allows the computer to disregard small changes in the first derivative due to noise. The program must then adjust the limit to find the optimum value that will reject the greatest proportion of the noise but still recognize sufficiently small peaks.

To rectify this problem, a method that employs a double limit was developed. This method can be described as follows. After a new data point is obtained and the first derivative is calculated, this derivative is compared with a relatively large limit to check for the start of a large, sharply rising peak. If the limit is not exceeded, the computer then compares the derivative with a second limit, which is much smaller than the first, to check for the beginning of a small peak. The large limit must be exceeded twice in succession to establish the start of a peak. In this case, the first derivative is determined between each new data point and the previous one.

The verification of the beginning of a small peak is more involved. First, the smaller limit must be exceeded several times in succession (in our case, nine times); second, the limit itself is incremented after each check; and third, the first derivative is determined between the present data point and the data point where the limit was first exceeded. This technique ensures that the small peak, although gently sloping, steadily increases in height during the verification period. The length of the verification step eliminates the small background fluctuations resulting from noise. Such fluctuations begin like small chromatographic peaks but soon drop toward the base line.

Elution Volume Calculation

The eluate from the high-pressure anion exchange system feeds a glass siphon that completely empties by a siphoning procedure after it accumulates a specific volume. Electrodes in the siphon are connected to contact points in the computer; these contact points close just before the siphon is filled and open as the siphon dumps. A computer program was written to instruct the computer to calculate the flow rate and accumulated volume as soon as contacts open. Since the siphon delivers a reproducible volume of fluid each time it dumps, the flow rate is easily calculated by dividing this volume by the elapsed time between each dump.

Once a peak maximum is found, its elution volume is determined in the following manner. The time of the last dump is subtracted from the time of the appearance of the maximum. This difference is multiplied by the flow rate that was determined at the last dump and then added to the accumulated volume (also determined at the last siphon dump).

WATER POLLUTION STUDIES

Much of the usable water supply in areas of high population density is polluted by various organic contaminants, including those present in industrial wastes and sanitary sewage as well as natural organic contaminants. If contamination levels become too high, additional processing steps will be necessary before waste streams are released to the environment or before water supplies are used by the human population. Although such contaminants have been analyzed in terms of gross organic content, only limited work has been done in determining their molecular constituents. Obviously, information of this type will be required to adequately design systems for removal or recovery of these contaminants.

Because of their sensitivity and capability for detecting and quantifying all, or essentially all, of the constituents in a sample, the high-resolution ion exchange chromatographs recently developed[17-20] at Oak Ridge National Laboratory appeared to be adaptable to the problem of analyzing for residual organic compounds present in water at low concentration levels.

17. C. D. Scott, J. E. Attrill, and N. G. Anderson, "Automatic, High-Resolution Analysis of Urine for Its Ultraviolet-Absorbing Constituents," *Proc. Soc. Exp. Biol. Med.* **125**, 181 (1967).

18. Charles D. Scott and Robert S. Melville, "Introduction to the Proceedings of the Symposium on Urinary Constituents of Low Molecular Weight," *Clin. Chem.* **14**, 287 (1968).

19. R. L. Jolley and M. L. Freeman, "Automated Carbohydrate Analysis of Physiologic Fluids," *Clin. Chem* **14**, 538 (1968).

20. Charles D. Scott, Robert L. Jolley, and Wayne F. Johnson, "Prototype Systems for the Automated High-Resolution Analyses of UV-Absorbing Constituents and Carbohydrates in Body Fluids," *Amer. J. Clin. Pathol.* **53**, 701 (1970).

Two types of high-resolution chromatographs have been developed for analyzing samples of body fluids. One of these, called the UV-analyzer, utilizes an acetate buffer (as the eluent) and ultraviolet photometry (for detection) to determine more than 200 compounds of biological origin in the concentration range of 100 ng to 100 μg/ml. The second chromatograph, called the carbohydrate analyzer, uses a borate eluent and a phenol–sulfuric acid color development system to determine more than 50 carbohydrate compounds of biological origin in the concentration range of 1 to 100 μg/ml. Many of these compounds and their degradation products are probably present in sewage effluents. Additional organic compounds of concern in sewage treatment[21,22] could also be analyzed using these instruments.[23] In view of such considerations, we have begun a program directed along four lines:

1. the selection of a technique for concentrating sewage effluent samples so that sufficient quantities of the individual constituents will be present to permit detection, and the testing of the method of choice for maintenance of sample integrity;
2. the development and testing of the analytical systems for reliability and reproducibility, and demonstration of their capabilities for the analysis of sewage effluents;
3. construction of an analytical system for the Advanced Waste Treatment Laboratory of the Water Quality Office;
4. the identification and quantification of the individual constituents in sewage samples.

12.14 PREPARATION OF SAMPLES

As was reported last year, a two-step procedure using both vacuum distillation and freeze-drying has been adopted as the technique for concentrating sewage effluent samples. The initial concentration of 10- to 30-fold is performed using the large vacuum still. The resulting concentrate is further reduced to a few milliliters by freeze-drying. A concentration factor of 500 was found to be adequate in most cases, but it appears to be dependent on a variety of sewage plant operating conditions, including temperature and residence time. For example, the effluent taken during the hot, dry summer periods required larger (>1000) concentration factors.

In order to test this concentration technique for maintenance of sample integrity, the total losses of noncarbonate carbon during the concentration of sewage effluent samples for the UV-analyzer were determined. Unfortunately, the method of analysis is not sufficiently sensitive to permit accurate determination of the carbon concentration in the sample of effluent before concentration. The results, however, indicated a carbon concentration of 22 μg/ml ± 100%. The method is satisfactory for analyzing the liquid concentrate and the separated solids. The carbon contents of the liquid and solid portions of two samples of concentrate (in each case, a volume of 3 liters of secondary effluent containing ~22 μg/ml of carbon concentrated to 6 ml) were as follows:

Sample	Carbon content (mg ± 10%)		Percent C in solid portion
	Liquid portion	Solid portion	
1	120	6.0	5.0
2	150	8.4	5.3

The carbon found in the solid portion may be biased high since the solid could not be washed and thus undoubtedly retained some liquid concentrate. The recovery of 95% or more of the noncarbonate carbon in the concentrated liquid and more than 85% of the original sample is considered to be quite satisfactory for the purpose of this application.

12.15 ANALYTICAL SYSTEMS

The analytical technique developed for polluted water samples consists of a concentration step (by a factor of 50 to 1000, depending on the history of the sample) followed by analysis on either the UV-analyzer or the carbohydrate analyzer (or both analyzers). Several sets of duplicate analyses using this technique with the UV-analyzer were made to demonstrate the reliability and reproducibility of the method. In each set, we started with two separate 3-liter volumes of sewage effluent and concentrated each to 6 ml; then we chromatographed 2 ml of each of the concentrates on a Mark II UV-analyzer. With the exception of some small differences in peak resolution, these duplicate analyses were in good agreement.

21. R. L. Bunch, E. F. Barth, and M. B. Ettinger, "Organic Materials in Secondary Effluents," *J. Water Pollut. Contr. Fed.* 33, 122 (1961).

22. D. W. Rychman, James W. Irvin, and Reginald H. F. Young, "Trace Organics in Surface Waters," *J. Water Pollut. Contr. Fed.* **39**, 661 (1967).

23. S. Katz and C. A. Burtis, "The Relationship between Chemical Structure and Elution Position in an Anion Exchange System," *J. Chromatogr.* **40**, 270 (1969).

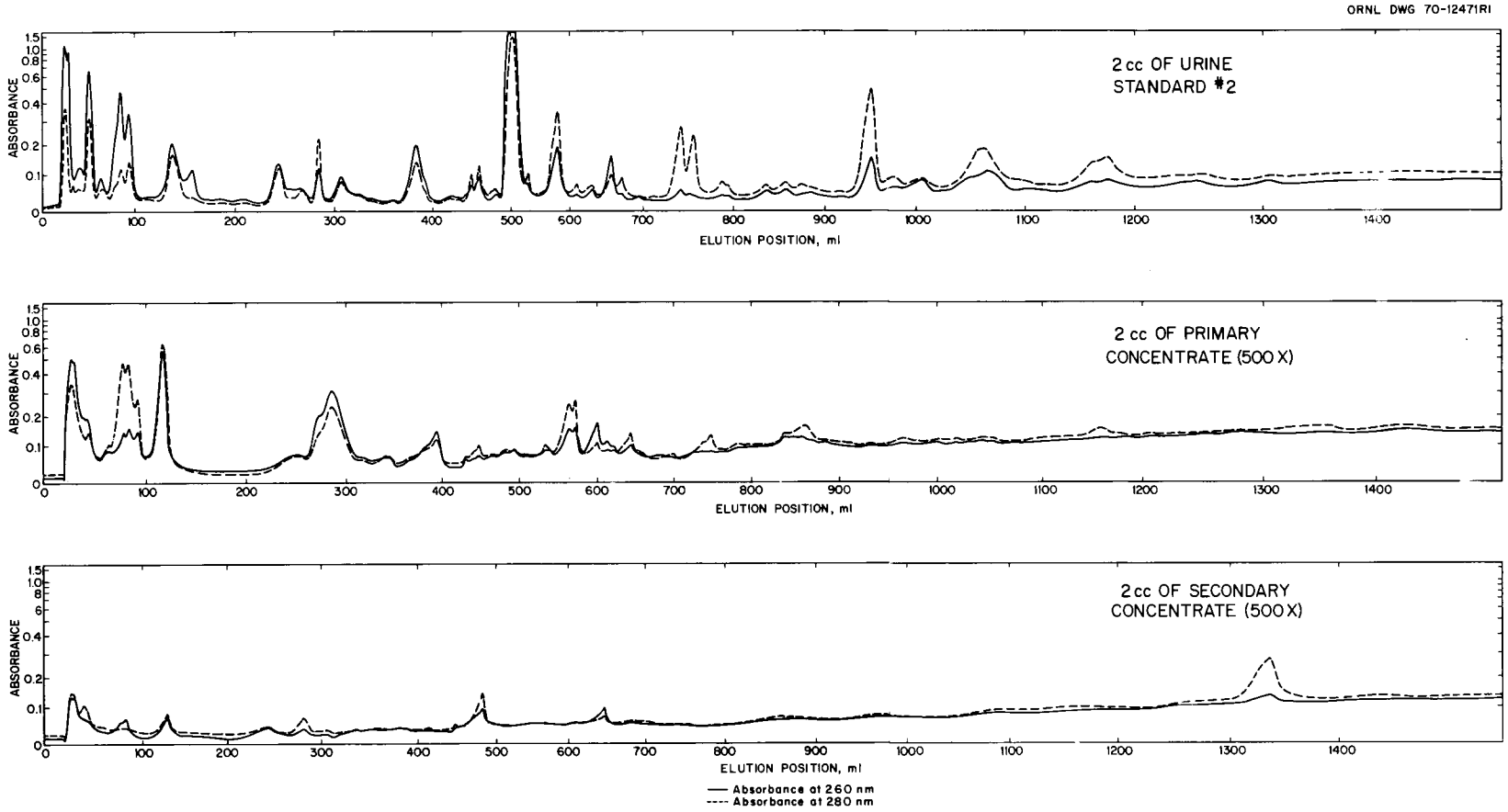

Fig. 12.18. Comparison of UV chromatograms of a primary effluent, secondary effluent, and urine.

The usefulness of the technique was demonstrated for primary and secondary sewage effluents from two different sewage treatment plants. One, the Oak Ridge East Waste Treatment Plant, processes essentially domestic wastes; the other, the Knoxville Third Creek Treatment Plant, handles primarily industrial wastes. Eleven samples of effluent were taken at intervals during the period of February 12 to September 14, 1970, from the Oak Ridge plant. As expected, the UV chromatograms from the primary effluent samples resemble, in a general way, those obtained from urine samples (Fig. 12.18). In general about 75 to 80 peaks were found. The UV chromatograms from secondary effluent usually contain only about half as many peaks as the primary effluent samples taken at the same time (Fig. 12.18).

Often a few of the peaks in the secondary effluent chromatograms are larger than the corresponding peaks in the primary effluent chromatogram; this indicates that the compounds responsible had "grown in," perhaps as decomposition products of compounds present in the primary effluent. A carbohydrate chromatogram for primary effluent, obtained by using the new Mark III carbohydrate analyzer, had 18 well-defined peaks (Fig. 12.19).

In order to demonstrate the general applicability of the analytical technique, samples of both primary and secondary effluents from a treatment plant handling industrial wastes were collected, filtered, and concentrated by a factor of 40. (Since the concentrations of organic compounds in streams handling industrial wastes are generally high, concentration by a factor of 40 to 100 is probably sufficient.) The UV chromatograms (Fig. 12.20) obtained from the primary and secondary effluent samples are remarkably similar to each other but distinctly dissimilar to normal urine chromatograms and those of domestic sewage samples. Not only are the pollutants present at much higher concentration levels than in domestic sewage, but they are also more stable and difficult to remove by standard secondary treatment.

A significant part of this program has been concerned with the construction of a UV-analyzer for use at the Advanced Waste Treatment Research Laboratory of the Water Quality Office (WQO). The Mark II UV-analyzer design was selected. However, a nine-chamber Varigrad was substituted for the original two-chamber gradient generator to provide flexibility in choosing a gradient. The use of this analyzer design will simplify the problem of identifying peaks since the identifications made and the techniques used in the parallel work of the Body Fluids Analyses Program will be directly applicable.

After the UV-analyzer had been fabricated, six test samples were run on it at ORNL to ensure satisfactory operation. Excellent results were obtained, and the resolution of peaks was found to be equal to that obtained with other Mark II UV-analyzers. The analyzer was then disassembled, shipped, reassembled (at the Advanced Waste Treatment Research Laboratory), and, with the assistance of personnel from ORNL, placed in operation.

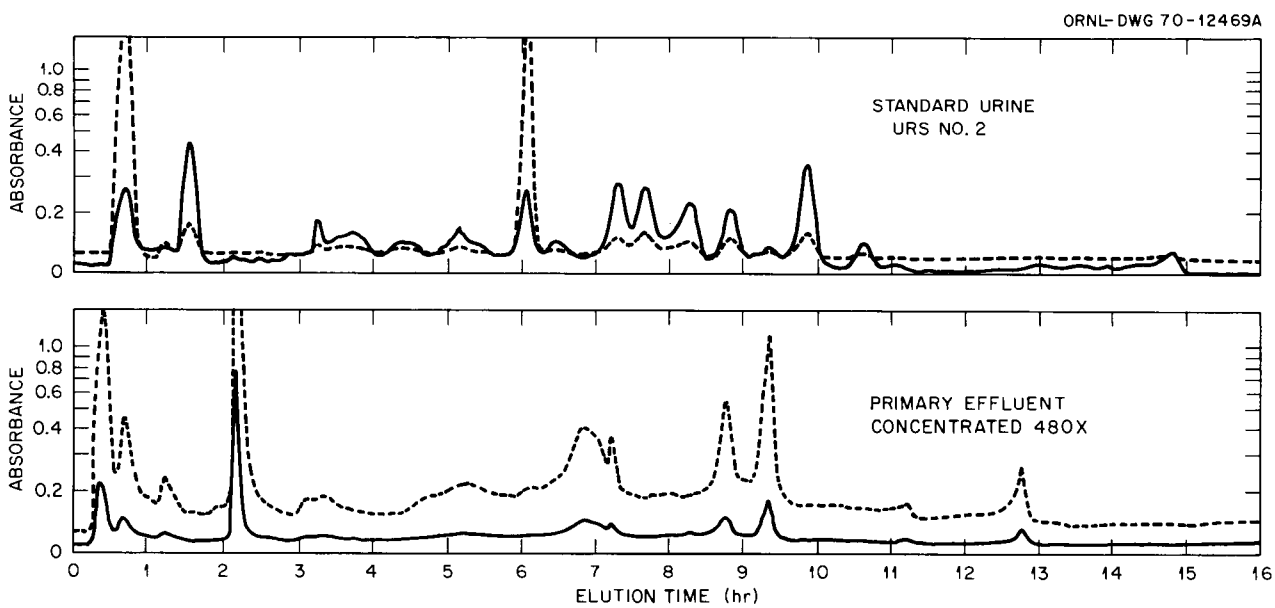

Fig. 12.19. Comparison of carbohydrate chromatograms of a primary effluent and a urine sample.

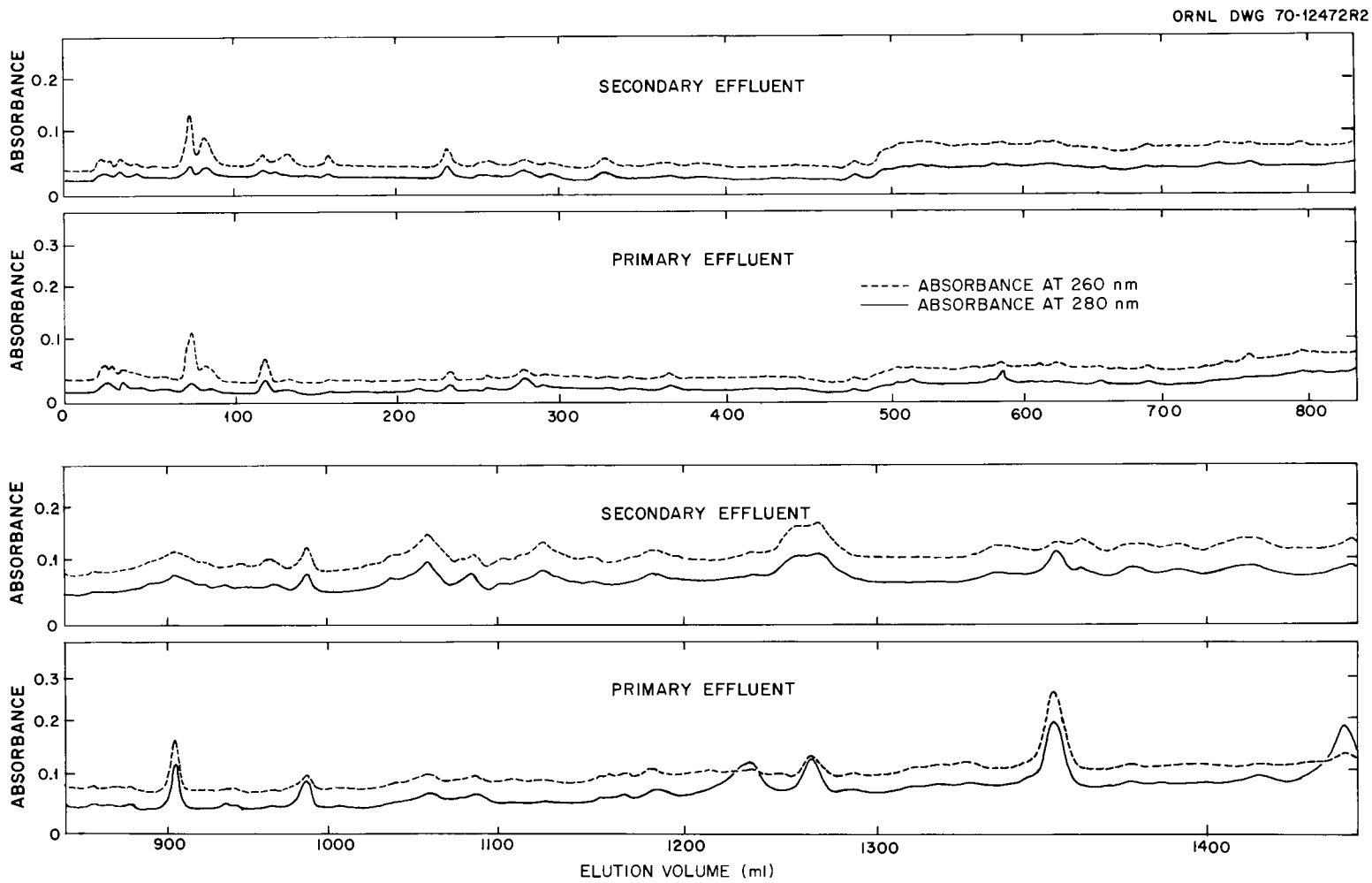

Fig. 12.20. Comparison of UV chromatograms obtained with primary and secondary industrial effluents.

An operating manual modified to reflect the changes made for the WQO analyzer was written and supplied with the Mark II instrument.

12.16 IDENTIFICATION OF REFRACTORY ORGANICS

The third effort of the experimental program, that of identifying the individual compounds found in sewage plant effluents, depended on the successful completion of the first two efforts and, hence, has only recently been initiated. The definitive identification effort, now under way, involves the collection of fractions from a large-scale preparative chromatograph and subsequent analyses of the fractions by auxiliary techniques such as cation exchange chromatography, ultraviolet spectroscopy, gas chromatography, and mass spectroscopy. As in the Body Fluids Analyses Program, such analyses are necessary to positively establish the identities of the chromatographic peaks. The 12 compounds listed in Table 12.5 have been identified with varying degrees of certainty. In addition to these compounds, excellent gas chromatographic and mass spectrographic data have been obtained from another peak that also appears in urine chromatograms. The compound has an apparent molecular weight of 153, but it has not been identified.

Table 12.5. Compounds identified in sewage effluents

Compound	Identification method[a]
Uracil	AC, CC
5-Acetylamino-6-amino-3-methyluracil	AC, CC
N^1-Methyl-2-pyridone-5-carboxamide	AC, CC
Caffeine	AC, GC, MS
Theobromine	AC, CC
7-Methylxanthine	AC, CC
1,7-Dimethylxanthine	AC, CC
3-Methylxanthine	AC, CC
1-Methylxanthine	AC, CC
Uroxanic acid	AC
Uric acid	AC, GC, MS
4-Hydroxyphenylacetic acid	AC, GC, MS

[a]AC = anion exchange cochromatography, CC = cation exchange cochromatography, MS = mass spectroscopy, and GC = gas chromatography.

13. Spectrophotometric Studies of Solutions of Lanthanides and Actinides

The major objective of this program is to develop and exploit spectrophotometric techniques for studying and utilizing the chemical properties of aqueous solutions, especially of the lanthanide and actinide elements, over wide ranges of experimental conditions. Some studies extend to nonaqueous and to solid solutions. The usual spectrophotometric techniques are used wherever materials and experimental conditions permit. A specially modified Cary model 14 spectrophotometer system has been built for use in extreme conditions and to permit study of the more highly alpha-active actinides. This system can be alpha-contained and is capable of operating at temperatures up to the critical point of water (374°C) and at pressures up to 10,000 psi. In conjunction with the spectrophotometric studies, the densities of aqueous solutions are being measured over the temperature range of 25 to 400°C to determine the concentration changes needed in the spectrophotometric studies and to obtain fundamental information.

13.1 HIGH-ENERGY ABSORPTION BANDS OF H_2O AND D_2O

The studies of the effects of temperature (25 to 380°C) on the near-infrared (5000 to 12,000 Å) absorption bands of H_2O and D_2O have been completed and reported in two papers. One has been published;[1] the abstract of the other follows:

"New Absorption Bands for H_2O and D_2O and the Effects of Temperature to 380°C on the Near IR Bands of Liquid and Vapor H_2O and D_2O," by J. T. Bell, N. A. Krohn, and D. M. Helton. *Abstract:* The changes in the four highest energy absorption bands of liquid and vapor H_2O and D_2O are related to the changing concentration over the temperature range 25 to 380°C. Two new bands for liquid H_2O are reported at 16,540 and 15,060 cm^{-1}, and two corresponding D_2O bands are reported at 13,580 and 11,770 cm^{-1}. The changes in the band energies and the intensities are shown to be linear functions of the molar concentrations, regardless of the liquid or vapor states. The linear relationships between the spectral changes and the molar concentrations may be used to support most any model for the structure of H_2O, but probably support the continuum models best. The data along with the assumption that the spectral changes result from changes in the molecular association of H_2O or D_2O lead to the conclusions that H_2O and D_2O are considerably associated at the critical points, where the concentration is ~17 *M*, and this association continues to concentrations near zero.

The discovery of two absorption bands at 6050 and 6640 Å for H_2O, and three bands at 7200, 8000, and 8500 Å for D_2O,[1] showed that the absorbance of H_2O and D_2O in cells with long path lengths (⩾10 cm) at wavelengths less than 7000 and 8800 Å, respectively, cannot be completely neglected in the spectral studies of aqueous solutions. The linear relation between the absorption band parameters and the molar concentrations at the various temperatures led to the conclusion that the H_2O or D_2O molecules are continuously dissociated over a concentration change of 55.5 to 0 *M*, regardless of the physical state. The positions and intensities of these new bands for H_2O and D_2O at 25°C (i.e., ~55 *M* water) were determined by extrapolating the band parameters as determined at higher temperatures and lower concentrations. Since that time, we have confirmed those band positions in the spectrum of H_2O in a 44-cm-path-length cell, and have determined more accurate values of 1.6×10^{-5} and 2.8×10^{-5} for the molar absorptivities of the bands at 6050 and 6640 Å respectively.

13.2 SPECTRAL STUDIES OF THE ACTINIDES

In experiments with concentrated (>1 *M*) solutions of $UO_2(ClO_4)_2$ we observed appreciable absorbance at wavelengths greater than 5000 Å, where the absorbance is generally assumed to be zero. The spectrum of 1.89

1. J. T. Bell and N. A. Krohn, *J. Phys. Chem.* 74, 4006 (1970).

M $UO_2(ClO_4)_2$ in 2 M $HClO_4$ in a 44.0-cm cell clearly showed an absorption band at 5077 Å and a poorly defined band at 5310 Å, with molar absorptivities of 6.9×10^{-3} and about 10^{-4} respectively. The intensities of these bands at 25°C are in good agreement with intensities calculated by the Boltzmann equation [Eq. (1)] for the transitions from the first and second vibrational levels of the ground state,

$$N/N_0 = e^{-1.44n\bar{\nu}/T}, \quad (1)$$

where N_0 = population of the ground state, N = population of the vibrational state, n = degeneracy of the vibrational state, $\bar{\nu}$ = vibrational frequency of the ground state (884 cm^{-1}), and T = temperature in °K. Furthermore, the observed increases in the band intensities for a temperature change of 17 to 95°C are almost exactly the same as the increases predicted for this temperature change according to Eq. (1). These relations are almost conclusive evidence that the new uranyl bands at 5077 and 5310 Å are "hot bands" originating from the first and second vibrational levels of the ground state. Details of this work have been submitted in a note to the *Journal of Molecular Spectroscopy.*

The thermodynamic quantities for the endothermic reaction for the formation of the 1:1 complex of Am^{3+} with iminodiacetic acid have been determined by spectrophotometric and pH methods. A paper summarizing the results has been accepted for publication in the *Journal of Inorganic and Nuclear Chemistry.* Its abstract follows:

"The Thermodynamics for the Formation of Americium–Iminodiacetic Acid Complexes as Determined by Spectrophotometric and pH Techniques," by J. T. Bell, R. D. Baybarz, and D. M. Helton. *Abstract:* The changes in the spectra and the pH of four solutions of Am^{3+} and iminodiacetic acid (IDA) have been observed over the 15–90°C range. Equilibrium constants for the reaction forming the 1:1 complex $AmIDA^+$ have been determined, and ΔH for the reaction was calculated to be 6.9 kcal $mole^{-1}$ from the linear plots of ln K vs. $1/T$. The free energy decreases from 3 to 2 kcal $mole^{-1}$ while the entropy is constant, 13.1 ± 3.7 e.u., over the 15–90°C range.

The heat of reaction for the first ionization of IDA was determined to be −1 kcal $mole^{-1}$, and the second ionization of IDA was indicated to also be exothermic. Therefore, the ionization of IDA cannot induce the endothermic character of reaction forming the 1:1 complex. The thermodynamics is likely controlled by the heat of dehydration of Am^{3+} which is expected to be about 200 kcal $mole^{-1}$.

13.3 EMISSION SPECTRA OF THE ACTINIDES

The emission spectra of the lanthanides and the electronic energy levels for the actinides indicate that some of the actinides have laser potentialities. The techniques for preparing a liquid laser of Nd^{3+} in $POCl_3$ and a laser of Nd^{3+} in $CaWO_4$ matrix have been refined and scaled down such that they have been applied to the preparation of an Am^{3+} laser.

The emission spectrum of Am^{3+} in $CaWO_4$ indicated a good possibility of a laser with a wavelength near 6900 Å. The calculated lifetimes for the 6900 Å emission also seemed adequate for Am^{3+} in $CaWO_4$, but the relatively low lifetimes for Am^{3+} in $POCl_3$ made a laser doubtful. Further testing showed no laser activity near 6900 Å for Am^{3+} in either matrix. However, an emission observed near 2.3 μ may make possible a 2.3-μ Am^{3+} laser.

13.4 DENSITIES OF AQUEOUS RARE-EARTH SOLUTIONS TO 340°C

The densities of solutions 0.05 to 0.44 M in $Pr(NO_3)_3$ and 0.1 to 0.63 M in HNO_3 were measured from 25 to 340°C. The effects of HNO_3 on these solutions were observed by measuring the densities of six HNO_3 solutions at 0.05 to 0.64 M over the same temperature range. The calculated apparent molal volumes of HNO_3 at 25°C are in good agreement with published data. At higher temperatures the apparent molal volume of HNO_3 decreases, and this decrease is inversely related to the HNO_3 concentration. The partial molal volumes of HNO_3 have been determined by extrapolating the plots of apparent molal volume vs the square root of the molality to zero concentration. The results, which were unexpected, are given in Table 13.1. A summary of this work is being prepared for publication.

Table 13.1. Partial molal volumes, ϕ_v^0, of HNO_3 in aqueous solutions at temperatures of 25 to 340°C

t (°C)	ϕ_v^0 (ml)	t (°C)	ϕ_v^0 (ml)
25	33.1	225	−567
50	−4.9	250	−969
75	−17.6	275	−2223
100	−49.3	300	−3974
125	−129	310	−6093
150	−337	320	−8091
175	−227	330	−8071
200	−302	340	−8924

13.5 PROTONIC WAVE FUNCTIONS AND SPECTRA

In the previous annual report, we described a method for solving Schrödinger's equation without using the

Born-Oppenheimer approximation.[2] Briefly, the coordinates of the molecule are transformed to center-of-mass coordinates, and the equation in the internal coordinates is solved variationally using Slater determinants as trial functions for the electrons and the protons. The calculations demonstrated that the protons have multiplet structure, analogous to the electronic multiplet structure, in addition to the so-called vibrational and rotational structure.[3]

It has been shown recently that the "vibrations" are protonic transitions of the type $nl \rightarrow (n+1)(l+1)$. For example, in HF, the calculated energy of the transition from the 108 s ground state of the proton to the 109 p excited state is 4277.4 cm^{-1}, which is within 10% of the experimental value of 3961.57 cm^{-1}. The "rotations" are transitions of the type $nl \rightarrow n(l+1)$.[4]

The effects of external homogeneous electric and magnetic fields on the protonic structure have also been studied. In the case of neutral hydrides, an external homogeneous electric field has the same effect on the protonic coordinates as on the electronic coordinates. However, for ionized hydrides, the effect is proportional to $(1 - Nm_p/M)$, where m_p and M are the protonic mass and the total molecular mass, respectively, and N is the degree of ionization. A homogeneous magnetic field affects the protonic coordinates through terms proportional to $H^2 m_p/M$ and $N_e(Hm_p/M)^2$, where H is the strength of the magnetic field and N_e is the number of electrons.[5] It has also been found that, in the presence of a homogeneous magnetic field, the center of mass of neutral atoms and molecules will vibrate in the plane perpendicular to the direction of the field with a frequency of $(N_e e^2H^2/4Mm_ec^2)^{1/2}$, where e is the electronic charge and c is the velocity of light.[5,6]

The multiplet theory for a single configuration for symmetric wave functions has been developed, and orthonormal eigenfunctions of L^2 and S^2 in terms of symmetric products of one particle wave function have been calculated for the s^2, sp, p^2, s^3, s^2p, sp^2, p^3, s^4, s^3p, s^2p^2, sp^3, and p^4 configurations.[7] With these eigenfunctions and the Hamiltonian matrix elements from a symmetric wave function,[8] the deuteron structure of a molecule with up to four deuterons can be studied.

At ORNL, experiments involving the use of photoelectron spectroscopy have shown that the vibrational transitions that are seen are dependent on the angle between the direction of the photoejected electron and the polarization of the incident photon.[9] The work on the selection rules for protonic transitions[10] was extended to include the photoeffect, and it was found that the vibrational transitions should have an angular dependence of the form $\alpha + (\beta - \alpha)\sin^2\theta$, where α and β are the absolute squares of the transition matrix elements and θ is the angle between the direction of the photoejected electron and the polarization of the photon.[11] A consequence of the above study is the prediction that protons can be photoejected from molecules in the same way as are electrons. Unfortunately, the cross section is large only at frequencies near the resonance frequency (i.e., the protonic binding energy).[12]

2. *Chem. Technol. Div. Annu. Progr. Rep. May 31, 1970*, ORNL-4572, pp. 233–35.

3. I. L. Thomas, "The Protonic Structure of Methane, Ammonia, Water, and Hydrogen Fluoride," *Chem. Phys. Lett.* 3, 705 (1969); I. L. Thomas, "The Protonic Structure of Molecules. I. Ammonia Molecules," *Phys. Rev.* **185**, 90 (1969); I. L. Thomas and H. W. Joy, "The Protonic Structure of Molecules. II. Methodology, Center-of-Mass Transformation, and the Structure of Methane, Ammonia, and Water," *Phys. Rev.* **A2**, 1200 (1970).

4. I. L. Thomas, "'Vibrational' and 'Rotational' Energy Levels as Protonic Structure in Molecules," *Phys. Rev.* **A3**, 565 (1971).

5. I. L. Thomas, "The Stark and Zeeman Effects on the Protonic Structure of Molecules," *Phys. Rev.* **A2**, 1675 (1970).

6. I. L. Thomas, "The Motion of the Center of Mass of Atoms and Molecules," *Phys. Rev.* **A3**, 1022 (1971).

7. I. L. Thomas, "Multiplet Theory for Symmetric Wave Functions," submitted for publication in the *Physical Review.*

8. I. L. Thomas, "Hamiltonian Matrix Elements from a Symmetric Wave Function," *Phys. Rev.* **A2**, 728 (1970).

9. T. A. Carlson and A. E. Jones, "Angular Distribution of Photoelectrons," *Chem. Div. Annu. Progr. Rep. May 20, 1970*, ORNL-4581, pp. 178-80.

10. I. L. Thomas, "Selection Rules and the Protonic Structure of Molecules," *Phys. Rev.* **A2**, 72 (1970).

11. I. L. Thomas, "The Angular Dependence of the Vibrational and Rotational Excitations Seen in Photoelectron Spectroscopy," submitted for publication in the *Physical Review.*

12. I. L. Thomas, "The Photoprotonic Effect in Hydrides," submitted for publication in the *Physical Review.*

14. Preparation and Properties of Actinide Oxides

14.1 THORIA DESINTERING STUDIES[1]

Experiments with thoria were continued[2] to determine the causes of desintering and the range of conditions under which it occurs. The development of a rational control of desintering could be useful for incorporating specified amounts, sizes, and geometries of porosity in nuclear fuel ceramic oxides. The continued determination of mercury porosities of desintered thoria to 15,000 psi indicated that most of the porosity is inaccessible in the majority of samples.

Fig. 14.1 shows representative desintering curves for sol-gel thoria, which had a density 99+% of the theoretical crystal density after prefiring in air at 1200°C for 2 hr. Although sol-gel thoria shows pronounced desintering effects, the density data in Fig. 14.2 for a representative selection of thoria powder compacts show that desintering may or may not occur in thoria powder pellets. With the exception of one sol-gel specimen for comparison, all the samples used in obtaining the data shown in Fig. 14.2 were compacts of thoria powder made by calcining thorium oxalate at 650 to 800°C and then carrying out the final firing at 1600 to 1800°C. The "DT" powders are characterized by a narrow-range ($\sigma_g \sim 1.1$) log-normal distribution of relic particle sizes near an average of 2 μ. Samples 305 and 355 were also calcined-oxalate thoria powders, but the digestion of sample 305 eliminated submicron oxalate particles that otherwise would have been present.

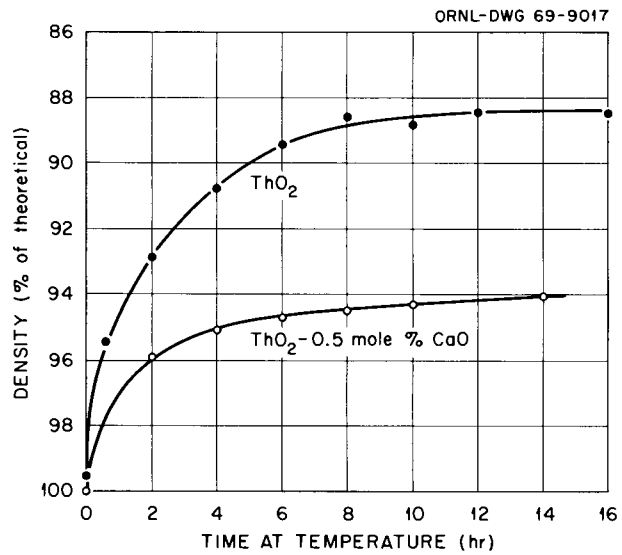

Fig. 14.1. Desintering of sol-gel thoria in air at 1600°C.

A number of possible mechanisms for void growth and desintering in oxide ceramics have been proposed. These include trapped gas pressure,[3] anisotropic crystal growth,[4] creep from externally applied stresses,[5] internal stressing by crystal growth and by thermal gradients,[6] and surface free-energy differentials induced by chemisorption.[7]

The simplest model for desintering is based on the Kelvin equation for surface-tension pressure in spherical fluid bubbles:

$$P = 2\gamma/r \,, \qquad (1)$$

1. Work done in cooperation with C. S. Morgan, Metals and Ceramics Division.

2. *Metals and Ceramics Div. Annu. Progr. Rep. June 30, 1970,* ORNL-4570, p. 26.

3. P. Vela and B. Russel, "Spontaneous Grain Boundary Swelling in Irradiated Copper-Boron Alloys," *J. Nucl. Mater.* **14,** 327–40 (1966).

4. R. S. Wilks, J. A. Desport, and J. A. G. Smith, *The Irradiation-Induced Macroscopic Growth of α Al_2O_3 Single Crystals,* AERE-R-5460, Harwell (1967).

5. L. E. Poteat and C. S. Yust, "Creep of Polycrystalline Thorium Dioxide," *J. Amer. Ceram. Soc.* **44,** 410–14 (1966).

6. S. E. Bronisz and D. L. Douglas, "Grain Growth in Thin Films of ThO_2, NpO_2 and PuO_2," *Phys. Status Solidi* **29,** K95 (1968); and "Annealing Effects in Thin Films of Thoria," *Proc. 26th Annu. Meeting, Electron Microsc. Soc. Amer. (1968).*

7. W. Missol, "Nature of Driving Force for Activated Sintering," *4th International Meeting on Powder Metallurgy, Dresden (1969),* CONF-690943, vol. 2.

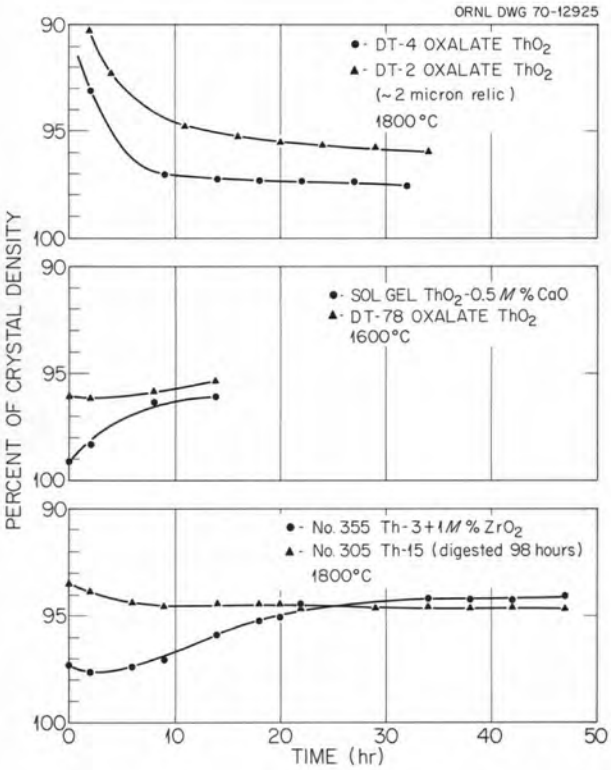

Fig. 14.2. Sintering and desintering of oxalate-relic thoria powder compacts.

where P is the equilibrium internal fluid pressure, γ is the surface specific free energy (surface tension), and r is the bubble radius. This equation is not directly applicable to the voids seen in desintered thoria, except possibly in the earliest stages of desintering, because the pores are elongated or faceted. Figure 14.3 is a scanning electron photomicrograph showing the nonsphericity and faceting of the pores, which are sometimes not highly obvious on lower-magnification optical metallographs such as Fig. 14.4. Both photographs are of thoria fired in air at 1600°C. Firing at 1800°C produces pores with somewhat greater rounding of the corners than firing at 1600°C, as shown in Fig. 14.5, but they are still highly elongated and comparatively flat-sided.

In developing a model for the desintering of the foregoing thoria products, it seems desirable to amplify and reinterpret Eq. (1) slightly, as follows:

$$P = (K\,\Delta\gamma/l) + P_e\,, \tag{2}$$

where K is a dimensionless geometric factor for shapes other than spherical ($K = 4$ for a cube when l is the edge length), l is a characteristic dimension, P_e is any externally applied overpressure, and $\Delta\gamma$ is the difference in surface tension between free surface in the pore and the grain boundaries, which are the extensions of

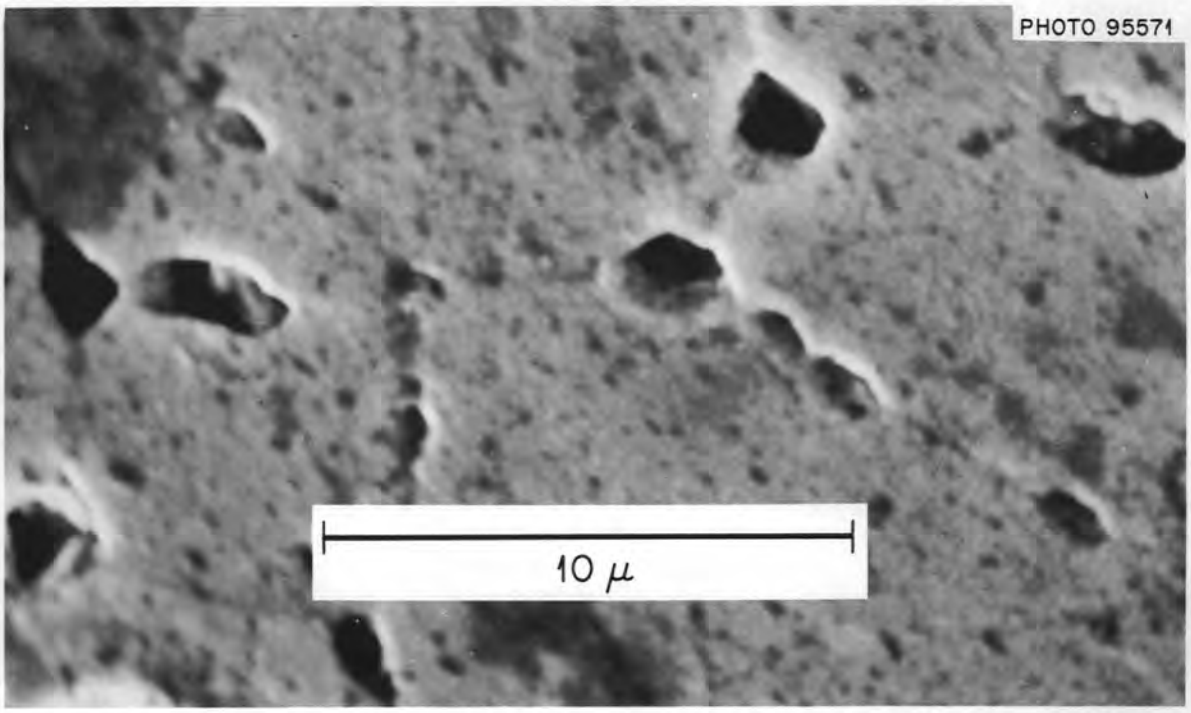

Fig. 14.3. Elongation and faceting of pores in sol-gel thoria fired in air for 8 hr at 1600°C. Scanning electron photomicrograph.

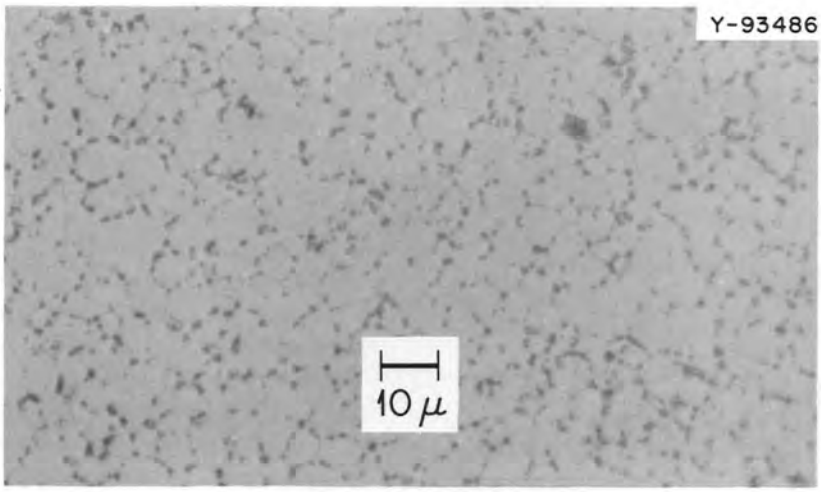

Fig. 14.4. Elongation of pores in sol-gel thoria fired in air for 8 hr at 1600°C. Optical metallograph.

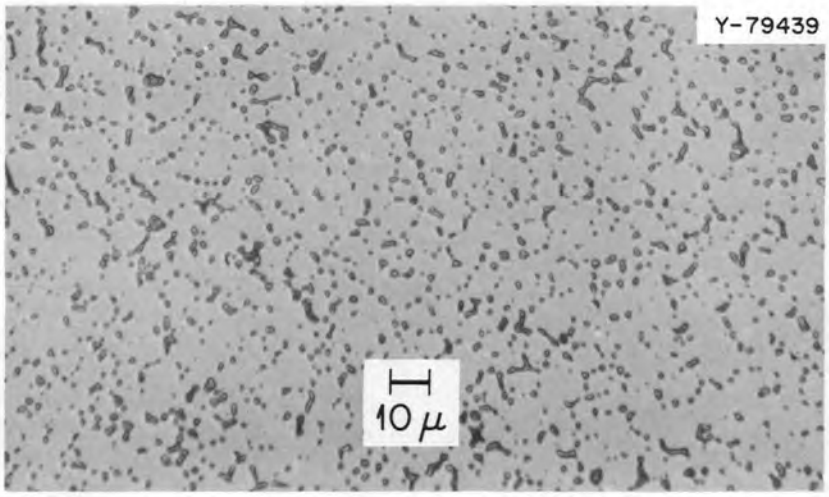

Fig. 14.5. Elongation of pores in sol-gel thoria fired in air for 1.5 hr at 1800°C. Optical metallograph.

the pore facets. Virtually all the porosity in desintered thoria is located in the grain boundaries. The observed elongated and prism shapes are reported to be characteristic of void formation when different facets are different crystallographic planes.[8]

Typical total gas release and composition data for sol-gel thoria and thoria-urania have been reported[9] in the range of 0.018 to 0.056 std cc/g for 1200°C-fired oxides fluxed or melted with Al_2O_3 or TiO_2 at 2000 to 2450°C in vacuum. A representative composition for thoria fired in air is: 0% argon, 41% CO_2, 3% (CO_2 + N_2), 2% H_2, 9% H_2O, 45% O_2, and 0% hydrocarbons.

Table 14.1 shows the equilibrium final densities predicted by Eq. (2) for thoria over a range of assumptions.

Comparison of these expected values of density in Table 14.1 with the final desintered densities in Figs. 14.1 and 14.2 shows approximate agreement in magnitudes. This indicates that the simple gas-pressure–surface-tension models may be valid. The calculated pore pressures suggested a further test, however. The

8. R. S. Nelson, D. J. Mazey, and R. S. Bower, "The Thermal Equilibrium Shape and Size of Holes in Solids," *Phil. Mag.* **11**(8), 91–112 (1965).

9. J. B. Cordiner and O. C. Dean, *A Study of Gas Evolution from Sol-Gel Thoria and Thoria-Urania,* ORNL-TM-2268 (1968).

Table 14.1. Predicted final equilibrium densities of desintered thoria using the modified Kelvin equation for cubical pores

Assumptions: $\Delta\gamma$ = 500 dynes/cm, perfect gases, no chemical reactions

Total gas (std cc/g)	Retained gas	Temperature (°C)	Pore radius (μ)	Nominal pore pressure (atm)	Equilibrium density[a] (g/cm^3)
0.056	A11	1800	5	4	5.4
0.056	CO_2, N_2, CO	1600	2	10	8.7
0.032	A11	1800	2	10	8.2
0.032	CO_2, N_2, CO	1600	2	10	9.2
0.018	A11	1800	2	10	8.9
0.018	CO_2, N_2, CO	1600	½	40	9.9

[a]Theoretical crystal density of thoria = 10.0 g/cm^3.

Table 14.2. Effect of lowering the external overpressure on "desintering" of sol-gel thoria

Sample	Prefiring condition	Initial density (g/cm^3)	Desintering conditions	Final density (g/cm^3)
1	1200°C, air, 4 hr	9.96	1800°C, vacuum, ½ hr	9.77
2-a	1800°C, air, 1½ hr	9.56	1800°C, vacuum, ¼ hr	9.65
2-b	Sample 2-a[a]	9.65	1800°C, vacuum, 2 hr	9.86
3-a	1800°C, air, 6 hr	9.38	1800°C, vacuum, 1 hr	9.44
3-b	Sample 3-a[a]	9.44	1800°C, air, 2 hr	9.40
4-a	1200°C, air, 2 hr	9.9 +	1800°C, vacuum, 1 hr	9.83
4-b	Sample 4-a[a]	9.83	1800°C, air, 2 hr	9.66

[a]After "desintering."

external gas overpressure is a detectably significant percentage of the total pore pressure in all cases: 2½% at the smallest and probably nearer 10%. If the external gas overpressure is reduced to zero, Eq. (2) predicts that the equilibrium density of 8.9 in Table 14.1 should decrease to 8.8. The results of desintering experiments performed in vacuum, to see if additional swelling could be induced, are given in Table 14.2. Setting P_e to zero significantly suppresses desintering, which is opposite to the effect predicted by the simple gas-pressure models.

The gases evolved during vacuum firing of samples 1, 2-a, and 2-b (Table 14.2) were analyzed for H_2, N_2, and (O_2 + CO + CO_2) chromatographically. Oxygen and the oxides are "lumped" because a molybdenum-lined graphite crucible had to be substituted for the available tungsten crucibles, which would have contributed excessive extraneous gas. Evolved hydrogen varied from 0.0001 wt % at 10 min to 0.001 wt % at 2 hr. Nitrogen hovered near the limit of detection, never exceeding 0.0003 wt %. The (O_2 + CO + CO_2) content varied from 0.02 wt % for 10 min to 0.08 wt % for 120 min. The high and progressive evolution of "oxygen" is probably an artifact of continuing oxygen dissociation from the thoria as the free oxygen reacted with the graphite.

The main conclusions from these data are that oxygen is unlikely to be able to contribute to gas pressure in voids, because of the ease of its progressive removal at 1800°C,[10] and that nitrogen is either virtually absent, in agreement with Cordiner and Dean,[9] or else is virtually nondiffusive in thoria at 1600 to 1800°C.

These results suggest that the gas-pressure model for desintering of thoria needs further testing despite the

10. The diffusion coefficient of oxygen is 10^4-10^6 times as great as that of thorium in thoria at 1600–1800°C, according to data of Poteat and Morgan and of Morgan and Yust: S. Peterson and C. E. Curtis, *Thorium Ceramics Data Manual*, ORNL-4530 (1970).

approximate reasonableness of the density values in Table 14.1.

Attempts to introduce controlled, known amounts of "inert gas" (nitrogen as $UN_{0.9}$) into sol-gel thoria failed because of the sensitivity of UN to traces of water and oxygen. We plan to try to introduce controlled amounts of CO_2 as "inert gas," although CO_2 is not as chemically inert as nitrogen toward thoria or toward dissociative reduction by vacuum. Experiments to determine gas release and composition from crushed desintered thoria are also in progress.

The desintering mechanism proposed by Bronisz and Douglas,[6] which suggests that internal stresses not caused by gas pressure may create voids in some circumstances, prompted a search for evidence of strain in the thoria products undergoing desintering. Sol-gel thoria fired at 1600 to 1800°C in air for desintering has fairly reproducible but anomalously low apparent x-ray crystal sizes as compared with the grain size seen by optical metallography. Table 14.3 shows some typical x-ray crystal sizes for thoria whose metallographic grain sizes are 5 μ and greater. Electron photomicrography of carbon replicas of polished, etched sections and of fracture surfaces discloses no visible subgrain structure of the sizes corresponding to these x-ray results, although occasionally structures that are neither normal grains nor 0.1-μ subgrains, as illustrated in Fig. 14.6, are seen. This pseudo-subgrain structure of Fig. 14.6 is from a replica of a metallographic section of sample 2 in Table 14.3. It gives the impression of being an artifact of polishing a very thin slice of a grain parallel to the face of an underlying grain boundary. That the

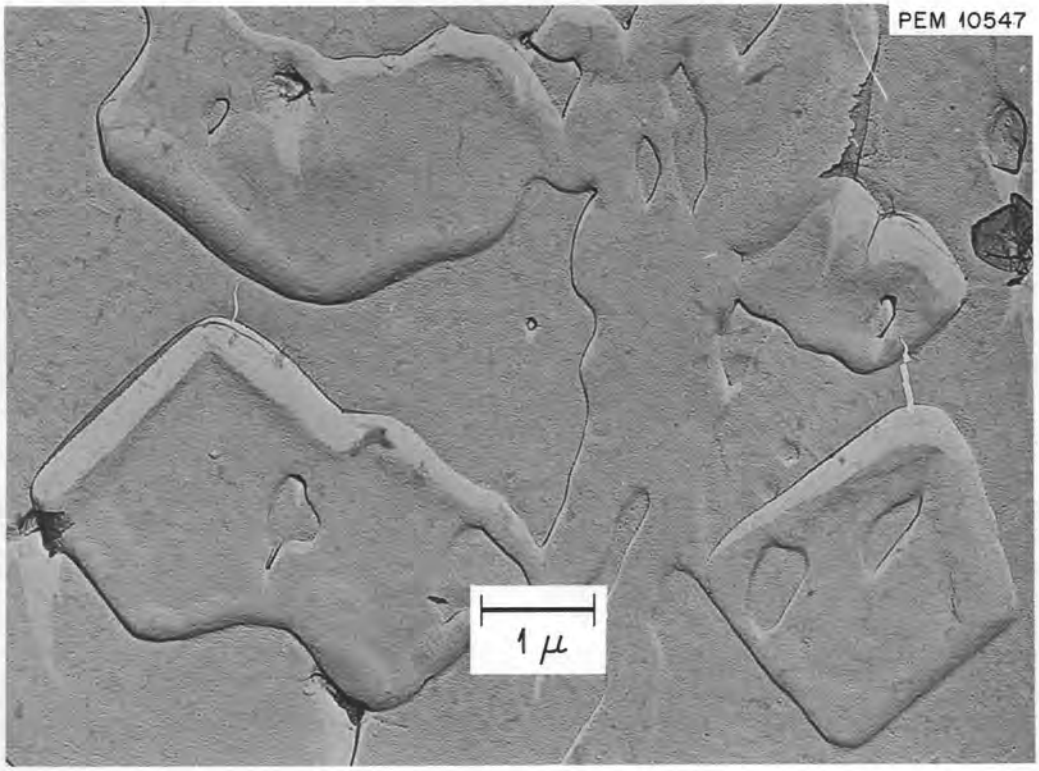

Fig. 14.6. Possible "subgrain" structure of sol-gel thoria fired in air for 0.5 hr at 1800°C. Scanning electron photomicrograph.

Table 14.3. Apparent x-ray crystallite size of sol-gel thoria fired at 1600–1800°C in air
Apparent metallographic grain sizes ≥5 μ

Sample	Composition	Firing temperature (°C)	Firing time (hr)	Crystal size (μ)		
				(111)	(220)	(311)
1	ThO_2	1600	8	0.1440	0.140	0.1545
1-a	ThO_2	1600	16	0.1635	0.1475	0.1325
2	ThO_2	1800	½	0.124	0.134	0.131
3	ThO_2–0.5 *M* CaO	1600	14	0.1445	0.174	0.164

small x-ray crystal sizes for samples fired at 1600 to 1800°C could be due to strain broadening seems unlikely; however, in the absence of reproducible and independent confirmation of subgrains in the 0.1-μ range, the interpretation of the x-ray results in terms of subgrain structure is tentative.

There is some independent evidence compatible with the hypothesis of large strains in the sol-gel thoria prefired at 1200 to 1400°C. Anomalously small and irregularly variable apparent x-ray crystal sizes have been found for sol-gel thoria fired at 1075 to 1270°C,[11] and cyclic grain growth and breakdown phenomena have been observed in sol-gel thoria undergoing low-temperature sintering.[12]

14.2 ADSORPTION OF NITRIC ACID ON THE SURFACE OF URANIA

The adsorption of nitric acid from solution on the surface of urania is important in stabilizing the colloidal urania particles in sol-gel processes for making nuclear fuel microspheres. However, the determination of isotherms and adsorption potentials for nitric acid adsorption on urania under the conditions encountered in processing practice is obscured by the circumstance that urania exists in both crystalline and amorphous states in the sol. The system is further complicated by the presence of a holding reductant, added to stabilize the uranium(IV).

For well-dispersed, fully crystallized dilute thoria sols it has been shown[13] that the ideal Donnan emf relation between adsorbed nitric acid and free nitric acid is valid:

$$pH_{app} = 2[\log_{10}(HNO_3)_F] - \log_{10}(HNO_3)_T , \qquad (1)$$

where

pH_{app} = apparent electrometric pH,
$(HNO_3)_F$ = free nitric acid concentration in solution,
$(HNO_3)_T$ = total nitric acid concentration, free and adsorbed, in the sol.

Since urania and thoria are homologous compounds which should be roughly similar, aside from redox properties, Eq. (1) was applied to pH, conductivity, and chemical data for a variety of ASPU-8 urania sols[14] to get the results shown in Table 14.4.

Examination of analytical error limits led to the expectation of about ±0.01 error in the HNO_3/U mole ratio; thus only the smallest difference (sample E) is explainable as data scatter.

Table 14.4. Correlation of urania sol adsorption equilibrium for nitric acid by the ideal Donnan emf

Sample	pH_{app}	pH_{cond}[a]	Total nitrate/U (mole ratio)		
			Eq. (1)	Chem. analysis	Difference[b]
B	2.10	1.92	0.09	0.20	0.11
C	2.33	2.09	0.07	0.24	0.17
D	2.26	2.35	0.08	0.12	0.04
E	2.51	2.11	0.10	0.09	−0.01
F	2.28	2.09	0.07	0.11	0.04

[a]Conductivity of the sol assumed to be due to free nitric acid only.
[b]Kinetically unavailable nitrate.

11. K. H. McCorkle, *Surface Chemistry and Viscosity of Thoria Sols,* ORNL-TM-1536 (June 1966), pp. 23, 205, 215–16.

12. B. D. Chun, *Properties of Colloidal Thoria* (Part I. "Grain Growth of Thoria Gel"), Ph.D. thesis, Dept. of Metallurgy, Univ. of Utah (1964).

13. K. H. McCorkle, *Surface Chemistry and Viscosity of Thoria Sols,* ORNL-TM-1536, p. 208 (June 1966).

14. Made by solvent extraction at 0.2 *M* U, 87–91% U(VI), by Unit Operations Section.

Table 14.5. Correlation of bound nitrate with amorphous urania

Sample	Amorphous urania fraction[a] ±0.20	Kinetically unavailable nitrate[b]/U (mole ratio ±0.01)	Crystal size in crystalline fraction (Å ± 3)
B	0.78	0.11	34
C	0.78	0.17	34
D	0.62	0.04	40
E	0	−0.01	39
F	0.45	0.04	37

[a]Determined by x-ray diffraction line intensities.
[b]From Table 14.4.

Table 14.6. Effect of surface oxidation on settled bed density of precipitated urania particle beds

Sample	Density, expressed as moles of U per liter of settled bed[a]	
	Before air exposure	After air exposure
1	0.30	0.40
2	0.33	0.58
3	0.36	0.58
4	0.36	0.63
5	0.40	0.72

[a]U(VI) content before air exposure, 6–9%; after air exposure, 15–17%; determined by difference from U(IV) analyses, with probable errors of around ±1%.

The "Difference" column in Table 14.4 was found to correlate roughly with the amorphous urania fraction in the sol, as shown in Table 14.5. This correlation indicates that nitric acid associated with amorphous urania is kinetically unavailable to the diffusion processes involved in generating the Donnan-like emf correction for electrometric pH measurement and that the rapid-equilibration adsorption effects are dominated by the urania surface of the crystalline fraction. Making the approximation that all the rapidly equilibrating adsorption is dependent on the crystalline urania surface alone allows us to calculate the adsorption potential for nitric acid, by the methods used for thoria,[15] to be (−2.5 ± 0.5) kcal/mole HNO_3 with 12% of the metal-ion surface sites occupied by nitric acid. This compares with about −6.5 kcal/mole HNO_3 on thoria.

Part of the foregoing difference can be attributed to the presence of formic acid (formate/U mole ratio of 0.5) during the adsorption of nitrate on urania, so that the potential refers to a displacement reaction instead of to simple adsorption. Urania sols containing nitric acid alone cannot be made reproducibly because of the erratically uncontrollable redox reaction between U(IV) and nitric acid and concomitant particle agglomeration. Formic acid diminishes the extent and the irreproducibility of these effects; however, even in the presence of formic acid at a formate/U mole ratio of 0.5, colloidal urania is slowly oxidized by the nitric acid. The rate of self-oxidation of the urania sol undergoes a change in slope at 80 ± 2% U(IV), which corresponds to about half of the crystallographically calculated surface urania ions. This oxidation to the 80% U(IV) level is accompanied by a release of nitric acid to the solution, despite the consumption of nitrate in the oxidation process, because of the loss of area by the particle agglomeration accompanying oxidation. The effect of additional surface oxidation on the agglomeration of urania particles is illustrated in Table 14.6. The extreme sensitivity of the colloidal urania to oxidation, and of agglomeration state to surface oxidation, makes adsorption data having well-defined thermodynamic meaning difficult to obtain.

14.3 PREPARATION OF CARBIDES AND CARBONITRIDES

Single-Step Conversion-Sintering of Carbides and Carbonitrides[16]

In concert with the continuing and growing interest in advanced types of nuclear fuels, studies have been carried out on the preparation of carbides and carbonitrides. One of the objectives of the work was to prepare the monocarbide or the carbonitride of uranium, uranium-plutonium, or plutonium in a single conversion-sintering step.

A sol-gel process for preparing the carbides and carbonitrides from oxides was investigated on a laboratory scale. In the process, stable colloidal solutions of the metal oxides and carbon are prepared, the sols are converted to solid gel forms, and the solids are then converted to the desired product by a high-temperature conversion step. The general preparation scheme has been previously described.[17] Low-nitrate plutonia sols and CUSP-type urania sols[18] were used as starting

15. K. H. McCorkle, *op. cit.*, pp. 56–87.

16. Work done in cooperation with L. G. Farrar, Analytical Chemistry Division.

17. *Chem. Technol. Div. Annu. Progr. Rep. May 31, 1970*, ORNL-4572, pp. 246–50.

18. *Chem. Technol. Div. Annu. Progr. Rep. May 31, 1968*, ORNL-4272, pp. 158–60; *Chem. Technol. Div. Annu. Progr. Rep. May 31, 1969*, ORNL-4422, pp. 223–28.

materials, and MO_2 + C sols were prepared by ultrasonically dispersing carbon black in the oxide sols. Stable fluid sols were obtained (1–2 *M* in metal content) with sufficient carbon to produce the monocarbide, sesquicarbide, or dicarbide. Sols used for preparing carbonitrides contained a carbon content consistent with the quantity required for a single-phase product. Depending on the method of preparation (evaporation, vacuum freeze drying, or extraction with water-immiscible solvents), the gels retain some volatile materials that are readily removed by low-temperature treatment (<800°C). The conversion to carbide or carbonitride is performed in a subsequent heating step.

The laboratory results have demonstrated the technical feasibility of the sol-gel procedure. The process offers several advantages in making the products from oxide – principally, the homogeneity of the starting materials, the flexibility of the product forms (microspheres, shards, powders), and the ease of adaptation to remote operations. The homogeneity of the MO_2 + C sols arises from the fact that the primary particles are very small (<500 Å in diameter).[19] Although aggregates are undoubtedly formed, the association of the MO_2 and carbon particles is maintained at the above magnitude. Theoretically, the small size of the reactants should provide faster conversion rates than are obtainable with mechanically ground material. However, in preparing shards or microspheres, the full potential of the faster rates cannot be utilized without destroying the macro bodies or creating unacceptable porosity. The intimate mixture does make it possible to obtain a ceramic body by using a single high-temperature conversion-sintering step.

The most recent work has been focused on the conversion-sintering step, using microspheres as the gel form. Although the prefiring (low-temperature step) and the conversion step could be combined, all the work has been done in a two-step sequence to define better the variables in the second step. The only difficulty with this procedure is that in uranium-bearing materials the UO_2 is very susceptible to oxidation and must be protected from oxygen. The carbides are converted in an argon atmosphere and are generally heated in vacuum at the end of the conversion to aid in the removal of oxygen from the system. The procedure for preparing the carbonitrides is similar except that nitrogen is introduced during the carbothermic reduction of the oxide. Since the mixtures used for preparing carbonitrides contain less carbon than would be required for making the carbide, the nitration must be done simultaneously with the reduction to conserve the proper stoichiometry. The subsequent evacuation of the carbonitride at an elevated temperature also serves to decompose any higher nitrides that may have formed. The conversion-sintering process is carried out at 1400 to 1600°C for plutonium preparations and at 1400 to 1750°C for uranium-plutonium mixtures. The specific procedures minimize the physical loss of reactants and the preferential volatilization of plutonium and reduce the porosity of the product.

The conversion step has been examined by thermogravimetry and by metallography at different stages. The results have shown that porosity develops very early in the conversion and at lower temperatures than originally anticipated. Excessive porosity formed early in the reduction cannot be removed during a subsequent sintering step. Further, there is evidence that the effect of increasing the sintering temperature to the point of particle deformation merely generates larger voids from microvoids. It appears that the initial stages of the reduction step must be closely controlled to achieve high-density products. The procedure must balance a rapid heating rate to minimize the sintering of the oxide particles with a rate that would avoid generating porosity or cracking. The most recent efforts have been directed toward examining this area of the procedure. With plutonium, the heating rates become important at temperatures as low as 1000 to 1100°C. The reduction of PuO_2 occurs in two steps. In argon, the first step starts at 1000 to 1100°C, and the carbide is formed above 1400°C.

Using the sol-gel procedure, it has been possible to prepare the monocarbides and carbonitrides of plutonium and uranium-plutonium mixtures as well as plutonium sesquicarbide. The corresponding uranium compounds have also been prepared by this technique.[18] Although it is difficult to completely avoid small amounts of other phases in the monocarbides, it is possible to prepare monocarbide which, according to x-ray analysis, is apparently single phase. Most of the metallographic examinations have been done on microsphere products, and the results have indicated that high-density carbides and carbonitrides can be obtained. The products generally had some internal porosity, usually in the form of small voids or microporosity. The densities of these products, as measured by mercury porosimetry, ranged from 88 to 95% of theoretical (based on calculated density from lattice parameters). To date, the plutonium carbonitride preparations have not been as satisfactory as the other products.

19. Work done by T. B. Lindemer, Metals and Ceramics Division.

Table 14.7. Sol-gel carbide and carbonitride preparations

Material	C/M[a] prior to conversion	Mole ratio by chemical analysis of products[a]				X-ray analysis[b]
		C/M	N/M	O/M	(C + N + O)/M	
I (U,Pu) carbides	3.1	1.10		0.039	1.14	MC (M_2C_3)
	3.0	1.04		0.002	1.04	MC
	2.9	0.92		0.008	0.93	MC
	2.8	0.88		0.042	0.92	MC
	2.7	0.74		0.085	0.82	MC
II (U,Pu) carbonitrides	2.8	0.80	0.18	0.059	1.04	MCN (M_2C_3)
	2.7	0.60	0.41	0.010	1.02	MCN
	2.4	0.40	0.61	0.002	1.01	MCN
	2.3	0.36	0.43	0.084	0.87	MCN
III Pu carbides	3.5	1.48		0.03	1.51	Pu_2C_3 (PuC)
	3.1	1.04		0.12	1.16	PuC + Pu_2C_3
	3.0	1.03		0.09	1.12	PuC + Pu_2C_3
	2.9	0.86		0.10	0.96	PuC (Pu_2C_3)
	2.6	0.73		0.20	0.93	PuC
IV Pu carbonitrides	2.4	0.49	0.58	0.09	1.16	PuCN, Pu_2C_3
	2.3	0.40	0.58	0.09	1.07	PuCN, Pu_2C_3
	2.2	0.22	0.75	0.20	1.17	PuCN, Pu_2C_3

[a]M = U + Pu.
[b]Parentheses denote minor phase.

The oxygen contents of the final materials prepared by the sol-gel process varied with the particular product and with the conditions under which it was made. Slightly higher values were observed with the plutonium monocarbides than with the corresponding uranium-plutonium material. However, the values may reflect the higher reactivity of the plutonium material. With the uranium-plutonium carbonitrides, lower oxygen contents were found for products that had C/M ratios of 0.5 to 0.8. It is possible to prepare products from the MO_2 + C sols that contain less than 1000 ppm of oxygen (some products had oxygen contents as low as 100–200 ppm); all the products can be readily prepared with less than 4000 ppm of oxygen. Typical results for the different types of products are given in Table 14.7. Figure 14.7 indicates the general appearance of some uranium-plutonium (25% Pu) (*b*) monocarbide and (*c*) carbonitride microspheres as compared with (*a*) the prefired (MO_2 + C) microspheres. The sizes of the microspheres shown are not directly comparable, although a reduction in size does occur during the conversion-sintering step.

In the work to date, the best results have been obtained with the monocarbides of uranium-plutonium (15–25% Pu) and plutonium, plutonium sesquicarbide, and the carbonitrides of uranium-plutonium. When the C/M ratio in the starting material was less than 2.4, it was more difficult to prepare satisfactory products, probably because of the lower carbon activity available during the reduction step. In the uranium-plutonium system, satisfactory products were obtained when a sufficient amount of carbon was used to produce a product that had a C/M ratio of 0.4 to 0.8. With plutonium, it was necessary to use a lower carbon content in order to obtain a single-phase carbonitride. The plutonium carbonitride products were the most difficult to prepare, and the experiments have indicated that a longer time may be needed for the conversion and that it may be more difficult to reduce the oxygen content in the products. Some of the preparation problems encountered are common to the general preparative method (carbothermic reduction of oxides), while others are unique to the single conversion-sintering step. Additional studies are planned, on a limited laboratory basis, to optimize further the variables of the system.

Kinetics of the Syntheses of Carbides, Carbonitrides, and Hypostoichiometric Oxides in the U-Pu-O-C-N System [19]

The kinetics of the reactions for producing carbides, nitrides, and carbonitrides in the uranium-plutonium system by the carbothermic conversion of sol-gel

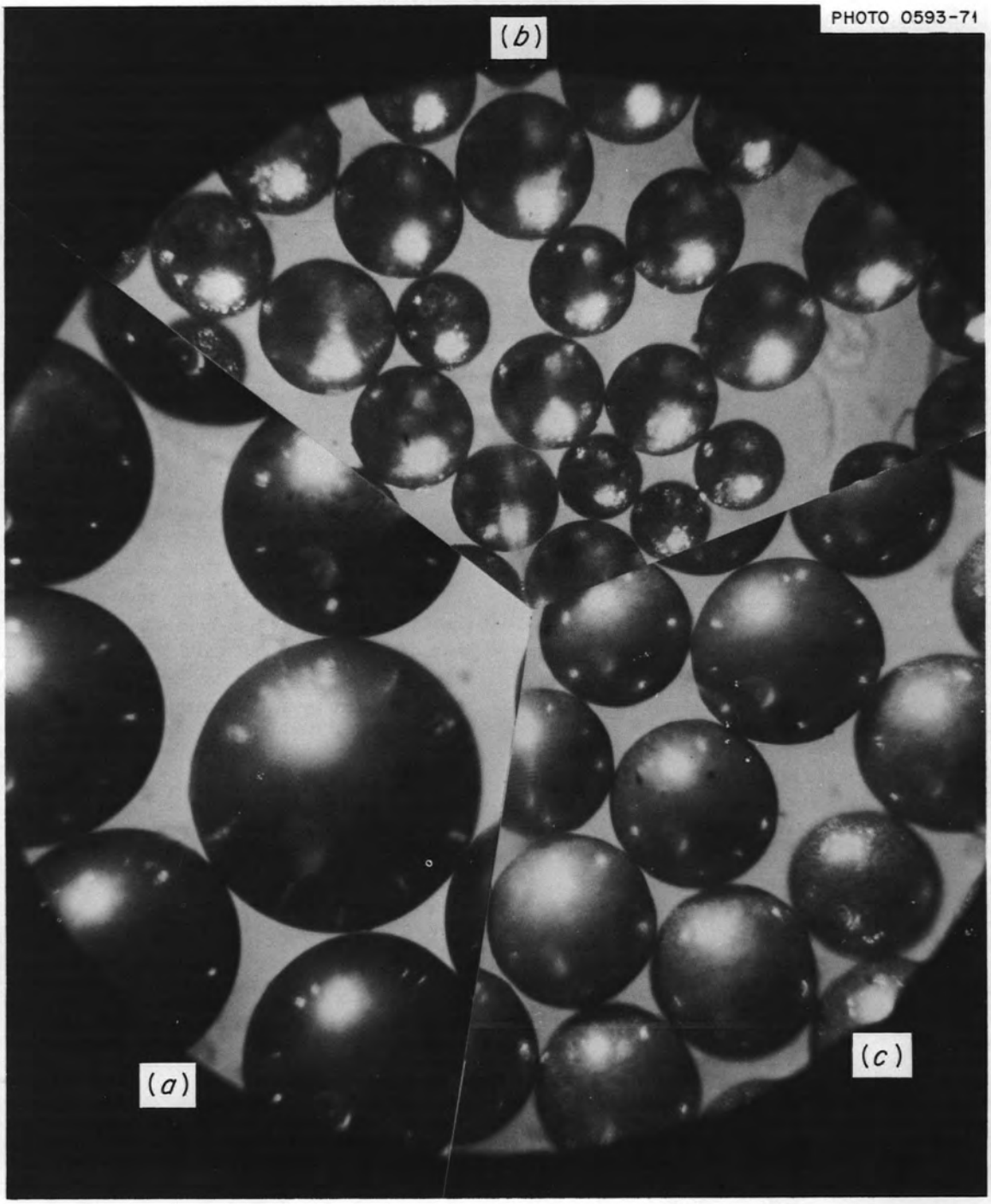

Fig. 14.7. Uranium-plutonium microspheres (25% Pu). (*a*) $(U,Pu)O_2$ + C, ~700 μ. (*b*) (U,Pu)C, ~300 μ. (*c*) (U,Pu)CN, ~450 μ.

oxide-carbon mixtures are being studied to ascertain the mechanisms controlling the conversion. This information is then applied to the design parameters of specific conversion equipment. Particular kinetics studies during this report period include those of UC with N_2,[20] UC_2 with N_2,[21] and UO_2 with C,[22] with the information being used to analyze the fluidized-bed conversion of oxide-carbon mixtures to fuel compounds in the U-Pu-C-N system.[23] The latter analysis was tested by converting 250 g of sol-gel $(U_{0.8}Pu_{0.2})O_2$-C shards to (U,Pu) (C,N) in a fluidized-bed reactor. These shards were pressed and sintered into 89%-dense, 0.63-cm-OD by 0.535-cm-long pellets that contained no second-phase compounds.[24]

A current kinetics study involves the simultaneous reaction of UO_2, C, and N_2 to produce U(C,N). This is being accomplished with oxide pellets so that quantitative weight change and metallographic techniques can be used to follow the progress of the reaction. At 1700°C, and with P_{CO} = 10 torrs and P_{N_2} = 380 torrs, the conversion is accomplished via two successive chemical reactions:

$$UO_2 + 0.78C + 0.27N_2 \rightarrow UO_{1.22}N_{0.54} + 0.78CO$$

and

$$UO_{1.22}N_{0.54} + 1.68C \rightarrow UC_{0.46}N_{0.54} + 1.22CO\,,$$

in which the $UO_{1.22}N_{0.54}$ is a composition in a solid-solution field that includes UO_2.[25,26] This sequence of reactions in the synthesis of U(C,N) has apparently never been reported in the literature. It is significant to note that UO_2 is converted to $UO_{1.22}N_{0.54}$ by the approximate replacement of each three atoms of oxygen by two of nitrogen and that the nitrogen present in the final U(C,N) appears to be incorporated in the system by the initial reaction.

A kinetics and thermodynamics analysis has been performed for the synthesis of $(U,Pu)O_{2-x}$ from $(U,Pu)O_2$.[27] The hypostoichiometric oxide enhances the compatibility of oxide fuel with cladding during burnup, but occurs at such low oxygen potentials that its synthesis often requires extremely long production times and high temperatures. The interrelations among the process variables for hydrogen reduction have been derived and shown to be consistent with experimental results; this permits, for the first time, an accurate prediction of the oxygen-to-metal ratio resulting from a given production process. Additionally, the parameters were developed and tested for reduction of oxide via the C-CO-CO_2 system; this technique reduces the processing time by at least an order of magnitude over that available in the hydrogen-reduction system.

20. J. M. Leitnaker, T. B. Lindemer, and C. M. Fitzpatrick, "Reaction of UC_2 with Nitrogen from 1475°C to 1700°C, *J. Amer. Ceram. Soc.* 53, 479–81 (1970).

21. T. B. Lindemer, J. M. Leitnaker, and M. D. Allen, "Kinetics of the Reaction of UC_2 and Nitrogen from 1500°C to 1700°C," *J. Amer. Ceram. Soc.* 53, 451–56 (1970).

22. T. B. Lindemer, M. D. Allen, and J. M. Leitnaker, "Reply to Discussion by Y. K. Rao," *J. Amer. Ceram. Soc.* 53, 581 (1970).

23. T. B. Lindemer, "Rate Controlling Factors in the Carbothermic Synthesis of Advanced Fuels," *Nucl. Appl. Technol.* 9, 711–15 (1970).

24. T. B. Lindemer, *LMFBR Fuel Cycle Studies Progress Report for October 1970, No. 20,* ORNL-TM-3217, pp. 43–46 (November 1970).

25. J. M. Martin, "Les Diagrammes de Phases U-UN-UO_2 et UO_2-UN-N_2," *J. Nucl. Mater.* 34, 81–85 (1970).

26. R. Benz, G. Balog, and B. H. Baca, "U-UO_2-UN_2 Phase Diagram," *High Temp. Sci.* 2, 221–51 (1970).

27. T. B. Lindemer and R. H. Bradley, "Kinetic Analysis of the Synthesis of $(U,Pu)O_{2-x}$ from Stoichiometric Oxide," presented at the annual meeting of the American Ceramic Society, Chicago, Apr. 26–28, 1971.

15. Chemical Engineering Research

The Chemical Engineering Research Program consists of several studies which are generally pertinent to the applied programs of the Chemical Technology Division; however, the studies are carried out in a more fundamental manner than that usually employed in applied programs. The areas of study may arise from needs for fundamental information in existing applied programs or from new ideas, which frequently mature into applied programs.

Much of the work performed under the Program can be more conveniently reported as part of the applied programs with which they are associated. In this section we are reporting only those studies not closely associated with the Molten-Salt Reactor (MSR) Program. Three particular studies that are carried out in support of the MSR program are summarized in this section; these studies are described in detail in Sect. 1.

We are also reporting a study made during an assignment to the Swiss Federal Institute for Reactor Research (EIR), Würenlingen, Switzerland.

15.1 MASS TRANSFER OF WATER FROM SOL DROPLETS

During the preparation of sol-gel microspheres, sol droplets must be suspended or fluidized in an organic phase until enough water is extracted from the aqueous sol to cause gelation. Mass transfer data have been obtained for single water and sol droplets fluidized in 2-ethyl-1-hexanol (2EH) at temperatures of 25, 40, and 50°C and in 2-methylpentanol and *n*-hexanol at 25°C. The Schmidt numbers for the three alcohol systems ranged between 5000 and 36,000, and the sphere Reynolds numbers varied from 0.2 to 30. A surface-active agent, Ethomeen S/15, was added to the organic phase to produce a "rigid" liquid drop with no induced circulation.

The controlling mass transfer resistance for a thoria sol drop fluidized at 25°C in 2EH is located in the organic-phase film surrounding the drop.[1] Thus, at identical hydrodynamic conditions, the mass transfer rates with either water or sol drops will be the same. The amount of solvent that transfers into the aqueous drop is negligible; therefore the change in the diameter of the drop is a direct measure of the amount of water that transfers into the organic phase. The mass flux can be related to the measured change in the diameter of the drop with time, as follows:

$$N = \frac{-\rho_w}{\pi D_p^{\,2}} \left(\frac{\pi}{6}\right) \frac{d(D_p^{\,3})}{d\theta} = \frac{-\rho_w}{2} \frac{dD_p}{d\theta} = K(C_s - C_0)\,, \qquad (1)$$

where

N = mass flux of water from the drop, g cm^{-2} sec^{-1},

ρ_w = density of water, g/cc,

D_p = diameter of drop, cm,

θ = time, sec,

K = mass transfer coefficient, cm/sec,

C_s = concentration of water in solvent at the interface of the drop, g/cc,

C_0 = concentration of water in bulk solvent, g/cc.

Equation (1) states that the mass transfer resistance within a thoria sol drop will be negligible during gelation; that is, water can be supplied to the interface fast enough to maintain C_s saturation.

The most commonly used mass transfer correlation for spheres in a flowing system expresses the Sherwood number, N_{Sh}, as a function of the product of the Schmidt number, N_{Sc}, to the $1/3$ power and the Reynolds number, N_{Re}, to the $1/2$ power. There is good evidence to believe that the exponent of the Reynolds number varies with Reynolds number, increasing from $1/3$ in the Stokes' law region to $2/3$ in the fully turbulent

1. S. D. Clinton, *Mass Transfer of Water from Single Thoria Sol Droplets Fluidized in 2-Ethyl-1-hexanol*, M.S. thesis, University of Tennessee, Knoxville; also published as ORNL-TM-2163 (June 1968).

region. For this reason, the mass transfer data were correlated on a log-log graph in which the Sherwood number divided by the Schmidt number to the ⅓ power was plotted against the sphere Reynolds number. The Reynolds number is based on the diameter of the drop and the fluidizing velocity of the organic phase. Runs with single water drops contributed 1785 data points, with the Reynolds number ranging from 0.2 to 30. The data are represented by the following equation:

$$N_{Sh} = 1.0 N_{Re}^{0.417} N_{Sc}^{0.333} . \tag{2}$$

Data from the thoria sol drop runs can also be correlated by Eq. (2) with a maximum deviation of ±10%. The use of a single correlation for both water and sol droplet data confirms that, until gelation occurs, the controlling mass transfer resistance is in the organic-phase film surrounding the sol drop.

An explicit relationship for the mass transfer coefficient can be derived by making use of experimental drag coefficient data in Eq. (2). The following equation defines the drag coefficient for flow around a sphere:

$$F = f_D \left(\frac{\rho_s U^2}{2g_c}\right)\left(\frac{\pi}{4} D_p^2\right) , \tag{3}$$

where

F = force exerted by the fluid on the sphere, dynes,

f_D = sphere drag coefficient,

ρ_s = density of continuous phase, g/cc,

U = fluidizing velocity, cm/sec,

g_c = dimensional constant, 1 g-cm dyne^{-1} sec^{-2}.

In Eq. (3) the first term in parentheses is the fluid kinetic energy per unit volume, and the second term in parentheses is the projected area of the sphere. The drag coefficient for the sphere was found experimentally to be a function of only the Reynolds number,

$$f_D = 33.7 N_{Re}^{-0.749} = 33.7 \left(\frac{D_p \rho_s U}{\mu}\right)^{-0.749} , \tag{4}$$

where μ is viscosity of continuous phase, g cm^{-1} sec^{-1}.

The following expression for the fluidizing velocity is derived from Eq. (3) when F is equal to the buoyant weight of the aqueous drop in the alcohol:

$$U = \left[\frac{4gD_p}{3\rho_s f_D}(\rho_p - \rho_s)\right]^{0.50} , \tag{5}$$

where g is acceleration of gravity, cm/sec^2, and ρ_p is density of sol drop, g/cc. Substituting Eq. (4) into Eq. (5) for the drag coefficient, an explicit relationship can be obtained for the fluidizing velocity which can then be used in Eq. (2) to evaluate the mass transfer coefficient. After elimination of the fluidizing velocity, Eq. (2) reduces to the following explicit relationship for the mass transfer coefficient:

$$K = 3.4 \frac{D_v^{2/3}}{\mu^{1/3}} (\rho_p - \rho_s)^{1/3} , \tag{6}$$

where D_v is diffusion coefficient, cm^2/sec.

With Eq. (6), an expression can be derived to predict the time required for the gelation of a fluidized sol drop. The difference between sol drop and solvent densities and the drop diameter can be related to the sol molarity by the following expressions:

$$\rho_p - \rho_s = 0.238 M_p + 0.175 ;$$

$$D_p = \left(\frac{M_c}{M_p}\right)^{1/3} D_c , \tag{7}$$

where

M_p = molarity of the thoria sol, moles/liter,

M_c = molarity of theoretically dense thoria, moles/liter,

D_c = diameter of theoretically dense thoria, cm.

Using Eqs. (6) and (7), Eq. (1) can be integrated to give the following relationship for the time required for gelation of a sol drop:

$$\theta_G = 2.7 \times 10^{-3} \frac{\mu^{1/3} D_c}{D_v^{2/3} (C_s - C_0)} \times \int_{M_I}^{M_G} \frac{dM_p}{M_p^{4/3} (0.238 M_p + 0.175)^{1/3}} , \tag{8}$$

where

θ_G = time required to gel fluidized sol drop, min,

M_I = initial molarity of thoria sol drop, moles/liter,

M_G = molarity of the gelled sphere, moles/liter.

The integral in Eq. (8) has been evaluated for molarity increments of 0.01, and values of the integral are tabulated (see Table 15.1) as a function of the sol

Table 15.1. Values of the sol molarity integral function

To find the value of the integral for a sol of initial molarity M_I which sets to a gel at a molarity of M_G, subtract the tabulated value at $X = M_G$ from that at $X = M_I$

X (moles/liter)	$\int_X^{20} \frac{dM_p}{M_p^{4/3}(0.238M_p + 0.175)^{1/3}}$
0.2	5.17
0.4	3.47
0.6	2.69
0.8	2.23
1.0	1.91
1.2	1.68
1.4	1.50
1.6	1.35
1.8	1.23
2.0	1.13
2.2	1.05
2.4	0.974
2.6	0.910
2.8	0.853
3.0	0.802
3.5	0.696
4.0	0.612
4.5	0.543
5.0	0.486
5.5	0.437
6.0	0.395
7.0	0.326
8.0	0.271
9.0	0.227
10.0	0.190
12.0	0.131
14.0	0.087
16.0	0.052
18.0	0.024
20.0	0.000

molarity. Gelation times have been calculated with Eq. (8) and compared with the experimentally determined gelation times of fluidized thoria sol drops (see Fig. 15.1). The calculated gelation times are plotted on the abscissa, and the experimental gelation times are shown on the ordinate. The variation between the calculated and experimental gelation times is less than ±10%.

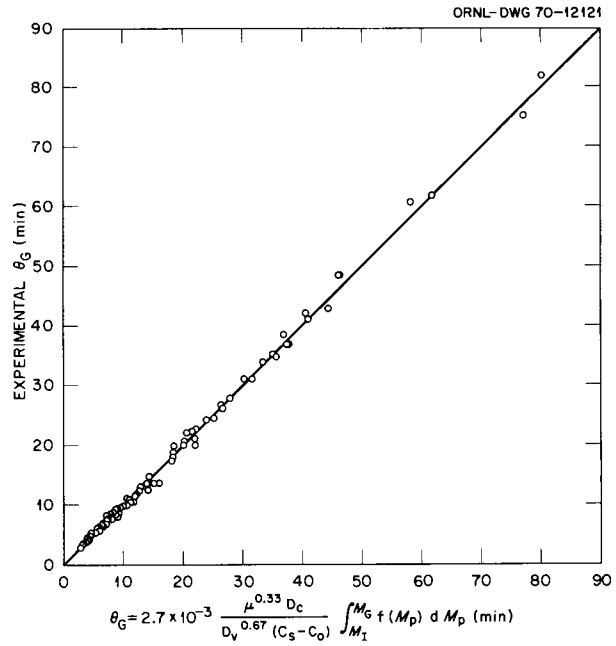

Fig. 15.1. Experimental gelation time vs calculated gelation time.

15.2 DEHYDRATION OF INDIVIDUAL SOL DROPLETS IN A MINICOLUMN[2]

A miniature tapered column (similar to a rotameter) has been used by Clinton to measure dehydration rates of individual sol droplets[1] (see also Sect. 15.1 of this report). A similar experimental approach was used to obtain qualitative data related to droplet deformation during the dehydration-gelation process. This work was performed by a Chemical Technology Division staff member at EIR under a cooperative agreement between EIR and ORNL; it has been reported in summary form (in German) in the EIR Plutonium Project Annual Report[3] and will be reported in detail in an EIR topical report[4] (in English). Highlights of the work are described below. Most of the work was done with UO_2-C sols in 2EH. The column, which was made of Plexiglas, had an overall height of 8 in. and a minimum diameter of $\frac{1}{8}$ in.

Microsphere deformation is a problem that is frequently encountered in the sol-gel process. Deformation has previously been studied, primarily by using a stepwise technique in which microspheres are formed under given conditions and then examined after gelation is complete. Such an approach provides very little information about the mechanics of deformation. The minicolumn, on the other hand, is ideally suited to this type of study since a single droplet can be observed

2. This work was done at the Swiss Federal Institute for Reactor Research (EIR), Würenlingen, Switzerland, while a staff member of the Chemical Technology Division was on assignment to the EIR Plutonium Project under a cooperative agreement between EIR and ORNL.

3. *Plutonium-Brennstoffprogramm Jahresbericht 1970,* EIR-Bericht Nr. 192 (in press).

4. K. J. Notz and K. J. Bischoff, *Dehydration of Individual Sol Droplets in a Minicolumn,* EIR Bericht No. 193 (in preparation).

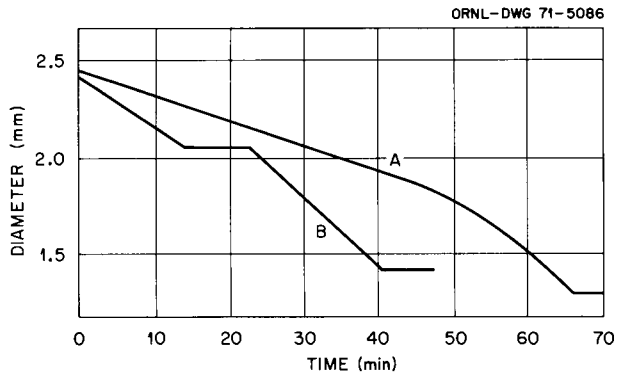

Fig. 15.2. Typical dehydration curves. *A*, for a droplet that remains spherical, *B*, for a droplet that develops a pit. Redrawn from EIR drawing.

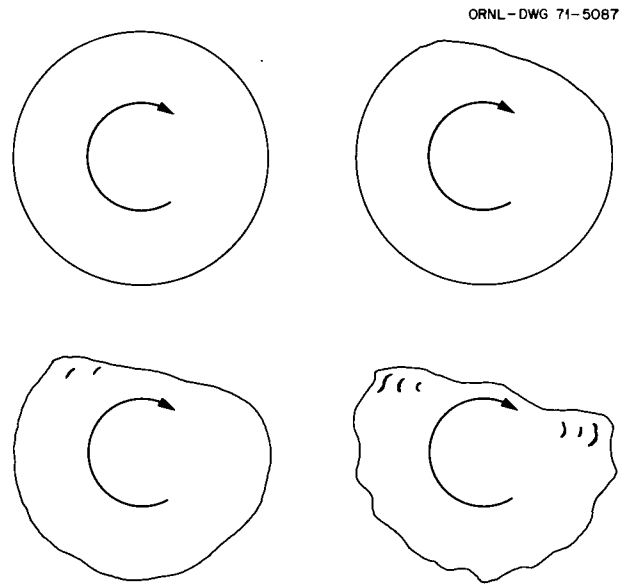

Fig. 15.3. Skin formation in a rotating droplet of sol showing the raisining type of deformation. Redrawn from EIR drawing.

continuously throughout its entire dehydration cycle.

Two general types of dehydration rate curves were obtained (Fig. 15.2). The smooth curve is typical of nondeforming droplets in the presence of a surfactant (which halts internal circulation, giving a stagnant droplet). This type of curve shows a linear shrinkage rate initially, with an increasing rate as the density of the sol increases, requiring an ever-increasing fluidizing velocity. This type of dehydration curve has been characterized by Clinton.[1] The other curve exhibits a "stepped" shrinkage rate which is typical of droplets that acquire a flat spot, which may later develop into a pit. During the time the pit is enlarging, the horizontal diameter of the droplet remains constant or nearly constant. The pit always appears at the top of the droplet for hydrodynamic reasons; a surfactant concentration gradient may also contribute to the orientation. During the time that the horizontal diameter remains constant, the settling velocity also remains constant.

Although sphere deformation takes many forms, there is a real basis for classifying these forms into two groups based on the present work: "cherry pitting" and "raisining." These terms describe the physical appearance of the two types of products as they leave a production-scale column. In the minicolumn, which normally causes the droplet to maintain a fixed orientation, raisining also appears as a single pit; in this case, the droplet has been reduced to a pitted hemisphere.

The difference between droplets exhibiting the cherry pit defect and those exhibiting the raisin type of deformation is further demonstrated by their response to rotation during dehydration. Rotation is easily accomplished by tilting the column slightly, causing the droplet to be displaced from the center of the axially symmetrical flow pattern. With rotation, droplets with the cherry pit deformation remained spherical, showing that any skin which might be present must be elastic. Droplets of the raisin type, however, clearly showed the presence of a flexible but nonelastic skin; while the volume of the droplet decreased due to extraction of water, the surface area remained constant, causing deformation at the top surface (Fig. 15.3). With continued water extraction, the deformed area became greater until it was finally fixed in position. With nondeforming droplets, high rotation rates (ca. 30 rpm) resulted in slower water extraction.

Settling velocities were calculated using the drag coefficient relationship[5] and were compared with experimental values. Although the data are well out of the Stokes' law region, they are in reasonable agreement with the calculated values (based on the appropriate Reynolds number) after a correction is made for the so-called wall effect.

The formation of a surfactant cap has been postulated on the basis of indirect evidence.[6] We have now actually seen such a cap form and grow (Fig. 15.4). Surfactant, an impurity in the solvent in this case, is carried to the droplet by the fluidizing solvent and is swept to the downstream side by viscous drag. Coverage of the upper hemisphere is rapid, but the lower half

5. J. H. Perry (ed.), *Chemical Engineer's Handbook*, 4th ed., pp. 5–59 to 5-62, McGraw-Hill, New York, 1963.

6. A. Frumkin and V. Levich, *Zh. Fiz. Khim.* **21**, 1183 (1947).

PHOTO 0900-71

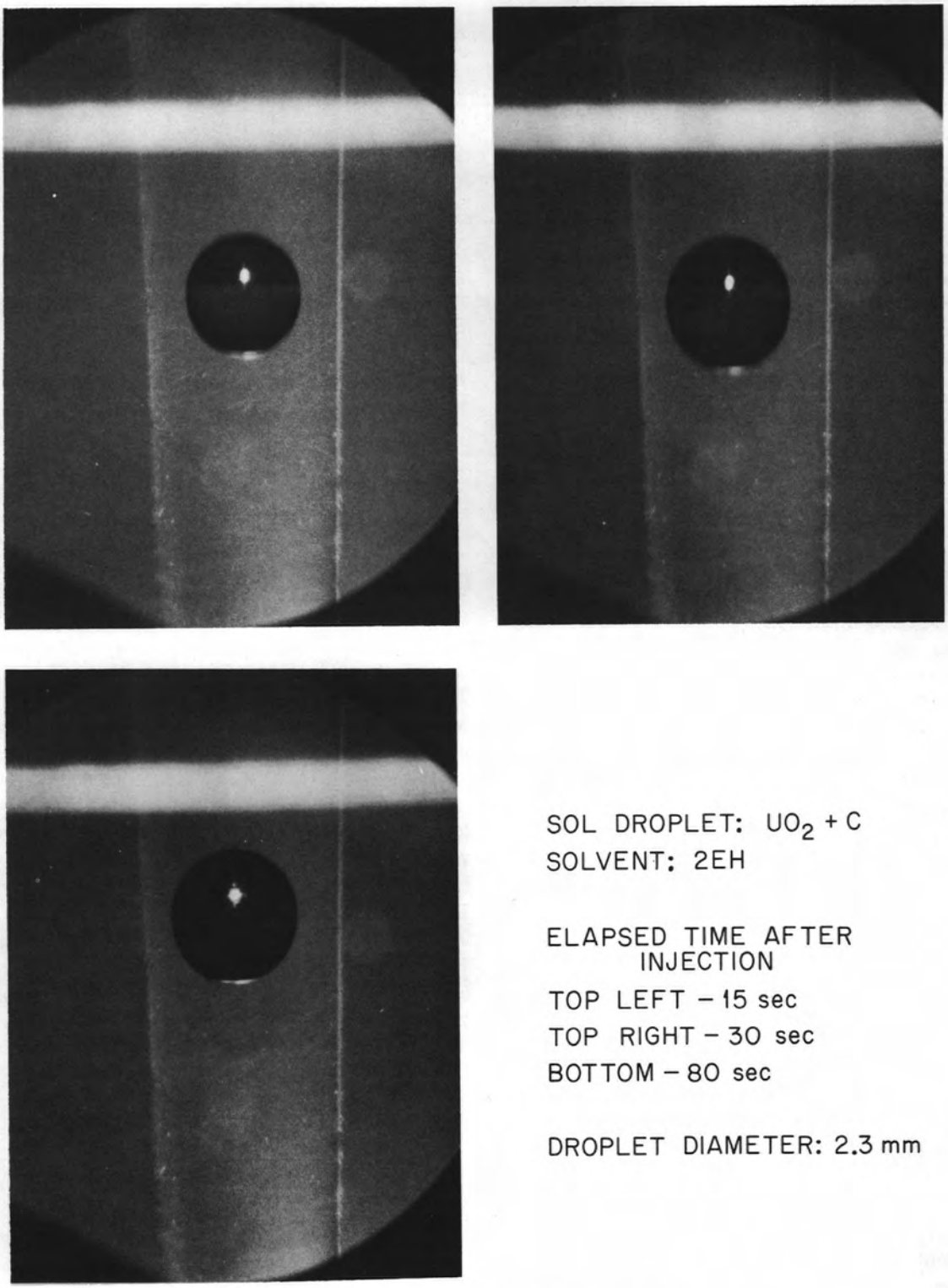

Fig. 15.4. Formation of surfactant cap. EIR photo.

ORNL-DWG 71-5088

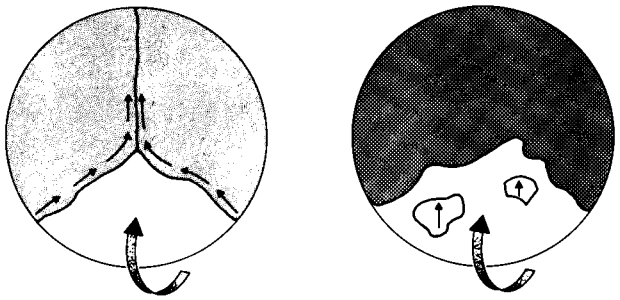

Fig. 15.5. Surface flow on a rotating sphere with partial surfactant coverage. Left, divergent-convergent type of flow. Right, floc type of flow. Arrows indicate direction of rotation. Redrawn from EIR drawing.

ORNL-DWG 71-5089

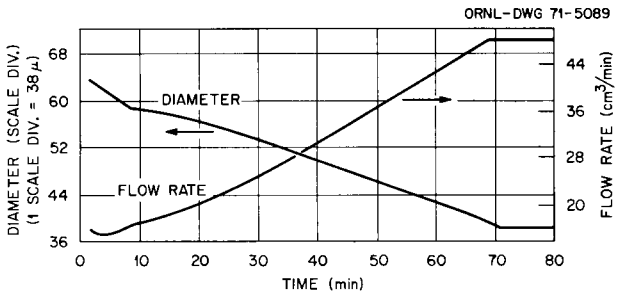

Fig. 15.6. Parameters for a spherical droplet with a surfactant cap. Sol: UO_2-C (C/U atom ratio of 3); solvent: 2EH + 1% H_2O + 0.01 *N* HNO_3; column diameter: ca. 4 mm at sphere location. Redrawn from EIR drawing.

tends to resist coverage because of the greater drag there. The droplet orientation remains fixed during coverage of the top half but becomes unstable thereafter, as shown in Fig. 15.4. If droplet rotation is induced, the surfactant layer can flow by either of two modes, as shown in Fig. 15.5. During the time the surfactant cap is growing, the settling rate goes through a minimum, as reflected by the flow rate required to maintain the droplet at a fixed altitude (Fig. 15.6). This is a consequence of the transition from an internally circulating to a stagnant (or "rigid") droplet, which causes an increase in the net surface velocity difference between solvent and droplet. When the surface coverage is complete, the rate of extraction decreases rapidly; this result is also due to the stagnant condition of the droplet.

Internal circulation patterns were observed in a translucent ZrO_2 sol containing a small amount of aluminum powder. Although a surfactant cap could not be seen, its presence was inferred by the gradual lowering of the circulation loop (Fig. 15.7). As the circulation path dropped lower, aluminum powder

ORNL-DWG 71-5090

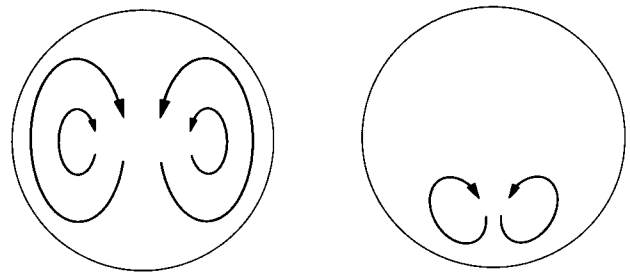

Fig. 15.7. Internal flow in a circulating droplet. Left, initial droplet; right, half covered with a surfactant cap. Redrawn from EIR drawing.

accumulated on the stagnant surface, shown at the halfway point in Fig. 15.8.

15.3 PRODUCTION OF SOL-GEL MICROSPHERES OF SMALL UNIFORM SIZE

Preliminary experiments have been made using ultrasonic vibrations to prepare small, uniform sol-gel spheres. Water was injected into 2-ethylhexanol through a hypodermic needle vibrated at various frequencies between 18 and 25 kHz by a Mullard ultrasonic drill. The experiments performed to date were rapid and only semiquantitative, but the water was shown to break up into drops of approximately the expected size (as calculated from the vibration frequency and the water flow rate). The droplets were much smaller than those formed without the vibration. Both axial and sidewise vibration of the needles have been tested; as expected, smaller droplets were formed with sidewise vibration. The droplets formed in these initial experiments are still larger than the 25- to 80-μ size that is our eventual goal. To reach these smaller drop sizes, it will be necessary to use higher-frequency disturbances (from either ultrasound or possible electrical stimulation) or to reduce the flow rate (capacity) through the nozzle.

15.4 PULSED CLONE CONTACTOR

A novel compact liquid-liquid contactor suitable for use in a glove box has been designed and briefly tested. The device consists of a cascade of hydroclones arranged so that the overflow part of the *N*th hydroclone is the underflow part of the (*N* + 1)th hydroclone. Spin is imparted to the clones intermittently by reciprocating pistons (one per clone) that alternately inject and remove fluid from the tangential port of each clone. Adjacent clones are 180° out of phase; fluid is

PHOTO 0901-71

DROPLET: ZrO_2 SOL
SOLVENT: 2EH
ADDED MATERIAL: ALUMINUM POWDER
TIME AFTER INJECTION: 1 min
DROPLET DIAMETER: 2.7 mm

Fig. 15.8. Preferred orientation of surface material. EIR photo.

injected into the Nth clone while fluid is removed from the $(N+1)$th and $(N-1)$th clones.

During operation with Amsco–15% TBP and uranyl nitrate, the unit had a satisfactory throughput capacity and satisfactory stage efficiencies. No further development of this unit is planned until a more immediate application is apparent.

15.5 AXIAL DISPERSION IN PACKED COLUMNS FOR CONTACTING LIQUIDS WITH A HIGH DENSITY DIFFERENCE

Packed columns operating with high-density fluids such as liquid metals and molten salts are important in the continuous processing of the fuel from molten-salt breeder reactors. A fundamental study of the flow of high-density fluids in packed columns was carried out since early studies showed that existing correlations for many properties of countercurrent flow in packed columns were either not reliable or incorrect when high-density liquids were used. These studies have included measurements of flooding, mass transfer, holdup, pressure drop, and axial dispersion in towers packed with Raschig rings and solid cylindrical packing. This work was supported largely by Chemical Engineering Research funds. Data on axial dispersion in packed columns are reported in detail in this section. Other work related to molten-salt reactor processing is summarized in Sect. 15.7 and is covered in detail in Sect. 1.

Measurement of Axial Dispersion in Packed Columns

We have continued to measure axial dispersion coefficients in packed columns during the countercurrent flow of mercury and water. The steady-state experimental technique used in this study was described

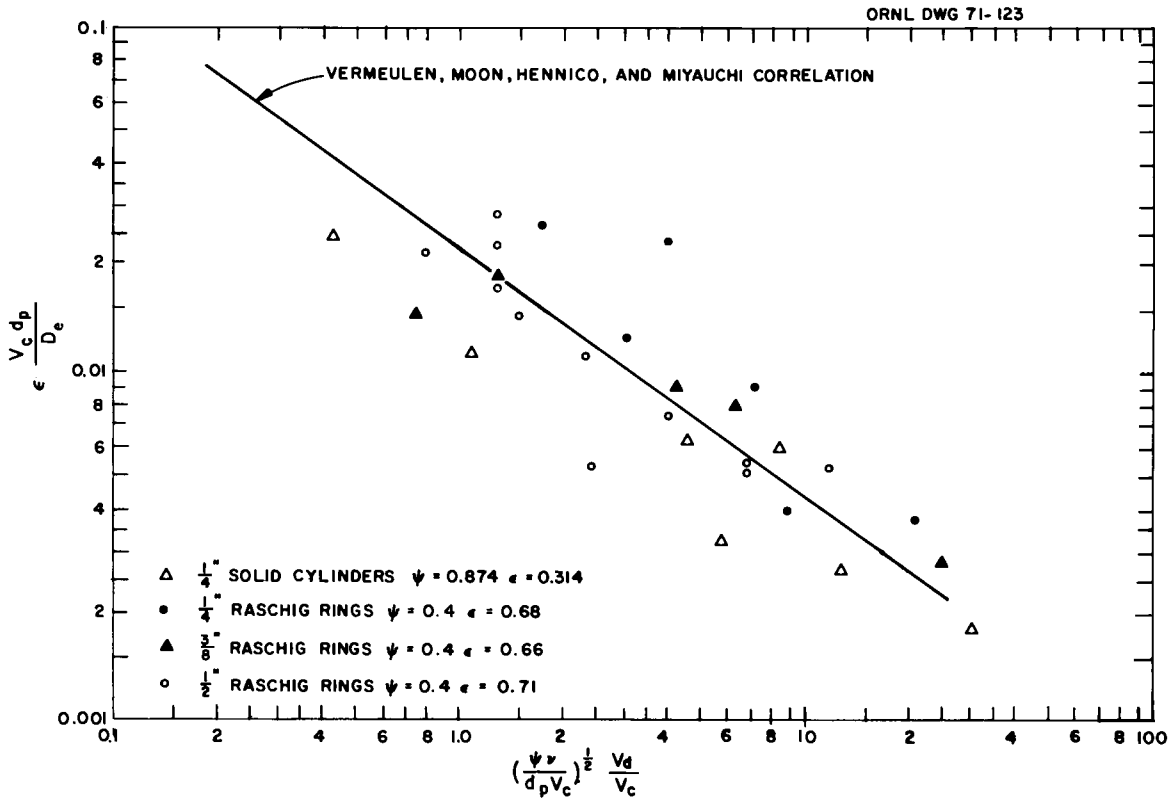

Fig. 15.9. Comparison of mercury-water data obtained in this study with the Vermeulen, Moon, Hennico, and Miyauchi correlation.

previously.[7] A tracer solution (dilute cupric nitrate) was pumped continuously into the top of a 2-in.-diam, 4-ft-long column. The steady-state tracer concentration in the continuous (aqueous) phase was then measured photometrically at several points down the column, that is, upstream. A plot of the logarithm of the tracer concentration vs distance down the column results in a straight line with a slope of $-V/D_e$, where V is the superficial continuous-phase (aqueous) rate and D_e is the dispersion coefficient.

Four different packing materials – 1/4-, 3/8-, and 1/2-in. Raschig rings and 1/4-in. solid cylindrical packing – were studied in a total of 37 runs. All of the packing was made of polyethylene, which is not wet by either phase.

The results are summarized in Fig. 15.9. The ranges of superficial mercury and water rates covered were 20 to 80 and 2.5 to 15 ft/hr respectively. The results are compared with a correlation proposed by Vermeulen et al.[8] Their correlation is based upon studies made with a variety of packing materials and several fluids having a range of physical properties. However, the authors pointed out that the fluids used in their study did not have a sufficiently wide range of differences in fluid densities to permit evaluation of the effect of fluid density.

In Fig. 15.9, the dimensionless quantity $\epsilon V_c d_p/D_e$ is plotted against the dimensionless quantity

$$(\psi V/d_p V_c)^{1/2} (V_d/V_c),$$

where

V_c, V_d = superficial velocities of continuous and dispersed phases,

d_p = packing diameter,

ϵ = packing void fraction,

V = kinematic viscosity of the continuous phase,

ψ = sphericity of the packing.

The agreement of the correlation with the recent experimental data is good. The scatter of the present data on this plot is not significantly greater than that of the original data. Axial dispersion, unlike flooding and holdup, can be described in both high- and low-density systems by a single correlation.

7. *Chem. Technol. Div. Annu. Progr. Rep. May 31, 1970*, ORNL-4572, p. 253.

8. T. Vermeulen et al., *Chem. Eng. Progr.* **62**, 95 (1966).

Reduction of Axial Dispersion in Packed Columns

We have continued studying column modifications that will reduce the effect of axial dispersion. In the last annual report, we described a device[9] that would reduce axial mixing to essentially any desired level by choosing the proper conditions. In the device, the dispersed phase flowed down through an annular region that functioned as an inverted bubble cap. This formed a seal that forced the continuous phase upward through a sieve plate. The axial dispersion was defined or described by the fraction of continuous phase flowing upward through the device which was recycled by back-mixing through the device. This "fraction back-mixing" was measured experimentally in a mercury-water column and was found to depend on the sieve opening size and on the water flow rate per opening. The only limitation of these devices was their limited capacity for handling dispersed phase. That is, when the mercury rate was increased, the columns flooded at relatively low rates as compared with a packed column that did not contain such devices.

A modified back-mixing preventer, which permits much higher metal rates, was tested during this report period. The modified device is illustrated in Fig. 15.10. The continuous-phase sieve openings are replaced with a vertical tube, which can be of any appropriate length. This releases the continuous phase at a position well above the metal-filled bubble cap. Flooding occurs when there is not sufficient driving force to provide the desired metal flow through the bubble cap without blocking the continuous-phase flow path. The modified design permits the metal level to rise to the bottom of the continuous-phase exit near the top of the vertical tube. In principle, this will allow enough pressure to force metal through the bubble cap seal at any desired rate. Thus an unproductive portion of the column (there is no useful two-phase contact between the preventer and the top of the continuous-phase outlet tube) is sacrificed in order to obtain increased metal capacity.

The device performed essentially as expected. Superficial metal rates up to 150 ft/hr were tested in a 2-in.-diam column; this approached the maximum rate obtainable in a packed column without preventers. Although the major effect of the modification was to increase the capacity of the column, there was a significant increase in back-mixing. However, this increase was tolerable and could be reduced by modifying the continuous-phase opening at the top of the vertical tube.

ORNL-DWG-70-8994

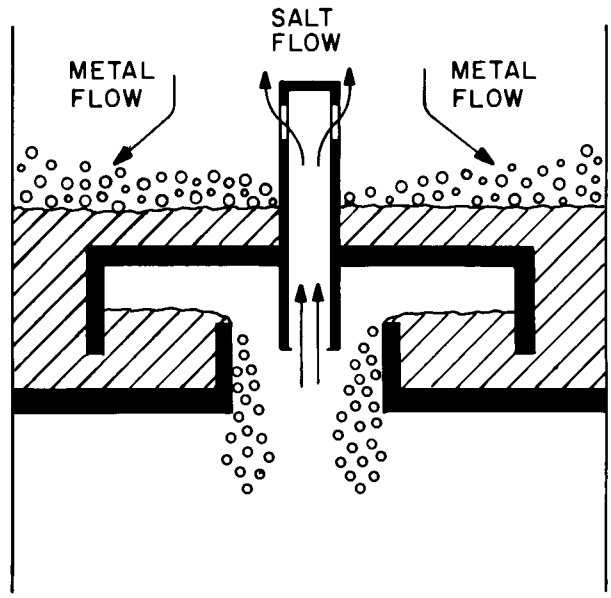

Fig. 15.10. Schematic diagram of an axial mixing preventer.

15.6 MULTICOMPONENT MASS TRANSFER IN ELECTROLYTE SYSTEMS

Calculations and correlations for mass transfer rates between two fluid phases are traditionally made in terms of fictive stagnant films on both sides of the interface. The diffusion coefficients and film thickness are "lumped together" into a mass transfer coefficient. There are two principal limitations to these techniques in several applications in the nuclear industry.

First, many applications involve the transfer of more than one component. When this occurs, there is usually no simple analytical (algebraic) expression that can be used to treat such columns, and investigations frequently resort to an analogous model which compares the system to a staged column. The staged model is not applicable over wide ranges of flow rates or compositions.

Second, many applications involve the transfer of materials that are ionic and possess electric charges in one of the phases, for example, an aqueous solution or molten salts. These applications will always be exchange processes unless a net flow of electric current is allowed. The transfer of ions is influenced by electric

9. *Chem. Technol. Div. Annu. Progr. Rep. May 31, 1970,* ORNL-4572, p. 254.

fields as well as by concentration gradients, and these fields may be generated by the difference in mobilities or the difference in valence of the diffusing ions. Solvent extraction by the so-called "liquid ion exchange" solvents and reductive extraction are two examples of situations in which ions are transferred.

A mathematical technique has been developed for treating such systems. It involves use of the Nernst-Planck equation to describe diffusion in the electrolyte phase, where the transferring components exist as charged ions. This equation is as follows:

$$J_i = D_i \left[\nabla C_i + \left(\frac{F}{RT} \right) C_i Z_i \nabla \phi \right],$$

where

J_i = the flux of component i,

D_i = diffusion coefficient of i,

C_i = local concentration of i,

F/RT = constant (Faraday constant divided by the gas constant and the absolute temperature),

Z_i = valence of i,

ϕ = electric potential.

The equilibrium at the interface is described by the relation:

$$\left(\frac{C_i \text{ solvent}}{C_i \text{ electrolyte}} \right) \left(\frac{C_j \text{ electrolyte}}{C_j \text{ solvent}} \right) \frac{Z_i}{Z_j} = \text{constant}.$$

In principle, any equilibrium expression could be used, but this equation is appropriate for many or most exchange processes of interest.

When the exchange involves more than two ions, the calculations involve a trial-and-error calculation of the flux of each component at various increments up the column, followed by a trial-and-error fit of the inlet conditions at the ends of the column. Yet, the computation times are reasonable for essentially all conditions of interest.

The importance of electric fields depends upon the valence of each ion involved, the difference in the diffusivities of the ions, the equilibrium constant, the relative total concentration in the two phases, and the presence of nontransferring ions in the electrolyte.

The importance of one of these quantities is illustrated in Fig. 15.11. The local flux for the binary exchange of two ions with like charges is plotted as a function of the ratio of the solvent flow to the nontransfer coefficient in the electrolyte phase. Three curves are shown; one curve corresponds to the diffusion of uncharged molecules, another corresponds to diffusion in an aqueous solution where the coion (usually the anion) is free to distribute nonuniformly in the electrolyte film, and the third corresponds to diffusion in molten salts where the anion concentration remains approximately constant across the electrolyte film. In these particular calculations, both diffusing ions have a valence of +1; the diffusion coefficients are equal in the solvent phase but differ by a factor of 5 in the electrolyte ($D_{2E}/D_{1E} = \alpha = 1/5$). Figure 15.11 was obtained by holding the mass transfer coefficient (D_{E2}/δ_E) for the electrolyte constant and changing the solvent-phase transfer coefficient. For low values of K, the major mass transfer resistance is in the solvent film (D_{S2}/δ_S), and there is no difference in the curves shown. As K increases, the resistance in the electrolyte film becomes more important and eventually controls the transfer rate. As the electrolyte film gains importance, the effects of electric potential gradients within the electrolyte film become important, and the three curves separate. The transfer rate of component 2 is enhanced by the electric fields generated by the more mobile component 1. The mobile anions act as "supporting" electrolyte and suppress the effects of electric fields in the aqueous system (case 1). Thus the transfer

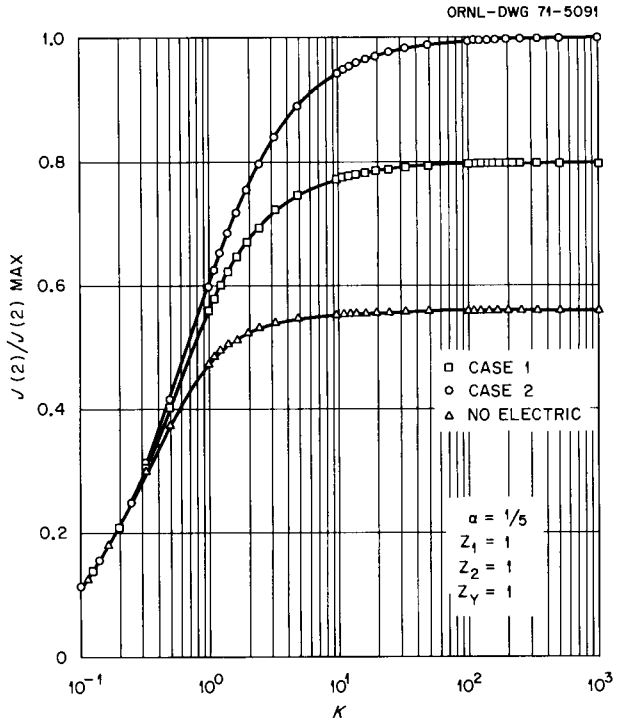

Fig. 15.11. Effect of $K\left(=\frac{D_{S2}/\delta_S}{D_{E2}/\delta_E}\right)$ on transfer rate.

rate is enhanced more in the salt system (case 2). The presence of any nontransferring ions has a similar effect.

The calculational procedure is presently equipped to handle up to ten ions, although there are no immediate plans to study any systems involving more than five. The results will be immediately applied to the analysis of reduction extraction systems, and we hope to obtain enough data from aqueous systems to test applicability or usefulness of the data in other situations.

15.7 CHEMICAL ENGINEERING RESEARCH STUDIES RELATED TO MSR PROCESSING

Frequently, some of the studies performed under the Chemical Engineering Research program can be reported more conveniently as part of the applied programs with which they are associated. Several studies that support or supplement the molten-salt reactor (MSR) program fall into this category and are mentioned only briefly here; a more detailed discussion will be found in Sect. 1. These studies were supported either partially or entirely by Chemical Engineering Research funds.

Reductive Extraction Engineering Studies (See Sect. 1.6)

Semicontinuous engineering experiments concerned with reductive extraction were performed using liquid bismuth and a molten fluoride salt in an 0.82-in.-ID, 24-in.-long column packed with ¼-in. Raschig rings. Measurements included hydrodynamic parameters and mass transfer rates.

Contactor Studies of a Simulated Molten-Salt–Liquid-Bismuth System (See Sect. 1.8)

The hydrodynamic behavior of packed columns and mixer-settlers was studied using mercury and water or an aqueous glycerin solution to simulate bismuth and molten salt.

Axial Dispersion in a Simulated Continuous Fluorinator (See Sect. 1.9)

Axial dispersion of liquid in an open column was measured with a gas bubbling through the liquid. Measurements were made with a variety of column diameters, gas inlets, and liquid properties.

16. Reactor Evaluation Studies

This program, which is a joint effort with the ORNL Reactor Division, has the primary purpose of assisting the USAEC in evaluating the technical feasibility and economics of various nuclear power concepts being developed, or being considered for development, under the U.S. Civilian Power Program. Work in this Division during the past year was devoted primarily to performing production calculations with the Oak Ridge Systems Analysis Code and developing systems analysis models for electric utility systems in cooperation with other members of the Joint Systems Analysis Study Group [Tennessee Valley Authority (TVA), Commonwealth Edison Company, Westinghouse Atomic Development Corporation (WADCO), and ORNL].

In other work, the reactor power cost code POWERCO[1,2] was revised for more effective handling of fuel cycle costs incurred prior to reactor startup. Formerly the cost of the initial core, including interest, was assigned to the first year of reactor operation. The code now assigns all preoperational costs to the time of actual occurrence.

The report "Reactor Fuel Cycle Costs for Nuclear Power Evaluation" was revised extensively and sent to the USAEC in a form ready for reproduction as WASH-1099.

16.1 OAK RIDGE SYSTEMS ANALYSIS CODE

The ORNL reactor systems analysis code ORSAC was described in a previous annual report.[3] Several changes were made to increase the speed and flexibility of the code, as follows:

1. The number of fossil fuel cost regions was increased from 10 to 13.
2. Separation of nuclear plants by fossil fuel cost regions was eliminated since this feature has been of little use thus far. This change reduced the number of equations in the linear programming calculation from 980 to about 320 and decreased the running time of the code by a factor of about 4.
3. Provision was made for fixing the known nuclear and fossil fuel plant startup schedule for the first several periods (e.g., through 1976).
4. The maximum number of linear segments in the capacity factor curve of a plant was increased from 2 to 6.
5. An improved routine was added for printing the results.
6. Cost constants for fuel cycle operations were updated to a 1970 basis.
7. The use of magnetic tapes was completely eliminated in favor of high-speed direct-access disk storage. This greatly improved the overall reliability of the system by eliminating tape failures.

A new series of ORSAC runs was made to provide data for use by the AEC in updating the 1969 LMFBR Cost-Benefit Analysis.[4] The plants that were entered as competitors for the electric power production market were fossil plants, light-water reactors, LMFBR's, and HTGR's, in various combinations. Updated capital costs were supplied by the ORNL Reactor Division. Use was made of the fuel cycle cost iteration feature of ORSAC, which permits the fuel cycle costs to be adjusted in accordance with the reactor mix obtained in the previous iteration. Essential convergence of the reactor mix was generally reached in three or four iterations.

1. R. Salmon, *A Procedure and a Computer Code (POWERCO) for Calculating the Cost of Electricity Produced by Nuclear Power Stations,* ORNL-3944 (June 1966).
2. R. Salmon, *A Revision of Computer Code POWERCO (Cost of Electricity Produced by Nuclear Power Stations) to Include Breakdowns of Power Cost and Fixed Charge Rates,* ORNL-4116 (August 1969).
3. D. E. Ferguson et al., *Chem. Technol. Div. Annu. Progr. Rep. May 31, 1969,* ORNL-4422, pp. 309–11.
4. *Cost-Benefit Analysis of the U.S. Breeder Reactor Program,* USAEC report WASH-1126 (April 1969).

16.2 OPTIMAL DISPATCHING OF ELECTRIC POWER GENERATING PLANTS

As a continuation of our effort in the Joint Systems Analysis Study Group,[5] an improved dynamic programming model was developed for determining the optimal short-term dispatching schedule of power generating plants in an electric utility system. This improved model is described in an ORNL report.[6]

16.3 ECONOMIC INTEGRATION OF NUCLEAR REACTORS IN ELECTRIC UTILITY SYSTEMS

During the year the Joint Systems Analysis Study Group formed three working groups in order to direct concerted effort toward the development of a strategic operating model for an electric utility system that contains nuclear generating plants. The Core Simulation Group will develop a model for in-core management of nuclear fuel. The Power Systems Simulation Group will develop models for power generation and transmission systems. The Systems Integration Group will develop a model for overall optimization that is based upon the work performed by the other two groups. The Chemical Technology Division has primary responsibility for the systems integration model and shares responsibility with TVA and Commonwealth Edison for the power systems simulation model. TVA and WADCO are primarily responsible for the core simulation model.

The time horizon for the strategic operating model has been selected as three to five years. This time period is sufficiently long to permit detailed analyses of outages, nuclear refueling, and seasonal loads, but short enough to provide a reliable projection of the status of the power generation and transmission systems. This strategic operating model will form the basis for future improvement of long-term expansion models such as ORSAC (Sect. 16.1) and short-term dispatching models (Sect. 16.2).

The following sections summarize the current status of the work, within the Division, involving development of models for power systems simulation and systems integration.

Power Systems Simulation

The initial developmental work on computer program SIMUL, which will be the basic model for power systems simulation, has been completed. Basically, this program calculates capacity factors of each generating plant in the system for each time period (usually one month) within the time horizon of the model. The program uses a probabilistic technique to incorporate the random effects of forced outages and load forecast error into prescribed load duration functions. The program has been transmitted to TVA, where other members of the Power Systems Simulation Group will develop a production version of the program and incorporate routines to develop an order of commitment of the individual plants based upon generating costs, transmission, and system reliability.

Systems Integration

Three computer programs are being developed as part of the overall systems integration model. Program MAIN schedules maintenance of all generating units. It also minimizes the probability of loss of load over the period of study in which system constraints are being considered. A second program, HYDRO, determines optimal usage of hydroelectric power and schedules the operations of all other types of power generating plants. Program REFCO calculates nuclear fuel cycle costs based upon a discounted cash flow procedure using continuous discounting. With REFCO, income tax deductions can be collected by fuel batches. This program must be supplied with a charge-discharge schedule for reactor fuel and with unit costs of fuel cycle services.

---

5. D. E. Ferguson et al., *Chem. Technol. Div. Annu. Progr. Rep. May 31, 1970,* ORNL-4572, pp. 236–38.

6. D. S. Joy, *A Dynamic Programming Approach for Determining the Optimal Dispatching Sequence for a Combined Hydro–Thermal–Pumped-Storage Utility System,* ORNL-4624 (December 1970).

17. Miscellaneous Programs

17.1 QUALITY ASSURANCE PROGRAM

Standard quality assurance procedures are being developed for the Chemical Technology Division and are being applied to many of the projects, primarily reactor support work, presently being carried out within the Division. As new projects or experiments are planned, the quality assurance requirements considered to be appropriate are applied by the Quality Assurance Coordinator (QAC) in cooperation with the Project Leader.

The QAC becomes involved in one of several ways. He may be contacted initially by a Project Leader, who makes an appointment to discuss a proposed project and put it into the proper perspective. This method of transferring information appears to be the most effective and is becoming the preferred method as personnel in the Division become cognizant of quality assurance and its importance. Also, the QAC reviews all new work orders that are opened each month and examines all applicable purchase requests. These two sources provide additional information about projects that might not have been brought to his attention otherwise.

Each project is assigned a quality level between 1 and 4; quality level 1 is the highest, and quality level 4 is the lowest. The quality level not only reflects the importance of the project but indicates whether failure of the project or experiments could cause: (1) significant delays in the overall project, (2) significant damage to the facility in which it is located, or (3) hazardous consequences. It is important to assign the proper quality levels to projects or experiments. A quality level that is too low might prove to be detrimental from the standpoint of safety and reliability. On the other hand, the higher the quality level assigned, the more expensive the project can become. Justification of the greater expense, then, resolves to a comparison of the cost of reliability with the cost of failure.

During this report period, more than 30 experiments in the Division were examined and assigned appropriate quality levels. A written program plan was required for each of the experiments involving quality level 2 (QL-2) work. This program plan outlines the method by which the project will be handled in all stages from design and development through operation and shutdown.

Standard procedures for use in the Division, including procedures for making engineering drawing changes, for QL-3 projects, and for incident reporting, have been written and approved. Additional procedures for the Division are currently being prepared.

Recently, an order was received from Argonne National Laboratory for 2.5 kg of dense $(U + Pu)O_2$ microspheres, which were to be prepared according to Argonne's "Specification FEFS-4, Uranium–Plutonium Dioxide Spheres (July 29, 1970)." To ensure that the material met the requirements of this specification, which arose from the planned end use of the material (i.e., fabrication of irradiation specimens), we were requested to write a Quality Verification Plan (QVP) stipulating the means employed to achieve product specifications and the accuracy to which the numbers could be determined. The plan, entitled "Quality Verification Plan for Production of $(Pu,U)O_2$ Spheres for Argonne National Laboratory (ANL)," was formally prepared at ORNL and approved by ANL. It will be useful as a guide for similar work for other projects.

17.2 EVALUATION OF THE RADIATION RESISTANCE OF SELECTED PROTECTIVE COATINGS (PAINTS)

Tests to evaluate commercial protective coatings for potential use in various nuclear facilities have been continued. A total of 108 coating systems were exposed in air and in water to a ^{60}Co source to obtain comparative ratings of coatings from 14 manufacturers with a recent or renewed interest in marketing their product in the nuclear field. Also, three different generic coating systems were irradiated for "steam-gamma" and "air-gamma" testing procedures followed by autoclave testing as part of the development of

Table 17.1. Gamma radiation resistance of several protective coatings

Radiation source: ^{60}Co with an intensity of 6×10^5 R/hr
Temperature: 40 to 50°C

Coating	Type	Manufacturer[a]	Substrate	Exposure[b] in Demineralized Water		Exposure in Air[b]	
				Dose (rads)	Effect[c]	Dose (rads)	Effect[e]
Amercoat No. 90	Modified phenolic	1	Steel	7.0×10^{9}[d]	F	1.0×10^{10}	---
Amercoat-90/Dimetcote-6	Modified phenolic	1	Steel	7.0×10^{9}[d]	F	1.0×10^{10}	---
Q-Kote	Phenolic	2	Steel	3.4×10^{9}[f]	C	$>8.5 \times 10^{9}$	---
Epoxy-Polyamide	Epoxy[e]	2	Steel	7.0×10^{9}[d]	F	$>8.5 \times 10^{9}$	---
			Concrete	3.4×10	C	$>7.8 \times 10^{9}$	---
Chem-Thane	Urethane	2	Steel	7.8×10^{9}[d]	F	$>8.5 \times 10^{9}$	---
			Concrete	$>9.0 \times 10^{9}$	---	$>7.8 \times 10^{9}$	---
Silicone-Alkyd	Alkyd	2	Steel	1.0×10^{8}[f]	B	6.8×10^{9}[d]	F
			Concrete	1.0×10^{8}[f]	B	$>7.8 \times 10^{9}$	---
63-139A (Epolon AE-7/Epolon Multi-Mil)	Epoxy	3	Concrete	1.5×10^{9}	A, C	$>8.3 \times 10^{9}$	---
68-139B (Vinyloid AE-98/Epolon Multi-Mil)	Vinyl	3	Concrete	2.0×10^{9}	B,F	$>8.3 \times 10^{9}$	---
68-121A (Epolon/Epolon Primer)	Epoxy[e]	3	Steel	8.0×10^{8}[f]	B	$>1.0 \times 10^{10}$	---
68-121B (Epolon/Metal Bond Primer)	Epoxy[e]	3	Steel	1.9×10^{9}[f]	B	$>1.0 \times 10^{10}$	---
68-139C (AE 14-69/Epolon)	Polyurethane	3	Concrete	$>3.4 \times 10^{9}$	---	$>2.4 \times 10^{9}$	---
68-139D (AE 15-69/Epolon)	Polyester	3	Concrete	1.0×10^{9}	A,C	$>2.4 \times 10^{9}$	---
Dur-A-Poxy No. 200	Epoxy	4	Steel	1.0×10^{9}	B	$>4.0 \times 10^{9}$	---
			Concrete	4.0×10^{9}	B	$>4.0 \times 10^{9}$	---
System-A (Engard Epoxy No. 437)	Epoxy	5	Steel	1.9×10^{9}	A,C	$>2.5 \times 10^{9}$	---
System-D (Engard Epoxy No. 437)		5	Concrete	1.0×10^{9}	B	$>1.5 \times 10^{9}$	---
System-B (Engard Epoxy No. 475)	Epoxy	5	Steel	$>2.4 \times 10^{9}$	---	$>2.4 \times 10^{9}$	---
System-E (Engard Epoxy No. 475)		5	Concrete	$>1.0 \times 10^{9}$	---	$>1.0 \times 10^{9}$	---
System-C (Engard Epoxy No. 480)	Epoxy	5	Steel	$>2.4 \times 10^{9}$	---	$>2.4 \times 10^{9}$	---
System-F (Engard Epoxy No. 480)		5	Concrete	$>1.0 \times 10^{9}$	---	$>1.0 \times 10^{9}$	---
Epoxy-Phenolic (Rust-Ban EP6846/EP6841)	Modified phenolic	6	Steel	4.5×10^{9}	F	$>9.0 \times 10^{9}$	---
			Concrete	3.3×10^{9}[f]	B,F	$>5.0 \times 10^{9}$	---
Epoxy-Polyamide (Rust-Ban EX6671/EX6664)	Epoxy[e]	6	Steel	4.5×10^{9}	F	$>9.0 \times 10^{9}$	---
			Concrete	4.1×10^{9}	A	$>5.0 \times 10^{9}$	---
Epoxy-Polyamide (Rust-Ban EX6671/EX6664 and No. 191)	Epoxy[e]	6	Steel	4.9×10^{9}	B	$>9.0 \times 10^{9}$	---
No. 1 (Vinyl Y-5280/Y-5296, Y-5295, Y-5290)	Vinyl	7	Steel	7.0×10^{8}	B	4.0×10^{9}	A,C
No. 2 (Nu-Pon Y-5240, Y-5242/Glid-Zinc 103)	Epoxy	7	Steel	1.5×10^{9}	B	$>6.4 \times 10^{9}$	---
No. 3 (Nu-Pon Y-5240, Y-5242/EGL-69722)	Epoxy	7	Steel	5.0×10^{9}	C	$>6.4 \times 10^{9}$	---
No. 4 (Nu-Pon Y-5240, Y-5242/Chromate Primer)	Epoxy	7	Steel	1.5×10^{9}	B	$>6.4 \times 10^{9}$	---
No. 5 (Glid-Tile Y-5596/Nu-Pon Cote Y-5240)	Epoxy	7	Steel	4.8×10^{8}	B	$>6.3 \times 10^{9}$	---
No. 6 (Nu-Pon Y-5240, Y-5242/Nu-Pon Mastic Y-5256)	Epoxy	7	Steel	$>6.3 \times 10^{9}$	---	$>6.3 \times 10^{9}$	---
No. 7 (water reducible enamel EGL-68144, -68146/EGL-68145, -68146 primer)	Epoxy	7	Steel	1.4×10^{9}	D	4.0×10^{9}	C
Nu-Pon Y-5240, Y-5242/Glid-Tile, Y-5512)	Epoxy	7	Concrete	1.9×10^{9}	C	$>2.4 \times 10^{9}$	---
Nu-Pon Y-5240, Y-5242/Nu-Pon Y-5256, Y-5257	Epoxy	7	Concrete	1.4×10^{9}	A,C	$>2.0 \times 10^{9}$	---
Glid-Tile, Y-5597, Y-5596/Glid-Tile Y-5512	Epoxy	7	Concrete	8.6×10^{8}	B,C	$>2.0 \times 10^{9}$	---
Water Reducible enamel-ELG-68144, -68146 ELG-68145, -68146, primer	Epoxy	7	Concrete	5.0×10^{8}	B	$>2.0 \times 10^{9}$	---
Vinyl Y-5280/Y-5285/Y-5283	Vinyl	7	Concrete	3.6×10^{8}	B	$>1.9 \times 10^{9}$	---
Glamorglaze	Epoxy	8	Steel	$>1.4 \times 10^{9}$	---	$>1.4 \times 10^{9}$	---
			Concrete	5.0×10^{8}	B	$>5.0 \times 10^{8}$	---
No. 200/No. 654 primer	Epoxy	8	Steel	$>1.4 \times 10^{9}$	---	$>1.4 \times 10^{9}$	---
			Concrete	5.0×10^{8}	B	---	---
No. 201/No. 654 primer	Epoxy	8	Steel	3.6×10^{8}	B	$>1.4 \times 10^{9}$	---
No. 201/Acrylic Surfacer	Epoxy	8	Concrete	5.0×10^{8}	B	---	---
Vinyl No. 403/400/No. 25 primer	Vinyl	8	Steel	$>3.6 \times 10^{8}$	B	$>1.4 \times 10^{9}$	---
Bitumastic No. 300-M	Epoxy (coal tar)	8	Steel	$>1.4 \times 10^{9}$	---	$>1.4 \times 10^{9}$	---
No. 800/810Torex/820 primer	Chlorinated Rubber	8	Steel	3.6×10^{8}	B	$>1.4 \times 10^{9}$	---
Organic Zinc W/Phenoxy resin	Organic Zinc	8	Steel	$>1.4 \times 10^{9}$	---	$>1.4 \times 10^{9}$	C
No. 1 (84-F-15/89-F-34, Mobilzinc-7)	Epoxy[e]	9	Steel	1.2×10^{9}[f]	A,B	1.0×10^{10}	C
No. 3 (78-D-7/Mobilzinc-7; amine cured)	Epoxy	9	Steel	1.2×10^{9}[f]	A,B	1.0×10^{10}[d]	C
No. 7 (84-F-15/89-F-34)	Epoxy[e]	9	1-Steel	1.6×10^{9}[f]	A,C	$>1.0 \times 10^{10}$	---
			2-Steel	3.8×10^{9}[f]	A,B	---	---
No. 15 (78-D-7, amine cured)	Epoxy	9	1-Steel	1.6×10^{9}[f]	A,C	$>1.0 \times 10^{10}$	---
			2-Steel	1.2×10^{9}[f]	B,C	---	---
No. 17 (Val-Chem/89-F-34)	Polyurethane	9	Steel	7.8×10^{9}[f]	C	$>1.0 \times 10^{10}$	---
No. 19 (84-F-15/89-F-34)	Epoxy[e]	9	1-Concrete	3.8×10^{8}[f]	B	$>1.0 \times 10^{10}$	---
			2-Concrete	2.0×10^{9}[f]	A,B	---	---
No. 23 (78-D-7, amine cured)	Epoxy	9	1-Concrete	5.9×10^{8}[f]	B	$>1.0 \times 10^{10}$	---
No. 24 (val-Chem/89-F-34)	Polyurethane	9	1-Concrete	3.1×10^{8}[f]	B	$>1.0 \times 10^{10}$	---
			2-Concrete	2.8×10^{9}	B	---	---

'able 17.1 (continued)

Coating		Manufacturer[a]	Substrate	Exposure[b] in Demineralized Water		Exposure[b] in Air	
				Dose (rads)	Effect[c]	Dose (rads)	Effect[c]
No. 25 (LM-115, "water dispersed")	Epoxy	9	Concrete	3.4×10^{8}[f]	B	$>1.0 \times 10^{10}$	---
No. 26 (78-W-102)	Modif	9	Concrete	3.8×10^{9}	B,C	---	---
No. 27 (LM-809, w/fiberglas cloth backing)	Epoxy	9	Concrete	4.3×10^{9}	A,F	---	---
N-1-S (No. 5671 thixopoxy)	Epoxy	10	Steel[g]	1.0×10^{9}[f]	B	1.0×10^{10}[d]	---
N-1 (No. 5671 thixopoxy)	Epoxy	10	Steel[h]	1.0×10^{9}[f]	A,B	1.0×10^{10}[d]	---
N-1-C (No. 5671 thixopoxy)	Epoxy	10	Concrete	1.3×10^{9}[f]	A,B,C	$\sim 8.0 \times 10^{9}$	C
N-2-C (No. 5697, polyamid epoxy)	Epoxy	10	Concrete	4.6×10^{9}	C	1.0×10^{10}	---
N-3-S (Nos. 5673 and 5627)	Epoxy	10	Steel[g]	1.0×10^{9}[f]	A,B,C	1.0×10^{10}[cd]	C
N-3 (Nos. 5673 and 5672)	Epoxy	10	Steel[h]	1.0×10^{9}[f]	A,B,C	1.0×10^{10}[d]	C
N-4-F (No. 1371, "4Z")	Inorg	10	Steel[g]	1.0×10^{9}[f]	E	1.0×10	---
N-5-S (No. 5627/5673/1371)	Epoxy	10	Steel[g]	1.0×10^{9}[f]	B	1.0×10^{10}[d]	F
N-6-S (No. 1357, "5Z")	Inorg	10	Steel[h]	9.5×10^{9}	E	1.0×10^{10}[d]	F
N-6 (No. 1357, "5Z")	Inorg	10	Steel[g]	9.5×10^{9}	E	1.0×10^{10}[d]	F
N-7-S (No. 5697/1357, "5Z")	Epoxy	10	Steel[h]	1.0×10^{10}	---	1.0×10^{10}[d]	---
N-7 (No. 5697/1357, "5Z")	Epoxy	10	Steel	1.0×10^{9}[f]	A,B,C	1.0×10^{10}[d]	C
Series-1 (DD-82/DD-82 primer)	Polyu	11	Concrete	$>2.3 \times 10^{9}$	B,D	$>3.4 \times 10^{9}$	---
Series-2 (DD-82/DD-81 primer)	Polyu	11	1-Concrete	1.0×10^{8}	A,B	$>3.4 \times 10^{9}$	---
			2-Concrete	2.3×10^{9}	B	---	---
Series-3 (100% solids epoxy)	Epoxy	11	Concrete	1.0×10^{8}	A,D	$>3.4 \times 10^{9}$	---
Series-4 (DD-82/HB epoxy primer)	Polyu	11	1-Concrete	6.0×10^{8}	B	---	---
			2-Concrete	3.5×10^{9}	A,D	$>2.4 \times 10^{9}$	---
System-1 (No. 545 and 520/545 primer)	Epoxy	11	Steel	1.4×10^{9}	A	$>1.0 \times 10^{10}$	---
			Concrete	4.3×10^{9}	B	$>1.0 \times 10^{10}$	---
System-4 (Epoxy-polyester/No. 545 epoxy primer)	Epoxy	11	Concrete	$>6.3 \times 10^{8}$	B	1.7×10^{9}[f]	A,B
System-5 (styrene copolymer/P-50, alkyd-phenolic)	Styre	11	Steel	2.0×10^{8}[f]	B	$>1.0 \times 10^{10}$	---
System-6 (Zp-200)	Inorg	11	Steel	6.0×10^{9}[d]	C,E	3.8×10^{9}[f]	C,D
			Concrete	6.0×10^{9}[d]	C	3.8×10^{9}[f]	C,D
System-7 (No. 520/Epoxy Primastic and ZP-200)	Epoxy	11	Steel	2.0×10^{8}[f]	B	$>1.0 \times 10^{10}$	---
			Concrete	6.0×10^{8}[f]	B	$>2.4 \times 10^{9}$	---
ME-1022 (Kem Cati-Coat Enamel and Primer)	Epoxy	12	Steel	1.0×10^{10}[d]	A,C	1.0×10^{10}	---
ME-1023 (Pexthane Enamel/Kem Cati-Coat Primer)	Polyu	12	Steel	1.0×10^{10}[d]	C	1.0×10^{10}	---
ME-1025 (Rexthane Enamel/Zinc Clad-7)	Polyu	12	Steel	3.0×10^{8}[f]	B	1.0×10^{10}	---
ME-1026 (Rexthane Enamel/latex-cement filter)	Polyu	12	Concrete	5.0×10^{8}[f]	B	1.0×10^{10}[d]	F
X-430 A (Capox EP System)	Modif	13	Steel	1.2×10^{9}[f]	A	1.0×10^{10}	---
X-430 B (Capox A HB System)	Epoxy	13	Steel	1.5×10^{9}[f]	B	1.0×10^{10}	---
X-430 D (Capox EP inorganic zinc system)	Modif	13	Steel	1.2×10^{9}[f]	A	1.0×10^{10}	---
X-430 F (Capox A HB system w/fiberglas)	Epoxy	13	Concrete	1.2×10^{9}[f]	B	1.0×10^{10}	---
System-1 (no. 92 Themec Zinc)	Inorg	14	Steel	3.0×10^{8}[f]	E	1.0×10^{10}	---
System-2 (HB Epoxoline)	Epoxy	14	Concrete	2.1×10^{9}[f]	B	1.0×10^{10}	---
System-3 (HB Epoxy/No. 92 Zinc)	Epoxy	14	Steel	3.0×10^{8}[f]	B	1.0×10^{10}	---
System-4 (HB Epoxy/HB Epoxy Primer)	Epoxy	14	Steel	1.0×10^{10}[d]	F	1.0×10^{10}	---
System-1A (No. 368 urethane/67-1241 epoxy)	Polyu	14	Concrete	1.8×10^{9}[f]	B	1.0×10^{10}[d]	F

[a]Manufacturer: (1) Amercoat Corp; (2) Chemline Div., Dixie Pa: Co., Inc.: (3) Con-Lux Paint Products, Inc.; (4) Dur-A-Flex, Inc.; (5) Engard Coatings, Corp.; (6) Enjay Chemical Co.; (7) Glidden-Durkee Div. of SCM Corp; (8) K; (9) Mobil Chemical Co.; (10) NAPCO, Inc.; (11) Prufcoat Div., Grow Chem. Coatings Corp.; (12) Sherwin-Williams Co., Inc.; (13) Subox Division, Wyandotte Che) TINEMEC Co.

[b]The coatings were inxpected for radiation damage at various exp -1 $\times 10^{8}$, 3 $\times 10^{8}$, and each additional 5 $\times 10^{8}$ rads exposure thereafter. The values listed represent the cumulative dose that had been received at the time adverse effect If no effects are entered, the exposure test is continuing, if less than 1 $\times 10^{10}$ rads.

[c]Radiation effects: A, chalked; B, blistered; C, embrittled; D, a; E,"sweating,"; F, checking (surface cracking).

[d]Earlier failure not detected. Appearance indicates that resist a that given.

[e]Polyamide-cured epoxy.

[f]Previously reported in ORNL-4572.

[g]Sandblasted steel.

[h]Pickled steel.

testing procedures for coatings to be used in reactor containment buildings. The procedures developed from the above tests were written into a proposed American National Standards Institute standard ANSI 101.2-1970, "Protective Coatings (Paints) for Light Water Reactor Containment Facilities."

The proposed ANSI 101.2-1970 standard was initially reviewed by a committee of 32 representatives of coating manufacturers, reactor designers, contractors, and private consultants. This standard is currently undergoing a second review, and we anticipate that it will be approved for publication within FY 1972. In addition, a new proposed standard, "Quality Assurance for Protective Coatings Applied to Nuclear Facilities," has been written in rough draft form and is now ready for the initial review.

The comparative resistances of the protective coating systems in deionized water–radiation tests show that selective systems of epoxies, modified phenolics, and polyurethanes would be satisfactory up to gamma exposures of 7×10^9 rads (see Table 17.1). All of the coating systems exposed in air indicate a resistance of at least 1×10^9 rads; about 50% of them would still be useful after exposures of up to 1×10^{10} rads. Tests of each of the various coating systems will be continued until the coating has failed or until it has received a cumulative exposure of 1×10^{10} rads. The average intensity of the ^{60}Co source is 6×10^5 R/hr, and the temperatures to which specimens are exposed range from 40 to 50°C.

As part of the protective coatings activities a paper entitled "Protective Coatings (Paints) for PWR and BWR Reactor Containment Facilities," by C. D. Watson, J. C. Griess, T. H. Row, and G. D. West, was written and will be published in *Nucl. Technol.* **10** (April 1971).

17.3 RESOURCE STUDIES

A wide-range program was begun partly as a National Science Foundation activity and partly as an independent effort to evaluate the long-term situation in regard to the availability of mineral resources and the future potentials for substitution and recycle to extend resource horizons of critical materials. Much of this work has been done in cooperation with Resources for the Future, Inc. (RFF). H. E. Goeller spent the summer of 1970 at the RFF offices in Washington, D.C., working with Joel Darmstadter, Hans Lansberg, and Samuel Schurr, who are economists on the RFF staff.

Thus far, the work has included studies involving: (1) evaluation of the resource-substitution-recycle situation for the major nonferrous metals (copper, lead, zinc, and tin), (2) a more comprehensive examination of all the chemical elements, and (3) preliminary evaluation of the resource and use pattern for mineral resources in the long-term future when many elements will be in short supply. The last two activities were undertaken after it was realized that a study of all mineral commodities was necessary to answer adequately all the problems inherent in the first activity. A comprehensive report on the last two areas of study is partially completed. This report is being written primarily for nontechnical readers in the social sciences in an attempt to familiarize them with the overall long-term situation on mineral resources; the major emphasis is on interrelations among mineral materials and their relationships to recycle and substitution. When this effort is completed, the study on copper, zinc, lead, and tin will be resumed and carried to completion; particular emphasis will be placed on future economics we can expect for these metals.

Some of the preliminary conclusions obtained from our studies are as follows:

1. About 17 of the chemical elements have near-infinite resource bases and will be available at fairly constant prices for as far in the future as we care to consider. These include oxygen, nitrogen, argon, neon, krypton, and xenon from the atmosphere; oxygen, hydrogen, sodium, chlorine, magnesium, bromine, potassium, boron, lithium, and iodine from seawater; and silicon, calcium, sodium, potassium, and chlorine from mineral sources.

2. Certain elements in limited supply with respect to presently used resources have near-infinite bases in alternative, but presently uneconomic, resources. For these, improved technology may counterbalance decreased resource quality (and, therefore, prices will remain stable); examples are iron, which will be obtained from taconite and laterite deposits when hematite deposits are exhausted, and aluminum, which will be won from high-alumina clays when bauxite is fully depleted. Recovery of other elements will proceed through a hierarchy of resources of decreasing quality in a way which will make it unlikely that improved technology can keep the price stable; for these elements, prices must certainly increase. The two principal examples are sulfur and carbon. The first will be obtained over the long term from native sulfur, sulfide ores, and pyrites; from fossil fuels; and ultimately from gypsum and seawater. Carbon (for nonfuel use) will be recovered from natural gas and petroleum, then from coal and oil shales, and finally from limestone. There will be a long period of oversupply of sulfur since its mandatory removal from fossil fuels (for pollution

control reasons) will yield quantities far in excess of world demand for this element.

3. A number of elements with presently limited market demand (e.g., Ga, Cs, Rb, Sc, Th, Nb, Hf, and the rare earths) now have long supply horizons. An insidious problem with these elements is that, in the event that new uses significantly increase the demand in the future, the long-time horizons could change rapidly to ones of very short duration.

4. Resources of nearly all other elements have time horizons of a century or less for recovery from reasonably economic resources. Since most uses of all elements are substitutable, the trend in the future for these elements must be toward (1) minimization or elimination entirely of dissipative uses, (2) essentially complete recycle of materials in nondissipative uses to provide a stable world pool for each material, and (3) development of methods for recovering multiple products from resources of ever-decreasing grade, including acceptable disposal methods for the rapidly increasing amounts of tailings or waste generated during recovery. For example, the world pool of copper will probably amount to about 1 billion tons in 50 to 100 years. Annual additions of a few million tons per year will be made to the pool from very low grade ores at prices greater than $1 per pound. Probably the most serious long-term resource problem is that of a perpetual supply of phosphorus, the only one of the three major plant nutrients with a noninfinite resource base. As soon as possible, means must be developed to maximize the recovery of phosphorus from phosphate rock (currently about 50% for acid processes and 75% for the electric furnace method) and minimize agricultural application to the lowest level possible to achieve acceptable crop yields. The problem with phosphorus is not only one of convenience but also may ultimately be a much more basic one – survival for a world with an equilibrium population of 12 to 20 billion people. Other elements with nearly unsubstitutable uses include lithium (fusion energy), manganese (steelmaking), fluorine (steel, aluminum, glass), helium (cryogenics and power), titanium (pigments at reasonable cost), tungsten (high temperature and hardness in toolmaking), and uranium and thorium (fission energy).

5. A century from now, we predict that the world will have the necessary quantities of nearly all minerals and metals required to sustain a materials-energy-oriented civilization, provided we have successfully completed the about-face from our present "use and dispose" philosophy to one of accepting substitution, recycle, and conservation as the standard way of life. To fill the gap resulting from increasing scarcities of many materials, we will live, even more than at present, in a world made principally of steel, aluminum, magnesium, glass, and ceramic and powered almost exclusively by nuclear energy. Petrochemical products such as plastics, solvents, synthetic fibers, etc., derived from coal, shale oil, and ultimately limestone, rather than from natural gas and petroleum, will still be in plentiful supply; however, the costs will be somewhat higher.

17.4 ENVIRONMENTAL QUALITY PROGRAM: PRODUCTIVE USES OF WASTE HEAT

The Environmental Quality Program was established in response to the increasing involvement of the Atomic Energy Commission in assessing the total impact of nuclear power plants on the environment. Productive uses of waste heat relate to the utilization of this thermal energy as a resource instead of the rejection of it as a waste.

In the conventional steam-electric power plant, up to 2 kW of thermal energy has to be dissipated for every kilowatt of electrical energy produced. Instead of indiscriminately discharging the heat to receiving waters, government regulatory agencies are enforcing legislation that requires electric utility companies to dissipate the heat into the atmosphere by cooling towers, by cooling ponds, or by more elaborate means such as closed cycle systems. This leads to an added expense to all consumers of electricity.

Alternatively, power plants may be conceived of as energy centers that produce electrical and thermal energy. And the cost of heat disposal might be minimized by maximizing the revenue-producing potential of the total energy output. Biological applications, particularly food cultivation in controlled environments, appear to be a promising way of utilizing at least a portion of the heat. Heating and cooling of urban areas, particularly new cities, might be another application, provided higher-temperature steam (300–400°F) is available and lower conversion efficiencies of thermal energy to electrical energy are tolerable.

Basic data indicate that temperature is one of the important variables to consider in the optimization of environmental conditions to increase growth and yields of cultivated foods.[1] Lettuce grows best at 55°F, tomatoes at 70°F, and cucumbers at 80°F. Chicken (broilers) and swine grow best at 68°F, and shrimp and

1. S. E. Beall, "Agricultural and Urban Uses of Low-Temperature Heat," presented at the Conference on Beneficial Uses of Thermal Discharges, Albany, N.Y., Sept. 16–18, 1970.

catfish at 85°F. All of these are within the range of temperatures of power plant effluents, which represent a potential year-round source of heat that could enhance food yield and modify seasonal variations in food supply.

Feasibility studies have been made to show the potential of thermal energy utilization. For greenhouse agriculture,[2] an analysis of the possible benefits was made for an established set of site conditions at the gas-cooled nuclear reactor at Fort St. Vrain, Colorado. "Greenhouse cooling towers" could be substituted for the specified conventional cooling towers at the same cost of $1 to $1.5 million. Instead of being dumped, the waste heat could be utilized to heat and cool 200 acres of enclosures in the exclusion area that surrounds the nuclear plant. The temperature of these greenhouses could be maintained at 75 to 80°F in the summer and about 65°F in the winter. Both the greenhouse operator and the utility would profit from such an operation.

In aquaculture,[3] a conceptual design was proposed for intensive year-round fish culture, utilizing published data on shrimp biology and technology to establish a model. Production was based on the availability of 1000 million gallons of flowing water per day, maintained at 80°F by blending power-plant effluent water with ambient-temperature water. At a yield of 25,000 lb of shrimp per acre-year over 400 acres of water surface in culture and a wholesale value of $1 per pound, a 23% return on investment was estimated for a specified set of conditions. A cost sensitivity analysis of the operation revealed that production cost is most sensitive to feed conversion ratio and least sensitive to labor factors; site improvement cost is intermediate.

In urban uses,[4] the concept of total energy utilization was examined in connection with new city planning for a population of 400,000 and a climatology similar to that for Philadelphia. An energy center of 2000 MW(t) was considered with a base load of 500 MW(e). Thermal heat was removed at various temperatures from the back-pressure turbine and utilized as follows: (1) almost 30% was used to heat water to 300°F, and the latter was piped to the downtown area for urban heating and cooling; (2) 24% was used for three different grades of process heat for urban industry; (3) 6% was employed for sewage distillation; and (4) 40% was available for greenhouse agriculture. Thermal energy was utilized and dispersed, rather than discharged as a point source to the surroundings. Use of high-temperature steam (400°F) reduced the turbine efficiency for electric power production to about 23%.

17.5 SYSTEMS ANALYSIS OF A NUCLEAR ENERGY CENTER

An economic model was developed[5] for determining (1) an optimum combination of industrial activities for a nuclear energy center as a function of energy cost and (2) the economic impact of the center on its economic region. The model is derived from the coupling of two research techniques, separable programming and input-output analysis, in a mutually consistent manner. Separable programming was used to optimize the mix of energy-intensive industries proposed for an energy center; maximization of premium worth at a 10% minimum acceptable rate of return was adopted as the optimization criterion. The program used energy cost as a parameter in order to study the variations in industrial activity and total energy demand as a function of energy cost.

Problems associated with the achievement of local optima in the separable program were corrected through development of a search routine based on inserting activity vectors into the basis of each prior solution and running the problem until an optimum that was believed to be reasonably close to the global optimum for this particular study was achieved.

Results of the separable program served as the data for an input-output program which examined the effect of the center on its economic region in terms of increases in gross product, employment, and capital demands. A feedback of information from the input-output program permitted adjustment of the capital and employment constraints in the separable program so that consistent relationships were maintained between the project demands and the resources of the economy. Projection of the input-output data to show the effects of an energy center over both short- and long-term time periods was developed employing a dynamic procedure which took into account the changes in the final demands of the economy as a function of the growth of gross product.

Puerto Rico was selected as a test region for this model because the commonwealth has (1) an interest in

2. S. E. Beall and G. Samuels, *The Use of Warm Water for Heating and Cooling Plant and Animal Enclosures,* to be published as an ORNL-TM report.

3. W. C. Yee, *Potential of Aquaculture at Nuclear Energy Centers – a Systems Study,* ORNL-4488 (to be published).

4. A. J. Miller et al., *Use of Steam-Electric Power Plants to Provide Thermal Energy to Urban Areas,* ORNL-HUD-14 (January 1971).

5. J. M. Holmes, "The Impact of Nuclear Energy Centers on the Economy of Puerto Rico," Ph.D. dissertation, University of Tennessee, Knoxville, July 1970.

the development of nuclear energy centers and desalting of seawater to obtain fresh water, (2) a rapid industrial growth, particularly in the heavy chemical industries, (3) an abundant supply of industrial labor, and (4) adequate economic information, including the data needed for input-output analysis. All data used for capital, labor, raw materials, and utility costs, income taxes, product values, and transportation rates were adjusted to represent current Puerto Rican conditions. A 1960 Puerto Rican input-output table that had been projected to 1975 by the Puerto Rico Planning Board was used as the basis for the economic impact phase of the study.

Industrial activities considered for the energy center included the production of elemental phosphorus, aluminum, magnesium, chlorine, caustic, vinyl chloride monomer, pig iron, steel, ammonia, and fresh water (seawater desalting). The feasibility of installing industrial activities at an energy center was established by comparing individual processes with competitive and, in some cases, non-power-intensive processes located elsewhere in Puerto Rico or on the mainland of the United States.

Results of the optimization phase indicate that, for an assumed base power rate of 4.1 mills/kWhr and comparable costs for steam, the energy center should produce elemental phosphorus, fabricated aluminum, chlorine-caustic, magnesium and steel ingot, desalted water, and a small amount of anhydrous ammonia. The total energy demand would be 890 MW(e) (including steam expressed as equivalent electrical megawatts), the capital cost would be $461 million (1975 dollars), and the center would employ about 5335 people. If a 12-year Puerto Rican tax exemption is not assumed, only the aluminum plant appears feasible, and the energy demand decreases to 209 MW(e).

The overall results of this study indicate that the impact of an energy center on the Puerto Rican economy would be significant, particularly on the demands for additional capital by the government and public services sectors. This additional capital demand for government and public services would total $464 million (including the nuclear reactor), which is equal to 101% of the cost of an energy center. The short- and long-term employment increase attributable to the complex (including those employed at the complex) was estimated at 8400 and 26,300 respectively. The long-term perturbation to the gross product would be an increase of $734 million, which is a factor of 6.55 times the value added by the complex alone.

17.6 APPLICATIONS OF ^{252}Cf

Two promising applications for ^{252}Cf which deal with neutron activation and neutron radiography are being investigated in cooperation with the Chemistry and the Analytical Chemistry Divisions. Preliminary experimentation was begun using a capture-gamma activation analysis technique for the detection of trace elements in an aqueous medium. The experiment consists of a ^{252}Cf source centrally located in two concentric polyethylene containers. The inner container is filled with the solution being analyzed, and the outer container is filled with a neutron shielding material. A Ge(Li) detector is placed outside the outer container to detect the secondary gamma rays produced.

The ANISN[6] computer program was used to select materials of construction that minimize the production of secondary gamma rays. The quantity of ^{252}Cf, size of the container, and distance between the container and the detector are some of the other parameters yet to be optimized.

To date, thermal-neutron radiography studies have used the two-dimensional DOT[7] computer program to analyze a proposed facility. The model used for this study is a 24-in.-long conical neutron collimator with a 1-in.-diam aperture, near the ^{252}Cf source, that increases to a 6-in.-diam opening at the imaging plane. The air-filled cone, submerged in water, is fabricated of aluminum and is lined with $\frac{1}{8}$- and $\frac{1}{2}$-in. thicknesses of boral and bismuth respectively. A 10-mg ^{252}Cf source is located 1 in. from the collimator, tangential to the opening. For such an arrangement, it was determined that a thermal-neutron flux of about 3.7×10^4 neutrons cm^{-2} sec^{-1} with radiation dose levels of approximately 130, 3, and 0.4 rem/hr from total neutrons and from primary and secondary gammas, respectively, would be produced at the imaging plane.

The objective of the study is to develop a design that maximizes the thermal-neutron flux at the imaging plane and minimizes the gamma radiation so that the film can be exposed with the neutron converter foil. If the gamma radiation is too high, the foil must first be exposed and then transferred to the film, thereby resulting in loss of image quality. A number of variables

6. W. W. Engle, Jr., *A Users Manual for ANISN*, K-1693, Oak Ridge Gaseous Diffusion Plant (March 1967).

7. F. R. Mynatt, F. J. Muckenthaler, and P. N. Stevens, *Development of a Two-Dimensional Discrete-Ordinates Transport Theory for Radiation Shielding*, CTC-INF-952 UCC (August 1969).

can be optimized more economically in an actual facility after the initial conceptual design is formulated with the aid of the computer. Some of the variables to be optimized are: (1) dimensions of the collimator, (2) thicknesses and types of material of construction, (3) the medium in and around the collimator, (4) the position of the shielding materials, and (5) the position of the ^{252}Cf source in relation to the collimator.

Publications, Speeches, and Seminars

BIOCHEMICAL TECHNOLOGY

Burtis, C. A.,[1] W. C. Butts,[2] and W. T. Rainey, Jr.,[2] "Separation of the Metabolites of Phenacetin in Urine by High-Resolution Anion-Exchange Chromatography," *Amer. J. Clin. Pathol.* **53**(5), 769–77 (1970).

Burtis, C. A.,[1] W. F. Johnson,[3] C. D. Scott, and N. G. Anderson,[1] "Increase in the Rate of Sample Throughput by Use of a 42-Cuvette GeMSAEC Fast Analyzer," presented at the Third Annual Symposium on High-Resolution Analyses and Advanced Analytical Concepts for the Clinical Laboratory, ORNL, Mar. 11 and 12, 1971.

Butts, W. C.,[2] and R. L. Jolley, "Gas-Chromatographic Identification of Urinary Carbohydrates Isolated by Anion-Exchange Chromatography," *Clin. Chem.* **16**, 722 (1970).

Chilcote, D. D., and J. E. Mrochek, "Automatic Digital Data Acquisition and On-Line Computer Analysis in High-Resolution Liquid Chromatography," presented at the Third Annual Symposium on High-Resolution Analyses and Advanced Analytical Concepts for the Clinical Laboratory, ORNL, Mar. 11 and 12, 1971.

Chilcote, D. D., and C. D. Scott, "Use of a Small, Dedicated Computer with a High-Resolution Liquid Chromatograph," presented at the Fourteenth Conference on Analytical Chemistry in Nuclear Technology, Gatlinburg, Tenn., Oct. 13–15, 1970.

Chilcote, D. D., and C. D. Scott, "Use of a Small, Dedicated Computer with a High-Resolution Chromatograph," presented at the Computer Aided Experimental Spectroscopy Study Group Conference, Midland, Mich., Nov. 4–6, 1970.

Egan, B. Z., J. E. Caton,[2] and A. D. Kelmers, "Use of Reversed-Phase Chromatography for Separating *E. coli* Ribosomal RNAs and Other Selected RNAs," presented at the 160th National Meeting of the American Chemical Society, Chicago, Ill., Sept. 13, 1970.

Egan, B. Z., R. W. Rhear, and A. D. Kelmers, "Solvent Extraction of Transfer Ribonucleic Acids," *Anal. Biochem.* **38**, 139 (1970).

Jolley, R. L., and C. D. Scott, "Preliminary Results from High-Resolution Analyses of Ultraviolet-Absorbing and Carbohydrate Constituents in Several Pathologic Body Fluids," *Clin. Chem.* **16**, 687 (1970).

Jolley, R. L., C. D. Scott, and N. E. Lee, "High-Resolution Column Chromatography of UV-Absorbing Constituents in Normal Body Fluids," presented at the 80th meeting of the Tennessee Academy of Science, Southwestern University, Memphis, Tenn., Nov. 20–21, 1970.

Jolley, R. L., K. S. Warren, C. D. Scott, J. L. Jainchill,[4] and M. L. Freeman, "Carbohydrates in Normal Urine and Blood Serum as Determined by High-Resolution Column Chromatography," *Amer. J. Clin. Pathol.* **53**(5), 793–802 (1970).

Katz, Sidney, "Some pH Control Problems in Gradient Elution Ion-Exchange Chromatography," *J. Chromatogr.* **53**, 415–19 (1970).

---

1. MAN Program.
2. Analytical Chemistry Division.
3. Instrumentation and Controls Division.
4. National Cancer Institute, Bethesda, Md.

Katz, S., S. R. Dinsmore, and W. W. Pitt, Jr., "A Small, Automated High-Resolution Analyzer for Determination of Carbohydrates in Body Fluids," presented at the Third Annual Symposium on High-Resolution Analyses and Advanced Analytical Concepts for the Clinical Laboratory, ORNL, Mar. 11 and 12, 1971.

Katz, S., W. W. Pitt, Jr., C. D. Scott, and A. A. Rosen,[5] "The Determination of Stable Organic Compounds in Water at PPB Levels by Automatic High-Resolution Ion Exchange Chromatography," presented at the American Chemical Society Meeting, Los Angeles, Mar. 28–Apr. 4, 1971.

Katz, S., C. D. Scott, R. L. Jolley, S. Dinsmore, and W. F. Johnson, "A Small, Automated High-Resolution Analyzer for Determination of Carbohydrates in Body Fluids," presented at the 18th Detroit Anachem Conference, Detroit, Mich., Oct. 14–16, 1970.

Kelmers, A. D., "Effect of Divalent Metal Ions on the Reversed-Phase Chromatographic Separation of Transfer Ribonucleic Acids," *Biochemistry* **9**, 4401 (1970).

Kelmers, A. D., "Effect of Divalent Metal Ions on the Reversed-Phase Chromatographic Separation of Transfer Ribonucleic Acids," presented at the Presymposium "tRNA: Structure and Function," IUPAC 7th International Symposium on the Chemistry of Natural Products, Riga, U.S.S.R., June 19, 1970.

Kelmers, A. D., J. E. Caton,[2] and B. Z. Egan, "Separation of *E. coli* Ribosomal RNAs and Mammalian RNAs by Reversed-Phase Chromatography," presented at the 7th International Symposium on the Chemistry of Natural Products, Latvian Academy of Sciences, Riga, U.S.S.R., June 21–27, 1970.

Mrochek, J. E., W. C. Butts,[2] W. T. Rainey, Jr.,[2] and C. A. Burtis,[1] "The Separation and Identification of Urinary Constituents Using Multiple Analytical Techniques," *Clin. Chem.* **17**, 72 (1971).

Mrochek, J. E., R. L. Jolley, W. C. Butts,[2] D. S. Young,[6] and W. J. Turner,[7] "The Metabolism of Nicotinic Acid and Nicotinamide by Humans as Determined by High-Resolution Ion Exchange Chromatography," presented at the Third Annual Symposium on High-Resolution Analyses and Advanced Analytical Concepts for the Clinical Laboratory, ORNL, Mar. 11 and 12, 1971.

Pitt, W. W., Jr., C. D. Scott, W. F. Johnson,[3] and Guy Jones, Jr., "A Bench-Top, Automated, High-Resolution Analyzer for Ultraviolet-Absorbing Constituents of Body Fluids," *Clin. Chem.* **16**, 637 (1970).

Pearson, R. L., J. F. Weiss, and A. D. Kelmers, "Improved Separation of Transfer Ribonucleic Acids on Polychlorotrifluoroethylene-Supported Reversed-Phase Chromatography Columns," *Biochem. Biophys. Acta* **228**, 770 (1971).

Ryon, A. D., and C. W. Hancher, "A Mechanical Mixer for Use in the Preparation of Reversed-Phase Chromatographic Packing," *Biotechnol. Bioeng.* **XII**, 1099 (1970).

Scott, C. D., "Development of High-Resolution Analyses of Body Fluids by High-Pressure Ion Exchange Chromatography," presented at the 22nd National Meeting of the American Association of Clinical Chemists, Buffalo, N.Y., July 1970.

Scott, C. D., "High-Pressure Ion Exchange Chromatography. Design and Operation of High-Resolution Systems," presented at the 160th National Meeting of the American Chemical Society, Chicago, Ill., Sept. 13, 1970.

Scott, C. D., "Development of High-Pressure Ion Exchange Chromatography for Automated, High-Resolution Analyses of Body Fluids," presented at the 63rd Annual A.I.Ch.E. Meeting, Chicago, Ill., Nov. 29–Dec. 3, 1970.

Scott, C. D., D. D. Chilcote, and W. W. Pitt, Jr., "Method for Resolving and Measuring Overlapping Chromatographic Peaks by Use of an On-Line Computer with Limited Storage Capacity," *Clin. Chem.* **16**, 637 (1970).

Scott, C. D., J. M. Jansen, Jr.,[3] and W. W. Pitt, "A Computer Technic for On-Line Analyses of Complex Column Chromatographic Data," *Amer. J. Clin. Pathol.* **53**, 739–47 (1970).

Scott, C. D., R. L. Jolley, W. W. Pitt, and W. F. Johnson,[3] "Prototype Systems for the Automated, High-Resolution Analyses of UV-Absorbing Constituents and Carbohydrates in Body Fluids," *Amer. J. Clin. Pathol.* **53**(5), 701–12 (1970).

5. Federal Water Quality Administration.
6. Clinical Center, NIH, Bethesda, Md.
7. Islip State Hospital, Central Islip, N.Y.

Scott, C. D., and R. S. Melville,[8] "Introduction, Proceedings of the First Annual Symposium on Automated, High-Resolution Analyses in the Clinical Laboratory," *Amer. J. Clin. Pathol.* **53**(5), 677–79 (1970).

Scott, C. D., and R. S. Melville,[8] "Introduction to the Proceedings of the Second Annual Symposium on Automated, High-Resolution Analyses in the Clinical Laboratory," *Clin. Chem.* **16**, 623 (1970).

Stevenson, R. L.,[9] and C. A. Burtis,[1] "High Resolution Liquid Chromatography of Complex Organic Mixtures," presented at the Third Annual Symposium on High-Resolution Analyses and Advanced Analytical Concepts for the Clinical Laboratory, ORNL, Mar. 11 and 12, 1971.

Thacker, L. H.,[3] W. W. Pitt, Jr., S. Katz, and C. D. Scott, "Miniature Photometers for Liquid Chromatography," *Clin. Chem.* **16**, 626 (1970).

Thacker, L. H.,[3] C. D. Scott, and W. W. Pitt, Jr., "A Miniaturized Ultraviolet Flow Photometer for Use in Liquid Chromatographic Systems," *J. Chromatogr.* **51**, 175–81 (1970).

Weeren, H. O., A. D. Ryon, D. E. Heatherly, and A. D. Kelmers, "Gram-Scale Purification of Arginine, Formylmethionine, Glutamic Acid, and Phenylalanine Transfer Ribonucleic Acids from *E. coli* K-12 MO7," *Biotechnol. Bioeng.* **XII**, 889 (1970).

CHEMICAL ENGINEERING

Watson, J. S., and H. D. Cochran, Jr., "A Simple Method for Estimating the Effect of Axial Backmixing on Countercurrent Column Performance," *Ind. Eng. Chem., Process Des. Develop.* **10**(1), 83–85 (1971).

Whatley, M. E., "Chemical Engineering at the Oak Ridge National Laboratory," presented to the Freshman Engineering Seminar at Tennessee Technological University, Nov. 16, 1970.

CHEMICAL PROCESSING FOR MOLTEN-SALT BREEDER REACTORS

Chandler, J. M., and S. E. Bolt,[10] "Uranium-233-Bearing Salt Preparation for the Molten Salt Reactor Experiment," *Nucl. Appl. Technol.* **9**(6), 807–13 (1970).

Ferris, L. M., J. C. Mailen, J. J. Lawrance,[11] F. J. Smith, and E. D. Nogueira,[12] "Equilibrium Distribution of Actinide and Lanthanide Elements between Molten Fluoride Salts and Liquid Bismuth Solutions," *J. Inorg. Nucl. Chem.* **32**, 2019–35 (1970).

Hightower, J. R., Jr., and L. E. McNeese, *Low-Pressure Distillation of Molten Fluoride Mixtures: Nonradioactive Tests for the MSRE Distillation Experiment,* ORNL-4434 (January 1971).

Mailen, J. C., F. J. Smith, and L. M. Ferris, "Solubility of PuF_3 in Molten $2LiF\text{-}BeF_2$," *J. Chem. Eng. Data* **16**(1), 68–69 (1971).

Smith, F. J., and L. M. Ferris, "Mutual Interactions of Thorium, Nickel and Bismuth in Th-Ni-Bi Solutions," *J. Inorg. Nucl. Chem.* **32**, 2863–68 (1970).

Smith, F. J., and L. M. Ferris, "The Distribution of Actinide and Lanthanide Elements between Molten Lithium Halide Salts and Liquid Bismuth Solutions," presented at the Southeast-Southwest Regional American Chemical Society Meeting, New Orleans, Dec. 2–4, 1970.

MISCELLANEOUS

Anderson, S. W.,[13] R. T. Jenkins,[14] David Joy, E. T. Merrill,[15] and T. D. Wolsko,[16] "Methods of Planning Generating Unit Operation," *Combustion* **42**(6), 17–21 (1970).

8. NIGMS, NIH, Bethesda, Md.
9. Varian Aerograph, Walnut Creek, Calif.
10. Reactor Division.
11. Australian Atomic Energy Commission, New South Wales.
12. Junta de Energia Nuclear, Madrid, Spain.
13. Commonwealth Edison Company.
14. Tennessee Valley Authority.
15. Battelle Northwest Laboratory.
16. Argonne National Laboratory.

Arnold, E. D., "Radiation and Environmental Characteristics of the Actinide Isotopes," presented at the 16th Annual Meeting of the American Nuclear Society, Los Angeles, June 28–July 2, 1970; *Trans. Amer. Nucl. Soc.* **13**(1), 219–20 (1970).

Arnold, E. D., "Shipping Containers for Irradiated Fuel Elements," subsection 10.1.1.3, pp. 12–19 in "Shield Design and Engineering," vol. 3 of *Engineering Compendium on Radiation Shielding* (R. G. Jaeger, E. P. Blizard, A. B. Chilton, M. Grotenhuis, A. Hönig, T. A. Jaeger, and H. H. Eisenlohr, eds.), Springer-Verlag, Berlin, 1970.

Arnold, E. D., "Shipping Containers for Fission Product Waste," subsection 10.1.1.4, pp. 19–23 in "Shield Design and Engineering," vol. 3 of *Engineering Compendium on Radiation Shielding* (R. G. Jaeger, E. P. Blizard, A. B. Chilton, M. Grotenhuis, A. Hönig, T. A. Jaeger, and H. H. Eisenlohr, eds.), Springer-Verlag, Berlin, 1970.

Arnold, W. D., and D. J. Crouse, "Radioactive Contamination of Oil Produced from Nuclear-Broken Shale," *Proceedings of the Symposium on Engineering with Nuclear Explosives, Held at Las Vegas, Nev., Jan. 14–16, 1970,* CONF-700101, vol. 2, p. 1597 (May 1970).

Bell, J. T., "Thermodynamics for the Formation of 1:1 Americium–Iminodiacetic Acid Complex," presented at the 1970 Combined Southeast-Southwest Regional Meeting of the American Chemical Society, New Orleans, La., Dec. 2–4, 1970.

Bell, J. T., and N. A. Krohn, "The Near Infrared Spectra of H_2O and D_2O at Temperatures between 25 and 390°C," *J. Phys. Chem.* **74**, 4006 (1970).

Boegly, W. J., Jr.,[17] W. L. Griffith,[17] and W. E. Clark, *Development of a Wet Oxidation Process for Municipal Refuse,* ORNL-HUD-15 (February 1971).

Coutant, C. C.,[18] and W. C. Yee, "Interactions of Thermal Power Plants and Aquaculture," presented at the European Inland Fisheries Advisory Commission Workshop on Aquaculture, Stuttgart, Ark., Sept. 10, 1970; to be published in the transcript of the meeting.

Crouse, D. J., W. D. Arnold, and F. J. Hurst, "Radioactive Contamination of Copper Produced Using Nuclear Explosives," *Proceedings of the Symposium on Engineering with Nuclear Explosives, Held at Las Vegas, Nev., Jan. 14–16, 1970,* CONF-700101, vol. 2, p. 1569 (May 1970).

Dickens, J. K.,[19] and R. D. Baybarz, "A Monoenergetic 6130-kev Gamma-Ray Source for Detector Calibration," *Nucl. Instrum. Methods* **85**, 143 (1970).

Gregg, J. L.,[20] J. M. Holmes, and H. E. Goeller, *Evaluation of a Power-Intensive Process for Iron and Steel Production at a Nuclear Energy Center,* ORNL-TM-2697 (Aug. 29, 1969).

Holmes, J. M., *Evaluation of Du Pont Arc Process for Acetylene and Vinyl Chloride Monomer Production,* ORNL-TM-2725 (Sept. 26, 1969).

Holmes, J. M., *Consideration of Nuclear Power Expansion for Puerto Rico, Including Surplus Capacity Penalties,* ORNL-TM-3142 (December 1970).

Joy, D. S., "Optimal Dispatching of Utility Systems," presented to the Chemical Engineering Department at Kansas State University, Manhattan, January 1970.

Joy, D. S., *A Dynamic Programming Approach for Determining the Optimal Dispatching Sequence for a Combined Hydro–Thermal–Pumped-Storage Utility System,* ORNL-4624 (December 1970).

Joy, D. S., "Optimal Dispatching of Utility Systems," presented to the Chemical Engineering Department at the University of Tennessee, Knoxville, January 1971.

Joy, D. S., and B. G. Kyle,[21] "Evaluation of Activity Coefficients from Ternary Liquid-Liquid Equilibria," *Ind. Eng. Chem., Process Des. Develop.* **9**, 244 (1970).

17. Civil Defense Project.
18. Ecological Sciences Division.
19. Neutron Physics Division.
20. Y-12 Plant consultant.
21. Department of Chemical Engineering, Kansas State University, Manhattan.

Kerr, H. T.,[10] M. J. Bell, and E. E. Bloom,[22] "Neutron Cross-Section Data Applied to the Materials Irradiation Studies at ORNL," presented at the Third Conference on Neutron Cross Sections and Technology, Knoxville, Tenn., Mar. 15–17, 1971; to be published in the proceedings.

Larson, R. E.,[23] F. J. Rees,[23] and J. P. Nichols, "Dynamic Programming for Expansion Planning of Nuclear Power Generation Systems," presented at the 16th Annual Meeting of the American Nuclear Society, Los Angeles, June 28–July 2, 1970.

Larson, R. E.,[23] F. J. Rees,[23] and J. P. Nichols, "Dynamic Programming for Expansion Planning of the Fuel Reprocessing Industry," presented at the 16th Annual Meeting of the American Nuclear Society, Los Angeles, June 28–July 2, 1970.

Meservey, A. B., "Decontamination and Film Removal," chap. 5 in *Decontamination of Nuclear Reactors and Equipment* (ed. by J. A. Ayres), The Ronald Press Co., New York, 1970.

Nichols, J. P., "Cells for Spontaneous Fission Sources," subsection 10.5.2, pp. 128–34 in "Shield Design and Engineering," vol. 3 of *Engineering Compendium on Radiation Shielding* (R. G. Jaeger, E. P. Blizard, A. B. Chilton, M. Grotenhuis, A. Hönig, T. A. Jaeger, and H. H. Eisenlohr, eds.), Springer-Verlag, Berlin, 1970.

Nichols, J. P., "Shipping Containers for Fission Sources," subsection 10.1.2.2, pp. 26–30 in "Shield Design and Engineering," vol. 3 of *Engineering Compendium on Radiation Shielding* (R. G. Jaeger, E. P. Blizard, A. B. Chilton, M. Grotenhuis, A. Hönig, T. A. Jaeger, and H. H. Eisenlohr, eds.), Springer-Verlag, Berlin, 1970.

Nugent, L. J.,[24] R. D. Baybarz, G. K. Werner,[24] and H. A. Friedman, "Intramolecular Energy Transfer and Sensitized Luminescence in an Einsteinium β-Diketone Chelate and the Lower Lying Electronic Energy Levels of Es(III)," *Chem. Phys. Lett.* 7, 179 (1970).

Peterson, J. R.,[25] J. A. Fahey,[26] and R. D. Baybarz, "The Preparation and Some Properties of Berkelium Metal," presented at the Fourth International Conference on Plutonium and Other Actinides, Oct. 5–9, 1970, Santa Fe, N.M.; published in the proceedings.

Sears, M. B., "Reactions of Uranium Carbonitrides and Uranium Nitride with Aqueous Solutions of Hydrochloric, Sulfuric, and Nitric Acids," *J. Inorg. Nucl. Chem.* 32, 2971–84 (1970).

Shappert, L. B., *Standard Quality Assurance Procedures for Quality Level III Projects in the Chemical Technology Division,* ORNL-TM-3084 (August 1970).

Shappert, L. B., "A Quality Assurance Program in the Design and Fabrication of a Radioactive Material Shipping Package," presented at the Seminar on Test Requirements for Packaging for the Transport of Radioactive Materials, Vienna, Austria, Feb. 8–12, 1971.

Shappert, L. B., and B. B. Klima, *The Savannah River Americium-Curium Slug Carrier,* ORNL-TM-3110 (Nov. 6, 1970).

Thomas, I. L., "Hamiltonian Matrix Elements from a Symmetric Wave Function," *Phys. Rev.* A2, 728 (1970).

Thomas, I. L., "Selection Rules and the Protonic Spectrum of Molecules," *Phys. Rev.* A2, 72 (1970).

Thomas, I. L., "The Stark and Zeeman Effects on the Protonic Structure of Molecules," *Phys. Rev.* A2, 1675 (1970).

Thomas, I. L., " 'Vibrational' and 'Rotational' Energy Levels as Protonic Structure in Molecules," *Phys. Rev.* A3, 565 (1971).

Thomas, I. L., "Motion of the Center of Mass of Atoms and Molecules," *Phys. Rev.* A3, 1022 (1971).

Thomas, I. L., and H. W. Joy,[27] "Protonic Structure of Molecules. II. Methodology, Center-of-Mass Transformation, and the Structure of Methane, Ammonia, and Water," *Phys. Rev.* A2, 1200 (1970).

22. Metals and Ceramics Division.
23. Systems Control, Inc., Palo Alto, Calif.
24. Chemistry Division.
25. Department of Chemistry, University of Tennessee, Knoxville.
26. Oak Ridge Graduate Fellow from the University of Tennessee under appointment from Oak Ridge Associated Universities.
27. Present address: Computation Center, Carnegie-Mellon University, Pittsburgh, Pa.

Watson, C. D., J. C. Griess,[10] T. H. Row,[10] and G. A. West, "Protective Coatings (Paints) for PWR and BWR Reactor Containment Facilities," presented at the 16th Annual Meeting of the American Nuclear Society, Los Angeles, June 28–July 2, 1970.

Watson, C. D., and G. A. West, "Protective Coatings – Paints," chap. 11 in *Decontamination of Nuclear Reactors and Equipment* (ed. by J. A. Ayres), The Ronald Press Co., New York, 1970.

Yee, W. C., "Economic Implications of Nuclear Desalination on Seawater Chemical Recovery," presented at the Third Symposium on Salt, Cleveland, Ohio, Apr. 21–24, 1969; pp. 121–32 in *Third Symposium on Salt,* ed. by Jon L. Rau and Louis F. Dellwig, The Northern Ohio Geological Society, Inc., Cleveland, 1970.

Yee, W. C., "Nuplex Concept May Lead to Livable Deserts," *Chem. Eng. News,* June 8, 1970, p. 16.

Yee, W. C., "Economics of Heated Effluent Utilization at Energy Centers," presented at the Symposium on Environmental Aspects of Nuclear Power Stations (sponsored by IAEA in cooperation with the USAEC), United Nations Headquarters, New York City, Aug. 10–14, 1970.

Yee, W. C., "Food Value from Heated Waters – an Overview," presented at the 32nd Annual Conference of The Chemurgic Council, Washington, D.C., Oct. 22–23, 1970; to be published in the proceedings.

Yee, W. C., "Heated Effluent Water Finds Productive Uses," *Chem. Eng. News,* Nov. 16, 1970, p. 51.

Yee, W. C., "Thermal Aquaculture Design," presented at the Second Annual Meeting of the World Mariculture Society, Galveston, Tex., Jan. 28–29, 1971; to be published in the proceedings.

POWER REACTOR FUEL PROCESSING

Arnold, E. D., and H. F. Soard, "Neutron Shielding Requirements for LMFBR and LWR Fuel Shipping Casks," presented at the American Nuclear Society Meeting, Los Angeles, June 28–July 2, 1970; *Trans. Amer. Nucl. Soc.* 13(1), 402 (1970).

Goode, J. H., and C. M. Cox,[22] *The Distribution of Fission Product Tritium in a Zircaloy-Clad UO_2 Blanket Rod from PWR-1,* ORNL-TM-2994 (June 1970).

Groenier, W. S., S. D. Clinton, D. E. Horner, and O. O. Yarbro, *Material-Balance Reference Flowsheets for the Aqueous Processing of LMFBR Fuels in an Existing Facility,* ORNL-TM-3108 (October 1970).

Irvine, A. R., L. B. Shappert, and R. L. Cox, "LMFBR Fuel Shipping – Containment and Heat Transport," presented at the ASME First Annual Conference on Fast Reactors, Palo Alto, Calif., Mar. 8–10, 1971; published by ASME as Publication 71-NE-6.

Irvine, A. R., L. B. Shappert, J. H. Evans,[28] and F. C. Davis,[28] "Destructive Tests Related to LMFBR Shipping Cask Development," presented at the International Atomic Energy Authority Seminar on Test Requirements for the Transport of Radioactive Materials, Vienna, Austria, Feb. 8–12, 1971.

Moore, J. G., and D. J. Crouse, *Solvent Stability in Nuclear Fuel Processing: Cyclic Irradiation Studies of 15 vol % TBP–n-Dodecane,* ORNL-4618 (November 1970).

Rollins, J. D.,[29] and J. H. Evans,[28] "Testing of a Uniquely Designed Shock Absorber to Demonstrate Ability of Type B Packaging to Pass the Free Drop Test," presented at the IAEA Seminar on Test Requirements for Packaging for the Transport of Radioactive Materials, Vienna, Austria, Feb. 8–12, 1971.

Shappert, L. B., J. H. Evans,[28] and W. C. Stoddart,[28] "Methods of Determining Compliance of Type B Packages with the Thermal, Mechanical, and Regulatory Requirements," presented at the Seminar on Test Requirements for Packaging for the Transport of Radioactive Materials, Vienna, Austria, Feb. 8–12, 1971.

Staff of the Chemical Technology Division, *Aqueous Processing of LMFBR Fuels – Technical Assessment and Experimental Program Definition,* ORNL-4436 (June 1970).

Unger, W. E., R. L. Cox, W. S. Groenier, A. R. Irvine, and C. D. Watson, "The Adaptation of Present Nuclear Fuel Reprocessing Technology for the Reprocessing of LMFBR Fuels," presented at the 63rd Annual A.I.Ch.E. Meeting, Chicago, Nov. 29–Dec. 3, 1970; to be published in the proceedings.

28. General Engineering Division.
29. Nuclear Fuel Services, Inc.

Yarbro, O. O., D. J. Crouse, and G. I. Cathers, "Iodine Behavior and Control in Processing Plants for Fast Reactor Fuels," presented at the 11th AEC Air Cleaning Conference, Richland, Wash., Aug. 31–Sept. 3, 1970; to be published in the proceedings.

PROGRESS REPORTS

Arnold, W. D., and D. J. Crouse, *Chemical Applications of Nuclear Explosions (CANE): Progress Report for January 1 to March 31, 1970,* ORNL-TM-3034 (June 16, 1970).

Arnold, W. D., and D. J. Crouse, *Chemical Applications of Nuclear Explosions (CANE): Progress Report for April 1 to June 30, 1970,* ORNL-TM-3116 (Aug. 25, 1970).

Arnold, W. D., and D. J. Crouse, *Chemical Applications of Nuclear Explosions (CANE): Progress Report for July 1 to September 30, 1970,* ORNL-TM-3181 (Nov. 20, 1970).

Burch, W. D., J. E. Bigelow, and L. J. King, *Transuranium Processing Plant Semiannual Report of Production, Status, and Plans for Period Ending December 31, 1969,* ORNL-4540 (June 1970).

Burch, W. D., J. E. Bigelow, and L. J. King, *Transuranium Processing Plant Semiannual Report of Production, Status, and Plans for Period Ending June 30, 1970,* ORNL-4588 (January 1971).

Hancher, C. W., A. D. Ryon, and F. L. Rogers, *Concentration and Desalting of Protein Solutions Program Progress Report for the Period Sept. 1 to Nov. 30, 1969,* ORNL-TM-3001 (August 1970).

Hancher, C. W., A. D. Ryon, and F. L. Rogers, *Concentration and Desalting of Protein Solutions Program Progress Report for the Period December 1, 1969, to February 28, 1970,* ORNL-TM-3073 (December 1970).

Hancher, C. W., A. D. Ryon, and F. L. Rogers, *Concentration and Desalting of Protein Solutions Program Progress Report for the Period March 1 to May 31, 1970,* ORNL-TM-3082 (Mar. 2, 1971).

Kelmers, A. D., *Biological Macromolecular Separations Technology Project Progress Report for the Period July 1, 1970, through September 30, 1970,* ORNL-TM-3150 (October 1970).

Kelmers, A. D., *Biological Macromolecular Separations Technology Project Progress Report for the Period October 1, 1970, through December 31, 1970,* ORNL-TM-3280 (February 1971).

McNeese, L. E., *Engineering Development Studies for Molten-Salt Breeder Reactor Processing No. 1,* ORNL-TM-3053 (November 1970).

McNeese, L. E., *Engineering Development Studies for Molten-Salt Breeder Reactor Processing No. 2,* ORNL-TM-3137 (February 1971).

Scott, C. D., et al., *Body Fluids Analyses Program Progress Report for the Period September 1, 1969, to February 28, 1970,* ORNL-TM-2966 (June 1970).

Scott, C. D., C. A. Burtis,[1] J. E. Caton,[2] J. E. Mrochek, and W. W. Pitt, Jr., *Biochemical Separation Systems Development Section of the Molecular Anatomy Program Progress Report for the Period March 1, 1970, to August 31, 1970,* ORNL-TM-3166 (December 1970).

Staffs of the Chemical Technology and the Metals and Ceramics Divisions, *LMFBR Fuel Cycle Studies Progress Report for April 1970, No. 14,* ORNL-TM-2996 (May 1970).

Staffs of the Chemical Technology and the Metals and Ceramics Divisions, *LMFBR Fuel Cycle Studies Progress Report for May 1970, No. 15,* ORNL-TM-3018 (June 1970).

Staffs of the Chemical Technology and the Metals and Ceramics Divisions, *LMFBR Fuel Cycle Studies Progress Report for June 1970, No. 16,* ORNL-TM-3072 (July 1970).

Staffs of the Chemical Technology and the Metals and Ceramics Divisions, *LMFBR Fuel Cycle Studies Progress Report for July 1970, No. 17,* ORNL-TM-3095 (August 1970).

Staffs of the Chemical Technology and the Metals and Ceramics Divisions, *LMFBR Fuel Cycle Studies Progress Report for August 1970, No. 18,* ORNL-TM-3127 (September 1970).

Staffs of the Chemical Technology and the Metals and Ceramics Divisions, *LMFBR Fuel Cycle Studies Progress Report for September 1970, No. 19,* ORNL-TM-3180 (October 1970).

Staffs of the Chemical Technology and the Metals and Ceramics Divisions, *LMFBR Fuel Cycle Studies Progress Report for October 1970, No. 20,* ORNL-TM-3217 (November 1970).

Staffs of the Chemical Technology and the Metals and Ceramics Divisions, *LMFBR Fuel Cycle Studies Progress Report for November 1970, No. 21,* ORNL-TM-3250 (January 1971).

Staffs of the Chemical Technology and the Metals and Ceramics Divisions, *LMFBR Fuel Cycle Studies Progress Report for December 1970, No. 22,* ORNL-TM-3281 (January 1971).

Staffs of the Chemical Technology and the Metals and Ceramics Divisions, *LMFBR Fuel Cycle Studies Progress Report for January 1971, No. 23,* ORNL-TM-3312 (February 1971).

Staffs of the Chemical Technology and the Metals and Ceramics Divisions, *LMFBR Fuel Cycle Studies Progress Report for February 1971, No. 24,* ORNL-TM-3345 (March 1971).

Staffs of the Chemical Technology and the Metals and Ceramics Divisions, *Thorium Fuel Cycle Development Progress Report, March 1970, No. 8,* ORNL-TM-3004 (June 1970).

Staffs of the Chemical Technology and the Metals and Ceramics Divisions, *Thorium Fuel Cycle Development Progress Report, April 1970, No. 9,* ORNL-TM-3015 (June 1970).

Staffs of the Chemical Technology and the Metals and Ceramics Divisions, *Thorium Fuel Cycle Development Progress Report, May 1970, No. 10,* ORNL-TM-3032 (June 1970).

Staffs of the Chemical Technology and the Metals and Ceramics Divisions, *Thorium Fuel Cycle Development Progress Report, June 1970, No. 11,* ORNL-TM-3088 (August 1970).

Staffs of the Chemical Technology and the Metals and Ceramics Divisions, *Thorium Fuel Cycle Development Progress Report, July 1970, No. 12,* ORNL-TM-3112 (August 1970).

Staffs of the Chemical Technology and the Metals and Ceramics Divisions, *Thorium Fuel Cycle Development Progress Report, August 1970, No. 13,* ORNL-TM-3124 (September 1970).

Staffs of the Chemical Technology and the Metals and Ceramics Divisions, *Thorium Fuel Cycle Development Progress Report, September 1970, No. 14,* ORNL-TM-3176 (October 1970).

Staffs of the Chemical Technology and the Metals and Ceramics Divisions, *Thorium Fuel Cycle Development Progress Report, October 1970, No. 15,* ORNL-TM-3204 (November 1970).

SEPARATIONS CHEMISTRY

Davis, W., Jr., and A. H. Kibbey, *Phase Decomposition of Tributyl Phosphate at 35 to 75°C in Nitric Acid Solutions,* ORNL-TM-3062 (August 1970).

Hurst, F. J., D. J. Crouse, and K. B. Brown, "Recovery of Uranium from Commercial Phosphoric Acids," presented at the 161st National American Chemical Society Meeting, Los Angeles, Mar. 28–Apr. 2, 1971.

McDowell, W. J., "Liquid Scintillation Counting Techniques for the Higher Actinides," presented at the International Conference on Liquid Scintillation Counting, University of California, San Francisco Medical Center, July 7–10, 1970; published in *Organic Scintillators and Liquid Scintillation Counting,* ed. by Donald L. Horrocks, pp. 937–50, Academic, New York, 1971.

McDowell, W. J., and C. F. Coleman, "Sulfate Complexes of the Transplutonium Actinides and Europium," presented at the Southeastern Regional Meeting of the American Chemical Society, New Orleans, Dec. 2–4, 1970.

Roddy, J. W., and C. F. Coleman, "A Versatile Empirical Equation for Interpolating Osmotic Coefficient Data," *J. Inorg. Nucl. Chem.* 32, 3956–58 (1970).

Roddy, J. W., and C. F. Coleman, "Reference Solutes for Isopiestic and Dynamic Vapor Pressure Osmometry in Organic Solvents: Triphenylmethane, Azobenzene, and Benzil in Dry Benzene," *J. Inorg. Nucl. Chem.* 32, 3891–98 (1970).

Roddy, J. W., and C. F. Coleman, "Mechanism of the Slow Extraction of Beryllium from Acid Perchlorate Solutions by Di(2-ethylhexyl)phosphoric Acid in *n*-Octane," presented at the 161st National Meeting of the American Chemical Society, Los Angeles, Mar. 28–Apr. 2, 1971.

SOL-GEL PROCESSES

Bond, W. D., ORNL-4587 (August 1970) (classified).

Haas, P. A., "Preparation of Sol-Gel Spheres Smaller than 200 Microns without Fluidization," *Nucl. Technol.* **10**, 283–92 (1971).

Haire, R. G., and T. E. Willmarth,[2] "Effect of Aging Media on the Morphology of $Pr(OH)_3$," presented at the Seventh International Congress on Electron Microscopy, Paris, France, Aug. 30–Sept. 5, 1970.

Kitts, F. G., R. E. Brooksbank, R. G. Haire, and M. H. Lloyd, *Mound Assistance Program: Development of a Sol-Gel Process and Equipment for the Production of Dense $^{238}PuO_2$ Microspheres,* ORNL-4565 (March 1971).

Luina, A. P.,[30] P. A. Haas, and C. C. Haws, Jr., *Ion Exchange for Recycle of 2-Ethyl-1-hexanol to Sol-Gel Preparation of Spheres,* ORNL-TM-3226 (Feb. 9, 1971).

McCorkle, K. H., and C. S. Morgan,[22] "Desintering of Thoria," presented at the Joint Fall Meeting, Basic Science and Nuclear Divisions, American Ceramic Society, Gatlinburg, Tenn., Nov. 3–6, 1970.

THESIS

Holmes, J. M., *The Impact of Nuclear Energy Centers on the Economy of Puerto Rico,* Ph.D. dissertation, University of Tennessee, Knoxville, July 1970.

TRANSURANIUM ELEMENT PROCESSING

Baybarz, R. D., "Recovery and Application of the Transuranium Elements ^{237}Np, ^{238}Pu, ^{241}Am, ^{242}Cm, ^{244}Cm, and ^{252}Cf," *At. Energy Rev.* 8(2), 327–60 (1970).

Hanson, C. L.,[31] M. S. Coops,[31] and E. D. Arnold, "Shielded Neutron Shipping Cask," presented at the 18th Conference on Remote Systems Technology, Washington, D.C., Nov. 17–19, 1970.

Jarvis, J. P., W. D. Burch, and J. M. Chandler, "Transfer of Californium Sources by Pneumatic Rabbit," presented at the 18th Conference of Remote Systems Technology, Washington, D.C., Nov. 17–19, 1970; to be published in the proceedings.

Peishel, F. L., W. D. Burch, and J. P. Jarvis, "Design and Installation of the TURF Californium Facility," presented at the 18th Conference on Remote Systems Technology, Washington, D.C., Nov. 17–19, 1970; to be published in the proceedings.

WASTE TREATMENT AND DISPOSAL

Bell, M. J., *An Analysis of the Diffusion of Radioactivity from Encapsulated Wastes,* ORNL-TM-3232 (February 1971).

Blanco, R. E., "Management of Radioactive Wastes," presented at the AEC-SINB Conference on Briefing for State and Local Government Officials on Nuclear Developments, Columbia, S.C., May 21–22, 1970.

Blanco, R. E., "General Discussion on Fuel Processing and Waste Disposal," presented at the Fifth Annual Tennessee Industries Week, University of Tennessee, Knoxville, Sept. 14–18, 1970.

Blanco, R. E., "Treatment and Disposal of Nuclear Power Reactor Wastes," presented in an ORAU seminar, Oak Ridge, Tenn., Jan. 7, 1971.

Blanco, R. E., "Management of Radioactive Wastes," presented at the Physics Division Seminar, ORNL, Jan. 15, 1971.

Blanco, R. E., "Management of Radioactive Wastes from Nuclear Power and Fuel Reprocessing Plants," presented at the Symposium on Technology for the Future to Control Industrial and Urban Wastes, University of Missouri, Rolla, Feb. 9, 1971.

---

30. Guest scientist from Spain.
31. Lawrence Radiation Laboratory, Livermore, Calif.

Blomeke, J. O., "A Salt Mine Repository for Radioactive Wastes," presented at the American Nuclear Society Meeting, Washington, D.C., Nov. 15–19, 1970.

Clark, W. E., *The Status of Pressurized Aqueous Combustion for Burning Solid Wastes Contaminated by Radionuclides,* ORNL-TM-3170 (October 1970).

Fitzgerald, C. L., H. W. Godbee, R. E. Blanco, and W. Davis, Jr., "The Feasibility of Incorporating Radioactive Wastes in Asphalt or Polyethylene," *Nucl. Appl. Technol.* **9**(6), 821–29 (1970).

Godbee, H. W., and J. P. Nichols, ORNL-TM-3277 (January 1971) (Official Use Only).

Perona, J. J.,[32] J. O. Blomeke, and R. S. Dillon, "Design and Safety Considerations in the Shipment of Solidified Wastes," presented at the Winter Meeting of the American Nuclear Society, Washington, D.C., Nov. 15–19, 1970.

Perona, J. J.,[32] R. S. Dillon, and J. O. Blomeke, *Design and Safety Considerations of Shipping Solidified High-Level Radioactive Wastes,* ORNL-TM-2971 (Dec. 30, 1970).

Rainey, R. H., W. L. Carter, and S. Blumkin,[33] *Completion Report – Evaluation of the Use of Permselective Membranes in the Nuclear Industry for Removing Radioactive Xenon and Krypton from Various Off-Gas Streams,* ORNL-4522 (April 1971).

Staff of the Oak Ridge National Laboratory, *Siting of Fuel Reprocessing Plants and Waste Management Facilities,* ORNL-4451 (July 1970).

Yee, W. C., F. DeLora,[34] and W. E. Shockley, *Low-Level Radioactive Waste Treatment: The Water Recycle Process,* ORNL-4472 (July 1970).

---

32. Consultant, University of Tennessee, Knoxville.
33. ORGDP.
34. Present address: Ministerio de Industria, Junta de Energia Nuclear, Madrid, Spain.

SEMINARS

1970

November 4	Analytical Services and Capabilities at ORNL	W. R. Laing[2] D. A. Costanzo[2]
November 11	Liquid Scintillation Counting for the Higher Actinides	W. J. McDowell
November 19	MSBR Fuel Processing	
	Chemical Studies Relating to the Metal Transfer Process	F. J. Smith
	Isolation of Protactinium and Californium	J. C. Mailen
December 2	Health Physics Tolerance Levels	K. Z. Morgan[35]
December 9	Colloid Flocculation	I. L. Thomas
December 16	Adsorption of Acid Species on Uranium Oxide Surface	K. H. McCorkle

1971

January 6	The Application of Quality Assurance Techniques to Applied Research and Development	L. B. Shappert
January 13	An Analysis of Head-End Heat Dissipation Problems in LMFBR Processing	R. L. Cox
	An Analysis of New LMFBR Dissolver Concepts	W. S. Groenier
January 20	Photochemical Bond Breaking in Cyclic Compounds by UV	R. T. Swindell[36]
January 27	Water Pollution Studies	S. Katz
February 9	Studies on the Chemical and Colloidal Nature of Pu(IV) Polymer	M. H. Lloyd
February 17	Thermodynamics of Lanthanide Complexes	G. Choppin[37]
February 25	Systems for Trapping Radioiodine	
	Solid Sorbents	R. D. Ackley J. G. Moore
	Liquid Scrubbers	G. I. Cathers
March 3	Studies of Iodine Chemistry	
	Volatilization from Solutions	G. I. Cathers
	Spectrophotometric Studies	A. H. Kibbey
March 17	Switzerland – Science and Scenery, or Fifty-Four Weeks Amidst Snow and Spheres	K. J. Notz
March 25	Engineering Studies of the Metal-Transfer Process for Removal of Rare Earths from an MSBR	E. L. Youngblood
	Hydrodynamics in Packed Columns During Countercurrent Flow of Fluids Having a Large Density Difference	J. S. Watson

35. Health Physics Division.
36. Tennessee Technological University, Cookeville.
37. Florida State University, Tallahassee.

CHEMICAL TECHNOLOGY DIVISION

MARCH 31, 1971

D. E. FERGUSON, DIRECTOR
K. B. BROWN, ASSISTANT DIRECTOR
ALICE McWILLIAMS, SECRETARY
JUNE REDMOND, SECRETARY
F. N. BROWDER, RADIATION AND SAFETY CONTROL OFFICER
A. T. GRESKY, SPECIAL ASSIGNMENT
MARTHA STEWART, REPORTS EDITOR

H. B. GRAHAM, ADMINISTRATIVE ASSISTANT
DONNA FITZGERALD, SECRETARY
W. O. GREEVER,[1] PROCUREMENT
LUCILLE KUYKENDALL, SECRETARY

LONG RANGE PLANNING COMMITTEE

J. P. NICHOLS, CHAIRMAN
E. D. ARNOLD
M. J. BELL
O. L. CULBERSON[2]
V. A. DeCARLO
D. S. JOY
J. T. ROBERTS[3]
R. SALMON
H. F. SOARD
F. G. WELFARE[4]
IMOGENE LOOPE, SECRETARY
LINDA KNAUER, PROGRAMMER
P. P. HAYOON, TECHNICIAN[8]

CHEMICAL DEVELOPMENT SECTION A

R. G. WYMER, SECTION CHIEF
R. E. LEUZE, ASSISTANT SECTION CHIEF
C. F. COLEMAN, ASSISTANT SECTION CHIEF
RUBY MILLER, SECRETARY
CAROLYN GREEN, SECRETARY
MARCIA CAMPBELL, SECRETARY

TECHNICIAN: C. F. KECK

SOL-GEL STUDIES

J. F. McBRIDE, GROUP LEADER
L. E. MORSE
W. L. PATTISON

TECHNICIAN: J. F. TALLEY

FUEL CYCLE STUDIES

W. D. BOND, GROUP LEADER
K. J. NOTZ
A. B. MESERVEY

TECHNICIAN: C. W. GREENE

SEPARATIONS CHEMISTRY RESEARCH FUNDAMENTAL CHEMISTRY

W. J. McDOWELL, PROBLEM LEADER
J. W. RODDY, PROBLEM LEADER

TECHNICIANS: G. N. CASE
J. E. THOMPSON

B. WEAVER, GROUP LEADER, SEPARATIONS RESEARCH
R. R. SHOUN

ACTINIDE SEPARATIONS AND ANALYSIS

D. O. CAMPBELL, PROBLEM LEADER

TRANSURANIUM ELEMENT PROCESSING

M. H. LLOYD, GROUP LEADER, TRU PROCESS DEVELOPMENT AND FINAL SEPARATIONS
S. R. BUXTON
J. M. CHILTON
J. B. KNAUER
P. B. ORR
O. K. TALLENT
J. R. FLANARY, FLOWSHEET IMPROVEMENT

TECHNICIANS: L. A. BYRD[8]
E. C. HENDREN[7]
C. H. JONES
A. S. LYLE
S. A. McCOSH

R. D. BAYBARZ, GROUP LEADER, TRU RESEARCH
F. A. KAPPELMANN
L. G. FARRAR[7]
H. A. FRIEDMAN[8]
B. J. STURM[8]

R. G. HAIRE, PROBLEM LEADER, ELECTRON MICROSCOPY, DTA, TGA

TECHNICIANS: R. L. HICKEY
D. H. NEWMAN
J. T. WIGGINS

ACTINIDE ELEMENT OXIDES AND COLLOID SYSTEMS

K. H. McCORKLE
I. L. THOMAS

HETEROGENEOUS SYSTEMS

N. A. KROHN,[9] GROUP LEADER

ACTINIDE ELEMENT SPECTROPHOTOMETRY

J. T. BELL, PROBLEM LEADER
N. A. KROHN[9]

TECHNICIAN: D. M. HELTON

BIOCHEMICAL SEPARATIONS

A. D. KELMERS, GROUP LEADER
B. Z. EGAN
R. L. PEARSON
J. F. WEISS

TECHNICIANS: J. P. EUBANKS
D. E. HEATHERLY
J. B. OVERTON

BODY FLUIDS ANALYSES

C. D. SCOTT, GROUP LEADER
M. R. BENNETT
J. C. MAILEN[9]

TECHNICIAN: N. E. LEE

J. E. MROCHEK, GROUP LEADER, BFA CHEMICAL IDENTIFICATION AND APPLICATIONS
W. C. BUTTS[7]
R. L. JOLLEY

TECHNICIAN: M. L. FREEMAN

W. W. PITT, GROUP LEADER, BFA SYSTEMS DEVELOPMENT: POLLUTION
D. O. CHILCOTE
S. KATZ

TECHNICIANS: S. R. DINSMORE[7]
G. JONES, JR.

CHEMICAL DEVELOPMENT SECTION B

R. E. BLANCO, SECTION CHIEF
D. J. CROUSE,[9] ASSISTANT SECTION CHIEF
L. M. FERRIS,[9] ASSISTANT SECTION CHIEF
SUE DAMEWOOD, SECRETARY
JO DeCARLO, SECRETARY
J. E. FARMER, DRAFTSMAN

SPECTROCHEMISTRY OF IODINE SOLUTIONS

W. DAVIS, JR., GROUP LEADER
A. H. KIBBEY

RADIOACTIVE WASTE STUDIES

H. W. GOODBEE, GROUP LEADER, CHARACTERIZATION OF SOLID PLUTONIUM-BEARING WASTES AND SOLIDIFIED HIGH-LEVEL WASTES

TECHNICIAN: M. V. CONNELLY[10]

W. E. CLARK, GROUP LEADER, COMBUSTION OF PLUTONIUM-BEARING SOLID WASTES

POWER REACTOR FUEL PROCESSING

V. C. A. VAUGHEN, GROUP LEADER, FLOWSHEET DEMONSTRATION ON RADIOACTIVE LMFBR, HTGR, AND LWR FUEL PROCESSING
J. H. GOODE
C. L. FITZGERALD

TECHNICIANS: G. D. DAVIS
O. L. KIRKLAND

L. M. FERRIS,[9] GROUP LEADER, MOLTEN SALT REACTOR FUEL PROCESSING
J. C. MAILEN
C. E. SCHILLING
F. J. SMITH

TECHNICIANS: J. F. LAND
C. T. THOMPSON

R. H. RAINEY, GROUP LEADER, SOLVENT EXTRACTION AND FUEL DISSOLUTION IN LMFBR FUEL PROCESSING AND REPURIFICATION OF ^{233}U
D. E. HORNER

TECHNICIANS: J. R. COLLINS
R. C. LOVELACE

G. I. CATHERS, GROUP LEADER, IODINE RETENTION IN LMFBR FUEL PROCESSING

TECHNICIANS: C. J. SHIPMAN
W. E. SHOCKLEY

SEPARATIONS PROCESSES RESEARCH

D. J. CROUSE,[9] GROUP LEADER
F. J. HURST
F. G. SEELEY

TECHNICIAN: W. B. HOWERTON

RADIOIODINE CHEMISTRY, RADIATION STABILITY OF SOLVENTS IN LMFBR FUEL PROCESSING

D. J. CROUSE,[9] GROUP LEADER
J. M. SCHMITT
J. G. MOORE

PLOWSHARE PROGRAM

D. J. CROUSE[9]
W. D. ARNOLD

TECHNICIAN: D. E. SPANGLER

UNIT OPERATIONS SECTION

M. E. WHATLEY, SECTION CHIEF
A. D. RYON,[9] ASST. SECTION CHIEF
JANICE SHANNON, SECRETARY
LINDA LOVEDAY, SECRETARY
MARCIA HENEGAR, SECRETARY

HTGR PROCESSING AND FUEL CYCLE STUDIES

P. A. HAAS, GROUP LEADER
B. C. FINNEY
R. W. GLASS
C. C. HAWS, JR.
R. S. LOWRIE
A. P. LUINA[11]

TECHNICIANS: R. D. ARTHUR
E. R. JOHNS[12]
K. LADD
D. A. McWHIRTER
C. H. TIPTON

MOLTEN SALT REACTOR PROCESSING

L. E. McNEESE, GROUP LEADER
B. A. HANNAFORD
J. R. HIGHTOWER
S. H. JURY[2]
C. W. KEE
R. B. LINDAUER
J. ROTH[13]
C. P. TUNG[14]
J. S. WATSON
H. G. WEEREN[9]
E. L. YOUNGBLOOD

TECHNICIANS: J. BEAMS
V. L. FOWLER
R. O. PAYNE
J. S. TAYLOR

BIOCHEMICAL SEPARATIONS

A. D. RYON,[9] GROUP LEADER
C. W. HANCHER
D. W. HOLLADAY
H. D. WEEREN[9]

TECHNICIANS: G. B. DINSMORE
F. G. KILPATRICK
F. L. ROGERS
W. G. SISSON[15]

LMFBR FUEL PROCESSING

C. D. WATSON, GROUP LEADER
S. D. CLINTON
R. L. COX
S. M. GOLDBERG[16]
W. S. GROENIER
H. F. JOHNSON[2]
G. A. WEST
W. M. WOODS

TECHNICIANS: J. C. ROSE
D. E. WILLIS

PROCESS DESIGN SECTION

H. E. GOELLER,[9] SECTION CHIEF
W. E. UNGER, ASSISTANT SECTION CHIEF
F. N. BROWDER,[9] DIVISION RADIATION AND SAFETY CONTROL OFFICER
H. E. GOELLER,[9] AGRO-INDUSTRIAL STUDY
F. E. HARRINGTON,[9] PLUTONIUM SOL-GEL STUDIES
J. M. HOLMES,[9] AGRO-INDUSTRIAL STUDY
F. L. PEISHEL, TRANSURANIUM ASSISTANCE
L. B. SHAPPERT,[9] DIVISION QUALITY ASSURANCE PROGRAM
W. G. STOCKDALE, ECONOMIC SURVEYS, SECTION EDITOR FOR NUCLEAR SAFETY, ENVIRONMENTAL QUALITY PROJECT ASSISTANCE, AND NSIC
MAY E. PEPPER, SECRETARY
MARY S. BROWN, SECRETARY
NANCY L. POPE, SECRETARY
K. F. STOOKSBURY, CLERK

DRAFTSMEN

D. E. DUNNING,[17] DRAFTING SUPERVISOR

B. G. DeVALL
A. J. FARMER
G. K. FORD[17]
J. H. FREELS[17]
A. H. GREGORY[17]
B. F. HENRY[17]
L. C. HUBBARD[17]
J. W. KIDD[17]
J. L. LUCKETT[18]
J. R. McINTOSH[17]
R. P. OLIVER[17]
J. D. PHILLIPS[17]
F. J. UNDERWOOD[17]

WASTE STUDIES — SALT MINE REPOSITORY

J. O. BLOMEKE, GROUP LEADER
B. F. BOTTENFIELD, PROJECT ENGINEER
F. N. BROWDER,[9] ORNL WASTE PRACTICES
R. S. DILLON, ECONOMIC EVALUATION
E. J. FREDERICK, ENGINEERING LIAISON
F. E. HARRINGTON,[9] LOW-LEVEL TREATMENT
J. M. HOLMES,[9] DESIGN EVALUATION
J. J. PERONA,[2] CONSULTANT, THERMAL TRANSPORT
W. C. ULRICH,[4] WET OXIDATION

MSR STUDIES

E. L. NICHOLSON, GROUP LEADER
W. L. CARTER, MSBR FUEL PROCESSING STUDIES
W. F. SCHAFFER, JR., MSBR EQUIPMENT DESIGN
E. L. YOUNGBLOOD, EQUIPMENT DEVELOPMENT

AQUEOUS LMFBR FUEL PROCESSING

A. R. IRVINE, GROUP LEADER
B. B. KLIMA, FUEL HANDLING AND SODIUM DEACTIVATION
S. MANN, PLUTONIUM STUDIES
A. M. ROM, FEED PREPARATION
L. B. SHAPPERT,[9] FUEL TRANSPORT STUDIES
O. O. YARBRO, IODINE STUDIES

Y-12 ENGINEERING ASSISTANCE

G. B. BERRY[17]
R. V. FOLTZ[17]
J. W. LANDRY
J. B. RUCH

THORIUM UTILIZATION

J. W. SNIDER,[9] GROUP LEADER
R. J. BRAATZ,[17] EQUIPMENT DESIGN
T. L. GOLSON,[17] MECHANICAL DESIGN

BETTIS LWBR SUPPORT PROGRAM

F. E. HARRINGTON,[9] PURIFICATION SYSTEMS
J. W. SNIDER,[9] $^{233}UO_2$ FACILITY
T. L. DOUGLASS, MECHANICAL DESIGN

PILOT PLANT SECTION

R. E. BROOKSBANK, SECTION CHIEF
W. D. BURCH,[9] ASSISTANT SECTION CHIEF
BOBBIE HOYLE, SECRETARY
WILMA BALDRY, SECRETARY
SHEILA FERREE, SECRETARY
BETTY McHARGUE, SECRETARY
R. B. WATERS, DRAFTSMAN

TRANSURANIUM PROCESSING PLANT

W. D. BURCH,[9] GROUP LEADER
L. J. KING, TECHNICAL GROUP
J. L. MATHERNE, ENGINEERING, PLANT SAFETY
F. R. CHATTIN, OPERATIONS
J. E. BIGELOW
E. D. COLLINS
W. W. EVANS
F. L. PEISHEL[19]
C. L. SHEPHERD
J. E. VAN CLEVE[20]
L. C. WILLIAMS[20]

PROCESS SUPERVISORS

O. B. OWSLEY
R. C. SHIPWASH
B. J. STRADER[20]
C. E. WADDELL

TECHNICIANS

W. G. BARRETT
K. P. BAYNE[20]
W. J. BRYAN
J. H. BROCK
E. W. BROWN
H. S. CALDWELL
E. B. CAGLE
J. E. EVE[20]
J. H. GROOVER
M. C. HILL
A. L. JOHNSON
R. R. LAXSON
J. F. LOCKMILLER
R. E. POTTER[20]
C. E. ROBERTS
O. W. SCATES
L. J. SHERSKY
W. M. SPROULE
J. L. STEPP
H. C. THOMPSON
A. V. WILDER
C. M. WILSON[20]
G. E. WOODALL

RADIOCHEMICAL OPERATIONS

J. R. PARROTT, GROUP LEADER, LWBR SUPPORT, ^{233}U DISPENSING
W. T. McDUFFEE,[9] QUALITY ASSURANCE
R. W. HORTON, SAFETY ANALYSIS
R. G. NICOL, PURIFICATION OPERATIONS
T. L. DOUGLASS,[21] OXIDE LINE OPERATIONS
W. R. WHITSON, IN-PLANT ENGINEERING

PROCESS SUPERVISORS

R. J. SHANNON
W. A. SHANNON

TECHNICIANS

A. L. BEETS
E. C. BRANTLEY
W. A. LINDSEY
C. W. MARTIN
R. E. PURKEY
J. H. WALKER

W. T. McDUFFEE,[9] GROUP LEADER, SOL-GEL PROGRAM
F. L. DALEY
F. G. KITTS

TECHNICIANS: C. W. BOATMAN
S. E. SHELL

HOT CELL FACILITY

V. C. A. VAUGHEN, GROUP LEADER, PLANT SAFETY

TURF FACILITY

J. M. CHANDLER,[22] GROUP LEADER

TECHNICIAN: W. T. BOSTIC

[1] ON LOAN FROM PLANT AND EQUIPMENT DIVISION.
[2] CONSULTANT, U.T.
[3] LEAVE OF ABSENCE.
[4] ON LOAN FROM REACTOR DIVISION.
[5] ON LOAN TO Y-12.
[6] ON LOAN FROM CHEMICAL DEVELOPMENT SECTION B.
[7] ASSIGNED TO THIS PROBLEM BY THE ANALYTICAL CHEMISTRY DIVISION.
[8] ASSIGNED TO THE TRANSURANIUM RESEARCH LABORATORY.
[9] DUAL CAPACITY.
[10] ON LOAN FROM ANALYTICAL CHEMISTRY DIVISION.
[11] GUEST SCIENTIST FROM SPAIN.
[12] ON LOAN FROM CHEMICAL DEVELOPMENT SECTION A.
[13] GUEST SCIENTIST FROM COMBUSTION ENGINEERING, WINDSOR, CONN.
[14] GUEST SCIENTIST FROM TAIWAN.
[15] ON LOAN TO CHEMISTRY DIVISION.
[16] ASSIGNEE FROM U.S. ATOMIC ENERGY COMMISSION.
[17] ON LOAN FROM GENERAL ENGINEERING DIVISION.
[18] PART TIME ON LOAN FROM NUCLEAR DATA PROJECT.
[19] ON LOAN FROM PROCESS DESIGN SECTION.
[20] ON LOAN FROM METALS AND CERAMICS DIVISION.
[21] ON LOAN TO PROCESS DESIGN SECTION.
[22] ON LOAN TO METALS AND CERAMICS DIVISION.

INTERNAL DISTRIBUTION

1. Biology Library
2–4. Central Research Library
5. Laboratory Shift Supervisor
6–7. ORNL – Y-12 Technical Library
Document Reference Section
8. MIT Practice School
9–28. Laboratory Records Department
29. Laboratory Records, ORNL R.C.
30. H. I. Adler
31. R. D. Baybarz
32. S. E. Beall
33. Arnold Berman
34. D. S. Billington
35. R. E. Blanco
36. J. O. Blomeke
37. W. D. Bond
38. C. J. Borkowski
39. G. E. Boyd
40. R. E. Brooksbank
41. J. C. Bresee
42. R. B. Briggs
43. F. N. Browder
44. K. B. Brown
45. F. R. Bruce
46. W. D. Burch
47. D. O. Campbell
48. G. I. Cathers
49. J. M. Chandler
50. W. E. Clark
51. C. F. Coleman
52. W. C. Colwell
53. J. A. Cox
54. D. J. Crouse
55. F. L. Culler
56. J. E. Cunningham
57. W. Davis, Jr.
58–257. D. E. Ferguson
258. L. M. Ferris
259. J. L. Fowler
260. J. H. Frye, Jr.
261. R. C. Fuller
262. J. H. Gillette
263. H. W. Godbee
264. H. E. Goeller
265. H. B. Graham
266. A. T. Gresky
267. W. R. Grimes
268. P. A. Haas
269. J. P. Hammond
270. C. S. Harrill
271. R. F. Hibbs
272. R. W. Horton
273. A. R. Irvine
274. R. L. Jolley
275. W. H. Jordan
276–282. P. R. Kasten
283. M. A. Kastenbaum
284. M. T. Kelley
285. A. D. Kelmers
286. F. Kertesz
287. L. J. King
288. E. Lamb
289. J. A. Lane
290. R. E. Leuze
291. R. B. Lindauer
292. J. L. Liverman
293. R. S. Livingston
294. M. H. Lloyd
295. F. C. Maienschein
296. J. P. McBride
297. W. J. McDowell
298. L. E. McNeese
299. R. A. McNees
300. A. B. Meservey
301. K. Z. Morgan
302. J. P. Nichols
303. E. L. Nicholson
304. K. J. Notz
305. G. D. Novelli
306–307. R. B. Parker
308. J. R. Parrott
309. Helen Raaen
310. R. H. Rainey
311. M. E. Ramsey
312. J. T. Roberts
313. A. F. Rupp
314. A. D. Ryon
315. C. D. Scott
316. H. E. Seagren
317. L. B. Shappert
318. M. J. Skinner
319. A. H. Snell
320. M. G. Stewart
321. D. A. Sundberg
322. E. H. Taylor
323. D. B. Trauger

324. W. E. Unger
325. V. C. A. Vaughen
326. C. D. Watson
327. B. S. Weaver
328. A. M. Weinberg
329. M. E. Whatley
330. J. C. White
331. R. G. Wymer
332. B. J. Young
333. Gale Young
334. E. L. Youngblood
335. P. H. Emmett (consultant)
336. J. J. Katz (consultant)
337. E. A. Mason (consultant)
338. C. H. Ice (consultant)
339. R. B. Richards (consultant)

EXTERNAL DISTRIBUTION

340. D. F. Cope, RDT Site Office (ORNL)
341. Richard Hamburger, AEC, Washington
342. J. A. Swartout, 270 Park Avenue, New York 17, New York
343. Dr. Barendregt, c/o COMPRIMO, Europahuis, James Wattstraat 79, Amsterdam, Holland
344. Bruce Deering, Black and Veatch Consulting Engineers, 1500 Meadowlake Parkway, P.O. Box 8405, Kansas City, Missouri
345. Giacomo Calleri, Comitato Nazionale per l'Energia Nucleare, Programma EUREX, Saluggia (Vc), Italy
346. D. J. Carswell, Radiochemical Laboratory, The New South Wales University of Technology, P.O. Box 1, Kensington, Sydney, N.S.W., Australia
347. E. Cerrai, Laboratori CISE, Casella Postale N. 3986, Milano, Italy
348. David Dyrssen, The Royal Institute of Technology, Department of Inorganic Chemistry, Kemisträgen 37, Stockholm 70, Sweden
349. Syed Fareeduddin, Indian Rare Earths Ltd., Army and Navy Building, 148 Mahatma Gandhi Road, Bombay 1, India
350. T. Ishihara, Division of Fuel Research and Development, Tokai Research Establishment, JAERI, Tokai-mura, Ibaraki-ken, Japan
351. A. S. Kertes, Hebrew University, Jerusalem
352. Jorgen Klitgaard, Atomic Energy Commission Res. Estab. Risö, Roskilde, Denmark
353. Y. Marcus, Israel Atomic Energy Commission, Tel Aviv, Israel
354. E. Glueckauf, Atomic Energy Research Establishment, Harwell, Berks, England
355. P. Regnaut, C.E.N. Fontenay-aux-Roses, Boite Postale No. 6, Fontenay-aux-Roses, Seine, France
356. R. Rometsch, Eurochemic, Mol, Belgium
357. A. J. A. Roux, Director of Atomic Energy Research, South African Council for Scientific and Industrial Research, Box 395, Pretoria, South Africa
358. Jan Rydberg, Department of Nuclear Chemistry, Chalmers Tekniska Hogskola, Gibraltargatan 5 H. Goteborg, Sweden
359. M. Shaw, AEC, Washington
360. Erik Svenke, Director, Department of Chemistry, Atomic Energy Company, Stockholm 9, Sweden
361. D. G. Tuck, Associate Professor, Department of Chemistry, Simon Fraser University, Burnaby 2, British Columbia, Canada
362. B. F. Warner, United Kingdom Atomic Energy Authority, Production Group, Windscale and Calder Works, Sellafield, Seascale, Cumberland, England
363. M. Zifferero, Comitato Nazionale per l'Energia Nucleare, Laboratorio Trattamento Elementi Combustibili, c/o Instituto di Chemica Farmaceutica e Tossicologica dell 'Universita, Piazzale delle Scienze, 5, Rome, Italy
364. M. Claude Jean Jouannaud, Department Head, Plutonium Extraction Plant, Marcoule (Gard), France
365. Prof. Louis Gutierrez-Jadra, Director de Planta Pilotos e Industriales, Junta de Energia Nuclear, Ciudad Universitaris, Madrid (3), Spain
366. W. G. Belter, AEC, Washington
367. J. A. Lieberman, AEC, Washington
368. W. H. Regan, AEC, Washington

369. H. Bernard, AEC, Washington
370. P. Schmid, Federal Institute for Reactor Research, Wurenlingen, AG, Switzerland
371. Atou Shimozato, Nuclear Reactor Design Section, Nuclear Power Plant Department, Hitachi Ltd., Hitachi Works, Hitachi-Shi, Ibaraki-Ken, Japan
372. R. S. Brodsky, Division of Naval Reactors, Atomic Energy Commission, Washington, D.C.
373. R. W. Barber, AEC, Washington
374. Theodore Rockwell III, Chairman AIF Safety Task Force, MPR Associates, Inc., 815 Connecticut Avenue, N.W., Washington, D.C.
375. Guenther Wirths, NUKEM, Hanau, Germany
376. Riki Kobayashi, Professor, Rice University
377. W. Pollard, Oak Ridge Associated Universities
378. Libarian, Department of Chemical Engineering and Chemical Technology, Imperial College, Prince Consort Road, London, S.W.7, England
379. Giuseppe Orsenigo, CNEN, Via Belisario 15, Rome, Italy
380. Werner Muller, European Transuranium Institute, Euratom, Postfach 2266, 75 Karlsruhe, West Germany
381. F. Baumgartner, Heidlberg University, Karlsruhe, Postfach 947, West Germany
382. Hugo Schumacher, Swiss Federal Institute for Reactor Research, Ch-5303 Wurenlingen, Switzerland
383. B. L. Vondra, NUMEC, Apollo, Pa.
384. W. H. McVey, AEC, Washington
385. E. E. Sinclair, AEC, Washington
386. A. R. Van Dyken, AEC, Washington
387. C. L. Sumrall, Gilbert Associates, Reading, Pa.
388. Dr. Narayamam Srinivasan, Head of Fuel Reprocessing Division, Bhabha Atomic Research Center, Bombay 74, India
389. D. M. Rafi, Pakistan Institute of Nuclear Science and Technology, P.O. Box Nilore, Rawal Pindi, Pakistan
390. D. E. Bloomfield, Battelle Northwest, Richland, Washington
391. P. A. DeJonghe, Centre d'Etude de l'Energie Nucleaire, Mol, Belgium
392. T. W. McIntosh, Division of Reactor Development and Technology, USAEC, Washington, D.C.
393. R. E. Pahler, AEC, Washington
394. D. R. Miller, AEC, Washington
395. J. J. Fardy, Australian Atomic Energy Commission, Lucas Heights, Sydney, Australia
396. R. E. Norman, Gulf General Atomic, P.O. Box 608, San Diego, California
397. H. O. G. Witte, Julich Nuclear Research Center, Julich, Germany
398. Alfred Richard Boettcher, Director, Julich Nuclear Research Center, Julich, Germany
399. Julich Nuclear Research Center Library, Julich, Germany
400. Hans W. Levi, Deputy Director, Hahn – Meitner – Institut fur Kernforschung Berlin, Sektor Kernchemie, Glienicker Strasse 100, 1 Berlin 39, Germany
401. William J. Lacy, Chief, Industrial Pollution Control Branch, Division of Applied Science and Technology, Federal Water Pollution Control Administration, Department of the Interior, Washington, D.C.
402. C. Djordjevic, Chemistry Department, College of William and Mary, Williamsburg, Virginia
403. G. Spaepen, Head, Chemical Technology, SCK-CEN, Mol, Belgium
404. P. S. Mathews, P. S. Mathew, Co., 5225 Wilshire Boulevard, Los Angeles, Calif. 90036
405. Ray W. Lambert, General Electric Company, Midwest Fuel Recovery Plant, Route 1, Box 219B, Morris, Ill. 60450
406. G. Rajan, Scientific Officer, Desalination and Effluent Engineering Division, Bhabha Atomic Research Centre, Bombay-85 AS, India
407. Laboratory and University Division, AEC, ORO
408. Patent Office, AEC, ORO

409–544. Given distribution as shown in TID-4500 under Chemical Separations Processes for Plutonium and Uranium category (25 copies – NTIS)